Tracer Development for the Molecular Imaging of Breast Cancer: Synthesis and Biological Evaluation of C-3 Modified 2,5-Anhydro-D-mannitol Derivatives as Potential Tracer Molecules

by

Venkata Pavan Kumar Kondapi

A thesis submitted in partial fulfillment of the requirements for the degree of

Doctor of Philosophy

Department of Chemistry
University of Alberta

Abstract

Mammography is the most frequently used imaging method for the detection of breast cancer. Despite the key role of mammography in the breast cancer detection, false-negative diagnosis by mammograms ranges from 4 to 34%. Positron emission tomography (PET), a tracer based molecular imaging method is an alternative to mammography for the detection of breast cancer. The most commonly used PET tracer [^{18}F]-2-fluoro-2-deoxy-D-glucose ([^{18}F]-FDG) also provides false-positive and false-negative diagnosis of breast cancer.

Mammalian hexose transporters (GLUTs) facilitate the transport of hexoses from the extracellular spacer to intracellular space and vice versa. To date, 14 different types of GLUTs, which exhibit difference in substrate specificity, are known. The ubiquitously expressed transporter protein GLUT1 transports [^{18}F]-FDG. Enzymatic phosphorylation of [^{18}F]-FDG with hexokinase prevents the back-transport of [^{18}F]-FDG by GLUT1. Due to minimal or complete lack of expression of GLUT1 in some breast cancer cells and ubiquitous expression of GLUT1 in some normal cells, relatively lower accumulation of [^{18}F]-FDG was observed in breast cancer cells over normal cells. After the discovery of GLUT5 in many breast cancer cells, tracers targeting this transporter were developed for the imaging of breast cancer. Unfortunately, these tracers were back transported from the breast cancer cells due to their inability to undergo enzymatic phosphorylation by hexokinase. Tracers that target the GLUT5 transporter protein and undergo enzymatic phosphorylation in the presence of hexokinase could significantly improve the efficiency of PET or optical imaging in the detection of certain types of breast cancers. This thesis comprises our studies of synthesis and biological evaluations of novel 2,5-anhydro-D-

mannitol (2,5-AM)-based scaffolds, to examine their ability to serve as tracers in the molecular imaging of early stage breast cancer.

Chapter 1 of this thesis provides a broad introduction to the hexose-based tracer development for the molecular imaging of breast cancer. Structural requirement of hexoses for the efficient GLUT-substrate binding is also overviewed in this Chapter. In Chapter 2, modification of the C-3 position of 2,5-AM *via* diastereoselective epoxide ring-opening of 2,5:3,4-dianhydro-D-allitol is described. Chapter 2 also discusses the solvent polarity effects on this epoxide ring-opening process. Chapter 3 presents the biological evaluation of 3-fluoro-3-deoxy-2,5-anhydro-D-mannitol whose ^{18}F-labeled version could potentially be used as a PET tracer for the detection of breast cancer. In addition, Chapter 3 also deals with the structure-activity relationship between GLUT5 and the C-3 modified 2,5-AM derivatives. D-Fructose and D-glucose transport inhibition into EMT-6 cells by C-3 modified 2,5-AM derivatives, followed by control experiments are used to determine the structural requirement of the C-3 modified 2,5-AM derivatives for GLUT recognition. In Chapter 4, synthesis and biological evaluations of a new probe 3-(*N*-(4-nitro-2,1,3-benzoxadiazol-7-yl))amino-2,5-anhydro-D-mannitol are described, along with docking studies performed by collaborators. Our studies demonstrate that this is the first GLUT5 targeting probe that exhibits low efflux from the murine breast tumor cells. Chapter 5 comprises the synthesis and biological evaluation of C-3 modified 2,5-AM bearing near-infrared emitting dyes as probes for the optical imaging of breast cancer.

Preface

A major part of Chapter 1 of this thesis will be published as a review article as V. P. K. Kondapi, T. Scully, P. Ghaly, O.-M. Soueidan, C. Cheeseman and F.G. West, "Structural Requirements of Hexose and GLUT for Mutual Binding: A Chemist's View of Hexose-GLUT Binding Process and its Applications in Tracer Development", *Manuscript in preparation*. The co-authors are involved in manuscript preparation. F. G. West and C. Cheeseman are the supervisory authors, involved in concept development and the manuscript preparation.

Chapter 2 of this thesis has been published as V. P. K. Kondapi, O.-M. Soueidan, S. N. Hosseini, N. Jabari and F. G. West, "Efficient and Easy Access to Optically Pure Tetrasubstituted Tetrahydrofurans *via* Stereoselective Opening of C_2-Symmetric Epoxide and Aziridine Rings", *European Journal of Organic Chemistry*, **2016**, 1367-1379. I was responsible for part of the experimental work, characterization of compounds and manuscript composition. The experimental work performed by the co-authors was briefly summarized in the Section 2.4.6. F. G. West was the supervisory author, involved in the manuscript preparation and concept development. R. MacDonald provided the X-ray data for compound **24**.

Chapter 3 of this thesis will be very soon published as V. P. K. Kondapi, O.-M. Soueidan, C. Cheeseman and F.G. West, "Hydrogen Bonding Property of the C-3 Substituent of D-Fructose Analogues: A Handle to Tune the GLUT-Hexose Binding Process", *Manuscript in preparation*. I was responsible for the experimental work, characterization of compounds, biological evaluations and manuscript preparation. O.-M. Soueidan experimentally verified some of the biological data to check the reproducibility.

F. G. West and C. Cheeseman were the supervisory authors, involved in concept development and the manuscript preparation. Further, the computational work presented in Section 3.9. will be published as R. Panigrahi, V. P. K. Kondapi, J. Lemieux, C. Cheeseman and F. G. West, *Manuscript in preparation*. R. Panigrahi was responsible for the computational work, which was supervised by J. Lemieux. I contributed to the manuscript preparation and providing biological experimental data, along with F. G. West and C. Cheeseman.

Chapter 4 will be soon published as V. P. K. Kondapi, R. Panigrahi, O.-M. Soueidan, J. Lemieux, C. Cheeseman and F.G. West, *Manuscript in preparation*. I was responsible for the experimental work, characterization of compounds, biological evaluations and manuscript preparation. O.-M. Soueidan experimentally verified some of the biological data to check the reproducibility. F. G. West and C. Cheeseman were the supervisory authors and were also involved in the manuscript preparation. R. Panigrahi was responsible for the computational work, which was presented in Section 4.10. The computational work was supervised by J. Lemieux.

Chapter 5 will be published as V. P. K. Kondapi, A. Belovodskiy, O.-M. Soueidan, C. Cheeseman and F.G. West, *Manuscript in preparation*. I was responsible for the experimental work, characterization of compounds, biological evaluations and manuscript preparation. F. G. West is involved in manuscript composition. Co-authors' findings were useful for the concept development, but not disclosed either in the Chapter 5 or the manuscript. F. G. West and C. Cheeseman were the supervisory authors and were also involved in the manuscript preparation.

Dedication

I deeply appreciate all the support given by my wife (Gayatri Kondapi) and my son (Karthikeya Abhirama Kondapi), during the course of my PhD study. I sincerely dedicate this thesis to my beloved wife and son. I also dedicate this thesis to my parents (Swarajya Lakshmi Kondapi & Subrahmanya Sarma Kondapi) and my brother (Hanumath Prasad kondapi).

Acknowledgements

I acknowledge, with gratitude, my debt of thanks to my PhD thesis supervisor Prof. F. G. West for his advice, encouragement, care and commitment to student learning.

I am very grateful to Prof. Christopher Cheeseman for his support during biological evaluation of hexose derivatives.

I would like to express my deepest appreciation to my external examiner Prof. Stephen G. Withers, University of British Columbia, Canada.

I sincerely thank my defense committee members – Prof. Dennis Hall, Prof. Derrick J. Clive, Prof. Todd L. Lowary, Prof. Stephen G. Withers and Prof. F. G. West.

I am indebted to all my family members for their support, especially, to my wife, my mother and my son.

I am very thankful to all the supporting staff of the Department of Chemistry, University of Alberta. I would like to thank the entire West group members for their support.

Last but not least, I would like to thank the cMIP (create Molecular Imaging Probe, NSERC) grant for their financial support.

Table of Contents

Chapter 4

Chapter 5

List of Tables

List of Figures

Chapter 1

Chapter 2

Chapter 3

Chapter 5

List of Schemes

Chapter 1

Chapter 2

Chapter 3

Chapter 4

Chapter 5

List of Symbols and Abbreviations

Ac	acetyl
Ac_2O	acetic anhydride
AcCl	acetyl chloride
$AlCl_3$	aluminum chloride
Ar	aryl
app	apparent (spectral)
2,5-AM	2,5-anhydro-D-mannitol
BF_3	boron trifluoride
Bn	benzyl
br	broad (spectral)
°C	degrees Celsius
CB	cytochalasin B
$CHCl_3$	chloroform
CsF	cesium fluoride
$CeCl_3$	cerium(III) chloride
$CHCl_3$	chloroform
cm^{-1}	wave numbers
CHO (cells)	Chinese hamster ovary cells
calcd	calculated
^{13}C NMR	carbon 13 nuclear magnetic resonance
^{14}C	an isotope of carbon

cal.	calories (units of energy)
DAST	diethylaminosulfur trifluoride
DIPEA	*N*,*N*-diisopropylethylamine
DCM	dichloromethane
DMF	*N*,*N*-dimethylformamide
DMSO	dimethyl sulfoxide
DEAD	diethyl azodicarboxylate
DIAD	diisopropyl azodicarboxylate
δ	chemical shift in parts per million downfield from tetramethylsilane
d	doublet (spectral)
dd	doublet of doublets
DMAP	4-dimethylaminopyridine
dq	doublet of quartets (spectral)
dr	diastereomeric ratio
dt	doublet of triplets (spectral)
ESI	electrospray ionization (mass spectrometry)
$_{+1}e^0$ or e^+	a positron
$_{+1}e^0$ or e^+	an electron
EtOAc	ethylacetate
EtOH	ethanol
EMT-6	murine breast tumor cells line
Et_2O	diethyl ether
Et	ethyl

ee	enantiomeric excess
^{18}F	an isotope of fluorine (also known as positron emitter)
^{19}F	the only stable isotope of fluorine
2-FDG	2-deoxy-2-fluoro-D-glucose
1-FDF	1-deoxy-1-fluoro-D-fructose
6-FDF	6-deoxy-6-fluoro-D-fructose
FPR	fluorescence plate reader
GLUT	membrane hexose transporter
$\Delta G^{\ddagger}$	activation energy
equiv	equivalent
g	gram
h	hour
Hz	hertz
HK	hexokinase
H^+	proton
^1H NMR	proton nuclear magnetic resonance
in vivo	referring to the studies performed in living organisms
in vitro	referring to the studies performed in cell culture or processed oocyte
IR-780	a near-infrared emitting chromophore
IR-783	a near-infrared emitting chromophore with anionic sulfonate groups
IC_{50}	concentration of the inhibitor required to achieve half maximal inhibition
J	coupling constant (in NMR)
KHF_2	potassium bifluoride

KF	potassium fluoride
Km	Michaelis constant
KHK	ketohexokinase (often referred as fructokinase)
k	kilo
$LiAlH_4$	lithum aluminum hydride (also referred as LAH)
L	litre(s)
µ	micro
M	metal atom; moles per litre
Me	methyl
MHz	megahertz
min	minute
m.p.	melting point
m	multiplet (spectral); milli
mol	number of moles
MeOH	methanol
MeONa	sodium methoxide
MS	mass spectrometry
$MgCl_2$	magnesium chloride
$NaBH_4$	sodium borohydride
N	normality
Nu	nucleophile
NMR	nuclear magnetic resonance
NBD	7-nitrobenz-2-oxa-1,3-diazole

^{18}O	an isotope of oxygen
OAc	acetate
OEt	ethoxy
OMe	methoxy
PET	positron emission tomography
py	pyridine
Piv	pivaloyl
Ph_3P	triphenylphosphine
i-Pr	isopropyl
Pg	protecting group
Ph	phenyl
q	quartet (spectral)
quant.	quantitative
R	generalized alkyl group of substituent
R_f	retention factor (chromatography)
RNA	ribonucleic acid
rt	room temperature
S_N1	unimolecular nucleophilic substitution
S_N2	bimolecular nucleophilic substitution
NaF	sodium fluoride
NaCl	sodium chloride
NaBr	sodium bromide
NaI	sodium iodide

NaN_3	sodium azide
$NaHCO_3$	sodium bicarbonate
$Sc(OTf)_3$	scandium triflate
SGLT	sodium-coupled glucose transporter
s	singlet (spectral); second
t	triplet (spectral)
T	temperature
TBS	*tert*-butyldimethylsilyl
TBDPS	*tert*-butyldiphenylsilyl
TMS	trimethylsilyl
TBAF	tetra-*N*-butylammonium fluoride
Tr	trityl
TFA	triluoroacetic acid
Tf	trifluoromethanesulfonyl; triflate
Ts	*p*-toluenesulfonyl; tosyl
THF	tetrahydrofuran
TM	trans-membrane (protein)
TOCSY	Total correlated spectroscopy
tert-AmOH	2-methyl-2-butanol
TEA	triethylamine (also referred as Et_3N)
TLC	thin layer chromatography
tert-AmOH	2-methyl-2-butanol
UV	ultra-violet

X	generalized heteroatom

Chapter 1

Tracer Development for the Molecular Imaging of Breast Cancer

1.1. The membrane hexose transporters

Hexoses are fuels for metabolic processes and energy sources for cells.[1] Due to polyhydroxy substitution, hexoses are very polar (hydrophilic) molecules, and thus cannot penetrate through plasma membranes by means of simple diffusion. Membrane hexose transporters facilitate the hexose traffic from extracellular space to intracellular space and vice versa (Figure 1.1.1). At least two distinct gene families, sodium-glucose transporters (SGLTs) and glucose transporters (GLUTs), are known to facilitate the transport of hexoses through cell membrane. SGLTs use the sodium ion gradient to drive the uptake of glucose, whereas GLUTs are passive transporters that use chemical or electrochemical gradients to transport hexoses.[2-8] In 1977, Kasahara and Hinkle purified the GLUT1 transport protein that was isolated from erythrocyte membrane.[9,10] In 1985, Mueckler and co-workers characterized GLUT1 as a 492-amino acid containing protein.[11]

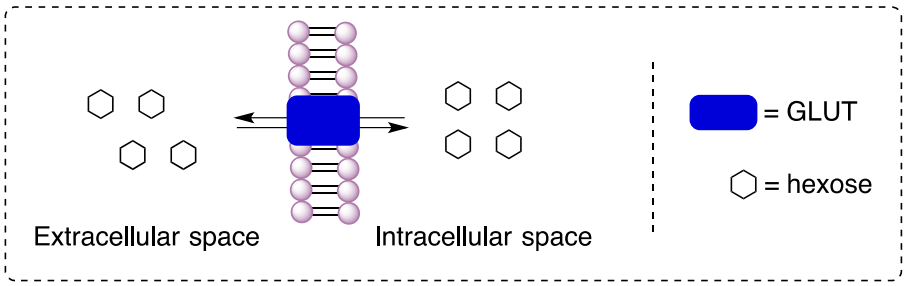

Figure 1.1.1. Transport of hexoses through plasma membrane by GLUTs.

1.2. GLUTs – Classification and substrate specificity

To date, there are fourteen known isoforms of GLUTs that are encoded by human SLC2A gene family. Each GLUT differs from the rest in structure, substrate specificity and substrate affinity. Based on amino acid sequence and degree of evolutionary divergence, GLUTs have been classified into three groups (Figure 1.2.1).[4,12] GLUTs 1-4 and 14 belong to Class-I, and primarily transport D-glucose (Table 1.2.1, entries 1-5).[2-8] GLUTs 1, 3 and 4 transport D-glucose with a high affinity (Km = 2 to 5 mM); in contrast, GLUT2 mediates D-glucose fluxes with a low affinity (Km ~ 11 mM).[2-8] Except GLUT4, Class-I GLUTs also transport D-galactose.[2] Insulin regulates the D-glucose transport through GLUT4. Though GLUT2 is primarily a D-glucose transporter, it also mediates D-fructose fluxes with lower affinity.[2-8]

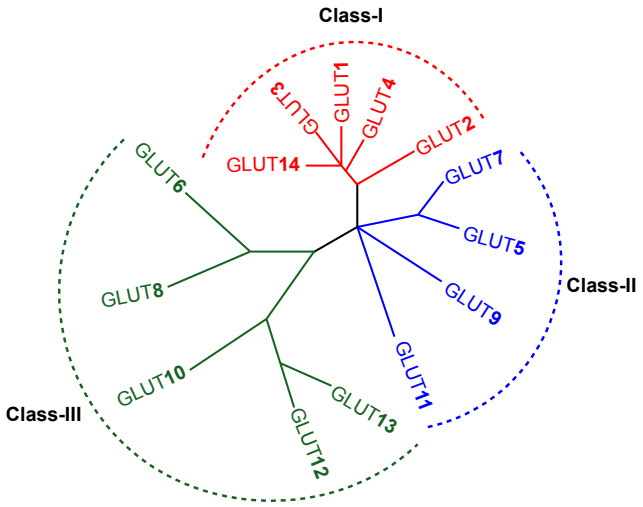

Figure 1.2.1. The relationship between the SLC2A gene family members. Originally created using PHYLIP 3.6 software. Distance between branches and length of the lines represent the degree of evolutionary divergence. (Reproduced from ref. 4).

Table 1.2.1. Classification and substrate specificity of GLUTs.

Class	Member	Substrate(s)
I	GLUT1	D-glucose and D-galactose
	GLUT2	D-glucose, D-galactose and D-fructose
	GLUT3	D-glucose and D-galactose
	GLUT4	D-glucose
	GLUT14	D-glucose and D-galactose
II	GLUT5	D-fructose (very low affinity for D-glucose)
	GLUT7	D-glucose and D-fructose
	GLUT9	D-glucose and D-fructose
	GLUT11	D-glucose and D-fructose
III	GLUT6	D-glucose (not well understood)
	GLUT8	D-glucose (very low affinity for D-fructose)
	GLUT10	D-glucose and D-galactose
	GLUT12	D-glucose, D-galactose and D-fructose
	GLUT13 (HMIT)	Myo-inositol

Class-II comprises GLUTs 5, 7, 9 and 11, which primarily transport D-fructose (Table 1.2.1, entries 6-9).[2-8] Excluding GLUT5, the rest of the Class-II family GLUTs also facilitate the transport of D-glucose.[2-8] GLUT5 is a high affinity D-fructose transporter and shows very limited or no affinity for D-glucose.[2-8] The Class-III GLUT

family is composed of GLUTs 6, 8, 10, 12 and 13 (Table 1.2.1, entries 10-14). The functional activity of Class-III GLUTs is poorly understood in comparison to the other two classes. Further, GLUTs 6, 8, 10 and 12 can facilitate D-glucose transport.[2-8] In addition, GLUTs 8 and 10 are capable of mediating D-galactose fluxes. GLUT13 transports myo-inositol **1**, an important polyhydroxycyclohexane utilized in cell membranes and signaling pathways (Figure 1.2.2). Accordingly, GLUT13 is also known as H^+- coupled myo-inositol transporter (HMIT).[2-8]

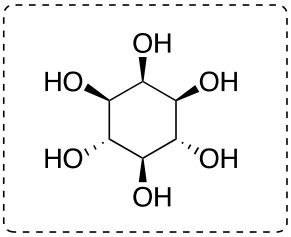

Figure 1.2.2. Structure of myo-inositol **1**.

1.3. GLUT expression in human tissues

Class-I GLUT expression in tissues: GLUT1 is ubiquitously expressed in mammalian cell types. GLUT1 expression was characterized particularly in the brain, blood-brain barrier and erythrocytes.[9,13,14] GLUT2 was found to be expressed in pancreatic β-cells, liver and kidney tissues.[15,16] GLUT3 is expressed in the brain (neurons).[17] GLUT4 is expressed in adipose tissue, heart and skeletal muscle.[18] Very importantly, D-glucose traffic through GLUT4 is regulated by insulin.[19]

Class-II GLUT expression in tissues: The high affinity D-fructose transporter, GLUT5 is found predominantly in the small intestine tissue, testes and the kidney tissue.[20] GLUT7 expression is not well known, but its expression is evident in intestine and

colon.[21,22] GLUT9 expression was identified in liver and kidney tissues.[21,23] GLUT11 was characterized in muscle, heart, placenta, kidney and pancreas.[21]

Class-III GLUT expression in tissues: GLUT6 expression was found in brain and spleen.[21] Expression of GLUT8 was located in testes, brain, placenta, kidney and spleen. Heart and lung tissue express GLUT10.[21] Insulin-sensitive tissues, intestine and prostate tissues express the transporter GLUT12.[21] Expression of HMIT was found in the brain.[21]

1.4. Mechanism of GLUT-mediated hexose transport

GLUT proteins are folded into twelve trans-membrane (TM) α–helices (Figure 1.4.1).[2-8,24,26] The Class-I and Class-II GLUT proteins contain a long intracellular loop connecting TM6 and TM7, and a long glycosylated extracellular loop between TM1 and TM2. Class-III GLUTs are also believed to have twelve TMs, but the long extracellular loop with the glycosylation site is between TMs 9 and 10. Available crystal structures of GLUTs and mutation studies indicate that TM7 is crucial for substrate binding.[2-8,24-26] Many models have been proposed to explain the transport mechanism of hexoses through GLUTs. It is widely accepted that hydrogen bonding interactions and hydrophobic interactions between the GLUT and hexose molecules are key for the recognition and GLUT-mediated transport of the hexoses.[2-8,24-30]

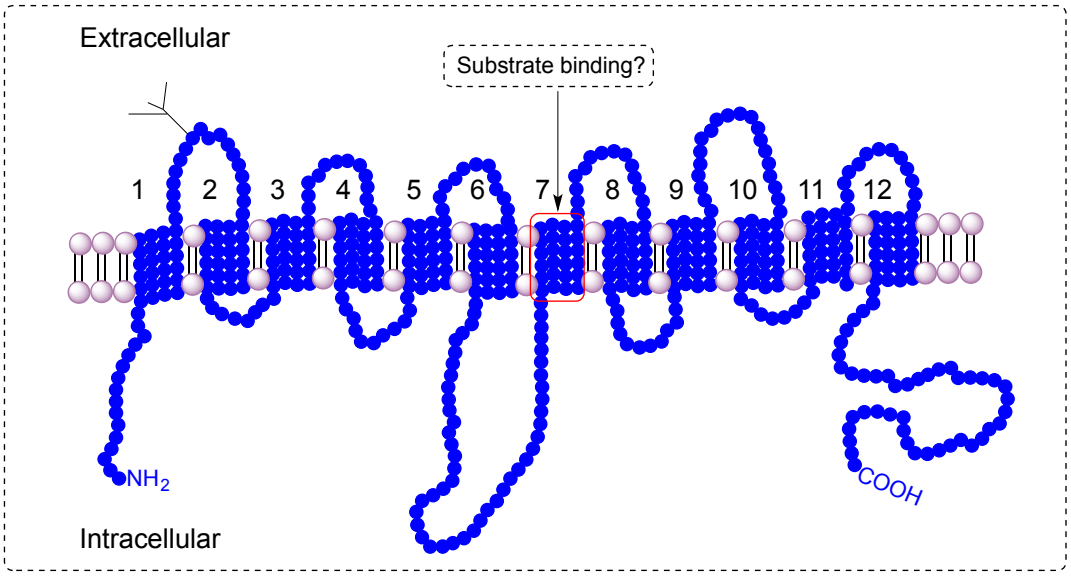

Figure 1.4.1. General structural representation of Class-I and Class-II GLUTs.

Figure 1.4.2 is a cartoon representation of the generally accepted mechanism of hexose transport by GLUTs.[2-8] First, the empty carrier (GLUT) opens to one side of the membrane (*cis* side) to allow substrate binding with the binding-pocket (Figure 1.4.2, Panel A). It was proposed that the nonpolar amino acid residues present in the side-chains (helices) of the three-dimensional protein structures interact with each other through hydrophobic interactions to achieve the compact folding of the protein. In this process, the hydrophobic residues squeeze the water molecules present in the first hydration shell to bury them in the protein binding pocket, to achieve a meta-stable state. This state is very prone to undergo conformational changes upon substrate binding, though such binding results in only small energetic changes. Upon substrate binding (Figure 1.4.2, Panel B), the protein translates its conformation to the *trans* side to release the hexose (Figure 1.4.2, Panels C and D). As the hexose is being released into intracellular space, the protein switches its conformation to open *cis* side for hexose binding.

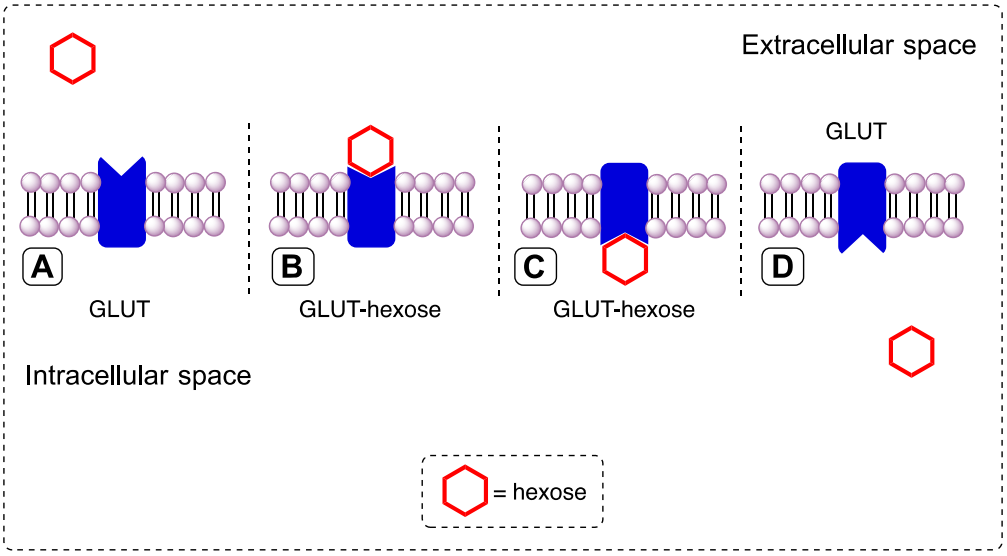

Figure 1.4.2. A general representation of the hexose transport mechanism by GLUTs. A) Extracellular hexose and GLUT in unbound state. B) Hexose binding with GLUT. C) Change in the GLUT conformation. D) Release of hexose into intracellular space.

Recent studies of crystal structures of mammalian hexose transporters, GLUTs 1, 3 and 5 provided more mechanistic insights into GLUT mediated hexose transport.[24-26] The N-terminal TMs 1-6 and C-terminal TMs 7-12 form the central aqueous pore or channel (Figure 1.4.3). Hexoses cross the lipid bilayer membrane through the central aqueous pore. In GLUT5, the N-terminal and C-terminal TMs undergo a rotational change of ~15° between the outward-open (**I**) and inward-open (**IV**) forms to facilitate hexose transport. TM1 and TM7 form cavity-closing interactions on the outside, whereas TM4 and TM10 form such interaction on the inside. TM7 and TM10 appear to have prominent roles in occluding the substrate binding site. Furthermore, TM7 and TM10 undergo gating conformational changes to transport hexoses from extracellular space to intracellular space and vice versa.[24-26]

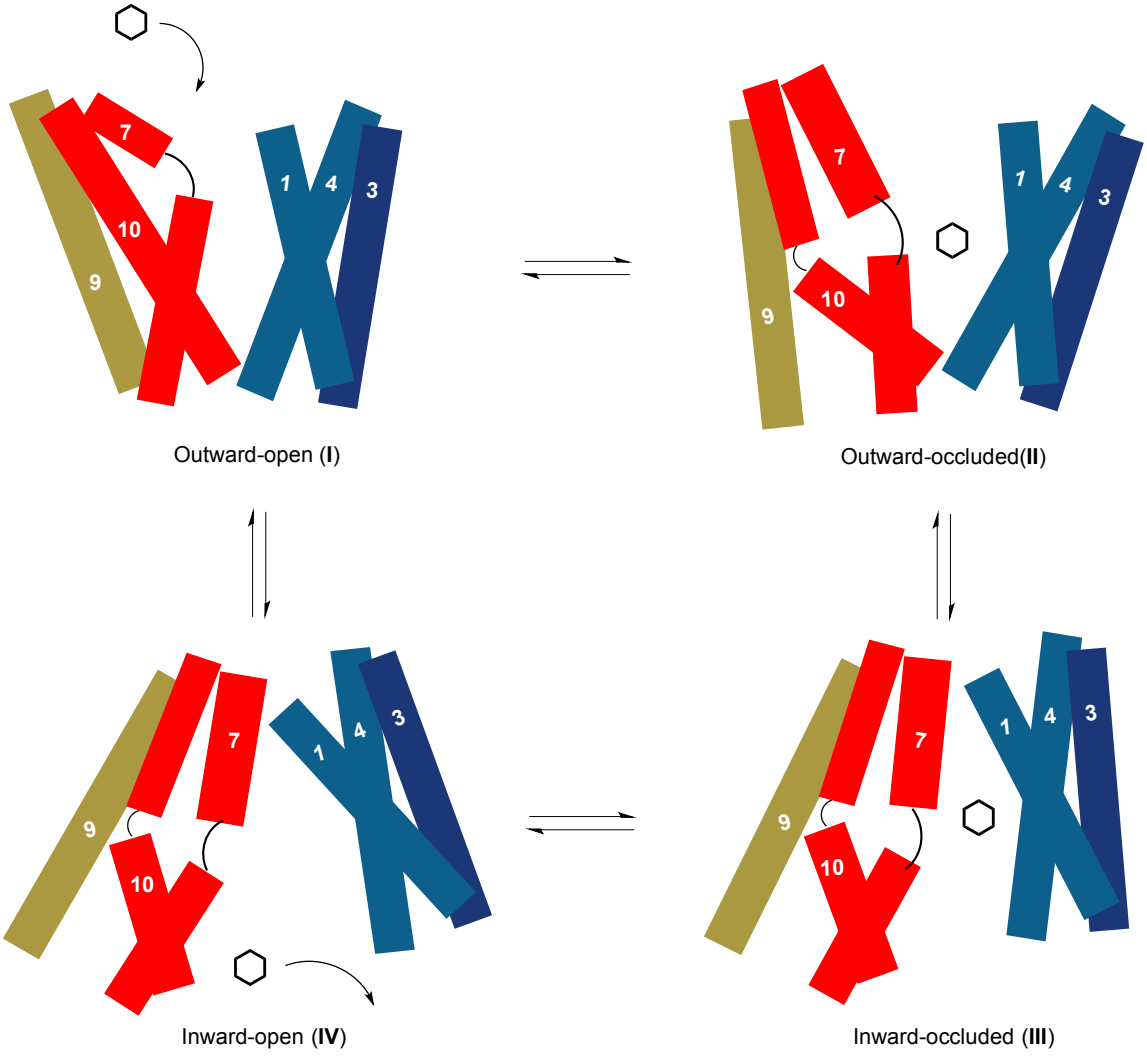

Figure 1.4.3. Role of TMs of the GLUT5 protein in hexose transport.

1.5. Enzymatic phosphorylation – A metabolic trap for hexoses

The hexoses that are transported into intracellular space by a GLUT could be transported back into extracellular space by the same GLUT. However, GLUTs are incapable of transporting hexose phosphates (Figure 1.5.1).[31] Thus, the hexose molecules that undergo enzymatic phosphorylation remain inside the cell. Enzymatic phosphorylation is a 'metabolic trap' for the hexoses, as it prevents the exit of the hexoses from the cell.

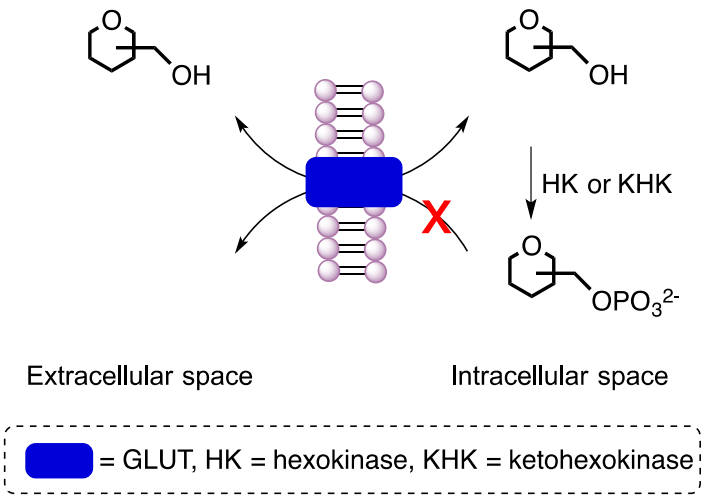

Figure 1.5.1. Inability of GLUTs to transport hexose phosphates

1.6. Role of hexose structure in the GLUT-mediated hexose transport process

In solution, D-hexose molecules exist as mixtures of various isomers (Figure 1.6.1 and 1.6.2).[32] In addition, the presence of extracellular ions such as Mg^{2+} or Ca^{2+} may change the conformation of the hexoses.[33] However, a GLUT recognition for one of the isomers of hexose is enough for its passage through the cell membrane. Figure 1.6.3 demonstrates the GLUT-mediated transport of a hexose "**H**", despite the GLUT recognition for only one of its isomers "$\mathbf{H_A}$", which was assumed to undergo phosphorylation inside the cells. As a result, the transport of a hexose by a particular GLUT does not reflect the affinity of that GLUT for all the isomers of the hexose (Figure 1.6.3). Crystallization of the GLUT-hexose complex can provide insights into the binding isomer of the hexose with the protein. In other cases, thorough screening of various hexose derivatives against a specified GLUT is required. In addition, docking analysis of the GLUT binding with all the possible hexose isomers might be useful to determine the structure-activity relationship.

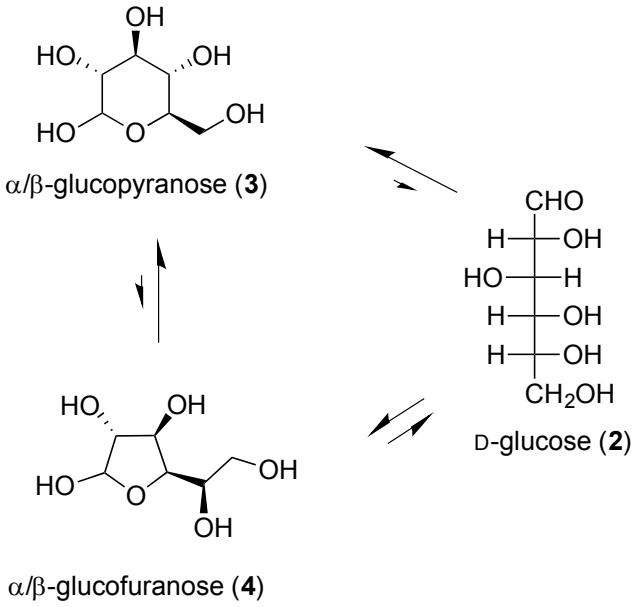

Figure 1.6.1. Various isomeric forms of D-glucose

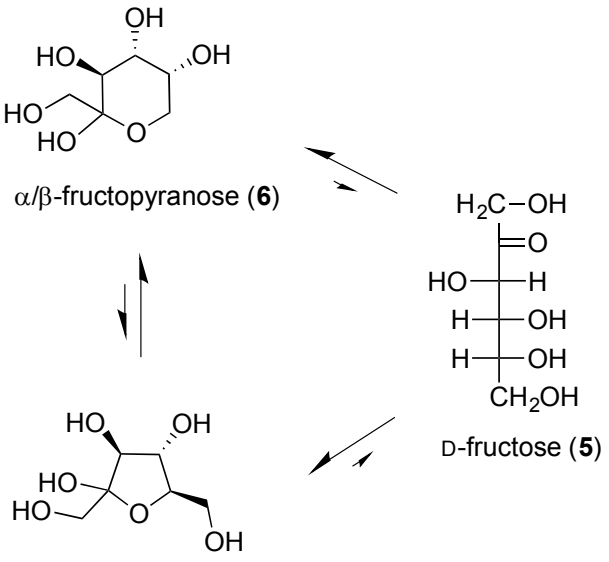

Figure 1.6.2. Various isomeric forms of D-fructose

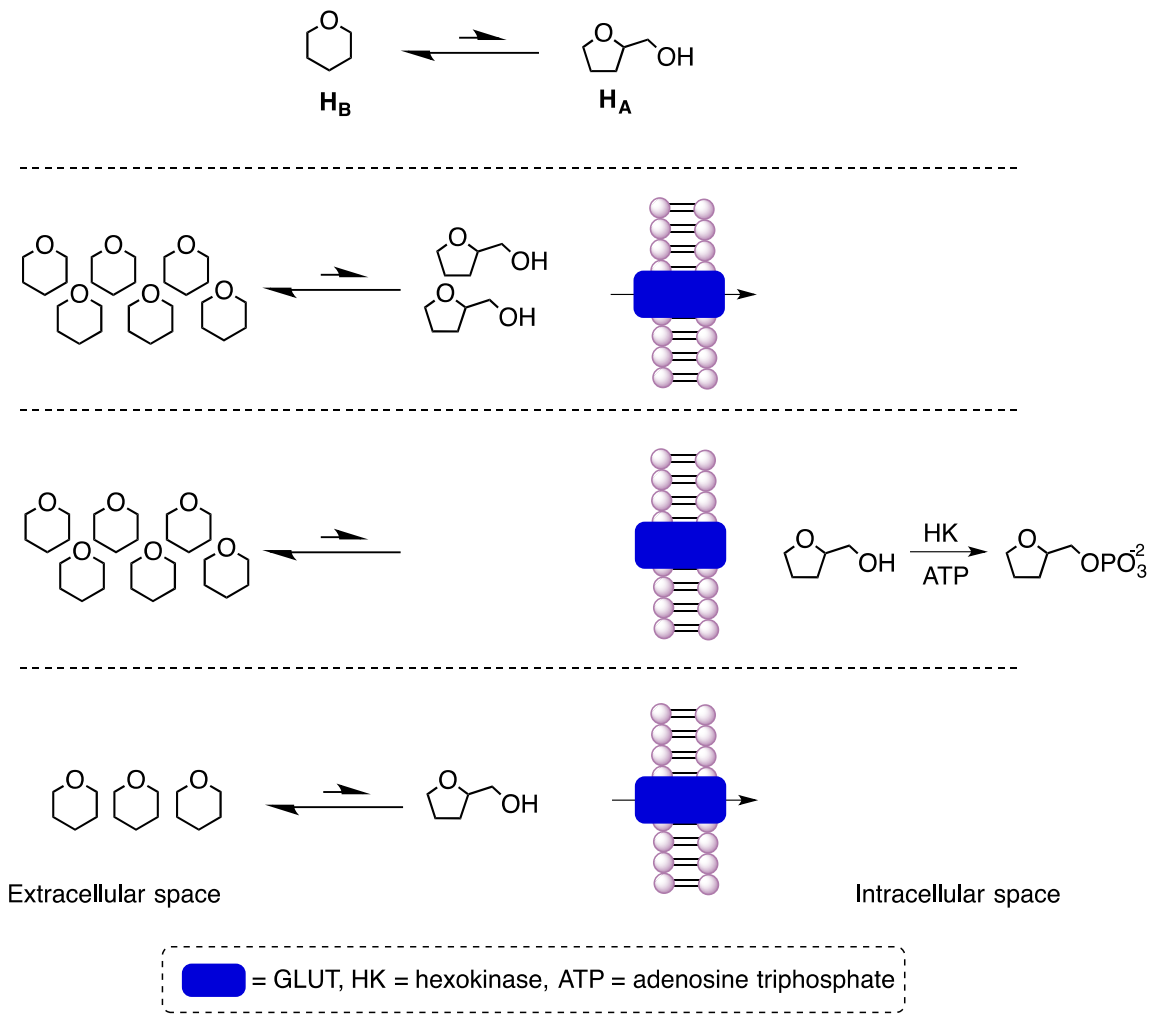

Figure 1.6.3. Transport of hexose "**H**" by GLUT when the GLUT recognizes only one isomer $\mathbf{H_A}$

On the other hand, the hydroxyl substituents on hexose also play a major role in the hexose-GLUT binding process. Certain hydroxyl substituents of hexoses are key to maintain hydrogen bonding interactions with GLUTs. Alteration of such hydroxyl groups would result in the loss of GLUT recognition for the hexose.[2-8] The hydroxyls which must be retained for the efficient GLUT-hexose binding are often referred "essential hydroxyl groups" or "critical hydroxyl groups".[2-8] The hydrocarbon skeleton of a hexose (*e.g.* CH and CH_2 units) is considered to be responsible for the nonpolar interactions between the hexose and hydrophobic amino acid residues of the GLUT. Similarly, certain

amino acid residues of the GLUTs are vital for the hexose-GLUT binding process, and mutation of such amino acids dramatically affects the hexose-GLUT binding process. A very recent report disclosed that a single point mutation of mammalian GLUT5 was enough to switch substrate preference from D-fructose to D-glucose.[25] Thus, mutation of the GLUT or modification of its natural ligand might result in loss of GLUT-hexose binding.

1.6.1. GLUT1 recognition for modified D-glucose derivatives

GLUTs 1, 2 and 3 are the major D-glucose transporters. However, only in the case of GLUT1 have the structural requirements for D-glucose been studied in detail. In general, GLUT1 exhibits higher tolerance for structural modification of D-glucose. Studies suggested that modification of positions C-1 to C-6 of D-glucose with certain functional groups such as alkoxy and amido functionalities is tolerated by GLUT1.[29-36] Despite the possibility of D-glucose to exist in various isomeric forms in solution, more than 99% of the D-glucose molecules exist in D-glucopyranose form as mixture of α and β anomers. GLUT1 exhibits a high affinity for D-glucose, and thus at least one of the anomers must attain GLUT1 recognition. It has been demonstrated that GLUT1 is capable of transporting both anomers **11** and **12** of methyl glycoside of glucose, though with different affinities (Figure 1.6.4).[34]

1,5-Anhydro-D-glucitol **8** is a C-1 modified D-glucose derivative which lacks both hydrogen bond donor and acceptor (except the oxygen atom that is part of pyranose ring) at the C-1 position. Regardless, **8** was recognized by GLUT1.[35] Furthermore, GLUT1

exhibited ten-fold lower affinity for 1-deoxy-D-glucopyranose **8** (K_i = 76 mM) when compared to D-glucose (K_i = 7.6 mM), indicating the importance of a polar substituent at C-1 for the efficient binding of GLUT-substrate. Interestingly, an appreciable difference in GLUT1 affinities for α-D-glucopyranosyl fluoride **9** and β-D-glucopyranosyl fluoride **10** was observed, demonstrating the importance of the orientation of hydrogen bond acceptor for efficient GLUT-substrate binding. In comparison to α-D-glucopyranosyl fluoride **9** (K_i = 80 mM), GLUT1 displayed higher affinity for β-D-glucopyranosyl fluoride **10** (K_i = 15 mM).[35] All of the above observations suggest that position C-1 modification of D-glucose is tolerated by GLUT1. However, the β-D-glucopyranose derivatives that contain a hydrogen bond acceptor at C-1 seem to bind more efficiently with GLUT1 than those lacking such substitution.

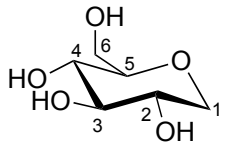

1,5-anhydro-D-glucitol (**8**)

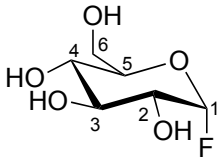

α-D-glucopyranosyl fluoride (**9**)

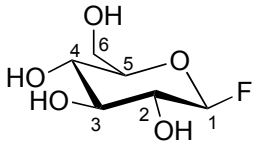

β-D-glucopyranosyl fluoride (**10**)

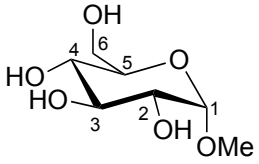

Methyl-α-D-glucopyranoside (**11**)

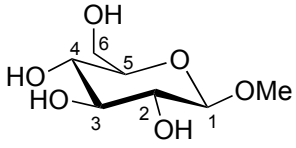

Methyl-β-D-glucopyranoside (**12**)

Figure 1.6.4. Structures of various C-1 modified D-glucopyranoses that are GLUT1 ligands

C-2 modified D-glucose derivatives were well studied as GLUT1 ligands. Functional group transformation of the C-2 hydroxyl group had a very limited effect on GLUT1-substrate binding process. C-2 modification with alkoxy, amido, fluoro, chloro or dichloro substituents yielded high affinity GLUT1 ligands (Figure 1.6.5, **13**-**19**).[35-39]

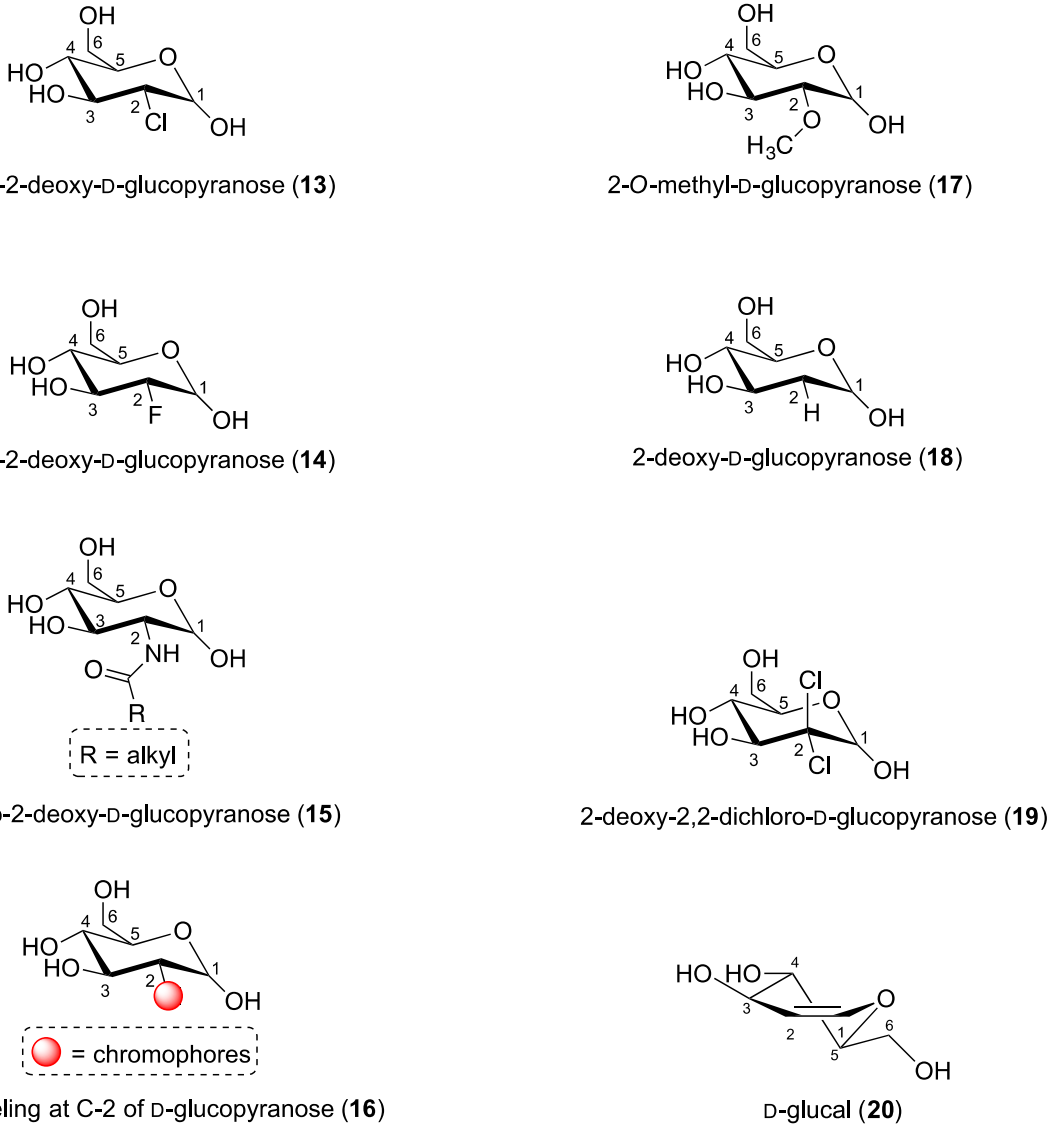

Figure 1.6.5. A selection of C-2 modified D-glucose derivatives that are recognized by GLUT1

Despite the loss of both hydrogen bond donor and acceptor property at position C-2, GLUT1 exhibited very high affinity for 2-deoxy-D-glucose **18**.[35] In addition, the steric bulk of the substituents present at C-2 is well tolerated by GLUT1 (Figure 1.6.5, **16**).[39] Importantly, D-glucal **20** (Figure 1.6.5), the C-1 / C-2 unsaturated D-glucose derivative also retains GLUT1 recognition.[35]

Only very few C-3 or C-4 modified D-glucose derivatives (*O*-alkylation of C-3 and C-4 hydroxyl groups) were evaluated as GLUT1 substrates. Further evaluations are required for complete assessment.[34] D-Galactose, the C-4 epimer of D-glucose is also a ligand for GLUT1,[4] indicating that alteration of the stereochemistry at C-4 position of D-glucose does not influence GLUT1 recognition. GLUT1 has exhibited tolerance for C-6 modified D-glucose derivatives.[36] However, the C-6 hydroxyl group of D-glucose is the site for enzymatic phosphorylation by hexokinase. Consequently, after the GLUT1 mediated transport of the C-6 modified D-glucose derivatives into intracellular space, efflux of these derivatives from the cell occurs due to lack of the metabolic trapping. Thus, C-6 modification of D-glucose attained lesser attention. All the above studies indicate the insensitivity of GLUT1 towards the positional modification of D-glucose (Figure 1.6.6).

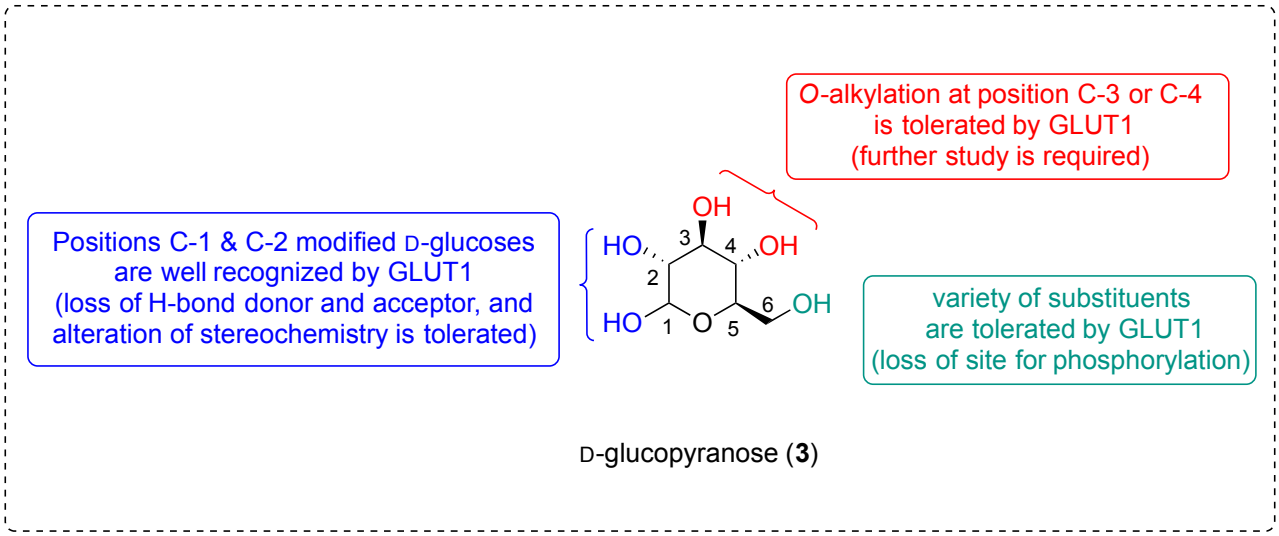

Figure 1.6.6. Summary of GLUT1 recognition for the modified D-glucoses

1.6.2. GLUT recognition for modified D-fructose derivatives

After the discovery of GLUT5 overexpression in breast cancer cells (detailed discussion is provided in Section 1.7), D-fructose derivatives were evaluated as GLUT5 ligands for the development of tracer molecules to detect breast cancer.[41-46] It appears that GLUT5 exhibits affinity for both D-fructofuranose and D-fructopyranose forms.[41] GLUT5 displayed very similar affinities for methyl-β-D-fructofuranoside **23** and methyl-β-D-fructopyranoside **24** (Figure 1.6.7).[41] Unfortunately, GLUT5 affinity for methyl-α-D-fructofuranoside **22** is unknown. Furthermore, stereochemistry of the C-2 position and substitution pattern at C-2 determine the affinity of GLUT5 for the modified D-fructose derivatives.[41]

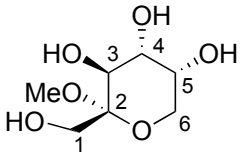

Methyl-α-D-fructopyranoside (**22**)

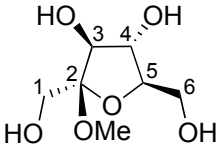

Methyl-β-D-fructofuranoside (**23**)

(K_i = 15.5 mM)

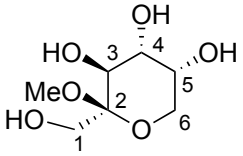

Methyl-β-D-fructopyranoside (**24**)

(K_i = 15.0 mM)

Figure 1.6.7. Comparison of GLUT5 affinity for the fructofunanose and fructopyranose forms

GLUT5 exhibited higher affinity for methyl-β-D-fructofuranoside **23** when compared to methyl-α-D-fructofuranoside **21** (Figure 1.6.8), indicating the importance of C-2 stereochemistry of fructofuranosides for the efficient GLUT-substrate binding.[41] Furthermore, GLUT5 affinity for furanose or pyranose forms of D-fructose was reduced with increase in the steric bulk of the substituent at C-2. GLUT5 displayed higher affinity for methyl-α-D-fructopyranoside **21** over allyl-α-D-fructopyranoside **25** (Figure 1.6.9).[41] Similarly, a higher affinity was displayed by GLUT5 for methyl-β-D-fructopyranoside **24** over allyl-α-D-fructopyranoside **27** (Figure 1.6.10).[41]

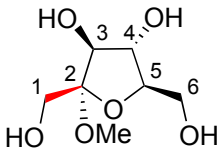

Methyl-α-D-fructofuranoside (**21**)

(K_i = 32.4 mM)

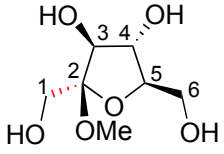

Methyl-β-D-fructofuranoside (**23**)

(K_i = 15.5 mM)

Figure 1.6.8. Comparison of GLUT5 affinity for α and β fructofuranoses

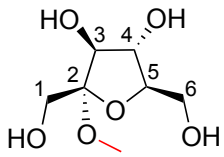

Methyl-α-D-fructofuranoside (**21**)

(K_i = 32.4 mM)

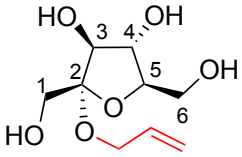

Allyl-α-D-fructofuranoside (**25**)

(K_i = 79.6 mM)

Figure 1.6.9. Comparison of GLUT5 affinity for α fructofuranoses

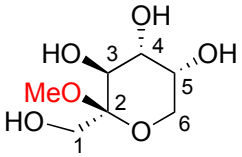

Methyl-β-D-fructopyranoside (**24**)

(K_i = 15.0 mM)

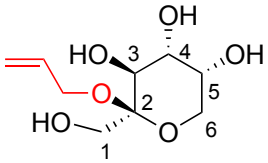

Allyl-β-D-fructopyranoside (**27**)

(K_i = 28.5 mM)

Figure 1.6.10. Comparison of GLUT5 affinity for C-2 modified fructofuranose and fructopyranose

Very few C-1 modified D-fructose derivatives were evaluated as GLUT5 substrates (Figure 1.6.11). Position C-1 modified D-fructose derivatives can equilibrate between furanose and pyranose forms. Modification of the C-1 hydroxyl group appears to reduce

the affinity of the GLUT5 transporter for the modified fructose derivatives. Loss of the hydrogen bond donor at the C-1 position results in loss of GLUT5 recognition. Though both 1-deoxy-1-fluoro-D-fructose **29** and allyl-D-fructose **30** retained the hydrogen bond acceptor functional group at the C-1 position, GLUT5 exhibited very poor or no affinity for **29** and **30**.[41] Surprisingly, despite the retention of both hydrogen bond donor and acceptor at the C-1, 1-(*N*-allyl)amino-D-fructose **28** was poorly recognized by GLUT5.[41] Protonation of the amine functionality of **28** at physiological pH could be the reason for lack of GLUT5 recognition for **28**. 1-(*N*-(4-Nitro-2,1,3-benzoxadiazol-7-yl))amino-D-fructose **31** possesses an aromatic amine substituent at position C-1, which remains unprotonated at physiological pH to retain the hydrogen bonding acceptor atom. However, **31** was also evaluated as very poor GLUT5 substrate.[40] Based on this observation, retention of both hydrogen bond acceptor and donor at C-1 appears to be insufficient on its own for GLUT5 recognition.

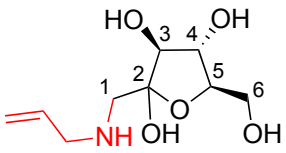

1-(*N*-allyl)amino-D-fructose (**28**)

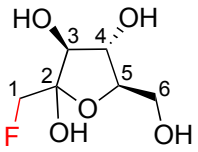

1-deoxy-1-fluoro-D-fructose (**29**)

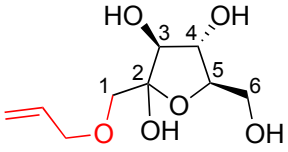

1-*O*-allyl-D-fructose (**30**)

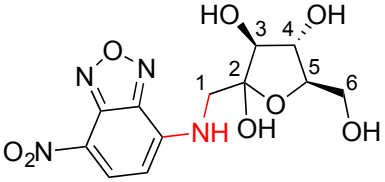

1-(*N*-(4-nitro-2,1,3-benzoxadiazol-7-yl))amino-D-fructose (**31**)

Figure 1.6.11. Position C-1 modified D-fructose drivatives

Although modified D-fructofuranose derivatives were evaluated several times as GLUT5 substrates, the secondary alcoholic positions *i.e.* C-3, C-4 and C-5 were not well studied. Evaluation of 3-*O*-allyl-D-fructose **32**, 4-*O*-allyl-D-fructose **34** and 5-*O*-allyl-D-fructose **36** (Figure 1.6.12) as GLUT5 substrates, indicated that derivatization of C-3 or C-4 or C-5 positions of D-fructose diminishes the GLUT5 affinity. Furthermore, D-psicose **33**, D-tagatose **35** and L-sorbose **36** were found to be poor GLUT5 substrates, which indicated the stereochemical requirement of the secondary alcoholic functionalities

for effective GLUT5-hexose binding.[41] In contrast to these results, GLUT1 exhibited greater tolerance for the stereoinversion of the hydroxyl group at position C-2 and C-4.

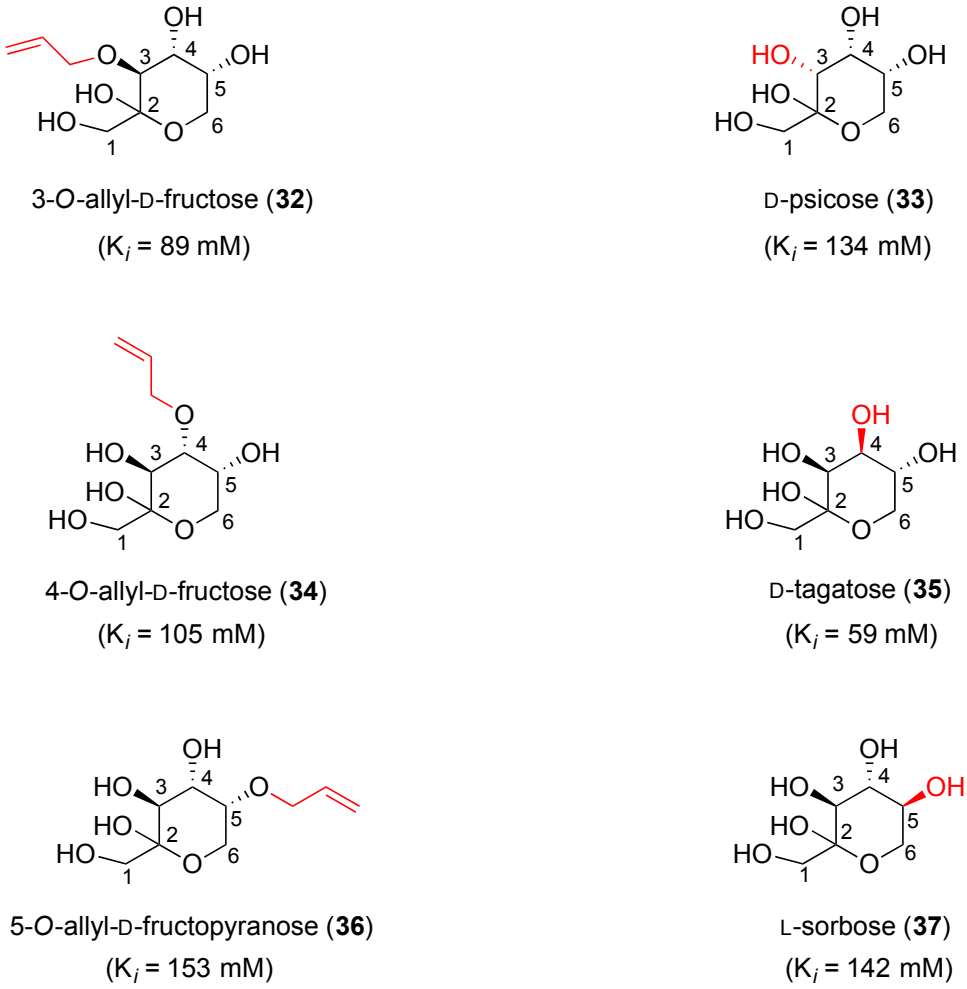

Figure 1.6.12. Position C-3, C-4 and C-5 modified D-fructose drivatives

Modification at C-6 of D-fructose was well tolerated by GLUT5. All the known C-6 modified D-fructose derivatives were successfully recognized by the GLUT5 transporter protein. Importantly, removal of the hydroxyl group at position C-6 limits the existence of D-fructose derivatives to the furanose form. Studies concluded very high GLUT5

affinity for 6-*O*-allyl-D-fructose **38** and 6-deoxy-6-fluoro-D-fructose **39**, indicating GLUT5 tolerance for the loss of a hydrogen bond donor at C-6.[41] To date, C-6 modified D-fructose derivatives which do not retain hydrogen bond acceptor at C-6 have not been evaluated as GLUT5 substrate. Thus, further studies are required to determine the

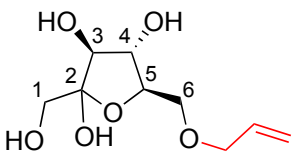

6-*O*-allyl-D-fructose (**38**)

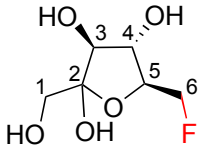

6-deoxy-6-fluoro-D-fructose (**39**)

Figure 1.6.13. Position C-6 modified D-fructoses

importance of a hydrogen bond acceptor at C-6 in hexose-GLUT5 binding process. Overall, unlike GLUT1, which appears to tolerate modification of all of the C-1 to C-6 positions of D-glucose, GLUT5 appears to be very sensitive to the substrate modifications, especially at the C-3 and C-4 secondary alcohol position (Figure 1.6.14).

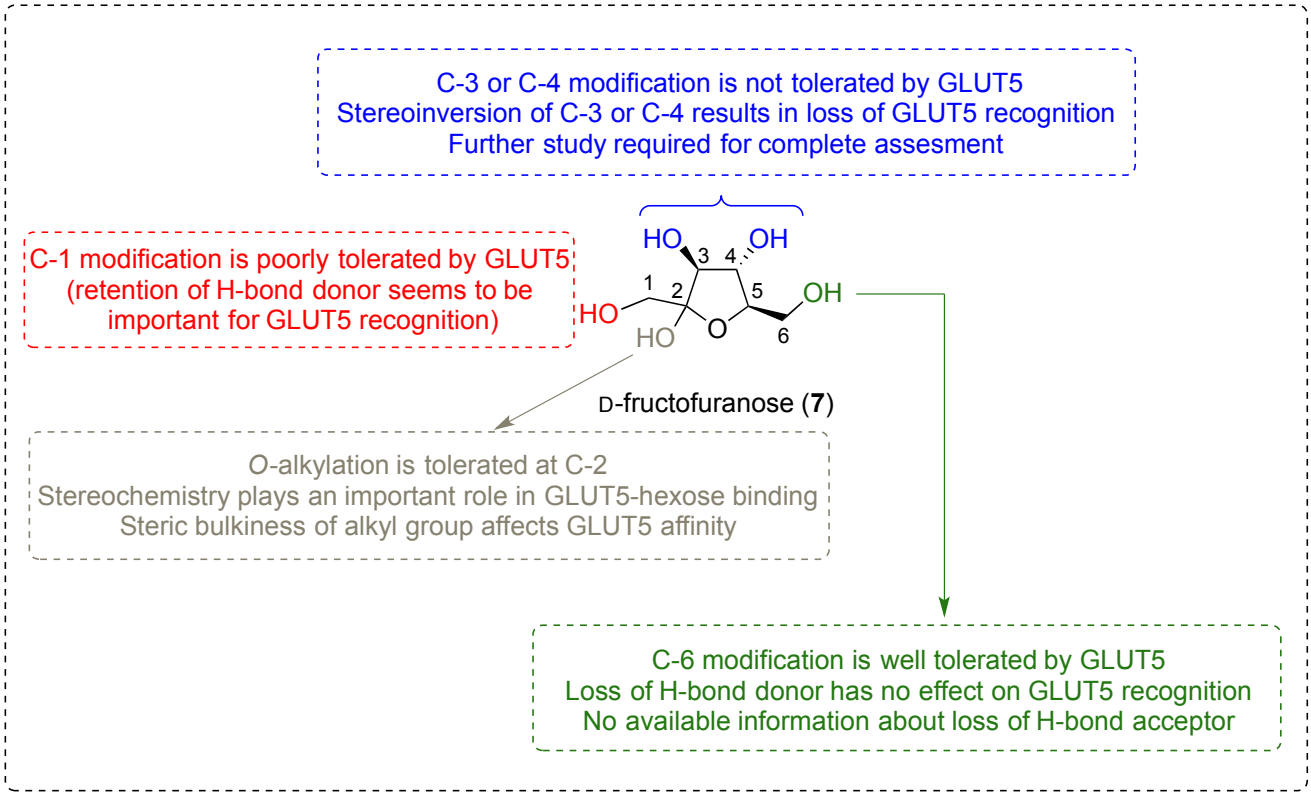

Figure 1.6.14. Summary of GLUT5 recognition for the modified D-fructoses

1.6.3. Development of 2,5-anhydro-D-mannitol based ligands for GLUT5

As mentioned previously, GLUT5 exhibited higher affinity for 2-*O*-methyl-β-D-fructofuranoside **23** when compared to *O*-methyl-α-D-fructofuranoside **21** (Figure 1.6.8). Furthermore, increasing steric bulk of the C-2 substituent decreases the GLUT5 affinity in the case of D-fructofuranose derivatives (Figure 1.6.9). 2,5-Anhydro-D-mannitol (2,5-AM, **40**) closely resembles the structure of a β-D-fructofuranoside (Figure 1.6.15) and it is therefore not surprising that GLUT5 displays very high affinity for 2,5-AM **40**.[43]

Methyl-β-D-fructofuranoside (**23**)

(K_i = 15.5 mM)

2,5-Anhydro-D-mannitol (**40**)

(K_i = 12.6 mM)

Figure 1.6.15. Structural comparison of **23** and **40**

Due to the C_2-symmetric structure, 2,5-AM **40** contains only three different types of carbon atoms. Position C-2 is part of the furanose ring and unmodifiable. Modification of position C-1 of 2,5-AM **40** is well tolerated by GLUT5 (Figure 1.6.16). Holman and coworkers have evaluated a variety of C-1 modified 2,5-AM derivatives as GLUT5 ligands. The C-1 modified 2,5-AM derivative 1-(*N*-2,4-dinitrophenyl)amino-2,5-anhydro-D-mannitol **41** was identified as a high affinity GLUT5 ligand.[45] Further, high GLUT5 affinity for 1-deoxy-1-fluoro-2,5-anhydro-D-mannitol **42** indicated the GLUT5 tolerance for the loss of a hydrogen bond donor at the C-1 position.[43-46] GLUT5 displayed high affinity for 1-amido-1-deoxy-2,5-anhydro-D-mannitol derivative **43**, indicating the tolerance of GLUT5 for long aliphatic substituents at C-1. Holman and coworkers had never focused on evaluation of C-3 modified 2,5-AM derivatives. Lack of synthetic protocols for the selective functionalization of 2,5-AM at C-3 and failure of C-3 modified D-fructose to obtain GLUT5 recognition could be two plausible reasons for not carrying the evaluation of C-3 modified 2,5-AM derivatives as GLUT5 substrates.

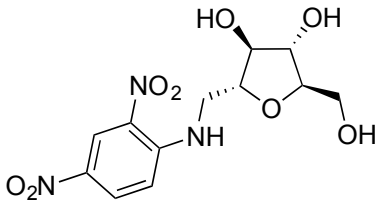

1-(*N*-(2,4-dinitrophenyl))amino-2,5-anhydro-D-mannitol (**41**)

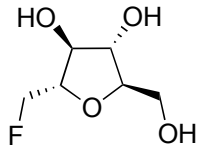

1-deoxy-1-fluoro-2,5-anhydro-D-mannitol (**42**)

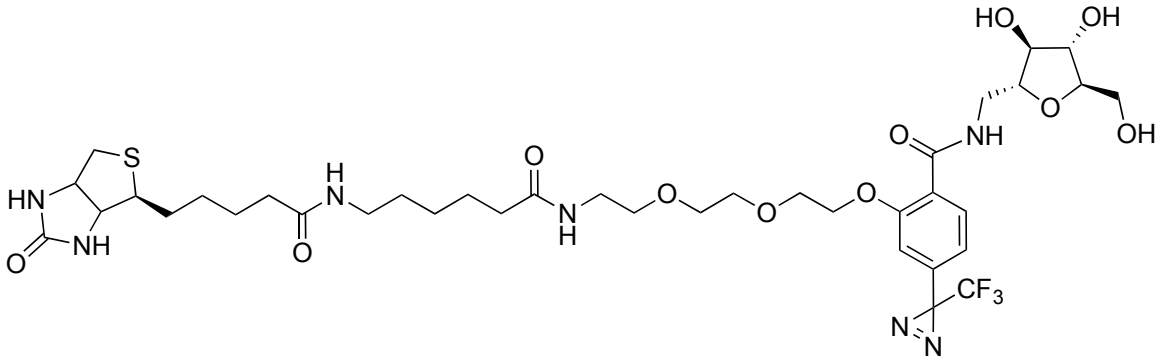

1-amido-1-deoxy-2,5-anhydro-D-mannitol derivative (**43**)

Figure 1.6.16. 2,5-AM based high affinity GLUT5 ligands

1.7. Overexpression of GLUTs in breast cancer

Cancer cells undergo faster cell division and exhibit altered metabolic profiles, which demands an excessive supply of hexoses.[47,48] As a result, the hexose transporters (GLUTs) are overexpressed in cancer cells. D-Glucose and D-fructose metabolism is the main source of energy for cancer cells. Due to high D-glucose consumption by many tumor cells, GLUT1 overexpression was widely found in various cancer cells (*e.g.* a recent analysis of 70 endometrial carcinoma cases found SLC2A1 mRNA in all the samples).[47-50] Anticancer gene p53 represses the expression of the GLUT1. Alteration to

the anticancer gene p53 could be one of the reasons for the overexpression of GLUT1 in cancer cells.[51]

Evidence for the overexpression of GLUT5 transport protein in breast cancer cells was reported in 1996.[52,53] Surprisingly, in contrast to many cancer cell types, 42% of the breast cancer cells were found to express low levels of GLUT1.[53] In addition, many of the breast cancer cells overexpressed D-fructose transporters (GLUT5 and GLUT2).[52] Very interestingly, despite overexpression of GLUT5 in breast cancer cells, GLUT5 expression was not found in normal breast cells.[53] Thus, GLUT5 could potentially be used as a portal for the delivery of vital molecules such as anticancer drugs and tracer molecules for molecular imaging of breast cancer.

1.8. An introduction to molecular imaging

Molecular imaging encompasses *in vivo* visualization, characterization and measurement of biological processes at molecular and cellular levels.[54,55] Positron emission tomography (PET), magnetic resonance imaging (MRI) and optical imaging fall under the category of molecular imaging.[54,55] The above-mentioned imaging techniques play a vital role in the disease diagnosis.[54,55] For imaging using methods such as PET and optical imaging, injection of a chemical substance (tracer) into patient body prior to diagnosis is required. The movement and location of a radioactive atom or a dye labeled chemical substance can be traced by various detection methods.[56] Radionuclide or dye labeling of a molecule that is selectively taken up by an organ or tissue can be used to develop diagnostic tracer molecules (Figure 1.8.1). Due to overexpression of GLUTs and

high hexose consumption in cancer cells, radiolabeled or dye labeled hexoses have the potential to serve as tracers in PET or optical imaging for the diagnosis of cancer.

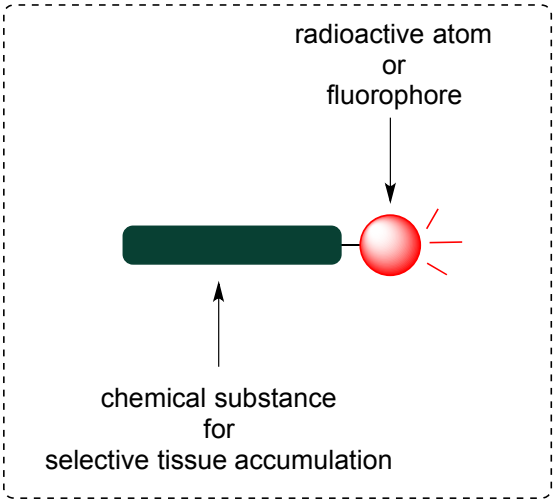

Figure 1.8.1. General representation of a tracer molecule for PET or optical imaging

1.8.1. Positron emission tomography (PET)

PET is a tracer-based imaging method, which operates through a positron-emitting tracer molecule.[57-59] After the injection of tracer into a patient's body, the positron emitted from tracer molecule reacts with an electron of the tissue, a phenomenon known as annihilation process (Scheme 1.8.1).[60] The annihilation produces two high-energy gamma rays, which exhibit high tissue penetration property. Consequently, gamma radiation emitted from the patient body can be detected and located by radiation detectors.

Scheme 1.8.1. Schematic representation of the annihilation process

Table 1.8.1. Selected list of radioisotopes that decay by positron emission

Isotope	$t_{1/2}$(min)	E_{max} (Mev)
^{11}C	20.4	0.959
^{13}N	9.96	1.197
^{15}O	2.03	1.738
^{18}F	109.8	0.633
^{68}Ga	68.3	1.898
^{82}Rb	1.25	3.40
^{94}Tc	52	2.44
^{124}I	6000	2.13

Positron-emitting isotope labeled carbohydrates, amino acids and nucleosides are used as tracers for PET.[61] The half-life of the positron emitting isotope and the kinetic energy of the emitted positron are two important factors that determine the usage of a positron emitting isotope as a radiolabel in PET (Table 1.8.1).[62] A longer half-life time of a positron emitting isotope allows the radiolabeling process to occur within the first half-life cycle of the radionuclide and thus provides sufficient time to run diagnostic imaging process before most of the activity has been lost. The distance a positron travels from the nucleus of emission is known as range. Positrons emitted from the radiolabel with high

kinetic energy travel longer ranges to lose kinetic energy, which results in the production of low-resolution diagnostic images (Figure 1.8.2).[62]

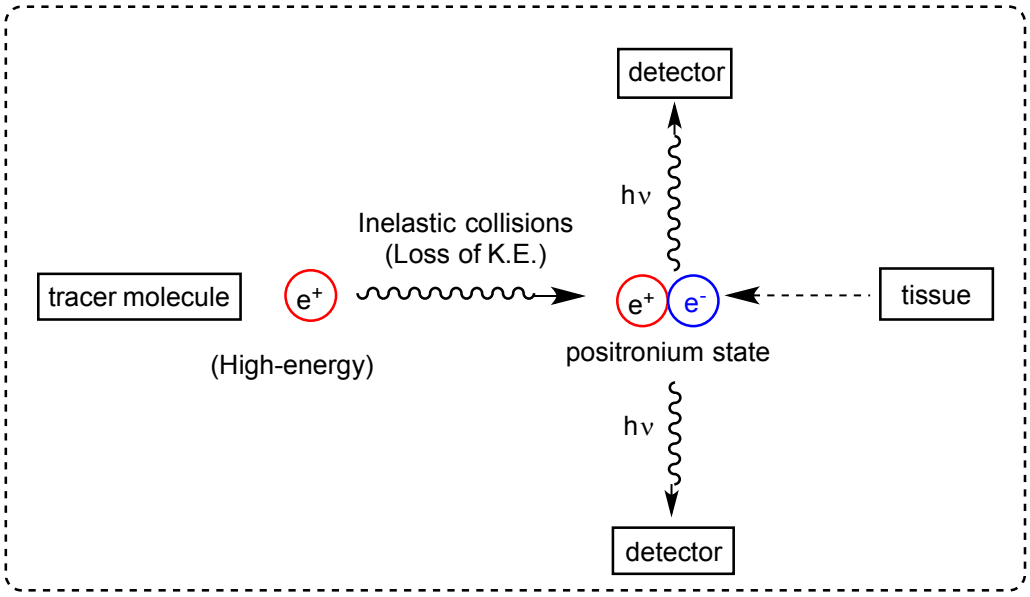

Figure 1.8.2. Schematic representation of the working principle of PET

The positrons emitted by the PET tracer rapidly lose their kinetic energy in inelastic collisions with atomic electrons of the tissue (Figure 1.8.2).[62] As the positron loses the kinetic energy, it combines with an electron to achieve the positronium state, which lasts for about 10^{-10} seconds. After the positronium state, when the positron and electron are almost at rest, the annihilation process occurs. Consequently, ejection of two gamma rays takes place. The gamma rays which are produced in the annihilation process travel at an angle of ~180° to each other (Figure 1.8.2).[57-59,62]

^{18}F is a commonly used isotope for the radiolabeling of the chemical substrates to synthesize radiotracers. The ^{18}F isotope emits low-energy positrons and consequently

produces diagnostic images with high resolution.[63] In addition, the half-life of the ^{18}F nucleus is 109.8 minutes, which is an adequate time to carry out the radiolabeling process. Moreover, after the positron decay, the ^{18}F nucleus is converted to the ^{18}O nucleus, a stable nonradioactive isotope (Scheme 1.8.2). Employment of ^{11}C and ^{94}Tc isotopes for the radiolabeling of PET tracers is also known.[64]

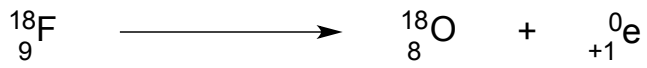

Scheme 1.8.2. Positron decay of ^{18}F isotope

Due to the overexpression of D-glucose transporters, particularly GLUT1, in many tumor cell types, hexoses are transported into the tumor cells at a faster rate in comparison to normal cells. Thus, radiolabelled or dye labeled hexoses could accumulate in the tumor region in greater quantities when compared to normal human tissue.[65] Consequently, many radiolabeled hexoses were synthesized and evaluated as tracers for PET imaging to locate the tumors. However, not all radiolabeled hexoses may serve as PET tracers for tumor detection. In order to serve as an optimal tracer for tumor imaging, the radiolabeled hexose must acquire the following properties; i) being transported by the GLUT which is overexpressed in the target tumor, and ii) capability to undergo enzymatic phosphorylation to allow metabolic trapping and accumulation in the tumor.[57-59,66]

Each tumor is unique in its expression of one particular GLUT or combination of several GLUTs. In order to localize the tracer molecule at the target tumor, at least one of the GLUTs that is overexpressed in the tumor must facilitate the transport of the tracer

into tumor cells. As the GLUTs are capable of back-transporting hexoses from intracellular space to extracellular space, the tracer may efflux from the cells. The efflux phenomenon, which reduces signal to noise ratio, must be prevented.[66] As it has been previously demonstrated (Section 1.5), enzymatic phosphorylation of the probe prevents its efflux from intracellular space to extracellular space.

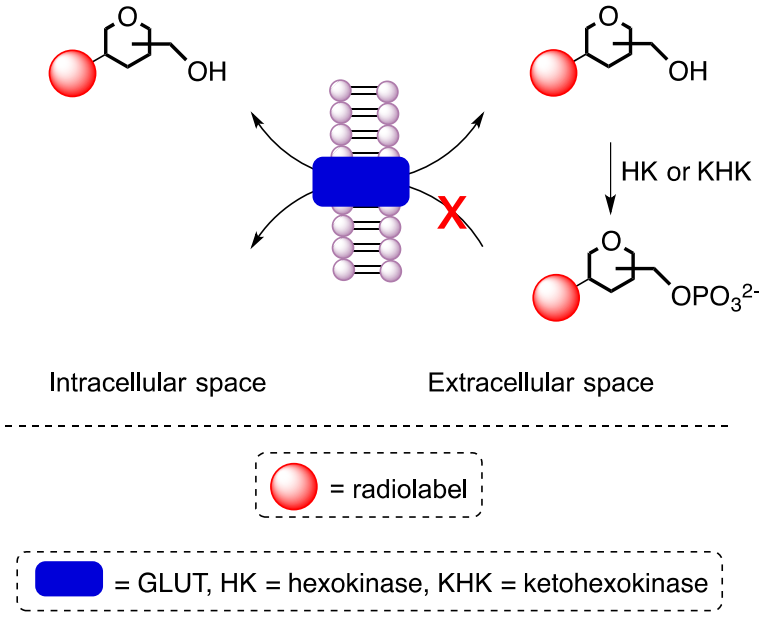

Figure 1.8.3. Importance of enzymatic phosphorylation to prevent the tracer efflux

1.8.2. Key stages in the PET tracer development

Any tracer development study starts with the labeling of hexose with ^{19}F, the naturally occurring and nonradioactive isotope of fluorine. Synthesis of ^{19}F-labeled hexose is essential to determine a particular GLUT recognition for the modified hexose. Any known electrophilic or nucleophilic fluorination method can be utilized for the ^{19}F labeling of hexoses.

In electrophilic fluorination, electron rich organic molecules react with electrophilic fluorine sources to yield organic fluorides. Fluorine is the most electronegative atom and thus the electrophilic fluorine sources are very strong oxidants. Fluorine gas itself is a source of electrophilic fluorine, but extremely reactive.[67] In addition, the physical state of F_2 (gas) also limits its usage as electrophilic fluorinating reagent. XeF_2 is an alternative electrophilic fluorine source, but exhibits poor functional group tolerance.[68]

In modern organic synthesis, the electrophilic fluorination of organic compounds is typically carried out with relatively more stable *N*-fluoro compounds, such as *N*-fluoro-pyridinium salts **44**, fluorobis(phenyl)sulfonimide (NFSI, **45**), 1-chloromethyl-4-fluoro-1,4-diazoniabicyclo-[2.2.2]-octane salts (Selectfluor, **46**), Accufluor **47** and fluoroiodane **48** (Figure 1.8.4).[69-76] The electrophilic fluorinating reagents commonly react with nucleophilic vinyl ethers to form organic fluorides (Schemes 1.8.3 and 1.8.4).[77,78] The organic nucleophile interacts with the $\sigma^*_{N\text{-}F}$ bond from the fluorine side as the nitrogen side is sterically hindered and inaccessible. Chiral NFSI **53** and chiral selectfluor **54** deliver electrophilic fluorine in enantioselective fashion (Figure 1.8.5).[76] However, **53** and **54** are not commonly employed as reagents in the fluorination of carbohydrates, which already exist in single enantiomeric form.

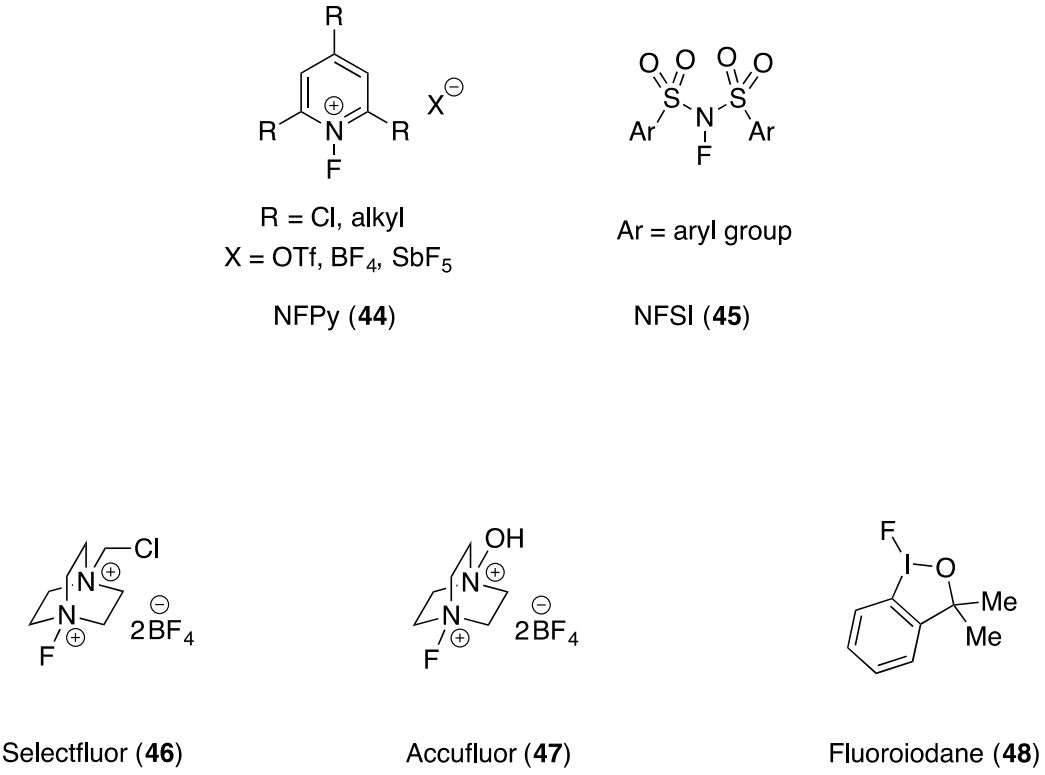

Figure 1.8.4. Electrophilic fluorination reagents

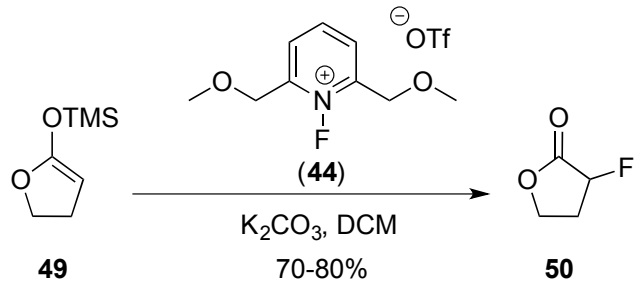

Scheme 1.8.3. Fluorination of silyl ether by *N*-fluoro- pyridinium salts **44**

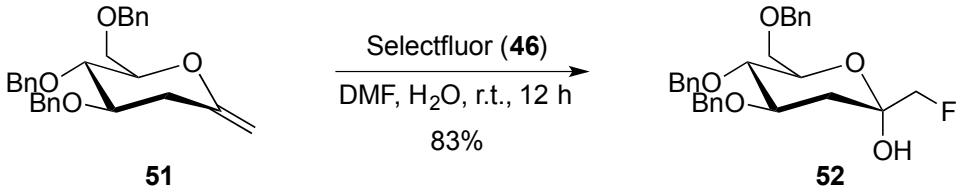

Scheme 1.8.4. Fluorination of vinyl ether by Selectfluor **46**

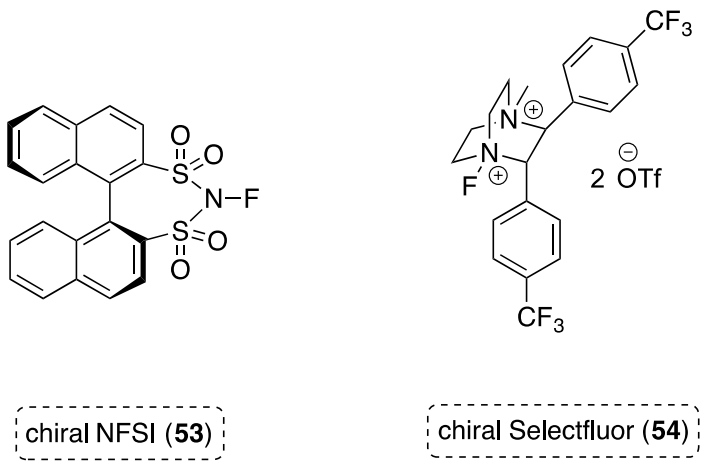

Figure 1.8.5. Chiral electrophilic fluorination reagents

Alkali metal fluorides (*e.g.* CsF, KF and KHF_2) are sources of nucleophilic fluoride ion and very commonly employed as reagents to fluorinate organic molecules.[79-82] However, alkali metal fluorides exhibit poor solubility in aprotic organic solvents. In addition, fluoride ions are less nucleophilic and more basic in nature. KHF_2 is very often used to incorporate fluorine in organic molecules *via* nucleophilic ring opening of epoxides (Scheme 1.8.5).[81] KF and CsF are used for the synthesis of organic fluorides by the S_N2 displacement of good leaving groups such as triflate, tosylate, bromide and iodide (Scheme 1.8.6).[82] Combination of KF with cation chelators such as crown ethers delivers very nucleophilic fluoride ions for S_N2 displacement reactions.

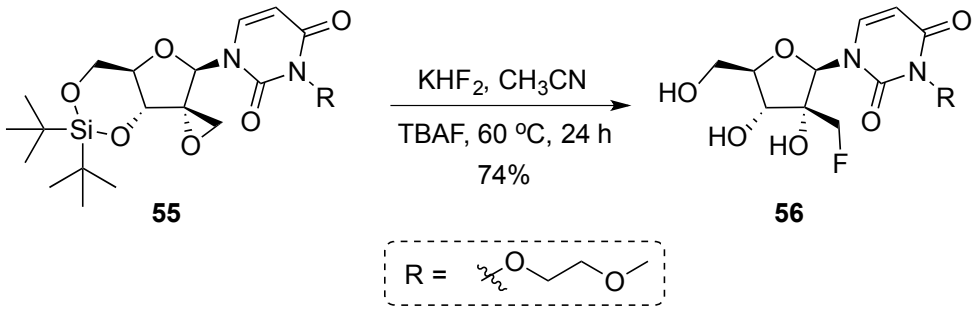

Scheme 1.8.5. Nucleophilic ring-opening of epoxide with KHF_2

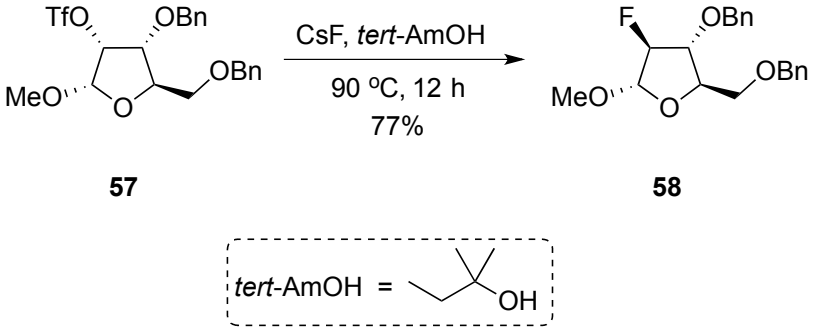

Scheme 1.8.6. Synthesis of organic fluorides by S_N2 displacement reaction

S_N2 displacement reactions with KF or CsF require conversion of the hydroxyl group of a hexose to a good leaving group. In addition, S_N2 displacement of halide, tosylate or triflate demands harsh reaction conditions and long reaction times.[82] Moreover, due to the basicity of fluoride ion, S_N2 displacement of good leaving groups with fluoride ion may also produce unwanted elimination products.[83] Organic sulfur fluorides (Figure 1.8.6) are nucleophilic fluorinating agents[76,84-87] that have the potential to convert free hydroxyl groups directly to organic fluorides (Scheme 1.8.7).[88]

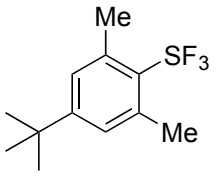

Fluolead (**59**)

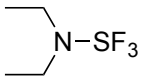

DAST (**60**)

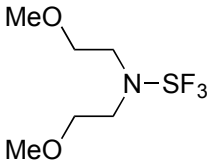

Deoxofluor (**61**)

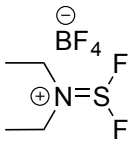

XtalFluor-E (**62**)

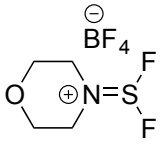

XtalFluor-M (**63**)

Figure 1.8.6. Nucleophilic fluorination reagents

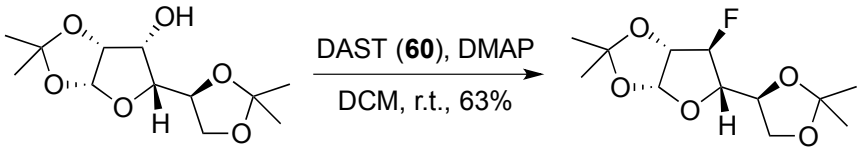

64 **65**

Scheme 1.8.7. DAST fluorination of a hydroxyl group

Synthesis of the "cold compound" (^{19}F-labeled hexose) is achieved using one of the above-mentioned fluorination methods. After the synthesis of the "cold compound", *in vitro* evaluations are performed to determine if the target GLUT has affinity for the ^{19}F labeled hexose. Competitive inhibition of [^{14}C]-D-glucose or [^{14}C]-D-fructose transport into the cells that express the target GLUT indicates the affinity of that particular GLUT

for ^{19}F-labeled hexose. If the ^{19}F-labeled hexose binds to the target GLUT, addition of modified hexose to the extracellular space inhibits the transport of the [^{14}C]-hexose into the cells (Figure 1.8.7). Upon observation of [^{14}C]-hexose transport inhibition by ^{19}F labeled hexose, several control experiments are performed to confirm the target GLUT affinity for the modified hexose.

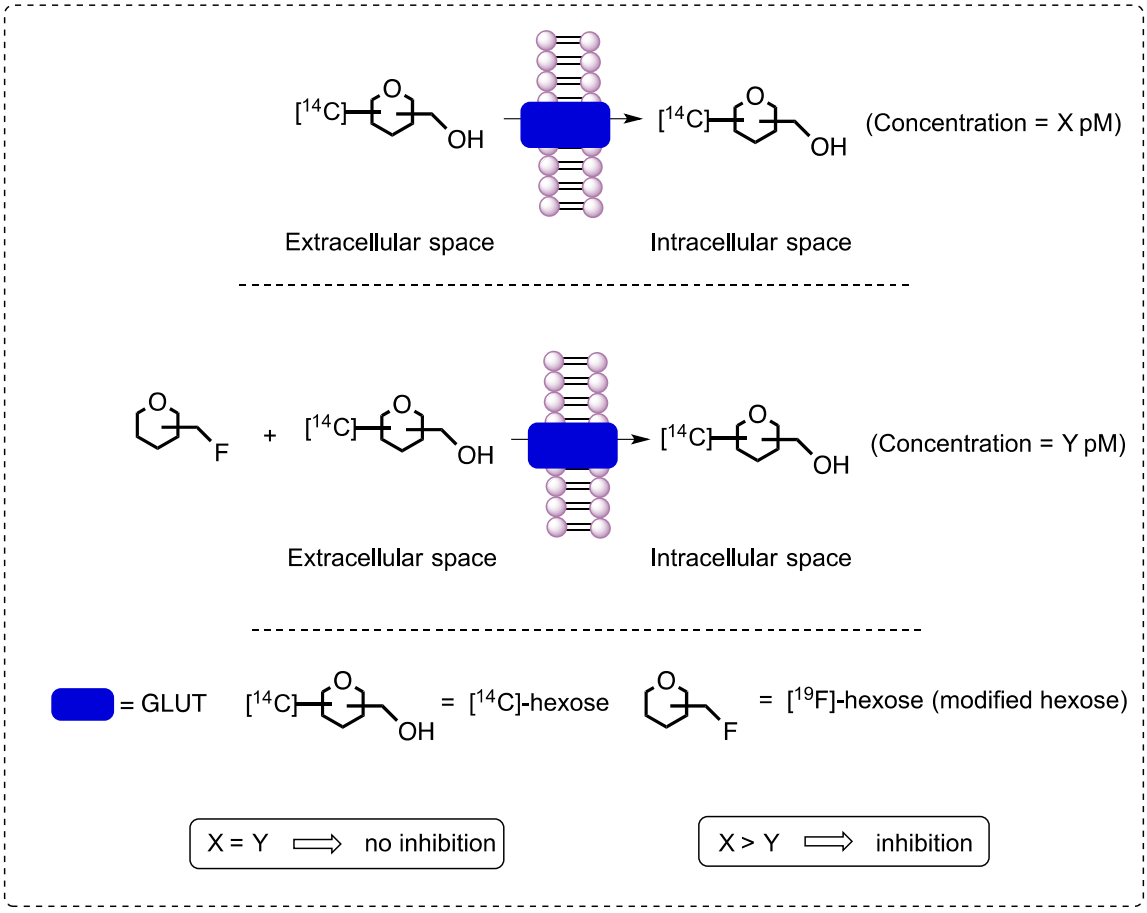

Figure 1.8.7. Preliminary evaluation of GLUT affinity for modified hexoses

Competitive inhibition study of [^{14}C]-D-hexose transport only indicates GLUT recognition for the ^{19}F-labeled hexose, but does not confirm the transport of the ^{19}F-labeled hexose into the tumor cells. To confirm transport the ^{19}F-labeled hexose into

tumor cells, evaluation of time-dependent uptake of the "hot compound" (^{19}F-labeled [^{14}C]-hexose) is necessary. If the "hot compound" is transported into tumor cells, optimization of the radiosynthesis of [^{18}F]-hexose is then required.

Synthesis of [^{18}F]-hexose is challenging due to the half-life of the ^{18}F isotope. Once the ^{18}F labeling of a hexose intermediate is performed, synthesis and purification of the [^{18}F]-hexose is required to be completed in less than the first one or two half-life cycles of the ^{18}F isotope. Thus, ^{18}F labeling of the hexose is often performed at the late-stage of the synthetic sequence.[89] Bombardment of [^{18}O]-H_2O with accelerated protons in cyclotron yields [^{18}F]-HF, which could be easily converted into the corresponding potassium salt (K^{18}F).[90] Upon chelation with Kryptofix 2.2.2 **66**, K^{18}F delivers very reactive fluoride nucleophile, which displaces good leaving groups such as OTf in S_N2 fashion to incorporate ^{18}F isotope in hexoses (Scheme 1.8.8).[91,44]

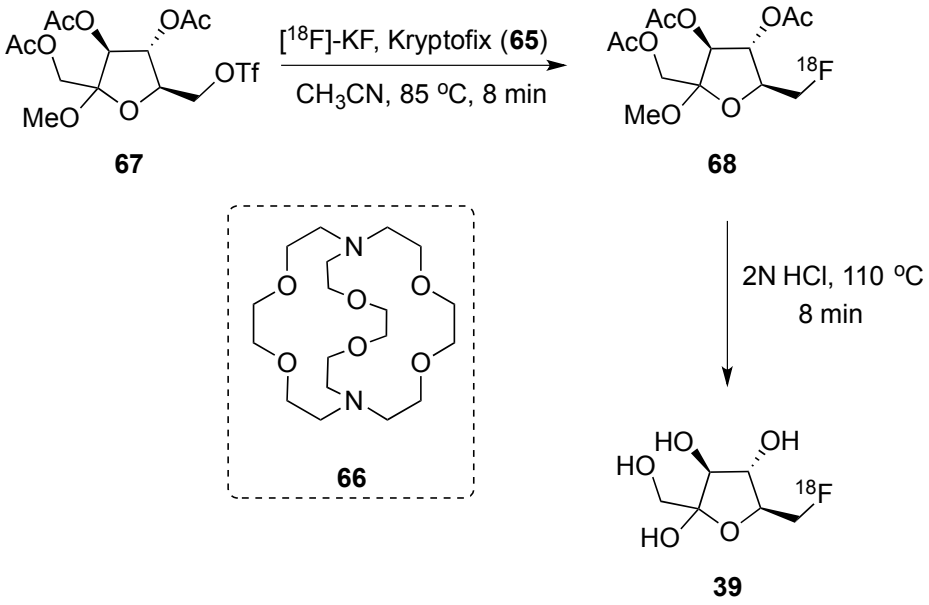

Scheme 1.8.8. ^{18}F labeling of D-fructose within the first half-life period of the isotope

Once the synthesis of [^{18}F]-hexose is accomplished, the *in vivo* evaluation of [^{18}F]-hexose is performed using small animal PET equipment. Injection of [^{18}F]-hexose into mice bearing the target tumor followed by PET scanning for a specific time period reveals the tumor diagnostic efficiency of the tracer. Upon the successful imaging of the tumor in a small animal, the [^{18}F]-hexose is ready for toxicology study and then clinical trials.

1.8.3. [^{18}F]-2-FDG – A commonly used PET tracer

[^{18}F]-2-Deoxy-2-fluoro-D-glucose ([^{18}F]-2-FDG **14**) is a very commonly used radiotracer in PET for cancer diagnosis.[92] As described previously (Section 1.6), D-glucose is a GLUT1 substrate and C-2 modification is tolerated by GLUT1. In addition, GLUT1 was found to be overexpressed in various cancer cell types when compared to normal cells (Section 1.7). Thus, [^{18}F]-2-FDG **14**, a glucose derivative with ^{18}F isotope labeling at

position C-2 has been successfully used as a tracer used in PET for tumor diagnosis (Figure 1.8.8).

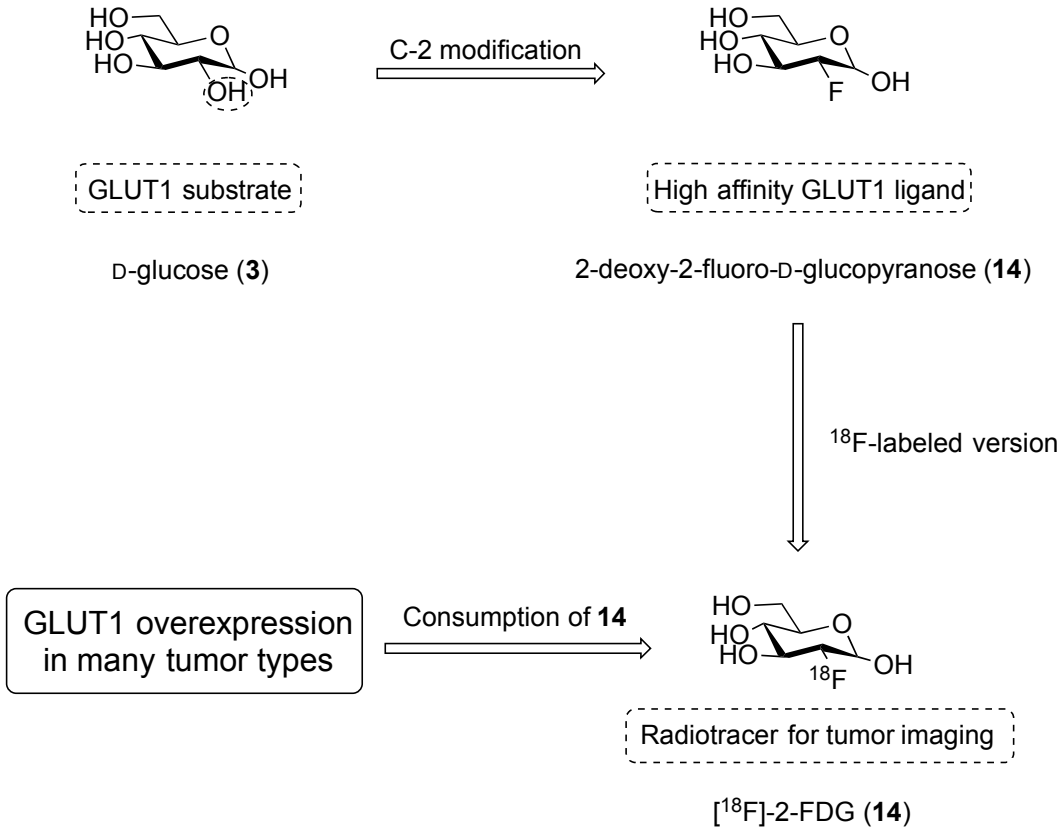

Figure 1.8.8. Structural features of [^{18}F]-2-FDG

Apart from being transported by GLUT1, [^{18}F]-2-FDG also undergoes enzymatic phosphorylation with hexokinase due to the presence of a C-6 hydroxyl group. In addition, the fluorine atom at position C-2 prevents [^{18}F]-2-FDG phosphate from undergoing further metabolic transformations (Figure 1.8.9). As a result, [^{18}F]-2-FDG gets metabolically trapped inside the tumor cells, which enhances the signal to noise ratio of the diagnostic image.[66] Furthermore, after the emission of a positron, [^{18}F]-2-FDG phosphate transforms into [^{18}O]-D-glucose and gets washed out from the patient body (Figure 1.8.9).

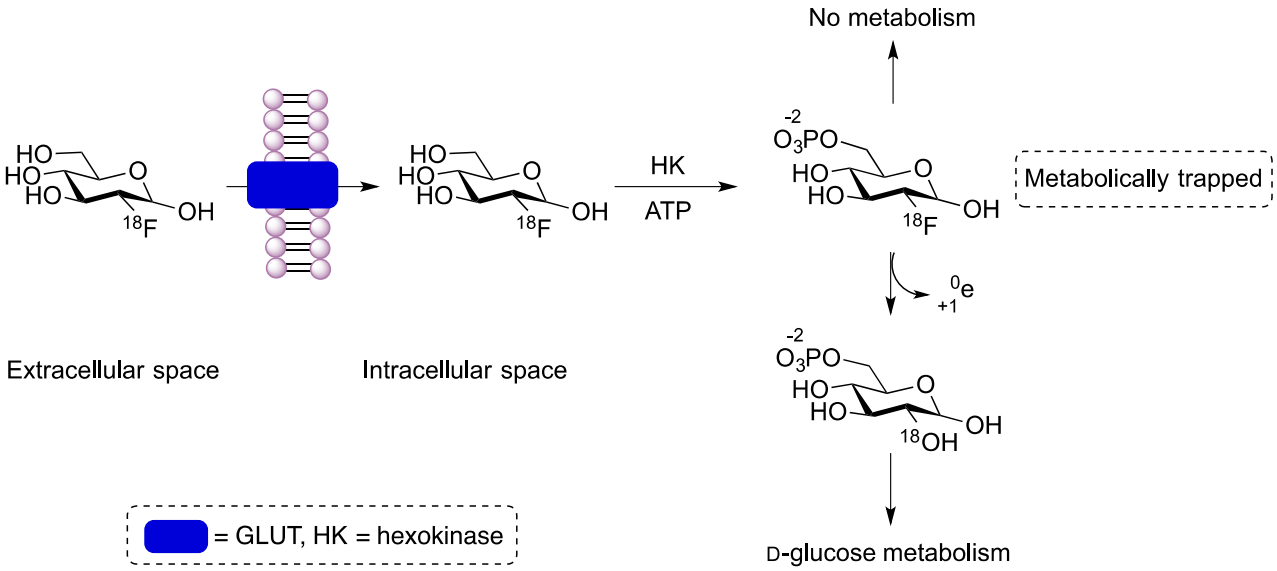

Figure 1.8.9. Post-transport changes of [^{18}F]-2-FDG

The first generation synthesis of [^{18}F]-2-FDG involved treatment of D-glucal **20** with [^{18}F]-F_2 and water (Scheme 1.8.9). This synthetic process also yields [^{18}F]-2-deoxy-2-fluoro-D-mannose **69**.[93]

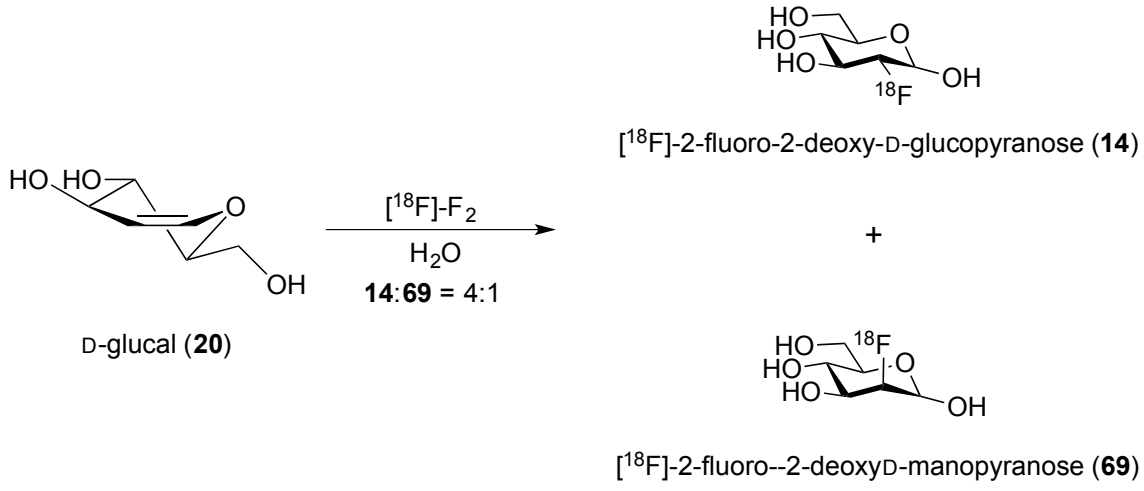

Scheme 1.8.9. The first generation synthesis of [^{18}F]-FDG

In 1987, a synthesis of [^{18}F]-2-FDG was reported by the displacement of protected mannose triflates **70** and **72** with fluoride ion (Scheme 1.8.10).[94] Currently, [^{18}F]-2-FDG is accessed by the displacement of peracetylated mannose triflate **74** with fluoride ion (Scheme 1.8.11).[95]

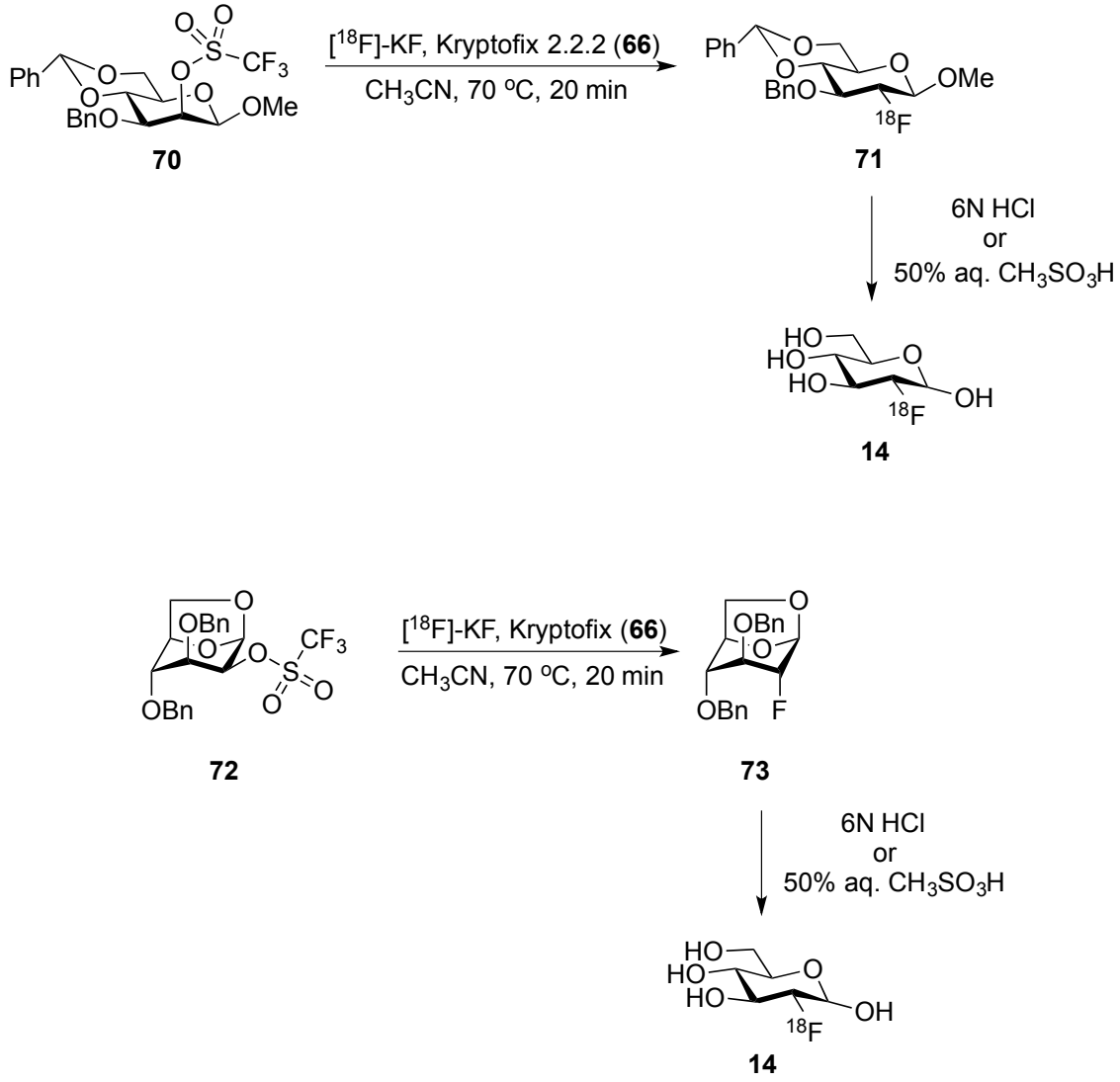

Scheme 1.8.10. The second generation synthesis of [^{18}F]-FDG

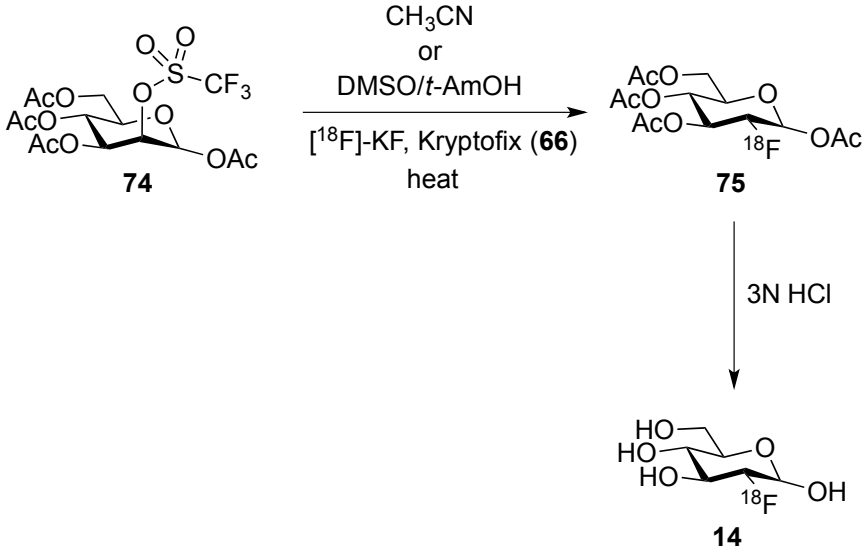

Scheme 1.8.11. The currently used synthesis of [^{18}F]-FDG

1.8.4. False diagnosis of early stage breast cancer with [^{18}F]-2-FDG

Breast cancer is the second leading cause of cancer related death in women. Early stage diagnosis of breast cancer is key for the patient survival.[96] In the late stages, metastasis of breast cancer diminishes the chances of patient survival.[97] Although [^{18}F]-2-FDG is a reliable tracer for tumor diagnosis, FDG imaging of breast cancer, especially during the early stages, can provide false diagnostic results. Low-to-negative expression of GLUT1 in breast cancer cells and ubiquitous expression of GLUT1 in normal breast cells (Figure 1.8.10) caused low signal to background ratios in FDG-PET diagnosis.[52] As a consequence, false positive and false negative diagnosis of the early stage breast cancer was observed with [^{18}F]-2-FDG PET.

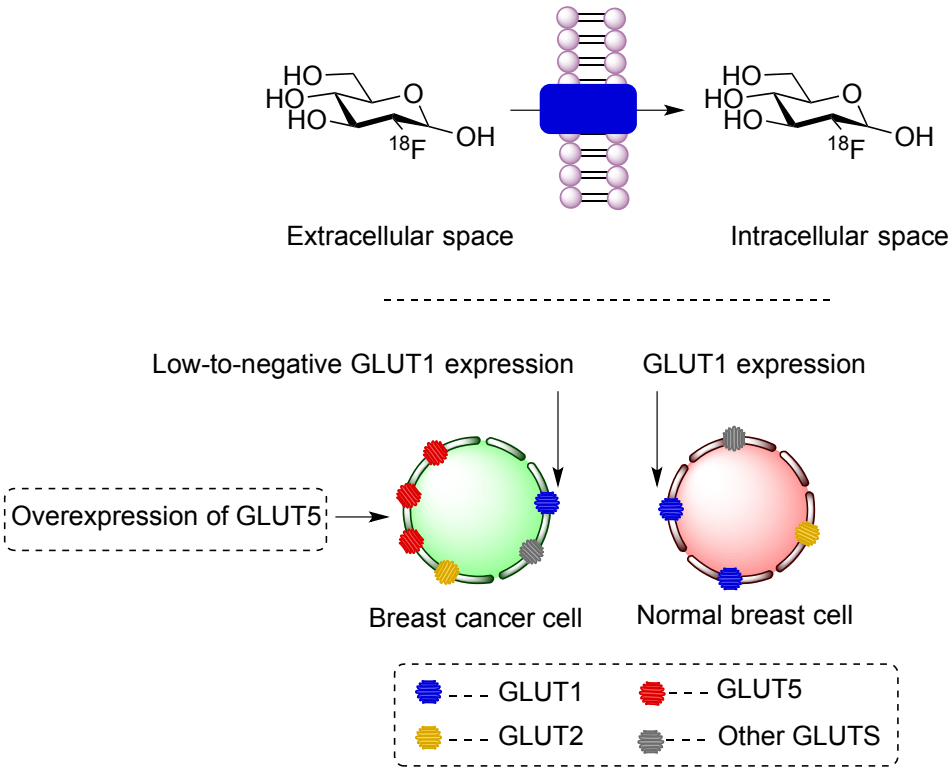

Figure 1.8.10. Expression of GLUTs in breast cancer and normal breast cells

As many breast cancer cells overexpress GLUT5,[52,53] which is not expressed in normal breast cells, development of PET tracers that exhibit high affinity for GLUT5 could improve signal to background ratio. Thereby, PET tracers that are transported by GLUT5 could be useful for the early stage diagnosis of breast cancer. Radiotracers [^{18}F]-1-FDF **29**, [^{18}F]-6-FDF **39** and [^{18}F]-1-FDAM **42** were developed for the early diagnosis of breast cancer (Figure 1.8.11).[44,46,98] As previously discussed (Section 1.7), GLUT5 exhibited very low affinity for C-1 modified D-fructoses. As a result, the usage of radiotracer [^{18}F]-1-FDF **29** in tumor diagnosis was not successful. The radiotracers [^{18}F]-6-FDF **39** and 1-FDAM **42** exhibited *in vivo* accumulation into EMT-6 tumor cells. However, **39** and **42** undergo enzymatic phosphorylation only by ketohexokinase (KHK), but not by hexokinase (HK).[44] Unfortunately, lack of ketohexokinase expression in breast

tumor cells precluded phosphorylation, leading to quick efflux of these probes from the tumor cells (Figure 1.8.12).

D-Glucose and C-2 modified D-glucose conjugates bind efficiently with hexokinase and undergo enzymatic phosphorylation.[66,99] Consequently, the D-glucose-based probes remain metabolically trapped inside tumor cells. Like D-glucose, D-fructose and its analogues undergo phosphorylation at the C-6 hydroxyl group. However, to preserve effective binding and transport by GLUT5, fructose analogues can be modified only at C-6, thus removing the only site for phosphorylation. As a result, to date, all the radiotracers ([^{18}F]-1-FDF **29**, [^{18}F]-6-FDF **39** and [^{18}F]-1-FDAM **42**) that target GLUT5 transport protein exhibited quick efflux from the tumor cells. Therefore, our goal is to develop probes that not only target the GLUT5 transporter protein, but also serve as competent substrates for hexokinase and undergo phosphorylation in the cytosol to prevent their efflux from the tumor cells.

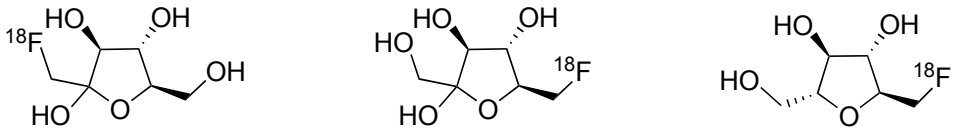

29 **39** **42**

Figure 1.8.11. Tracers developed to target the GLUT5 transporter

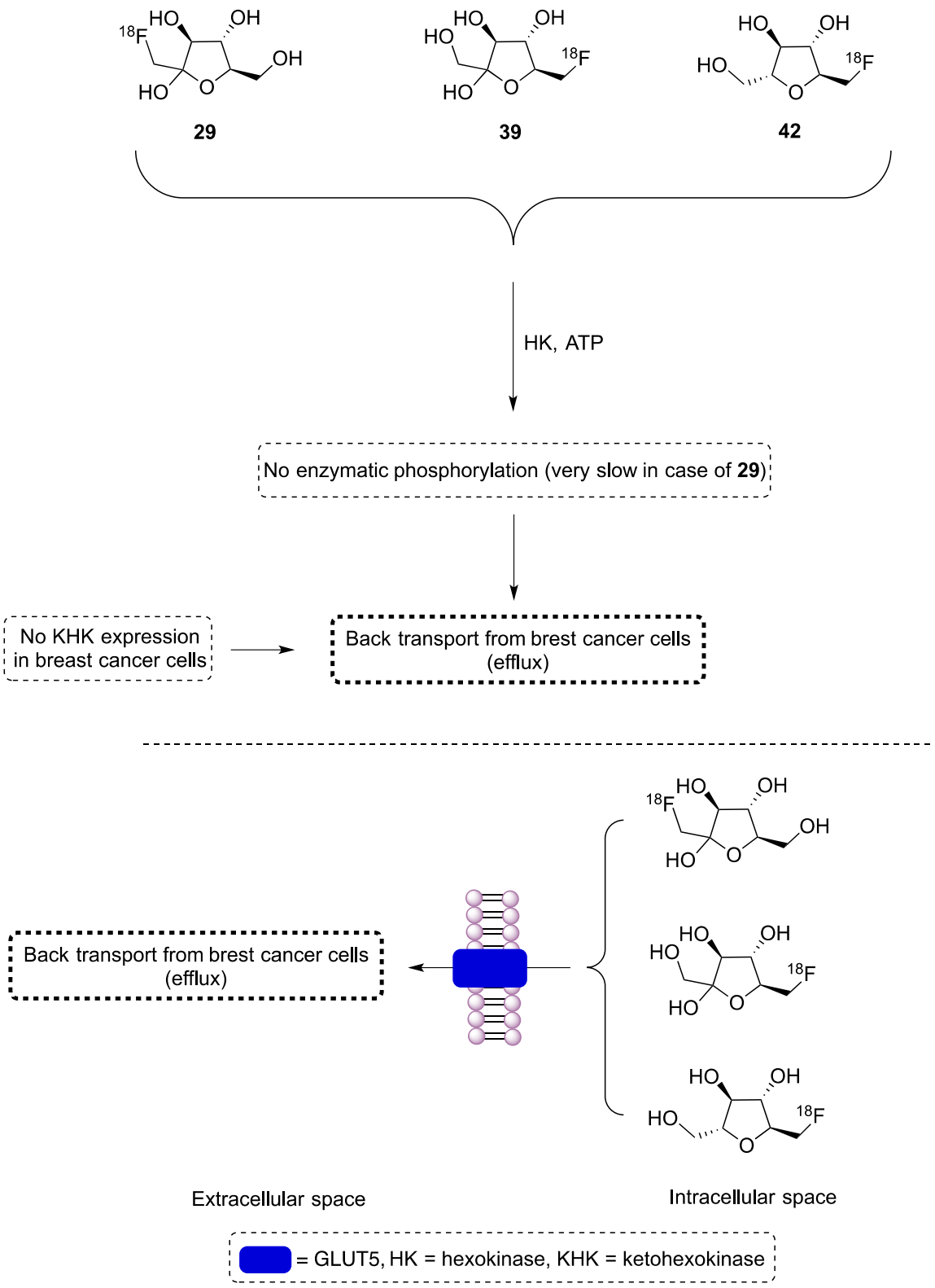

Figure 1.8.12. Efflux of tracers that target GLUT5 transporter

2,5-AM **40** was previously described as a high affinity GLUT5 ligand. In addition, 2,5-AM **40** undergoes enzymatic phosphorylation in the presence of hexokinase or ketohexokinase (Scheme 1.8.12).[99] The 2,5-AM based probe 1-FDAM **42** is prepared by the incorporation of the radiolabel ^{18}F at position C-1. 1-FDAM **42** was quickly back-transported from tumor cells, despite the presence of one primary hydroxyl group at C-6 for enzymatic phosphorylation. Development of a 2,5-AM based tracer which retains both primary alcoholic groups could lead to a substrate for enzymatic phosphorylation by hexokinase, due to its ability to closely mimic the 2,5-AM. In order to retain both primary hydroxyl groups in a 2,5-AM based probe, the radiolabel ^{18}F would need to be incorporated at the C-3 position.

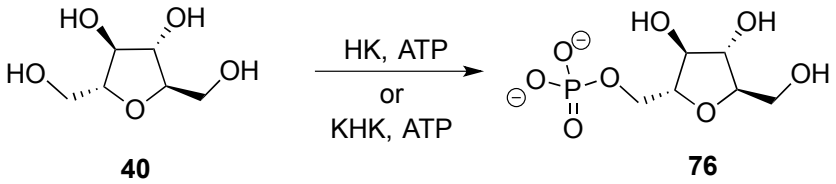

40 **76**

HK = hexokinase, KHK = ketohexokinase

Scheme 1.8.12. Enzymatic phosphorylation of 2,5-AM **40**

We designed a new PET tracer molecule [^{18}F]-3-FDAM **77**, which retains both primary hydroxyl groups and was expected to be transported by GLUT5 transport protein (Figure 1.8.13). However, the C-3 modified 2,5-AM derivatives had not been evaluated as GLUT5 substrates to date. Thus, the importance of the C-3 hydroxyl group for GLUT5 recognition was unknown. In addition, no synthetic protocol was previously described to access C-3 modified 2,5-AM derivatives (Scheme 1.8.14).

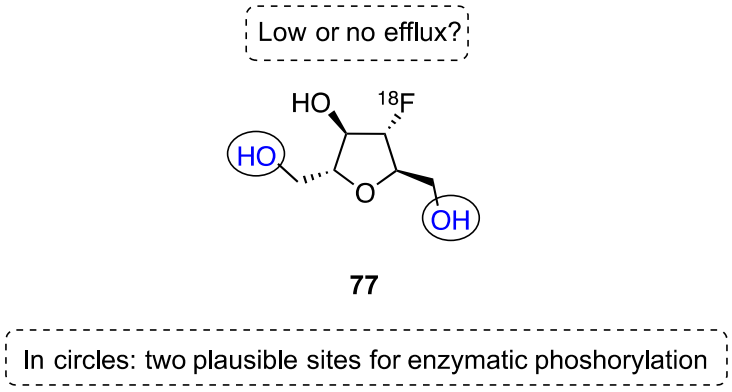

Figure 1.8.13. Design of a new PET tracer

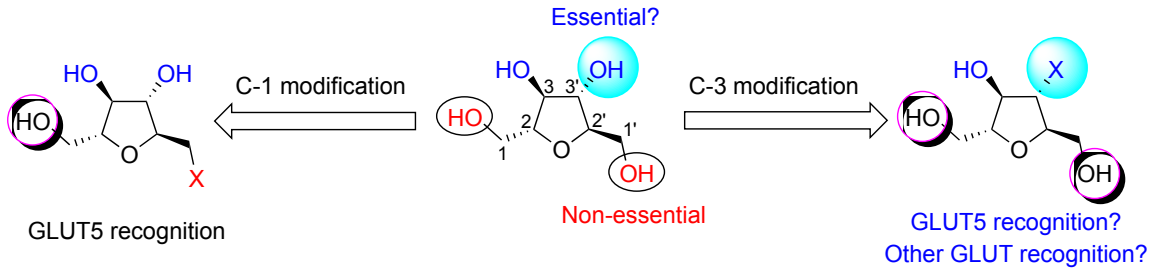

Figure 1.8.14. Overview of reported work and planned future work on modified 2,5-AM derivatives

C-1 modified 2,5-AM derivatives can be easily accessed from 2,5-AM **40** (Scheme 1.8.13).[40] Selective protection of one of the primary alcohols with TrCl yields 1-*O*-trityl-2,5-anhydro-D-mannitol **78**. Acetylation of compound **78** provides access to 1-*O*-trityl-3,4,6-*O*-tri-acetyl-2,5-anhydro-D-mannitol **79**. Selective deprotection of trityl group with AcOH affords 1,3,4-tri-*O*-acetyl-2,5-anhydro-D-mannitol **80**. Treatment of the unprotected primary alcoholic group of **80** with TsCl provides access to compound **81**. Nucleophilic displacement of the leaving group followed by deprotection of acetate functionality yields C-1 functionalized 2,5-AM derivative **82**. Thus, selective protection of primary hydroxyl functionality with an acid sensitive protecting group is the key to

access C-1 functionalized 2,5-AM. Unfortunately, this strategy cannot be applied to the synthesis of C-3 functionalization of 2,5-AM derivatives **83**.

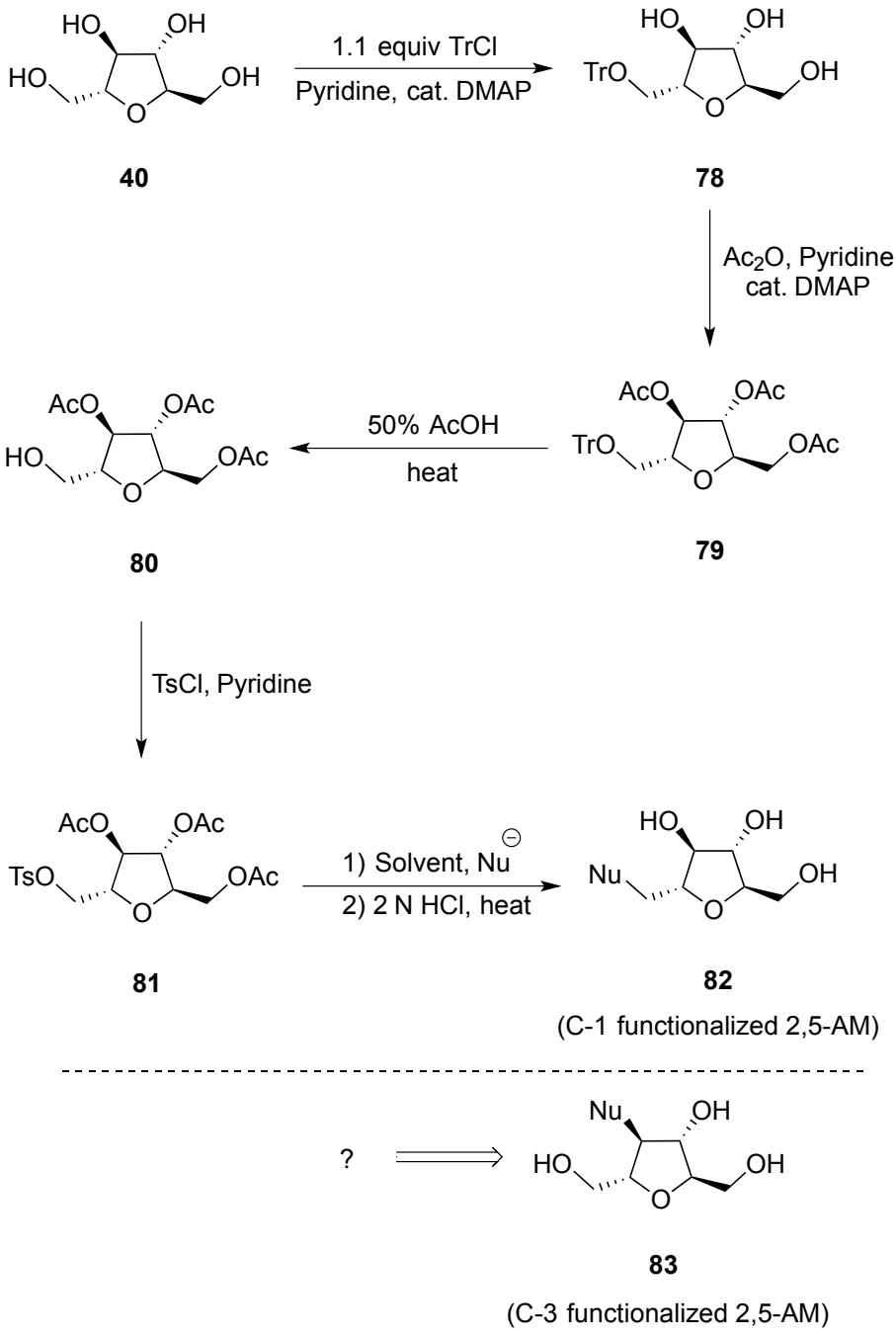

Scheme 1.8.13. C-1 functionalization of 2,5-AM and the lack of synthetic strategy for C-3 modification

1.9. Conclusion

Facilitated hexose transporter proteins (GLUTs) associate with cell membranes, and transport hexoses from intracellular space to extracellular space and vice versa. However, GLUTs do not transport hexose phosphates. Each GLUT exhibits specific affinity towards one or more hexoses. Tumor cells overexpress GLUTs due to altered hexose metabolism. Thus, GLUTs have the potential to serve as portals for the selective delivery of tracer molecules into tumor cells. GLUT1 is a D-glucose transporter and tolerates modification of primary and secondary hydroxyl groups of D-glucose. In contrast, GLUT5 transports D-fructose and does not tolerate the alteration of secondary alcoholic groups of D-fructose.

Breast cancer is one of the leading causes of cancer-related death in women. Early stage detection of breast cancer is crucial for patient survival. False positive and false negative diagnosis of early stage breast cancer was observed with [^{18}F]-2-FDG PET imaging. Transport of [^{18}F]-2-FDG by ubiquitously expressed GLUT1 and low-to-negative GLUT1 expression in breast cancer cells are considered to be two major reasons for the false diagnosis by [^{18}F]-2-FDG PET. Developing tracers that operate through the GLUT5 transport protein, which was found to be overexpressed in breast cancer cells but not in normal breast cells, could provide early stage diagnosis of breast cancer. Initial tracer molecules that target GLUT5 displayed quick efflux from tumor cells, which compromises signal to noise ratio. 2,5-AM **40** undergoes enzymatic phosphorylation with hexokinase and ketohexokinase. Two primary alcoholic positions that are crucial for enzymatic phosphorylation can be retained by the incorporation of radiolabel at position

C-3 of 2,5-AM. Such tracers are expected to overcome the problem of quick efflux. Moreover, no synthetic protocols were reported to accomplish the stereoselective C-3 functionalization of 2,5-AM **40**.

In Chapter 2, diastereoselective modification of the C-3 position of 2,5-anhydro-D-mannitol is described. Chapter 3 presents the biological evaluation of 3-deoxy-3-fluoro-2,5-anhydro-D-mannitol whose ^{18}F-labeled version could potentially be used as a PET tracer for the detection of breast cancer. In addition, Chapter 3 also deals with the structure-activity relationship between GLUT5 and C-3 modified 2,5-AM derivatives. In Chapter 4, synthesis and biological evaluation of a new probe 3-(*N*-(4-nitro-2,1,3-benzoxadiazol-7-yl))amino-2,5-anhydro-D-mannitol are described, along with interesting docking studies performed by collaborators. Chapter 5 comprises the synthesis and biological evaluation of C-3 modified 2,5-AM bearing near-infrared emitting dyes as probes for the optical imaging of breast cancer. In Chapter 5, we have also presented our efforts to synthesize 2,5-anhydro-D-mannitol mimicking aza-sugar based probes.

1.10. References

1) Dashty, M. A quick look at biochemistry: Carbohydrate metabolism. *Clin. Biochem.* **46**, 1339-1352 (2013).
2) Thorens, B. & Mueckler, M. Glucose transporters in the 21st century. *Am. J. Physiol. Endocrinol. Metab*. **298**, E141-E145 (2010).
3) Gould, G. & Holman, G. D. The glucose transporter family: Structure, function and tissue specific expression. *Biochem. J*. **295**, 329-341 (1993).

4) Manolescu, A. R., Witkowska, K., Kinnaird, A., Cessford, T. & Cheeseman C. Facilitated hexose transporters: New perspectives on form and function. *Physiology* **22**, 234-240 (2007).

5) McQuade, D. T., Plutschack, M. B. & Seeberger, P. H. Passive fructose transporters in disease: A molecular overview of their structural specificity. *Org. Biomol. Chem*. **11**, 4909-4920 (2013).

6) Mueckler, M. & Thorens, B. The SLC2 (GLUT) family of membrane transporters. *Mol. Aspects Med*. **34**, 121-138 (2013).

7) Long, W. & Cheeseman, C. I. Structure and functional insights into GLUT family of membrane transporters. *Cell Health and Cytoskeleton*. **7**, 167-183 (2015).

8) Deng, D. & Yan, N. GLUT, SGLT, and SWEET: Structural and mechanistic investigation of the glucose transporters. *Protein Sci.* **25**, 546-558 (2016).

9) Kasahara, M. & Hinkle P. C. Recognition and purification of D-glucose transporter from human erythrocytes. *J. Biol. Chem.* **252**, 7384-7390 (1977).

10) Sogin, D. C. & Hinkle, P. C. Characterization of the glucose transporter from human erythrocytes. *J. Supramol. Struct.* **8**, 447-453 (1978).

11) Mueckler, M., Caruso, C., Baldwin, S. A., Panico, M., Blench, I., Morris, H. R., Allard, W. J., Lienhard, G. E. & Lodish, H. F. Sequence and structure of a human glucose transporter. *Science*. **229**, 941-945 (1985).

12) Joost, H-G, Bell, G. I, Best, J. D, Birnbaum, M. J., Charron, M. J., Chen, Y. T., Doege, H., James, D. E., Lodish, H. F., Moley, K. H., Moley, J. F., Mueckler, M., Rogers, S., Schurmann, A. & Seino, S., Thorens, B. Nomenclature of the

GLUT/SLC2A family of sugar/poloyl transport facilitators. *Am. J. Physiol. Endocrinol. Metab.* **282**, E974-E976 (2002).

13) Morgello, S., Uson, R. R., Schwartz, E. J. & Haber, R. S. The human blood-brain barrier glucose transporter (GLUT1) is a glucose transporter of gray matter astrocytes. *Glia.* **14**, 43-54 (1995).

14) Kumagai, K. A. Glucose transport in brain and retina: Implications in the management and complications of diabetes. *Diabetes Metab. Res Rev.* **15**, 261-273 (1999).

15) Postic, C., Burcelin, R., Rencurel, F., Pegorier, J-P., Loizeau, M., Girard, J. & Leturque, A. Evidence for a transient inhibitory effect of insulin on GLUT2 expression in the liver: Studies *in vivo* and *in vitro*. *Biochem. J.* **293**, 119-124 (1993).

16) Pang, K., Mukonoweshuro, C. & Wong, G. G. Beta cells arise from glucose transporter 2 (GLUT2)-expressing epithelial cells of the developing rat pancreas. *Proc. Natl. Acad. Sci. USA*. **91**, 9559-9563 (1994).

17) Maher, F., Davies-Hill, T. M., Lysko, P. G., Henneberry, R. C. & Simpson, I. A. Expression of two glucose transporters, GLUT1 and GLUT3, in cultured cerebellar neurons: Evidence for neuron-specific expression of GLUT3. *Mol. Cell. Neurosci.* **2**, 351-360 (1991).

18) Haung, S. & Czech, P. The GLUT4 glucose transporter. *Cell Metab.* **5**, 237-252 (2007).

19) Leto, D. & Saltiel, A. Regulation of glucose transport by insulin: Traffic control of GLUT4. *Mol. Cell Biol.* 13, 383-396 (2012).

20) Band, E. B., Depaoli, A. M., Davidson, N. O, Bell, C. I. & Burant, C. F. Sequence, tissue distribution, and functional characterization of the rat fructose transporter GLUT5. *Am. J. Physiol. Gastrointest. Liver Physiol.* **264**, G1169-1176 (1993).

21) Zhao, F-Q. & Keating, A. F. Functional properties and genomics of glucose transporters. *Curr. Genomics* **8**, 113-128 (2007)

22) Cheeseman, C. GLUT7: A new intestinal facilitated hexose transport. *Am. J. Physiol. Endocrinol. Metab.* **295**, E238-E241(2008).

23) Preitner, F., Bonny, O., Laverriere, A., Rotman, S., Firsov, D., Costa, A. D., Metref, S. & Thorens, B. GLUT9 is a major regulator of urate homostasis and its genetic inactivation induces hyperuricosuria and urate nephropathy. *Proc. Natl. Acad. Sci. USA*. **106**, 15501-15506 (2009).

24) Deng, D., Xu, C., Sun, P., Wu, J., Yan, C., Hu, M. & Yan, N. Crystal structure of the human glucose transporter GLUT1. *Nature.* **510**, 121-125 (2014).

25) Nomura, N., Verdon, G., Kang, H. J., Shimamura, T., Nomura, Y., Sonoda, Y., Hussien, S. A., Qureshi, A. A., Coincon, M., Sato, Y., Abe, H., Nakada-Nakura, Y., Hino, T., Arakawa, T., Kusano-Arai, O., Iwanari, H., Murata, T., Kobayashi, T., Hamakubo, T., Kasahara, M., Iwata, S. & Drew, D. Structure and mechanism of mammalian fructose transporter GLUT5. *Nature.* **526**, 397-401 (2015).

26) Deng, D., Xu, C., Sun, P., Yan, C., Ke, M., Jiang, X., Xiong, L., Ren, W., Hirata, K., Yamamoto, M., Fan, S. & Yan, N. Molecular basis of ligand recognition and transport by glucose transporters. *Nature*. **526**, 391-396 (2015).

27) Manolescu, A. R., Augustin, R., Moley, K., & Cheeseman, C. A highly conserved hydrophobic motif in the exofacial vestibule of fructose transporting SLC2A proteins

acts as a critical determinant of their substrate selectivity. *Mol. Membr. Biol.* **24**, 455–463 (2007).

28) Sheena, A., Mohan, S. S., Haridas, N. P. A. & Anilkumar, G. Elucidation of the glucose transport pathway in glucose transporter 4 *via* steered molecular dynamics simulations. *PLoS One.* **6**, e25747 (2011).

29) Carruthers, A., DeZutter, J., Ganguly, A. & Devaskar, S. U. Will the original glucose transporter isoform please stand up. Am. J. Physiol. *Endocrinol. Metab.* **297**, E836-E848 (2009).

30) Mueckler, M. & Makepeace, C. Transmembrane segment 12 of the GLUT1 glucose transporter is an outer helix and is not directly involved in the transport mechanism. *J. Biol. Chem.* **281**, 36993-36998 (2006).

31) Gallagher, B. M., Fowler, J. S., Gutterson, N. I., MacGregor, R. R., Wan, C-N. & Wolf, A. P. Metabolic trapping as a principle of radiopharmaceutical design: Some factors responsible for the biodistribution of [^{18}F]-2-deoxy-2-fluoro-D-glucose. *J. Nucl. Med.* **19**, 1154-1161, (1978).

32) Angyal, S. J. The composition and conformation of sugars in solution. *Angew. Chem. Int. Ed. Engl.* ***8***, 157-166 (1969).

33) Tajmir-Riahi, H. A. Carbohydrate complexes with alkaline earth metal ions. Interactions of D-glucono-1,5-lacton with the Mg (II), Ca (II), Sr (II) and Ba (II) cations in the crystalline solid and aqueous solution. *J. Inorg. Chem.* **39**, 33-41 (1990).

34) Gatley, S. J. Labeled glucose analogs in the genomic era. *J. Nucl. Med.* **44**, 1082-1086 (2003).

35) Barnett, J. E. G., Holman, G. D. & Munday, K. A. Structural requirement for binding to the sugar-transport system of the human erythrocyte. *Biochem. J.* **131**, 211-221 (1973).

36) Calvaresi, E. C. & Hergenrother. P. J. Glucose conjugation for specific targeting and treatment of cancer. *Chem. Sci.* **4**, 2319-2333 (2013).

37) Som, P., Atkins, H. L., Bandopadhyay, D., Fowler, J. S., MacGregor, R. R., Matsui, K., Oster, H., Sacker, D. F., Shiue, C. Y., Tuner, H., Wan, C-N., Wolf, A. P. & Zabnski, V. A fluorinated glucose analog, 2-fluoro-2-deoxy-D-glucose (F-18): Nontoxic tracer for tumor detection. *J. Nucl. Med*. **21**, 670-675 (1980).

38) Avril, N. GLUT1 expression in tissue and ^{18}F-FDG uptake. *J. Nucl. Med*. **45**, 930-932 (2004).

39) Guo, J., Du, C., Shan, L., Zhu, H., Xue, B., Quian, Z., Achilefu, S. & Gu, Y. Comparison of near-infrared fluorescent deoxyglucose probes with different dyes for tumor diagnosis in vivo. *Contrast Media Mol. Imaging*. **7**, 289-301 (2012).

40) Z. Cheng, J. Levi, Z. Xiong, O. Gheysens, S. Keren, X. Chen & S. S. Gambhir. Near-infrared fluorescent deoxyglucose analog for tumor optical imaging in cell culture and in living mice. *Bioconjugate Chem.* **17**, 662-669 (2006).

41) Tatibouet, A., Yang, J., Morin, C. & Holman, G. D. Synthesis and evaluation of fructose analogues as inhibitors of the D-fructose transporter GLUT5. *Bioorg. Med. Chem.* **8**, 1825-1833 (2000); Haradahira, T. *et al.* Radiosynthesis, rodent biodistribution, and metabolism of 1-deoxy-1-[^{18}F]-fluoro-D-fructose. *Nucl. Med. Biol.* **22**, 719–725 (1995).

42) Girniene, J., Tatibouët, A., Sackus, A., Yang, J., Holman, G. D. & Rollin, P. Inhibition of the D-fructose transporter protein GLUT5 by fused-ring glycol-1,3-oxazolidin-2-thiones and oxazolidin-2-ones. *Carbohydrate Res.* **338**, 711-719 (2003).

43) Yang, J., Dowden, J., Tatibouet, A., Hatanaka, Y. & Holman, G. D. Development of high-affinity ligands and photoaffinity labels for the D-fructose transporter GLUT5. *Biochem. J.* **367**, 533-539 (2002).

44) Wuest, M., Trayner, B. J., Grant, T. N., Jans, H. S., Mercer, J. R., Murray, D., West, F. G., McEwan, A. J. B., Wuest, F. & Cheeseman, C. I. Radiopharmacological evaluation of 6-deoxy-6-[^{18}F]fluoro-D-fructose as a tracer for PET imaging of breast cancer. *Nucl. Med. Biol.* **38**, 461-475 (2011).

45) Tanasova, M., Plutschack, M., Muroski, M. E., Sturla, S. J., Struouse, G. F. & McQuade, D. T. Fluorescent THF-based fructose analogue exhibits fructose-dependent uptake. *ChemBioChem*. **14**, 1263-1270 (2013).

46) Soueidan, O. M., Trayner, B. J., Grant, T. N., Henderson, J. R., Wuest, F., West, F. G. & Cheeseman, C. I. New fluorinated fructose analogs as selective probes of hexose transport protein GLUT5. *Org. Biomol. Chem.* **13**, 6511-6521 (2015).

47) Medina, R. A. & Owen, G. I. Glucose transporters: Expression, regulation and cancer. *Biol. Res.* **35**, 9-26 (2002).

48) Adekola, K., Rosen, S.T. & Shanmugam M. Glucose transporters in cancer metabolism. *Curr. Opin. Oncol.* **24**, 650-654 (2012).

49) Carvalho, K. C., Cunha, I. W., Rocha, R. M., Ayala, F. R., Cajaiba, M. M., Begnami, M. D., Vilela, R. S., Paiva, G. R., Andrade, R. G. & Soares, F. A. GLUT1 expression

in malignant tumors and its use as an immunodiagnostic marker. *Clinics*. **66**, 965-972 (2011).

50) Schwartzenberg-Bar-Yoseph, F., Armoni, M. & Karniel, E. The tumor suppressor p53 down-regulates glucose transporters GLUT1 and GLUT4 gene expression. *Cancer Res.* **64**, 2627-2633 (2004).

51) Krzeslak, A., Wojcik-Krowiranda, K., Forma, E., Jozwiak, P., Romanowicz, A. & Brys, M. Expression of GLUT1 and GLUT3 glucose transporters in endometrial and breast cancer. *Pathol. Oncol. Res.* **18**, 721-728 (2012).

52) Godoy, A., Ulloa, V., Rodriguez, F., Reinicke, K., YaÑez, A. J., GarcÍa, M. A., Medina, R. A., Carrasco, M., Barberis, S., Castro, T., MartÍnez, F., Koch, X., Vera, J. C., Poblete. M. T., Figueroa, C.D., Peruzzo, B., PÉrez, F., Nualart, F. Differential subcellular distribution of glucose transporters GLUT1-6 and GLUT9 in human cancer: Ultrastructural localization of GLUT1 and GLUT5 in breast tumor cells. *J. Cell. Physiol.* **207**, 614-627 (2006).

53) Zamora-Leon, S. P., Golde, D. W., Concha, I. I., Rivas, C. I., Delgado-López, F. & Vera, J. C. Expression of the fructose transporter GLUT5 in human breast cancer. *Proc. Natl. Acad. Sci. USA*. **93**, 1847-1852 (1996).

54) James, M. L. & Gambhir, S. S. A molecular imaging primer: Modalities, imaging agents, and applications. *Physiol. Rev.* **92**, 897-965 (2012).

55) Wang, D. S., Dake, M. D., Park, J. M. & Kuo, M. D. Molecular imaging: A primer for interventionalists and images. *J. Vasc. Interv. Radiol.* **17**, 1405-1423 (2006).

56) Nolting, D. D., Nickels, M. L., Guo, N. & Pham, W. Molecular imaging probe development: A chemistry perspective. *Am. J. Nucl. Med. Mol. Imaging.* **2**, 273-306 (2012).

57) Gambhir, S. S. Molecular imaging of cancer with positron emission tomography. *Nat. Rev. Cancer.* **2**, 683-693 (2002).

58) Imam, S. K. Review of positron emission tomography tracers for imaging of tumor hypoxia. *Cancer Biother. Radiopharm.* **25**, 365–74 (2010).

59) Muehllehner, G. & Karp, J. S. Positron emission tomography. *Phys. Med. Biol.* **51**, R117–37 (2006).

60) Zanzonico, P. Positron emission tomography: a review of basic principles, scanner design and performance, and current systems. *Semin. Nucl. Med.* **34**, 87–111 (2004).

61) Couturier, O., Luxen, A., Chatal, J. F., Vuillez, J. P., Rigo, P. & Hustinx, R. Fluorinated tracers for imaging cancer with positron emission tomography. *Eur. J. Nucl. Med. Mol. Imaging* **31**, 1182–206 (2004); Wood, K. A., Hoskin, P. J. & Saunders, M. I. Positron emission tomography in oncology: a review. *Clin. Oncol. (R. Coll. Radiol).* **19**, 237–55 (2007).

62) Pagani, M., Stone-Elander, S. & Larsson, S. A. Alternative positron emission tomography with non-conventional positron emitters: effects of their physical properties on image quality and potential clinical applications. *Eur. J. Nucl. Med.* **24**, 1301–27 (1997).

63) Maschauer, S. & Prante, O. Sweetening pharmaceutical radiochemistry by ^{18}F fluoroglycosylation: A short review. *BioMed. Res. Int.* Article ID 214748 (2014).

64) Miller, P. W., Long, N. J., Vilar, R. & Gee, A. D. Synthesis of ^{11}C, ^{18}F, ^{15}O, and ^{13}N radiolabels for positron emission tomography. *Angew. Chem. Int. Ed.* **47**, 8998–9033 (2008).

65) Berger, A. How does it work? Positron emission tomography. *Brit. Med. J.* **326,** 1449 (2003).

66) Czernin, J. & Phelps, M. E. Positron emission tomography scanning: current and future applications. *Annu. Rev. Med.* **53**, 89–112 (2002).

67) Rozen, S. Elemental fluorine as a legitimate reagent for selective fluorination of organic compounds. *Acc. Chem. Res.* **21**, 307–312 (1988).

68) Ramsden, C. A. Xenon difluoride in the organic laboratory: a tale of substrates, solvents and vessels. *Arkivoc* **2014**, 109 (2013).

69) Furuya, T., Kamlet, A. S. & Ritter, T. Catalysis for fluorination and trifluoromethylation. *Nature* **473**, 470–7 (2011).

70) Lal, G. S., Pez, G. P. & Syvret, R. G. Electrophilic NF Fluorinating Agents. *Chem. Rev.* **96**, 1737–1756 (1996).

71) Singh, R. P. & Shreeve, J. M. Recent highlights in electrophilic fluorination with 1-chloromethyl-4-fluoro-1,4-diazoniabicyclo[2.2.2]octane bis(tetrafluoroborate). *Acc. Chem. Res.* **37**, 31–44 (2004).

72) Nyffeler, P. T., Durón, S. G., Burkart, M. D., Vincent, S. P. & Wong, C.-H. Selectfluor: mechanistic insight and applications. *Angew. Chem. Int. Ed.* **44**, 192–212 (2004).

73) Umemoto, T., Harasawa, K., Tomizawa, G., Kawada, K. & Tomita, K. N-F 19-fluorine nuclear magnetic resonance of N-fluoropyridinium salts. *J. Fluor. Chem.* **53**, 369–377 (1991).

74) Kiselyov, A. S. Chemistry of N-fluoropyridinium salts. *Chem. Soc. Rev.* **34**, 1031–7 (2005).

75) Stavber, S. Recent advances in the application of Selectfluor^{TM} F-TEDA-BF4 as a versatile mediator or catalyst in organic synthesis. *Molecules* **16**, 6432–64 (2011).

76) Champagne, P. A., Desroches, J., Hamel, J.-D., Vandamme, M. & Paquin, J.-F. Monofluorination of Organic Compounds: 10 Years of Innovation. *Chem. Rev.* **115**, 9073–174 (2015).

77) Umemoto, T. *et al.* Power- and structure-variable fluorinating agents. The N-fluoropyridinium salt system. *J. Am. Chem. Soc.* **112**, 8563–8575 (1990).

78) Waschke, D., Leshch, Y., Thimm, J., Himmelreich, U. & Thiem, J. Synthesis of fluorinated ketoheptoses as specific diagnostic agents. *Eur. J. Org. Chem.* **2012**, 948–959 (2012).

79) Nguyen, T.-H., Abarbri, M., Guilloteau, D., Mavel, S. & Emond, P. Nucleophilic fluorination of alkynyliodonium salts by alkali metal fluorides: access to fluorovinylic compounds. *Tetrahedron* **67**, 3434–3439 (2011).

80) Kim, D. W., Jeong, H. J., Lim, S. T., Sohn, M. H., Katzenellenbogen, J. A. & Chi, D. Y. Facile nucleophilic fluorination reactions using tert-alcohols as a reaction medium: significantly enhanced reactivity of alkali metal fluorides and improved selectivity. *J. Org. Chem.* **73**, 957–62 (2008).

81) Akiyama, Y., Hiramatsu, C., Fukuhara, T. & Hara, S. Selective introduction of a fluorine atom into carbohydrates and a nucleoside by ring-opening fluorination reaction of epoxides. *J. Fluor. Chem.* **127**, 920–923 (2006).

82) Soueidan, O.-M., Trayner, B. J., Grant, T. N., Henderson, J. R., Wuest, F., West, F. G. & Cheeseman, C. I. New fluorinated fructose analogs as selective probes of the hexose transporter protein GLUT5. *Org. Biomol. Chem.* **13**, 6511–21 (2015).

83) Tsuchiya, T., Takahashi, Y., Endo, M., Umezawa, S. & Umezawa, H. Synthesis of 2′,3′-dideoxy-2′-fluorokanamycin A. *J. Carbohydr. Chem.* **4**, 587–611 (2007).

84) Singh, R. P. & Shreeve, J. M. Recent advances in nucleophilic fluorination reactions of organic compounds using deoxofluor and DAST. *Synthesis (Stuttg).* **2002**, 2561–2578 (2002).

85) L'Heureux, A. Beaulieu, F., Bennettl, C., Bill, D. R., Clayton, S., LaFlamme, Mirmehrabi, M., Tadayon, S., Tovell, D. & Couturier, M. Aminodifluorosulfinium salts: selective fluorination reagents with enhanced thermal stability and ease of handling. *J. Org. Chem.* **75**, 3401–11 (2010).

86) Ni, C., Hu, M. & Hu, J. Good partnership between sulfur and fluorine: sulfur-based fluorination and fluoroalkylation reagents for organic synthesis. *Chem. Rev.* **115**, 765–825 (2015).

87) Furuya, T., Kuttruff, C. A. & Ritter, T. Carbon-fluorine bond formation. *Curr. Opin. Drug Discov. Devel.* **11**, 803–19 (2008).

88) Raju, R., Castillo, B. F., Richardson, S. K., Thakur, M., Severins, R., Kronenberg, M. & Howell, A. R. Synthesis and evaluation of 3''- and 4''-deoxy and -fluoro analogs of

the immunostimulatory glycolipid, KRN7000. *Bioorg. Med. Chem. Lett.* **19**, 4122–5 (2009).

89) Cole, E. L., Stewart, M. N., Littich, R., Hoareau, R. & Scott, P. J. H. Radiosyntheses using fluorine-18: the art and science of late stage fluorination. *Curr. Top. Med. Chem.* **14**, 875–900 (2014).

90) DeJesus, O. T., Martin, J. A., Yasillo, N. J., Gatley, S. J. & Cooper, M. D. [18F]Fluoride from a small cyclotron for the routine synthesis of [18F]2-Fluoro-2-deoxy-d-glucose. *Int. J. Rad. Appl. Instrum. A.* **37**, 397–401 (1986).

91) Bouvet, V. Jans, H. S., Wuest, M., Soueidan, O.-M., Mercer, J., McEwan, A. J. B., West, F. G., Cheeseman, C.I. & Wuest, F. Automated synthesis and dosimetry of 6-deoxy-6-[(18)F]fluoro-D-fructose (6-[(18)F]FDF): a radiotracer for imaging of GLUT5 in breast cancer. *Am. J. Nucl. Med. Mol. Imaging* **4**, 248–59 (2014).

92) Castellucci, P. Perrone, A. M., Picchio, M., Ghi, R., Farsad, M., Nanni, C., Messa, C., Meriggiola, M. C., Al-Nahhas, A., Rubello, D., Fazio, F. & Fanti, S. Diagnostic accuracy of 18F-FDG PET/CT in characterizing ovarian lesions and staging ovarian cancer: correlation with transvaginal ultrasonography, computed tomography, and histology. *Nucl. Med. Commun.* **28**, 589–95 (2007).

93) Diksic, M. & Jolly, D. New Synthesis of 2-Deoxy-2-fluoro-D-hexoses by Fluorination in Water. *J. Carbohydr. Chem.* **4**, 265–271 (2006).

94) Haradahira, T., Maeda, M. & Kojima, M. Alternative synthesis of no-carrier-added 2-deoxy-2-[18F]fluoro-D-glucose using [^{18}F] fluoride ion. *J. Label. Compd. Radiopharm.* **25**, 497–507 (1988).

95) Lee, C.-C. *et al.* Multistep synthesis of a radiolabeled imaging probe using integrated microfluidics. *Science* **310**, 1793–6 (2005).

96) Ferrini, K., Ghelfi, F., Mannucci, R. & Titta, L. Lifestyle, nutrition and breast cancer: facts and presumptions for consideration. *Ecancermedicalscience* **9**, 557 (2015).

97) Weigelt, B., Peterse, J. L. & van 't Veer, L. J. Breast cancer metastasis: markers and models. *Nat. Rev. Cancer* **5**, 591–602 (2005).

98) Haradahira, T. *et al.* Radiosynthesis, rodent biodistribution, and metabolism of 1-deoxy-1-[18F]fluoro-D-fructose. *Nucl. Med. Biol.* **22**, 719–725 (1995).

99) Ravshel, F. M. & Cleland, W. W. The substrate and anomeric specificity of fructokinase. *J. Biol. Chem.* **248**, 8174-8177 (1973); Hanson, R. L., Ho, R. S., Wiseberg, J. J., Simpson, R., Younathan, E. S. & Blair, J. B. Inhibition of glucongenesis and glycongenolysis by 2,5-anhydro-D-mannitol. *J. Biol. Chem.* **259**, 218-223 (1984).

Chapter 2

Synthesis of C-3 Modified 2,5-Anhydro-D-mannitol Derivatives *via* Diastereoselective Epoxide Ring-Opening of 2,5:3,4-Dianhydro-D-allitol

2.1. Introduction

2.1.1. Applications of 2,5-anhydro-D-mannitol derivatives in asymmetric catalysis

In the previous Chapter, 2,5-anhydro-D-mannitol (Figure 2.1.1, 2,5-AM **1**) derivatives were described as ligands for GLUT5, and potential substrates for the development of tracers used in the molecular imaging of GLUT5 expressing cancers (*e.g.* breast cancer and prostate cancer). Furthermore, 2,5-AM **1** derivatives are chiral ligands used in asymmetric homogeneous catalysis.[1-3] In homogeneous catalysis, ligand screening is the crucial step to achieve high reactivity and stereoselectivity. Sugar molecules exist in single enantiomeric form in nature and often serve as ligand in asymmetric catalysis.[1-4] Functionalization of secondary hydroxyl groups of 2,5-AM **1** with donor heteroatoms, such as phosphorus, sulfur or nitrogen would allow these ligands to bind with metal centers to develop asymmetric homogeneous catalysts (Figure 2.1.1, **i**).[1-3] Enantioselectivity of a reaction catalyzed by 2,5-AM **1** based ligands could be tuned by the derivatization of the primary hydroxyl functionalities with bulky protecting groups (Figure 2.1.1). 2,5-AM derivatives functionalized with phosphinite, phosphonite or phosphoramidite groups were well employed as chiral ligands in asymmetric catalysis.[1-3]

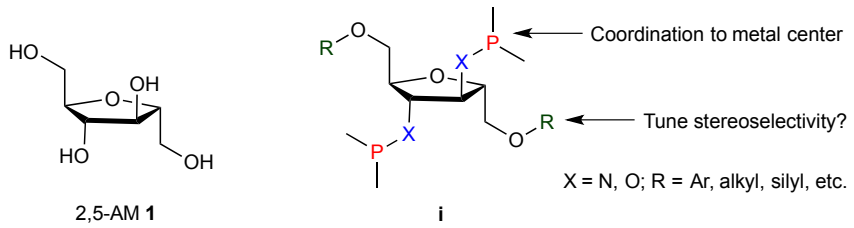

Figure 2.1.1. General representation of 2,5-AM based chiral ligand

In 2008, Claver and coworkers demonstrated the catalytic ability of 2,5-AM-based ligands through enantioselective synthesis of allylamine **4** (Scheme 2.1.1).[3] A palladium (II) catalyzed allylic substitution reaction was carried out in the presence of a 2,5-AM-based phosphite ligand **2** (Figure 2.1.2) to achieve a high enantio-induction. In this reaction, racemic 1,3-diphenyl-3-acetoxy-prop-1-ene **3** underwent substitution of the acetoxy group with primary amine in the presence of $[Pd(\mu\text{-}Cl)(\eta^3\text{-}C_3H_5)]_2$ and ligand **2** to yield enantioenriched allylamine **4** (98% ee) (Scheme 2.1.1).[3]

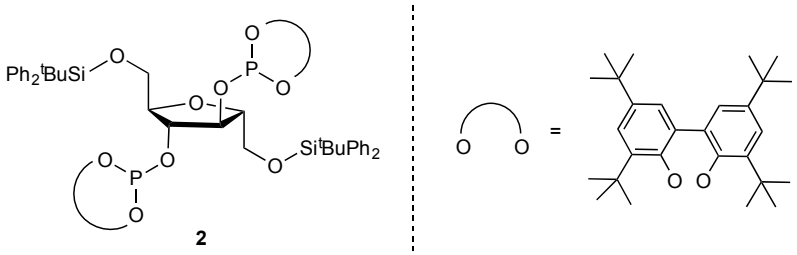

Figure 2.1.2. Structure of 2,5-AM based chiral phosphite ligand

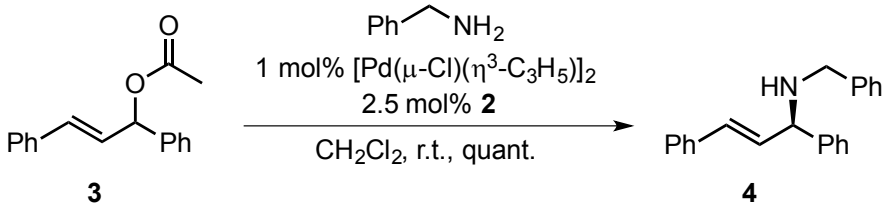

Scheme 2.1.1. Enantioselective synthesis of allylamine

2.1.2. Synthesis of epoxides

Epoxidation of olefins or ring-closure of β-functionalized alcohol such as β-hydroxy bromides are two common methods to access epoxides.[5-9] Under acidic conditions, vicinal diols also react to yield epoxides.[10] Typically, this process involves *in situ* conversion of one of the hydroxyl groups to a good leaving group followed by the nucleophilic attack of the remaining alcohol. Scheme 2.1.2 illustrates the conversion of a vicinal diol **5** to an epoxide **6** under acidic conditions.[10]

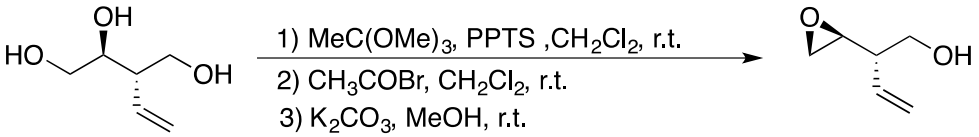

5 **6**

Scheme 2.1.2. Epoxide formation from 1,2-diols

2.1.3. Reactivity of epoxides

Small ring systems are strained molecules (**ii**, **iii** and **iv**) and have been often used as versatile synthetic intermediates in organic synthesis (Figure 2.1.3).[11] Typically, the reactivity of small rings increases as the ring size decreases.

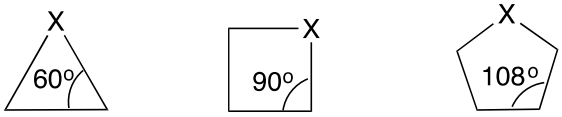

ii **iii** **iv**

X = O, S, CR_2, NR, SiR_2

Figure 2.1.3. General representation of bond angles in small sized rings

There are three key factors that contribute to the net strain of an epoxide ring system; i) angle strain, ii) torsional strain, and iii) steric strain (Figure 2.1.4).[12-16] Among these three types of strains, angle strain is the most important contributing factor towards the reactivity of three membered ring systems. According to Baeyer strain theory, the amount of strain present in a polygon is equal to the half of the difference between the tetrahedral value (bond angle in a perfect tetrahedron, 109° 28′) and the internal angle of the polygon. The Baeyer angle strain at any methylene group of an unsubstituted cyclopropane is 24°44' (comes from [109° 28' – 60°]/2), the highest value among all the simple cycloalkane systems.[17] Experimentally determined strain values for cyclopropane, aziridine and oxirane are 27.5, 26.7 and 26.3 kcal/mol, respectively.[12,13,15,16] Small decrease in ring strain values from cyclopropane to aziridine and aziridine to oxirane are plausibly due to the decrease in number of eclipsed interactions (reduction of torsional strain, Figure 2.1.4). In addition to angle strain and torsional strain, bulky substituents on epoxide ring carbons can cause steric strain.[14,15]

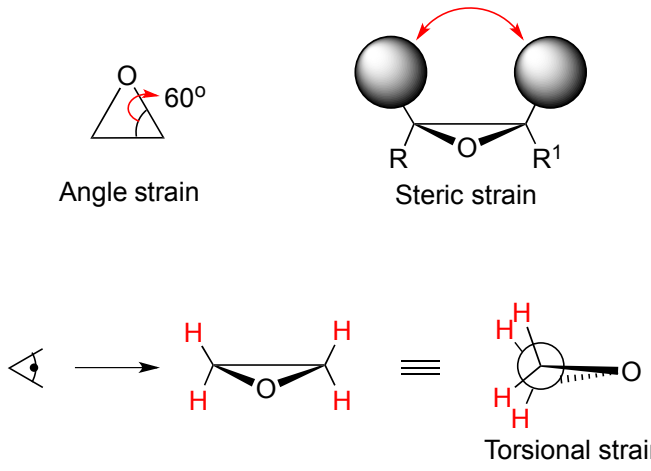

Figure 2.1.4. Components causing strain in three-membered rings

2.1.4. Solvent effects on nucleophilic epoxide ring-opening reaction

Nucleophilic epoxide ring-opening reaction could occur in S_N1 or S_N2 fashion, depending upon factors such as, substitution at the epoxide ring carbons, solvent, and reagents (Scheme 2.1.3).[18] Usually, polar protic solvents decrease the rate of S_N2 epoxide ring-opening processes by the formation of hydrogen bonds with the nucleophile, which reduce nucleophilicity of the nucleophile.[18-21] Nucleophilic ring-opening of an epoxide (**vi**) in S_N2 fashion incorporates the nucleophile on the sterically less hindered carbon (**vii**). On the other hand, the S_N1 mechanistic pathway installs the nucleophile on the carbon with greater substitution (**viii**).[18] Furthermore, the S_N2 process yields one stereoisomer, whereas S_N1 process could result in the formation of a stereoisomeric mixture.[19-21]

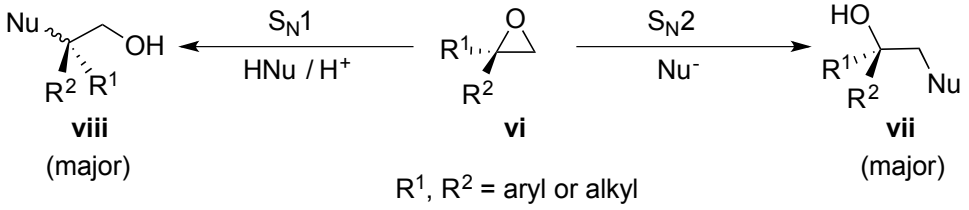

Scheme 2.1.3. Nucleophilic epoxide ring opening

According to the Hughes-Ingold rules, solvation of a molecule or transition state is a function of charge magnitude (Table 2.1.1), and the following rules were postulated;[22-26]

1) Increase in the magnitude of charge increases solvation,
2) Increase in charge dispersal decreases solvation,
3) Charge destruction results in a greater decrease in solvation.

Table 2.1.1. Effect of solvent polarity on various types of S_N1 processes

Type	Reactants	Activated complex	Charge alteration during TS	Effect of increased solvent polarity on rate
I	Nu + R-X	$Nu^{\delta+}$----R----$X^{\delta-}$	separation	Large increase
II	Nu + $R\text{-}X^{+}$	$Nu^{\delta+}$----R---- $X^{\delta+}$	dispersion	Small decrease
III	Nu^{-}+ R-X	$Nu^{\delta-}$----R---- $X^{\delta-}$	dispersion	Small decrease
IV	Nu^{-}+ $R\text{-}X^{+}$	$Nu^{\delta-}$----R---- $X^{\delta+}$	destruction	Large decrease

Nu = nucleophile, R = alkyl group and X = a group that undergoes displacement with Nu

Nucleophilic ring opening of an epoxide can be considered as either of Type-I or Type-III reactions, depending on the nature of the nucleophile (Table 2.1.1). Reaction of epoxide (**ix**) with a neutral nucleophile falls under Type-I category (Scheme 2.1.4), whereas reaction with an anionic nucleophile belongs to Type-III category (Scheme 2.1.5). As charge separation occurs during the reaction transition (**TS-I**), Type-I epoxide ring-opening reactions are vulnerable to solvent polarity effects (Scheme 2.1.4).

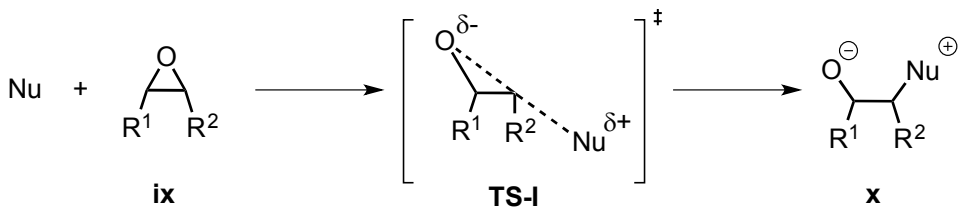

Scheme 2.1.4. Charge separation during the TS of epoxide ring-opening with neutral nucleophile

As charge dispersion takes place in the transition state of Type-III process (**TS-II**), the rate of the epoxide ring-opening process with a charged nucleophile is less sensitive to solvent polarity effects (Scheme 2.1.5). However, in some cases the Type-III nucleophilic ring-opening process is also vulnerable to solvent effects as the solvents are capable of changing the ground state energies of the reactants, through interactions such as, hydrogen bonding.

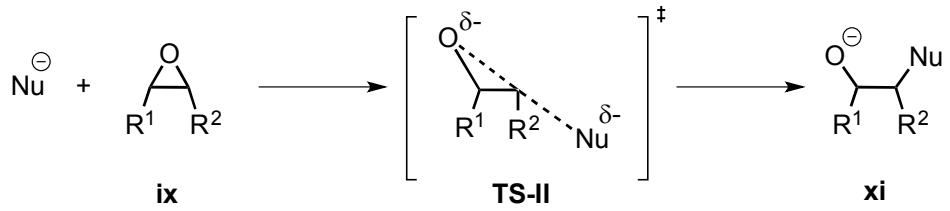

Scheme 2.1.5. Charge dispersion during the TS of epoxide ring-opening with neutral nucleophile

In 1979, Christian Reichardt performed a systematic study and ranked the solvent polarity based on an empirical solvent polarity measure called $E_T(30)$.[27] Relative solvent polarities of a few common organic solvents (based on $E_T(30)$ value) are furnished in Table 2.1.2. Among all the solvents, water, 2,2,2-trifluoroethanol, methanol, ethanol and acetic acid have higher dielectric constants, which indicates high polarity of these solvents.

Table 2.1.2. Relative solvent polarity chart

Solvent polarity rank	Solvent	$E_T(30)$
1	Water	63.1
2	2,2,2-Trifluoroethanol	59.5
3	Methanol	55.5
4	Ethanol	51.9
5	Acetic acid	51.2
6	Nitromethane	46.3
7	Acetonitrile	46.0
8	Dimethylsulfoxide	45.0
9	N,N-Dimethylformamide	43.8
10	*t*ert-Amyl alcohol	41

2.2. Strategy for the synthesis of C-3 modified 2,5-AM derivatives

Epoxides are synthetic intermediates that provide quick access to β-functionalized alcohols. C-3 modified 2,5-AM derivatives **xii** can be obtained by the ring opening of C_2-symmetric epoxide, 2,5-anhydro-D-allitol **7** (Scheme 2.2.1), which can be obtained from 2,5-AM **1**.

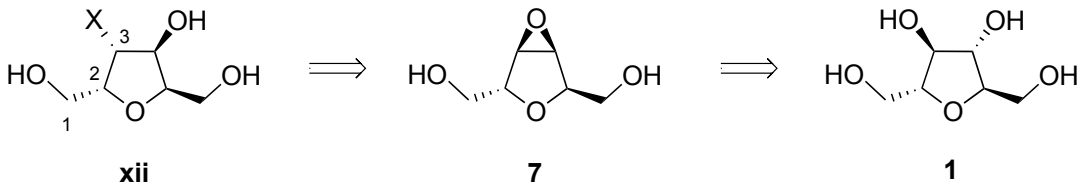

xii **7** **1**

Scheme 2.2.1. Synthetic strategy to access C-3 modified 2,5-AM derivatives

However, upon nucleophilic ring-opening of epoxide **7**, it produces a diastereomeric mixture (Scheme 2.2.2). Nucleophilic attack on the C-3 carbon of **7** yields a C-3 modified 2,5-AM derivative **xii**, whereas C-4 attack of the nucleophile produces an unwanted C-4 modified 2,5-anhydro-D-iditol derivative **xiii**. Our goal was to improve the diastereomeric ratio of this process by limiting the formation of **xiii**. Though epoxides are reactive due to the associated ring strain, the substitution pattern on the epoxide carbon participating in S_N2 displacement may reduce the reactivity of the epoxides. Nucleophilic ring opening of epoxide **7** might be difficult as the epoxide is associated with two electronically equivalent secondary carbons. Moreover the hydroxymethyl substituents on the C-2 and C-5 positions of the tetrahydrofuran ring of **7** are the only stereocontrol elements in this process. As a result, accomplishing high yield and simultaneously maintaining higher diastereoselectivity in this transformation could be challenging.

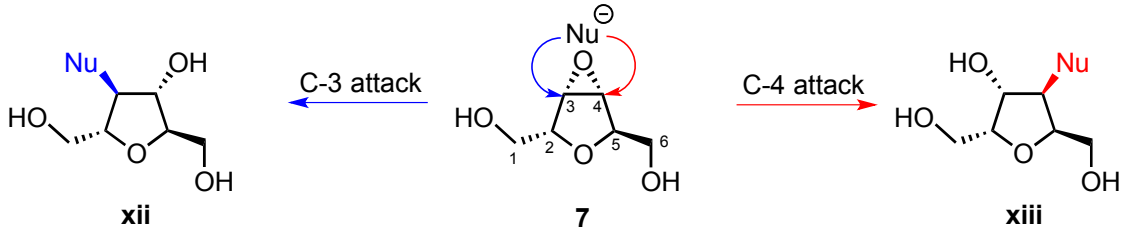

xii **7** **xiii**

Scheme 2.2.2. Possibility of two diastereomers from ring-opening of epoxide **7**

2.3. Synthesis of 2,5-anhydro-D-mannitol and 2,5:3,4-dianhydro-D-allitol

2,5-AM **1** was synthesized according to the literature procedure.[28] To an acidified solution of D-glucosamine hydrochloride **8** at 5 °C, sodium nitrite was added in portions. Diazotization of the amino group produced the unstable diazonium salt, which spontaneously underwent ring contraction reaction to form the tetrahydrofuran core with an exocyclic aldehyde substitution (Scheme 2.3.1, 2,5-anhydro-D-mannose **9**). The stereochemistry of the intermediate (Scheme 2.3.1, **Int-1**) at C-2 is critical for the

formation of aldehyde **9**. The anti-bonding molecular orbital $\sigma^*_{C\text{-}N}$ bond must be coplanar to the C-O bond to achieve ring contraction of the intermediate (Figure 2.3.1, **Int-1**). Upon treatment with $NaBH_4$, 2,5-anhydro-D-mannose **9** yielded impure 2,5-AM **1** (Scheme 2.3.2).

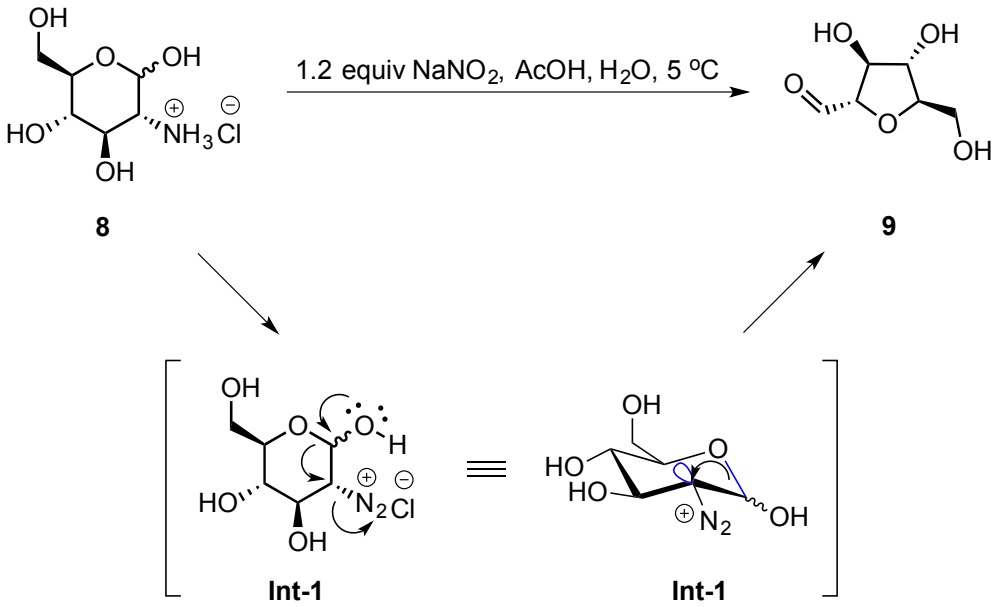

Scheme 2.3.1. Synthesis of impure 2,5-AM

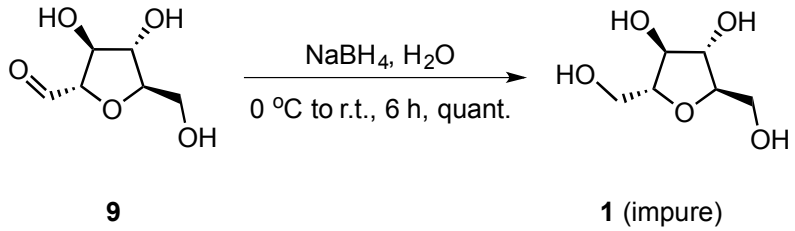

Scheme 2.3.2. Preparation of impure 2,5-AM **1** by the reduction of **9**

In order to obtain analytically pure 2,5-AM **1**, it was first converted to peracetylated compound, 1,3,4,6-tetra-*O*-acetyl-2,5-anhydro-D-mannitol **10**. Treatment of impure 2,5-

AM **1** with acetic anhydride in pyridine (Scheme 2.3.3) yielded peracetylated compound **10**. All the inorganic salts were separated from **10** by liquid-liquid extraction technique. The crude mixture of compound **10** was purified by column chromatography to yield pure form of **10** (81-90%). Compound **10** was treated with MeONa in MeOH to remove the acetyl groups, which yielded pure 2,5-AM **1** as crystals in quantitative yield (Scheme 2.3.3).

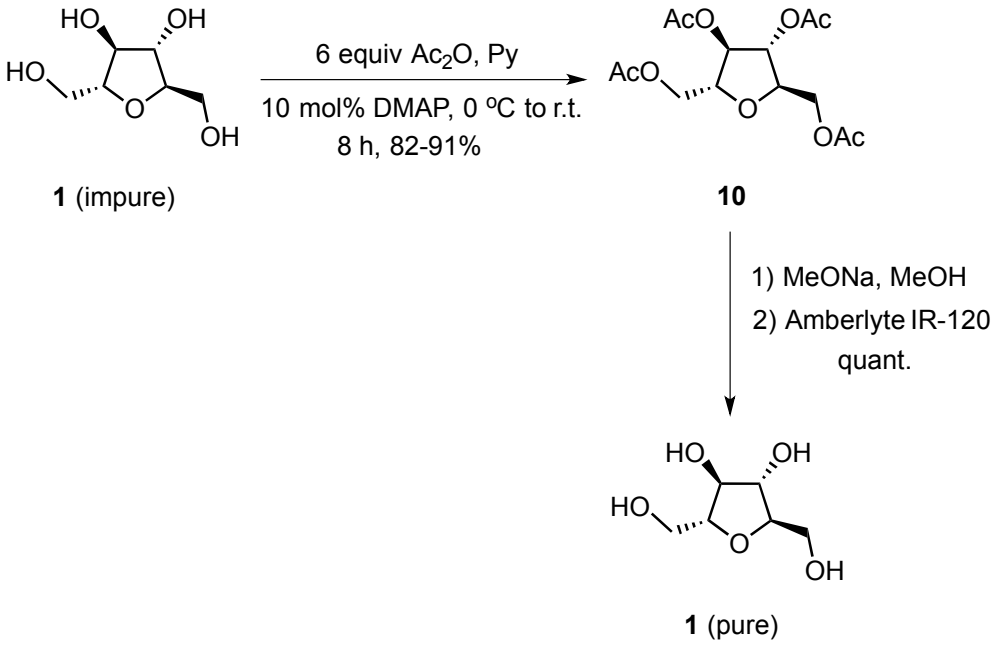

Scheme 2.3.3. Purification of 2,5-AM **1**

The epoxide 2,5:3,4-dianhydro-D-allitol **7** was synthesized from 2,5-AM **1**, which contains two hydroxyl groups that are *anti* to each other at C-3 and C-4. However, our efforts to convert **1** into epoxide **7** were unsuccessful under acidic conditions. Mitsunobu reaction is an alternative to acidic conditions to convert the vicinal diol functionalities into epoxides.[29] Treatment of 2,5-AM **1** under Mitsunobu reaction conditions yielded 2,5:3,4-dianhydro-D-allitol **7** (Scheme 2.3.3).[30]

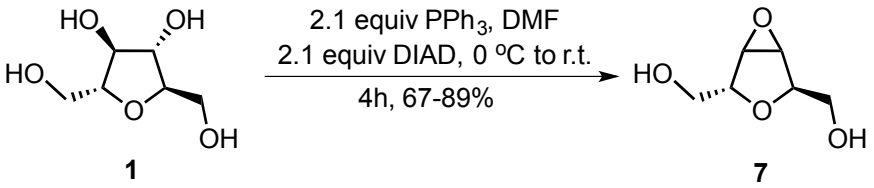

Scheme 2.3.4. Synthesis of 2,5:3,4-dianhydro-D-allitol **7** from 2,5-AM **1**

The primary alcohols of 2,5-AM **1** are sterically less hindered than secondary alcohols and should exhibit high reactivity with the active catalyst (betaine intermediate) present in the Mitsunobu reaction mixture. Nonetheless, the secondary alcohols of 2,5-AM **1** underwent Mitsunobu reaction in the presence of primary hydroxyls to provide epoxide **7**. Despite the high yields observed in this transformation, the reaction demands the usage of two equivalents of the reagents (PPh_3 and DIAD) to convert **1** into epoxide **7**. Treatment of 2,5-AM **1** with one equivalent of the reagents reagent did not yield epoxide **7**. Plausibly, one of the primary alcohols first reacts with one equivalent of Ph_3P-DIAD complex (Scheme 2.3.4, Panel A). However, no nucleophilic alcohol exists in close proximity to the leaving group in **Int-I**. As a result, one of the secondary alcohols of **Int-I** reacts with the second equivalent of Ph_3P-DIAD complex to yield intermediate **Int-II**. Unlike the activated primary alcohol of **Int-I**, the activated secondary alcohol present in **Int-II** has an *anti* vicinal hydroxyl group, which undergoes ring closing reaction to yield **Int-III**. During the work-up process, oxyphosphonium salt (**Int-III**) undergoes hydrolysis to form epoxide **7**.

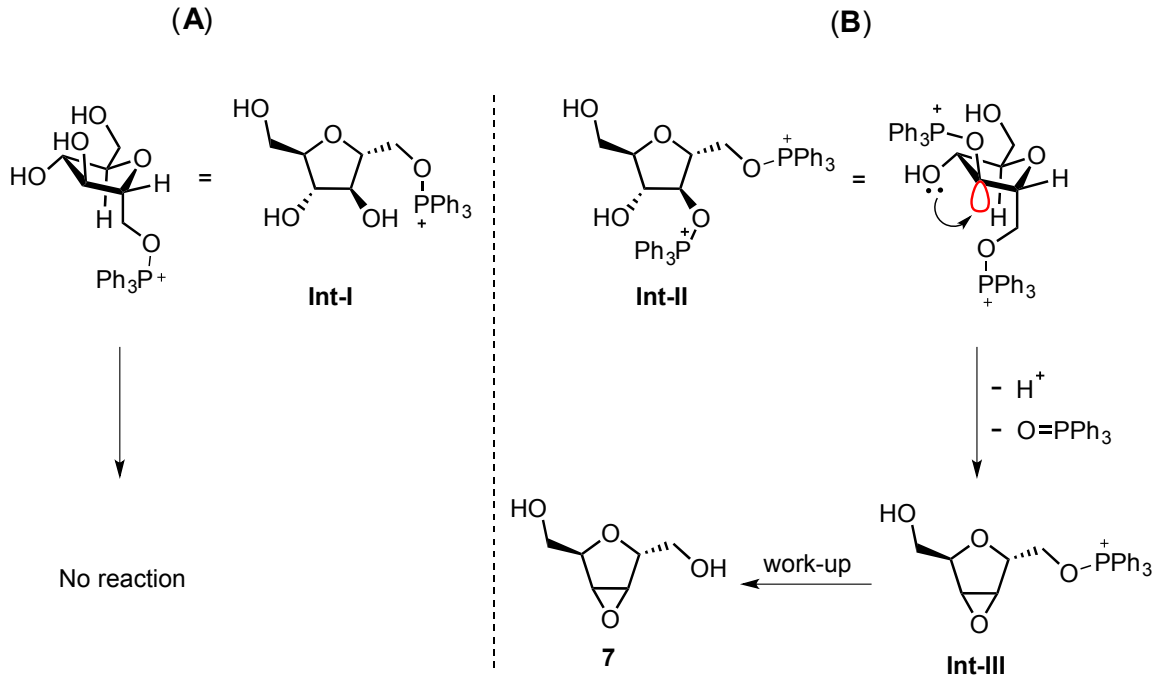

Scheme 2.3.4. Reaction mechanism of epoxide **7** formation

2.4. Diastereoselective epoxide ring-opening of 2,5:3,4-dianhydro-D-allitol

2.4.1. Epoxide ring-opening of 2,5:3,4-dianhydro-D-allitol 7 with fluoride ion

Epoxide **7** underwent ring-opening by reacting with KHF_2 in ethylene glycol to yield a diastereomeric mixture of 3-fluoro-3-deoxy-2,5-anhydro-D-mannitol **11a** (3-FDAM) and its diastereomer **11b** in 62% yield (Scheme 2.4.1, **11a**:**11b** = 5:1). Unfortunately, the diastereomeric mixture is inseparable. In order to accurately evaluate 3-FDAM **11a** as a ligand for GLUT5, greater than 95% purity of the compound **11a** was required.

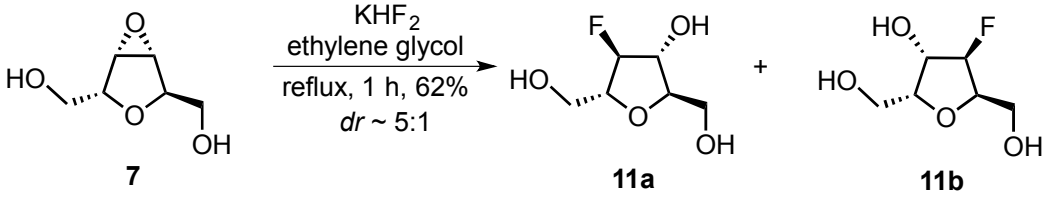

Scheme 2.4.1. Epoxide ring-opening of **7** with fluoride ion

2.4.2. Optimization of diastereoselective epoxide ring-opening of 7

We envisioned the improvement of diastereomeric ratio by the protection of primary hydroxyl groups of epoxide **7** with bulky protecting groups. We expected the bulky protecting groups to increase the diastereomeric ratio by sterically hindering of the C-4 for nucleophilic attack, which could block the nucleophile to attack the sterically more hindered C-4 carbon (Figure 2.4.1). The pivaloyl group is used extensively in carbohydrate chemistry and we expected the ^{t}butyl group of the pivaloyl ester to block the nucleophilic attack at C-4 carbon. Synthesis of 1,5-di-*O*-pivaloyl-2,5:3,4-anhydro-D-mannitol **12** was carried out in pyridine by treating epoxide **7** with pivaloyl chloride (Scheme 2.4.2). Triethylamine was added to neutralize the acidic pyridinium hydrochloride formed in this reaction, which could facilitate the epoxide ring-opening.

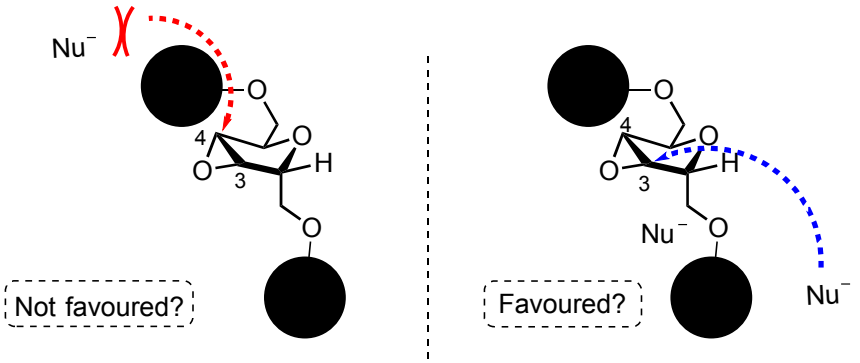

Figure 2.4.1. Envision of bulky protecting groups blocking the nucleophilic attack at C-4 of epoxide **7**

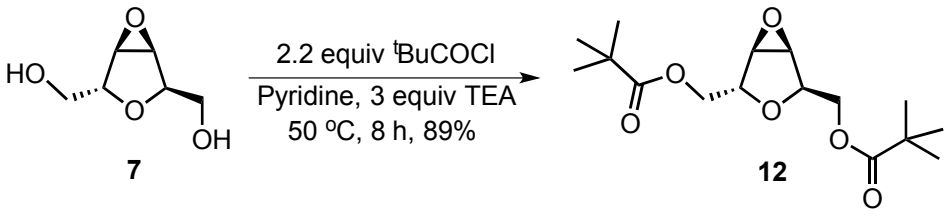

7 **12**

Scheme 2.4.2. Synthesis of epoxide **12**

During attempted fluorination under refluxing conditions in ethylene glycol, epoxide **12** underwent pivaloyl migration from primary carbon to secondary carbon. Pivaloyl migration was also observed in Lewis acidic and thermal conditions (Scheme 3). Migration of esters group under Brønsted acidic conditions is a known process.[31] The proposed mechanism for the acid catalyzed migration involves coordination of the Lewis acid to the epoxide ring oxygen to activate the epoxide ring (Scheme 2.4.3, **Int-I**). Then, the nucleophilic attack of the carbonyl oxygen atom on the activated epoxide carbon results in a bicyclic intermediate (Scheme 2.4.3, **Int-II**). During the work-up process, the bicyclic intermediate reacts with water to give migration product **13**. However, this mechanism does not represent migration of the pivaloyl group under heating conditions with fluoride ion. Ester migrations under basic conditions are well studied and the basic nature of the fluoride ion could be the reason for ester migration under such conditions.[32]

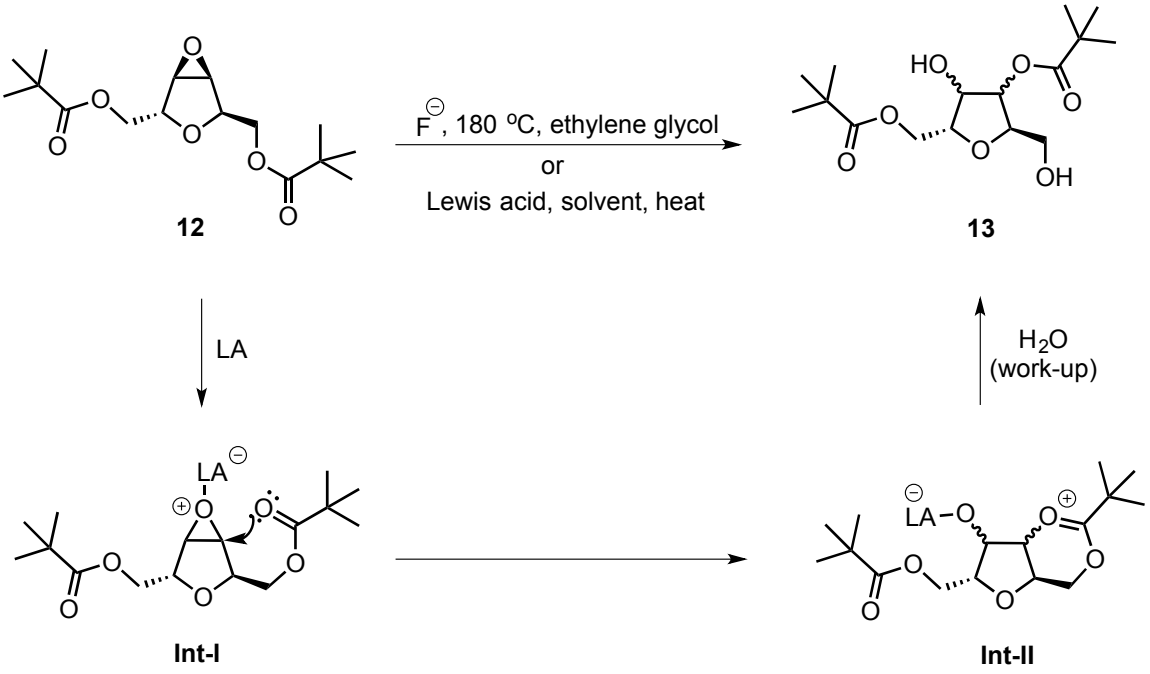

Scheme 2.4.3. Migration mechanism of pivaloyl group under Lewis acidic conditions

Furthermore, the ester migration was confirmed by ^{1}H NMR and mass spectrometric analysis. As shown in Figure 2.4.2, the downfield shift of the C**H**-COO^{t}Bu resonance suggested the migration of ester from primary carbon to secondary carbon. Further, mass spectrometric analysis (molecular weight of **13** = molecular weight of **12** + molecular weight of H_2O) suggested the formation of compound **13**.

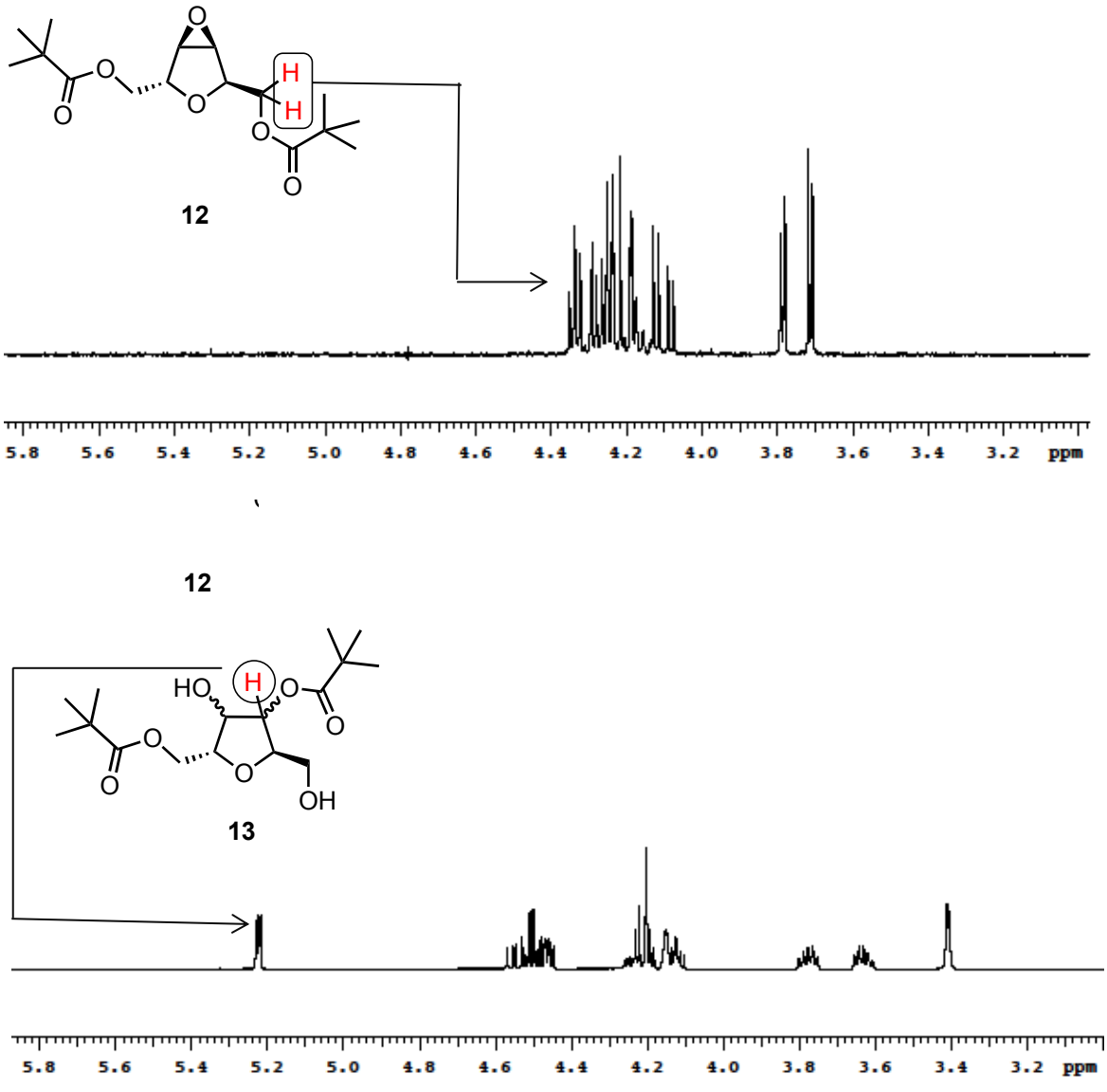

Figure 2.4.2. ^{1}H NMR spectral comparison between **12** and **13**

Due to the observed incompatibility of pivaloyl group under fluorination conditions, protected-epoxides **14** and **15** (Schemes 2.4.4) were synthesized, in order to evaluate the directing ability of different protecting groups. The primary hydroxyl groups on C-1 and C-6 of epoxide **7** were protected with benzyl and trityl groups in the epoxides **14** and **15**, respectively. Steric bulk of the protecting group on C-1 and C-6 of the epoxide was expected to increase in the following order; epoxide **7** (Pg = H) < epoxide **14** (Pg = Bn) < epoxide **12** (Pg = Piv) < epoxide **15** (Pg = Tr). Since fluorination of epoxides usually requires harsh reaction conditions, we decided to investigate the more reactive azide as a standard nucleophile. Moreover, it can undergo further chemical transformations to provide access to nitrogen containing functionalities such as, amines and amides. Epoxide **7** was treated with NaH in DMF followed by benzyl bromide to yield epoxide 1,6-di-*O*-benzyl-2,5:3,4-anhydro-D-allitol **14** in quantitative yield (Scheme 2.4.4). 1,6-di-*O*-trityl-2,5:3,4-anhydro-D-allitol **15** was synthesized by heating epoxide **7** with trityl chloride in pyridine. 4-(*N,N*-dimethyl)amino pyridine (DMAP) was employed as a catalyst (Scheme 2.4.4).

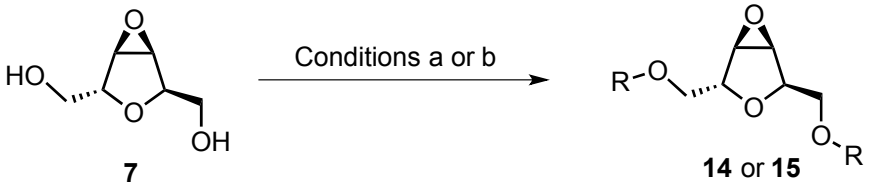

7 **14** or **15**

Conditions (a): 2.2 equiv BnBr, NaH, DMF, r.t., 8h, quant, R = Bn (**14**)

Conditions (b): 2.2 equiv TrCl, 50 mol% DMAP pyridine 50 ºC, 8 h, 69%, R = Tr (**15**)

Scheme 2.4.4. Synthesis of epoxides **14** and **15**

After accessing epoxides **7**, **12**, **14** and **15**, we proceeded to investigate the ability of the protecting groups at C-1 and C-6 to block the azide nucleophilic attack at C-4 carbon during the epoxide ring-opening process. NH_4Cl or $CeCl_3$ catalyzed epoxide ring-opening

with sodium azide is a known protocol to synthesize β-azido-alcohol, under mild conditions.[33] Upon ring-opening of epoxide **7** with sodium azide in EtOH, we obtained a mixture of 3-azido-3-deoxy-2,5-anhydro-D-mannitol **16a** and 3-azido-3-deoxy-2,5-anhydro-D-iditol **16b** in 83% yield with a diastereomeric ratio of 80:20 in favor of **16a** (Table 2.4.1, entry 1). The diastereomeric ratio obtained during the ring-opening of **7** (**16a**: **16b** = 80:20) was used as a benchmark to study the directing ability of various protecting groups.

Nucleophilic ring-opening of epoxide **14** was carried out with sodium azide to yield a mixture of diastereomers 1,6-di-*O*-benzyl-3-deoxy-3-azido-2,5-anhydro-D-mannitol **17a** and 1,6-di-*O*-benzyl-3-deoxy-3-azido-2,5-anhydro-D-iditol **17b** in 70:30 ratio, respectively (Table 2.4.1, entry 2). As we observed a poor diastereomeric ratio during the epoxide ring-opening of benzyl protected epoxide **14**, we extended our study to the epoxide **12**, in which two primary hydroxyl groups of **7** were protected with bulkier pivaloyl protecting groups. Subjection of epoxide **12** to sodium azide in EtOH resulted in the corresponding β-azido-alcohol in high yield (Table 2.4.1, entry 3) as a mixture of 1,6-di-*O*-pivaloyl-3-deoxy-3-azido-2,5-anhydro-D-manitol **18a** and 1,6-di-*O*-pivaloyl-3-deoxy-3-azido-2,5-anhydro-D-iditol **18b** in 80:20 diastereomeric ratio, which suggested the inability of the pivaloyl group to direct the nucleophile.

Table 2.4.1. Study of the epoxide ring-opening of **7**, **12**, **14** and **15** with azide

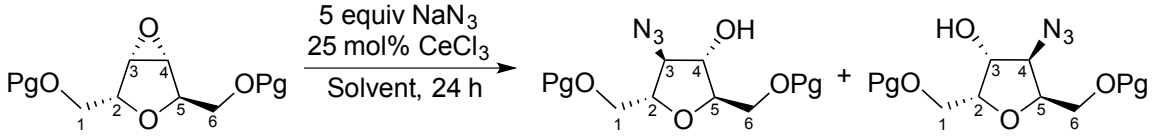

Pg = H (**7**)
Pg = Piv (**12**)
Pg = Bn (**14**)
Pg = Tr (**15**)

Pg = H (**16a**)
Pg = Bn (**17a**)
Pg = Piv (**18a**)

Pg = H (**16b**)
Pg = Bn (**17b**)
Pg = Piv (**18b**)

Entry	Solvent	Pg	T (^oC)	Product	dr (a:b)	Yield (%)[a]
1	EtOH	H (**7**)	75	**16**	~80:20	83[b]
2	EtOH	Bn (**14**)	78	**17**	70:30	54[c]
3	EtOH	Piv (**12**)	78	**18**	~83:17	72[c]
4	EtOH	Tr (**15**)	90	-	No reaction[d]	
5	DMF	Piv (**12**)	85	**18**	~83:17	81[c, e]
6	DMF	Bn (**14**)	85	**17**	70:30	60[c, e]
7	DMF	H (**7**)	85	**16**	95:5	88[b, e]
8	DMSO	H (**7**)	85	**16**	95:5	86[c, e]

[a]Combined yield of two diastereomers. [b]*dr* was determined by ^{1}H NMR analysis *via* integration of methine protons C**H**-OH. [c]Ratio was determined by ^{1}H NMR analysis *via* integration of methine protons C**H**-N_3. [d]Only starting material was observed by ^{1}H NMR. [e]Amberlyst 15 (dry form) (1.1 e□uiv) was used as catalyst instead of $CeCl_3$.

We next turned our attention to the bulkier trityl group, which is not only larger than the pivaloyl group, but also remains in close proximity with the sugar core. Thus we expected the trityl group to block the nucleophilic attack at C-4 more efficiently. Our efforts to open trityl epoxide **15** with azide were unsuccessful, as the expoxide **15** was unreactive below 90 ^{o}C (Table 2.4.1, entry 4). Heating **15** in the presence of variety of Lewis acids led to decomposition. However, a literature report demonstrated the epoxide-ring opening of **15** with lithium amide under basic conditions at 120 ^{o}C, leading to the formation of a diastereomeric mixture (observed *dr* = 80:20).[34]

Given the moderate selectivity seen with bulky protecting groups, we shifted our focus towards the study of solvent effects on the epoxide ring-opening process. In most cases, the solvent is the most abundant chemical present in the reaction mixture. Thus, solvent can influence a chemical process in numerous ways, such as tuning the nucleophilicity of the nucleophile, stabilization of reactive intermediates, and changing the rate of the reaction through stabilization of transition state or ground state. Since the epoxide **7** exhibited poor solubility in many aprotic solvents like DCM, ether, THF and dioxane, we decided to examine the effect of polar aprotic solvent DMF. We screened various Lewis acids to find an optimal catalyst for efficient ring-opening of the epoxides in DMF. However, we did not observe efficient catalysis by many Lewis acids such as $BF_3.Et_2O$, $AlCl_3$, $CeCl_3$ and $Sc(OTf)_3$. Competing coordination of Lewis acids with DMF could be a reason for the inability of Lewis acids to catalyze the reaction. Finally, a convenient and environmentally benign polystyrene resin-bound sulfonic acid Amberlyst 15 was used in dry form to promote the ring-opening in DMF. However, changing to a polar aprotic solvent had no impact on the diastereomeric ratio observed during epoxide ring-opening of **12** and **14**.

Surprisingly, during the epoxide ring-opening of **7** with azide nucleophile in DMF, we observed a dramatic increase in diastereomeric ratio (Table 2.4.1, entry 7). The same diastereomeric ratio was observed during the epoxide-ring opening of **7** in DMSO (Table 2.4.1, entry 8), which suggested that polar aprotic solvents yield optimal diastereomeric ratios. Furthermore, we observed a faster rate of conversion of epoxide **7** with azide in DMF in comparison to the reaction in EtOH (90% conversion of epoxide **7** in EtOH at 80

°C after 24 h and 100% conversion was observed in DMF after 17 h at the same temperature). The slower rate of epoxide ring-opening of **7** in polar protic solvent compared to the polar aprotic solvent could be due to a relatively low energy ground state of reactants in protic solvents. As shown in Figure 2.4.3, the nucleophile is more stabilized in the polar protic solvents through hydrogen bonding, whereas the reactivity of the nucleophile was enhanced in polar aprotic solvents by solvation of the counter cation. In addition, the higher degree of hydrogen bond formation of epoxide **7** in polar protic solvents also lowers the ground state of epoxide **7**. These two factors contribute towards relatively low energy ground state of the reactants in polar protic solvents.

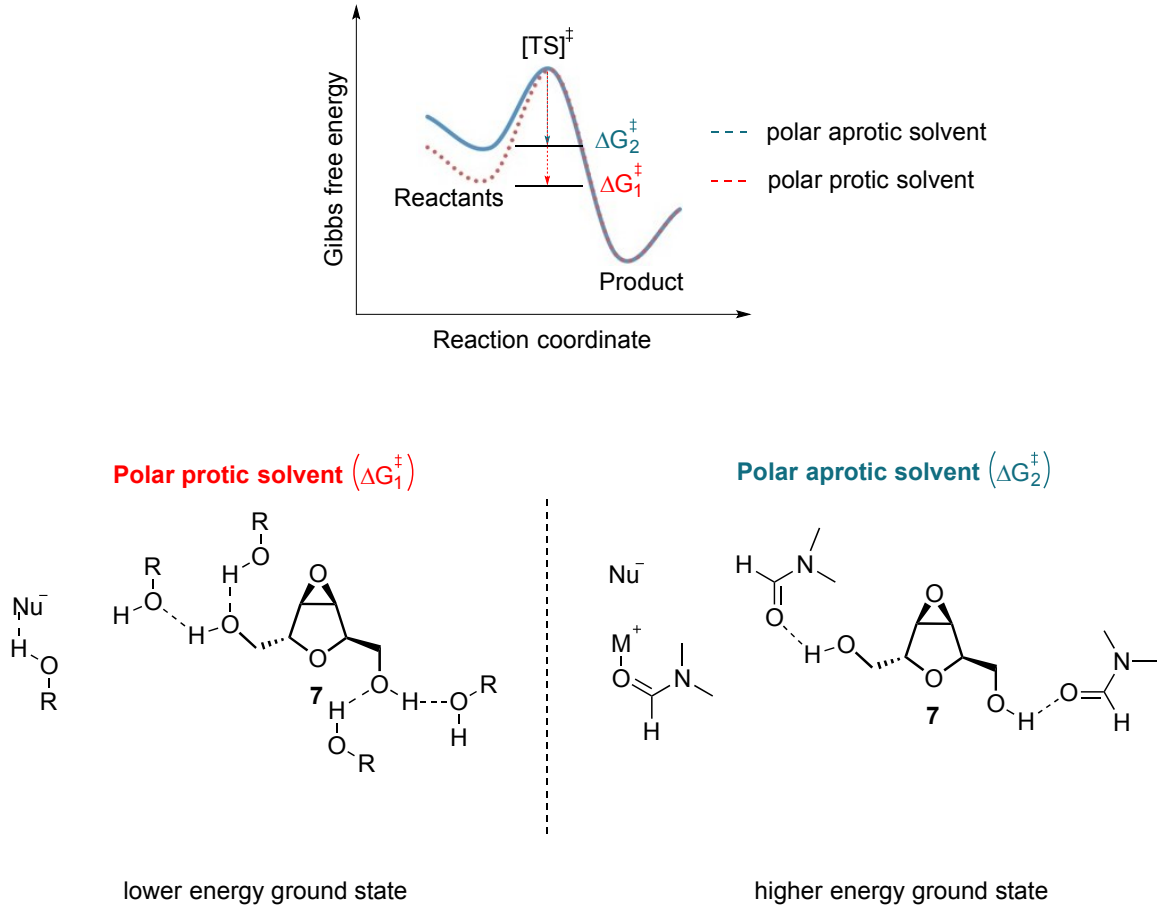

Figure 2.4.3. Hydrogen bonding effect of the solvent on the ground state of the reactants

With the optimized conditions for the epoxide ring-opening of **7** with azide in hand, we proceeded to synthesize our target fluoro-sugar (3-FDAM, **11**). However, synthesis of the fluoro-sugar **11** *via* epoxide ring-opening of **7** also required further optimization and screening of fluoride ion sources. Usage of various fluoride ion sources such as, NaF, KF or CsF, in the ring-opening process of epoxide **7** did not yield **11**. The usage of the [18]-crown-6 as a cation-chelating ligand to enhance the nucleophilicity of fluoride ion sources did not cause the epoxide ring-opening of **7**. Ultimately, he ring-opening of epoxide **7** was accomplished by treatment with KHF_2 in DMF at reflux, to yield 67% of 3-fluoro-3-deoxy-2,5-AM **11** with excellent diastereoselectivity (**11a:11b** = 96:4, Scheme 2.4.5). With **11a** of purity greater than 95% in hand, the *in vitro* studies can be performed. However, this protocol is not suitable for the radiosynthesis of [^{18}F]-3-FDAM **11a** due to the long reaction time.

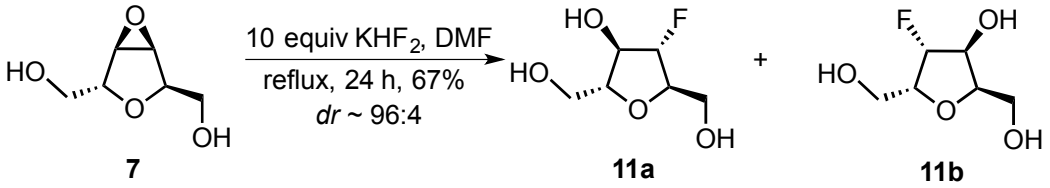

Scheme 2.4.5. Epoxide ring-opening of **7** with fluoride ion

Table 2.4.2. Summary of diastereoselective nucleophilic epoxide ring-opening of **7**

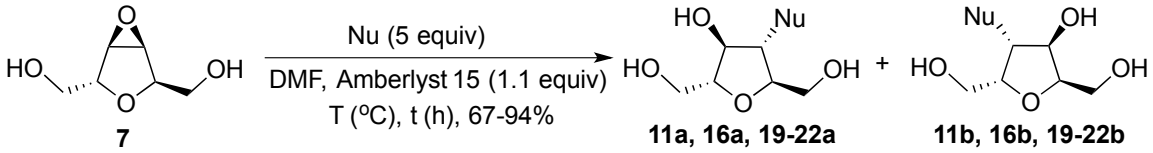

Entry	Nu	T (°C)	t (h)	Product	*dr* (a:b)	Yield (%)[a]
1	NaSMe	75	15	**19**	90:10	74 [b]
2	NaCl	-40 to rt	8	**20**	≥97:3	84[c]
3	NaBr	-40 to rt	8	**21**	≥97:3	91[c]
4	NaI	-40 to rt	8	**22**	≥97:3	94[c]
5	KHF_2	153	24	**11**	96:4	67[d,e,f]
6	NaN_3	85	15	**16**	95:5	88 [b]

[a]Isolated yield after purification by column chromatography. [b]dr was determined by ^{1}H NMR analysis *via* integration of SCH_3 protons. [c]*dr* was determined by ^{1}H NMR analysis *via* integration methine protons C**H**-OH. [d]10 equiv of KHF_2 was added. [e]*dr* was determined by ^{19}F NMR analysis. [f]Amberlyst 15 was not added to the reaction mixture

In order to explore further the scope of this protocol, we investigated the ring-opening of epoxide **7** with a sulfur-based nucleophile. At 75 °C, epoxide **7** reacted with sodium thiomethoxide resulting β-hydroxy-thioether **19** in good yield (86%) and good diastereoselectivity (**19a**:**19b** = 90:10, Table 2.4.2, entry 1). We then examined the compatibility of this protocol with halide ions (Table 2.4.2, entries 2, 3 and 4). Ring-opening of epoxide **7** was successfully accomplished using chloride, bromide and iodide ions at lower temperatures, resulting in the corresponding halo alcohols 3-chloro-3-deoxy-2,5-anhydro-D-mannitol **20**, 3-bromo-3-deoxy-2,5-anhydro-D-mannitol **21** and 3-iodo-3-deoxy-2,5-anhydro-D-mannitol **22** in high yields and excellent diastereoselectivity (**20a-22a**:**20b-22b** ≥ 97:3).

2.4.3. Rationale for the high diastereoselectivity in aprotic solvents

The observed diastereoselectivity in the epoxide ring-opening of compounds **7**, **12** and **14** was affected by three factors; i) substitution on the C-1 and C-6 hydroxyl groups, ii) the nature of the nucleophile and iii) nature of the solvent. Only epoxide **7**, which contains free hydroxyl groups at C-1 and C-6 yielded high diastereomeric ratios in polar aprotic solvents. In polar protic solvents, epoxide ring-opening of **7** yielded low diastereomeric ratios. Irrespective of the solvent nature, epoxides **12** and **14**, which have protecting groups at C-1 and C-6, resulted in low diastereomeric ratios. Thus, a fine combination of solvent and substrate was essential to obtain the desired diastereomeric ratio. As shown in Figure 2.4.4 (Panel M), Path-I involves attack of the nucleophile on C-3, whereas Path-II represents attack of nucleophile on C-4. Nucleophilic attack at C-4 is less favored in general, due to steric clash between incoming nucleophile and substituents on C-6. As a result, nucleophilic attack on C-3 carbon (Figure 2.4.4, Path-I) is always favored over the nucleophilic attack on C-4 carbon (Figure 2.4.4, Path-II). Both protic and aprotic solvents form hydrogen bonding with **7** (Figure 2.4.4, Panel N). However, the degree of hydrogen bond formation of protic solvents with epoxide **7** is greater in comparison to aprotic solvents, as polar protic solvents contain both hydrogen bond donor and acceptor groups. On the other hand, polar aprotic solvents are only hydrogen bonded with the primary hydroxyl groups of **7**. Therefore, the steric repulsion is higher between substituent on C-6 and nucleophile in polar protic solvents compared to polar aprotic solvents (Figure 2.4.4, Panel N), which should result in higher diastereomeric ratio in the polar protic solvents. But, experimentally, higher amount of the major diastereomer formation (from Path-I) was observed in polar aprotic solvents. This could be due to the possibility of several

competing paths in polar protic solvents, which reduce the diastereoselectivity (Figure 2.4.4, **TS-I** and **TS-II**). Polar aprotic solvents cannot initiate competing paths **TS-I** and **TS-II** (Figure 2.4.4). Thus, polar aprotic solvents only

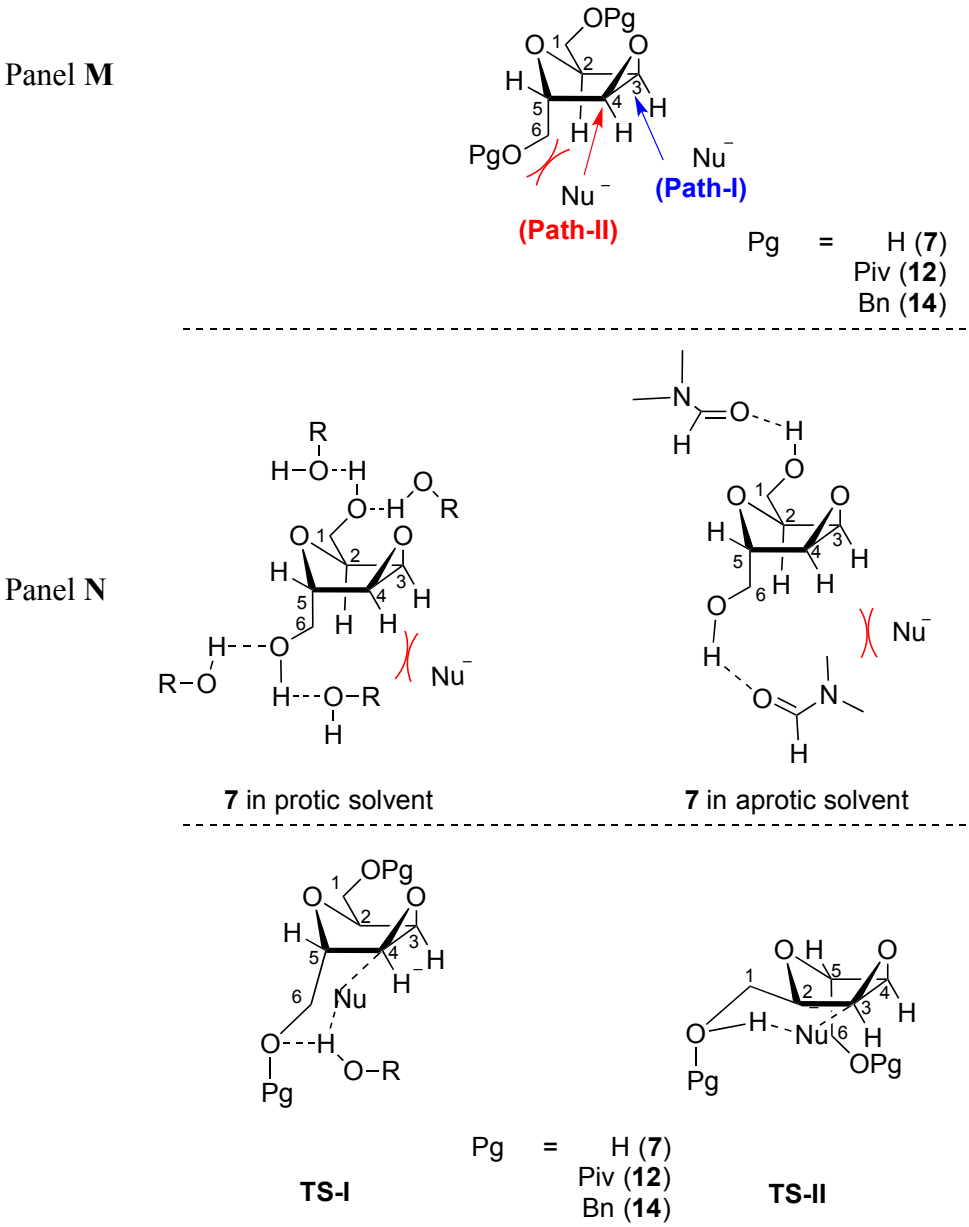

Figure 2.4.4. Proposed solvent hydrogen bonding effect on epoxide ring-opening

enhance the steric repulsions between the substituents on C-6 carbon and the incoming nucleophile through hydrogen bond formation with the hydroxyl groups of **7** (Figure 2.4.7, Panel N), which possibly enhances the formation of major diastereomers **11a**, **16a** and **19a-22a**. This hypothesis is in agreement with the observed low diastereomeric ratio when C-1 and C-6 hydroxyl groups are protected. As protected epoxides **12** and **14** are incapable of forming hydrogen bonding with polar aprotic solvents, they yielded poor diastereoselectivity.

2.4.4. Stereochemistry determination of epoxide ring-opening products

In the ^{1}H NMR spectra of major products **11a**, **16a** and **19a-22a**, the hydroxyl-substituted methine proton was observed as an apparent triplet with coupling constant values of ~7.2 Hz (in case of **22a** ~8 Hz). Based on *J* values, we concluded that all major products obtained in this protocol have the same relative stereochemistry on the furanose ring, but it cannot be unequivocally determined based on *J* values. It is worth mentioning that the relative stereochemistry of these products also cannot be determined by 2D-TROESY as the chemical shifts of key protons were overlapping. Thus, we focused on crystalizing the epoxide ring-opening products **11a**, **16a** and **19a-22a**. Unfortunately, none of these products was crystalline and our efforts to crystalize these derivatives was unsuccessful, which led us to focus on the synthesis and crystallization of derivatives of the epoxide ring opening products.

Azido-sugar **16a** was converted into the corresponding amide **24** through a one-pot procedure. The azide functionality of compound **16a** was reduced to the

corresponding amine **23** by Pd/C catalyzed hydrogenolysis in MeOH, which upon treatment with *N*-acetoxy succinimide produced the amide **24** in 53% overall yield (Scheme 2.4.6). After screening several solvent systems, we successfully crystalized the amide **24** in a binary solvent system of MeOH-dioxane.

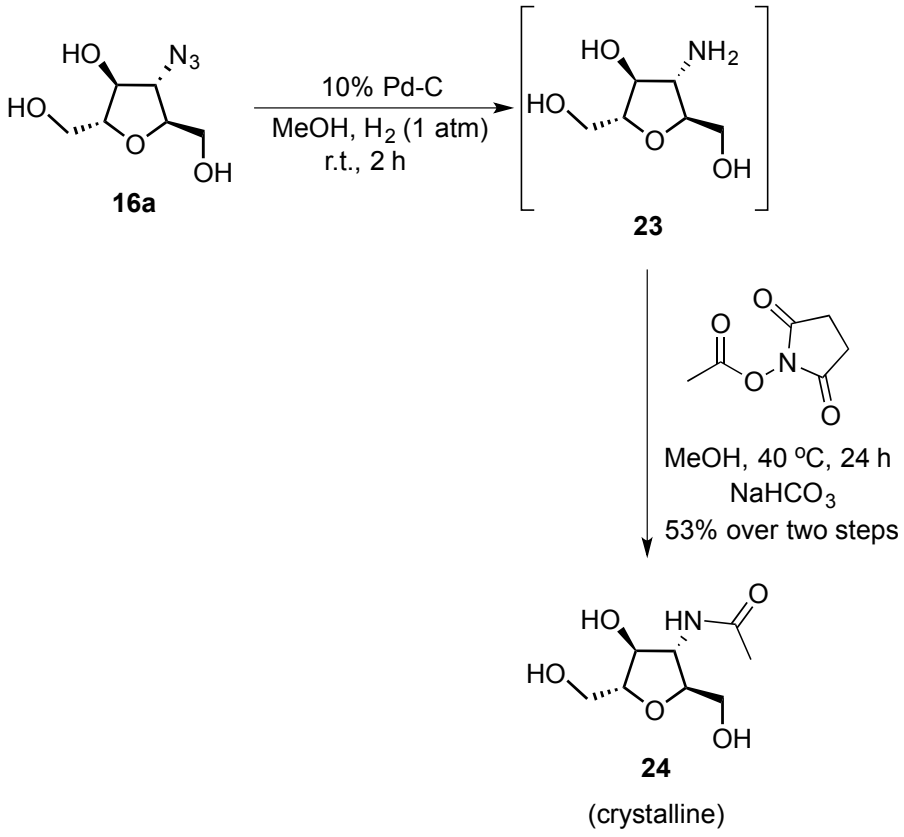

Scheme 2.4.6. One-pot synthesis of amide **24**

X-ray crystallography confirmed that the relative stereochemistry of **24** is identical to the all-*trans* 2,5-AM **1** stereochemistry (Figure 2.4.5). Amide **24** was synthesized from azide **16a** in two steps, which involved functional group transformations with no change in the stereochemistry of the furanose ring. Hence, the relative *trans*-stereochemistry of **11a**, **16a** and **19a-22a** was assigned by analogy.

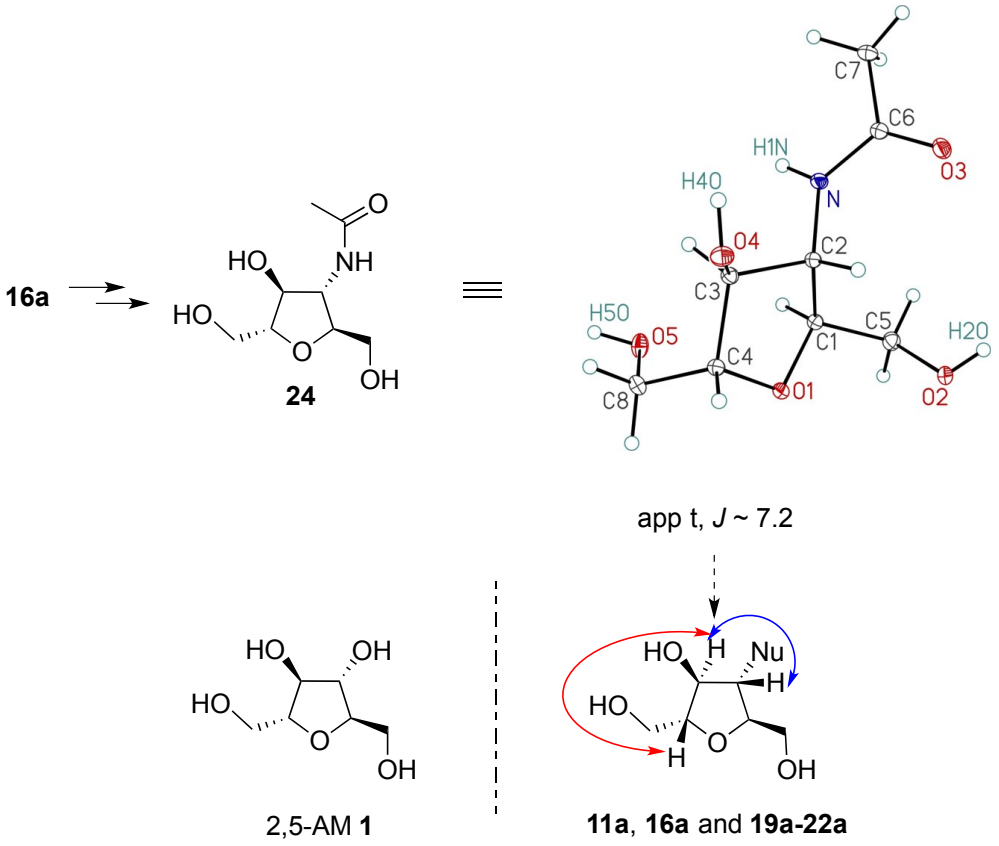

Figure 2.4.5. X-ray structure of **24** and coupling pattern of **11a**, **16a** and **19a-22a**

However, the above assignment does not provide stereochemical information of the major and minor diastereomers (**17a-18a** and **17b-18b**) obtained during the epoxide ring-opening of epoxides with protecting groups on C-1 and C-6 carbons (**12** and **14**). To determine the stereochemistry of epoxides **18a** and **18b**, each diastereomer in its pure form was treated with sodium methoxide in MeOH to cleave the pivaloyl protecting

group (Scheme 2.4.7). The ^{1}H NMR spectrum of the product obtained by deprotection of **18a** was compared to the ^{1}H NMR spectrum of diastereomeric mixture of **16a** and **16b**. In the event, spectral data for the product obtained by deprotection of **18a** matched the ^{1}H NMR spectrum of the major diastereomer **16a**. A similar observation in the case of the minor diastereomer confirms that the relative stereochemistry of major and minor diasteromers obtained during epoxide-ring opening of **7**, **12** and **14** is the same irrespective of the presence of a protecting group on primary hydroxyl groups.

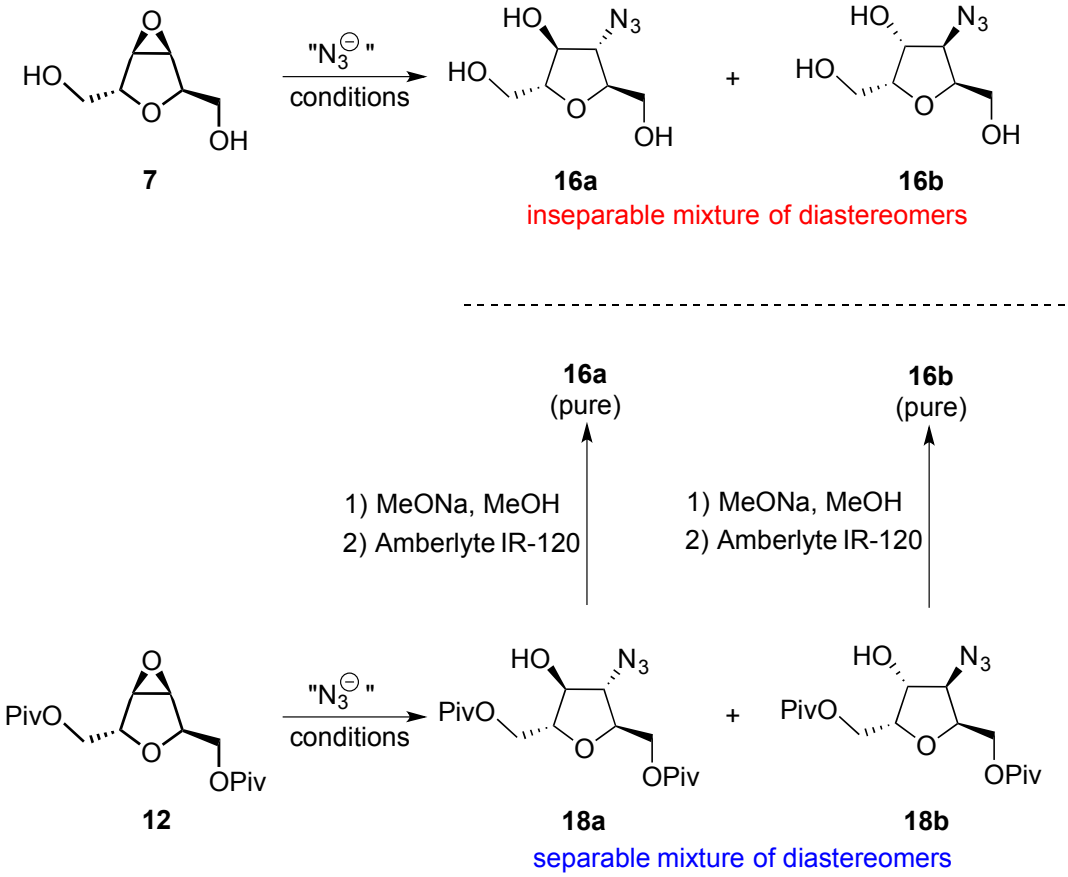

Scheme 2.4.7. Synthesis of **16a** and **16b** from the pure forms of **18a** and **18b**

2.4.5. Accurate determination of the diastereomeric ratio

We have used various NMR techniques to determine *dr* values. ^{19}F NMR analysis was used to determine the ratio of 3-fluoro-3-deoxy-2,5-anhydro-D-mannitol **11a** to its minor diastereomer **11b**, whereas ^{1}H NMR analysis was used to determine the *dr* value in all other cases. Both 3-thiomethoxy-3-anhydro-D-mannitol **19a** and its minor diastereomer **19b** had singlet and non-overlapping methyl (CH-S**Me**) resonances, which were integrated to determine the *dr* value as 8.8:1. In all other cases (**16a** and **20a-22a**), overlap of ^{1}H NMR resonances of major and minor diastereomers could potentially cause error in determination of the *dr* value. To determine the *dr* values of **16a** and **20a-22a** with greater accuracy, the resonances corresponding to the minor diastereomer in ^{1}H NMR spectrum were separated from the resonances of major diastereomer, with the assistance of 1D-TOCSY experiments. Resonances of major and minor diastereomers, which were not overlapping with each other, were integrated to determine the diastereomeric ratio. As shown in Figure 2.4.6, first ^{1}H NMR spectrum of mixture of diastereomers (**16a** and **16b**) was recorded (Figure 2.4.6, spectrum A). Using the 1D-TOCSY experiment, resonances of the minor diastereomer were determined (Figure 2.4.6, spectrum B). 1D TOCSY irradiation of any of the furanose ring protons of **16b** separated the resonances corresponding to **16b** from the ^{1}H NMR spectrum of the diastereomeric mixture of **16a** and **16b**. To confirm the efficiency of 1D-TOCSY to generate the full ^{1}H NMR spectrum corresponding to the minor diastereomer, the actual ^{1}H NMR spectrum of **16b** (Figure 2.4.9, spectrum C) was compared to the 1D-TOCSY generated ^{1}H NMR spectrum of **16b** (Figure 2.4.9. spectrum B). To our delight, the ^{1}H

NMR spectrum of **16b** generated by 1D-TOCSY is identical to the original ^{1}H NMR spectrum of **16b**. Thus, to determine the

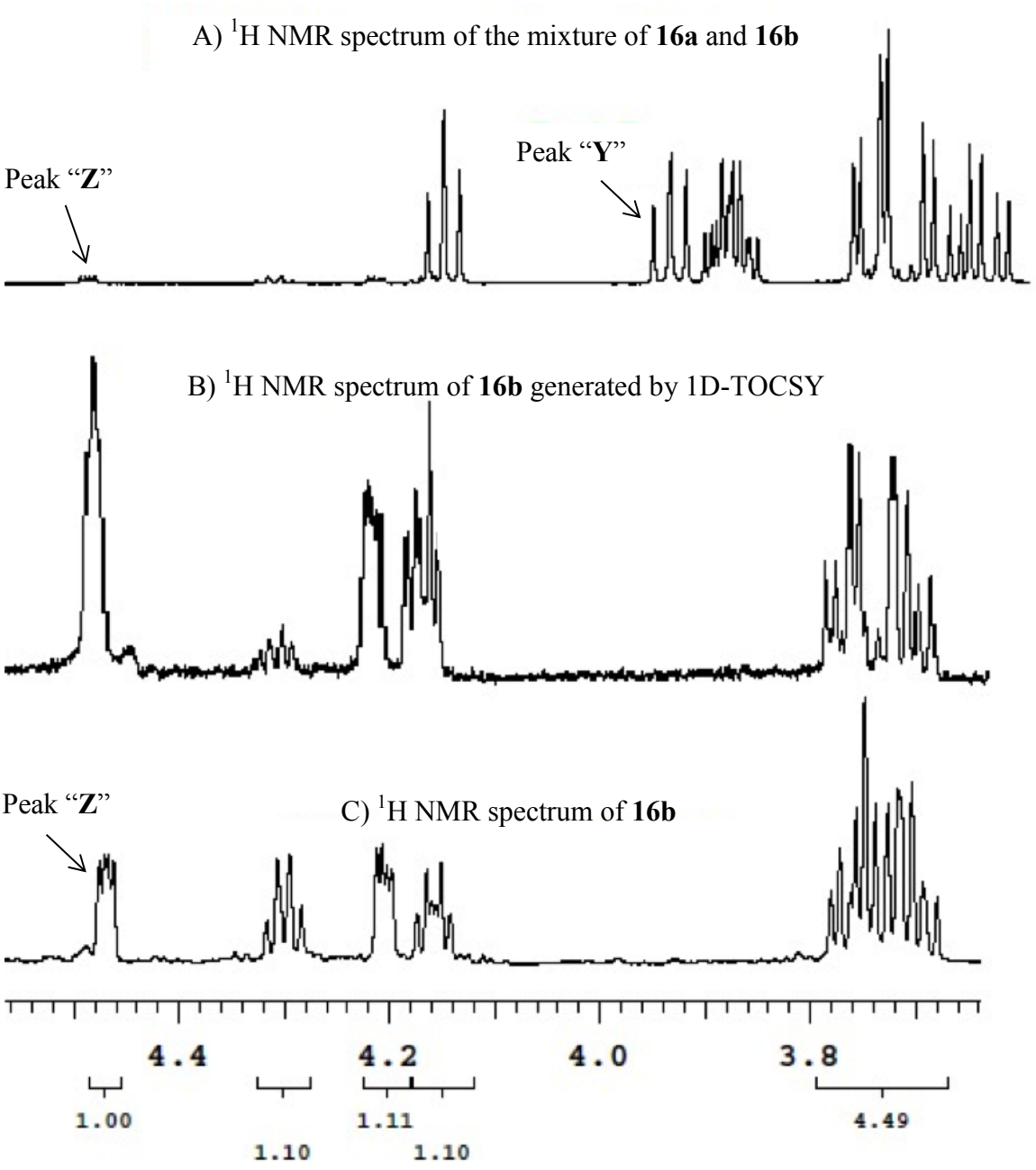

Figure 2.4.6. A strategic way to determine diastereomeric ratio by ^{1}H NMR analysis

accurate diastereomeric ratio, we first generated the ^{1}H NMR spectrum of the minor diastereomers (**12b**, **20-22b**) by 1D-TOCSY and the resonance of the major diastereomer,

which did not overlap with any of the minor diastereomer resonances, was integrated to determine the *dr* value. For example, to determine the ratio of **16a** to **16b**, we first generated the ^{1}H NMR spectrum of **16b** using 1D-TOCSY to find resonances corresponding to **16b**. The resonances "**Y**" and "**Z**" corresponding to **16a** and **16b**, respectively (Figure 2.4.9, Spectrum A and C), were integrated to determine the diastereomeric ratio.

2.4.6. Application towards the synthesis of C-3 and C-4 modification of 2,5-AM derivatives

Diastereoselective epoxide ring-opening methodology was extrapolated to the synthesis of C-3 and C-4 modified 2,5-AM derivatives. My co-worker Dr. Olivier Soueidan had synthesized a aziridine **25** starting from the azido-sugar **17**, which was obtained by epoxide ring-opening of **14**. Aziridine **25** underwent ring-opening reactions with various nucleophiles, which provided access to C-3 and C-4 modified 2,5-AM derivatives (Scheme 2.4.8).

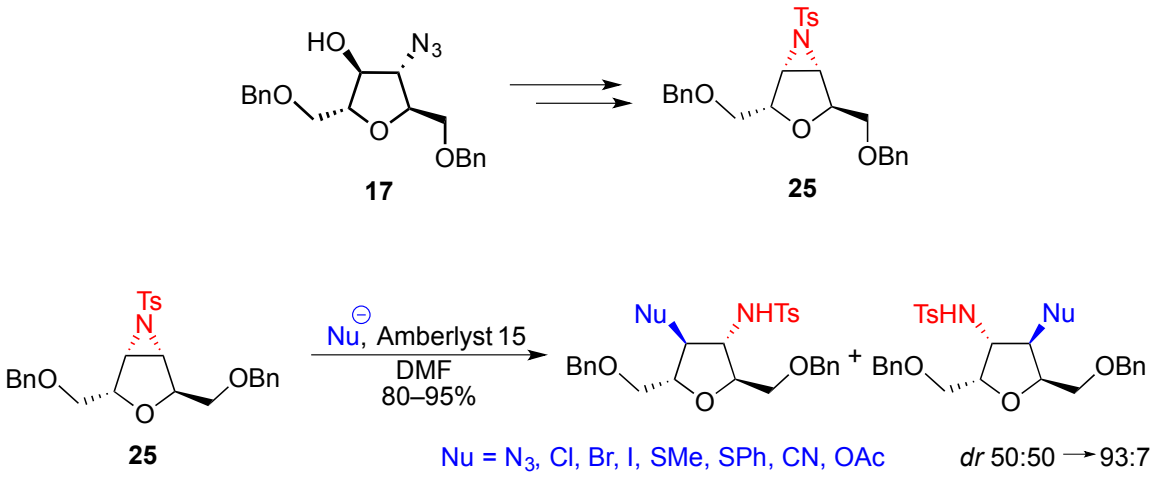

Scheme 2.4.8. Extrapolation of epoxide ring-opening methodology to C-3 & C-4 modification of 2,5-AM

2.5. Conclusion

We studied the effect of C-1 and C-6 protecting groups and solvents on the epoxide ring-opening of **7** with various nucleophiles. Consequently, we developed a versatile method to synthesize C-3 modified 2,5-AM derivatives by diastereoselective ring-opening of C_2-symmetric epoxide **7**. Ring-opening of the epoxide occurred under mild conditions in DMF using Amberlyst 15 as an additive. This method is protecting group free and provides direct access to C-3 functionalized 2,5-AM derivatives in high yields and excellent diastereoselectivity (Scheme 2.5.1).

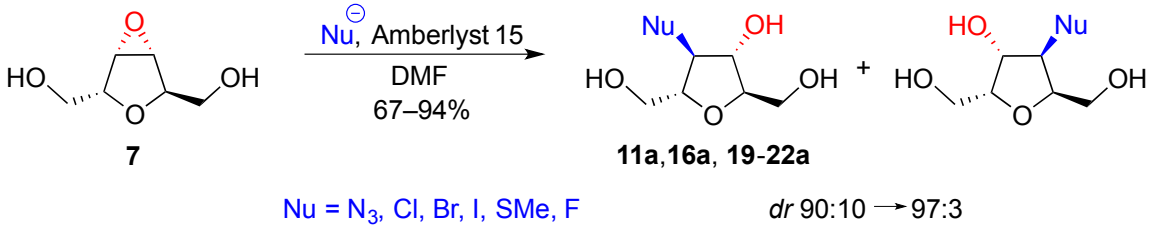

Scheme 2.5.1. Overview of diastereoselective ring-opening of epoxide **7**

2.6. Future directions

Our efforts to accomplish the ring-opening of epoxide **7** with nucleophiles such as cyanide, primary amines and silyl vinyl ethers was unsuccessful. Thus, further optimization is required to improve the scope of this protocol. Further, azide **16a** can be derivatized with different functional groups to develop ligands for the use in asymmetric transition-metal catalysis. We are also interested in exploring the scope of **16a** in organocatalysis. Preparation of variety of amine derivatives from **16a** and thorough screening of these derivatives for a particular chemical transformation could yield efficient organocatalysts.

2.7. Experimental section

Reactions were carried out in flame-dried glassware under a positive argon atmosphere unless otherwise stated. Transfer of anhydrous solvents and reagents was accomplished with oven-dried syringes or cannulae. Solvents were distilled before use: dichloromethane (CH_2Cl_2) and dimethylformamide (DMF) from calcium hydride, tetrahydrofuran (THF) from sodium/benzophenone ketyl and pyridine from KOH. All the commercially available solvents and reagents were used without further purification. Reagents were purchased from Sigma-Aldrich company. Thin layer chromatography was performed on glass plates precoated with 0.25 mm silica gel. For the spot visualization, TLCs were treated with 2.5% *p*-anisaldehyde in AcOH-H_2SO_4-EOH (1:3:86) and heated until color development. Flash chromatography columns were packed with 230–400 mesh silica gel with the specified solvent system. Optical rotations (deg cm^2 g^{-1}) were measured with Perkin Elmer 241 polarimeter, using the D-line of sodium lamp (λ = 589.3 nm) at 22 ± 2 °C. Proton nuclear magnetic resonance spectra (^{1}H NMR) were recorded at 400 MHz or 500 MHz in indicated deuterated solvents and were reported in ppm in the presence of TMS as internal standard. The coupling constants (*J*) were reported in hertz (Hz) and standard notation was used to describe the multiplicity of signals observed in ^{1}H NMR spectra: broad (br), multiplet (m), singlet (s), doublet (d), triplet (t), etc. Carbon nuclear magnetic resonance spectra (^{13}C NMR) were recorded at 100 MHz or 125 MHz. The spectra were referenced to the residual solvent present in the deuterated solvent (*e.g.* $CDCl_3$: δ = 77.26 ppm, ^{13}C; 7.26 ppm, ^{1}H). Infrared (IR) spectra were measured with a Nic-Plan FTIR Microscope. IR spectra were recorded neat and reported in cm^{-1}. Mass

spectra were determined on a high-resolution electrospray positive ion mode spectrometer.

2,5-Anhydro-D-mannitol (1).

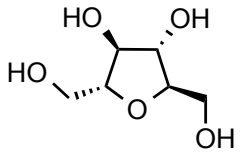

Compound **1** was synthesized by following a reported procedure.[28]

3,4:2,5-Dianhydro-D-allitol (7).

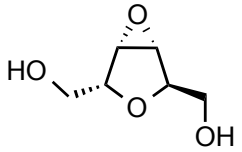

A one-neck round bottom flask, maintained under Ar atmosphere was charged with 2,5-AM **2** (1.64 g, 10.0 mmol) and PPh_3 (5.78 g, 22.0 mmol). DMF (18 mL) was then added and the resulting mixture was stirred at room temperature until the solids were completely dissolved. This solution was cooled to 10 °C and DIAD (4.4 mL, 2.2 mmol) was added dropwise but quickly. The reaction mixture was allowed to attain room temperature, before being stirred at 40 °C for 2 h. DMF was evaporated under reduced pressure to result viscous syrup, which was partitioned between water (150 mL) and diethyl ether (100 mL). Aqueous layer was collected and washed again with diethyl ether (100 mL). The aqueous layer was concentrated under reduced pressure and the crude product was subjected to silica gel column chromatography, eluted with DCM and acetone solvent mixture (3:1 to 2:3). Fractions containing product were combined and concentrated to yield compound **7** (1.26 g, 86%) as white solid that matched with

previously reported characterization data.[30] R_f 0.37 (50:50, DCM:acetone); ^{1}H NMR (400 MHz, D_2O): δ 4.22-4.17 (m, 2H), 4.02 (br d, *J* = 3.0 Hz, 1H), 3.91 (br d, *J* = 3.0 Hz, 1H), 3.78-3.60 (m, 4H); ^{13}C NMR (100 MHz, D_2O): δ 79.7, 78.9, 62.8, 61.5, 58.3, 57.2.

1,6-Di-*O*-pivaloyl-3,4:2,5-dianhydro-D-allitol (12).

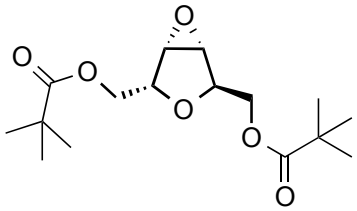

To a stirred solution of epoxide **7** (1.46 g, 10.0 mmol) in pyridine (15 mL) under Ar atmosphere, triethylamine (3 mL) and DMAP (0.31 g, 2.50 mmol) were added. This mixture was cooled to 0 °C and pivaloyl chloride (2.6 mL, 22 mmol) was added dropwise. The reaction mixture was warmed to room temperature and stirred for 5 hours at room temperature. Solvent was evaporated under reduced pressure to yield viscous syrup, which was diluted with DCM (150 mL). Organic layer was washed with saturated $NaHCO_3$ solution (100 mL) and subsequently with brine solution (100 mL). DCM layer was dried over anhydrous Na_2SO_4, filtered and concentrated under vacuum to yield crude product. The crude product was subjected to column chromatography on silica gel and eluted with hexane and ethyl acetate (80:20) to yield compound **12** as colorless oil. R_f 0.47 (20:80, EtOAc: Hexane); $[\alpha]_D^{20}$ +31.9 (*c* 0.65, MeOH); IR (cast film) 2974, 2937, 1734, 1481, 1461, 1398, 1161, 1086, 1037, 941 cm^{-1}; ^{1}H NMR (400 MHz, $CDCl_3$): δ 4.29 (app t, *J* = 4.2 Hz, 1H), 4.24-4.04 (m, 4H), 4.05 (dd, *J* = 12.0, 4.5 Hz, 1H) 3.74 (d, *J* = 3.0 Hz, 1H), 3.67 (d, *J* = 3.0 Hz, 1H), 1.18 (s, 9H), 1.17 (s, 9H); ^{13}C NMR (100 MHz,

$CDCl_3$): δ 177.6, 177.5, 75.7, 74.9, 63.5, 61.9, 56.7, 56.1, 38.23, 38.20, 26.63, 26.61; HRMS (ESI) calcd for $C_{16}H_{26}O_6$ [M+Na^+] 337.1629; found 337.1622.

1,6-Di-*O*-benzyl-3,4:2,5-dianhydro-D-allitol (14).

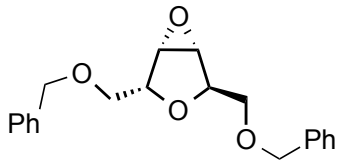

Compound **7** (0.20 g, 1.4 mmol) was dissolved in dry DMF (5 mL) and NaH 60% (0.12 g, 3.1 mmol) was added in a single portion at 0 °C. After 10 min, BnCl (0.36 mL, 3.1 mmol) was added neat at 0 °C and the reaction mixture was warmed to room temperature and stirred for 4 hours. After reaction completion, the mixture was quenched by water (5 mL) and the aqueous layer was extracted by DCM (3 × 5 mL). The combined organic layers were dried over $MgSO_4$, filtered and concentrated under reduced pressure. The crude product was used in the next step without further purification: R_f 0.80 (98:2, DCM: acetone); $[\alpha]_D^{20}$ -60.0 (*c* 1.40, CH_2Cl_2); IR (cast film) 3062, 3030, 2862, 1496, 1453, 1406, 1361, 1089 cm^{-1}; ^1H NMR (500 MHz, $CDCl_3$) δ 7.38-7.29 (m, 10H), 4.62 (d, *J* = 12.0 Hz, 1H), 4.58 (d, *J* = 12.0, 1H), 4.56 (d, *J* = 12.0, 1H), 4.52 (d, *J* = 12.0 Hz, 1H), 4.24-4.26 (m, 2H), 3.83 (d, *J* = 3.0 Hz, 1H), 3.76 (d, *J* = 3.0 Hz, 1H), 3.65 (d, *J* = 6.5 Hz, 2H), 3.59 (d, *J* = 4.5 Hz, 2H); ^{13}C NMR (125 MHz, $CDCl_3$) δ 138.1, 138.0, 128.5, 128.4, 127.9, 127.8, 127.7, 127.5, 77.3, 76.7, 73.6, 73.5, 70.5, 69.0, 58.0, 57.2; HRMS (ESI) calcd for $C_{20}H_{22}NaO_4$ [M + Na]$^+$ 349.1410; found 349.1409.

1,6-Dityrityl-3,4:2,5-dianhydro-D-allitol (15).

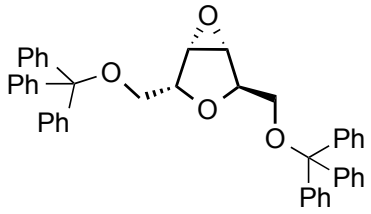

One-neck round bottom flask, maintained under Ar atmosphere was charged with epoxide **7** (1.46 g, 10.0 mmol), triethylamine (3 mL) and pyridine (15 mL). After the epoxide was completely dissolved, trityl chloride (6.4 g, 2.3 mmol) and DMAP (0.31 g, 2.50 mmol) were added. The reaction mixture was heated at 60 °C for 10 hours, before being cooled to room temperature. Pyridine was removed under reduced pressure to result viscous syrup, which was subjected to silica gel column chromatography using hexanes and ethyl acetate (95: 5) to yield pure compound **15** as white solid (3.85 g, 66%) that matched with previously reported characterization data.[34] R_f 0.47 (5:95, EtOAc: Hexanes); ^{1}H NMR (400 MHz, $CDCl_3$): δ 7.57–7.23 (m, 30H), 4.35 (t, *J* = 6.3 Hz, 1H), 4.24 (t, *J* = 4.2 Hz, 1H), 4.02 (d, *J* = 3.0 Hz, 1H), 3.75 (d, *J* = 3.0 Hz, 1H), 3.45-3.32 (m, 3H), 3.19 (dd, *J* = 10.0, 3.6, Hz, 1H).

1,6-Di-*O*-pivaloyl-3-azido-3-deoxy-2,5-anhydro-D-mannitol (18).

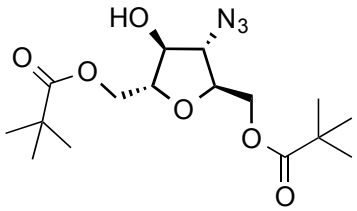

Epoxide **12** (1.50 g, 4.78 mmol) was dissolved in mixture of EtOH:H_2O (25 mL, 9:1). To this solution, NaN_3 (3.27 g, 48.0 mmol) and $CeCl_3.7H_2O$ (0.93 g, 2.50 mmol) were added.[35] This mixture was stirred at 75 °C for 24 hours. Solvents were evaporated under

reduced pressure to yield crude compound, which was then subjected to column chromatography on silica gel, eluted with (95:5, DCM:Acetone). Both diastereomers were separated and pure fractions corresponding to each diastereomer were combined. Removal of solvent resulted major diastereomer (1.22 g, 67%) and minor diastereomer (0.24 g, 14%). Both diastereomers were isolated as colorless oils with combined yield of 81% (1.47 g).

Major **18a**. R_f 0.61 (5:95, acetone: DCM); $[\alpha]_D^{20}$ +71.5 (*c* 1.50, MeOH); IR (cast film) 3473, 2975, 2937, 2876, 2107, 1733, 1481, 1398, 1366, 1284, 1160, 1036, 942, 770 cm^{-1}; ^1H NMR (500 MHz, $CDCl_3$): δ 4.32-4.19 (m, 4H), 4.12 (ddd, *J* = 5.0, 5.0, 4.8 Hz, 1H), 4.04-3.97 (m, 1H), 3.91 (apt, *J* = 7.2 Hz, 1H), 2.9 (d, *J* = 4.9 Hz, 1H), 1.26 (s, 9H), 1.24 (s, 9H) ; ^{13}C NMR (125 MHz, $CDCl_3$): δ 179.0, 178.2, 80.8, 78.5, 76.8, 67.5, 63.5, 63.2, 38.95, 38.91, 27.2, 27.1; HRMS (ESI): calculated for $C16H27N3NaO6$ $[M+Na]^+$ 380.1792; found 380.1787.

Minor **18b**. (partial data) R_f 0.63 (95:5, acetone: DCM); $[\alpha]_D^{20}$ 7.8 (*c* 1.15, MeOH); IR (cast film) 3478, 2974, 2910, 2108, 1733, 1481, 1399, 1284, 1164, 1092, 1036, 940, 771 cm^{-1}; ^{13}C NMR (125 MHz, $CDCl_3$): δ 179.8, 178.1, 81.8, 78.6, 75.2, 68.6, 62.4, 61.2, 38.9, 38.7, 27.2, 27.1; HRMS (ESI): calculated for $C16H27N3NaO6$ $[M+Na]^+$ 380.1792; found 380.1792.

1,6-Di-*O*-benzyl-3-azido-3-deoxy-2,5-anhydro-D-mannitol (17).

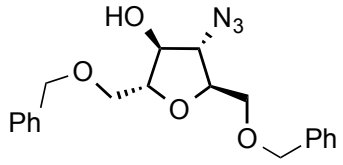

To a solution of compound **14** (4.1 g, 13 mmol) in dry DMF (50 mL), Amberlyst 15 (1.8 g, 25 mmol) was added followed by careful addition of NaN_3 (4.1 g, 63 mmol) in several portions.[35] The reaction mixture was stirred at 120 °C for 2 days. The Amberlyst 15 was filtered off and the crude product was purified by column chromatography after evaporation of DMF under reduced pressure. Desired product was obtained as a mixture of two inseparable isomers (70:30) as pale yellow oil (2.7 g, 60%).

Major **13a**: R_f 0.50 (95:5, DCM: acetone); IR (cast film) 3430, 3030, 2864, 2105, 1486, 1453, 1363 cm^{-1}; ^1H NMR (500 MHz, $CDCl_3$): δ 7.36-7.26 (m, 10H), 4.64 (d, J = 11.9 Hz, 1H), 4.57 (d, J = 3.0 Hz, 2H), 4.56 (d , J = 11.9 Hz, 1H), 4.12-4.10 (m, 2H), 4.02-4.00 (m, 2H), 3.69 (dd, J = 10.5, 3.0 Hz, 1H), 3.63-3.60 (m, 2H), 3.55 (dd, J = 10.5, 5.5 Hz, 1H), 3.15 (d, J = 7.5 Hz, 1H); ^{13}C NMR (100 MHz, $CDCl_3$) δ 137.5, 136.9, 128.2, 128.1, 127.7, 127.5, 127.5, 127.4, 83.1, 80.6, 77.3, 73.4, 73.2, 70.2, 69.9, 68.2; HRMS (ESI) calcd for $C_{20}H_{23}N_3NaO_4$ $[M + Na]^+$ 392.1581; found 392.1573.

Minor **13b.** (partial data): R_f 0.50 (95:5, DCM: acetone); ^1H NMR (500 MHz, CDCl3) δ 4.48 (ddd, J = 6.0, 6.0, 4.5 Hz, 1H), 4.45 (ddd, J = 6.7, 6.7, 2.2 Hz, 1H), 4.20 (m, 1H); ^{13}C NMR (100 MHz, $CDCl_3$) δ 128.0.

General procedure to synthesize (16) and (19). To a stirred heterogeneous mixture of compound **7** (1.46 g, 10.0 mmol) and NaNu (Nu = N_3 and SMe, 50.0 mmol) in DMF (30 mL), Amberlyst 15 (2.73 g, 10.0 mmol) was added.[35] This mixture was heated (at 85 °C

for Nu = N_3 and 75 °C for Nu = SMe) for 17 hours. DMF was removed under reduced pressure and to yield paste. To the crude mixture, 1:1 mixture of DCM:acetone was added and stirred for 15 minutes. Solids were filtered under vacuum and filtrate was concentrated to yield crude compound. The crude compound was subjected to silica gel flash chromatography, eluted with DCM:acetone (50:50) solvent mixture. Fractions containing compound were combined and evaporated to yield a colorless oil, **16** or **19** as mixture of inseparable diastereomers.

3-Azido-3-deoxy-2,5-anhydro-D-mannitol (16).

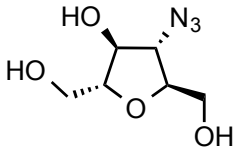

Pale yellow viscous oil (*d.r* = 95:5, 1.66 g, 88%). R_f 0.37 (50:50, DCM:acetone); $[\alpha]_D^{20}$ +26.1 (*c* 0.95, MeOH); IR (cast film) 3357, 2930, 2883, 2106, 1376, 1258, 1043, 857, 696 cm^{-1}; ^1H NMR (500 MHz, D_2O): δ 4.16 (app t, *J* = 7.0 Hz, 1H), 3.95 (dd, *J* = 8.0, 7.0 Hz, 1H), 3.92-3.86 (m, 2H), 3.77 (dd, *J* = 12.5, 3.5 Hz, 2H), 3.70 (dd, *J* = 12.5, 4.9 Hz, 1H), 3.66 (dd, *J* = 12.4, 5.2 Hz, 1H); ^{13}C NMR (125 MHz, D_2O): δ 82.2, 80.4, 75.0, 66.3, 61.0, 60.8; HRMS (ESI) calcd for $C_6H_{11}N_3O_4Na$ $[M+Na^+]$ 212.0642; found 212.0638.

3-Thiomethyl-3-deoxy-2,5-anhydro-D-mannitol (19).

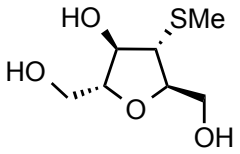

Pale yellow viscous oil (*d.r* = 90:10,1.43 g, 74%). R_f 0.37 (50:50, DCM:acetone); $[\alpha]_D^{20}$ +44.4 (*c* 0.38, MeOH); IR (cast film) 3359, 2922, 2876, 1429, 1387, 1320, 1239, 1184, 1041, 900, 829, 664 cm^{-1}; ^1H NMR (500 MHz, D_2O): δ 4.07 (dd, *J* = 7.6, 7.3 Hz, 1H), 3.94 (ddd, *J* = 9.0, 4.9, 2.8 Hz, 1H), 3.84 (ddd, *J* = 7.2, 5.3, 3.0 Hz, 1H), 3.78 (dd, *J* = 12.4, 2.8 Hz, 1H) 3.77 (dd, *J* = 11.2, 3.0 Hz, 1H), 3.70 (dd, *J* = 12.5, 5.0 Hz, 1H), 3.60 (dd, *J* = 12.4, 5.4 Hz, 1H), 3.0 (dd, *J* = 9.0, 8.0 Hz, 1H), 2.15 (s, 3H); ^{13}C NMR (125 MHz, D_2O): δ 82.9, 81.9, 75.0, 61.5, 60.9, 50.3, 12.3; HRMS (ESI) calcd for $C_7H_{14}SO_4Na$ $[M+Na^+]$ 217.0505; found m/z 217.050.

General procedure to synthesize (20), (21) and (22). Epoxide **7** (0.540 g, 3.78 mmol) was dissolved in DMF (10 mL) and cooled to -40 °C. To this solution, Amberlyst 15 (1.1 g, 4.0 mmol) and NaX (X = Cl, Br and I, 19 mmol) were added. Resulting heterogeneous mixture was stirred for 4 hours and slowly allowed to attain room temperature over a period of 3 hours. After the reaction mixture was warmed to room temperature, stirring was continued for an additional 1 hour. DMF was removed under reduced pressure to result in a paste. To the crude mixture a 1:1 mixture of DCM:acetone (50 mL) was added and stirred for 15 minutes. Solids were filtered under vacuum and the filtrate was concentrated to yield the crude compound. The crude compound was subjected to silica

gel flash chromatography, eluted using DCM:acetone (50:50) solvent mixture. Fractions containing compound were combined and the solvent was evaporated to yield pure compounds **20**, **21** and **22**.

3-Chloro-3-deoxy-2,5-anhydro-D-mannitol (20).

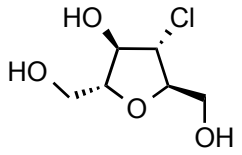

Colorless viscous syrup (0.56 g, d.r ≥ 97:1, 84%). R_f 0.37 (50:50, DCM:acetone); $[\alpha]_D^{20}$ +38.2 (*c* 3.72, MeOH); IR (cast film) 3349, 2928, 1360, 1390, 1040, 901, 823 cm^{-1}; ^1H NMR (500 MHz, D_2O): δ 4.26 (app t, *J* = 7.2 Hz, 1H), 4.14-4.06 (m, 2H), 3.92-3.86 (m, 1H), 3.84-3.77 (m, 2H), 3.75-3.66 (m, 2H); ^{13}C NMR (125 MHz, D_2O): δ 85.6, 84.7, 79.8, 63.5, 62.5, 62.3; HRMS (ESI) calcd for $[M+Na^+]$ $C_6H_{11}ClO_4Na$ 205.0238; found m/z 205.0239.

3-Bromo-3-deoxy-2,5-anhydro-D-mannitol (21).

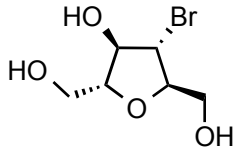

Pale yellow viscous syrup (d.r ≥ 97:1, 0.76 g, 91%). R_f 0.37 (50:50, DCM:acetone); $[\alpha]_D^{20}$ +30.3 (*c* 0.74, MeOH); IR (cast film) 3365, 2927, 2879. 1383, 1230, 1183, 1041, 896, 776 cm^{-1}, ^1H NMR (500 MHz, D_2O): δ 4.33 (app t, *J* = 7.6 Hz, 1H), 4.17 (ddd, *J* = 9.0, 2.9, 2.8 Hz, 1H), 4.09 (dd, *J* = 9.0, 8.0 Hz, 1H), 3.88-3.66 (m, 5H); ^{13}C NMR (125

MHz, D_2O): δ 84.2, 83.1, 78.5, 61.8, 60.7 49.9; HRMS (ESI) calcd for $C_6H_{11}BrO_4Na$ [M+Na^+] calcd 248.9733; found 248.9731.

3-Iodo-3-deoxy-2,5-anhydro-D-mannitol (22).

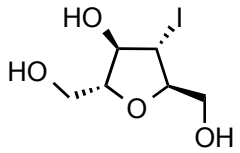

Pale yellow viscous syrup (d.r ≥ 97:1, 0.94 g, 94%). R_f 0.37 (50:50, DCM:acetone); $[\alpha]_D^{20}$ +17.9 (*c* 3.60, MeOH); IR (cast film) 3377, 2926, 2881, 1385, 1327, 1221, 1184, 1156, 1036, 896, 834, 741, 663 cm^{-1}; ^1H NMR (500 MHz, D_2O): δ 4.34 (app t, *J* = 8.5 Hz, 1H), 4.22 (m, 1H), 4.04 (dd, *J* = 9.9, 9.7 Hz, 1H), 3.9-3.75 (m, 4H), 3.68 (dd, *J* = 12.2, 4.7 Hz, 1H); ^{13}C NMR (125 MHz, D_2O): δ 84.9, 82.4, 79.3, 61.0, 59.7, 23.9; HRMS (ESI) calcd for $C_6H_{11}IO_4Na$ [M+Na^+] 296.9594; found 296.9590.

3-Fluoro-3-deoxy-2,5-anhydro-D-mannitol (11).

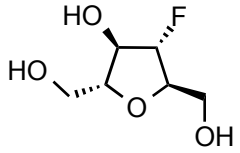

KHF_2 (3.21 g, 41.1 mmol) was added to a solution of epoxide **7** (0.60 g, 4.11 mmol) in DMF (12 mL). The heterogeneous mixture was heated at 100 °C for 6 hours, before being refluxed for 18 hours. DMF was removed under reduced pressure and acetone (30 mL) was then added. Solids were filtered off and evaporation of acetone from the filtrate resulted crude compound. The crude was subjected to silica gel column chromatography, eluted using DCM:acetone (50:50). Fractions containing the compound were combined

and concentrated to yield compound **11** as a colorless viscous syrup (*d.r* = 96:1, 0.47 g, 67%). R_f 0.37 (50:50, DCM:acetone); $[\alpha]_D^{20}$ +35.9 (*c* 0.50, MeOH); IR (cast film) 3380, 2937, 1387, 1320, 1217, 1054, 911, 853 cm^{-1}; ^1H NMR (400 MHz, D_2O): δ 4.94 (app dt, *J* = 53.5, 3.8 Hz, 1H), 4.32 (ddd, *J* = 20.2, 5.7, 3.5 Hz, 1H), 4.21 (ddd, *J* = 21.6, 9.5, 5.2 Hz, 1H), 3.97 (ddd, *J* = 5.6, 5.6, 3.9 Hz, 1H), 3.76-3.62 (m, 4H); ^{19}F NMR (375 MHz, D_2O): δ (ppm) -189.7 (app dt, *J* = 53.51, 20.8 Hz); ^{13}C NMR (100 MHz, D_2O): δ□98.2 (d, J_{C-F} = 181.6 Hz), 83.5 (d, J_{C-F} = 5.4 Hz), 81.8 (d, J_{C-F} = 25.1 Hz), 75.1 (d, J_{C-F} = 24.7 Hz), 60.8 (d, J_{C-F} = 1.5 Hz), 60.5 (d, J_{C-F} = 7.2 Hz); HRMS (ESI) calcd for) $C_6H_{11}FO_4Na$ [M+Na^+] 189.0534; found 189.0529.

3-Acetamido-3-deoxy-2,5-anhydro-D-mannitol (24).

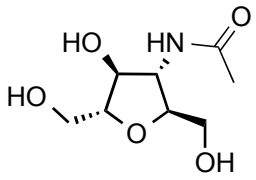

A 50 mL round bottomed flask was charged with azide **16** (0.25g, 1.32 mmol) and MeOH (25 mL). To this mixture, 10% Pd/C (0.05 g, 20% by weight) was added and the resulting heterogeneous mixture was stirred at room temperature, under a hydrogen atmosphere (1 atm). After stirring for 2 hours, solids were filtered out and washed with MeOH (10-20 mL). Filtrate was taken into a 100 mL round bottom flask and MeOH was partially evaporated to concentrate the solution (ca. 25 mL). To this mixture, activated ester (5.0 mmol, 0.79 g of *N*-acetoxy succinimide) and excess of $NaHCO_3$ were added. This heterogeneous mixture was heated at 40 °C for 24 hours. Solids were filtered and washed with excess of MeOH. Evaporation of MeOH under reduced pressure yielded a viscous

syrup, which was subjected to silica gel column chromatography using DCM:MeOH mixture (100:0 to 80:20). Fractions with compound were combined and concentrated under vacuum to yield clear crystals (0.142 g, 53% over two steps). R_f 0.2 (80:20, DCM:MeOH); m.p. 34.2-36.1 °C; $[\alpha]_D^{20}$ +33.6 (*c* 0.70, MeOH); IR (cast film) 3288, 2930, 2878, 1654, 1557, 1432, 1376, 1312, 1047, 958 cm^{-1}; ^1H NMR (400 MHz, D_2O): δ 4.19 (app t, *J* = 7.5 Hz, 1H), 4.06 (app t, *J* = 7.5 Hz, 1H), 3.88 (ddd, *J* = 7.6, 4.9, 2.6 Hz, 1H), 3.83 (ddd, *J* = 8.3, 5.2, 3.0 Hz, 1H), 3.73 (dd, *J* = 12.5, 3.0 Hz, 1H), 3.68 (dd, *J* = 12.5, 3.0 Hz, 1H), 3.63 (dd, *J* = 12.5, 5.2 Hz, 1H), 3.58 (dd, *J* = 12.5, 5.2 Hz, 1H), 1.83 (s, 3H); ^{13}C NMR (100 MHz, D_2O): δ 174.5, 82.4, 80.7, 74.6, 61.4, 60.9, 56.6, 21.9; HRMS (ESI) calcd for $[M+Na^+]$ $C_8H_{15}NO_5Na$ 228.0842.1105; found 228.0841.

2.7. References

1) Axet, M. R. *et al.* Chiral Diphosphite-Modified Rhodium(0) Nanoparticles: Catalyst reservoir for styrene hydroformylation. *Eur. J. Inorg. Chem.* **2008,** 3460–3466 (2008).
2) Axet, M. R., Benet-Buchholz, J., Claver, C. & Castillón, S. New C2-symmetric diphosphite ligands derived from carbohydrates: Effect of the remote stereocenters on asymmetric catalysis. *Adv. Synth. Catal.* **349,** 1983–1998 (2007); Favier, I. *et al.* Efficient recycling of a chiral palladium catalytic system for asymmetric allylic substitutions in ionic liquid. *Chem. Commun.* **47,** 7869–71 (2011).
3) Balanta Castillo, A. *et al.* An outstanding palladium system containing a C2-symmetrical phosphite ligand for enantioselective allylic substitution processes. *Chem. Commun.* 6197–6199 (2008).

4) Gual, A. *et al.* Diphosphite ligands derived from carbohydrates as stabilizers for ruthenium nanoparticles: promising catalytic systems in arene hydrogenation. *Chem. Commun.* 2759–61 (2008); Gual, A., Godard, C., Claver, C. & Castillón, S. C 1 - Symmetric Diphosphite Ligands Derived from Carbohydrates: Influence of Structural Modifications on the Rhodium-Catalyzed Asymmetric Hydroformylation of Styrene. *Eur. J. Org. Chem.* **2009,** 1191–1201 (2009); Sanhes, D., Gual, A., Castillón, S., Claver, C., Gómez, M. & Teuma, E. New chiral diphosphites derived from substituted 9,10-dihydroanthracene. Applications in asymmetric catalytic processes. *Tetrahedron: Asymmetry* **20,** 1009–1014 (2009).

5) Padwa, A. & Murphree, S. Epoxides and aziridines - a mini review. *ARKIVOC* **2006,** 6-33 (2005).

6) De Faveri, G., Ilyashenko, G. & Watkinson, M. Recent advances in catalytic asymmetric epoxidation using the environmentally benign oxidant hydrogen peroxide and its derivatives. *Chem. Soc. Rev.* **40,** 1722–60 (2011).

7) Xia, Q.-H., Ge, H.-Q., Ye, C.-P., Liu, Z.-M. & Su, K.-X. Advances in homogeneous and heterogeneous catalytic asymmetric epoxidation. *Chem. Rev.* **105,** 1603–62 (2005).

8) Marigo, M., Franzén, J., Poulsen, T. B., Zhuang, W. & Jørgensen, K. A. Asymmetric organocatalytic epoxidation of alpha,beta-unsaturated aldehydes with hydrogen peroxide. *J. Am. Chem. Soc.* **127,** 6964–5 (2005); Corey, E. J., Shibata, S. & Bakshi, R. K. An efficient and catalytically enantioselective route to (S)-(-)-phenyloxirane. *J. Org. Chem.* **53,** 2861–2863 (1988); Kang, J. Y. & Connell, B. T. Synthesis of substituted acetylenic epoxides followed by indium-catalyzed rearrangement to 2,3,5-

trisubstituted furans. *J. Org. Chem.* **76,** 2379–83 (2011); Träff, A., Bogár, K., Warner, M. & Bäckvall, J.-E. Highly efficient route for enantioselective preparation of chlorohydrins via dynamic kinetic resolution. *Org. Lett.* **10,** 4807–10 (2008).

9) Tu, Y., Wang, Z.-X. & Shi, Y. An Efficient Asymmetric epoxidation method for trans-olefins mediated by a fructose-derived Ketone. *J. Am. Chem. Soc.* **118,** 9806–9807 (1996); Marigo, M., Franzén, J., Poulsen, T. B., Zhuang, W. & Jørgensen, K. A. Asymmetric organocatalytic epoxidation of α,β-unsaturated aldehydes with hydrogen peroxide. *J. Am. Chem. Soc.* **127,** 6964–5 (2005).

10) Hanazawa, T., Koiwa, M., Hareau, G. P.-J. & Sato, F. Optically active trans-4-(tert-butyldimethylsiloxymethyl)-5-(tert-butyldimethylsiloxy)-2-cyclohexenone as a useful chiral building block for preparation of substituted cyclohexane rings: synthesis and its highly stereoselective reaction with RCu(CN)Li. *Tetrahedron Lett.* **41,** 2659–2662 (2000).

11) Schneider, C. Synthesis of 1,2-difunctionalized fine chemicals through catalytic, enantioselective ring-opening reactions of epoxides. *Synthesis* **2006,** 3919–3944 (2006); 1. Battistini, C., Crotti, P., Macchia, B., Macchia, F. & DePuy, C. H. Nucleophilic step of ring-opening reactions of cyclopropanes with electrophiles. Electronic substituent effects on stereoselectivity of reactions of some 1-arylbicyclo[4.1.0]heptanes with mercuric salts. *J. Org. Chem.* **43,** 1400–1404 (1978); Bisol, T. B., Bortoluzzi, A. J. & Sá, M. M. Nucleophilic ring-opening of epoxide and aziridine acetates for the stereodivergent synthesis of β-hydroxy and β-amino γ-lactams. *J. Org. Chem.* **76,** 948–62 (2011); Dieter, R. K. & Pounds, S. Ring opening reactions of electrophilic cyclopropanes. *J. Org. Chem.* **47,** 3174–3177 (1982).

12) Ferguson, L. N. Ring strain and reactivity of alicycles. *J. Chem. Educ.* **47,** 46 (1970).

13) Dudev, T. & Lim, C. Ring strain energies from ab initio calculations. *J. Am. Chem. Soc.* **120,** 4450–4458 (1998).

14) Robert D. Bach & Dmitrenko, O. The effect of carbonyl substitution on the strain energy of small ring compounds and their six-member ring reference compounds. *J. Am. Chem. Soc.* **128,** 4598-4611 (2006).

15) Bach, R. D. & Dmitrenko, O. The Effect of substitutents on the strain energies of small ring compounds. *J. Org. Chem.* **67,** 2588–2599 (2002).

16) Cremer, D. & Gauss. Cyclopropane and cyclobutane – CC and CH bond energies, 1,3 interactions and σ-aromaticity. *J. Am. Chem. Soc.* **108,** 7467-7477 (1986); Stirling, C. J. M. Evaluation of strain effects on the reactivity of small rings. *Isr. J. Chem.* **21,** 111–118 (1981).

17) de Meijere, A. Adolf von Baeyer: winner of the Nobel prize for chemistry 1905. *Angew. Chem. Int. Ed.* **44,** 7836–40 (2005) and cited references.

18) Bonollo, S., Lanari, D. & Vaccaro, L. Ring-opening of epoxides in water. *Eur. J. Org. Chem.* **2011**, 2587–2598 (2011).

19) Nielsen, L. P. C. and Jacobsen, E. N. Catalytic Asymmetric epoxide ring-opening chemistry. In *aziridines and epoxides in organic synthesis* (ed A. K. Yudin), 229-269 (Wiley-VCH Verlag GmbH & Co. KGaA, 2006).

20) Jacobsen, E. N. Asymmetric catalysis of epoxide ring-opening reactions. *Acc. Chem. Res.* **33**, 421–431 (2000).

21) Schaus, S. E. & Jacobsen, E. N. Asymmetric ring opening of meso epoxides with TMSCN catalyzed by (pybox)lanthanide complexes. *Org. Lett.* **2,** 1001–1004 (2000).

22) Hughes, E. D. & Ingold, C. K. Mechanism of substitution at a saturated carbon atom. Part IV. A discussion of constitutional and solvent effects on the mechanism, kinetics, velocity, and orientation of substitution. *J. Chem. Soc.* 244-255 (1935).

23) Martins, F., Leitão, R. E. & Moreira, L. Solvation effects in the heterolyses of 3-X-3-methylpentanes(X = Cl, Br, I). *J. Phys. Org. Chem.* **17,** 1061–1066 (2004).

24) Akeroyd, F. M. The foundations of modern organic chemistry: The rise of the Hughes and Ingold theory from 1930–1942. *Found. Chem.* **2,** 99–125 (2000).

25) Gawley, R. E. A proposal for (slight) modification of the Hughes-Ingold mechanistic descriptors for substitution reactions. *Tetrahedron Lett.* **40,** 4297–4300 (1999).

26) Brown, D. C. Teaching solvent effects on S_N2 reactions by the introduction of ionic liquids. *Chem. Educ.* **11**, 64-66 (2006).

27) Reichardt, C. Empirical parameters of solvent polarity as linear free-energy relationships. *Angew. Chemie Int. Ed. Engl.* **18,** 98–110 (1979).

28) Soueidan, O.-M. *et al.* New fluorinated fructose analogs as selective probes of the hexose transporter protein GLUT5. *Org. Biomol. Chem.* **13,** 6511–21 (2015).

29) Castejón, P., Pastó, M., Moyano, A., Pericàs, M. A. & Riera, A. A convenient, stereodivergent approach to the enantioselective synthesis of N-Boc-aminoalkyl epoxides. *Tetrahedron Lett.* **36,** 3019–3022 (1995).

30) Gutheie, R. D., Jenkins, I. D., Watters, J. J., Wright, M. W. & Yamasaki, R. Synthesis of some derivatives of 2,5-anhydro-D-mannitol. *Aust. J. Chem.* **35**, 2169-21773 (1982).

31) Otero, D. A. & Simpson, R. 2,5-anhydro-D-hexitols: syntheses of 2,5-anhydro-d-altritol and 2,5-anhydro-D-iditol. *Carbohydr. Res.* **128,** 79–86 (1984).

32) Chevallier, O. P. & Migaud, M. E. Investigation of acetyl migrations in furanosides. *Beilstein J. Org. Chem.* **2,** 14 (2006).

33) Amantini, D., Fringuelli, F., Piermatti, O. & Tortoioli, S. Nucleophilic ring opening of 1,2-epoxides in aqueous medium. *ARKIVOC* **2006,** 293-311 (2002); Sabitha, G., Babu, R. S., Rajkumar, M. & Yadav, J. S. Cerium(III) chloride promoted highly regioselective ring opening of epoxides and aziridines using NaN_3 in acetonitrile: A facile synthesis of 1,2-azidoalcohols and 1,2-azidoamines. *Org. Lett.* **4,** 343–345 (2002).

34) Nair, V., Chun, B. K. & Vadakkam J. Ring-expanded analogues of natural oxetanocin. *Tetrahedron* **45**, 10261-10268 (2004).

35) Given their potential sensitivity, care should be taken using sodium azide and isolating the product organic azides on multigram scales.

Chapter 3

Evaluation of C-3 Modified 2,5-Anhydro-D-mannitol Derivatives as GLUT5 Ligands

3.1. Design of a new tracer for PET based on the work of Holman and coworkers

As it has been discussed in Chapter 1, Holman and coworkers evaluated various derivatives of D-fructose and 2,5-anhydro-D-mannitol (2,5-AM, **2**) as GLUT5 substrates. Based on Holman's work the new tracers [^{18}F]-6-fluoro-6-deoxy-D-fructose (6-FDF, **3**) and [^{18}F]-1-fluoro-1-deoxy-2,5-anhydro-D-mannitol (1-FDAM, **4**) were developed for use in positron emission tomography (PET) for breast cancer diagnosis (Figure 3.1.1).[1,2] GLUT5 was found to be overexpressed in breast cancer cells in a tissue specific manner[3] and allows selective accumulation of the tracers [^{18}F]-6-FDF **3** and [^{18}F]-1-FDF **1** in breast cancer cells. The low expression of ketohexokinase in breast cancer cells and the failure of [^{18}F]-6-FDF **3** and [^{18}F]-1-FDF **1** to undergo enzymatic phosphorylation in the presence of hexokinase (very slow in case of [^{18}F]-1-FDF **1**)[4] led to the quick efflux of the probes from cancer cells. But, lack of probe efflux is critical to attain high quality diagnostic image.[5]

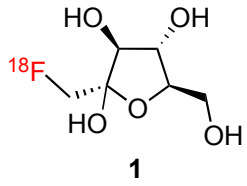

1

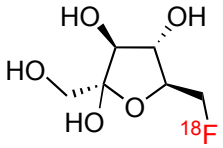

3

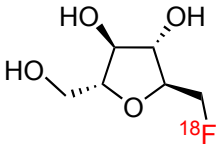

4

Figure 3.1.1. D-Fructose analogues used as PET tracers for breast cancer imaging

To date, all the probes that target GLUT5 transport protein (C-1 or C-6 modified D-fructose **1** or 2,5-AM **3**), underwent efficient efflux. To overcome the efflux problem, we have designed a new tracer, 3-fluoro-3-deoxy-2,5-anhydro-D-mannitol (3-FDAM **5**). The C-3 position of 2,5-AM is functionalized with a fluorine atom (Figure 3.12) to retain both primary hydroxyl groups at positions C-1 and C-6. As a result, 3-FDAM **5** closely mimics 2,5-AM and could potentially undergo enzymatic phosphorylation with hexokinase. Thus, we envisioned the ^{18}F labeled 3-FDAM **5** to be an optimal tracer for breast cancer imaging. However, the role of the C-3 hydroxyl group in binding and transport of **2** by GLUT5, is unknown. Therefore, before we proceeded forward to the synthesis and *in vivo* evaluations of [^{18}F]-3-FDAM **5**, it was important to perform *in vitro* study to determine the affinity of GLUT5 for the cold form of 3-FDAM **5**.

Y = H (1-FDAM, **4**) Y = OH (6-FDF, **3**) 3-FDF (**5**)

In circles: site for enzymatic phosphorylation by hexokinase

Figure 3.1.2. Structural advantage of 3-FDAM over 1-FDAM and 3-FDF

3.2. Evaluation of 3-FDAM 5 as a GLUT5 substrate

In the previous chapter, we demonstrated diastereoselective synthesis of 3-FDAM **5** (Chapter 2, Scheme 2.4.5). Given ready access to the target molecule with excellent diateroselectivity *via* stereoselective epoxide ring-opening of 2,5:3,4-dianhydro-D-allitol, we proceeded further for the *in vitro* evaluation of 3-FDAM **5**. Since GLUT5 is selectively overexpressed in many breast cancer cells, exhibition of potency towards GLUT5 is highly desirable for a potential tracer molecule to diagnose breast cancer. GLUT5 is a transporter of D-fructose and a potential GLUT5 substrate should inhibit D-fructose transport into GLUT5 expressing cells. To determine the GLUT5 recognition for 3-FDAM **5**, a [^{14}C]-D-fructose transport inhibition study with 3-FDAM **5** was performed and a GLUT5 characterized EMT-6 cell line was used as standard cell model. Western blot analysis of EMT-6 cells indicated the expression of GLUTs 1, 2 and 5 in the EMT-6 cells (Figure 3.2.1).

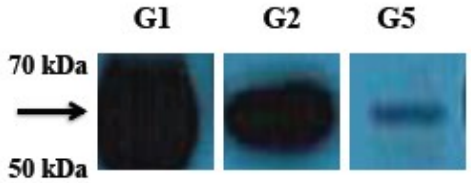

Figure 3.2.1. Western blot analysis showing presence of GLUTs 1, 2 and 5 in EMT6 cells

(Western blot analysis was performed by D. O′Neill)

To our surprise, 3-FDAM **5** failed to inhibit uptake of [^{14}C]-D-fructose into EMT-6 cells, which indicates poor or no affinity of GLUT5 for 3-FDAM **5** (Figure 3.2.2). Given this result, the C-3 hydroxyl group appeared to be an essential functionality for the substrate-GLUT binding process. To date, many hexose-based tracers were developed by the replacement of nonessential hydroxyl groups.[1,2] However, a detailed structure-activity relationship was not performed to retain GLUT recognition for hexoses through the modification of essential hydroxyl groups. As the C-3 hydroxyl group of 2,5-AM appeared to be essential for the GLUT5-hexose binding process, we undertook a study to evaluate substituent effects at C-3 in 2,5-AM derivatives.

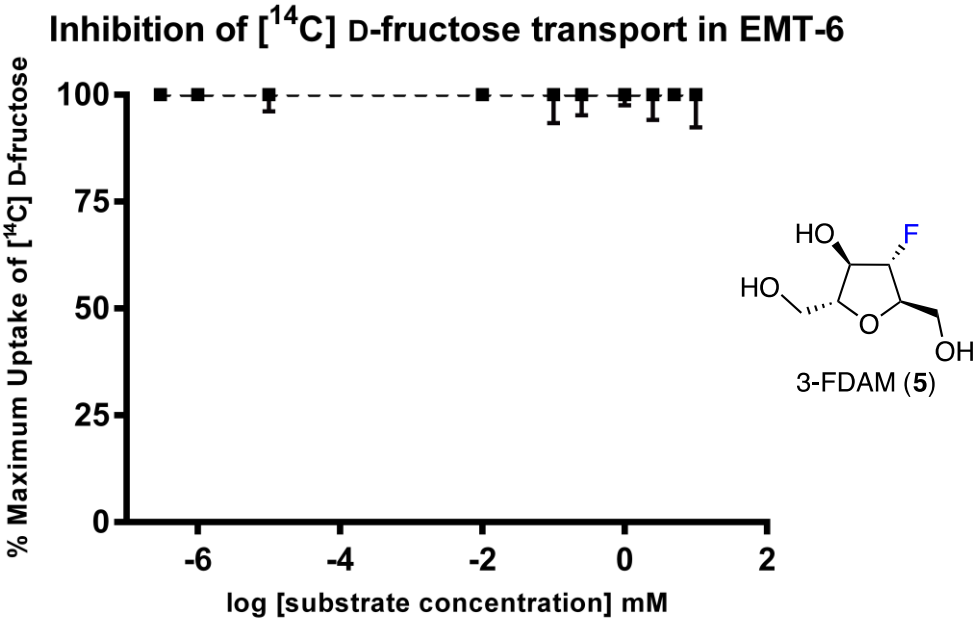

Figure 3.2.2. Concentration dependent [^{14}C]-D-fructose uptake inhibition by 3-FDAM **5** after 25 min incubation at 25 °C into EMT-6 cells. Error bars represent the SEM of triplicates.

3.3. A systematic evaluation of a library of 2,5-AM derivatives

The absence of GLUT5 recognition for 3-FDAM not only eliminates the plausibility of its utility as tracer for PET to diagnose breast cancer, but also raises questions about the general feasibility of C-3 modified 2,5-AM derivatives in tracer development for breast cancer imaging. It is widely surmised that GLUT-mediated hexose transport operates through a hydrogen bond network.[6-12] Substrate recognition by a GLUT for a particular hexose was summarized in terms of essentiality of retaining a hydroxyl group.[6-12] For example, the hydroxyl group at C-6 of D-fructose was concluded to be nonessential for GLUT5 recognition, whereas the C-3 hydroxyl group was concluded to be critical.[13,14] Consequently, tracers were always designed so that the essential hydroxyl groups remained unmodified (e.g. [^{18}F]-6-FDF **3** and [^{18}F]-1-FDAM **4**). However, an essential hydroxyl group can be viewed as a group that possesses both hydrogen bond donor and acceptor properties, and it might be plausible that either or both the hydrogen bonding aspects are crucial for the GLUT recognition for a hexose. Therefore, loss of hydrogen bond donor property at C-3 of 3-FDAM **5** could be the reason for the poor binding of GLUT5 transporter protein with **5**.

As noted in Chapter 1, GLUT1 exhibits higher tolerance towards substrate modification; in contrast, GLUT5 does not tolerate modification of any secondary hydroxyl groups. To understand the role of the C-3 substituent in the hexose-GLUT5 binding, we designed a selection of 2,5-AM derivatives, which exhibit different hydrogen bond donor/acceptor properties (Figure 3.3.1). Systematic evaluation of C-3 modified 2,5-AM derivatives as GLUT5 ligands not only assists in the development of 2,5-AM

based tracers, but might also provide valuable information regarding the transport mechanism of hexoses involving GLUT5.

As shown in Figure 3.3.1, 2,5-AM **2** has a hydroxyl group at C-3 position, while 3-(*N*-2,4-dinitrophenyl)amino-2,5-anhydro-D-mannitol (DNAM **9**) is functionalized with an aromatic amine group at the same position. Thus, both 2,5-AM **2** and DNAM, **9** contain hydrogen bond donor and acceptor functionalities at C-3.[15,16] On the other hand 3-deoxy-2,5-anhydro-D-arabino-hexitol (3-DAM **10**) lacks any polar substituents at the C-3 position for the intermolecular hydrogen bond formation. 3-FDAM **5** and 3-azido-3-deoxy-2,5-anhydro-D-mannitol (3-AZAM, **6**) contain only hydrogen bond acceptor functionalities (fluorine and azide, respectively).[17] 3-Acetamido-3-deoxy-2,5-anhydro-D-mannitol (3-ADAM, **7**) and 3-trifluoroacetamido-3-deoxy-2,5-anhydro-D-mannitol (3-TDAM, **8**) contain amide functionalities at C-3, and are chosen as they both exhibit different hydrogen bond donor acceptor strengths, while maintaining structural similarity.[18]

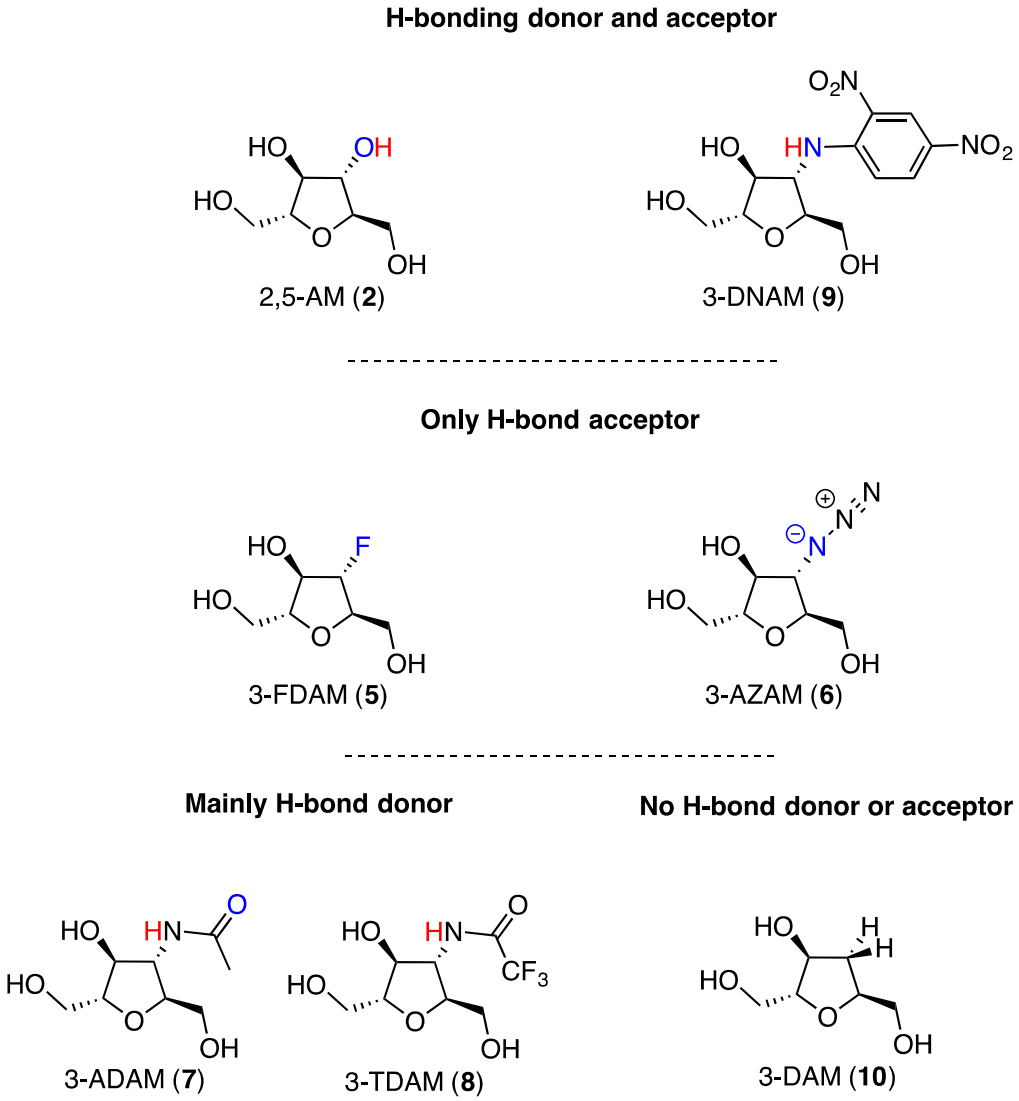

Figure 3.3.1. A selection of C-3 modified 2,5-AM derivatives for systematic evaluation of C-3 substituent effects on modified 2,5-AM-GLUT binding process.

3.4. Synthesis of library of C-3 modified 2,5-AM derivatives

Synthesis of 2,5-AM **2**, 3-FDAM **5**, 3-AZAM, **6** and 3-ADAM **7** was described in Chapter 2 (Section 2.4). The azide **6** was reduced to amine by Pd/C catalyzed hydrogenation to yield amine **11**. Amide **8** was prepared in good yield (73% over two

steps) by treating the amine **11** with ethyl trifluoroacetate under basic conditions (Scheme 3.4.1).

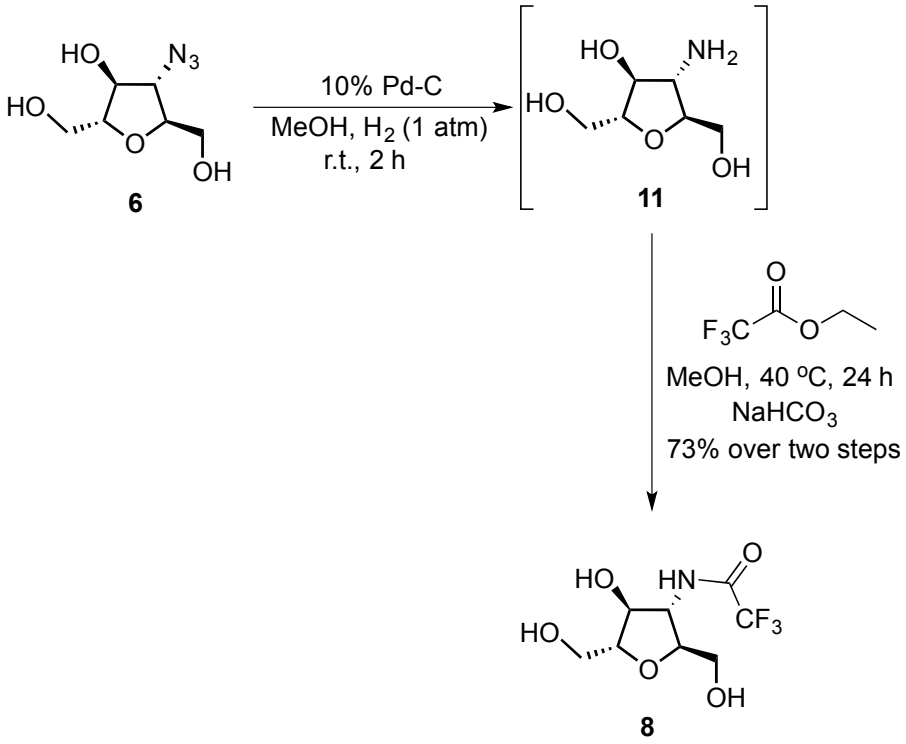

Scheme 3.4.1. Synthesis of amide **8**

3-DNAM **9** was synthesized from azide **6** in four steps (Scheme 3.4.2). Despite several efforts to purify compounds **12-14**, we failed to obtain them in pure form. Since the synthetic route to access 3-DNAM **9** from 3-AZAM **6** involved only simple functional group transformations, the impure intermediates were carried forward. Treatment of azide **6** with *tert*-butyldimethylsilyl chloride in the presence of imidazole resulted in protection of the primary hydroxyl groups as silyl ethers. The azide functionality of the intermediate **12** was reduced to amine by Pd catalyzed hydrogenation reaction. The amine **13** underwent ipso substitution reaction with 1-chloro-2,4-

dinitrobenene to yield **14**, which was treated with trifluoroacetic acid in MeOH to cleave the silyl ethers, resulting in DNAM **9** in 32% overall yield.

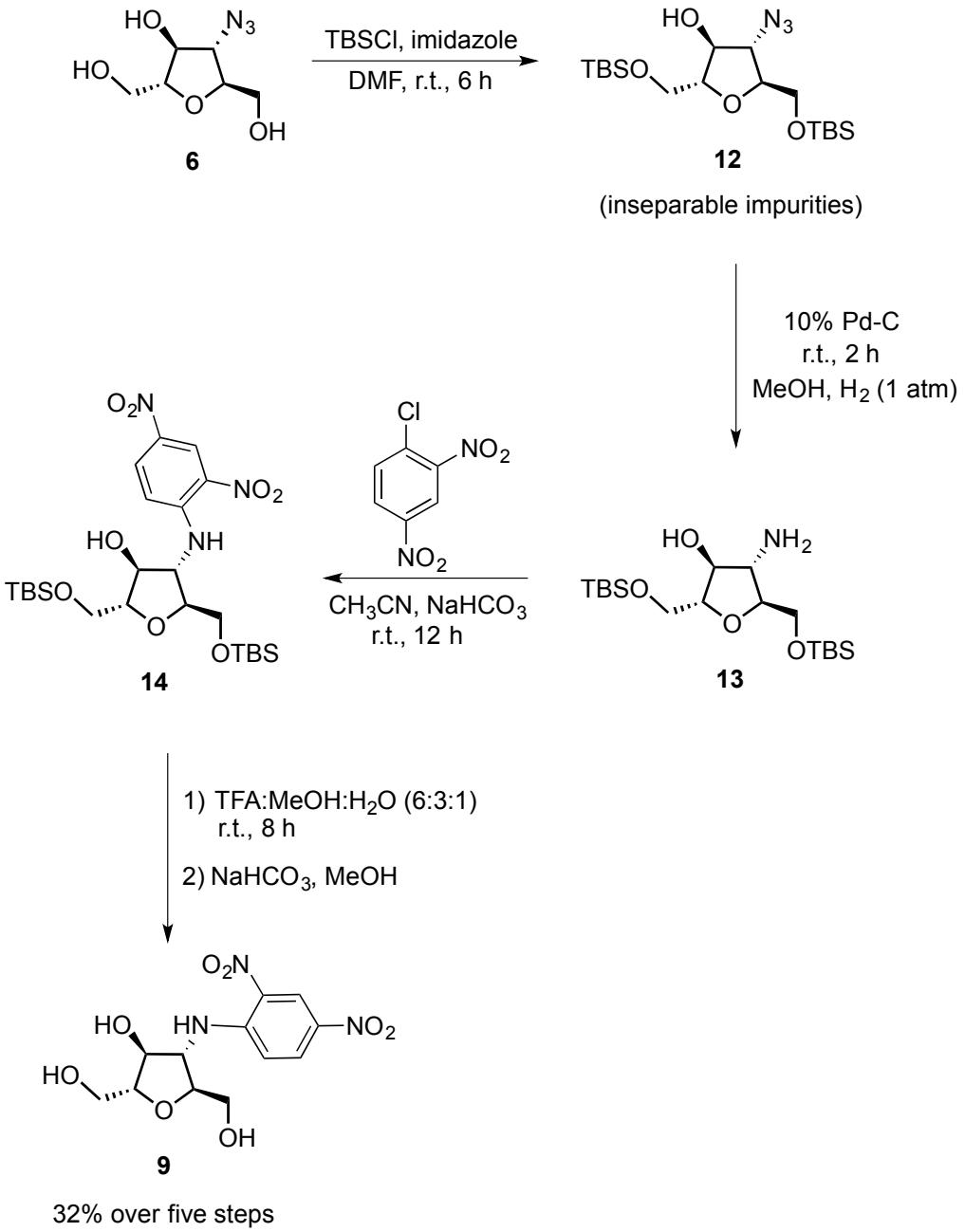

Scheme 3.4.2. Synthesis of arylamine **9**

3-DAM **10** was prepared by following a reported procedure.[19] Synthesis of 2,5:3,4-dianhydro-D-allitol **12** was demonstrated in the Chapter 2 (Section 2.3). Epoxide **15** was hydrogenated in the presence of Pd/C to yield 3-DAM **10**, with excellent diastereoselectivity. The reported diastereomeric ratio was 99:1 (**10a**: **10b**), whereas we did not observe the minor diastereomer by ^{1}H NMR. Though the authors did not provide any rationale for the observed diastereoselectivity, it could be due to participation of the hydroxyl groups in the hydrogenation process. The primary hydroxyl groups of **12** could coordinate with the palladium catalyst to direct the hydrogenolysis process. Hydroxyl group directed metal hydrogenation reactions of imines, carbonyls and epoxides have been studied.[20] As shown in Scheme 3.4.3, both transition states **TS**, the primary hydroxyl groups are involved in the delivery of metal activated hydrogen to provide the major diastereomer **10a**.

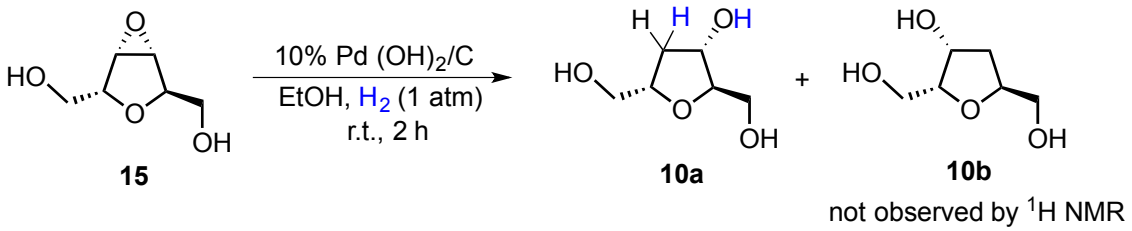

Scheme 3.4.3. Synthesis of 3-DAM **10** and responsible transition states for the formation of **10a**.

3.5. [^{14}C]-D-hexose transport inhibition studies with C-3 modified 2,5-AM derivatives

EMT-6 cells express GLUT5, GLUT1 and GLUT2 (Figure 3.2.2). Thus, EMT-6 cells could also be used as cell models for the evaluation of GLUT1 and GLUT2 affinity for hexoses. To date, studies described GLUT5 as the only transporter of 2,5-AM, without a thorough evaluation against other GLUTs.[13] An *in vitro* study with C-3 functionalized 2,5-AM derivatives in EMT-6 cells might provide information about the GLUTs that recognize 2,5-AM derivatives.

Previously, we observed no [^{14}C]-D-fructose transport inhibition by 3-FDAM **5** in EMT-6 cells (Figure 3.2.2). This observation indicates that D-fructose transporters do not recognize 3-FDAM **5**. However, other GLUT recognition for 3-FDAM **5** cannot be ruled out based on this observation. A [^{14}C]-D-glucose transport inhibition study in EMT-6 cells would provide information about D-glucose transport recognition for 3-FDAM **5**. In the event, [^{14}C]-D-glucose transport into EMT-6 cells was inhibited by 3-FDAM **5**, confirming D-glucose transporter recognition for 3-FDAM **5** (Figure 3.5.1).

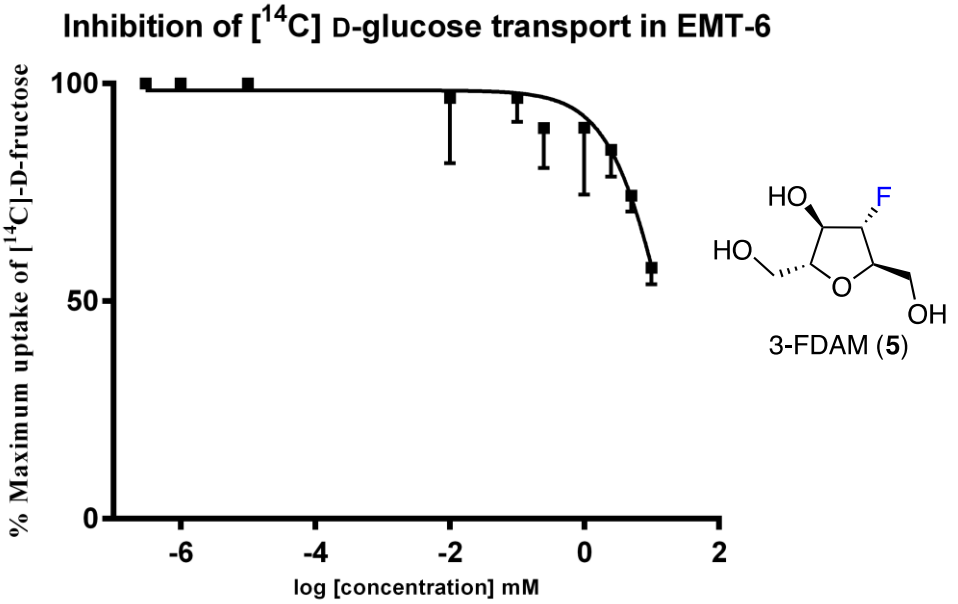

Figure 3.5.1. Concentration dependent [^{14}C]-D-glucose uptake inhibition by 3-FDAM **5** after 25 min incubation at 25 °C into EMT-6 cells. Error bars represent the SEM of triplicates.

Though 2,5-AM **2** was described as a GLUT5 ligand, we observed specific recognition of 3-FDAM **5** by D-glucose transporters. Thus, substitution of the C-3 hydroxyl group of 2,5-AM **2** with a fluorine atom (3-FDAM **5**) led to a switch of the recognition from a D-fructose transporter (GLUT5) to D-glucose transporters. In order to gain more structure-activity relationship, we performed [^{14}C]-D-fructose and [^{14}C]-D-glucose transport inhibition studies with 2,5-AM **2**.

As we expected, the GLUT5 ligand, 2,5-AM **2** inhibited [^{14}C]-D-fructose transport into EMT-6 cells (Figure 3.5.2). To our surprise, 2,5-AM **2** also inhibited [^{14}C]-D-glucose transport into EMT-6 cells (Figure 3.5.3). Both 2,5-AM **2** and FDAM **5** inhibited [^{14}C]-D-glucose, but only 2,5-AM **2** inhibited [^{14}C]-D-fructose transport into EMT-6 cells. Although both 2,5-AM **2** and FDAM **5** contain a hydrogen bond acceptor at C-3, only

2,5-AM **2** possesses a hydrogen bond donor at C-3. In light of these results, we hypothesized that the presence of a hydrogen bond donor at C-3 position is crucial for D-fructose transporter recognition. We also hypothesized that elimination of the hydrogen bond donor property at the C-3 position of 2,5-AM derivatives affords specific recognition by D-glucose transporters.

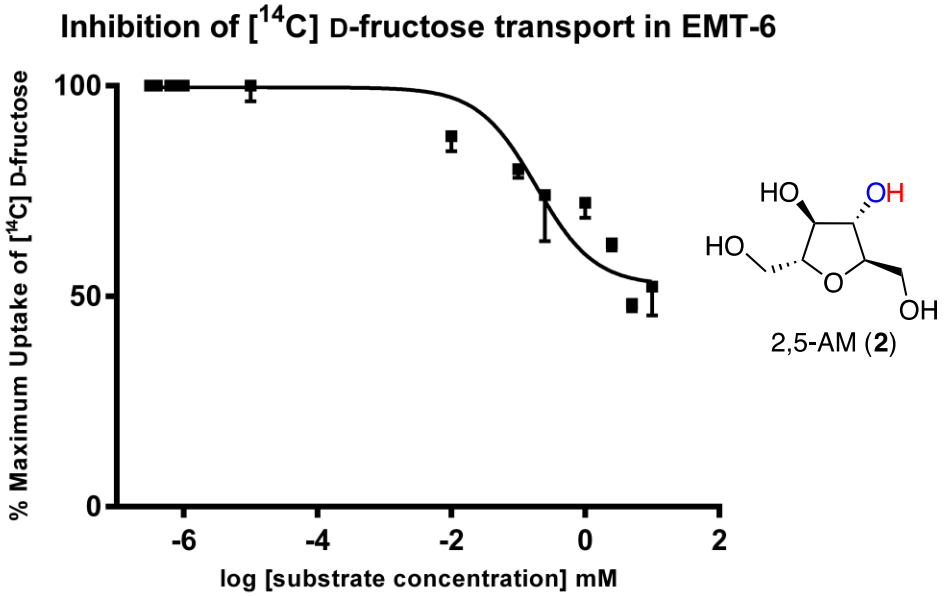

Figure 3.5.2. Concentration dependent [^{14}C]-D-fructose uptake inhibition by 2,5-AM **2** after 25 min incubation at 25 °C into EMT-6 cells. Error bars represent the SEM of triplicates.

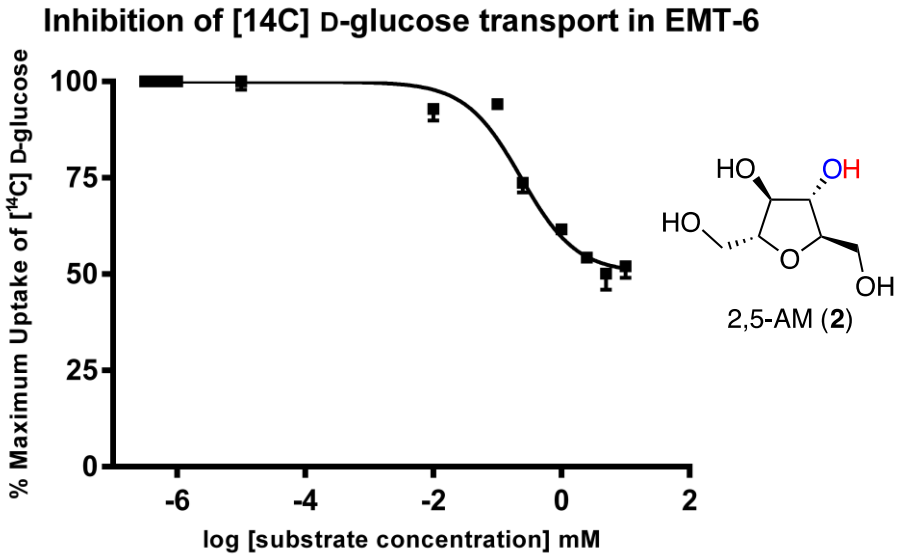

Figure 3.5.3. Concentration dependent [^{14}C]-D-glucose uptake inhibition by 2,5-AM **2** after 25 min incubation at 25 °C into EMT-6 cells. Error bars represent the SD of triplicates.

Very similar to 3-FDAM **5**, 3-AZAM **6** also contains a hydrogen bond accepting azide at the C-3 position, but lacks a hydrogen bond donor. In accordance with our hypothesis, 3-AZAM **6** also did not inhibit [^{14}C]-D-fructose transport (Figure 3.5.4), but inhibited [^{14}C]-D-glucose transport into EMT-6 cells (Figure 3.5.5). Based on the results seen with 3-FDAM **5** and 3-AZAM **6**, it seems clear that 2,5-AM derivatives lacking a hydrogen bond at C-3 are not recognized by fructose transporters (*e.g.* GLUT5).

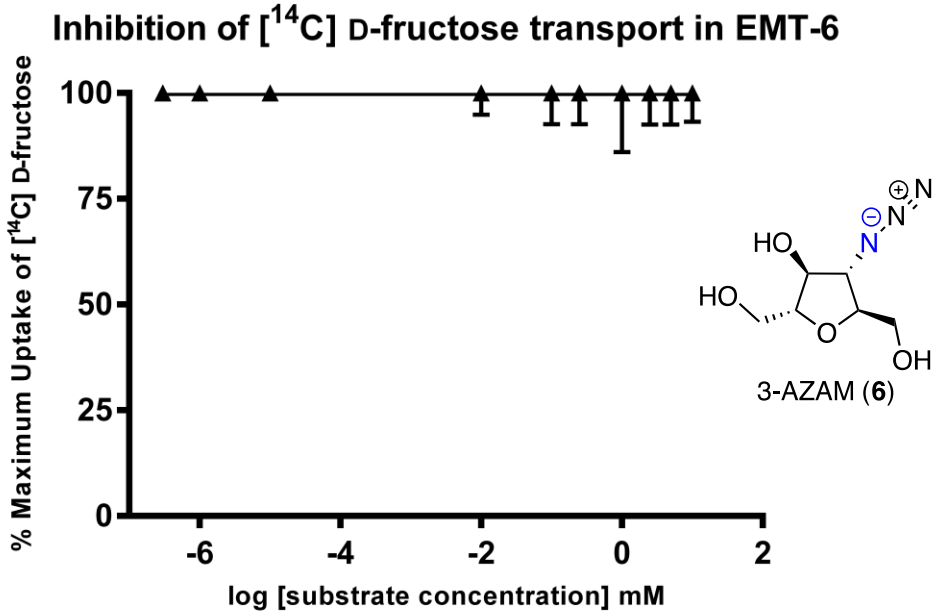

Figure 3.5.4. Concentration dependent [^{14}C]-D-fructose uptake inhibition by 3-AZAM **6** after 25 min incubation at 25 °C into EMT-6 cells. Error bars represent the SEM of triplicates.

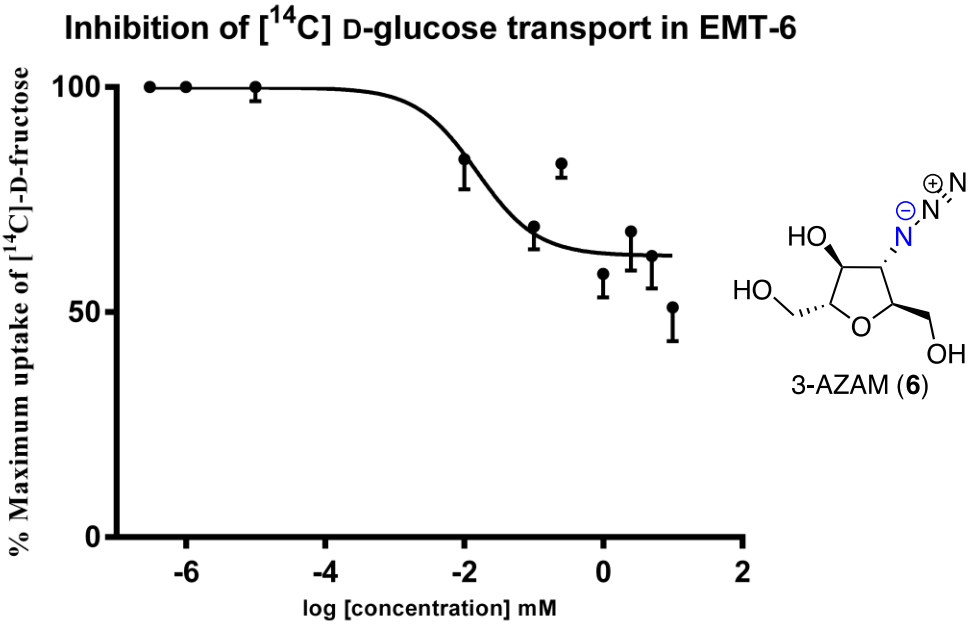

Figure 3.5.5. Concentration dependent [^{14}C]-D-glucose uptake inhibition by 3-AZAM **6** after 25 min incubation at 25 °C into EMT-6 cells. Error bars represent the SED of triplicates.

In comparison to 3-FDAM **5** (IC_{50} = 3.16 mM), 3-AZAM **6** (IC_{50} = 15.2 μM) inhibited D-glucose transport with a lower IC_{50} value (Figure 3.5.5). Based on this observation, it appeared that variation in hydrogen bond acceptor strength of the C-3 functionality changed the affinity for the D-glucose transporter.[21-23] To investigate the importance of hydrogen bond acceptor property of the C-3 substituent for D-glucose transporter recognition, the ability of 3-DAM **10** to inhibit the [^{14}C]-D-glucose transport into EMT-6 cells was examined. 3-DAM **10** possesses neither a hydrogen bond donor nor an acceptor at the C-3 position, and failed to inhibit [^{14}C]-D-glucose transport into EMT-6 cells (Figure 3.5.6). This result confirms that retention of C-3 hydrogen bond acceptor is required for glucose transporter recognition of 2,5-AM derivatives.

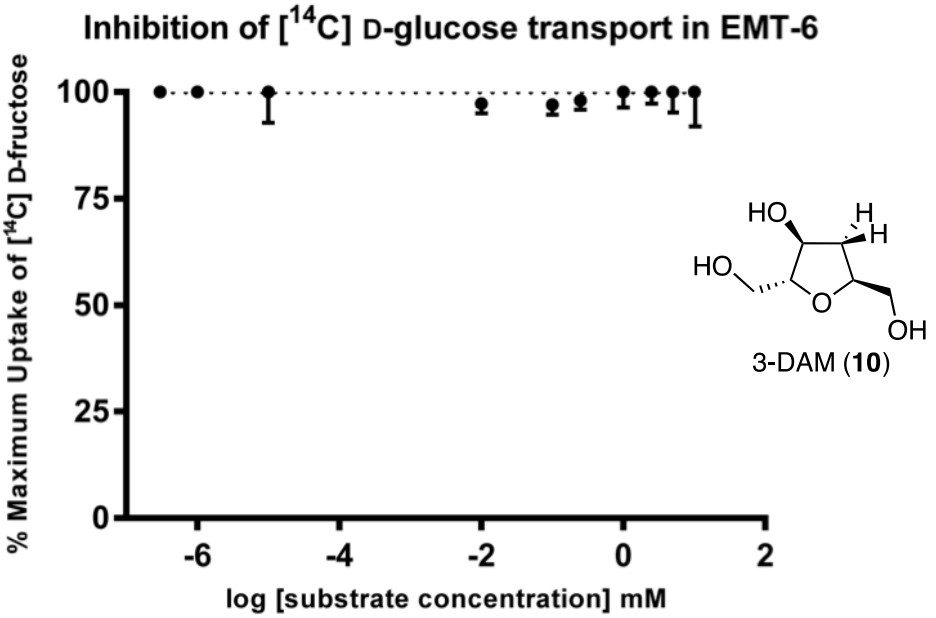

Figure 3.5.6. Concentration dependent [^{14}C]-D-glucose uptake inhibition by 3-DAM **10** after 25 min incubation at 25 °C into EMT-6 cells. Error bars represent the SEM of triplicates.

Next, we explored the ability of 3-ADAM **7** and 3-TDAM **8** to inhibit [^{14}C]-D-glucose transport. 3-ADAM **7** and 3-TDAM **8** are functionalized with amides at the C-3

position, differing from –OH, F and N_3 in the position of hydrogen bond acceptor atom (Figure 3.5.7). With the hydrogen bond acceptor atom no longer directly attached to the C-3 carbon of 2,5-AM derivative, study of the [^{14}C]-D-glucose transport inhibition by

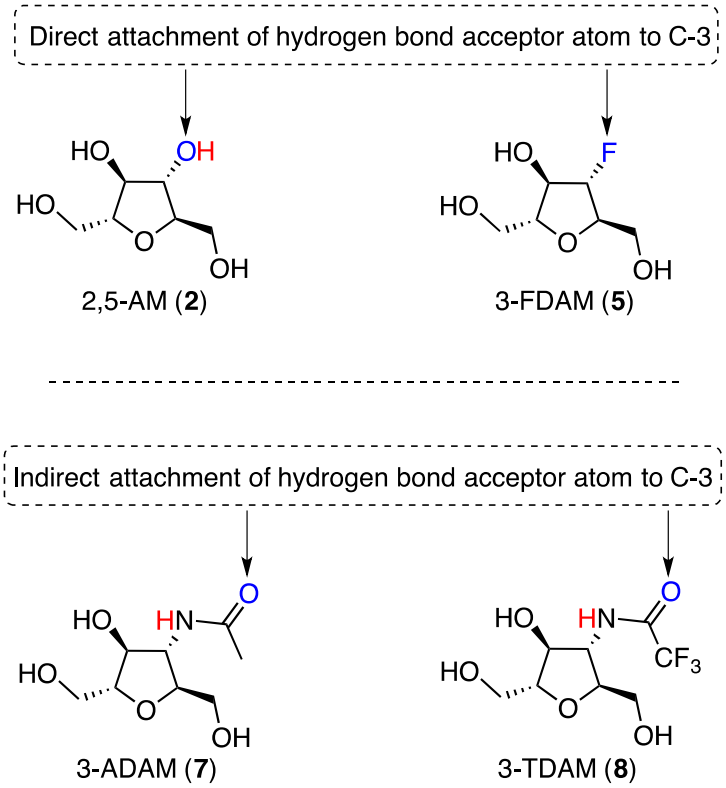

Figure 3.5.7. Difference in the hydrogen bond acceptor atom position in 2,5-AM derivatives

amides **7** and **8** might provide more insights into the GLUT-hexose structure-activity relationship. Furthermore, 3-TDAM **8** is functionalized with trifluoroacetamide functionality at the C-3 position, while 3-ADAM **7** contains acetamide functionality. Therefore, 3-ADAM **7** possesses a better hydrogen bond acceptor, in comparison to 3-TDAM **8**, at position C-3. We observed no inhibition of [^{14}C]-D-glucose transport by 3-TDAM **8**, but 3-ADAM **7** inhibited [^{14}C]-D-glucose transport at higher substrate

concentrations (Figure 3.5.8). No [^{14}C]-D-glucose transporter recognition for 3-TDAM **8** can be attributed to the poor hydrogen bond accepting ability of 3-TDAM **8** (in comparison to 3-ADAM **7**).[18,21]

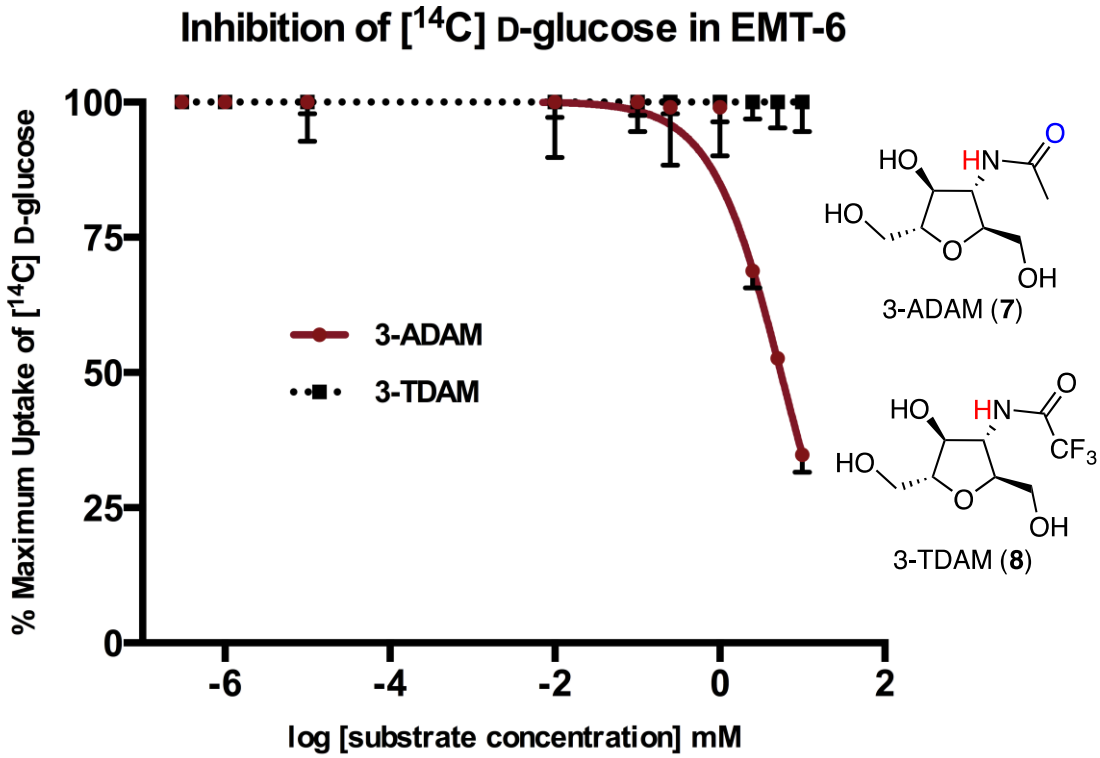

Figure 3.5.8. Concentration dependent [^{14}C]-D-glucose uptake inhibition by 3-ADAM **7** after 25 min incubation at 25 °C into EMT-6 cells. Error bars represent the SEM of triplicates.

In order to investigate the effect of sterically demanding C-3 substituent on the GLUT-substrate binding process, we examined the [^{14}C]-hexose transport inhibition by 3-DNAM **9**. Typically, arylamines are less basic than aliphatic amine and remain unprotonated at physiological pH (approx. 7.4). As a result, an arylamine should retain its hydrogen bond acceptor property at physiological pH. In the event, despite the presence of a bulky 2,4-dinitroaniline substituent at the C-3 position, 3-DNAM **9** displayed very similar inhibition of [^{14}C]-D-glucose uptake to that of 2,5-AM **2** (Figure 3.5.9). All the

above results support the hypothesis that the D-glucose transporter recognition for C-3 modified 2,5-AM derivatives is only a function of the hydrogen bond acceptor property of the C-3 substituent.

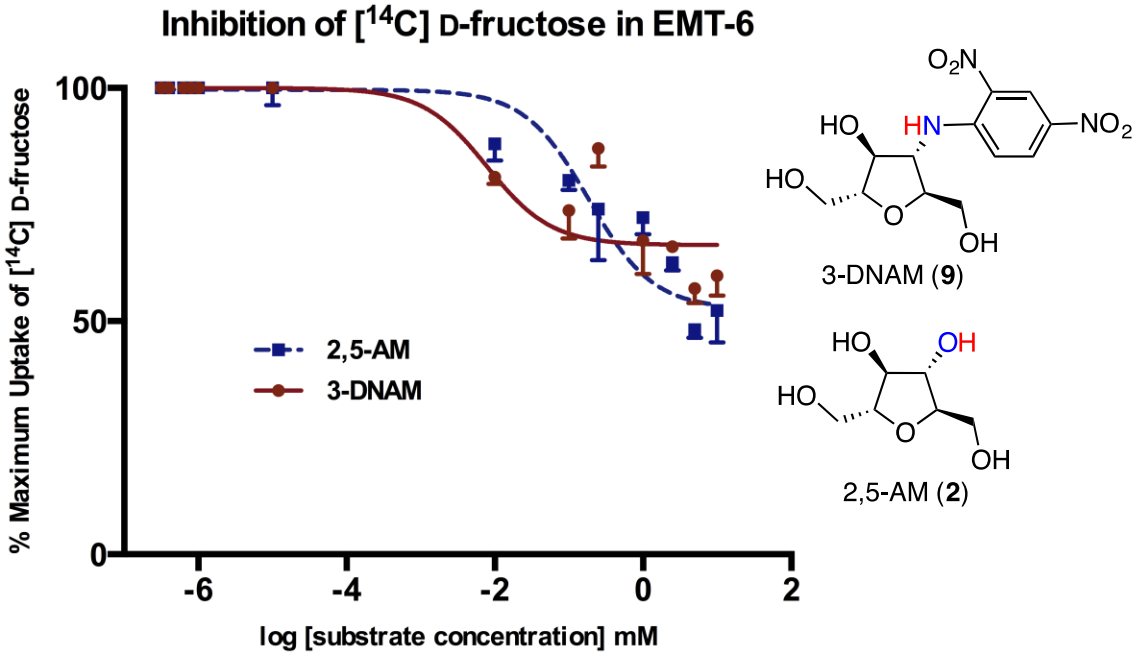

Figure 3.5.9. Comparison of [^{14}C]-D-glucose uptake inhibition by 3-DNAM **9** and 2,5-AM **2**, after 25 min incubation at 25 °C into EMT-6 cells. Error bars represent the SEM of triplicates.

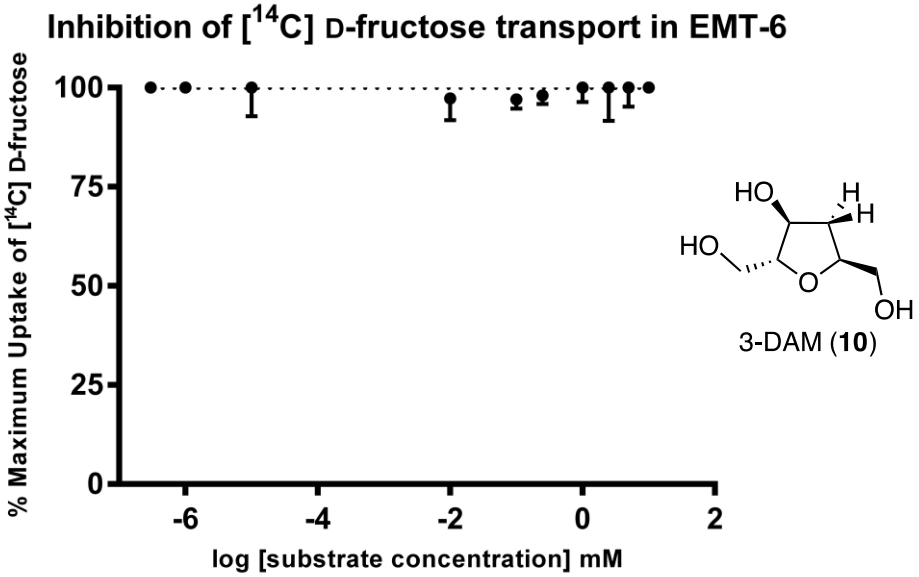

Figure 3.5.10. Concentration dependent [^{14}C]-D-fructose uptake inhibition by 3-DAM **10** after 25 min incubation at 25 °C into EMT-6 cells. Error bars represent the SEM of triplicates.

Given the observed importance of hydrogen bond accepting capability at C-3 of 2,5-AM derivatives, we proceeded to examine the functional group requirement at C-3 of 2,5-AM derivatives for D-fructose transporter recognition. We used 3-DAM **10** as a control, since it lacks both hydrogen bond donor and acceptor at C-3. As we expected, [^{14}C]-D-fructose uptake was not inhibited by **10** (Figure 3.5.10). However, we previously studied the [^{14}C]-D-fructose transport inhibitory ability of 3-FDAM **5** and 3-AZAM **6**, finding them unable to block [^{14}C]-D-fructose transport into EMT-6 cells (Figures 3.2.2 and 3.5.4). These results indicate that the presence of only a hydrogen bond acceptor at C-3 is not sufficient for recognition by D-fructose transporters. Furthermore, 2,5-AM **2**, which possesses both hydrogen bond donor and acceptor, inhibited [^{14}C]-D-fructose transport into the EMT-6 cell line (Figure 3.5.2). Retention of a hydrogen bond donor or both hydrogen bond donor and acceptor at C-3 position appears to be a requirement for D-fructose transporter recognition. To further evaluate the hydrogen bonding

requirements at C-3, the effect of DNAM **9** on [^{14}C]-D-fructose uptake was studied. Though 2,5-AM **2** and 3-DNAM **9** differ in the functional group at the C-3 position, they possess both hydrogen bond donor and acceptor. In support our hypothesis, despite the difference in the nature of the functional groups at the C-3 position, 3-DNAM **9** also inhibited the [^{14}C]-D-fructose transport into EMT-6 cells (Figure 3.5.11). Furthermore, this result indicates that steric hindrance of the C-3 substituent atom is tolerated by D-fructose transporters.

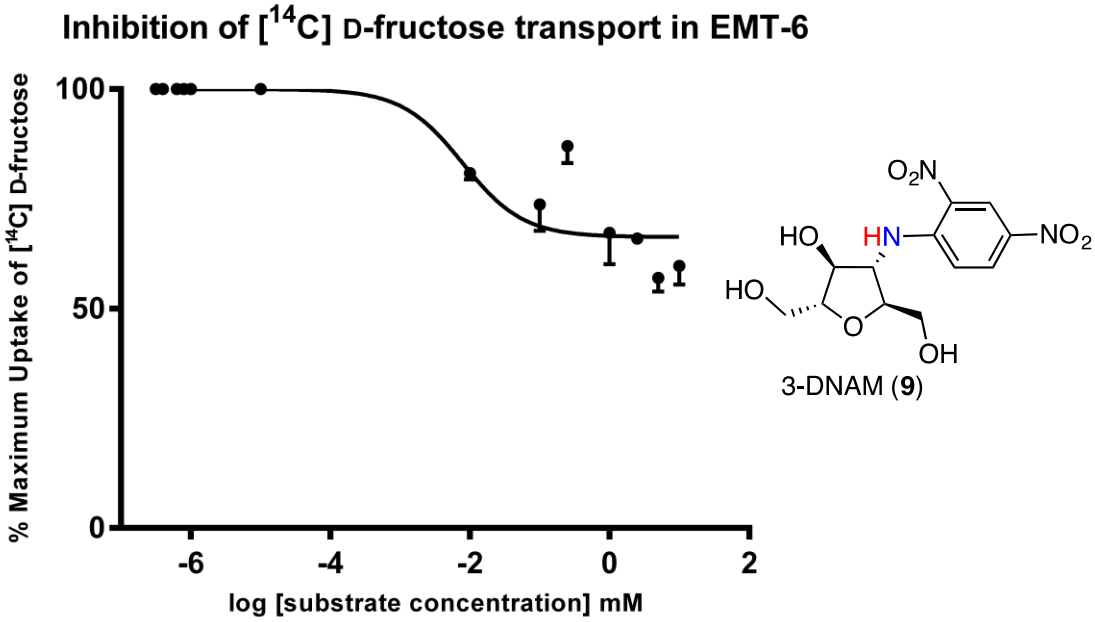

Figure 3.5.11. Concentration dependent [^{14}C]-D-fructose uptake inhibition by 3-DNAM **9** after 25 min incubation at 25 °C into EMT-6 cells. Error bars represent the SEM of triplicates.

To understand the effect of hydrogen bond donor strength of the C-3 substituent on hexose-GLUT recognition, we performed [^{14}C]-D-fructose transport inhibition study with C-3 amides, 3-ADAM **7** and 3-TDAM **8**. Despite similar structural features, amides 3-ADAM **7** and 3-TDAM **8** differ in hydrogen bond donor strength,[18,21] which could help understanding the effect of hydrogen bond donor strength on GLUT-hexose binding. In

comparison to amide **7**, inductively withdrawing CF_3- group present in **8** reduces the electron density at the amide nitrogen atom of **8**, which enhances the hydrogen bond donor ability of the amide functionality of **8**. Both 3-ADAM **7** and 3-TDAM **8** successfully inhibited [^{14}C]-D-fructose transport into EMT-6 cells (Figures, 3.5.12 and 3.5.13).

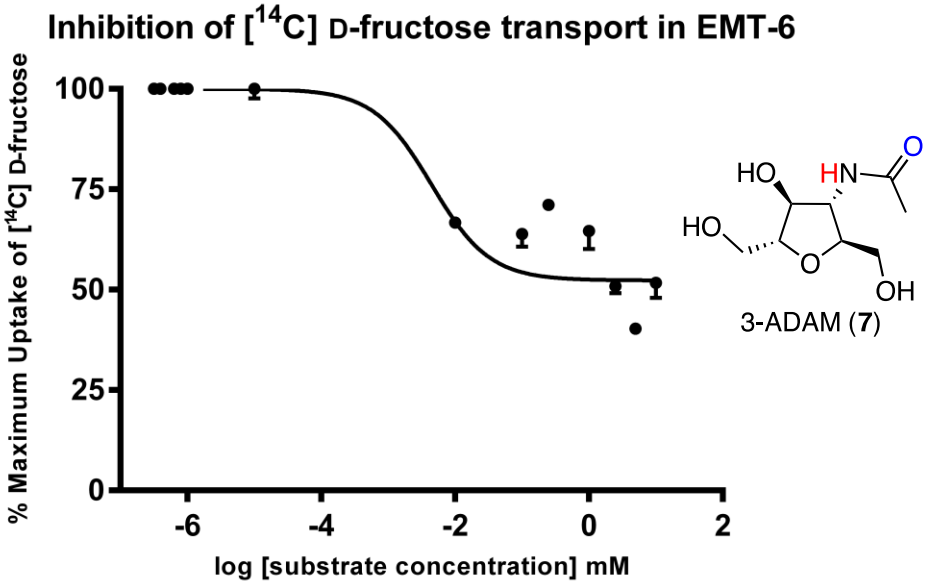

Figure 3.5.12. Concentration dependent [^{14}C]-D-fructose uptake inhibition by 3-ADAM **7** after 25 min incubation at 25 °C into EMT-6 cells. Error bars represent the SEM of triplicates.

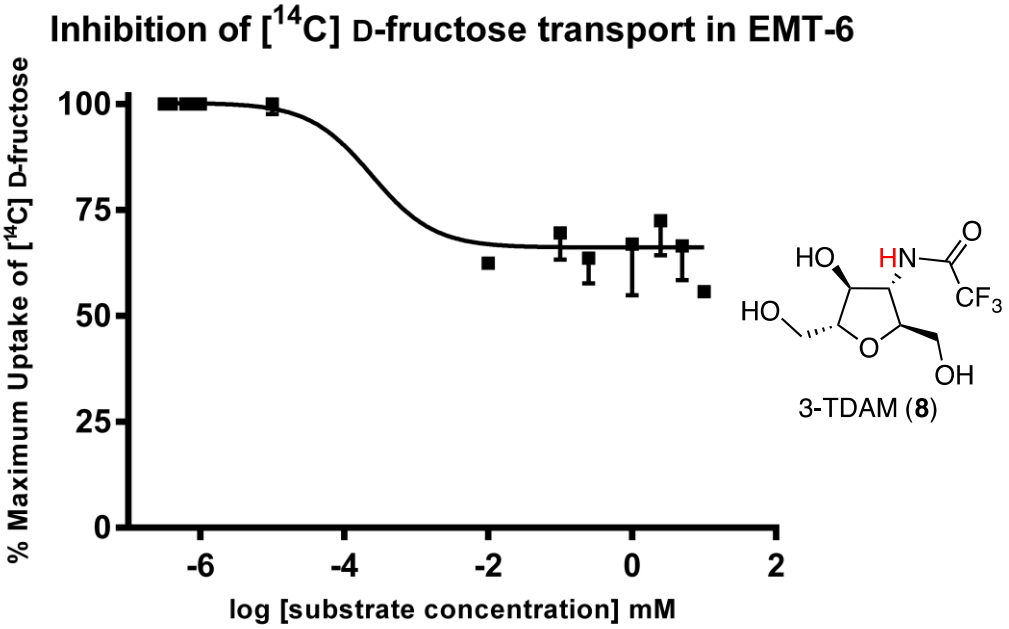

Figure 3.5.13. Concentration dependent [^{14}C]-D-fructose uptake inhibition by 3-TDAM **8** after 25 min incubation at 25 °C into EMT-6 cells. Error bars represent the SEM of triplicates.

Interestingly, 3-TDAM **8**, which holds a stronger hydrogen bond donor, inhibited [^{14}C]-D-fructose transport with lower IC_{50} value (Table 3.5.1), indicating that hydrogen bond donor strength can influence GLUT-substrate binding process. In addition, 3-TDAM **8** inhibited only [^{14}C]-D-fructose transport into EMT-6 cells, but not [^{14}C]-D-glucose transport, indicating specificity for D-fructose transporters. Lack of D-glucose transporter recognition for the trifluoroacetamide **8** could be attributed to the presence of week hydrogen bond acceptor at C-3.[18,21] Importantly, lack of a good hydrogen bond acceptor at C-3 did not influence the D-fructose transporter recognition for TDAM **8**. Thus, presence of the hydrogen bond donor at the C-3 position of the modified 2,5-AM appears to be the only requirement for the D-fructose transporter recognition.

Table 3.5.1 comprises the IC_{50} values observed during the [^{14}C]-D-hexose inhibition by the C-3 modified 2,5-AM derivatives and therefore describes the relative affinity exhibited by the D-glucose and D-fructose transporters for these derivatives. Figure 3.5.14 is a comparison of the [^{14}C]-D-fructose transport inhibitory ability of 2,5-AM derivatives with the natural hexose D-fructose. The C-3 modified 2,5-AM derivatives with amide substituents at C-3 had shown more potency towards the D-fructose transporters than comparison D-fructose. Figure 3.5.15 demonstrates the lower affinity of the D-glucose transporters for the C-3 modified 2,5-AM derivatives when compared to the natural hexose D-glucose.

Table 3.5.1. Summary of D-glucose and D-fructose transporter recognition for C-3 modified 2,5-AM

Derivative	**Donor**[a]	**Acceptor**[b]	**IC_{50} (µM)**[c]	**IC_{50} (µM)**[d]
3-DAM **9**	No	No	No inhibition	No inhibition
3-FDAM **5**	No	Yes	No inhibition	3160
3-AZAM **6**	No	Yes	No inhibition	15.2±0.9
3-TDAM **8**	Yes	Weak	2.4±0.5	No inhibition
3-ADAM **7**	Yes	Yes	4.4±0.4	764±14
3-DNAM **9**	Yes	Yes	8.3±0.2	623±33
2,5-AM **2**	Yes	Yes	226±17	206±21

[a] "Donor" represents the presence of hydrogen bond donor atom at position C-3 of 2,5-AM. [b] "Acceptor" represents the presence of hydrogen bond donor atom at position C-3 of 2,5-AM. [c]IC_{50} values corresponding to the [^{14}C]-D-fructose transport inhibition. [d]IC_{50} values corresponding to the [^{14}C]-D-glucose transport inhibition.

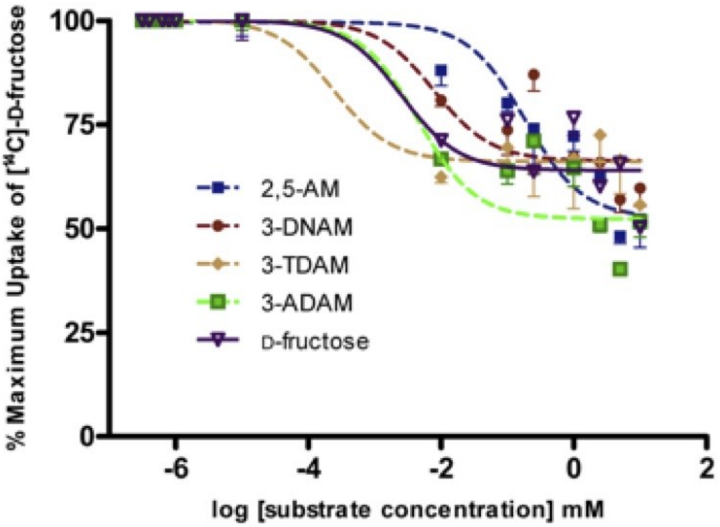

Figure 3.5.14. Comparison of the D-fructose transport inhibitory ability of C-3 modified derivatives with D-fructose. Error bars represent SEM (N=3).

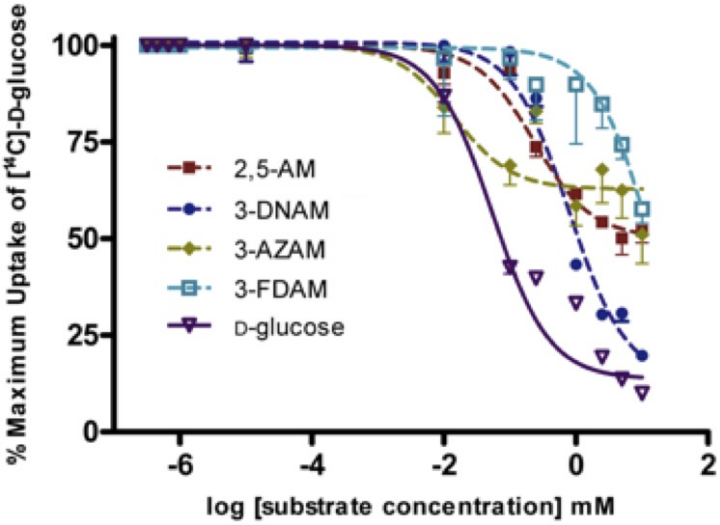

Figure 3.5.15. Comparison of the D-glucose transport inhibitory ability of C-3 modified derivatives with D-glucose. Error bars represent SEM (N=3).

3.6. Ruling out the involvement of conformational and steric aspects induced by the C-3 substituent in the hexose-GLUT recognition process

Conformational changes may play a substantial role in the hexose-GLUT recognition process. Modification of the C-3 substituent could potentially induce changes in the conformation of the hexose molecule. However, involvement of conformation effects as a factor to affect the GLUT-hexose recognition process seems unlikely based the following observations; i) no D-glucose transporter recognition was observed for 3-DAM **10**, whereas sterically similar 3-FDAM **5** displayed D-glucose transporter recognition, ii) 3-TDAM **8** had no D-glucose transporter recognition, but 3-ADAM **7** showed D-glucose transporter recognition, iii) both 2,5-AM **2** and 3-DNAM **9** were recognized by the D-fructose transporter recognition (Figure 3.6.1).

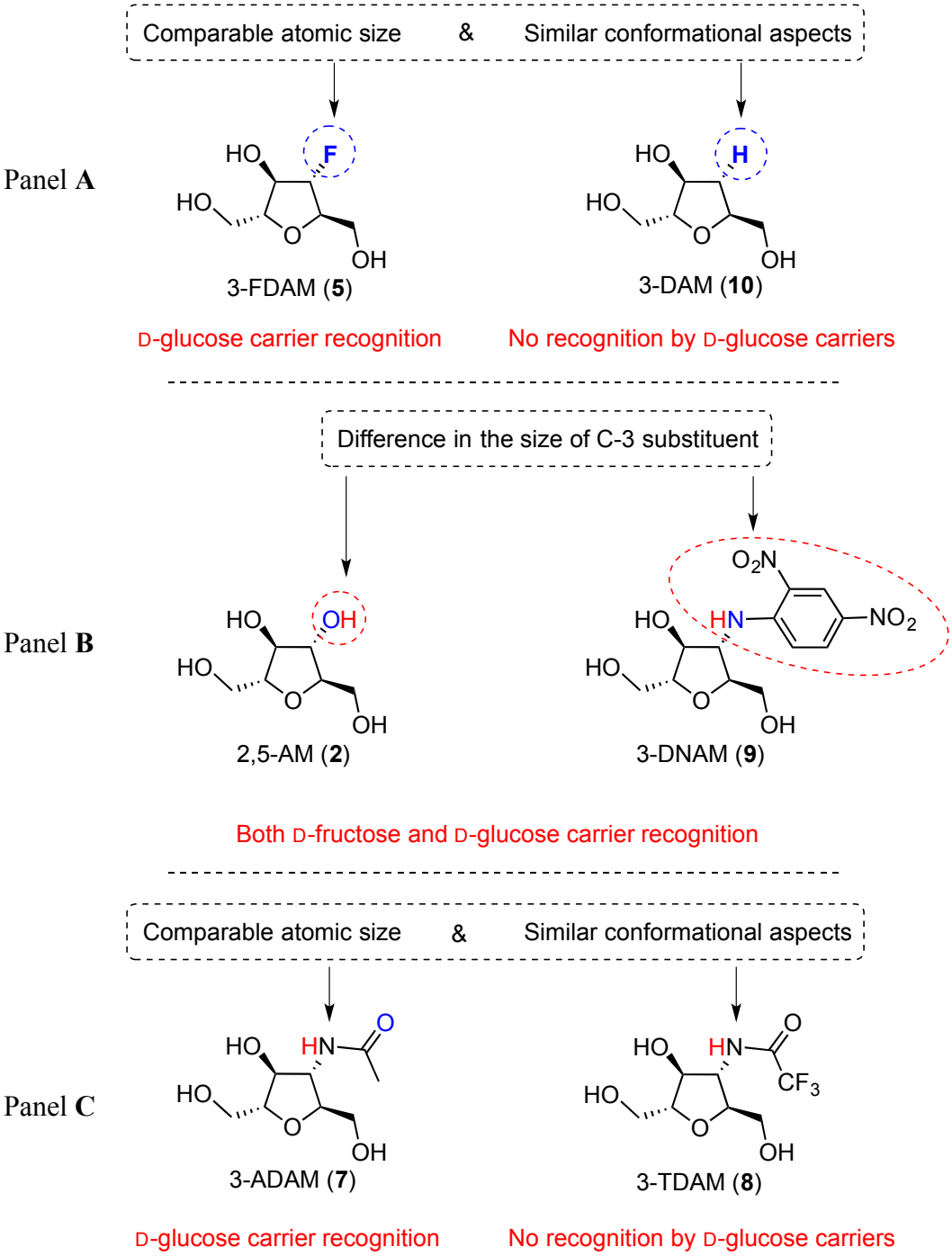

Figure 3.6.1. Illustration of conformational independent GLUT recognition for the C-3 modified 2,5-AM

When a hydrogen atom is replaced with an electronegative atom such as fluorine, it could change the conformational preference of the molecule.[17] However, in Chapter 2, we showed that protons on the furanose ring of compounds **2**, **5**-**10** exhibited similar *J* values in ^{1}H NMR spectrum, indicating the conformational similarity of these compounds. As a result, we expected 3-DAM **10** and 3-FDAM **5** to exist in very similar conformation. Further, due to the comparable atomic size of substituents at C-3 position (hydrogen in the case of 3-DAM **10** and fluorine in the case of 3-FDAM **5**), **5** and **10** exhibit similar steric demands at C-3. Despite the similar conformations and steric bulkiness at the position C-3 of the two molecules, only 3-FDAM **5** displayed D-glucose transporter recognition (Figure 3.6.1, Panel A). Moreover, 3-ADAM **7** and 3-TDAM **8** are expected to have nearly identical steric demand at C-3, yet while both compounds inhibited [^{14}C]-D-fructose uptake, only **7** inhibited [^{14}C]-D-glucose uptake (Figure 3.6.2, Panel C). In the absence of any significant steric or conformational distinction, difference **7** and **8** may derive from their hydrogen bonding properties. Furthermore, a sterically demanding dinitroaromatic substituent at C-3 position did not affect 3-DNAM-GLUT recognition process, indicating the tolerance of GLUTs for steric bulk at C-3 (Figure 3.6.2, Panel B). These observations eliminate the plausibility of the conformational and steric aspects to interfere in the GLUT-hexose process and thereby support our hypothesis of hydrogen bond property of the C-3 substituent playing a substantial role in the GLUT-hexose binding process.

3.7. [^{14}C]-D-hexose transport inhibition studies in the presence of Cytochalasin B

Based on the [^{14}C]-D-hexose transport inhibition studies, GLUTs that are involved in the recognition of the C-3 modified 2,5-AM derivatives cannot be assigned. In order to identify the GLUTs that recognize these derivatives, further evaluations are required. Cytochalasin B (CB, **11**, Figure 3.7.1) is a well-known non-competitive inhibitor of hexose transport through Class-I GLUTs.[24] By repeating [^{14}C]-D-hexose transport inhibition studies with C-3 modified 2,5-AM derivatives in the presence of CB further information about the GLUTs affected by 2,5-AM derivatives can be obtained. Accordingly, we examined [^{14}C]-D-fructose and [^{14}C]-D-glucose transport inhibition by C-3 modified 2,5-AM derivatives in the presence of 100 μM extracellular CB **11**.

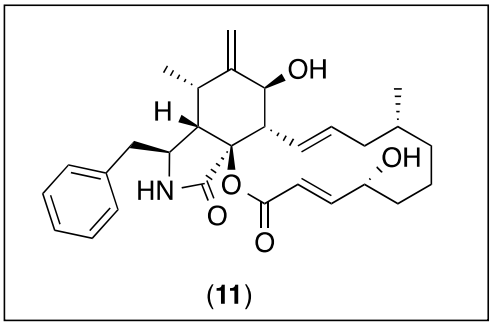

(**11**)

Figure 3.7.1. Structure of CB, a Class-I GLUT inhibitor

As shown in Figure 3.7.2, after the incubation of EMT-6 cells with 100 μM CB, [^{14}C]-D-glucose transport into EMT-6 cells was measured in the presence of 5 mM concentration of extracellular modified 2,5-AM derivative. No further inhibition of [^{14}C]-D-glucose transport was observed into EMT-6 cells when 100 μM CB was co-incubated (Figure 3.7.2). This result confirms that only Class-I D-glucose transporters recognize C-

3 modified 2,5-AM derivatives. Based on Western blot studies, GLUT1 and GLUT2 are the two major D-glucose transporters that are overexpressed in EMT-6 cells (Figure 3.2.1). GLUT1 and GLUT2 facilitate most of the [^{14}C]-D-glucose transport into EMT-6 cells. GLUT1 is a D-glucose transporter, whereas GLUT2 transports D-fructose as well as D-glucose. Both 3-FDAM **5** and 3-AZAM **6** inhibited the transport of [^{14}C]-D-glucose into EMT-6 cells, but not [^{14}C]-D-fructose transport. [^{14}C]-D-Glucose uptake inhibition by 3-FDAM **5** and 3-AZAM **6** in a specific manner (without affecting the D-fructose transport) rules out the possibility of GLUT2 recognition for 3-FDAM **5** and 3-AZAM **6**. In addition, in the presence of CB, no [^{14}C]-D-glucose transport inhibition by 3-FDAM **5** or 3-AZAM **6** was observed. Thus, 3-FDAM **5** or 3-AZAM **6** were identified as GLUT1 ligands.

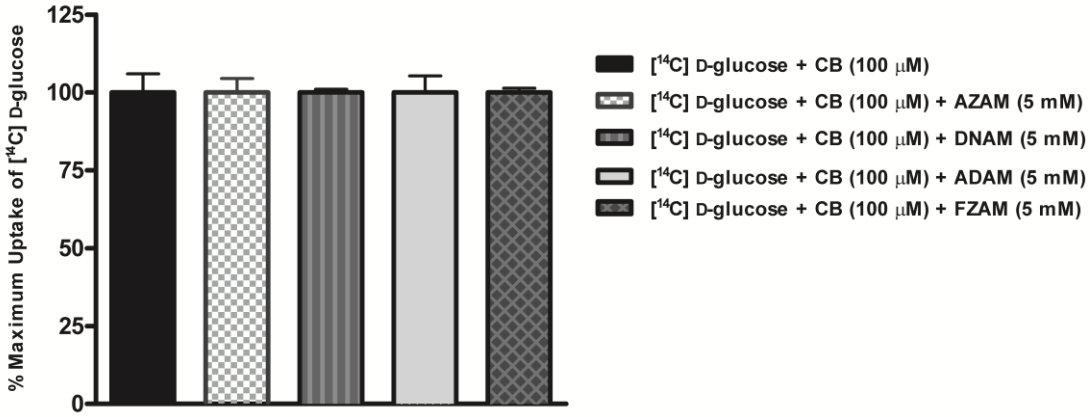

Figure 3.7.2. [^{14}C]-D-Glucose transported into EMT-6 cells after 25 min incubation with a 2,5-AM derivative at 25 °C, pre-incubated with 100 μM CB. Error bars represent the SEM of triplicates.

Figure 3.7.3 shows net [^{14}C]-D-fructose transport inhibition by 3-DNAM **9**, 3-ADAM **7** and 3-TDAM **8** in the presence of CB. This result indicates recognition for these derivatives by Class-II D-fructose transporters, as CB only blocks the transport of

hexoses through Class-I GLUTs. In addition, GLUT5 (a Class-II GLUT) only transports D-fructose, but not D-glucose. Thus, [^{14}C]-D-fructose uptake inhibition by 3-TDAM **8** in a specific manner was an indication of GLUT5 recognition for this substrate. 3-DNAM **9** or 3-ADAM **7** inhibit [^{14}C]-D-glucose transport into EMT-6 cells only in the absence of CB, but not in the presence of extracellular CB. Moreover 3-DNAM **9** or 3-ADAM **7** also inhibit [^{14}C]-D-fructose transport irrespective of the presence of extracellular CB. Clearly, Class-I D-glucose transporters and Class-II D-fructose transporters recognize 3-DNAM **9** and 3-ADAM **7**. Furthermore, previously, GLUT1 recognition was concluded for 3-AZAM **6** and 3-FDAM **5**, which contain the hydrogen bond acceptor functionality at C-3 position. 3-DNAM **9** and 3-ADAM **7** also possess hydrogen bond acceptor functionalities at C-3 and are structurally similar to 3-AZAM **6** and 3-FDAM **5**. As a result, GLUT1 recognition is also likely for 3-DNAM **9** and 3-ADAM **7**. However, to confirm the GLUT1 and/or GLUT5 recognition for the C-3 modified 2,5-AM derivatives further studies are required.

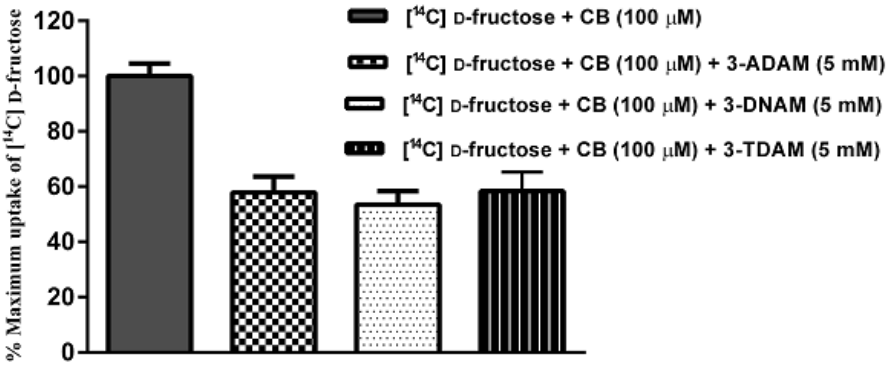

Figure 3.7.3. [^{14}C]-D-fructose transported into EMT-6 cells after 25 min incubation with a 2,5-AM derivative at 25 °C, pre-incubated with 100 μM CB. Error bars represent the SEM of triplicates.

3.8. Study with GLUT1 and GLUT5 mRNA injected Xenopus laevis oocytes

To confirm GLUT5 recognition, we studied the potential of the C-3 modified 2,5-AM derivatives to inhibit the net [^{14}C]-D-fructose transport facilitated by GLUT5. To measure fructose transport by GLUT5, we used Xenopus laevis oocytes as GLUT5 negative cell model. These oocytes were surgically removed and processed by D. O′Neill. We first measured the amount of D-fructose transported into water-injected oocytes, mediated by the natural transporters expressed in oocytes (background). Next, we measured fructose transported into oocytes injected GLUT5 mRNA. By subtracting the amount of [^{14}C]-D-fructose transported by natural D-fructose transporters found in oocytes from the amount of [^{14}C]-D-fructose transported into GLUT5 injected oocytes, we measured the net transport of fructose facilitated by GLUT5. We then measured net fructose transport by GLUT5 in the presence of 5 mM concentrations of 3-DNAM **9**, 3-ADAM **7** and 3-TDAM **8**. We observed significant inhibition of net fructose transport facilitated by GLUT5 in the presence of extracellular 3-DNAM **9**, 3-ADAM **7** and 3-TDAM **8** (Figure 3.8.1). Consequently, GLUT5 recognition for C-3 modified 2,5-AM derivatives was confirmed.

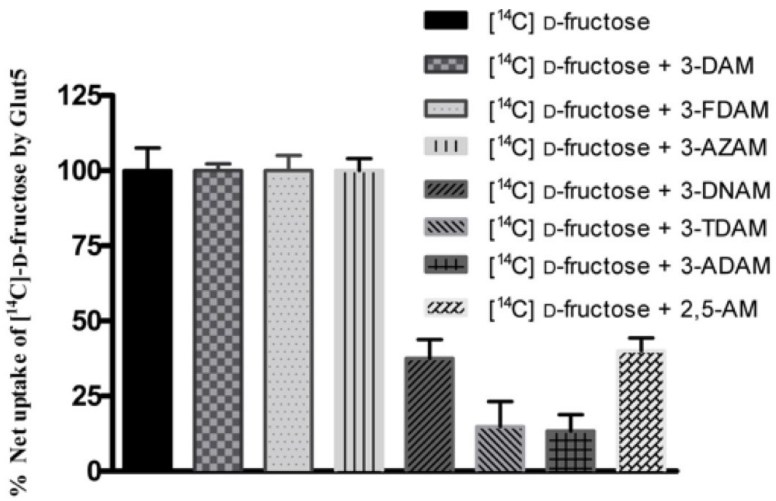

Figure 3.8.1. Inhibition of GLUT5 facilitated [^{14}C]-D-fructose transport by C-3 modified 2,5-AM derivatives, after 40 min incubation at 25 °C into GLUT5 mRNA injected oocytes. Error bars represent the SEM of triplicates.

As discussed in the previous section, the net [^{14}C]-D-hexose transport that is mediated by a particular GLUT can be calculated by experiments with water and GLUT mRNA injected oocytes. We used oocytes injected with either GLUT1 mRNA or water to determine glucose transport mediated by GLUT1. Figure 3.8.2 shows the inhibition of net [^{14}C]-D-glucose transport facilitated by GLUT1 with the addition of 5 mM extracellular concentration of 3-AZAM **6**, 3-DNAM **9**, 2,5-AM **2** and 3-ADAM **7**, affirming GLUT1 recognition for these C-3 modified 2,5-AM derivatives.

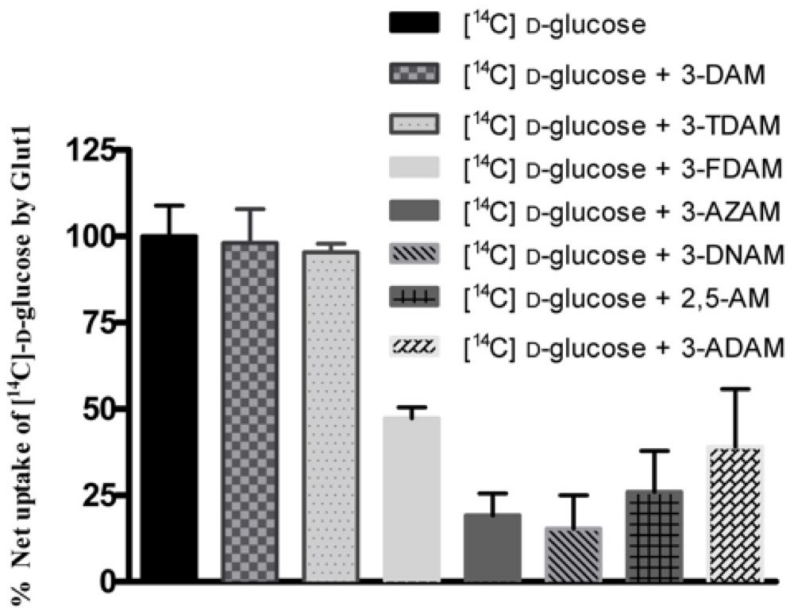

Figure 3.8.2. Inhibition of GLUT1 facilitated [^{14}C]-D-glucose transport by C-3 modified 2,5-AM derivatives, after 40 min incubation at 25 °C into GLUT1 mRNA injected oocytes. Error bars represent the SEM of triplicates.

3.9. Docking study with C-3 modified 2,5-AM derivatives

The X-ray crystal structures of the human glucose transporter proteins GLUT1 and GLUT5 were obtained from the protein data bank. *In silico* docking studies were performed by R. Panigrahi and J. Lemieux using AutoDock® software to compare with the experimental results. To our delight, we observed correlation between experimental and computational results. The C-3 functionalized 2,5-AM derivatives that retained a hydrogen bond acceptor at the C-3 position (3-FDAM **5**, 3-AZAM **6**, 3-ADAM **7** and 3-DNAM **9**) displayed binding to the inward-open conformation of GLUT1. Importantly, C-3 modified 2,5-AM derivatives were demonstrated to bind to the same binding pocket to which D-glucose is known to bind (Figure 3.9.1). As it has been observed experimentally, 3-DAM **10** did not bind to the inward-open configuration of GLUT1.

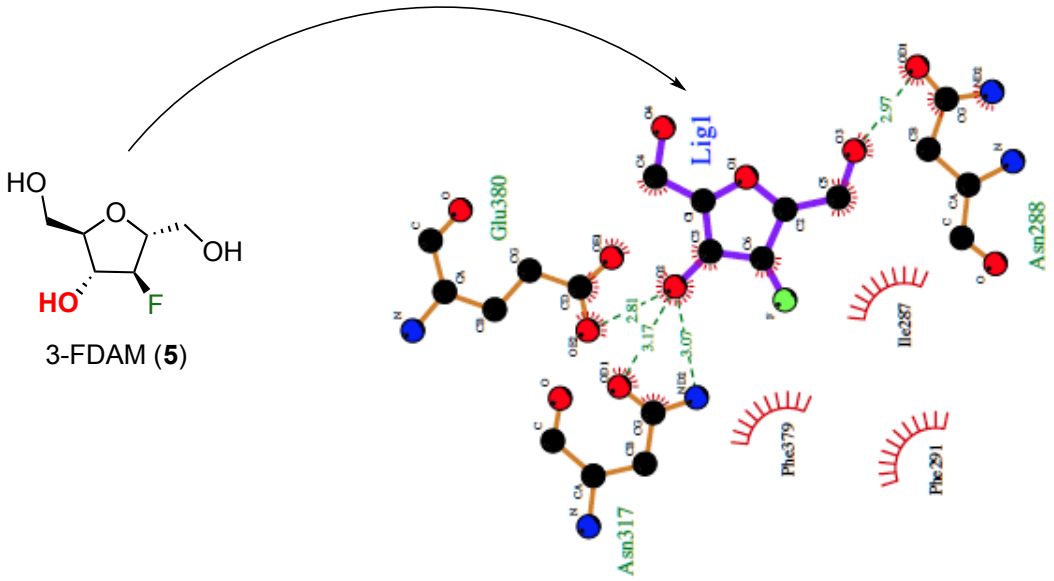

Figure 3.9.1. A cartoon to demonstrate the *in silico* binding analysis of 3-FDAM **5** with the inward-open conformer of GLUT1.

Very similar to the experimental results, the C-3 functionalized 2,5-AM derivatives that retained a hydrogen bond donor at the C-3 position (2,5-AM **2**, 3-ADAM **7**, 3-TDAM and 3-DNAM **9**) displayed binding to the inward-open conformation of GLUT5. Importantly, C-3 modified 2,5-AM derivatives were demonstrated to bind to the same binding pocket to which D-fructose is known to bind (Figure 3.9.2). As it has been observed experimentally, 3-FDAM **5** that lacked a hydrogen bond donor at C-3 did not bind to the inward-open configuration of GLUT5.

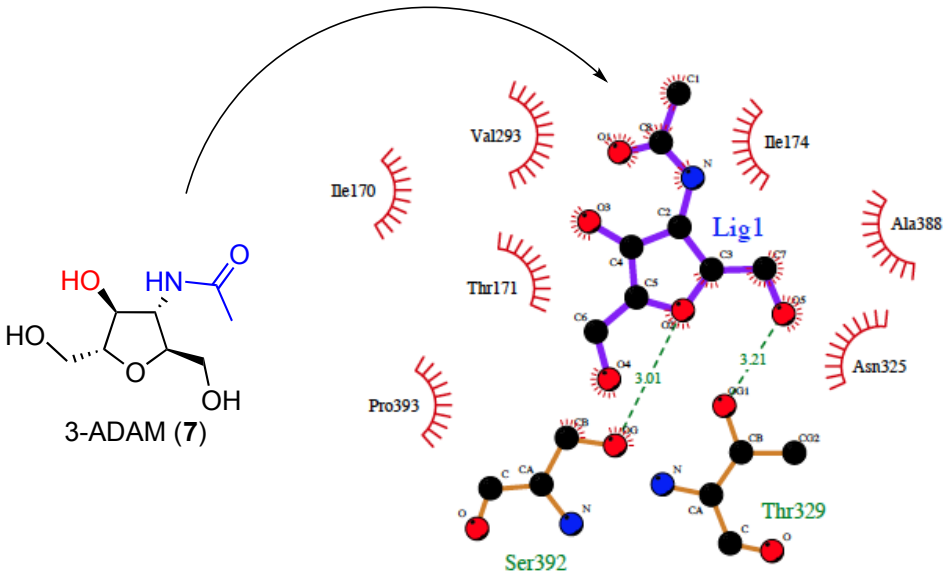

Figure 3.9.2. A cartoon to demonstrate the *in silico* binding analysis of 3-ADAM **7** with the inward-open conformer of GLUT5.

3.10. Conclusion

We investigated the D-hexose transport inhibition of selected 2,5-AM derivatives and performed various control experiments to conclude GLUT recognition for these derivatives. All the above results conclude that retention of a hydrogen bond donor at C-3 position is key for GLUT5 recognition, whereas hydrogen bond acceptor retention is crucial for GLUT1 recognition for C-3 modified 2,5-AM derivatives. Our studies also emphasize that the C-3 position of 2,5-AM is pivotal for tuning the selectivity between GLUT1 and GLUT5, which provides fundamental guidelines to develop 2,5-AM based probes for breast cancer diagnosis. A recent report demonstrated that single point mutation of GLUT5 changes the substrate affinity from D-fructose to D-glucose, indicating similarity between GLUT1 and GLUT5 binding pockets.[25] In complement to the mutation result, we observed modification of a single position (C-3) of a hexose (2,5-AM) changes the transport protein recognition from GLUT5 to GLUT1. In Table 3.10.1,

a summary of variety of 2,5-AM derivatives and their recognition by GLUT1/GLUT5 is found. In general, the hydroxyl groups that are key for the GLUT-hexose recognition process, are labeled as "essential hydroxyl groups". Such hydroxyl groups are untouched during hexose based tracer development to retain a particular GLUT recognition. Our results concluded that GLUT-hexose recognition is a function of hydrogen bond donor/acceptor properties, and demonstrated the modification of one of the "essential hydroxyl group" while retaining hexose recognition by the GLUT.

Table 3.10.1. Summary of GLUT recognition for C-3 modified 2,5-AM derivatives

Derivative	H-bond donor	H-bond acceptor	Recognition
3-DAM	No	No	--
3-FDAM	No	Yes	GLUT1
3-AZAM	No	Yes	GLUT1
3-TDAM	Yes	Weak	GLUT5
3-ADAM	Yes	Yes	GLUT5 + GLUT1
3-DNAM	Yes	Yes	GLUT5 + GLUT1
3-AM	Yes	Yes	GLUT5 + GLUT1

To date, D-glucose derivatives were known to be transported by GLUT1 and GLUT2, whereas D-fructose derivatives were demonstrated to target GLUT2 and GLUT5. In this study, 2,5-AM-based scaffolds were demonstrated to target both GLUT1 and GLUT5. Such scaffolds could be useful to develop tracers that can be used for the diagnosis of wide-range of cancer types, irrespective of the metabolic needs of the cancer cells (D-fructose or D-glucose).

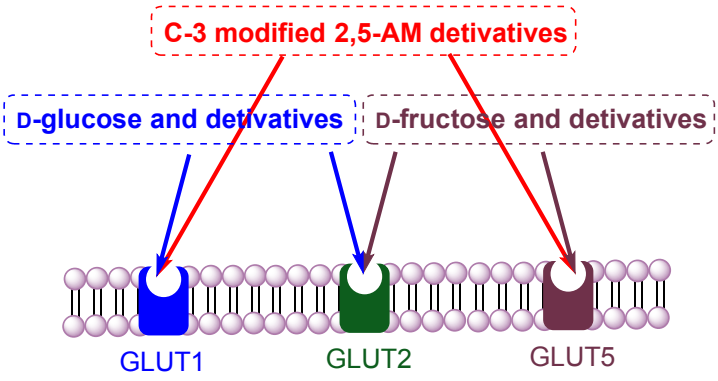

Figure 3.10.1. Comparison of 2,5-AM derivatives to D-fructose and D-glucose derivatives, in terms of GLUT targeting.

3.11. Future directions

The C-3 modified 2,5-AM derivatives can serve as scaffolds for the development of highly selective probes to target GLUT1 or GLUT5. Given ready access to the X-ray structures of GLUT1 and GLUT5, the amino acids that interact with these derivatives can be identified by molecular dynamics simulation of GLUT-ligand complexes. Mutation study of the mRNA could confirm the key amino acids involved in GLUT-substrate binding. Importantly, these scaffolds could be useful to develop tracers that can target both GLUT1 and GLUT5 for the molecular imaging. Such tracers could serve efficiently in the diagnosis of a wide variety of tumors.

3.12. Experimental section

Reactions were carried out in flame-dried glassware under a positive argon atmosphere unless otherwise stated. Transfer of anhydrous solvents and reagents was accomplished with oven-dried syringes or cannulae. Solvents were distilled before use (except MeOH and CH_3CN): dimethylformamide (DMF) from calcium hydride and pyridine from KOH.

MeOH and CH_3CN were purchased from Sigma-Aldrich® company, and were used without distillation. All the commercially available solvents and reagents were used without further purification. Reagents were purchased from Sigma-Aldrich company. Thin layer chromatography was performed on glass plates precoated with 0.25 mm silica gel. For the spot visualization, TLCs were treated with 2.5% *p*-anisaldehyde in AcOH-H_2SO_4-EOH (1:3:86) and heated until color development. Flash chromatography columns were packed with 230–400 mesh silica gel with the specified solvent system. Optical rotations (deg cm^2 g^{-1}) were measured with Perkin Elmer 241 polarimeter, using the D-line of sodium lamp (λ = 589.3 nm) at 22 ± 2 °C. Proton nuclear magnetic resonance spectra (^{1}H NMR) were recorded at 400 MHz or 500 MHz in indicated deuterated solvents and were reported in ppm in the presence of TMS as internal standard. The coupling constants (*J*) are reported in hertz (Hz) and standard notation was used to describe the multiplicity of signals observed in ^{1}H NMR spectra: broad (br), multiplet (m), singlet (s), doublet (d), triplet (t), etc. Carbon nuclear magnetic resonance spectra (^{13}C NMR) were recorded at 100 MHz or 125 MHz. The spectra were referenced to the residual solvent present in the deuterated solvent (*e.g.* $CDCl_3$: δ = 77.26 ppm, ^{13}C; 7.26 ppm, ^{1}H). Infrared (IR) spectra were measured with a Nic-Plan FTIR Microscope. IR spectra were recorded neat and reported in cm^{-1}. Mass spectra were determined on a high-resolution electrospray positive ion mode spectrometer.

Beckman LS 6500 multi-purpose scintillation counter was used for the determination ^{14}C isotope concentration. Glucose free Krebs-Ringer buffer solution (120 mM NaCl, 25 mM $NaHCO_3$, 4 mM KCl, 1.2 mM KH_2PO_4, 2.5 mM $MgSO_4$, 70 μM

$CaCl_2$, pH 7.4) was used to for the studies with EMT-6 cells. Modified Barth's medium (MBM buffer) was used for the studies with oocytes (88 mM NaCl, 1 mM KCl, 0.33 mM $Ca(NO_3)_2$, 0.82 mM $MgSO_4$, 2.4 mM $NaHCO_3$, 0.4 mM $CaCl_2$, 20 mM HEPES, pH 7.4). [^{14}C]-D-hexoses with specified activity were purchased from Moravek Biochemicals.

3-Acetamido-3-deoxy-2,5-anhydro-D-mannitol (8).

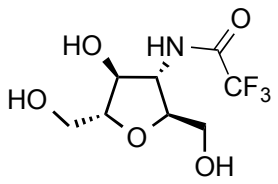

A 50 mL round bottom flask was charged with azide **6** (0.25 g, 1.3 mmol) and MeOH (25 mL). To this mixture, 10% Pd/C (0.05 g, 20% by weight) was added and the resulting heterogeneous mixture was stirred at room temperature, under H_2 atmosphere (1 atm). After stirring for 2 h, solids were filtered out and washed with MeOH (10-20 mL). The filtrate was taken into a 100 mL round bottom flask and MeOH was partially evaporated to concentrate the solution (ca. 25 mL). To this mixture, activated ester ethyl trifluoroacetate (1.20 mL, 10.1 mmol) and excess of $NaHCO_3$ were added. This heterogeneous mixture was heated at 40 ^{o}C for 24 h. Solids were filtered off and washed with excess of MeOH. Evaporation of MeOH under reduced pressure yielded a viscous syrup, which was subjected to silica gel column chromatography using DCM:MeOH mixture (gradient from 100:0 to 80:20). Fractions with compound were combined and concentrated under vacuum to yield clear crystals of **8** (0.243 g, 73% over two steps). R_f

0.37 (DCM: MeOH, 85:15,); m.p. 58.9-60.7 ^{o}C; $[\alpha]_D^{20}$ +30.3 (*c* 1.60, MeOH); IR (cast film) 3305, 3099, 2932, 2882, 1708, 1567, 1385, 1216, 1189, 1161, 1053, 935, 898 cm^{-1}; ^{1}H NMR (500 MHz, D_2O): δ 4.37 (app t, *J* = 7.9 Hz, 1H), 4.23 (app t, *J* = 7.5 Hz, 1H) 4.01 (ddd, *J* = 8.3, 5.0, 3.0 Hz, 1H) 3.96 (ddd, *J* = 7.5, 5.0, 3.0 Hz, 1H), 3.80 (dd, *J* = 12.6, 3.0 Hz, 1H), 3.75 (dd, *J* = 12.6, 3.0 Hz, 1H), 3.68 (dd, *J* = 12.6, 4.6 Hz, 1H), 3.65 (dd, *J* = 12.6, 4.8 Hz, 1H); ^{13}C NMR (125 MHz, D_2O): δ 159.2 (q, J_{C-F} = 37.9 Hz), 115.7 (q, J_{C-F} = 285.8 Hz), 82.5, 80.0, 74.1, 61.1, 60.7, 57.0; HRMS (ESI) calcd for $C_8H_{12}NF_3O_5Na$ [M+Na^+] 282.0560; found 282.0562.

3-(*N*-2,4-Dinitrophenyl)amino-2,5-anhydro-D-mannitol (9).

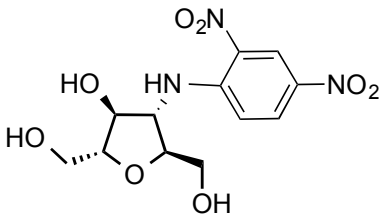

Azide **6** (0.25g, 1.3 mmol) and of DMF (10 mL) were stirred in a 50 mL round bottom flask under Ar atmosphere. After 5 min stirring, imidazole (0.21 g, 3.0 mmol) and *tert*-butyl(chloro)dimethylsilane (0.45 g, 3.0 mmol) were added to the flask and the stirring was continued for 6 h. The crude reaction mixture was diluted with 100 mL of DCM and washed with brine solution (2 x 25 mL). The organic layer was dried over Na_2SO_4. Solids were filtered and the organic solvent was evaporated under reduced pressure to yield a thick oil, which was carried on directly to the next step.

The thick oil obtained from the previous transformation was dissolved in MeOH (25 mL). To this homogeneous solution, 10% Pd/C (0.05 g, 20% by weight) was added and the resulting heterogeneous mixture was stirred at room temperature under H_2 atmosphere (1 atm). After stirring for 2 h, solids were filtered out and washed with MeOH (20 mL). The filtrate was taken into a 50 mL round bottom flask in portions and MeOH was completely evaporated under reduced pressure to yield a thick syrup.

The syrup obtained from the previous transformation was dissolved in acetonitrile (10 mL) under argon and an excess of (ca. 0.5 g) of Na_2CO_3 was added. To this heterogeneous mixture, (0.6 g, 3.0 mmol) of 1-chloro-2,4-dinitro-benzene was added and vigorous stirring was continued for 12 h. Excess Na_2CO_3 was separated from the reaction mixture by filtration. The filtrate was concentrated under reduced pressure to yield a yellow paste, which was dissolved in 15 mL of MeOH. To the yellow colored homogeneous mixture, 4 mL of 90% trifluoroacetic acid solution was added. After 8 h of stirring at rt, solvents were evaporated from the reaction mixture to yield a yellow syrup. The resultant syrup was dissolved in 30 mL of MeOH and 2 g of Na_2CO_3 was added. The heterogeneous mixture was vigorously stirred for 2 hours, before the solids removed by filtration. The filtrate was evaporated under vacuum and the crude compound was subjected to silica gel column chromatography using DCM:MeOH mixture (100:0 to 80:20). Fractions with compound were combined and concentrated under vacuum to yield yellow oil (0.1 g, 32%). R_f 0.25 (DCM: MeOH, 80:20); $[\alpha]_D^{20}$ +31.9 (*c* 1.60, MeOH); IR (cast film) 3345, 3104, 2930, 1617, 1522, 1503, 1428, 1284, 1139, 1057, 765 cm^{-1}; ^1H NMR (500 MHz, CD_3OD): δ 9.04 (d, J = 2.7 Hz, 1H), 8.30 (dd, J = 9.5, 2.7 Hz, 1H),

7.54 (d, J = 9.5 Hz, 1H), 4.36 (app t, J = 5.5 Hz, 1 H), 4.28 (app t, J = 5.5 Hz, 1H), 4.07 (dt, J = 5.5, 4.4 Hz, 1H), 4.01-3.97 (m, 1H), 3.81 (dd, J = 11.9, 4.4 Hz, 1H), 3.77 (dd, J = 12.0, 2.7 Hz, 1H), 3.67 (dd, J = 12.0, 4.4 Hz, 1H), 3.65 (dd, J = 11.9, 2.7 Hz, 1H); ^{13}C NMR (125 MHz, CD_3OD): δ 148.0, 136.1, 130.7, 129.6, 123.2, 115.2, 85.3, 83.3, 77.3, 61.65, 61.60, 61.2; HRMS (ESI) calcd for $C_{12}H_{16}N_3O_8$ [M+H$^+$] 330.0932; found 330.0932.

3-Deoxy-2,5-anhydro-D-arabino-hexitol (10).

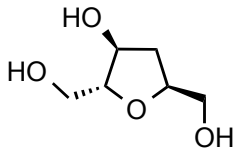

2,5:3,4-Dianhydro-D-allitol (0.31 g, 2.1 mmol) was dissolved in EtOH (50 mL). To this mixture, 20% $Pd(OH)_2/C$ (0.06 g, 20% by weight) was added and the resulting heterogeneous mixture was stirred at room temperature, under H_2 atmosphere (1 atm). After stirring for 2 h, solids were filtered out and washed with MeOH (20 mL). The filtrate was evaporated under reduced pressure to yield a colorless oil in quantitative yields. Spectral data matches to the literature report.[19] ^{13}C NMR (125 MHz, D_2O): δ 79.2, 77.7, 61.3, 60.4, 57.7, 57.5.

Cell culture: EMT-6 cells were grown in a 5% CO_2 incubator at 37 °C in Gibco® DMEM-F12 media supplemented with 15 mM HEPES, L-GLUTamine, 10% Fetal

Bovune and 1% Penicillin/Streptomycin with media renewal every 2 to 3 days. (K. Wong grew the EMT-6 cells for the [^{14}C]-hexose uptake inhibition studies).

General procedure for the [^{14}C]-D-hexose transport inhibition study.

Radioactive "Hot" flux solutions were prepared by mixing 5 μL of [^{14}C] D-glucose or [^{14}C] D-fructose (solution in EtOH, specific activity approximately 1 mCi/mL), 50 μL of 100 mM D-fructose or D-glucose and 945 μL Krebs-Ringer solution of a substrate with specified concentration. EMT-6 cells were grown to confluence in 12 well NEST® cell culture plates with media removal every 2 days. One hour before performing the flux study, EMT-6 cells were washed twice with Krebs-Ringer buffer solution. To each well 1 mL of Krebs-Ringer buffer was added and incubation at 37 °C was continued for one h, in order to deplete the nutrients present in the cells. After one h of incubation, Krebs-Ringer buffer was removed and 300 μL of radioactive "Hot" flux solution was added into each well. After incubation at 25 °C for 25 min, media was aspirated and each well was rinsed twice with ice-cold Krebs-Ringer solution. To each well 500 μL of 5% trifluoroacetic acid was added to lyse the cells. After one hour of cell lysing, 400 μL of cell lysate from each well was transferred into scintillation vials containing 5 mL of Scinti-Safe™ liquid scintillation fluid for counting in a liquid scintillation counter.

[^{14}C]-D-hexose transport inhibition study in the presence of CB: Radioactive "Hot" flux solutions were prepared by mixing 5 μL of [^{14}C]-D-glucose or [^{14}C]-D-fructose (solution in EtOH, specific activity approximately 1 mCi/mL), 50 μL of 100 mM D-fructose or D-glucose, 10 μL of 10 mM CB (purchased from SIGMA-ALDRICH®) and 935 μL of Krebs-Ringer solution of a substrate with specified concentration. EMT-6 cells

were grown to confluence in 12 well NEST® cell culture plates with media removal every 2 days. One h before performing the flux study, EMT-6 cells were washed twice with Krebs-Ringer buffer solution. To each well 1 mL of Krebs-Ringer buffer was added and incubation at 37 °C was continued for one h, in order to deprive the nutrients present in the cells. After one h of incubation, Krebs-Ringer buffer was removed and 300 μL of radioactive "Hot" flux solution was added into each well. After incubation at 25 °C for 25 min, media was aspirated and each well was rinsed twice with ice-cold Krebs-Ringer solution. To each well 500 μL of 5% trifluoroacetic acid was added to lyse the cells. After one hour of cell lysing, 400 μL of cell lysate from each well was transferred into scintillation vials containing 5 mL of Scinti-Safe™ liquid scintillation fluid for counting in a liquid scintillation counter.

Inhibition of D-hexose uptake by 2,5-AM derivatives in GLUT1 or GLUT5 mRNA injected oocytes: Xenopus laevis oocytes were surgically removed, processed and injected with mRNA by D. O′Neill. Radioactive "Hot" flux solutions were prepared by mixing 5 μL of [^{14}C]-D-glucose or [^{14}C]-D-fructose (solution in EtOH, specific activity approximately 1 mCi/mL), 50 μL of 100 mM D-fructose and 945 μL of MBM buffer solution or 945 μL of MBM buffer solution with 5 mM substrate. Four clean test tubes were labeled as W1, W2, G1 and G2. To each of W1 and W2 test tubes, 15 water injected oocytes were added. Similarly, to each of G and G2 test tubes, 15 GLUT (GLUT1 or GLUT5) mRNA injected oocytes were added. Oocytes in the test tubes W1 and G1 were subjected for incubation with 500 μM of hot flux solution that does not contain substrate, for 45 min at room temperature. To the test tubes W2 and G2, 500 μM of hot flux

solution that contain 5 mM concentration of a particular substrate was added and incubation was continued for 45 min at room temperature. After the incubation period, the flux solution from each test tube was aspirated and carefully washed with cold MBM buffer (10x1 mL). To each test tube, 500 μL of 1% SDS lysing buffer was added and the oocytes were thoroughly lysed with the assistance of pipette tip. 400 μL of the cell lysate from each test tube was transferred into scintillation vials containing 5 mL of Scinti-Safe^{TM} liquid scintillation fluid for counting in a liquid scintillation counter (Beckman LS 6500 multi-purpose scintillation counter).

Data analysis

In the inhibition experiments performed, counts per minute (CPM) were normalized to standards by the subtraction of the background levels and then plotted against the maximum uptake of the radiolabeled hexose (i.e. [^{14}C]-D-fructose or [^{14}C]-D-glucose). For time courses, values were corrected with standards and to the protein levels present per well. IC_{50} values (concentration at which half maximum inhibition of cellular uptake of a radiotracer was observed) were determined using non-linear regression analysis in GraphPad Prism 5 (GraphPad Software, San Diego, CA, USA), and significance was determined at $p < 0.05$ using a Student's t-test.

3.13. References

1) Wuest, M., Trayner, B. J., Grant, T. N., Jans, H. S., Mercer, J. R., Murray, D., West, F. G., McEwan, A. J. B., Wuest, F. & Cheeseman, C. I. Radiopharmacological

evaluation of 6-deoxy-6-[^{18}F]fluoro-D-fructose as a tracer for PET imaging of breast cancer. *Nucl. Med. Biol.* **38**, 461-475 (2011).

2) Soueidan, O. M., Trayner, B. J., Grant, T. N., Henderson, J. R., Wuest, F., West, F. G. & Cheeseman, C. I. New fluorinated fructose analogs as selective probes of hexose transport protein GLUT5. *Org. Biomol. Chem.* **13**, 6511-6521 (2015).

3) Godoy, A., Ulloa, V., Rodriguez, F., Reinicke, K., YaÑez, A. J., GarcÍa, M. A., Medina, R. A., Carrasco, M., Barberis, S., Castro, T., MartÍnez, F., Koch, X., Vera, J. C., Poblete. M. T., Figueroa, C.D., Peruzzo, B., PÉrez, F., Nualart, F. Differential subcellular distribution of glucose transporters GLUT1-6 and GLUT9 in human cancer: Ultrastructural localization of GLUT1 and GLUT5 in breast tumor cells. *J. Cell. Physiol.* **207**, 614-627 (2006); Zamora-Leon, S. P., Golde, D. W., Concha, I. I., Rivas, C. I., Delgado-López, F. & Vera, J. C. Expression of the fructose transporter GLUT5 in human breast cancer. *Proc. Natl. Acad. Sci. USA*. **93**, 1847-1852 (1996).

4) Haradahira, T. *et al.* Radiosynthesis, rodent biodistribution, and metabolism of 1-deoxy-1-[^{18}F]fluoro-D-fructose. *Nucl. Med. Biol.* **22**, 719–725 (1995).

5) Czernin, J. & Phelps, M. E. Positron emission tomography scanning: current and future applications. *Annu. Rev. Med.* **53**, 89–112 (2002).

6) Thorens, B. & Mueckler, M. Glucose transporters in the 21st century. *Am. J. Physiol. Endocrinol. Metab*. **298**, E141-E145 (2010).

7) Gould, G. & Holman, G. D. The glucose transporter family: Structure, function and tissue specific expression. *Biochem. J.* **295**, 329-341 (1993).

8) Manolescu, A. R., Witkowska, K., Kinnaird, A., Cessford, T. & Cheeseman C. Facilitated hexose transporters: New perspectives on form and function. *Physiology* **22**, 234-240 (2007).

9) McQuade, D. T., Plutschack, M. B. & Seeberger, P. H. Passive fructose transporters in disease: A molecular overview of their structural specificity. *Org. Biomol. Chem*. **11**, 4909-4920 (2013).

10) Mueckler, M. & Thorens, B. The SLC2 (GLUT) family of membrane transporters. *Mol. Aspects Med*. **34**, 121-138 (2013).

11) Long, W. & Cheeseman, C. I. Structure and functional insights into GLUT family of membrane transporters. *Cell Health and Cytoskeleton*. **7**, 167-183 (2015).

12) Deng, D. & Yan, N. GLUT, SGLT, and SWEET: Structural and mechanistic investigation of the glucose transporters. *Protein Sci.* **25**, 546-558 (2016).

13) Tatibouet, A., Yang, J., Morin, C. & Holman, G. D. Synthesis and evaluation of fructose analogues as inhibitors of the D-fructose transporter GLUT5. *Bioorg. Med. Chem.* **8**, 1825-1833 (2000); Haradahira, T. *et al.* Radiosynthesis, rodent biodistribution, and metabolism of 1-deoxy-1-[^{18}F]-fluoro-D-fructose. *Nucl. Med. Biol.* **22**, 719–725 (1995).

14) Girniene, J., Tatibouët, A., Sackus, A., Yang, J., Holman, G. D. & Rollin, P. Inhibition of the D-fructose transporter protein GLUT5 by fused-ring glycol-1,3-oxazolidin-2-thiones and oxazolidin-2-ones. *Carbohydrate Res.* **338**, 711-719 (2003).

15) Fileti, E. E., Chaudhuri, P. & Canuto, S. Relative strength of hydrogen bond interaction in alcohol–water complexes. *Chem. Phys. Lett.* **400,** 494–499 (2004).

16) Brammer, L., Bruton, E. A. & Sherwood, P. Understanding the behavior of halogens as hydrogen bond acceptors. *Cryst. Growth Des.* **1,** 277–290 (2001).

17) Schneider, H.-J. Hydrogen bonds with fluorine. Studies in solution, in gas phase and by computations, conflicting conclusions from crystallographic analyses. *Chem. Sci.* **3,** 1381-1394 (2012); Hunter, L. The C-F bond as a conformational tool in organic and biological chemistry. *Beilstein J. Org. Chem.* **6,** 38 (2010).

18) Platts, J. A., Maarof, H., Harris, K. D. M., Lim, G. K. & Willock, D. J. The effect of intermolecular hydrogen bonding on the planarity of amides. *Phys. Chem. Chem. Phys.* **14,** 11944–52 (2012); Johansson, A., Kollman, P., Rothenberg, S. & McKelvey, J. Hydrogen bonding ability of the amide group. *J. Am. Chem. Soc.* **96,** 3794–3800 (1974).

19) Garcia, J. G., Voll, R. J. & Younathan, E. S. Stereoselective carbohydate synthesis *via* palladium hydroxide catalyzed epoxide hydrogenolysis. *Tetrahedron Lett*. **32**, 5273-5276, (1991).

20) Machado, A. S., Olesker, A., Castillon, S. & Lukacs, G. Hydroxy group directed hydrogenation with rhodium and iridium catalysts. Synthesis of a protected chiral carbocyclic analogue of daunosamine. *J. Chem. Soc. Chem. Commun.* 330 (1985); Stork, G. & Kahne, D. E. Stereocontrol in homogeneous catalytic hydrogenation via hydroxyl group coordination. *J. Am. Chem. Soc.* **105,** 1072–1073 (1983).

21) Steiner, T. The hydrogen bond in the solid state. *Angew. Chem. Int. Ed.* **41,** 49–76 (2002).

22) Bräse, S., Gil, C., Knepper, K. & Zimmermann, V. Organic azides: an exploding diversity of a unique class of compounds. *Angew. Chem. Int. Ed.* **44,** 5188–240 (2005).

23) No direct comparison of the hydrogen bond acceptor strengths between organic fluorides and organic azides was found. Organic azides are 1,3-dipoles with negative charge localization on the nitrogen atom directly attached to carbon (ref. 22), allowing this nitrogen atom to serve as a hydrogen bond acceptor. Based on the observed hydrogen bond acceptor trends (ref. 21) and poor hydrogen bond acceptor ability of organic fluorides (ref. 17), we considered the organic azides to be better hydrogen bond acceptors when compared to organic fluorides.

24) Jung, C. Y. & Rampal, A. L. Cytochalasin B binding sites and glucose transport carrier in human erythrocyte ghosts. *J. Biol. Chem.* **252,** 5456–63 (1977).

25) Nomura, N., Verdon, G., Kang, H. J., Shimamura, T., Nomura, Y., Sonoda, Y., Hussien, S. A., Qureshi, A. A., Coincon, M., Sato, Y., Abe, H., Nakada-Nakura, Y., Hino, T., Arakawa, T., Kusano-Arai, O., Iwanari, H., Murata, T., Kobayashi, T., Hamakubo, T., Kasahara, M., Iwata, S. & Drew, D. Structure and mechanism of mammalian fructose transporter GLUT5. *Nature.* **526**, 397-401 (2015).

Chapter 4

Synthesis and Biological Evaluation of a New Fluorescent Probe 3-NBD-AM

4.1. Introduction to fluorescent hexose probes

In order to obtain a high quality diagnostic image of the tumor under investigation, localization of the tracer in the tumor cells over normal cells is required.[1] As GLUT1 is often overexpressed in many tumor cells, scaffolds that exhibit a high affinity for GLUT1 were used to achieve a higher tracers accumulation in the tumor location.[2] Despite the ubiquitous expression of GLUT1, the tracers that were transported by GLUT1, such as 2-fluoro-2-deoxy-D-glucose (2-FDG), were demonstrated to exhibit high accumulation in cancer cells over normal cells.[1] However, GLUT1 expression levels in the early-stage breast cancer cells were proven to be inconsistent.[3,4] Moreover, GLUT5 was found to be overexpressed along with the D-fructose transporter proteins GLUT1 and GLUT2.[3,4] Consequently, studies towards the development of probes to target the GLUT5 transporter protein have received attention in the past decade.[4,5]

However, despite the overexpression of GLUT5 in many breast cancer cells, some of these cells were determined to express lower levels of GLUT5 as well.[6-7] Development of a tracer that targets GLUT5 and shows some propensity for GLUT1 could potentially enhance the tracer accumulation in breast cancer cells, irrespective of the variation in GLUT1 and GLUT5 expression levels. The ability of such probes to undergo enzymatic phosphorylation could further improve the quality of diagnostic image through the

prevention of probe efflux.[1] To prove this hypothesis, we decided to design, synthesize and evaluate a fluorescent probe that has the potential to display a very high affinity for GLUT5. In addition, assistance of GLUT1 in the transport of such probes could allow the probe accumulation in a wide variety of breast cancer cells. Furthermore, exhibition of low efflux property by the probe will intensify its accumulation in the tumor cells to obtain a high signal to noise ratio. Other than studying the concept of high probe accumulation in the breast tumor cells, fluorescent hexose molecules have various applications in physiology that includes, but are not limited to the characterization and study of a particular GLUT expression in various tissue types.[8-10] In addition, there has been search for GLUT5 selective probes to understand the mechanism of D-fructose uptake in healthy and tumor cells.

4.1.1. Previously known GLUT1 or GLUT5 targeting probes

Many groups, including our group, have synthesized and studied D-glucose, D-fructose and 2,5-anhydro-D-mannitol (structurally similar to D-fructofuranose) based probes to target GLUT1 or GLUT5 (Figure 4.1.1). GLUT1 transports 2-NBD-G **1** from extracellular space to intracellular space and vice versa.[11] The assistance of GLUT2 in the transport of 2-NBD-G **1** shall not be denied, but never evaluated. 1-NBD-AM **2** and 6-NBD-F **3** were synthesized to target D-fructose transporters.[4,12,13] 1-NBD-AM **2** was reported as a fluorescent probe whose transport into cells was extracellular D-fructose dependent. The authors had designed probe **2** based on the hypothesis that 2,5-AM moiety present in this probe would undergo phosphorylation inside the cells by hexokinase to prevent back transport. However, majority of the probe was back

transported from intracellular space, after multiple washes over regular time periods. This result suggested either no enzymatic phosphorylation of the probe by hexokinase or slow rate of phosphorylation of the probe. The probe **2** was not systematically evaluated to find the GLUTs involved in its transport. On the other hand, 6-NBD-F **3** exhibited GLUT5 dependent transport into breast tumor cells. The probe **3** was determined to target GLUT5 in a very selective manner. Nonetheless, both probe **3** was also quickly back transported from the intracellular space to extracellular space, indicating the requirement for a new probe development to suppress the efflux problem.

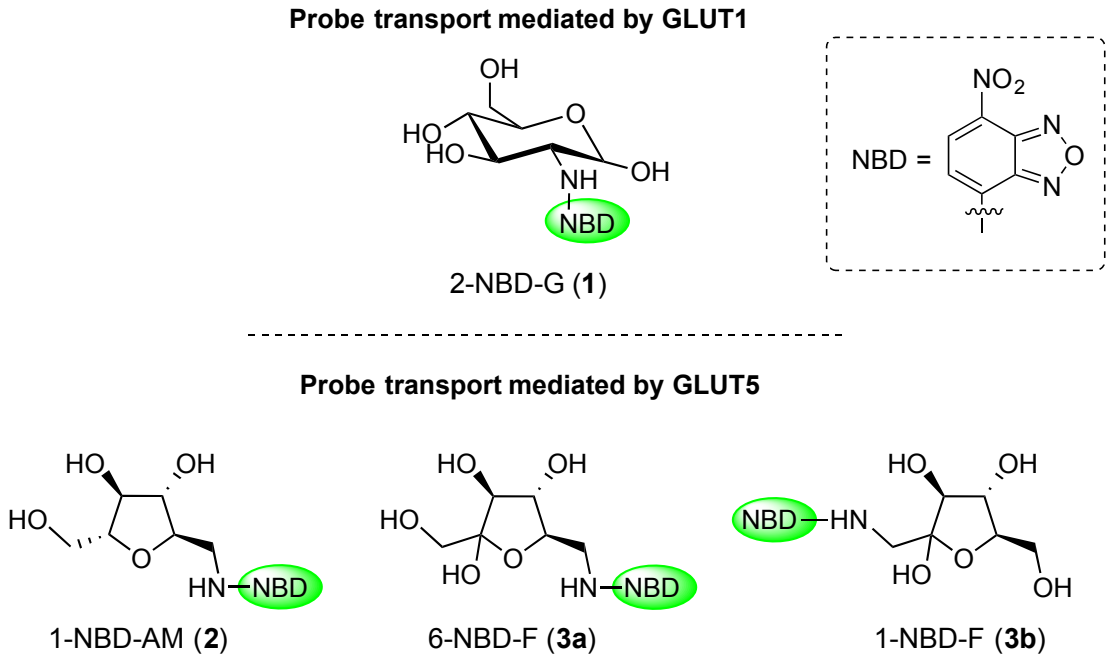

Figure 4.1.1. Structural representation of previously reported NBD-hexose probes

4.1.2. Design of new fluorescent probe – 3-NBD-AM

In Chapter 3, GLUT1 or GLUT5 recognition for 2,5-AM derivatives was summarized as a function of hydrogen bonding property of the C-3 substituent. The presence of a hydrogen bond donor at the C-3 of 2,5-AM derivatives provided high affinity GLUT5

ligands. In addition, presence of a hydrogen bond acceptor at the C-3 position of 2,5-AM derivatives provided moderate GLUT1 affinity. However, hexose-GLUT binding does not represent the transport of the hexose by the GLUT and thus the ability of GLUT5 or GLUT1 to transport 2,5-AM derivatives must be evaluated. To understand the transport mechanism of C-3 modified 2,5-AM derivatives by GLUTs and to evaluate the uptake of these molecules by tumor cells, we designed a fluorescent probe, 3-NBD-AM **4** (Figure 4.1.2). At C-3, 3-NBD-AM **4** retains both hydrogen bond donor and acceptor, and is expected to obtain dual GLUT recognition. By measuring the relative NBD (7-nitro-1,2,3-benzoxadiazole) fluorescence present inside the tumor cells, amount of the probe taken up by the tumor cells can be measured. Furthermore, position C-3 modified 2,5-AM derivatives contain two primary hydroxyl groups and closely mimic the structure of the parent hexose, which may enhance the likelihood of enzymatic phosphorylation of the probe by hexokinase (Chapter 1, Scheme 1.8.12). Thus, 3-NBD-AM **4** was expected to exhibit a low efflux. Upon the exhibition of GLUT5-dependent uptake and no efflux by the probe **4**, the C-3 modified 2,5-AM scaffolds could serve as potential tracers in the molecular imaging of breast cancer.

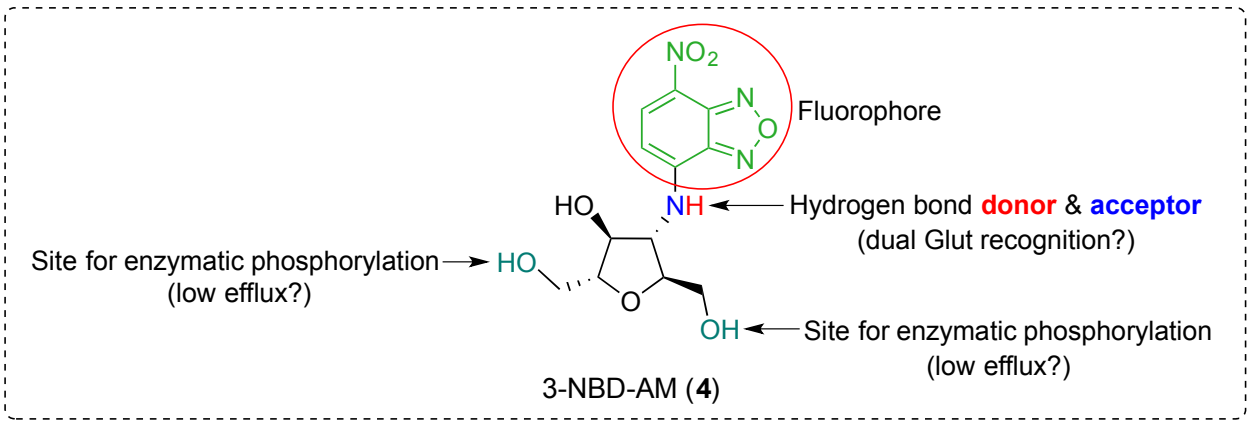

Figure 4.1.2. Structural advantages of 3-NBD-AM **4**

4.2. Synthesis of 3-NBD-AM

Typically, labeling of hexose with NBD group is performed by the treatment of primary amino functionality of an unprotected sugar with NBD-Cl **5** under mild basic conditions.[2,12,13] Often, low product yields were observed under these conditions. In comparison to NBD-Cl **5**, NBD-F **6** exhibits very high reactivity in ipso substitution reactions with primary amines and thiols.[14-16] NBD-Br **7** is known to show poor reactivity with the amines and thiols, mainly due to the higher atomic size of Br (Figure 4.2.1). The utility of NBD-I **8** as a reagent in the NBD labeling process has not yet been reported, but it is predicted to be the least reactive NBD-halide towards the ipso substitutions based on the reactivity trend exhibited by the rest of the NBD-halides. In spite of the higher reactivity of NBD-F **6**, most often NBD-Cl **5** is employed as reagent for the NBD labeling of amines and thiols, due to its significantly lower price.[12-16]

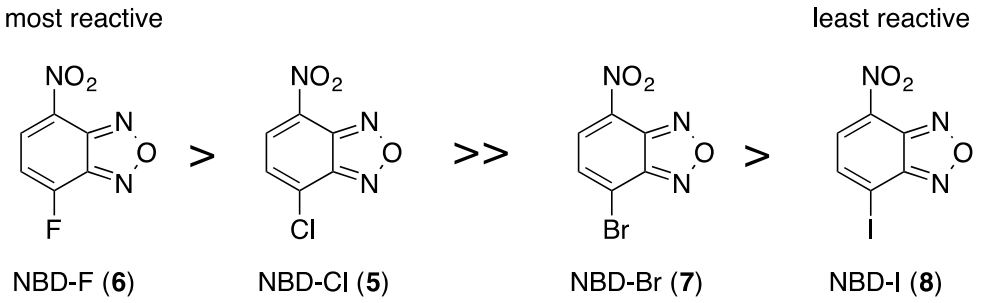

Figure 4.2.1. Reactivity of NBD-halides towards ipso substitution with amines/thiols

In Chapter 3, we showed that 3-amino-2,5-anhydro-D-mannitol (Scheme 4.2.2, **11**) could undergo efficient *N*-arylation under the specified conditions of nucleophilic aromatic substitution. During *N*-arylation of the C-3 amine functionality of a 2,5-AM derivative, we observed poor reactivity of 1-chloro-4-nitrobenzene (mono-nitro substituted aryl halide) with the amine functionality, in comparison to 1-chloro-2,4-

dinitrobenzene. However, despite the similar mono-nitro substitution on the aromatic ring, NBD-Cl **5** reacted efficiently with the amine functionality of 2,5-AM derivative at room temperature. The higher reactivity of NBD-Cl **5** could be attributed to the electron withdrawing nature of benzoxadiazole ring.[13]

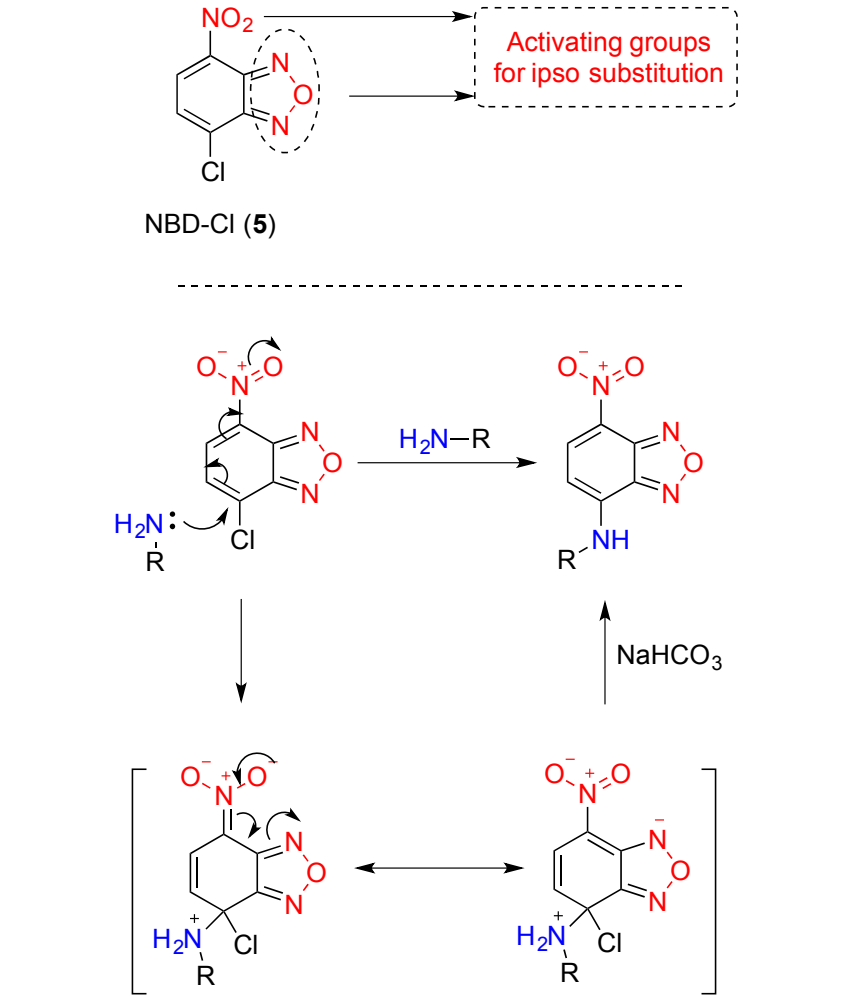

Scheme 4.2.1. Structure and reactivity of NBD-Cl with a primary amine

3-NBD-AM **4** was synthesized in impure form the amine **11** (Scheme 4.2.2), which was accessed from **10** by reduction. In Chapter 2, the synthesis of azide **10** was demonstrated from D-glucosamine hydrochloride **9**. However, by reacting the amine **11** with NBD-Cl **5** under basic conditions in MeOH, we obtained lower yields of 3-NBD-AM **4** (Scheme 4.2.2). Moreover, the product obtained from this transformation was found to be impure. The primary amine functional group of amino-sugar **11** is bound to a secondary carbon (C-3) and in addition, the oxygen atoms of amine **11** are inductively withdrawing. Hence, the amine functionality of compound **11** is a relatively poor nucleophile and does not participate very actively in ipso substitution reactions.

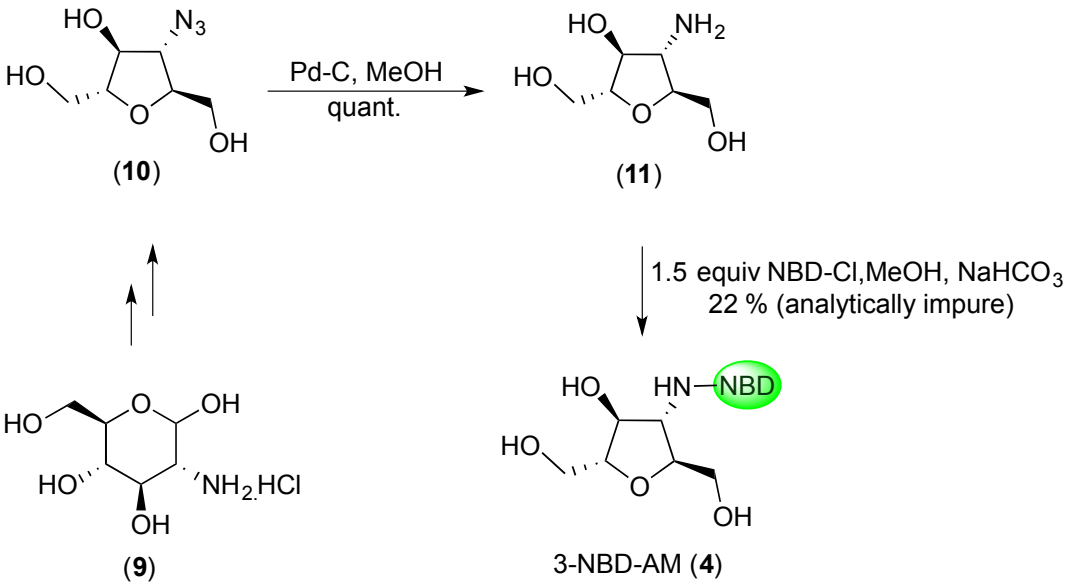

Scheme 4.2.2. Protecting group free synthesis of 3-NBD-AM **4**

To avoid the interference of the primary hydroxyl groups during the reaction between the amine group of 2,5-AM derivative and NBD-Cl **5**, silyl protecting groups were introduced on the primary alcohols. The target molecule 3-NBD-AM **4** was

synthesized in multiple steps starting from azide **10** (Scheme 4.2.3). Primary hydroxyl groups of compound **10** were protected as triisopropylsilyl (TIPS) ethers by treatment with TIPSCl and imidazole in DMF. The crude product was subjected to palladium catalyzed hydrogenation to reduce azido functional group. The amine, obtained from the previous chemical transformation was treated with NBD-Cl in acetonitrile to provide access to 3-(*N*-7-nitro-2-1,3-benzoxadiazol-4-yl)amino)-1,6-*O*-triisopropylsilyl-2,5-anhydro-Dmannitol **12** in 57% yield over three steps. Compound **12** was subjected to trifluoroacetic acid to carry out the deprotection of silyl protecting groups to yield 3-NBD-AM **4** (88%).

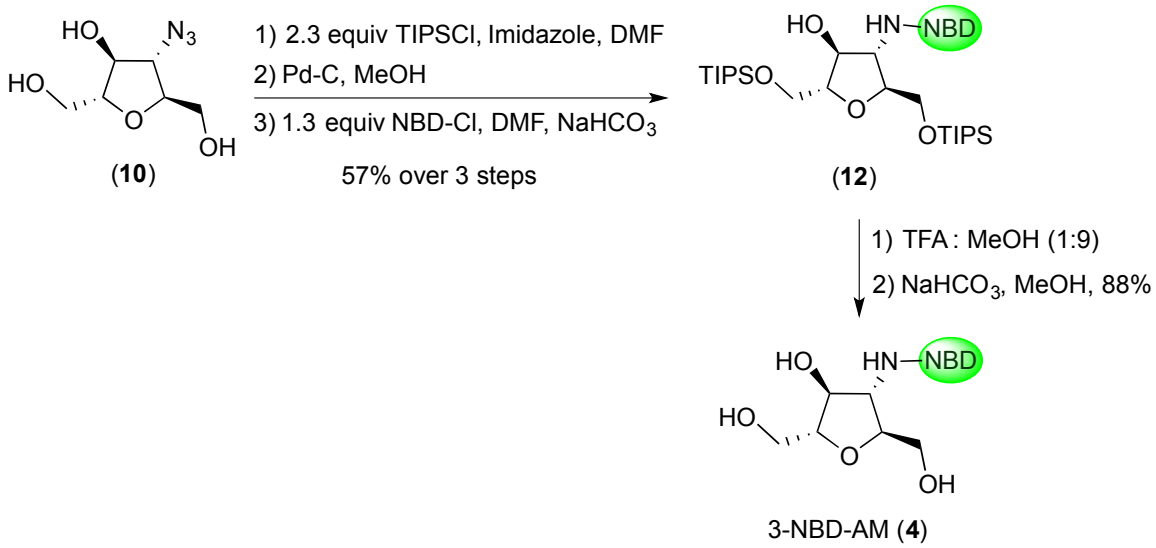

Scheme 4.2.3. Higher yield synthesis of 3-NBD-AM **4**

With **4** in hand in analytically pure form, we proceeded to its *in vitro* evaluation. Compound **4** contains the NH-NBD fluorophore, which allows measurement of the NBD fluorescence present inside the cells *via* a fluorescence plate reader (FPR) study.

4.3. Measurement of 3-NBD-AM transport into EMT-6 cells

4.3.1. Introduction to Fluorescence Plate Reader (FPR)

A multi mode FPR is a very useful instrument to study variety of fluorophores that emit broad spectrum of wavelengths in cell culture. Typically, a multi mode FPR consists of monochromators. Light, a composition of various wavelengths, passes through a monochromator on the excitation side, which usually transmits more than 60% of the desired wavelength range to the sample-well. As applied light excites the sample, it emits a specific fluorescent signal, generally at a longer wavelength in comparison to the applied light. An emission monochromator cleans the fluorescent signal and transmits at least 60% of the desired wavelength to the detector.

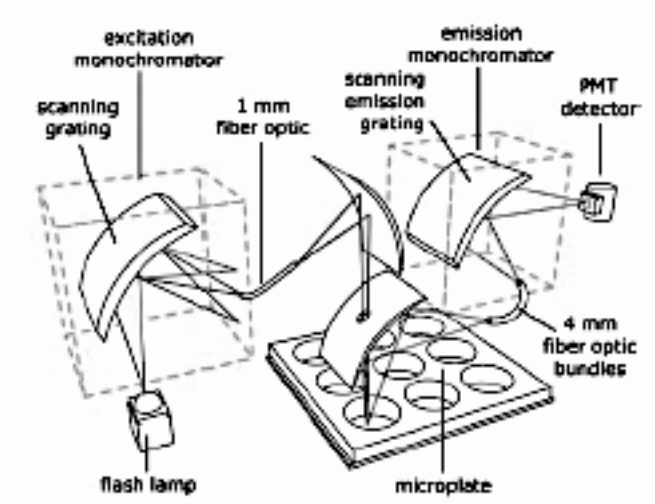

Figure 4.3.1. Schematics of optical settings of FPR

(Taken from ref. 12 with permission)

The λ_{max} (absorption) and λ_{max} (emission) values of 3-NBD-AM **4** were determined prior to the FPR study. In MeOH, λ_{max} (absorption) for 3-NBD-AM **4** was measured to be 465 nm and the λ_{max} (emission) was determined to be 550 nm. The

absorption maximum and emission maximum wavelengths were incorporated in the FPR method before any measurements were taken.

4.3.2 Measurement of 3-NBD-AM taken up by EMT-6 cells under various conditions

Hexose transporters are inactive at low temperatures (ca. 0 ^{o}C) due to their inability to change conformations to transport the hexoses across the cell membrane.[11] To examine GLUT-dependent transport of 3-NBD-AM **4**, we studied the effect of temperature on the transport of 3-NBD-AM **4**. EMT-6 cells were incubated with 3-NBD-AM at 4 ^{o}C and 37 ^{o}C for 45 min. Only 3% of NBD fluorescence was observed in EMT-6 cells that were incubated at 4 ^{o}C with 300 μM of **4**, in comparison to the EMT-6 cells incubated at 37 ^{o}C (Figure 4.32), eliminating the plausibility of the transport of **4** by simple diffusion mechanism. As shown in Figure 4.3.3, a steady increase in NBD fluorescence inside EMT-6 cells was observed by increasing the incubation time, which confirmed the time dependent uptake of **4** into EMT-6 cells.

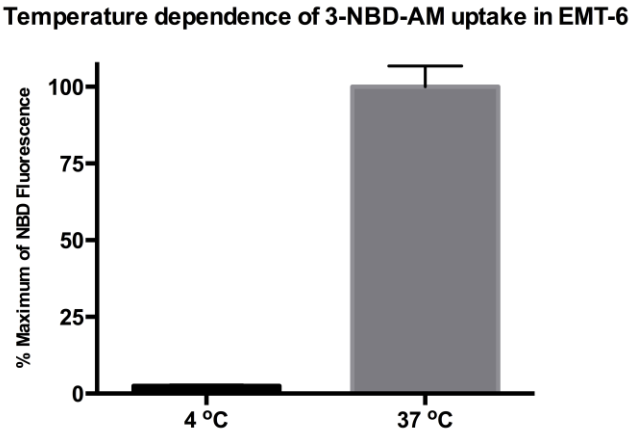

Figure 4.3.2. % maximum of NBD fluorescence measured by FPR in EMT-6 cells at 0 ^{o}C and 37 ^{o}C after 45 min incubation with 3-NBD-AM (300 μM). Error bars represent the SEM of triplicates.

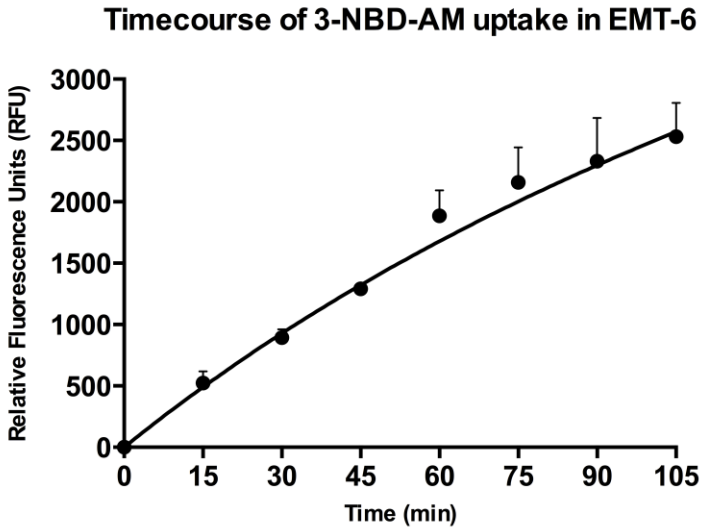

Figure 4.3.3. The observed NBD fluorescence in EMT-6 cells after incubation with 3-NBD-AM (300 μM) over time period of 105 min at 37 ^{o}C. Error bars represent the SEM of triplicates.

To inspect the extracellular hexose dependent uptake of 3-NBD-AM **4**, transport of **4** into EMT-6 cells was measured after co-incubation with 50 mM of D-glucose or D-fructose with 300 μM 3-NBD-AM **4**. The presence of D-fructose in the extracellular space showed a strong inhibitory effect on NBD fluorescence of EMT-6 cells (Figure 4.3.4). Only a minor drop in NBD fluorescence was observed in the presence of D-glucose. The higher inhibitory effect on the 3-NBD-AM **4** uptake by extracellular D-fructose can be attributed to higher affinity of D-fructose carriers for 3-NBD-AM **4**.

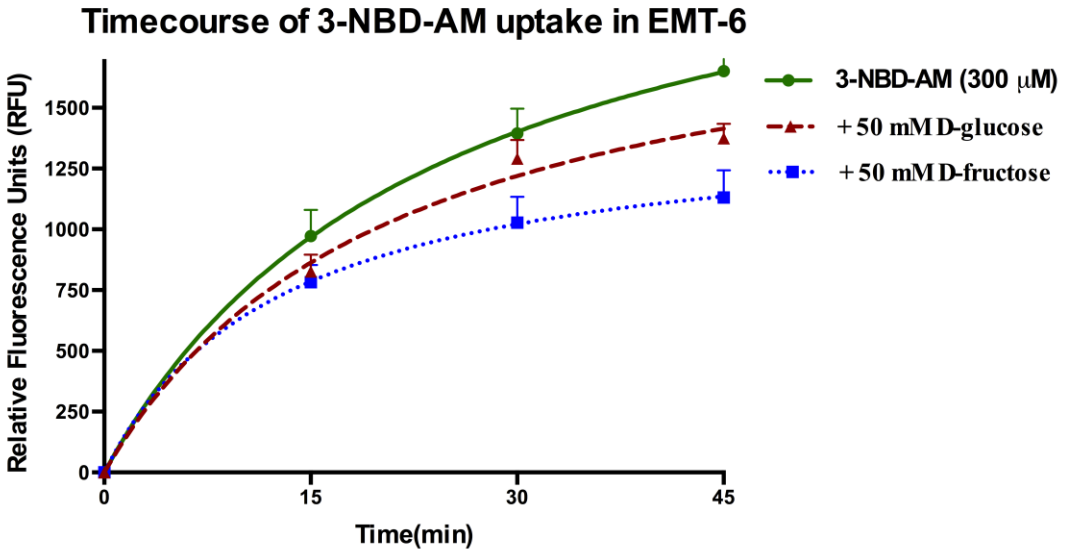

Figure 4.3.4. Effect of 50 mM D-glucose and D-fructose co-incubation with 3-NBD-AM on NBD fluorescence in EMT-6 cells at 37 ^{o}C over 45 min period. Error bars represent the SEM of triplicates.

To further assess the affinity of D-fructose carriers for 3-NBD-AM **4**, we studied the uptake of 3-NBD-AM **4** in a cell line that expresses low levels of D-fructose transporters. Thus, we measured the uptake of [^{14}C]-D-fructose and [^{14}C]-D-glucose in both CHO and EMT cells (Figure 4.3.5), to assess the levels of D-fructose carriers in CHO cells. EMT-6 cells took up higher amount of [^{14}C]-D-fructose and [^{14}C]-D-glucose than CHO cells. In addition, relatively, a very low amount of [^{14}C]-D-fructose was transported into CHO cells in comparison to the amount of [^{14}C]-D-glucose transported; this study suggested a low level expression of D-fructose carriers in CHO cells, when compared to EMT-6 cells. Therefore, the study of extracellular hexoses on the uptake of 3-NBD-AM **4** in CHO cells might provide further information about the transporters involved in its transport. Uptake of 3-NBD-AM **4** into CHO cells was heavily influenced by the presence of extracellular D-glucose or D-fructose (Figure 4.3.6). Additionally, the

amount of the 3-NBD-AM **4** transported into CHO cells in the presence of a large excess of extracellular D-glucose represented the probe transport by D-fructose carriers. Accordingly, almost the same amount of uptake of 3-NBD-AM **4** was seen by the addition of extracellular D-fructose or D-glucose. In other words, similar uptake of 3-NBD-AM **4** was seen in the presence of a high levels of the D-glucose transporters and low levels of D-fructose transporters. This may reflect a higher affinity of the probe for D-fructose carriers.

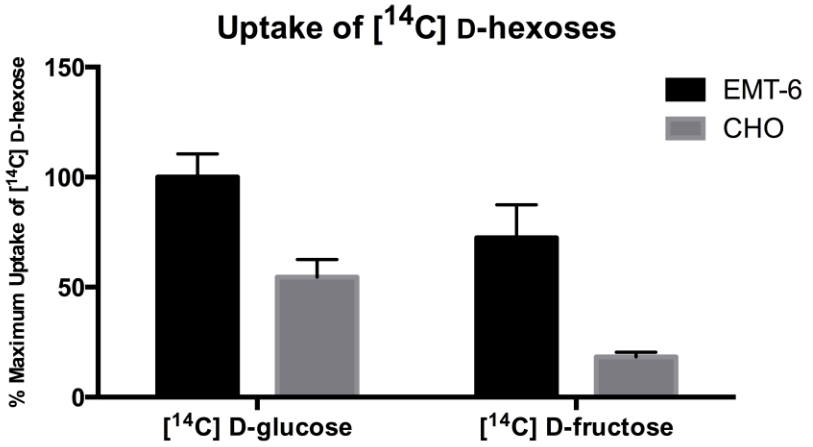

Figure 4.3.5. Comparison of [^{14}C]-D-fructose and [^{14}C]-D-glucose uptake in CHO and EMT-6 cells at 25 ^{o}C. Error bars represent the SEM of triplicates.

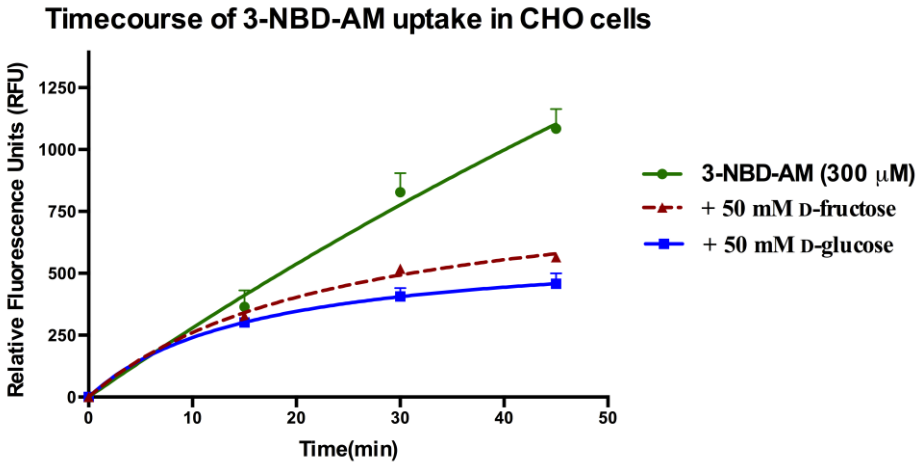

Figure 4.3.6. Fluorescence in CHO cells after co-incubation of D-glucose and D-fructose with 3-NBD-AM. Error bars represent the SEM of triplicates.

4.4. [^{14}C]-D-Hexose transport inhibition study with 3-NBD-AM

The uptake studies using FPR measurements indicated higher uptake of 3-NBD-AM **4** by D-fructose carriers. To confirm higher affinity of the D-fructose transporters for 3-NBD-AM **4**, we studied the [^{14}C]-D-hexose transport inhibitory capability of **4**. We observed [^{14}C]-D-fructose transport inhibition by 3-NBD-AM into EMT-6 cells at 25 ^{o}C, with a very low IC_{50} value (12.6±0.05 μM), confirming very high affinity towards D-fructose carriers (Figure 4.41). Also, [^{14}C]-D-fructose transport inhibitory abilities of 2,5-AM, D-fructose and 3-NBD-AM were compared. Our results suggested very high affinity of D-fructose carriers for the probe **4** over 2,5-AM.

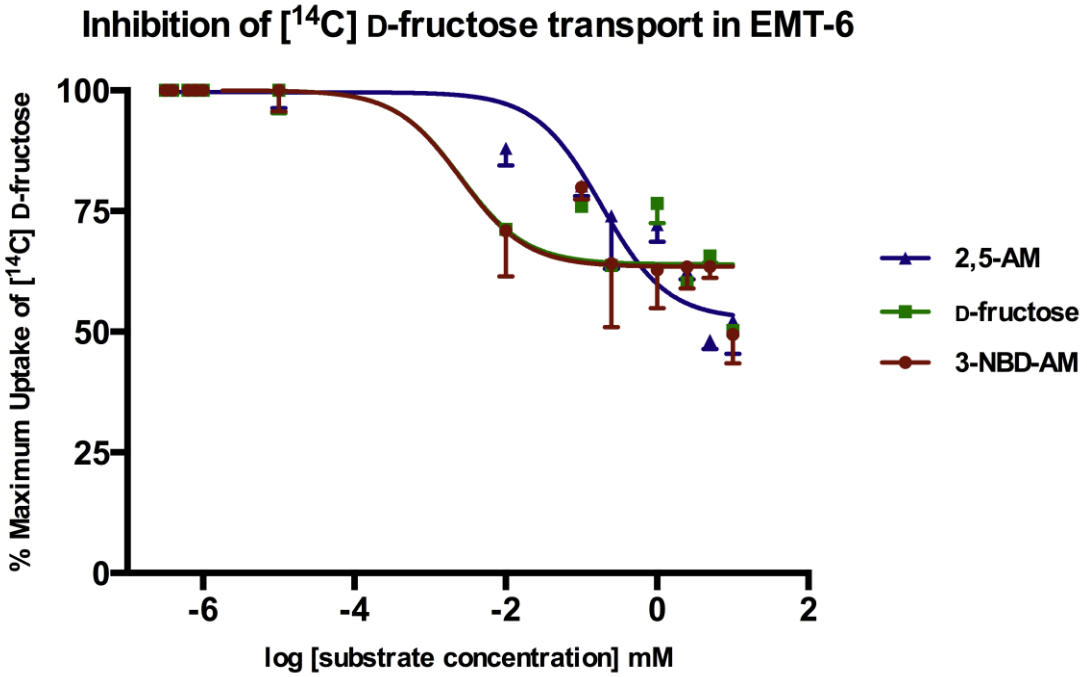

Figure 4.4.1. [^{14}C]-D-Fructose uptake inhibition by 3-NBD-AM after 25 min incubation at 25 ^{o}C with EMT-6 cells. Error bars represent the SEM of triplicates.

To determine affinity of the D-glucose carriers for 3-NBD-AM **4**, a [^{14}C]-D-glucose transport inhibition study was performed. Appreciable level of D-glucose carrier

recognition was observed for 3-NBD-AM **4** based on this [^{14}C]-D-glucose inhibition study (Figure 4.4.2). However, relatively higher IC_{50} value (668±24 μM) was observed for 3-NBD-AM **4** in comparison to the natural ligand D-glucose or the parent hexose 2,5-AM (IC_{50} = 206±21). Based on all the above observation, we concluded that 3-NBD-AM **4** is mainly a substrate for the D-fructose carriers, with some affinity for D-glucose carriers.

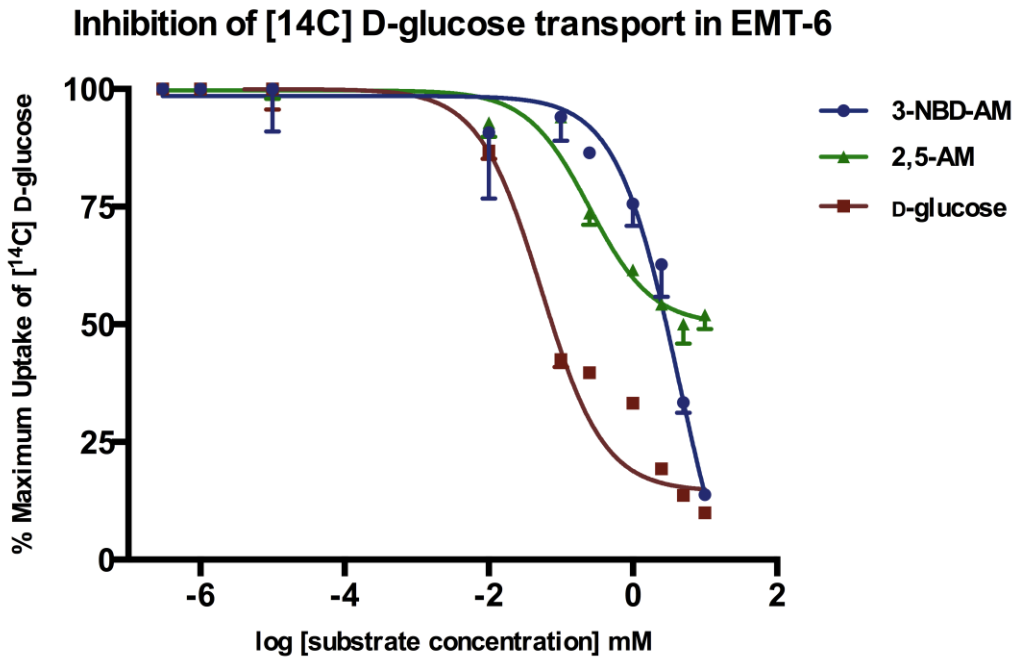

Figure 4.4.2. [^{14}C]-D-Glucose uptake inhibition by 3-NBD-AM after 25 min incubation at 25 ^{o}C with EMT-6 cells. Error bars represent the SEM of triplicates.

To identify the GLUTs that are involved in the transport of 3-NBD-AM **4**, we studied the ability of 3-NBD-AM **4** to inhibit [^{14}C]-hexose transport in the presence of 100 μM CB, a noncompetitive hexose transport inhibitor of Class-I GLUTs.[18] In the presence of CB, 3-NBD-AM **4** did not inhibit the transport of [^{14}C]-D-glucose into EMT-

6 cells (Figure 4.4.4). Based on this observation we concluded that the D-glucose transporters belonging to the Class-I are involved in the recognition of 3-NBD-AM **4**. Among the Class-I D-glucose transporters, GLUT1 and GLUT2 are the principal D-glucose transporters in EMT-6 cells and thus either of GLUT1 or GLUT2 is involved in the recognition of 3-NBD-AM **4**.

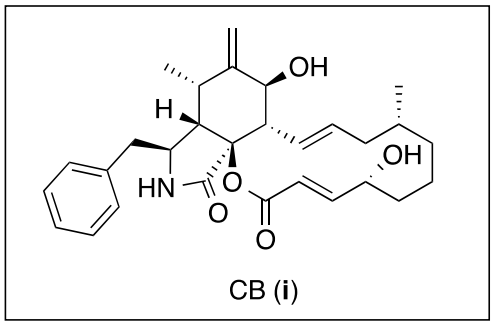

Figure 4.4.3. Structure of Cytochalasin B, a Class-I GLUT inhibitor

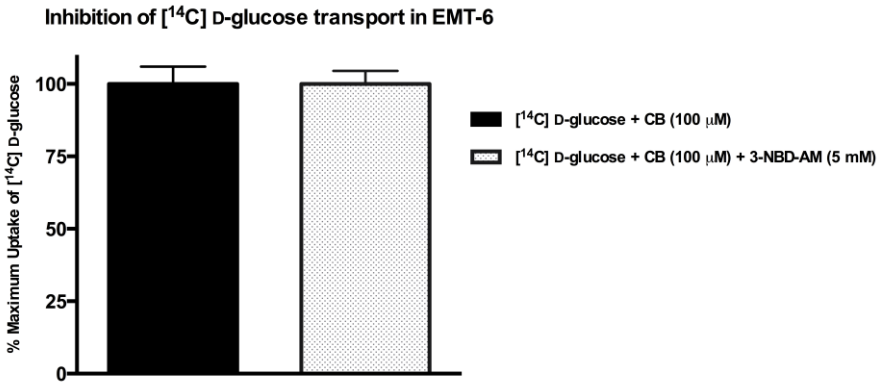

Figure 4.4.4. [^{14}C]-D-Glucose uptake inhibition by 3-NBD-AM in the presence of CB, after 25 min incubation at 25 ^{o}C with EMT-6 cells. Error bars represent the SEM of triplicates.

As shown in Figure 4.4.5, [^{14}C]-D-fructose transport into EMT-6 cells was partially blocked by 3-NBD-AM **4**, in the presence of 100 μM CB, indicating that Class-II or/and Class-III GLUTs that carry D-fructose are involved in the recognition of 3-

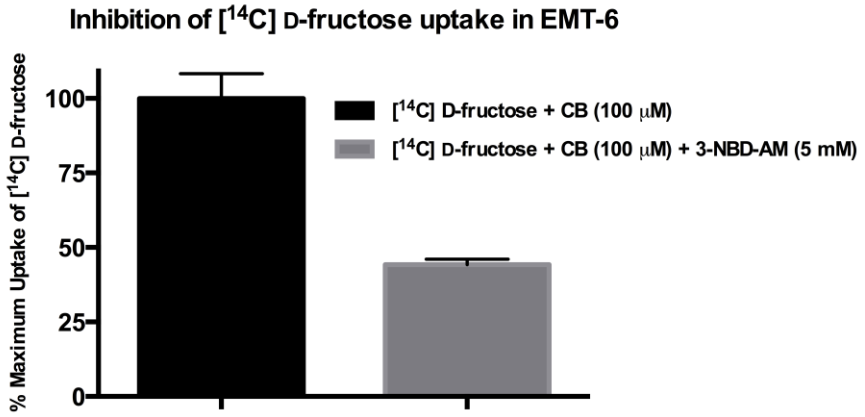

Figure 4.4.5. [^{14}C]-D-glucose uptake inhibition by 3-NBD-AM in the presence of CB, after 25 min incubation at 25 ^{o}C with EMT-6 cells. Error bars represent the SEM of triplicates.

NBD-AM **4**. Furthermore, to study GLUT2 involvement in the transport of the probe, we measured the uptake of the probe in the presence of GLUT2 inhibitors, quercetin and phloretin (Figure 4.4.6).[19] We observed no inhibition of 3-NBD-AM **4** transport by either of the GLUT2 inhibitors (Figure 4.4.7). This experiment rules out the involvement of the GLUT2 transporter protein in the transport of 3-NBD-AM **4**. Previously (Figure 4.4.4), based on [^{14}C]-D-glucose transport inhibition by **4** in the presence of CB, we found the involvement of either of GLUT1 or GLUT2 in the transport of 3-NBD-AM **4**. As we observed no change in the uptake of 3-NBD-AM **4** in the presence of GLUT2 inhibitors, we concluded the GLUT1 assisted transport of 3-NBD-AM **4**.

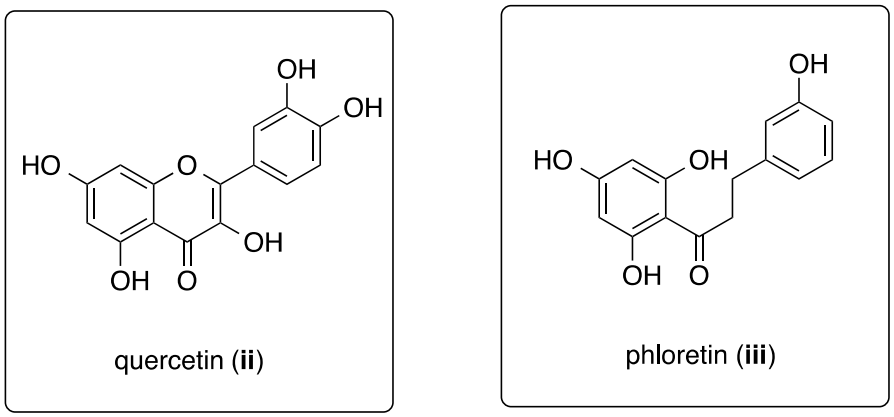

Figure 4.4.6. Structures of quercetin and phloretin

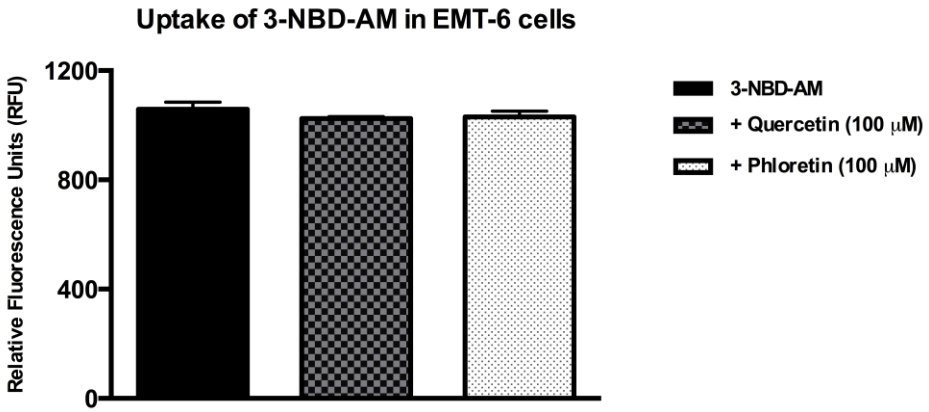

Figure 4.4.7. Comparison of 3-NBD-AM uptake into EMT-6 cells in the presence and absence of GLUT2 inhibitors. Error bars represent the SEM of triplicates.

As the involvement of GLUT2 in the transport of 3-NBD-AM **4** is eliminated, it was clear that one of the Class-II or Class-III GLUTs that carry D-fructose and GLUT1 were involved in the transport of **4**. Apart from GLUT5, the rest of the Class-II and class-III GLUTs that transport D-fructose also transport D-glucose.[20] Further, no inhibition of [^{14}C]-D-glucose transport by 3-NBD-AM **4** in the presence of CB (which only blocks the D-glucose transport through the Class-I GLUTs), indicated that the Class-II or Class III

GLUTs that transport D-glucose, were not recognizing the probe **4**. Thus, GLUT5, the only D-fructose transporter from Class-II and Class-III GLUTs that does not transport D-glucose, must be involved in the transport of 3-NBD-AM **4**.

To confirm GLUT5-dependent transport of 3-NBD-AM **4** into EMT-6 cells, we compared the uptake of 3-NBD-AM into normal CHO cells and CHO cells that were transfected with GLUT5. Both normal CHO cells and GLUT5 transfected CHO cells were incubated with 3-NBD-AM for 30 min at 37 ^{o}C and NBD fluorescence inside the CHO cells was measured using FPR. We observed higher uptake of 3-NBD-AM into transfected CHO cells in comparison to that of normal CHO cells (Figure 4.4.8), indicating the GLUT5 dependent transport of 3-NBD-AM **4**. However, even the normal CHO cells were determined to be GLUT5 positive (by Western blot analysis). Thus, to assess the probe accumulation into GLUT5 negative cells, further studies were required.

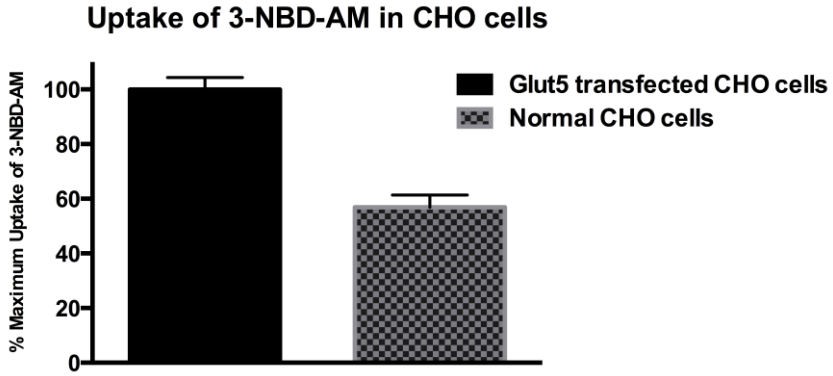

Figure 4.4.8. Fluorescence plate reader comparison of 3-NBD-AM uptake into GLUT5 transfected CHO cells and normal CHO cells measured after 45 min incubation with EMT-6 (300 μM) at 37 ^{o}C. Error bars represent the SEM of triplicates.

For better understanding of the role of GLUT5 in the transport of 3-NBD-AM **4**, it was required to perform inhibition studies with GLUT5 negative cells. Unfortunately, we did not have access to cells which do not express GLUT5. Further, knocking down all the GLUTs except GLUT5 from CHO or EMT-6 cells is a very time consuming, expensive and difficult process. Alternatively, GLUT5 negative Xenopus laevis oocytes were used to perform uptake experiments with **4**.[5]

The oocytes were collected, processed and then were separated into two batches. Once batch of oocytes was injected with water and the other batch was injected with the GLUT5 mRNA (oocyte isolation and processing was performed by D. O′Neill). The same number of oocytes from each batch was incubated with the probe for 45 min and the extracellular space was washed until it was free from 3-NBD-AM **4**. After lysing the oocytes, supernatant isolated from each batch of cells was taken into two different wells of a 12-well plate and NBD fluorescence in each well was measured. To our delight, we observed very high NBD fluorescence in the supernatant that corresponded to the GLUT5 injected oocytes (Figure 4.4.9). On the basis of this study, it can be concluded that GLUT5 has very high affinity for 3-NBD-AM **4**. A small uptake of 3-NBD-AM **4** into oocytes could be due to the transport facilitated by GLUT1, which is expressed in water injected oocytes.

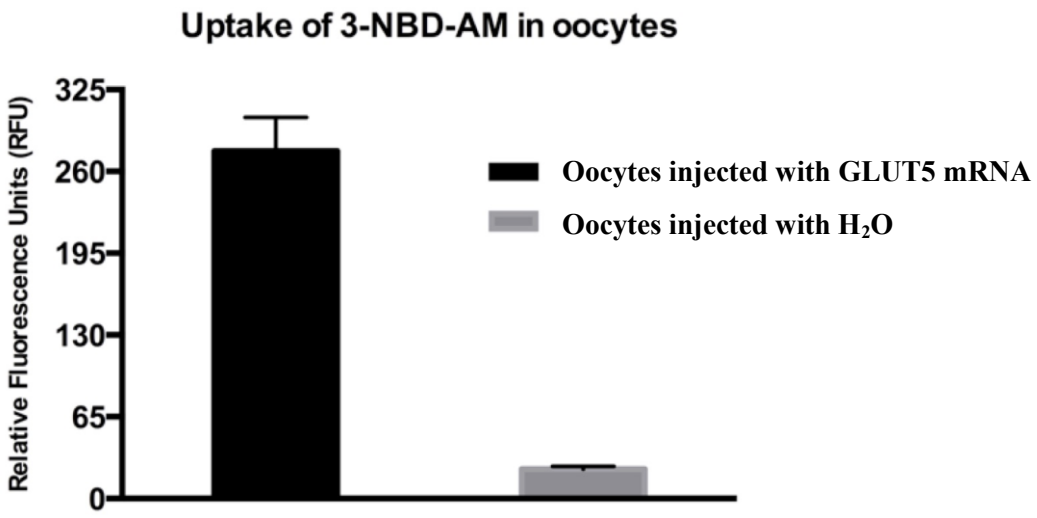

Figure 4.4.9. Fluorescence plate reader comparison of 3-NBD-AM taken up by water injected oocytes and GLUT5 injected oocytes, measured after 45 min incubation with EMT-6 (300 μM) at 25 ^{o}C. Error bars represent the SEM of triplicates.

Finally to conclude that the D-fructose transport inhibition by 3-NBD-AM **4** into EMT-6 cells was due to its recognition by GLUT5, we performed [^{14}C]-D-fructose transport inhibition studies with GLUT5 mRNA injected Xenopus laevis oocytes. The background [^{14}C]-D-fructose transport that is facilitated by natural transporters expressed in oocytes was subtracted from the overall [^{14}C]-D-fructose transported into GLUT5 mRNA injected oocytes to determine the net [^{14}C]-D-fructose transport that is facilitated by GLUT5. As shown in Figure 4.4.10, we observed good inhibition of net [^{14}C]-D-fructose transport by GLUT5 in the presence of 5 mM concentration 3-NBD-AM **4**. Furthermore, the uptake of 3-NBD-AM **4** into EMT-6 cells was measured in the presence and absence of Class-I GLUT inhibitor CB; only ~10-15% of the uptake of **4** was blocked by CB, indicating that GLUT1 is not the primary transporter of the probe. NBD fluorescence study of the uptake of 3-NBD-AM **4** (Figure 4.4.9) and its ability to inhibit

[^{14}C]-D-fructose transport in GLUT5 mRNA injected oocytes (Figure 4.4.10), concluded that 3-NBD-AM **4** is mainly a probe for GLUT5.

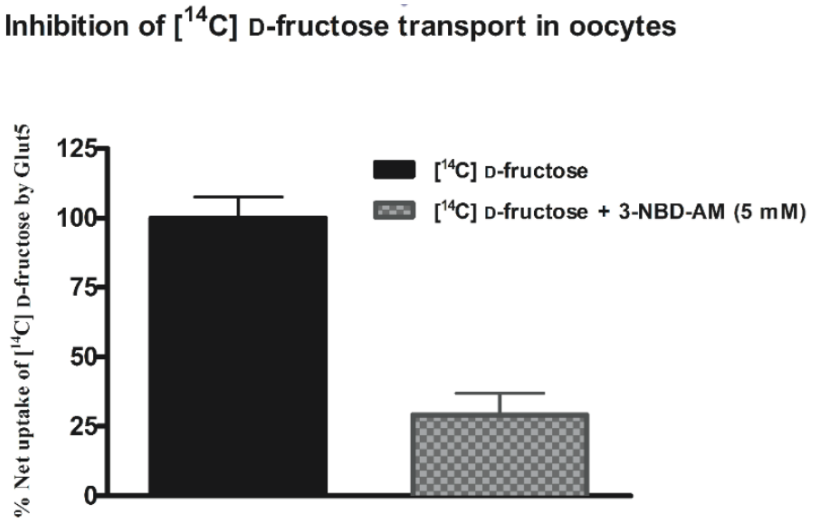

Figure 4.4.10. [^{14}C]-D-fructose uptake (by GLUT5) inhibition into oocytes by 3-NBD-AM. Error bars represent SEM of triplicates.

4.5. Km determination for 3-NBD-AM

To determine affinity of the transporter for 3-NBD-AM **4**, we measured uptake of **4** into EMT-6 cells. Figure 4.5.1 represents the dose-dependent uptake of 3-NBD-AM **4** into EMT-6 cells. From the Michaelis-Menten curve, we determined the Km value for 3-NBD-AM **4** to be 1.2 ± 0.1 mM. As we observed very low Km value for 3-NBD-AM compared to the reported Km value for D-fructose (~6 mM),[20] it can be concluded that the 3-NBD-AM **4** is a high affinity GLUT5 probe.

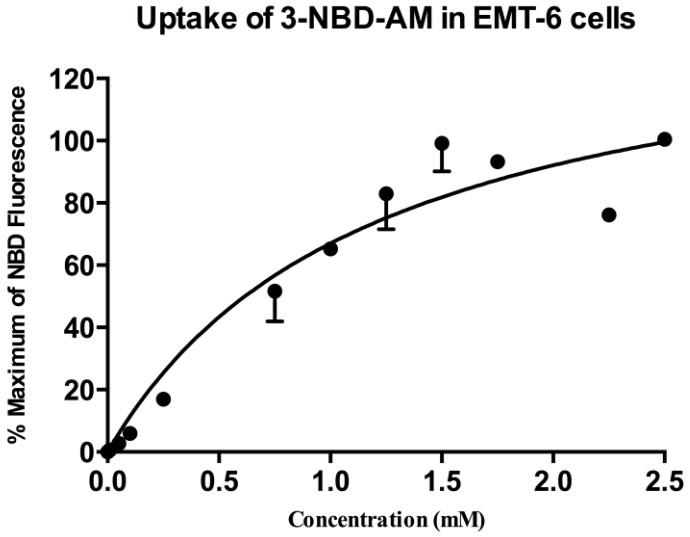

Figure 4.5.1. Michaelis-Menten curve obtained by plotting dose-dependent uptake of 3-NBD-AM. Error bars represent SEM of triplicates.

4.6. Comparison of 3-NBD-AM uptake into EMT-6 cells with existing GLUT5 probes

1-NBD-AM **2** was a D-fructose transporter targeting probe that was reported by McQuade and coworkers.[4] Further, our group member Dr. Soueidan studied 6-NBD-F to target GLUT5.[12] We designed the 3-NBD-AM **4** not only to be used as a probe for GLUT5, but also to evaluate its efficiency to accumulate in the tumor cells in comparison to the existing probes. We measured the uptake of 6-NBD-F **3a**, 1-NBD-AM **2** and 3-NBD-AM **4** into EMT-6 cells at 37 ^{o}C for a period of 45 min. As shown in Figure 4.6.2, we observed almost the same amount of NBD fluorescence in those EMT-6 cells that were incubated with NBD-F **3a** or 1-NBD-AM **2**, whereas a substantial increase in NBD-fluorescence was observed in the case of 3-NBD-AM **4**. This study concluded relatively higher uptake of 3-NBD-AM **4**. This higher accumulation of 3-NBD-AM **4** could be due to i) higher GLUT5 affinity for 3-NBD-AM **4**, and ii) GLUT1 assistance in the transport of 3-NBD-AM **4**.

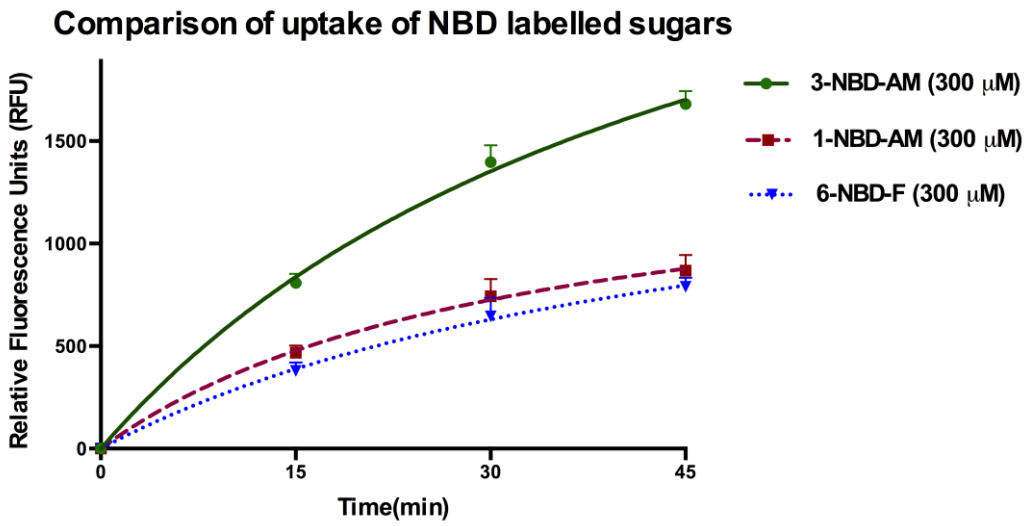

Figure 4.6.1. Comparison of uptake of 6-NBD-F, 1-NBD-AM and 3-NBD-AM uptake into EMT-6 cells at 37 ^{o}C for 45 min. Error bars represent SEM of triplicates.

4.7. Efflux study of 3-NBD-AM

As 3-NBD-AM **4** closely mimics the hexose 2,5-AM, which was proven to undergo enzymatic phosphorylation with both hexokinase and ketohexokinase to prevent efflux,[21] we also expected this probe to exhibit no efflux. Thus, an efflux comparison study was performed with 1-NBD-AM **2** and 3-NBD-AM **4** to verify the back transport of these two probes from EMT-6 cells. We observed quick efflux of 1-NBD-AM **2** from EMT-6 cells at 37 ^{o}C. Only ~23% of the maximum NBD fluorescence of **2** remained inside the cells after 75 min. In the case of 3-NBD-AM **4** at 37 ^{o}C, 73% of maximum NBD fluorescence remained in EMT-6 cells after 75 min (Figure 4.7.1). This study clearly demonstrates the advantage of C-3 modified 2,5-AM derivatives as candidates for the tracer development to use in molecular imaging for the breast cancer detection.

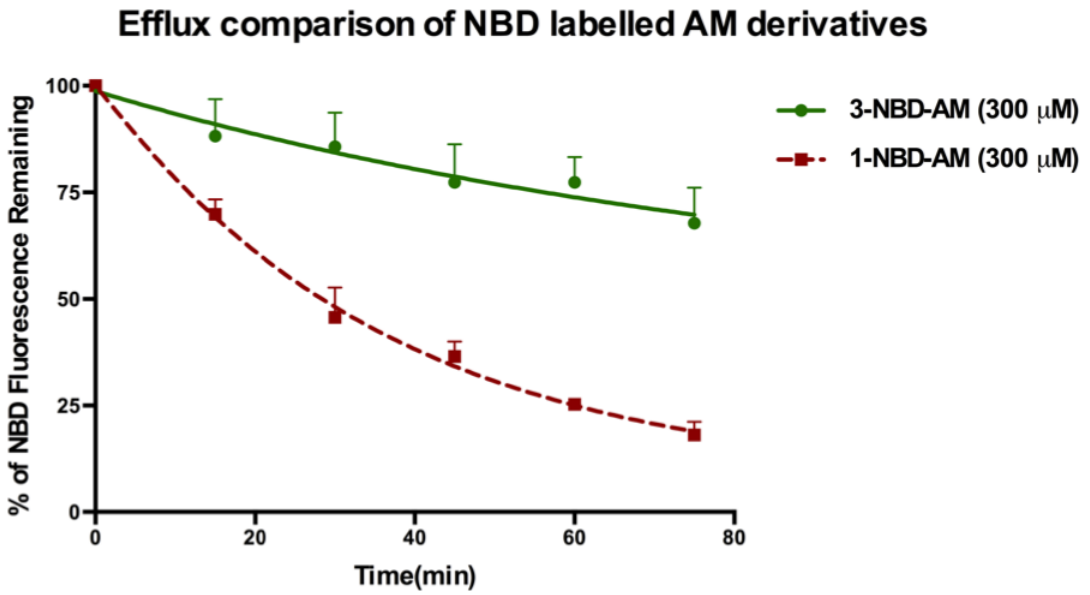

Figure 4.7.1. Comparison of efflux of 3-NBD-AM and 1-NBD-AM from EMT-6 cells at 37 ^{o}C. Error bars represent SEM of the triplicates.

After we observed 73% of maximum of fluorescence due to the presence of 3-NBD-AM **4** inside the EMT-6 cells after 75 min, we prolonged the observation time to 120 min to study the efflux profile of the probe over a longer time period. Figure 4.7.2 demonstrates a slow efflux of the probe up to 90 min and no further efflux after 90 min. It appears that the probe **4** slowly undergoes enzymatic phosphorylation, which allowed initial efflux of a small amount of the probe.

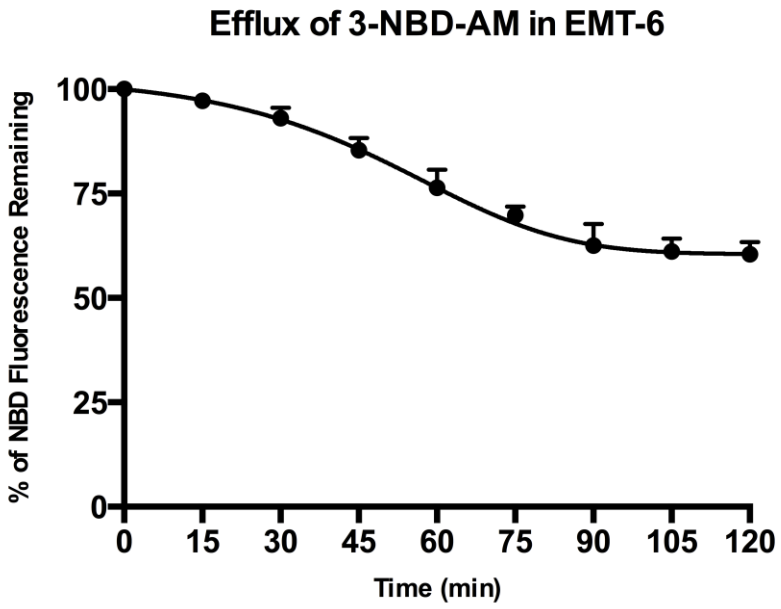

Figure 4.7.2. Study of 3-NBD-AM efflux from EMT-6 cells (incubated with 300 μM 3-NBD-AM for 45 min) at 37 ^{o}C over a period of 2 h. Error bars represent SEM of the triplicates

4.8. Confocal imaging of EMT-6 cells with 3-NBD-AM

Measurement of NBD fluorescence in EMT-6 cells after incubation with a very low concentration of 3-NBD-AM **4** (ca. 20 μM) *via* FPR generates error. To avoid this problem, we relied on confocal imaging techniques, in which the fluorescence of EMT-6 cells can be seen with the assistance of a microscope. By confocal imaging technique, we observed barely any green fluorescence from EMT-6 cells that were not incubated with 3-NBD-AM **4** (Figure 4.8.1, Panel A). Those EMT-6 cells which were incubated with 20 μM 3-NBD-AM **4** solution for a period of 45 min at 37 ^{o}C displayed substantial green fluorescence. Addition of a large excess of extracellular D-fructose had a minor effect the NBD fluorescence of EMT-6 cells. However, addition of large excess of D-fructose caused dramatic reduction in the NBD fluorescence of EMT-6 cells. The confocal study

of EMT-6 cells clearly demonstrates that GLUT5 is the principal transporter of the probe **4** and GLUT1 only assists the transport of the probe **4**, but not the main transporter of **4**.

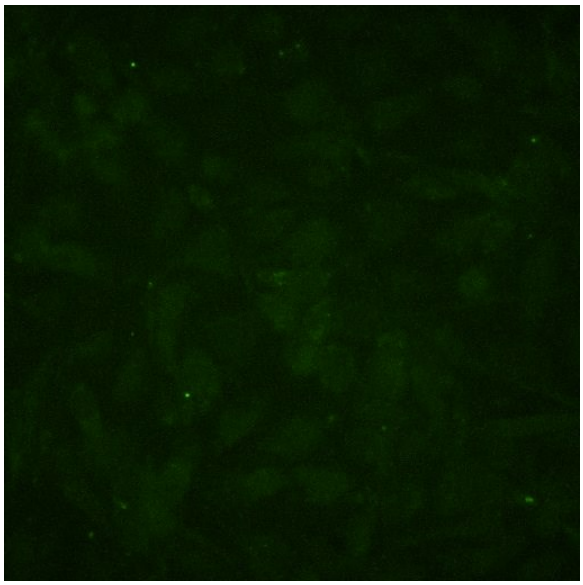

Background (**A**)

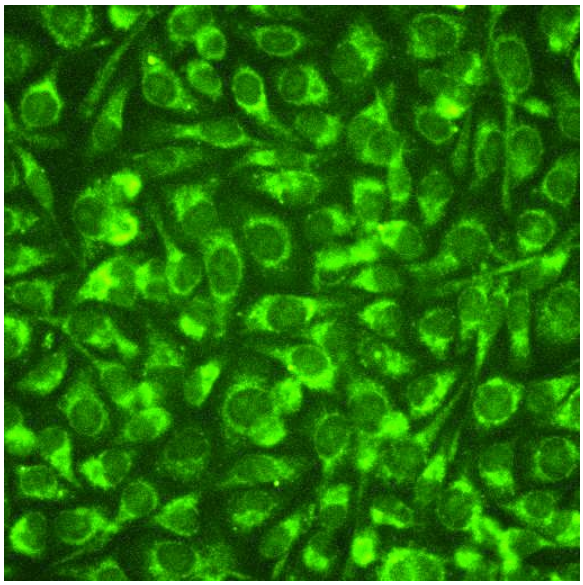

Incubation with 3-NBD-AM (20 μM) (**B**)

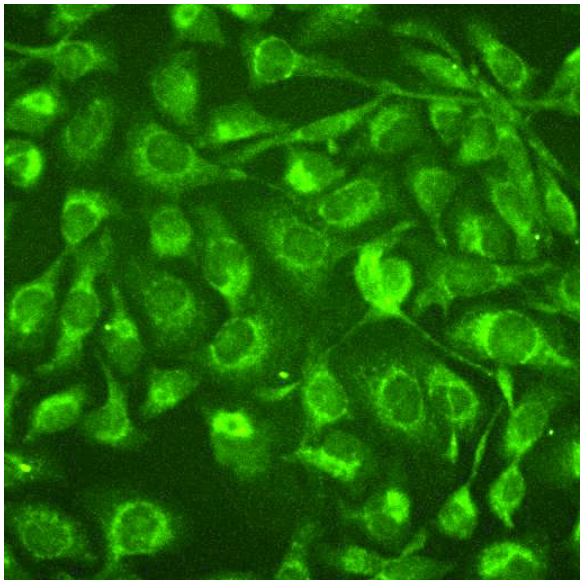

Incubation with 3-NBD-AM (20 μM) + 50 mM D-glucose (**C**)

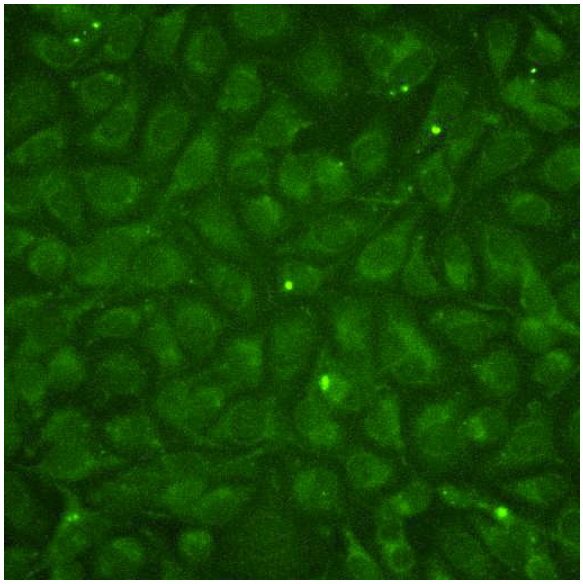

Incubation with 3-NBD-AM (20 μM) + 50 mM D-fructose (**D**)

Figure 4.8.1. Confocal imaging of EMT-6 cells with 3-NBD-AM

4.9. Hexokinase recognition for 3-NBD-AM

In section 4.7, the low efflux property of 3-NBD-AM **4** was discussed. Further, no efflux of the probe was observed after ~90 min, which denoted the enzymatic phosphorylation of the probe **4**. Thus, to study the hexokinase and ketohexokinase recognition for 3-NBD-AM **4**, enzymatic phosphorylation assays were prepared with hexokinase and ketohexokinase. After the subjection of 3-NBD-AM **4** to the hexokinase or ketohexokinase assays, we analyzed them by LCMS. In addition, we subjected 3-NBD-AM **4** to the assay in the absence of the enzymes hexokinase or ketohexokinase. We determined the molecular ion peak of 3-NBD-AM in the positive mode, in the absence of enzymes hexokinase or ketohexokinase. However, the molecular ion was not found in the presence of enzymes hexokinase or ketohexokinase (sometimes, greater reduction of the molecular ion peak was observed). These results indicate that the low efflux of the probe **4** is due to enzymatic phosphorylation of **4** by hexokinase and/or ketohexokinase.

4.10. Docking study with C-3 modified 2,5-AM derivatives

The crystal structures of the human hexose transporters GLUT1 and GLUT5 were obtained from the protein data bank. The *in silico* docking studies were performed by our collaborators R. Panigrahi and J. Lemieux using AutoDock® software to verify the experimental results. Our collaborators calculated *in silico* binding energies of 3-NBD-AM **4** with GLUT1 and GLUT5. In outward conformation, GLUT5 exhibited higher affinity for 3-NBD-AM (-7.5 kcal/mol), whereas lower affinity binding was displayed by GLUT1 (-6.5 kcal/mol) (Figure 4.10.1). Furthermore, it was found that GLUT1 and GLUT5 both showed equal affinity for 3-NBD-AM **4** in inward conformation. However,

the binding of outward conformers of GLUT1 and GLUT5 with 3-NBD-AM **4** is the critical step in the transport of the probe into cells. The inward binding energy of the probe with GLUT1 and GLUT5 contributes to the efflux of the probe. As we did not observed back-transport of the probe, plausibly due to the enzymatic phosphorylation, the binding affinities of the inward conformers of GLUT1 and GLUT5 for the probe are likely to be less relevant.

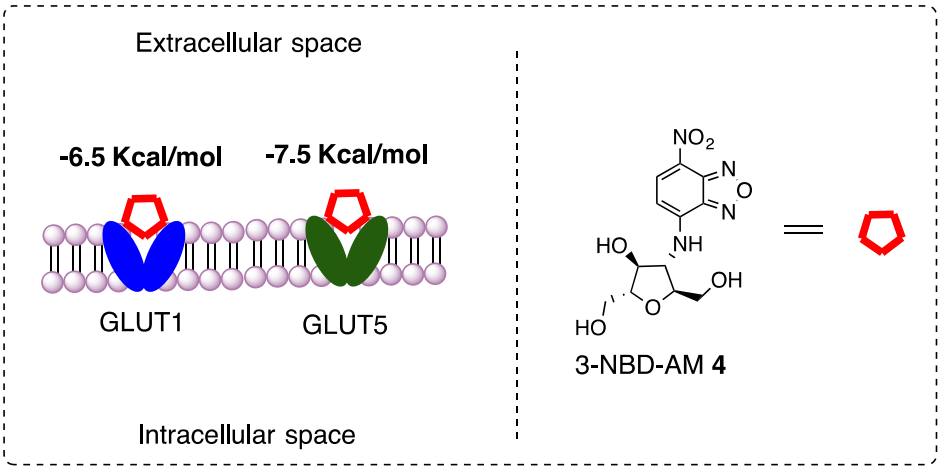

Figure 4.10.1. A cartoon demonstrates higher affinity binding of 3-NBD-AM to GLUT5 over GLUT1

4.11. Conclusions

In conclusion we developed a probe (3-NBD-AM **4**) that exhibited very high affinity towards GLUT5. Additionally, GLUT1 assisted the transport of this probe. We also observed superior uptake of the probe **4** by EMT-6 cells when compared to other known probes **2** and **3a**. Furthermore, very low efflux of the probe was observed over a period of 90 min and thereafter no further efflux of the probe was observed, indicating slow metabolic trapping of the probe. Biological evaluation of the probe **4** not only provides

access to a high affinity GLUT5 targeting probe, but also remains as the first GLUT5 targeting probe that exhibited no efflux after 90 min.

4.12. Future directions

As 3-NBD-AM **4** demonstrated the plausibility of the development of GLUT5 targeting tracers that can remain trapped inside tumor cells. Thus, the radiolabeling of C-3 modified 2,5-AM derivatives could yield efficient tracers for the PET imaging of breast cancer. The radiolabeling of 2,5-AM at C-3 should be performed through linkers such as, amide or arylamine to retain the hydrogen bond donor, which was demonstrated to be crucial for efficient GLUT5-substrate binding and transport of these derivatives.

4.13. Experimental section

Reactions were carried out in flame-dried glassware under a positive argon atmosphere unless otherwise stated. Transfer of anhydrous solvents and reagents was accomplished with oven-dried syringes or cannulae. Solvents were distilled before use (except MeOH and CH_3CN): dimethylformamide (DMF) from calcium hydride and pyridine from KOH. MeOH and CH_3CN were purchased from SIGMA-ALDRICH® company, and were used without distillation. All the commercially available solvents and reagents were used without further purification. Reagents were purchased from Sigma-Aldrich® company. Thin layer chromatography was performed on glass plates precoated with 0.25 mm silica gel. For the spot visualization, TLCs were treated with 2.5% *p*-anisaldehyde in AcOH-H_2SO_4-EOH (1:3:86) and heated until color development. Flash chromatography columns were packed with 230–400 mesh silica gel with specified solvent system. Optical

rotations (deg cm^2 g^{-1}) were measured with Perkin Elmer 241 polarimeter, using the D-line of sodium lamp (λ = 589.3 nm) at 22 ± 2 °C. Proton nuclear magnetic resonance spectra (^{1}H NMR) were recorded at 400 MHz or 500 MHz in indicated deuterated solvents and were reported in ppm in the presence of TMS as internal standard. The coupling constants (*J*) are reported in hertz (Hz) and standard notation was used to describe the multiplicity of signals observed in ^{1}H NMR spectra: broad (br), multiplet (m), singlet (s), doublet (d), triplet (t), etc. Carbon nuclear magnetic resonance spectra (^{13}C NMR) were recorded at 100 MHz or 125 MHz. The spectra were referenced to the residual solvent present in the deuterated solvent (*e.g.* $CDCl_3$: δ = 77.26 ppm, ^{13}C; 7.26 ppm, ^{1}H). Infrared (IR) spectra were measured with a Nic-Plan FTIR Microscope. IR spectra were recorded neat and reported in cm^{-1}. Mass spectra were determined on a high-resolution electrospray positive ion mode spectrometer.

Beckman LS 6500 multi-purpose scintillation counter was used for the determination ^{14}C isotope concentration. Glucose free Krebs-Ringer buffer solution (120 mM NaCl, 25 mM $NaHCO_3$, 4 mM KCl, 1.2 mM KH_2PO_4, 2.5 mM $MgSO_4$, 70 μM $CaCl_2$, pH 7.4) was used to for the studies with EMT-6 cells. Modified Barth's medium (MBM buffer) was used for the studies with oocytes (88 mM NaCl, 1 mM KCl, 0.33 mM $Ca(NO_3)_2$, 0.82 mM $MgSO_4$, 2.4 mM $NaHCO_3$, 0.4 mM $CaCl_2$, 20 mM HEPES, pH 7.4). [^{14}C]-D-hexoses with specified activity were purchased from Moravek Biochemicals. Cold phosphate-buffered saline (1XPBS) was used to wash the extracellular 3-NBD-AM probe (137 mM NaCl, 2.7 mM KCl, 10 mM Na_2HPO_4, 2 mM KH_2PO_4). Synergy™ MX BioTek® fluorescent plate reader was used to measure the NBD fluorescence of EMT-6

cells. Confocal imaging of EMT-6 cells was performed using Leica TCS SP5 fluorescence microscope located in the Katz building, at the University of Alberta.

3-(*N*-7-nitro-2-1,3-benzoxadiazol-4-yl)amino)-1,6-*O*-triisopropylsilyl-2,5-anhydro-D-mannitol (12).

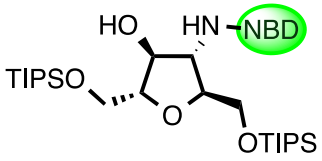

In a 50 mL round bottom flask, azide **10** (0.50g, 2.6 mmol) and DMF (20 mL) were stirred under Ar atmosphere for 5 min. To the resulting homogeneous mixture, imidazole (0.42 g, 6.0 mmol) and triisopropyl(chloro)silane (1.28 mL, 6.0 mmol) were added. The reaction mixture was stirred at room temperature for 6 h. The crude reaction mixture was diluted with 250 mL of DCM, before being transferred into a separatory funnel. The organic layer was washed with brine solution (3 x 25 mL) and dried over Na_2SO_4. Solids were filtered and the organic solvent was evaporated under reduced pressure to yield thick oil that was used in the next step without purification.

The crude product was placed in a 100 mL round bottom flask and 50 mL of MeOH was added. The homogeneous mixture was charged with 10% Pd/C (0.11 g, 20% by weight) and stirred at room temperature under an H_2 atmosphere for 2 h. Solids were separated from the reaction mixture through filtration and washed with MeOH (50 mL).

The filtrate was taken into a 100 mL round bottom flask (in portions) and MeOH was completely evaporated under reduced pressure to yield a thick, pale yellow syrup.

The crude product, obtained from the previous transformation was dissolved in 20 mL acetonitrile under argon and an excess of Na_2CO_3 (ca. 1.5 g) was added. To the heterogeneous mixture, of 4-chloro-2,4-dinitrobenzene (1.2 g, 6.0 mmol) was added and the reaction mixture was vigorously stirred for 12 hours. Excess Na_2CO_3 was separated from the reaction mixture by filtration and the residue was washed with 40 mL of DCM. Evaporation of the organic solvents under vacuum yielded crude compound **12**. The crude product was subjected to silica gel column chromatography, eluting with hexanes:DCM (gradient of 100:0 to 70:30) to yield a thick, orange paste (0.95 g, 57%). R_f 0.32 (Hexane:DCM, 70:30); $[\alpha]_D^{20}$ +1.6 (*c* 0.3, MeOH); IR (cast film) 3361, 3088, 3045, 2943, 2867, 1633, 1527, 1451, 1385, 1340, 1053, 894, 733 cm^{-1}; ^1H NMR (500 MHz, $CDCl_3$): δ 8.46 (d, *J* = 8.6 Hz, 1H), 6.58 (br s, 1H), 6.52 (d, *J* = 8.6 Hz, 1H), 4.51 (br s, 1H), 4.47-4.42 (m, 2H), 4.22 (td, *J* = 4.1, 2.6 Hz, 1H), 4.17 (dt, *J* = 5.2, 3.5, 1H) 4.07 (dd, *J* = 10.8, 4.1 Hz, 1H), 3.98 (dd, *J* = 10.5, 3.5 Hz, 1H), 3.93 (dd, *J* = 10.8, 2.6 Hz, 1H), 3.88 (dd, *J* = 10.8, 5.3 Hz, 1H), 1.23-1.16 (m, 6 H), 1.13 (d, *J* = 3.3 Hz, 9H), 1.11 (d, *J* = 3.3 Hz, 9H), 1.08 (d, *J* = 2.8 Hz, 9H), 1.06 (d, *J* = 2.8 Hz, 9H); ^{13}C NMR (125 MHz, CD_3OD): δ 144.2, 143.7, 143.2, 136.3, 124.4, 100.1, 85.7, 83.8, 79.0, 64.5 (2C), 63.1, 17.9, 17.8, 11.9, 11.8; HRMS (ESI) calcd for $C_{30}H_{55}N_4O_7Si_2Na$ [$M+Na^+$] 661.3423; found 661.3424.

3-(*N*-7-Nitro-2-1,3-benzoxadiazol-4-yl)amino)-2,5-anhydro-D-mannitol (4).

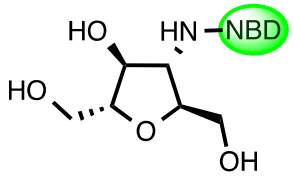

Compound **12** (0.63 g, 1.0 mmol) was dissolved in 50 mL of MeOH. To the orange colored homogeneous mixture, 15 mL of 90% trifluoroacetic acid solution was added. After 8 h of stirring at room temperature, solvents were evaporated from the reaction mixture to yield an orange syrup. The syrup was dissolved in 50 mL of MeOH and excess (ca. 4.0 g) of Na_2CO_3 was added. The heterogeneous mixture was vigorously stirred for 2 h, before the solids were separated by filtration. The filtrate was evaporated under vacuum and the crude compound was subjected to silica gel column chromatography using DCM:MeOH mixture (gradient of 100:0 to 90:20). Fractions with compound were combined and concentrated under vacuum to give an orange solid (0.29 g, 88%). R_f 0.28 (MeOH:DCM, 10:90); m.p. 82-84 ^oC; $[\alpha]_D^{20}$ +63.5 (*c* 8.0, MeOH); IR (cast film) 3311, 3076, 3025, 2937, 1621, 1586, 1492, 1313, 1137, 1034, 847, 734 cm^{-1}; ^1H NMR (500 MHz, CD_3OD): δ 8.51 (d, *J* = 8.5 Hz, 1H), 6.63 (d, *J* = 8.5 Hz, 1H), 4.46 (bs, 1H), 4.35 (app t, *J* = 6.3 Hz, 1H), 4.12 (dt, *J* = 7.0, 4.1 Hz, 1H), 4.04-3.98 (m, 1H) 3.83-3.76 (m, 2H), 3.7-3.62 (m, 2H); ^{13}C NMR (125 MHz, DMSO-D6): δ 145.7, 145.0, 144.5, 138.3, 121.5, 100.3, 84.7, 81.1, 76.2, 62.1, 61.8, 61.5; HRMS (ESI) calcd for $C_{12}H_{14}N_4O_7Na$ $[M+Na^+]$ 349.0755; found 349.0752.

EMT-6 cell culture: EMT-6 cells were grown in a 5% CO_2 incubator at 37 ^oC in Gibco® DMEM-F12 media supplemented with 15 mM HEPES, L-GLUTamine, 10% Fetal Bovune and 1% Penicillin/Streptomycin with media renewal every 2 to 3 days.

[^{14}C] D-Fructose and [^{14}C] D-glucose transport inhibition study: Radioactive "Hot" flux solutions were prepared by mixing 5 μL of [^{14}C] D-glucose or [^{14}C] D-fructose (solution in EtOH, specific activity approximately 1 mCi/mL), 50 μL of 100 mM D-fructose or D-glucose and 945 μL Krebs-Ringer solution of 3-NBD-AM **4** with specified concentration. EMT-6 cells were grown to confluence in 12 well NEST® cell culture plates with media removal every 2 days. One h before performing the flux study, EMT-6 cells were washed twice with Krebs-Ringer buffer solution. To each well 1 mL of Krebs-Ringer buffer was added and incubation at 37 ^oC was continued for one h, in order to deplete the nutrients present in the cells. After one hour of incubation, Krebs-Ringer buffer was removed and 300 μL of radioactive "Hot" flux solution was added into each well. After incubation at 25 ^oC for 25 min, media was aspirated and each well was rinsed twice with ice-cold Krebs-Ringer solution. To each well 500 μL of 5% trifluoroacetic acid was added to lyse the cells. After one hour of cell lysing, 400 μL of cell lysate from each well was transferred into scintillation vials containing 5 mL of Scinti-Safe™ liquid scintillation fluid for counting in a liquid scintillation counter. (**Note:** The same procedure was followed to study [^{14}C]-D-fructose and [^{14}C]-D-glucose transport inhibition by 3-NBD-AM **4** in CHO cells).

[^{14}C]-D-Fructose and [^{14}C] D-glucose transport inhibition study in the presence of CB: Radioactive "Hot" flux solutions were prepared by mixing 5 μL of [^{14}C] D-glucose or [^{14}C]-D-fructose (solution in EtOH, specific activity approximately 1 mCi/mL), 50 μL of 100 mM D-fructose or D-glucose, 10 μL of 10 mM CB and 935 μL of Krebs-Ringer solution of 3-NBD-AM **4** with specified concentration. EMT-6 cells were grown to confluence in 12 well NEST® cell culture plates with media removal every 2 days. One hour before performing the flux study, EMT-6 cells were washed twice with Krebs-Ringer buffer solution. To each well 1 mL of Krebs-Ringer buffer was added and incubation at 37 ^{o}C was continued for one hour, in order to deprive the nutrients present in the cells. After one hour of incubation, Krebs-Ringer buffer was removed and 300 μL of radioactive "Hot" flux solution was added into each well. After incubation at 25 ^{o}C for 25 min, media was aspirated and each well was rinsed twice with ice-cold Krebs-Ringer solution. To each well 500 μL of 5% trifluoroacetic acid was added to lyse the cells. After one hour of cell lysing, 400 μL of cell lysate from each well was transferred into scintillation vials containing 5 mL of Scinti-Safe™ liquid scintillation fluid for counting in a liquid scintillation counter (Beckman LS 6500 multi-purpose scintillation counter).

Studies with fluorescence plate reader (FPR).

Temperature dependent uptake of 3-NBD-AM (4) into EMT-6 cells: EMT-6 cells were grown to confluence in two sets of 12-well NEST® cell culture plates with media removal every 2 days. One h before performing the uptake study, EMT-6 cells of the each well were washed twice with Krebs-Ringer buffer solution (plates were labeled as A and B). To each well 1 mL of Krebs-Ringer buffer was added and incubation of plates (A

& B) was continued for one h at 37 ^{o}C. After one h of incubation, plate-B was stored in a cold room for 10 min to attain low temperature (T = 4 ^{o}C), while Plate-A was continued to be stored in the incubator to maintain temperature of 37 ^{o}C. The Krebs-Ringer buffer was removed from each well of both the plates (A & B) and charged with freshly prepared 500 μL of 300 μM 3-NBD-AM solution in Krebs-Ringer buffer. After the addition of 300 μM 3-NBD-AM solution, plate-A was incubated at 37 ^{o}C and plate-B was stored in the cold room at 4 ^{o}C. After a time period of 30 min, extracellular media was aspirated and each well was rinsed four-times with cold PBS buffer over a period of 3 min. To each well 1 mL of PBS buffer added and the fluorescence count in each well was counted with fluorescent plate reader (Synergy^{TM} MX BioTek®).

Uptake of 3-NBD-AM (4) into EMT-6 cells and uptake inhibition by D-hexose: EMT-6 cells were grown to confluence in 12 well NEST® cell culture plates with media removal every 2 days. One h before performing the flux study, EMT-6 cells were washed twice with Krebs-Ringer buffer solution. To each well 1 mL of Krebs-Ringer buffer was added and incubation at 37 ^{o}C was continued for one h. After incubation, Krebs-Ringer buffer was removed and 500 μL of 300 μM of freshly prepared 3-NBD-AM solution or 500 μL of (300 μM 3-NBD-AM + 50 mM D-hexose) solution in Krebs-Ringer buffer was added. After incubation for a specified period of time at 37 ^{o}C, extracellular media was aspirated and each well was rinsed four-times with cold PBS buffer over a period of 3 min. To each well 1 mL of PBS buffer was added and fluorescence count in each well was measured *via* fluorescent plate reader (Synergy^{TM} MX BioTek®). Net fluorescence

value corresponding to a particular well was calculated by subtracting the background fluorescence value (auto-fluorescence of a well with EMT-6 cells and PBS buffer).

Uptake of 3-NBD-AM (4) into EMT-6 cells in the presence of GLUT inhibitors: EMT-6 cells were grown to confluence in NEST® cell culture plates with media removal every 2 days. One h prior to the flux study, EMT-6 cells were washed twice with Krebs-Ringer buffer solution. To each well 1 mL of Krebs-Ringer buffer was added and incubation was continued for one h at 37 ^{o}C. After one hour of incubation, Krebs-Ringer buffer was removed and 500 μL of freshly prepared Krebs-Ringer buffer solution of 3-NBD-AM (concentration = 300 μM) or 500 μL of Krebs-Ringer buffer solution of 3-NBD-AM with GLUT inhibitor (net concentration of 3-NBD-AM = 300 μM; net concentration of the GLUT inhibitor = 100 μM) was added. GLUT inhibitors (CB, quercetin and phloretin) were purchased from SIGMA-ALDRICH® company in solid form. 10 mM solutions of these inhibitors were prepared to use as stock solutions. After incubation for a specified period of time, extracellular media was aspirated and each well was rinsed four-times with cold PBS buffer over a period of 3 min. To each well 1 mL of PBS buffer was added and fluorescence count in each well was measured *via* fluorescent plate reader (Synergy™ MX BioTek®). The net fluorescence value corresponding to a particular well was calculated by subtracting the background fluorescence value (auto-fluorescence of a well with EMT-6 cells and Krebs-Ringer buffer)

Inhibition of D-fructose uptake by 3-NBD-AM (4) in GLUT5 mRNA injected oocytes: Radioactive "Hot" flux solutions were prepared by mixing 5 μL of [^{14}C] D-

fructose (solution in EtOH, specific activity approximately 1 mCi/mL), 50 μL of 100 mM D-fructose and 945 μL of MBM buffer solution or 945 μL of MBM buffer solution with 5 mM 3-NBD-AM **4**. Four clean test tubes were labeled as W1, W2, G1 and G2. To each of W1 and W2 test tubes, 15 water injected oocytes were added. Similarly, to each of G and G2 test tubes, 15 GLUT5 mRNA injected oocytes were added. Oocytes in the test tubes W1 and G1 were subjected for incubation with 500 μM of hot flux solution that does not contain 3-NBD-AM for 45 min at room temperature. To the test tubes W2 and G2, 500 μM of hot flux solution that contain 5 mM concentration of 3-NBD-AM was added and incubation was continued for 45 min at room temperature. After the incubation period, the flux solution from each test tube was aspirated and carefully washed with cold MBM buffer (10x1 mL). To each test tube, 500 μL of 1% SDS lysing buffer was added and the oocytes were thoroughly lysed with the assistance of pipette tip. 400 μL of the cell lysate from each test tube was transferred into scintillation vials containing 5 mL of Scinti-Safe^{TM} liquid scintillation fluid for counting in a liquid scintillation counter (Beckman LS 6500 multi-purpose scintillation counter).

Study of uptake of 3-NBD-AM (4) into GLUT5 mRNA injected oocytes: Xenopus laevis oocytes were surgically removed, processed and injected with mRNA by D. O′Neill. An equal number of GLUT5 mRNA injected oocytes and water injected oocytes were taken in two separate test tubes. The test tube containing water injected oocytes was labeled as ‘W’ and the test tube containing GLUT5 mRNA injected oocytes was labeled as ‘G’. To each of these test tubes, 500 μL of 300 μM solution of 3-NBD-AM in MBM buffer was added and the incubation was continued for 45 min at room temperature. After

the incubation period, extracellular media was carefully removed from each test tube and oocytes were carefully washed six-times with cold MBM buffer solution. After thorough washing, to each test tube 1mL of MBM buffer was added and the oocytes were lysed with the pipette tip. The entire solution from each test tube (W and G) was transferred into two 1.5 mL graduated micro test tubes with sealable top (also labeled as W and G). These micro test tubes were sealed and subjected to centrifugal force for 3 minutes. 900 μL of supernatant from each test tube was transfered to one of the wells of 12 well NEST® cell culture plate. To one the wells 900 μL of MBM buffer was added to obtain background reading. Fluorescence of each well was measured with fluorescence plate reader (FPR) and subtraction of background value from the crude FPR value provided the net fluorescence value corresponding to a particular well.

Confocal imaging of EMT-6 cells with 3-NBD-AM: Murine breast cancer cell line EMT-6 was grown in Gibco DMEM-F-12 supplemented with 15 mM HEPES, L-glutamine, 10% fetal bovine serum and 1% penicillin/streptomycin with media renewal every 2–3 days. Both cell lines were grown in a CO_2 incubator at 37 °C. Prior to the cell imaging experiments, media was removed and cells were washed two times with Krebs-Ringer buffer. Krebs-Ringer buffer, and 3-NBD-AM (20 μM) or 3-NBD-AM (20 μM) + D-hexose (50 mM) were added to the coverslips placed in the cell culture plate, respectively. This set up was incubated at 37 °C for 30 min. After incubation, the cells were rinsed two times with Krebs-Ringer buffer. Ethanol (1 mL, 95%) was added to each coverslip to fix the cells in the cell culture plate, and incubation was continued for another 30 min. Cells were rinsed four times with PBS, and PBS-rinsed coverslips were

then mounted onto microscopy slides using 20 µL drops of polyvinyl alcohol-based mounting media supplemented with 0.1% n-propyl gallate as anti-fade and 4',6-diamidino-2-phenylindole (DAPI) (50 μgmL^{-1}). Then, cells were imaged using corresponding lasers visualizing DAPI (blue nuclear staining) and Fluorescein isothiocyanate (FITC, green emission) with a Plan-Apochromat 40X/1.3 oil DIC M27 lens on a Leica TCS SP5 confocal laser scanning microscope. Imaging experiments were carried out two times using different batches of cells. (Note: While studying the effect of extracellular D-hexoses on 3-NBD-AM uptake *via* confocal imaging, all the parameters of microscope must remain the same throughout the study)

Data analysis

In the inhibition experiments performed, counts per minute (CPM) were normalized to standards by the subtraction of the background levels and then plotted against the maximum uptake of the radiolabeled hexose (i.e. [^{14}C]-D-fructose or [^{14}C]-D-glucose). For time courses, values were corrected with standards and to the protein levels present per well. IC_{50} values (concentration at which half maximum inhibition of cellular uptake of a radiotracer was observed) were determined using non-linear regression analysis in GraphPad Prism 5 (GraphPad Software, San Diego, CA, USA), and significance was determined at $p < 0.05$ using a Student's t-test.

4.13. References.

1) Pauwels, E. K. Ribeiro, M. J., Stoot, J. H. M. B, McCready, V. R., Bourguigon, M. & Maziere, B. FDG accumulation and tumor biology. *Nucl. Med. Biol.* **25,** 317–322 (1998); Czernin, J. & Phelps, M. E. Positron emission tomography scanning: current and future applications. *Annu. Rev. Med.* **53**, 89–112 (2002).

2) Medina, R. A. & Owen, G. I. Glucose transporters: Expression, regulation and cancer. *Biol. Res.* **35**, 9-26 (2002); Adekola, K., Rosen, S.T. & Shanmugam M. Glucose transporters in cancer metabolism. *Curr. Opin. Oncol.* **24**, 650-654 (2012); Carvalho, K. C., Cunha, I. W., Rocha, R. M., Ayala, F. R., Cajaiba, M. M., Begnami, M. D., Vilela, R. S., Paiva, G. R., Andrade, R. G. & Soares, F. A. GLUT1 expression in malignant tumors and its use as an immunodiagnostic marker. *Clinics*. **66**, 965-972 (2011).

3) Godoy, A., Ulloa, V., Rodriguez, F., Reinicke, K., YaÑez, A. J., GarcÍa, M. A., Medina, R. A., Carrasco, M., Barberis, S., Castro, T., MartÍnez, F., Koch, X., Vera, J. C., Poblete. M. T., Figueroa, C.D., Peruzzo, B., PÉrez, F., Nualart, F. Differential subcellular distribution of glucose transporters GLUT1-6 and GLUT9 in human cancer: Ultrastructural localization of GLUT1 and GLUT5 in breast tumor cells. *J. Cell. Physiol.* **207**, 614-627 (2006).

4) Tanasova, M., Plutschack, M., Muroski, M. E., Sturla, S. J., Struouse, G. F. & McQuade, D. T. Fluorescent THF-based fructose analogue exhibits fructose-dependent uptake. *ChemBioChem*. **14**, 1263-1270 (2013).

5) Wuest, M., Trayner, B. J., Grant, T. N., Jans, H. S., Mercer, J. R., Murray, D., West, F. G., McEwan, A. J. B., Wuest, F. & Cheeseman, C. I. Radiopharmacological

evaluation of 6-deoxy-6-[^{18}F]fluoro-D-fructose as a tracer for PET imaging of breast cancer. *Nucl. Med. Biol.* **38**, 461-475 (2011); Soueidan, O. M., Trayner, B. J., Grant, T. N., Henderson, J. R., Wuest, F., West, F. G. & Cheeseman, C. I. New fluorinated fructose analogs as selective probes of hexose transport protein GLUT5. *Org. Biomol. Chem.* **13**, 6511-6521 (2015).

6) Zamora-Leon, S. P., Golde, D. W., Concha, I. I., Rivas, C. I., Delgado-López, F. & Vera, J. C. Expression of the fructose transporter GLUT5 in human breast cancer. *Proc. Natl. Acad. Sci. USA*. **93**, 1847-1852 (1996).

7) Gowrishankar, G., Zitzmann-Kolbe, S., Junutula, A., Reeves, R., Levi, J., Srinivasan, A., Bruus-Jensen, K., Cry, J., Dinkelborg, L. & Gambhir, S. S. GLUT 5 is not over-expressed in breast cancer cells and patient breast cancer tissues. *PLoS One* **6,** e26902-e26902 (2011).

8) Loaiza, A., Porras, O. H. & Barros, L. F. Glutamate triggers rapid glucose transport stimulation in astrocytes as evidenced by real-time confocal microscopy. *J. Neurosci.* **23,** 7337–42 (2003).

9) Visualizing sweetness: increasingly diverse applications for fluorescent-tagged glucose bioprobes and their recent structural modifications. *Sensors (Basel).* **12,** 5005–27 (2012).

10) TeSlaa, T. & Teitell, M. A. Techniques to monitor glycolosis. *Methods Enzymol.* **542,** 91-114 (2014).

11) Yoshioka, K., Takashashi, H., Homma, T., Saito, M., Oh, K. B., Nemomoto, Y. & Matsuoka, H. A novel fluorescent derivative of glucose applicable to the assessment of glucose uptake activity of Escherichia coli. *Biochim. Biophys. Acta* **1289,** 5–9

(1996); Cheng, Z., Levi, J., Xiong, Z., Gheysens, O., Keren, S., Chen, X. & Gambhir, S. S. Near-infrared fluorescent deoxyglucose analog for tumor optical imaging in cell culture and in living mice. *Bioconjugate Chem.* **17**, 662-669 (2006).

12) Soueidan, O. M., Scully, T. W., Kaur, J., Panigrahi, R. Belovodskiy, A. Do, V., Matier, C., Lemieux, J., Wuest, F., Cheeseman, C. I. & F. G. West. Fluorescent Hexose Derivatives Demonstrate Stringent Stereochemical Requirement for Recognition and Transport by GLUT1 and GLUT5. *Manuscript in preparation*.

13) Levi, J. Cheng, Z., Gheysens, O., Patel, M., Chan, C. T., Wang, Y., Namavari, M. & Gambhir, S. S. Fluorescent fructose derivatives for imaging breast cancer cells. *Bioconjug. Chem.* **18,** 628–34

14) Ghosh, P. B. & Whitehouse, M. W. 7-chloro-4-nitrobenzo-2-oxa-1,3-diazole: a new fluorigenic reagent for amino acids and other amines. *Biochem. J.* **108,** 155–6 (1968).

15) Toyo'oka, T., Watanabe, Y. & Imai, K. Reaction of amines of biological importance with 4-fluoro-7-nitrobenzo-2-oxa-1,3-diazole. *Anal. Chim. Acta* **149,** 305–312 (1983).

16) del Rosso, M. D., di Nunno, L., Florio, S. & Amorese, A. Reactivity of 7-halogeno-4-nitrobenzofurazans towards thiophenols. A kinetic investigation. *J. Chem. Soc. Perkin Trans. 2* 239 (1980).

17) Instrumentation for fluorescence spectroscopy. In *Principles of Fluorescence Spectroscopy*. Edn. 3. (eds. Lakowicz, J. R.) 27-61 (Springer Science+Business Media, LLC, 233 Spring Street, New York, NY 10013, USA, 2006).

18) Jung, C. Y. & Rampal, A. L. Cytochalasin B binding sites and glucose transport carrier in human erythrocyte ghosts. *J. Biol. Chem.* **252,** 5456–63 (1977).

19) Song, J. *et al.* Flavonoid inhibition of sodium-dependent vitamin C transporter 1 (SVCT1) and glucose transporter isoform 2 (GLUT2), intestinal transporters for vitamin C and Glucose. *J. Biol. Chem.* **277,** 15252–60 (2002); Kwon, O. *et al.* Inhibition of the intestinal glucose transporter GLUT2 by flavonoids. *FASEB J.* **21,** 366–77 (2007) and cited references.

20) Manolescu, A. R., Witkowska, K., Kinnaird, A., Cessford, T. & Cheeseman C. Facilitated hexose transporters: New perspectives on form and function. *Physiology* **22**, 234-240 (2007).

21) Ravshel, F. M. & Cleland, W. W. The substrate and anomeric specificity of fructokinase. *J. Biol. Chem.* **248**, 8174-8177 (1973); Hanson, R. L., Ho, R. S., Wiseberg, J. J., Simpson, R., Younathan, E. S. & Blair, J. B. Inhibition of gluconeogenesis and glycogenolysis by 2,5-anhydro-D-mannitol. *J. Biol. Chem.* **259**, 218-223 (1984).

5. Synthesis and *In vitro* Evaluation of Near-Infrared Emitting Fluorescent Hexoses for the Optical Imaging of Tumors

5.1. Introduction to optical imaging

Molecular imaging is an important tool used in biomedical research and tumor detection.[1-2] Positron emission tomography (PET) and optical imaging, are two different modalities of the molecular imaging that play a vital role in the detection of tumors. Optical imaging has a wide range of applications in cell biology and pharmacology.[3-9] In recent years, optical imaging is emerging as a powerful tool for disease diagnosis.[3-9] Unlike positron emission tomography (PET) which operates through a positron emitting tracer, optical imaging operates through a fluorescent, near-infrared light emitting tracer (Figure 5.1.1). Due to the poor absorption of chromophores present in mammalian tissues in the near-infrared region, the tissues become relatively transparent in this region.[3] This phenomenon allows the employment of near-infrared emitting compounds as tracers for the target detection. The tracers used in the PET imaging technique are radioactive and unstable. On the other hand, the tracers used in optical imaging are nonradioactive and storable. However, the poor penetrability of the near-infrared fluorescent light limits the applications of optical imaging in the diagnosis of tumors, which exist in the deeper tissue.[3-9]

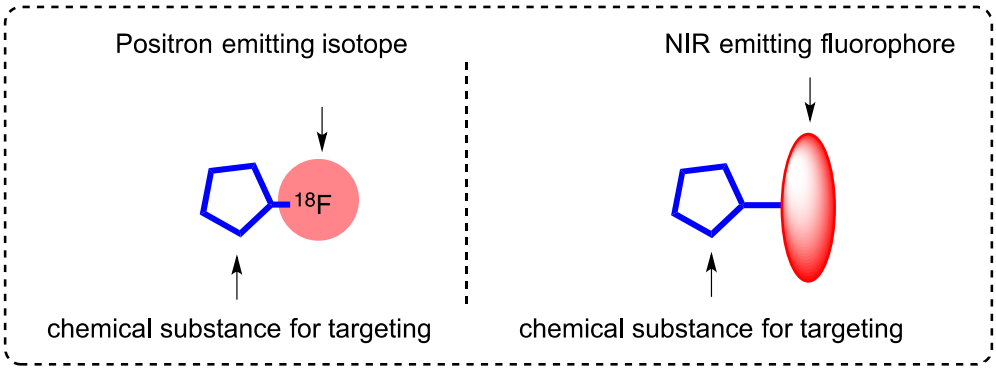

Figure 5.1.1. Comparison of tracers used in PET and optical imaging

5.2. Previous reports on near-infrared emitting hexoses

As the GLUTs are overexpressed in tumor cells (Chapter 1, Section 1.7) to facilitate the transport of hexoses at a faster rate, near-infrared dye labeling of hexoses might provide access to tracers for optical imaging of tumors. To date, only a few reports demonstrated the synthesis of near-infrared emitting hexose-based tracers for tumor imaging. In 2006, Gambhir and coworkers synthesized near-infrared emitting D-glucoses by labeling the C-2 position of D-glucosamine with a Cy5 dye (Figure 5.2.1).[10] Though these near-infrared emitting D-glucose derivatives (Cy5.5-2DG **1** and Cy5.5-2DG-H **2**) were taken up by the tumor cells, extracellular D-glucose did not affect the uptake. Furthermore, Cy.5.5-NHS **3** (Figure 5.2.2), a Cy5 dye that was not attached any hexose moiety was also taken up by the tumor cells. Based on these observations, the authors concluded a non-GLUT mediated uptake path for the near-infrared labeled hexoses.

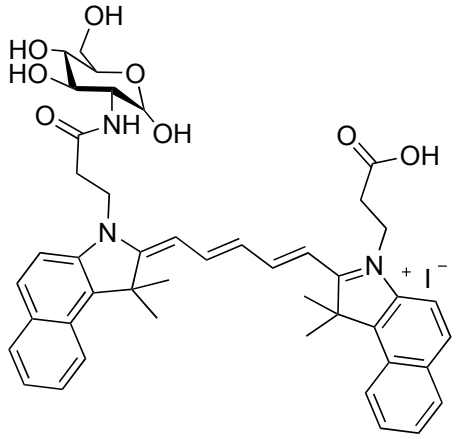

Cy5.5-2DG (**1**)

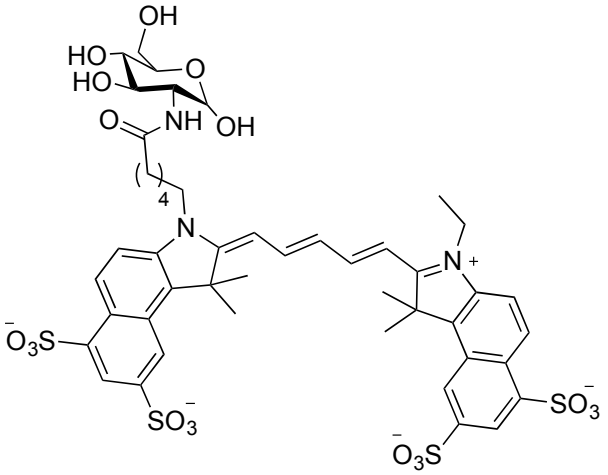

Cy5.5-2DG-H (**2**)

Figure 5.2.1. Near-infrared emitting hexoses reported by Gambhir and co-workers

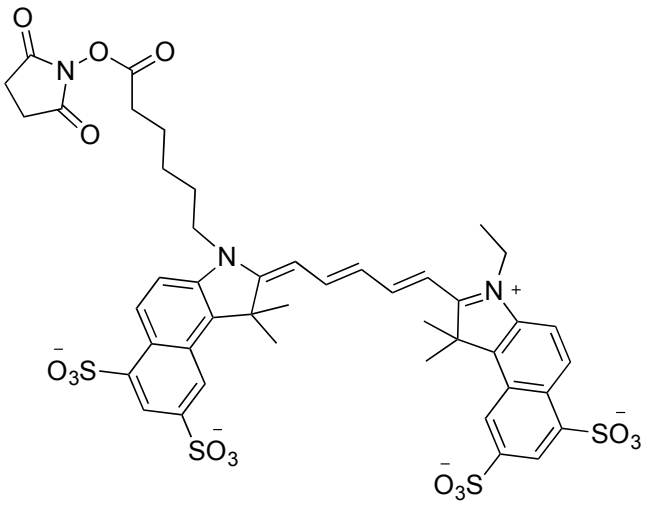

Cy5.5-NHS (**3**)

Figure 5.2.2. Structure of Cy.5.5-NHS

In 2007, Park and co-workers reported the synthesis and evaluation of D-glucose based near-infrared emitting hexose Cy3-G **4** (Figure 5.2.3). The Cy3 dye was conjugated with D-glucose through a glycosidic linkage. The transport of this hexose **4** was affected as the extracellular D-glucose was added. Accordingly, the fluorescent hexose derivative **4** was reported as GLUT1 substrate.[11]

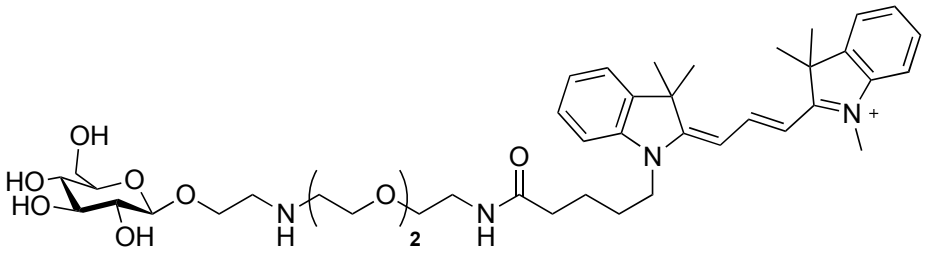

Cy3-G (**4**)

Figure 5.2.3. A Cy3-labeled D-glucose derivative reported by Park and coworkers

In 2009, Kovar and coworkers reported 800CW (near-infrared emitting dye) labeled D-glucose derivative (2-800CW-DG **5**, Figure 5.2.4) and concluded that uptake of 2-800CW-DG **5** into tumor cells was GLUT1 dependent. However, this report does not provide a clear picture of the uptake mechanism. GLUTs are known for their inability of transporting anionic species, such as hexose phosphates. Thus, GLUT1 mediated transport of anionic 800CW labeled D-glucose could be a receptor-mediated endocytosis process, which plausibly involves recognition of the hexose moiety by GLUT1, followed by endocytosis of the entire **5**-GLUT1 complex rather than transport through the protein pore.[12] However, no mechanistic study is available to explore the mechanism of uptake of these molecules.

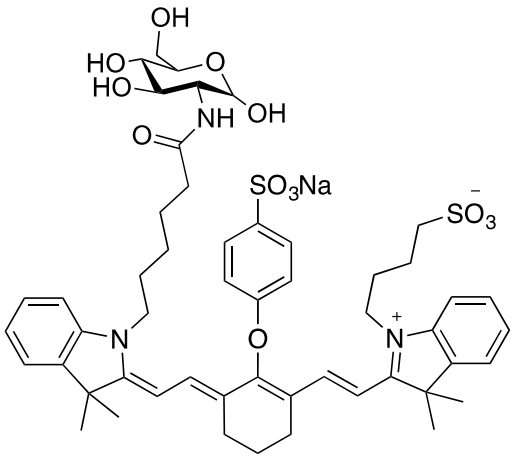

2-800CW-DG (**5**)

Figure 5.2.4. Structure of near-infrared emitting hexose 2-800CW-DG

Very recently, Gu and coworkers also reported D-glucose dependent uptake of a near-infrared emitting D-glucose derivative by tumor cells. Unlike previous reports, Gu and coworkers had synthesized a dual D-glucose labeled near-infrared emitting probe 2-

Cypate-DG **6** (Figure 5.2.5).[13] The uptake mechanism of 2-Cypate-DG **6** by GLUTs is not well understood.

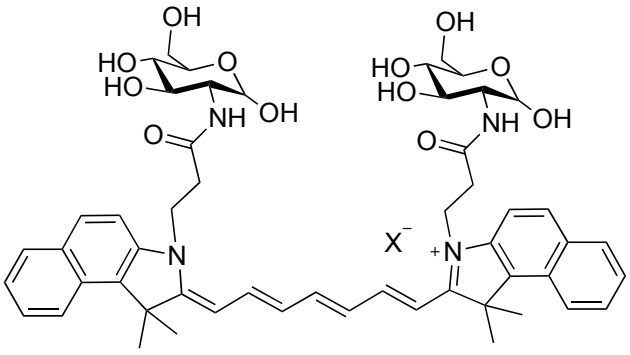

2-Cypate-DG (**6**)

Figure 5.2.5. A dual hexose labeled near-infrared emitting chromophore

According to the study by Gambhir and coworkers, GLUTs do not mediate the transport of near-infrared emitting hexoses,[10] whereas the other studies suggest a GLUT-mediated uptake path.[11-13] Irrespective of various conflicting reports on the near-infrared emitting hexoses, there are two plausible transport mechanisms for the uptake of these near-infrared emitting hexoses by tumor cells; i) Receptor (GLUT) mediated endocytosis, and ii) Transport by GLUTs

To understand the transport mechanism of the near-infrared emitting hexoses into tumor cells, further studies are required. In addition, the reported near-infrared emitting hexoses were not thoroughly characterized (often relying exclusively upon mass spectrometric analysis for the characterization of the dye-hexose conjugates). As a result, there exists a possibility of presence of some impurities that could alter the experimental observations. Furthermore, the known near-infrared emitting hexoses were developed to

target GLUT1, a D-glucose transporter. But, we are interested in developing GLUT5 targeting near-infrared emitting hexoses, which have never been reported. Thus, our goal is to synthesize thoroughly characterized (using various analytical methods such as NMR, IR and mass spectrometry) near-infrared emitting hexoses to target GLUT5. Development of such near-infrared emitting hexoses might allow the optical imaging of tumors that overexpress GLUT5.

5.3. Near-infrared labeled hexoses to target GLUT5

5.3.1. Design of near-infrared emitting dyes for GLUT5

The general structure of the near-infrared emitting hexose that could potentially target GLUT5 is presented in Figure 5.3.1. Conjugation of a hexose scaffold that exhibits a high affinity for GLUT5 with a near-infrared emitting dye could yield a GLUT5 targeting near-infrared hexose. To separate the hexose moiety from the bulky near-infrared emitting dye, a linker should be added. Though the linker increases the hydrophobicity of the probe, it is useful to prevent the interference of near-infrared emitting chromophore in substrate-GLUT binding process.

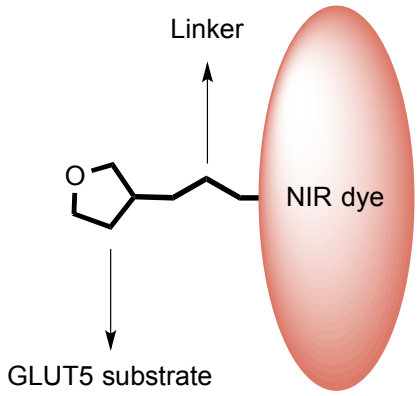

Figure 5.3.1. General representation of near-infrared hexose for GLUT5 targeting

The proposed conjugates **7**, **8** (Figure 5.3.2) were designed to compare the relative affinities of GLUT5 for D-fructose verses 2,5-AM based targeting moieties. On the other hand, probes **8** and **9** (Figure 5.3.2) were designed to study the effect of overall charge (as mediated by anionic sulfonate functionalities) on the uptake of near-infrared emitting hexoses by tumor cells.

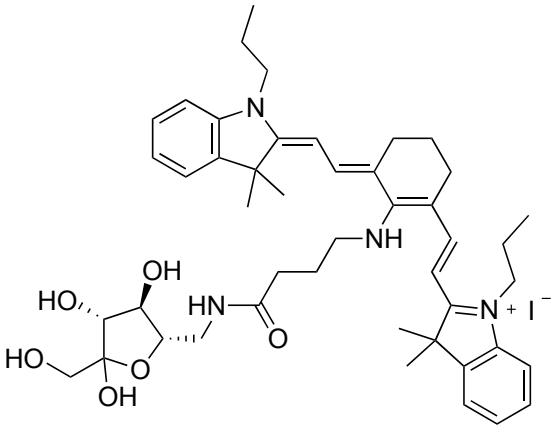

6-IR780-F (**7**)

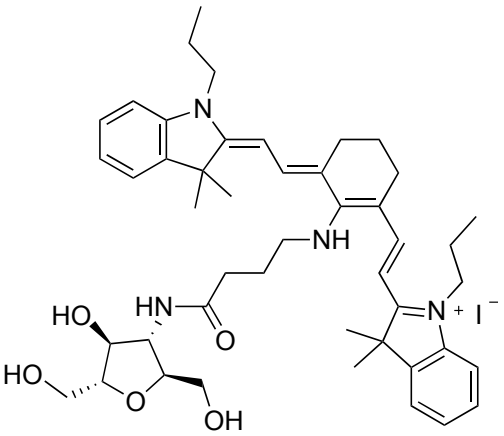

3-IR780-AM (**8**)

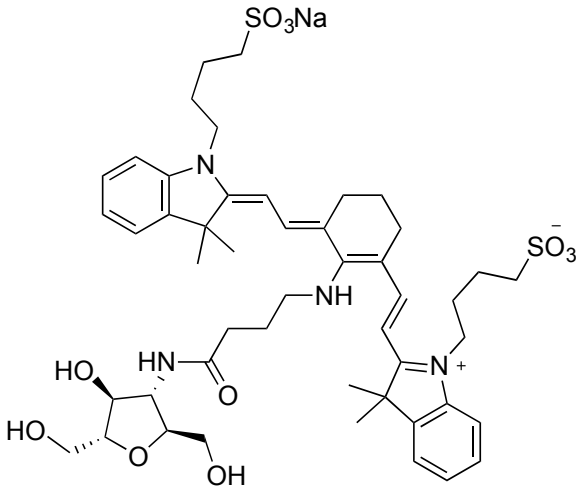

3-IR783-AM (**9**)

Figure 5.3.2. New near-infrared emitting hexoses to target GLUT5 transport protein

5.3.2. Usage of IR-780 iodides as near-infrared emitting chromophores

Previously, the D-glucose-based near-infrared emitting hexoses **ii** were accessed by the treatment of D-glucosamine hydrochloride with the *N*-alkanoicsuccinimides **i** (Scheme 5.3.1) under mild basic conditions.[10-13]

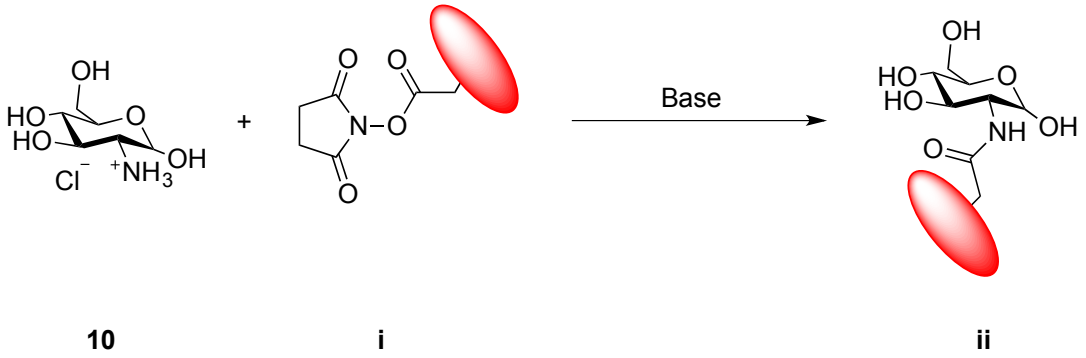

10 **i** **ii**

Scheme 5.3.1 Previous approach to synthesize near-infrared emitting hexoses

As shown in Figure 5.3.1, the vinyl chloride functionality present in IR-780 iodide dye is conjugated to the iminium ion and expected to react with nucleophiles such as primary amines. Therefore, our strategy is to incorporate a linker on the hexose moiety that is functionalized with a primary amine group. The near-infrared dye labeling could be performed by reacting the primary amine on the linker **iii** with IR-780 iodide **17** to yield the near-infrared hexose **iv** (Scheme 5.3.2).

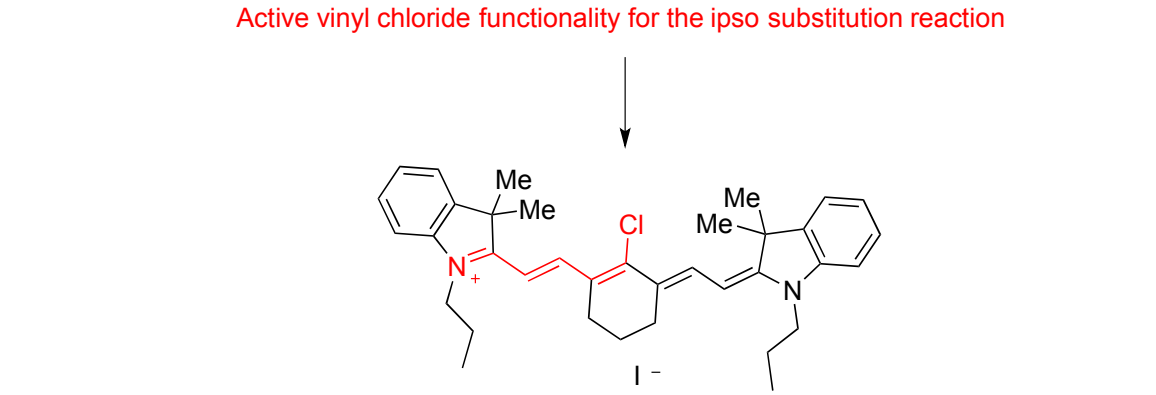

Figure 5.3.3. Highlight of the active vinyl chloride functionality of IR dyes

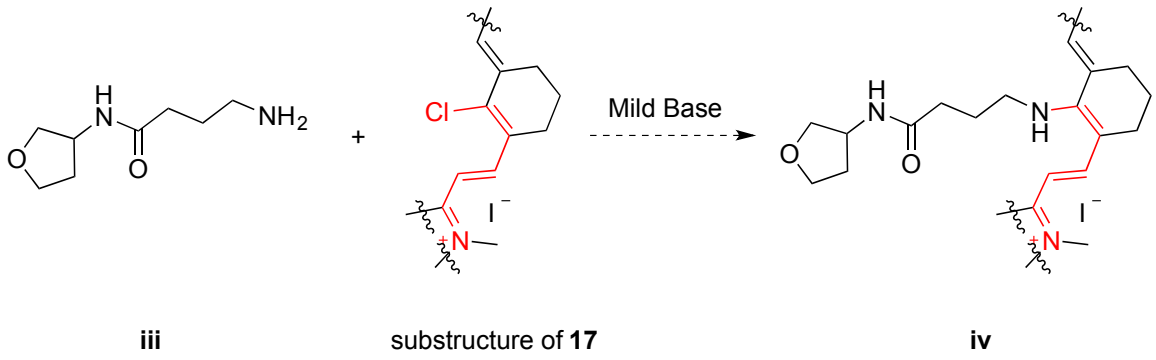

Scheme 5.3.2. Our approach to synthesize near-infrared emitting hexoses *via* ipso substitution

In addition to the presence of synthetically useful active vinyl group, the IR-780 iodide **17** has been demonstrated to provide higher quantum yields when compared to the Cy5 dyes (Figure 5.2.2). Moreover, the IR-780 iodide has been used as photosensitizer in the photodynamic therapy (PDT) of tumors.[14] Thus, if conjugation of IR-780 with a GLUT5 ligand (hexose) leads to accumulation in the tumor cells, these conjugates could be used for both imaging and PDT.

5.4. Synthesis of IR-780 iodide dye

IR-780 iodide dye **17** was synthesized by following a reported protocol.[14] 2-Chloro-3-(hydroxymethylene)-1-cyclohexene-1-carboxylaldehyde **12** was prepared in 92% yield by reacting cyclohexanone **11** with the Vilsmeier formylation reagents (Scheme 5.4.1). Condensation of phenylhydrazine hydrochloride **13** with methyl isopropyl ketone **15** in AcOH afforded quantitative amount of 2,3,3-trimethyl-3*H*-indole **14**. *N*-Propyl-2,3,3-trimethyl-3*H*-indolium iodide **16** was prepared in quantitative yield by the *N*-alkylation of 2,3,3-trimethyl-3*H*-indole **14** with *N*-propyl iodide in CH_3CN at reflux (Scheme 5.4.2). Condensation of the aldehyde **12** with *N*-propyl-2,3,3-trimethyl-3*H*-indolium iodide **16** resulted the formation of IR-780 dye **17** in 64% yield (Scheme 5.4.3).

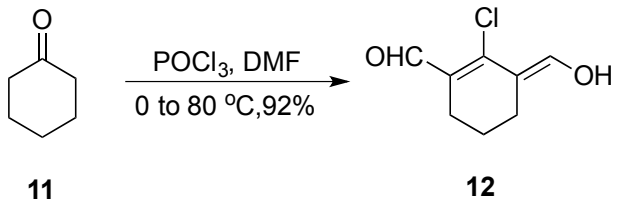

11 **12**

Scheme 5.4.1. Preparation of aldehyde **2**

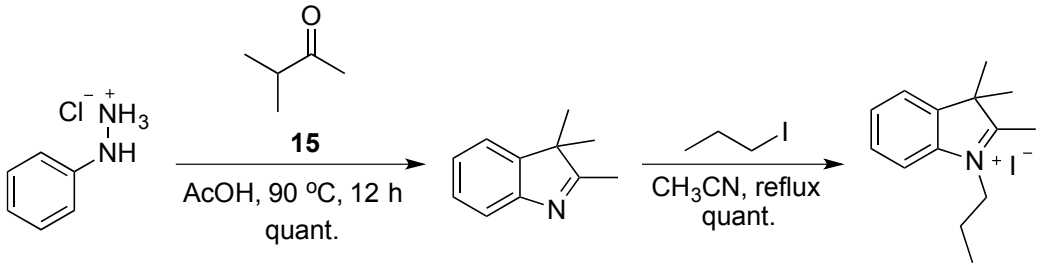

13 **14** **16**

Scheme 5.4.2. Synthesis and *N*-alkylation of 1,1-dimethyl-1*H*-isoindole

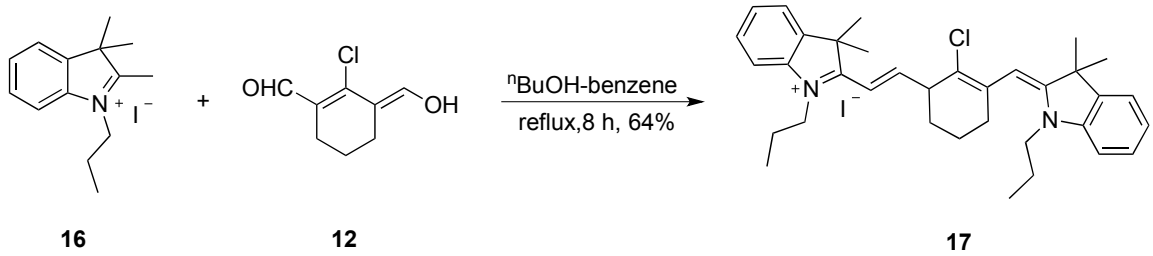

16 12 17

Scheme 5.4.3. Synthesis of IR-780 iodide dye **17** by the condensation of **12** with **16**

5.5. Efforts towards the synthesis of D-fructose based near-infrared emitting hexose

Scheme 5.5.1 represents the retrosynthetic analysis of the near-infrared emitting fructose (3-IR780-F, **7**). Target molecule **7** can be accessed by the deprotection of ketal functionality of compound **22**. We envisioned the synthesis of ketal-protected near-infrared emitting hexose **22** by the ipso substitution of vinyl chloride present in IR-780 dye **17** with amine **21**. Reduction of azide **20** can afford the amine **21**. A chemoselective amidation of the compound **19** can install the linker on the ketal-protected D-fructose moiety to yield **20**. Finally, reduction of the azide **18** provides access to the amine **19**. The synthesis of azide **18** was carried out from D-fructose following a literature protocol.[15]

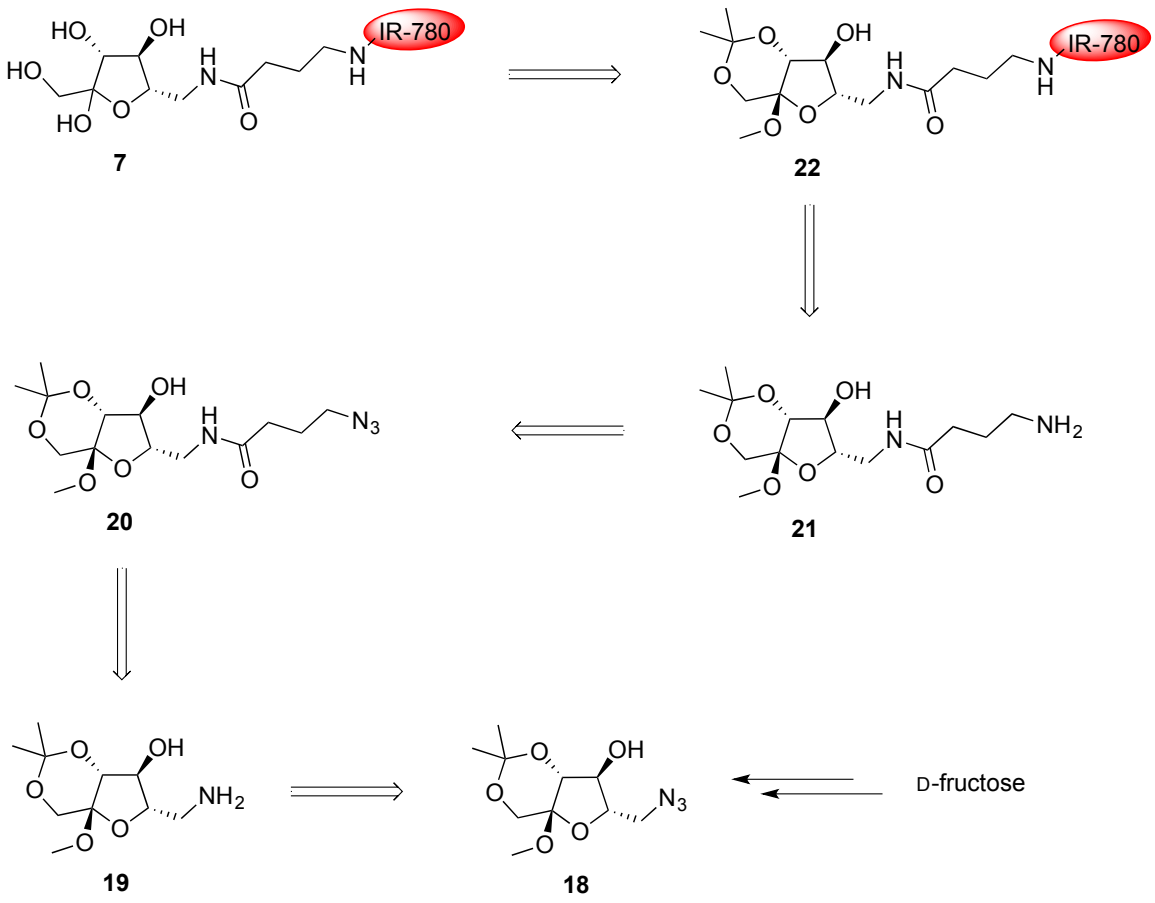

Scheme 5.5.1. Retrosynthetic analysis of 6-IR780-F **7**

5.5.1. Forward synthesis of near-infrared emitting D-fructose 7

Glycosidation and ketal protection of D-fructose was carried out in one-pot by following a literature procedure.[15] Under acidic conditions, D-fructose reacted with MeOH to generate 1:1 mixture of anomers **23a** and **23b**. Treatment of the resulting mixture with 2,2-dimethoxy-propane for a period of 1 h yielded methyl-1,3-*O*-isopropylidene-fructofuranoside **24**, in 62-73% yield over two steps (Scheme 5.5.2).

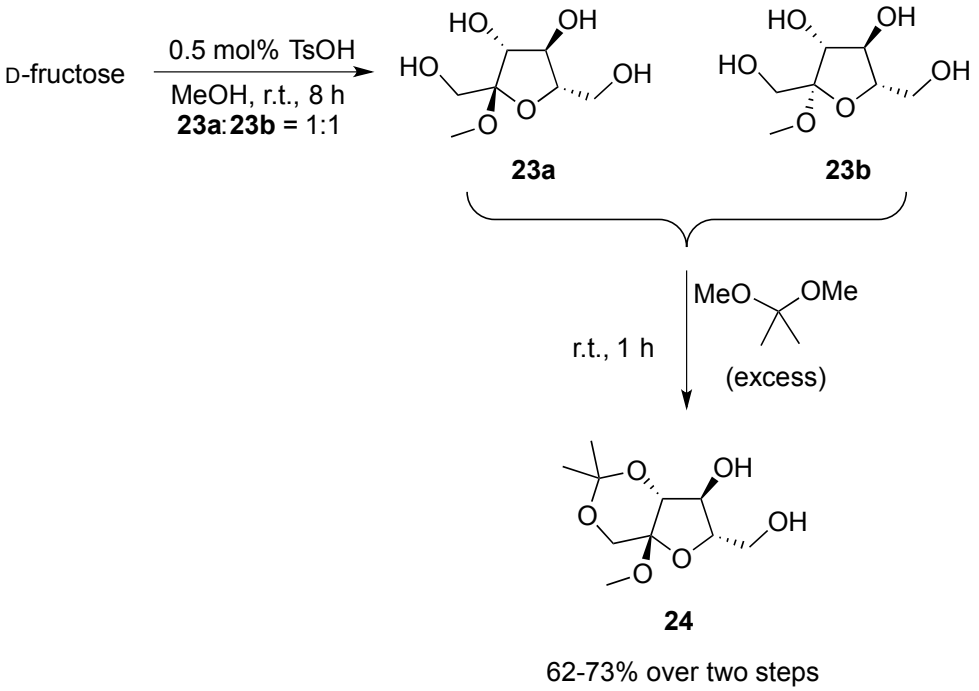

Scheme 5.5.2. Synthesis of ketal-protected D-fructose derivative

Regioselective tosylation of the primary hydroxyl group of compound **24** afforded methyl-1,3-*O*-isopropylidene-6-*O*-(p-toluene)sulfonyl-fructofuranoside **25**. S_N2 displacement of the tosyl group of **25** with sodium azide in hot DMF yielded 86% of methyl-6-azido--6-deoxy-1,3-*O*-isopropylidene-fructofuranoside **18** (Scheme 5.5.3).

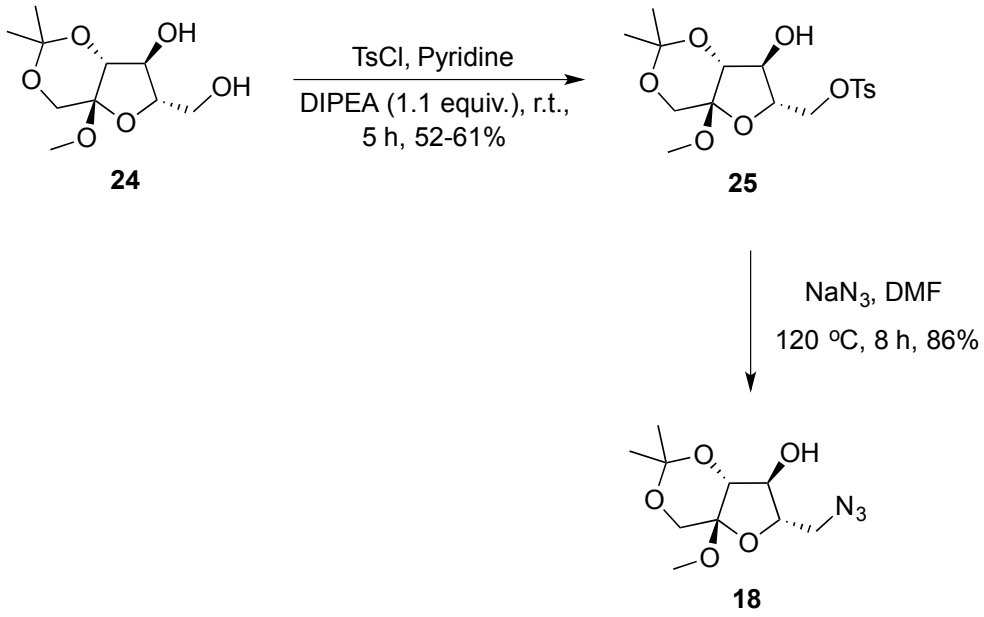

Scheme 5.5.3. Functionalization of the C-6 position of D-fructose with azide

As we accessed the precursor **18**, we focused on the synthesis of the 4-azidobutanoic acid **28**, which will later be used as linker in the near-infrared labeling of hexoses. Ethyl 4-bromobutyrate **26** reacted with sodium azide under heating conditions to produce ethyl 4-azidobutyrate **27** *via* displacement of the bromide ion. Further, the saponification of ethyl 4-azidobutyrate **27** under basic conditions provided access to 4-azidobutanoic acid **28**.[19] Compound **26** was converted into **28** in two steps with a overall yield of 62%.

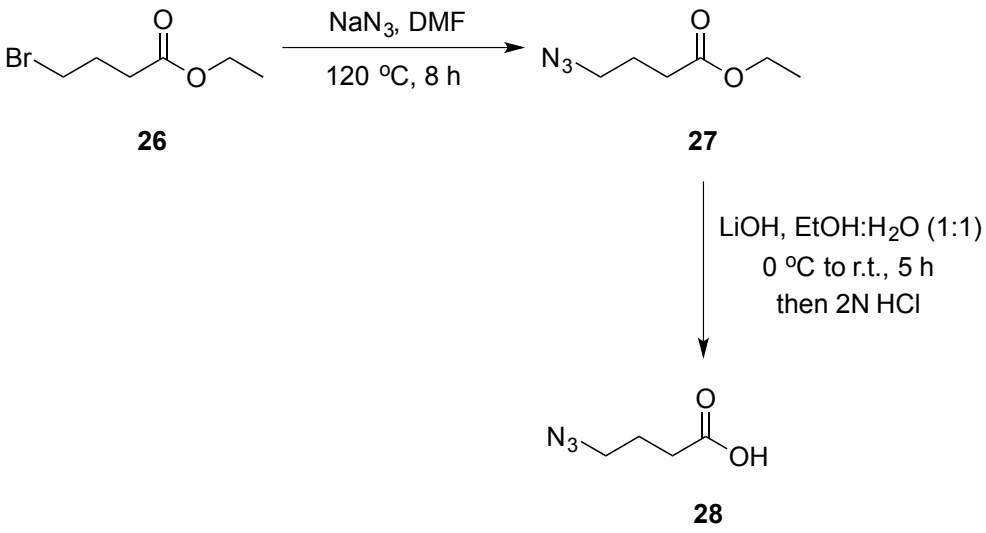

Scheme 5.5.4. Synthesis of 4-azidobutyric acid

4-Azidobutanoic acid **28** reacted with oxalyl chloride to yield 4-azidobutyryl chloride **29**. Acid chloride **29** was then treated with *N*-hydroxysuccinimide to access *N*-(4-azido)butyroxy succnimide **30** in quantitative yield (Scheme 5.5.5).

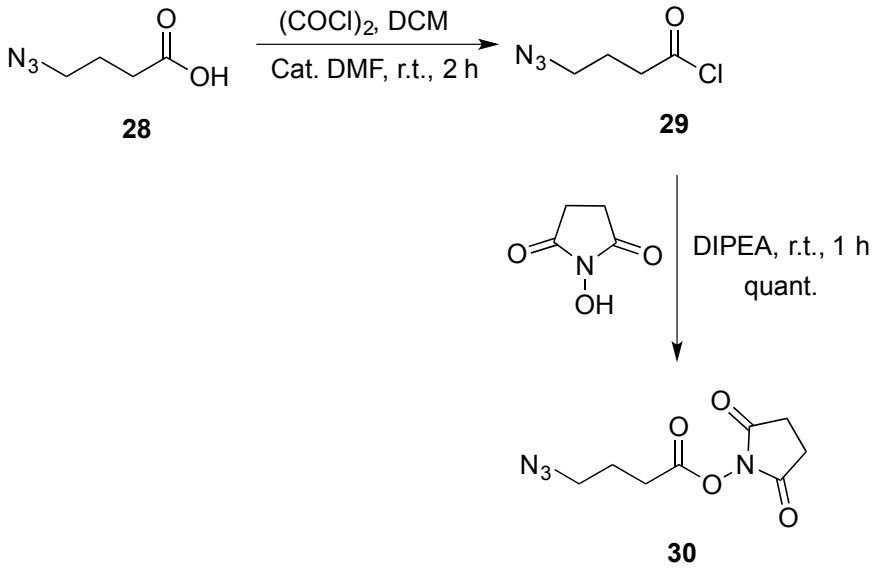

Scheme 5.5.5. Synthesis of active ester **30**

On the other hand, the azide **18** was reduced with $LiAlH_4$ in ether to afford 6-amino-1,3-*O*-isopropylidene-2-*O*-methyl-fructofuranoside **19** in quantitative yields. The crude form of the amine **19** reacted with the active ester **30** in MeOH to produce 6-(4-azido)butyramido-6-deoxy-1,3-*O*-isopropylidene-fructofuranoside **20** (Scheme 5.5.6).

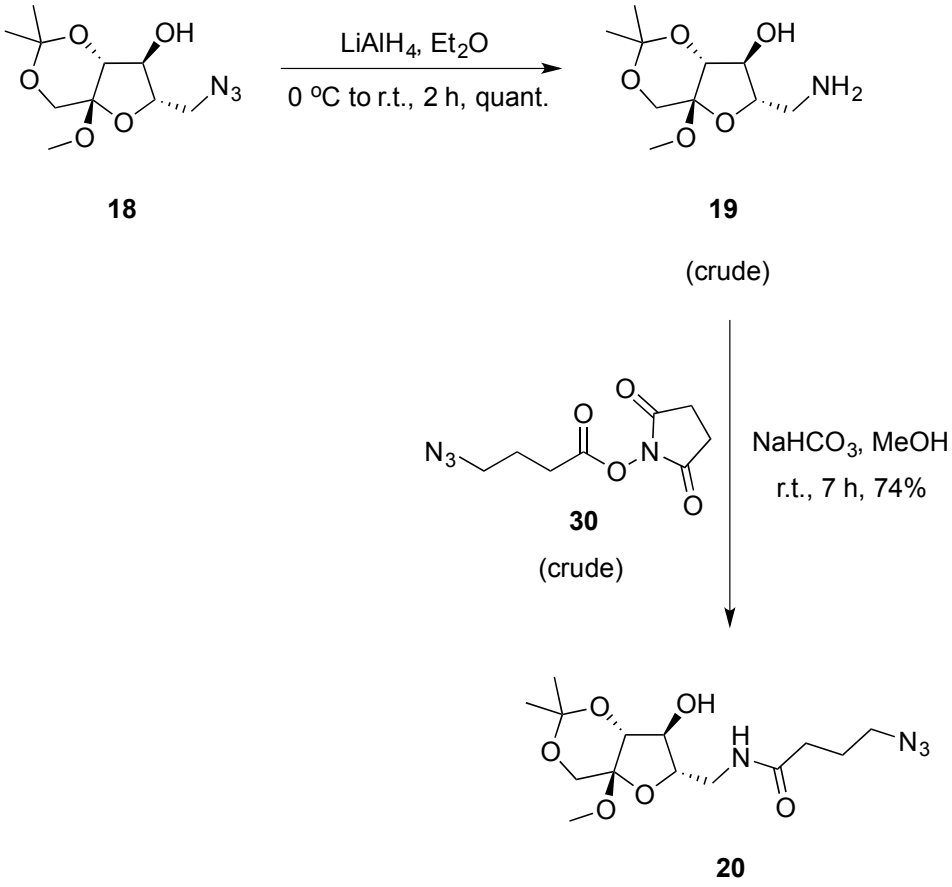

Scheme 5.5.6. Incorporation of 4-azido-linker into D-fructose derivative

The azide functionality of **20** was reduced to by palladium catalyzed hydrogenolysis in EtOAc to yield 6-(4-amino)butyramido-6-deoxy-1,3-*O*-isopropylidene-2-*O*-methyl-fructofuranoside **21** (Scheme 5.5.7). As we synthesized the precursor amine

21, we proceeded to the optimization of ipso substitution reaction of IR-780 dye **17** with amine **21**.

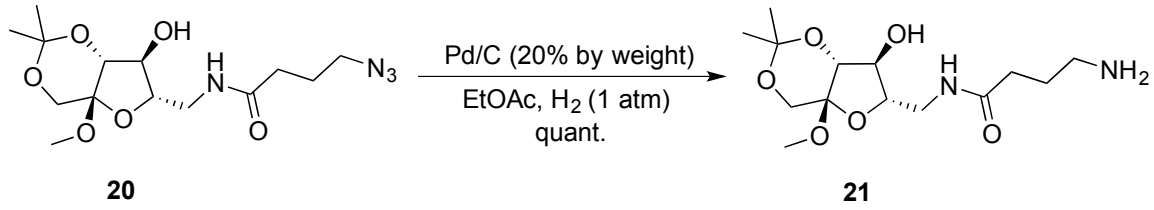

20 **21**

Scheme 5.5.7. Palladium-catalyzed hydrogenolysis of reduction the 4-azidoamide

Table 5.5.1 shows the observed yields of ipso substitution product **22** under different reaction conditions. In protic solvent MeOH, lower yields of the product were observed, irrespective of the nature of the base additive (Table 5.5.1, entries 1 and 2). However, a slight increase in the product yield was observed when $NaHCO_3$ was used as base instead of triethylamine. This could be due to the reactivity of triethylamine as nucleophile. A slight improvement in the product yield was observed when the solvent was changed from MeOH to aprotic DCM (Table 5.5.1, entries 3 and 4). Though the reaction appeared to proceed cleanly under the DCM/$NaHCO_3$ conditions, we observed low conversion of the starting materials (Table 5.5.1, Entry 4). With the slight increase in solvent polarity by the usage of THF as a solvent instead DCM, we observed almost no change in product yields (Table 5.5.1, entry 5). Finally, a greater increase in the product formation was observed as we changed the solvent to polar aprotic DMF (Table 5.5.1, entries 6 and 7). To our surprise, utilization DIPEA as base led to the formation of small amounts of inseparable impurities (observed in the product ^{1}H NMR spectrum). Such impurities were not observed when $NaHCO_3$ was utilized as base.

Table 5.5.1. Optimization of the ipso substitution reaction of IR-780 **17** dye with amine **34**

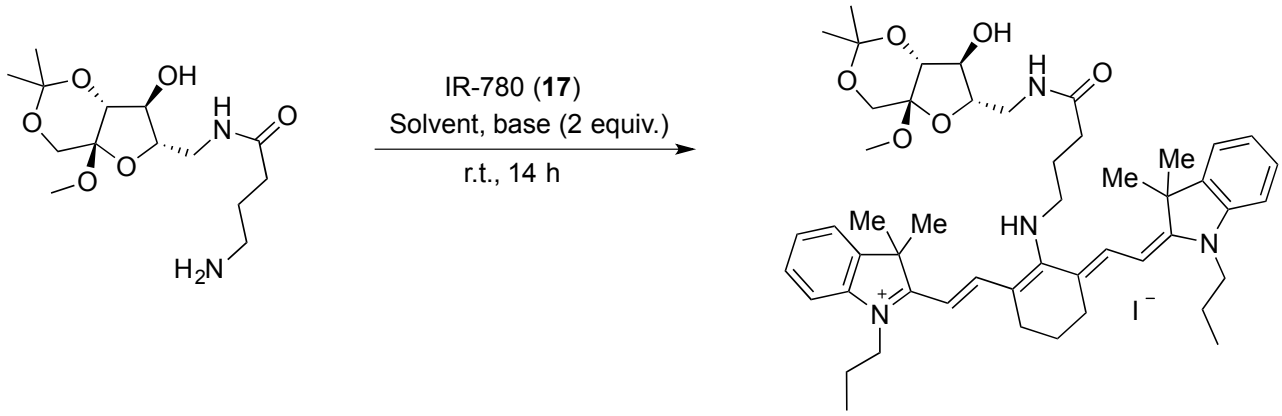

21 **22**

Entry	Solvent	Base	Yield
1	MeOH	Et_3N	30[a]
2	MeOH	$NaHCO_3$	44[a]
3	DCM	Et_3N	41[a,b]
4	DCM	$NaHCO_3$	50[b]
3	THF	$NaHCO_3$	44[b]
4	DMF	DIPEA	68[c]
5	DMF	$NaHCO_3$	78[d]

[a]Complete conversion of the IR-780 iodide dye **17** was observed. [b]IR-780 iodide dye **17** was not completely consumed. [c]Unknown impurities were observed by the ^{1}H NMR analysis of the product. [d]Reaction time was increased to 24 h.

Table 5.5.2. Unfruitful attempts to access the target near-infrared emitting hexose **7** via deprotection of ketal functionalities of compound **35**

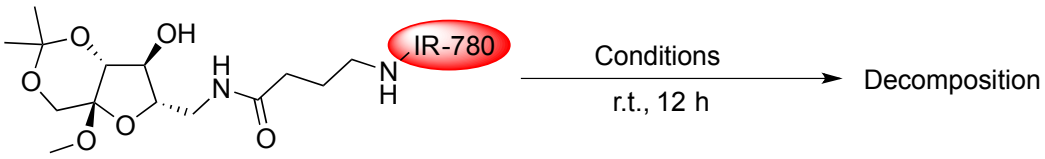

22

Entry	Solvent	Catalyst
1	MeOH	HCl[a]
2	MeOH	PPTS[b]
3	MeOH	AcOH[a,b]
4	DMF	PPTS [b,c]
5	DMF	AcOH[b,c]
6	MeOH	I_2[b]

[a]1% of H_2O in MeOH was used. [b]10 mol% of catalyst was used.
[c]1.1 equiv. of ethane-1,2-dithiol was added.

Despite several attempts to cleave the anomeric *O*-methyl and ketal group of compound **35** to access the target near-infrared emitting hexose **7**, we remained unsuccessful (Table 5.3.2). Under the strong acidic conditions, we observed decomposition of the starting material **35** (Table 5.3.2, entry 1). Next, we attempted selective deprotection of the ketal functionality in the presence of PPTS or AcOH in MeOH; however, even under these milder conditions we observed decomposition of

compound **35** (Table 5.5.2, entries 2 and 3). We changed the solvent from aqueous/MeOH to DMF to prevent the plausible hydrolysis of the chromophore and 1,2-ethane-dithiol was added to capture the acetone molecule generated in the ketal deprotection process (Table 5.5.2, entries 4 and 5). Unfortunately, the all these efforts led to decomposition of **35**. Molecular iodine catalyzed deprotection of ketal functionality was previously demonstrated.[16] By considering the acid sensitivity of the chromophore, we attempted the selective deprotection the ketal functionality under these mild conditions, but, remained unsuccessful (Table 5.5.2, entries 6).

5.6. Synthesis of 2,5-anhydro-D-mannitol based near-infrared emitting hexose

5.6.1. Retrosynthesis of 2,5-anhydro-D-mannitol based near-infrared emitting hexose 8

We previously demonstrated the successful ipso substitution of the vinyl chloride functionality of IR-780 iodide dye **17** with primary amine functionality. The target near-infrared emitting hexose **8** could be accessed by the ipso substitution of the vinyl chloride functionality of IR-780 dye **17** with the amine **34**. A palladium catalyzed hydrogenolysis of compound **34** not only reduces the azide functionality, but also cleaves the benzyl ether functionalities to yield the amine precursor **35**. Treatment of 3-amino-2,5-anhydro-D-mannitol **33** with acid chloride **29** affords the azide **34**. Protection of alcoholic groups of the azido-sugar **31**, followed by the reduction of the azido functionality could provide access to the amine **33** (Figure 5.6.1).

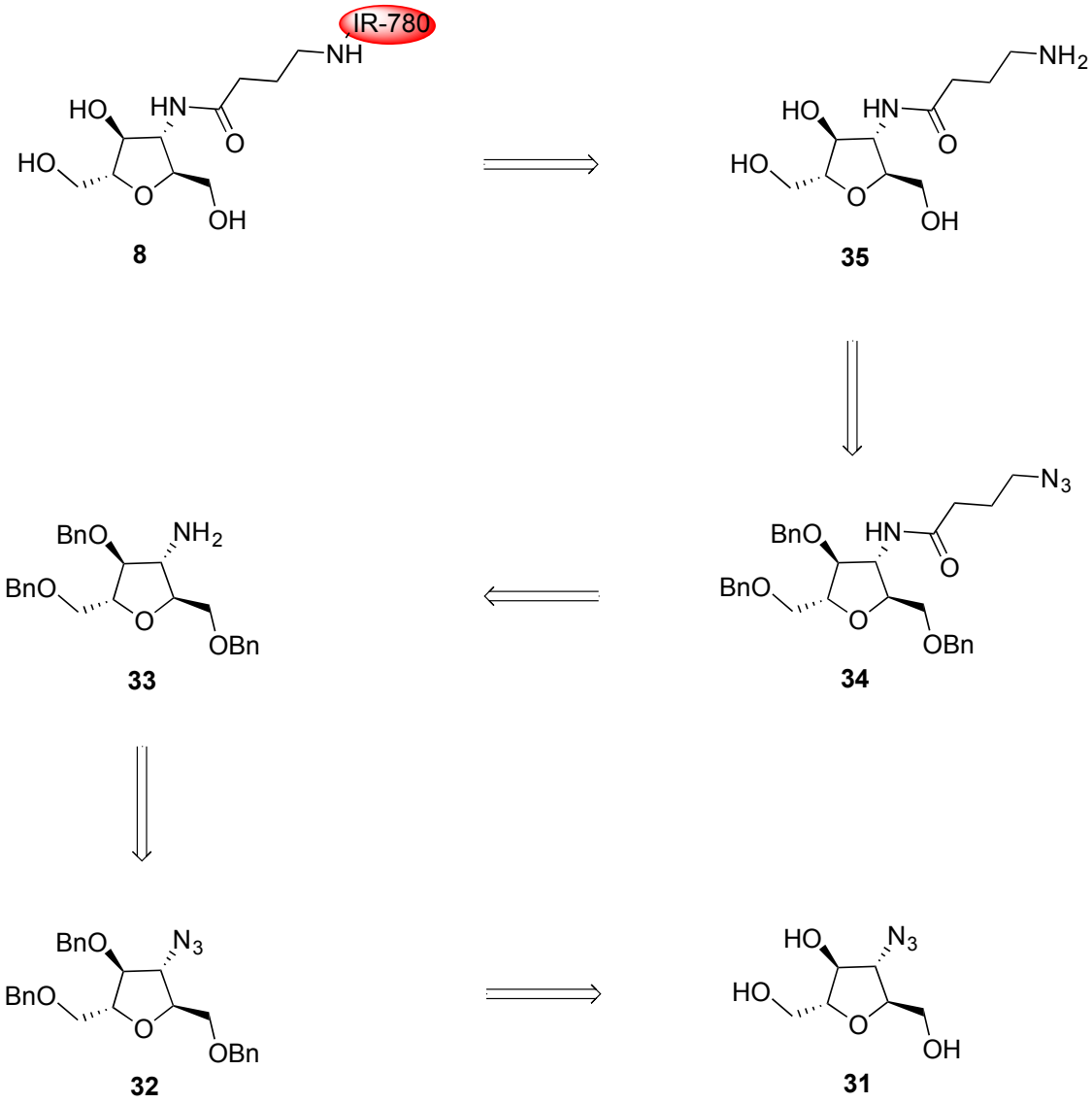

Scheme 5.6.1. Retrosynthetic analysis of the compound **8**

In Chapter 2 (Section 2.4), we demonstrated synthesis of 3-azido-3-deoxy-2,5-anhydro-D-mannitol **31** *via* diastereoselective ring-opening of 2,5:3,4-dianhydro-D-allitol. Hydroxyl groups of **31** were protected as benzyl ethers by treating with sodium hydride and benzyl bromide in DMF to yield 94% of 3-azido-3-deoxy-1,4,6-tri-*O*-benzyl-2,5-anhydro-D-mannitol **32** (Scheme 5.6.2). The azide functionality of compound **32** was

reduced with $LiAlH_4$ to produce 1,4,6-tri-*O*-benzyl-3-amino-2,5-anhydro-D-mannitol **33** in quantitative yields (Scheme 5.6.2).

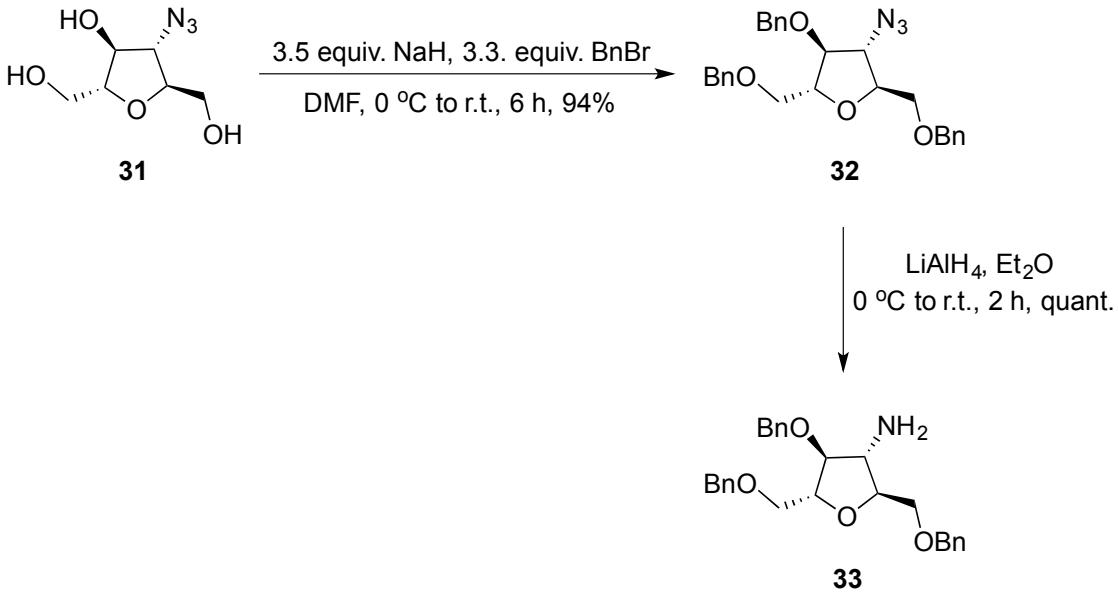

Scheme 5.6.2. Synthesis of amine intermediate **33**

The amine **33** reacted with 4-azidobutyryl chloride **29** to incorporate the linker moiety on the hexose scaffold, providing 96% yield of 3-(4-azido)butyramido-3-deoxy-1,4,6-tri-*O*-benzyl-2,5-anhydro-D-mannitol **34** (Scheme 5.6.3). Further, the reduction of the azido functionality of the linker moiety and cleavage of the benzyl ethers present on the hexose moiety were accomplished in a single step. The palladium catalyzed hydrogenolysis of **34** in acidified MeOH afforded corresponding amine hydrochloride salt **35** in quantitative yield (Scheme 5.6.3).

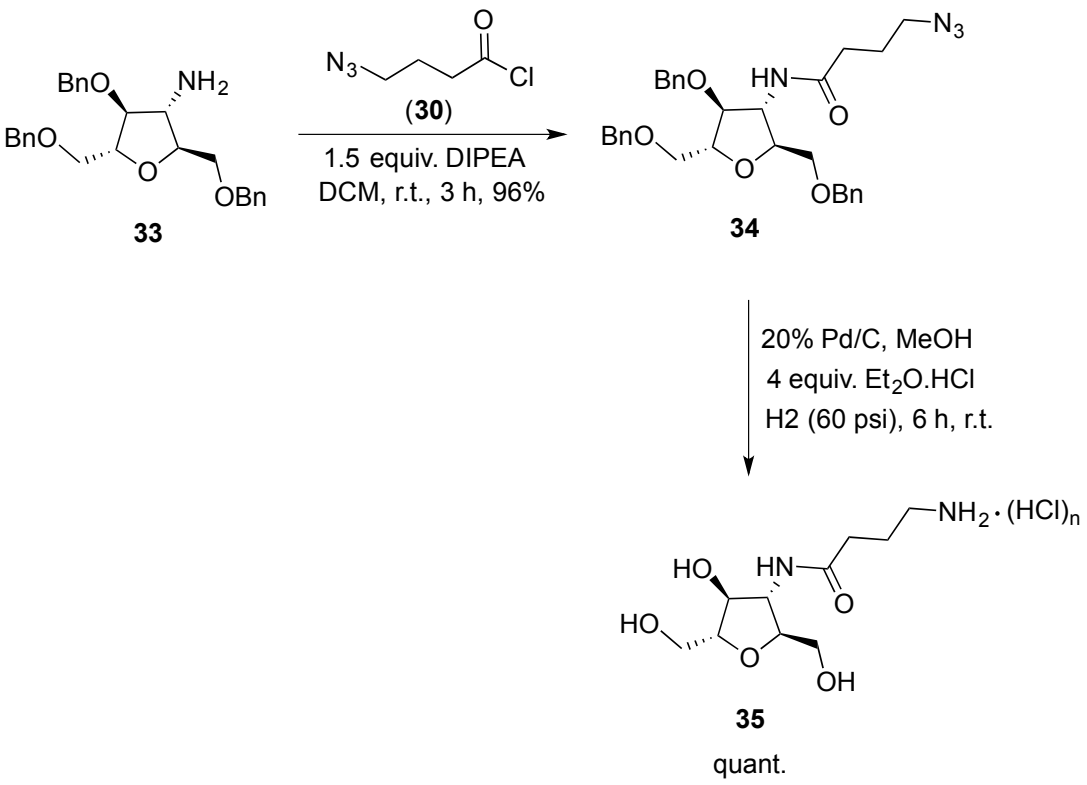

Scheme 5.6.3. Synthesis of 2,5-AM derivative with amido-linker

After accessing the precursor amine hydrochloride, we proceeded for the labeling of **35** with a near-infrared emitting chromophore. We previously optimized the ipso substitution reaction between the primary amine and IR-780 iodide (Table 5.5.1), which contains active vinyl chloride functionality. The amine hydrochloride was stirred with an excess of $NaHCO_3$ in DMF to generate the amine from the corresponding hydrochloride salt **35**. The amine reacted with IR-780 iodide **17** under the optimized conditions to access the target near-infrared emitting hexose **8** in good yields (Scheme 5.6.4).

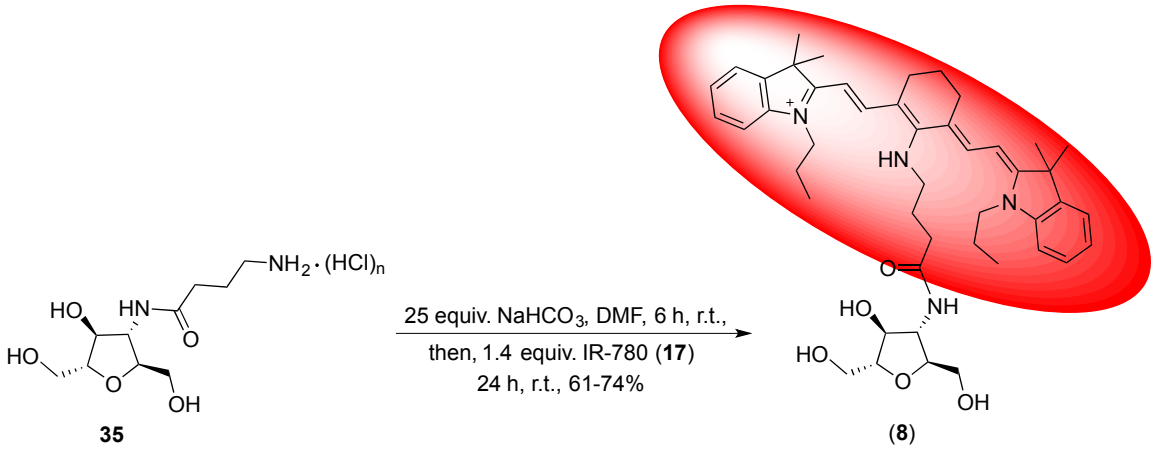

Scheme 5.6.4. IR-780 labeling of C-3 modified 2,5-AM derivative

After the successful synthesis of **8**, labeling of the amine precursor **35** was carried out with IR-783 iodide **36** (Figure 5.6.1). Though we observed good conversion of the starting materials during the reaction between the corresponding amine of compound **35** and IR-783 dye **36** (Figure 5.6.1), due to difficulties associated with the purification process, we observed moderate to low yields of the product **9** (Scheme 5.6.5).

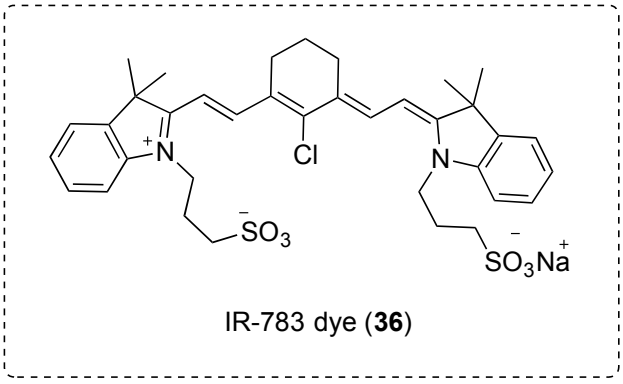

Figure 5.6.1. Structure of IR-783 dye

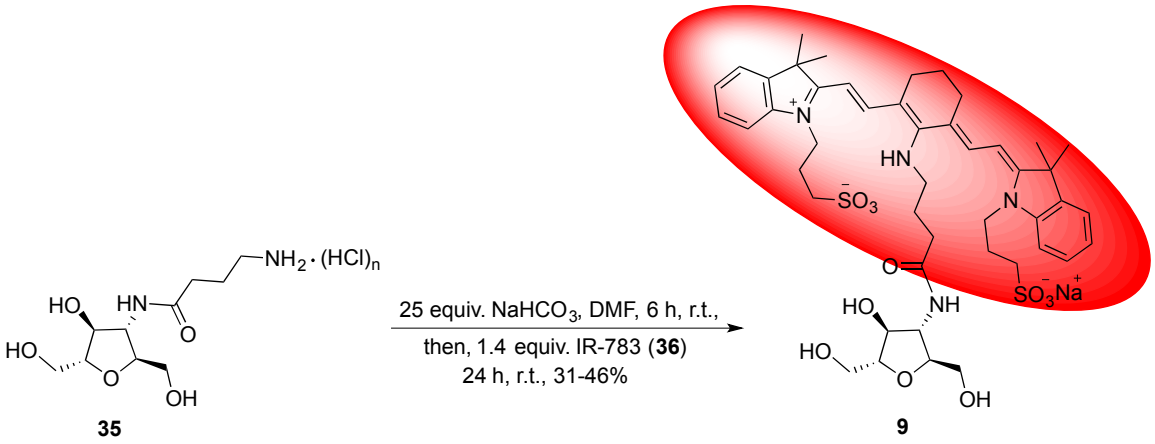

Scheme 5.6.5. IR-783 labeling of C-3 modified 2,5-AM derivative

5.7. Biological evaluation of the new near-infrared emitting hexoses 8 and 9

Given the access to two near-infrared hexoses (3-IR780-AM **8** and 3-IR783-AM **9**) that have the potential to target GLUT5, we proceeded to *in vitro* evaluation of **8** and **9**. Despite the very similar structural features of **9** and **8**, the hexose derivative **9** contains anionic sulfonate groups. Thus, by comparing the transport of **9** and **8**, it is possible to assess the sensitivity of GLUT5 to transport hexoses bearing anionic payloads.

We incubated the EMT-6 cells with 150 μM **8** or **9** over a period of 45 min and the fluorescence remaining in the cells was measured by fluorescence plate reader (FPR). For this study, Krebs buffer that contained 1% DMSO was used to overcome the solubility issues with 3-IR780-AM **8**. Clearly, 3-IR783-AM **8** exhibited superior accumulation into EMT-6 cells over the 3-IR783-AM **9** (Figure 5.7.1).

Figure 5.7.1. Uptake comparison of 3-IR780-AM **8** and 3-IR-783-AM **9** in EMT-6 cells. The EMT-6 cells were incubated for 60 min at 37 °C incubation with **8** an **9**. Error bars represent SEM of the triplicates.

However, 3-IR780-AM **8** is less hydrophilic in nature than 3-IR783-AM **9**, and there is a plausibility of the adsorption of **8** to the cell surface. Thus, we employed an alternative technique, confocal imaging. As shown in Figure 5.7.2, the confocal images were obtained after the 60 min incubation of EMT-6 cells with 10 μM extracellular concentration of 3-IR780-AM **8**, 3-IR783-AM **9** and IR783 **36**, respectively. It is important to mention that, after an incubation period of 60 min, before we mounted the cells on a glass coverslip for the confocal study, the cells were washed thoroughly with EtOH. As a result, no 3-IR780-AM **8** molecule is expected to remain in the extracellular space. Therefore, the uptake comparison between the near-infrared emitting compounds *via* confocal imaging may be more reliable method than the fluorescence plate reader method.

As shown in Figure 5.7.2, very high fluorescence of EMT-6 cells that were incubated with 3-IR780-AM **8** confirmed the accumulation of 3-IR780-AM **8** in EMT-6

cells. On the other hand, 3-IR783-AM **9** and IR783 iodide **36** exhibited poor accumulation and resulted in low fluorescence of EMT-6 cells. Previously, near-infrared emitting dyes were demonstrated to show accumulation into tumor cells even without hexose labeling.[10] But, based on the comparison made between the uptake of **7**, **9** and **41** by EMT-6 cells *via* confocal imaging, it appeared that there is a significant difference in the relative transport of these near-infrared emitting compounds.

Further, confocal imaging is a technique that can be only used for the comparison of relative uptake of probes. Our results with confocal imaging study only concludes the higher uptake of fructose analogue-labeled chromophores by breast cancer cells, but does not rule out the complete lack of uptake of near-infrared emitting chromophores by tumor cells. Hence, these results only show the poor accumulation of the near-infrared emitting compounds IR-783 iodide dye **36** and 3-IR783-AM **9** when compared to the probe 3-IR780-AM **8**. Our results also emphasize that by avoiding the incorporation of anionic functionalities in the dye structure, the efficiency of the tracer used in optical imaging can be increased.

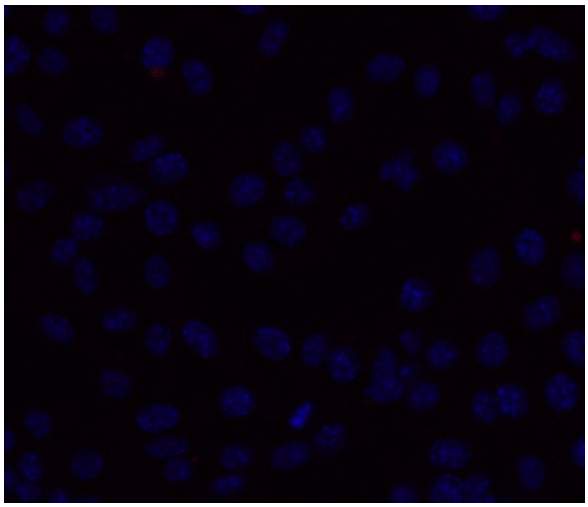

EMT-6 cells incubated with Krebs buffer

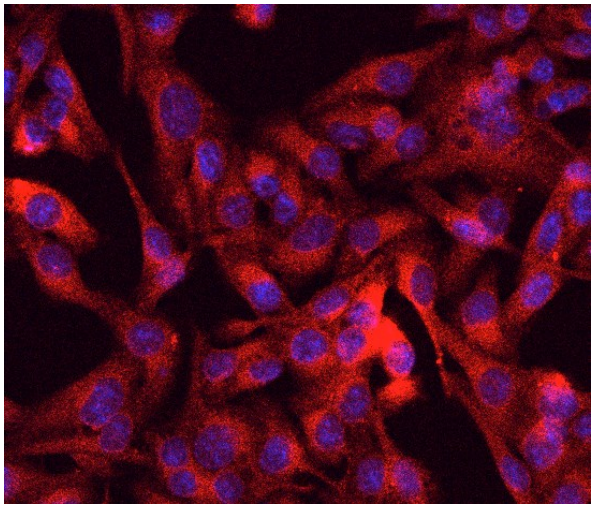

EMT-6 cells incubated with 3-IR780-AM **8**

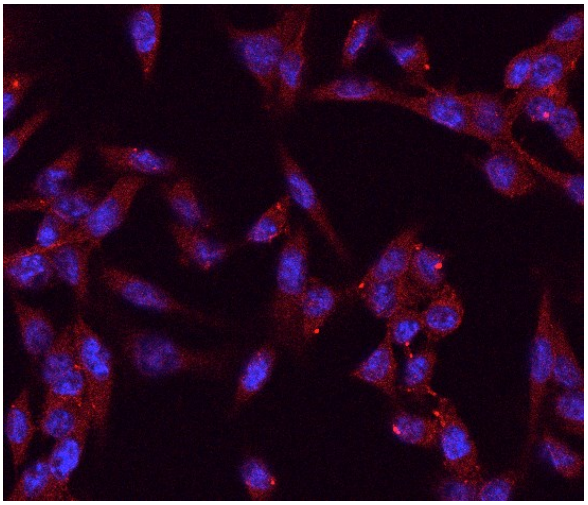

EMT-6 cells incubated with 3-IR783-AM **9**

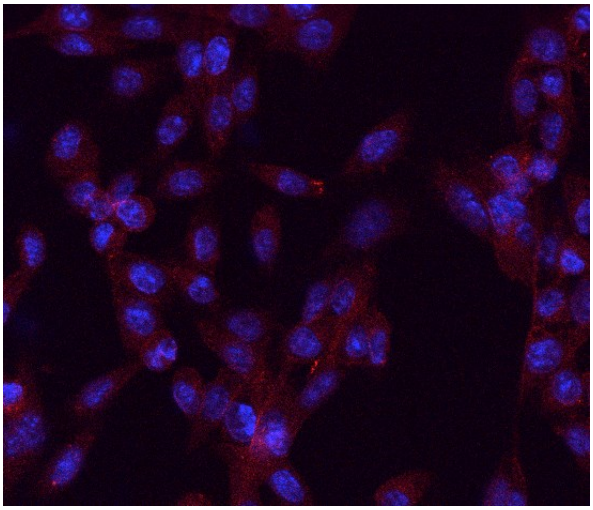

EMT-6 cells incubated with IR783 dye **36**

Figure 5.7.2. Confocal imaging of EMT-6 cells performed after the treatment with 10 μM extracellular concentration of various near-infrared emitting hexoses for 45 min at 37 °C. The nuclei are stained with DAPI.

Previous experiments only concluded the low accumulation of 3-IR783-AM **9** when compared to 3-IR780-AM **8**, but did not provide any information about the uptake path of these hexoses. In order to understand the transport mechanism of **8** and **9**, further studies were required. Encouraged by the uptake studies *via* FPR and confocal imaging, we proceeded further to study the ability of 3-IR780-AM **8** and 3-IR783-AM **9** to inhibit [^{14}C]-hexose transport into EMT-cells. To our surprise, **9** did not inhibit the transport of either [^{14}C]-D-fructose or [^{14}C]-D-glucose transport into EMT-6 cells. This study eliminates the plausible receptor (GLUT)-mediated endocytosis uptake path of 3-IR783-AM **9**. Lack of GLUT recognition for 3-IR783-AM **9** could be due to presence of anionic sulfonate functionalities. Very low accumulation of 3-IR783-AM **9** into EMT-6 cells, observed by confocal imaging technique (Figure 5.7.2), could be due to alternative paths such as endocytosis. This observation is in agreement with the studies conducted by Gambhir and co-workers.[10]

To our delight, we observed both [^{14}C]-D-fructose and [^{14}C]-D-glucose transport inhibition into EMT-6 cells by 3-IR780-AM **8** (Figures 5.7.3 and 5.7.4). The hexose scaffold present in 3-IR780-AM **8** is a 2,5-AM derivative that is functionalized with amide group at position C-3. This scaffold was previously demonstrated to target GLUT5 with higher affinity and GLUT1 with low affinity (Chapter 3). Very similar to our previous observation, we observed greater ability of 3-IR780-AM **8** to block [^{14}C]-D-fructose transport into EMT-6 cells when compared to the ability to inhibit [^{14}C]-D-glucose transport.

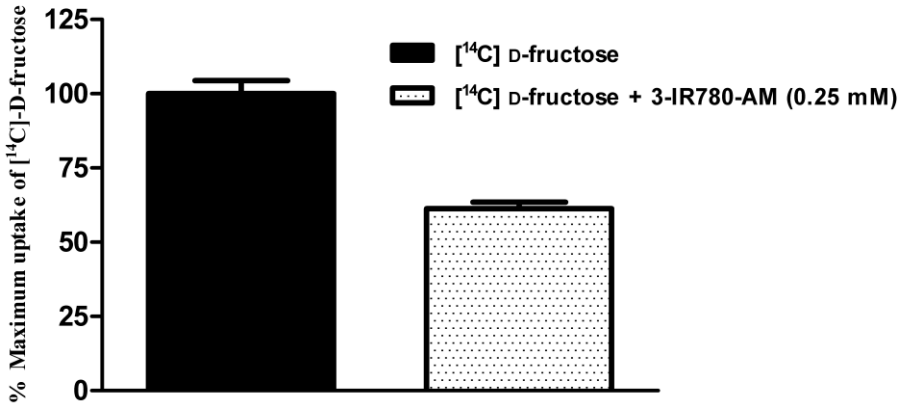

Figure 5.7.3. Inhibition of [^{14}C]-D-fructose transport into EMT-6 cells by 0.25 mM extracellular 3-IR780-AM **8** after 25 min at 25 °C. Error bars represent the SEM of triplicates.

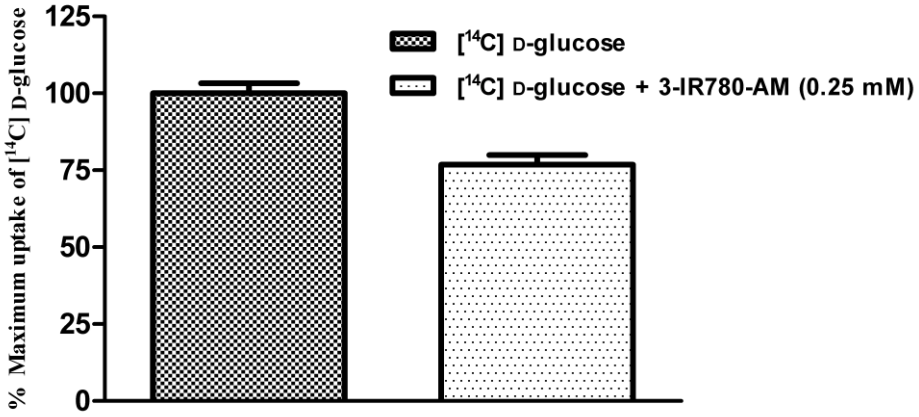

Figure 5.7.4. Inhibition of [^{14}C]-glucose transport into EMT-6 cells by 0.25 mM extracellular 3-IR780-AM **8** after 25 min at 25 °C. Error bars represent the SEM of triplicates.

Furthermore, 3-IR780-AM **8** also inhibited [^{14}C]-D-fructose transport in the presence of 100 μM extracellular CB, but not [^{14}C]-D-glucose transport (Figures 5.7.5 and 5.7.6, respectively). As it was previously demonstrated (Chapters 3 and 4) CB is a noncompetitive Class-I GLUT inhibitor. Inability of **8** to block the D-glucose transport in the presence of CB confirms the involvement of Class-I D-glucose transporters. The D-glucose transport inhibition by **8** confirms the recognition of Class-II or III D-fructose transporters. Thus, transport of 3-IR780-AM **8** is facilitated by at least two transporters. Previously, the C-3 modified 2,5-AM derivative labeled with chromophore NBD also exhibited similar properties. Based on our studies furnished in Chapter 4, we concluded GLUT1 and GLUT5 recognition for the NBD labeled probe. Similar results with 3-IR780-AM **8** denote GLUT1 and GLUT5 recognition for 3-IR780-AM **8**

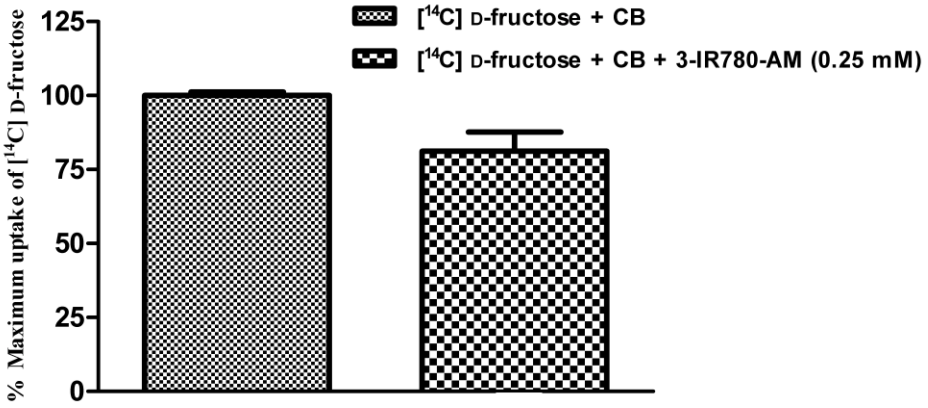

Figure 5.7.5. Inhibition of [^{14}C]-D-fructose transport into EMT-6 cells treated with 100 μM CB and then 0.25 mM extracellular 3-IR780-AM and 100 μM D-fructose for 25 min at 25 °C. Error bars represent the SEM of triplicates.

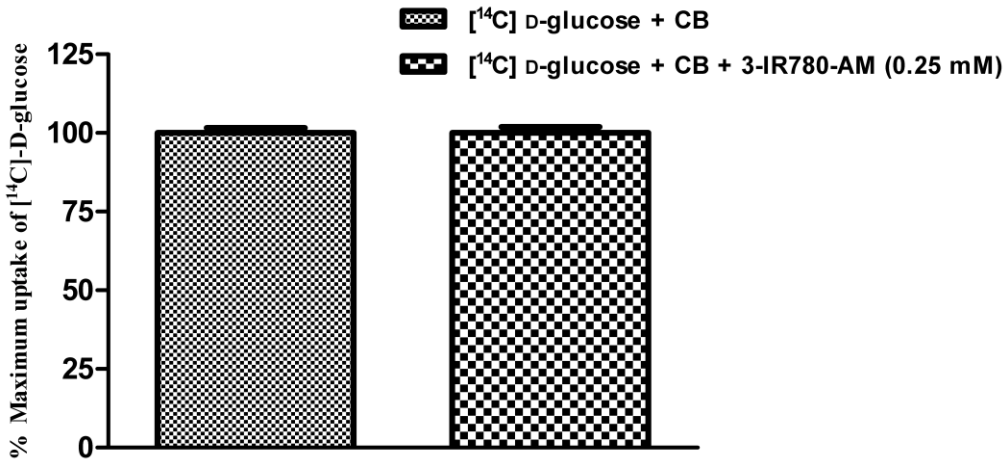

Figure 5.7.6. Inhibition of [^{14}C]-D-glucose transport into EMT-6 cells treated with 100 μM CB and then 0.25 mM extracellular 3-IR780-AM and 100 μM D-glucose for 25 min at 25 °C. Error bars represent the SEM of triplicates.

Having observed the ability of **8** to mimic natural hexose GLUT ligands, we studied the effect of extracellular hexoses on the transport of 3-IR780-AM **8** into EMT-6 cells. We observed reduction in the uptake of 3-IR780-AM **8** by EMT-6 cells in the presence of D-fructose and D-glucose (Figure 5.7.7). In the presence of extracellular D-fructose, greater reduction of IR780-AM **8** transport into EMT-6 cells was observed when compared to uptake in the presence of D-glucose. The above study concludes the ability of IR780-AM **8** to closely mimic D-fructose analogue.

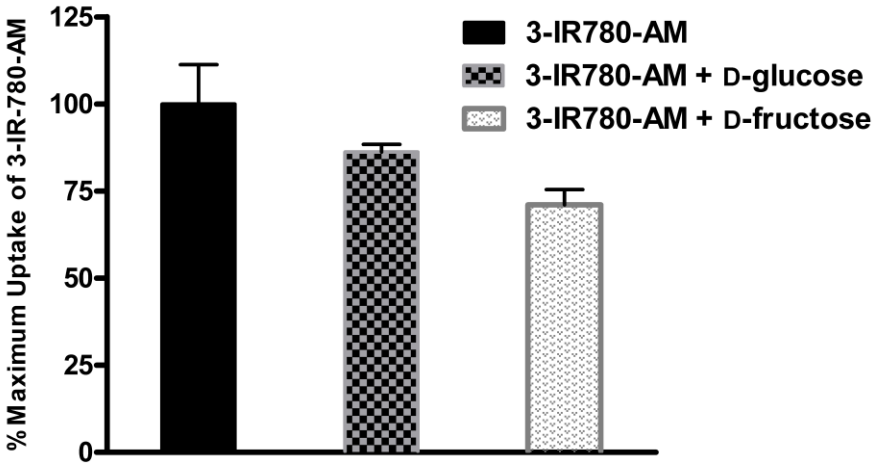

Figure 5.7.7. Inhibition of [^{14}C]-glucose transport into EMT-6 cells by 0.25 mM extracellular 3-IR780-AM after 25 min at 25 °C. Error bars represent the SEM of triplicates.

EMT-6 cells incubated with 3-IR780-AM **8** for 45 min at 25 °C

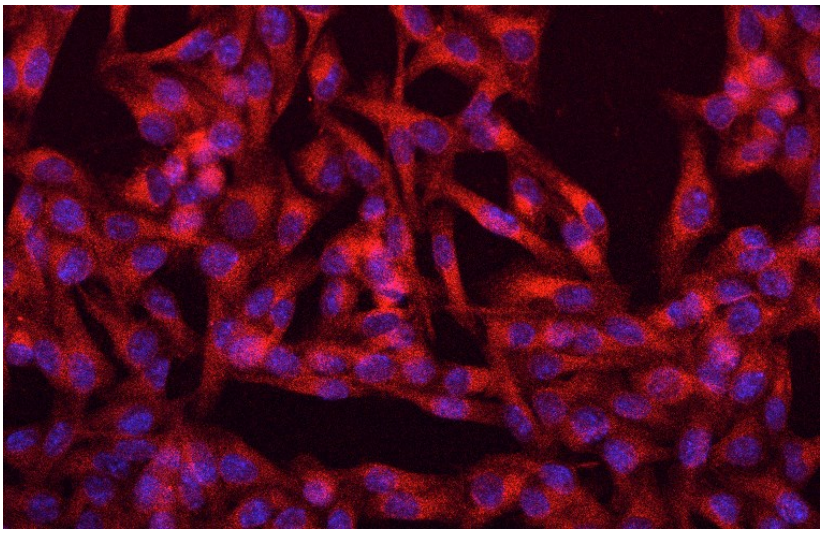

EMT-6 cells incubated with 3-IR780-AM **8** and 50 mM D-glucose for 45 min at 25 °C

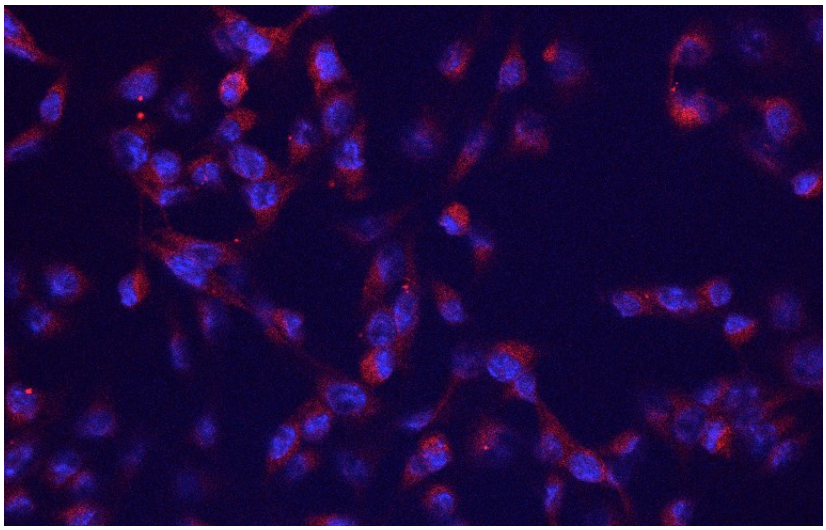

EMT-6 cells incubated with 3-IR780-AM **8** and 50 mM D-fructose for 45 min at 25 °C

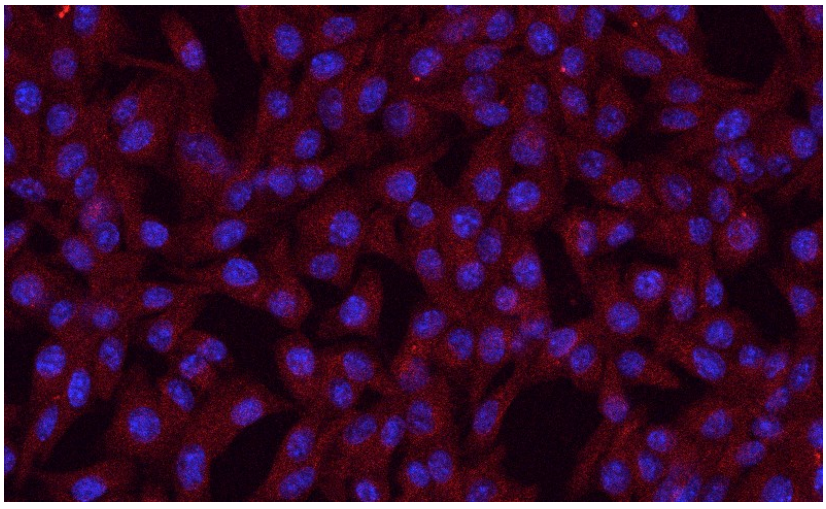

Figure 5.7.8. Study of extracellular hexose presence on the transport of 3-IR780-AM **8** into EMT-6 cells. DAPI was used to stain the nuclei.

Furthermore, we studied the effect of a large excess of extracellular hexoses on the transport of 3-IR780-AM **8** into EMT-6 cells *via* confocal imaging (Figure 5.7.8). We observed great reduction in the near-infrared fluorescence of EMT-6 cells that were incubated with 10 μM 3-IR780-AM **8** and 50 mM hexose when compared to the EMT-6 cells that were incubated only with 3-IR780-AM **8**. Addition of extracellular D-glucose or D-fructose had shown very similar effect on the probe uptake by EMT-6 cells. We previously studied NBD fluorophore labeling of position C-3 modified 2,5-AM derivative (Chapter 4) and observed greater reduction the fluorescence of EMT-6 cells with the addition of extracellular D-fructose, in comparison to the presence of extracellular D-glucose.

To confirm the GLUT5 dependent transport of 3-IR780-AM **8**, we studied the uptake of 3-IR780-AM **8** into water-injected and GLUT5 mRNA-injected oocytes. The oocytes collected and processed, and then were separated into two batches. Once batch of oocytes was injected with distilled water and the other batch was injected with GLUT5 mRNA (oocyte isolation and processing was performed by D. O′Neill). Clearly, superior uptake of the probe by GLUT5 mRNA-injected oocytes demonstrated the GLUT5-mediated uptake of 3-IR780-AM **8** (Figure 5.7.9).

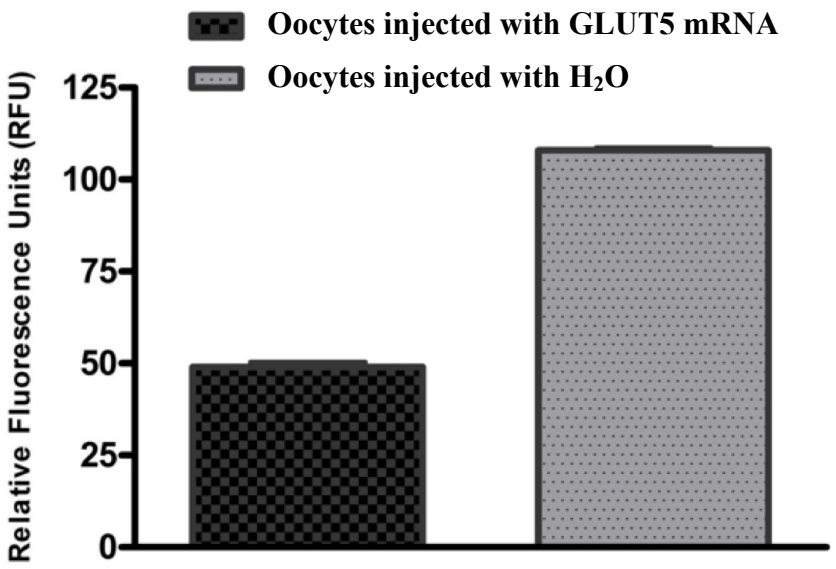

Figure 5.7.9. Study of 3-IR780-AM 8 into oocytes injected with water and GLUT5 mRNA injected oocytes at 25 °C in 45 min. Error bars represent SEM of duplicates.

5.8. Design and efforts towards synthesis of aza-sugar based near-infrared emitting probes

In Chapter 1, a fructose analogue 2,5-AM was demonstrated as a high affinity GLUT5 ligand. In Chapter 3, the importance of hydrogen bond donating functionality at the C-3 was demonstrated. In the current Chapter, we demonstrated the synthesis of near-infrared emitting 2,5-AM based hexoses to target GLUT5. However, 2,5-AM based near-infrared emitting hexoses have exhibited poor water solubility due to the hydrophobic chromophore moiety. Our efforts to increase the hydrophilicity by utilizing a near-infrared chromophore functionalized with anionic sulfonates was unfruitful, due to lack of GLUT recognition for such probes. Alternatively, incorporation of more hydrophilic scaffold could enhance the water solubility of the probe. An aza-sugar, 2,5-dihydroxymethyl-3,4-dihydroxypyrrole (DMDP **37**, Figure 5.8.1), which resembles the

structure of 2,5-AM. In terms of the absolute stereochemistry and the relative positions of hydrogen bond donors and acceptors, DMDP **37** very closely mimics the hexose 2,5-AM. Evaluation of fluorescent dye labeled DMDP **37** as a GLUT5 substrate may yield novel scaffolds to target GLUT5 (Figure 5.8.2). In addition, ligands based upon the aza-sugar DMDP **37** can be attached to dye or radiolabels through the ring heteroatom, which is not possible in the case of 2,5-AM as the valency of the ring oxygen cannot be extended further in the non-ionic state. Consequently, such probes are expected to exhibit better water solubility when compared to the 2,5-AM based probes. At physiological pH, aza-sugar DMDP **37** exists as a dialkylammonium salt, due to the basic secondary amine functionality. Thus, it is important to convert the amine functionality of the ring nitrogen atom to less basic functionalities such as arylamine or amide, which remain unprotonated at physiological pH. After considering the above mentioned factors, we designed the following fluorescent hexoses **38** and **39**.

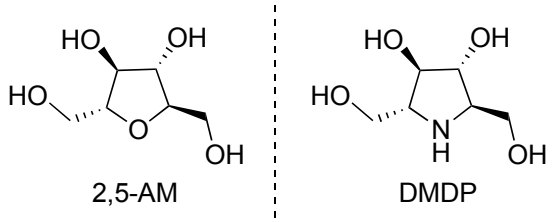

Figure 5.8.1. Structural similarity between 2,5-AM and DMDP **37**

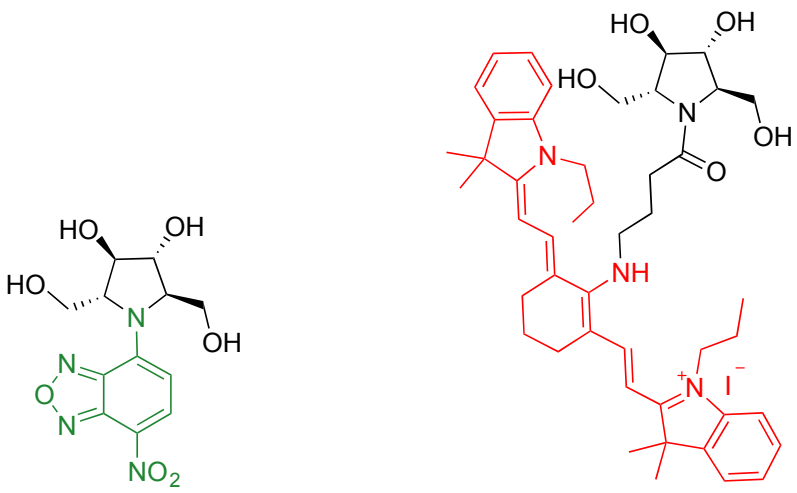

38 **39**

Figure 5.8.2. New aza-hexose based fluorescent probes

DMDP **37** was synthesized following a published protocol, reported by García Fernández and co-workers.[17] The advanced intermediate **46** was synthesized from D-fructose in seven steps. Diketal protection of D-fructose was carried out in acetone in the presence of a catalytic amount of para-toluenesulfonic acid (PTSA) to yield 61% of 1,2:4,5-di-*O*-isopropylidene-α-D-fructopyranose **40** (Scheme 5.8.1). Treatment of the alcoholic functionality of compound **40** with NaH yielded an alkoxide intermediate, which reacted with α,α'-dibromo-o-xylene to afford 81% of 3-*O*-(2-bromomethyl)benzy-l,2:4,5-di-*O*-isopropylidene-α-D-fructopyranose **41**. Regioselective hydrolysis of one of the ketal groups of diketal **41** in the presence of AcOH, yielded 71% of 3-*O*-(2-bromomethyl)benzy-l,2-*O*-isopropylidene-α-D-fructopyranose **42**. Upon activation of the alcoholic group at C-4, compound **42** underwent intramolecular benzylation reaction to yield 3,4-*O*-(o-xylenyl)-l,2-*O*-isopropylidene-α-D-fructopyranose **43**. Further, the C-5 hydroxyl group of compound **43** was converted to corresponding iodide **44** by Appel reaction in 94% yield.

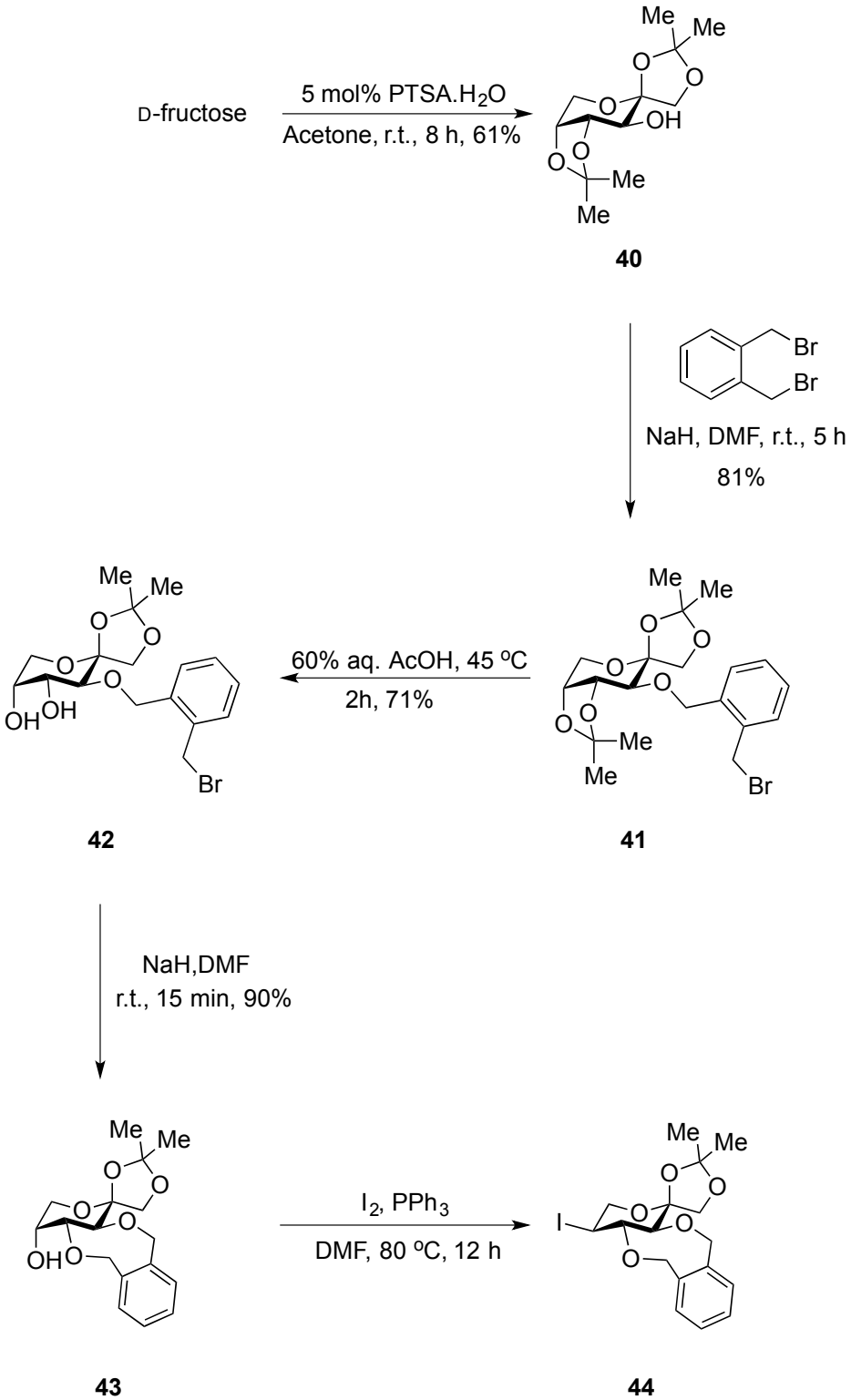

Scheme 5.8.1. Synthesis of intermediate **44** from D-fructose

Displacement of the iodide functionality with azide afforded 84% of 3,4-*O*-(o-xylenyl)-l,2-*O*-isopropylidene-5-azido-5-deoxy-α-D-fructopyranose 4**5** (Scheme 5.8.2). Under acidic conditions, the ketal functionality of **45** was removed to provide access to the key intermediate, 3,4-*O*-(o-xylenyl)-5-azido-5-deoxy-α-D-fructopyranose **46** in 88% yield.

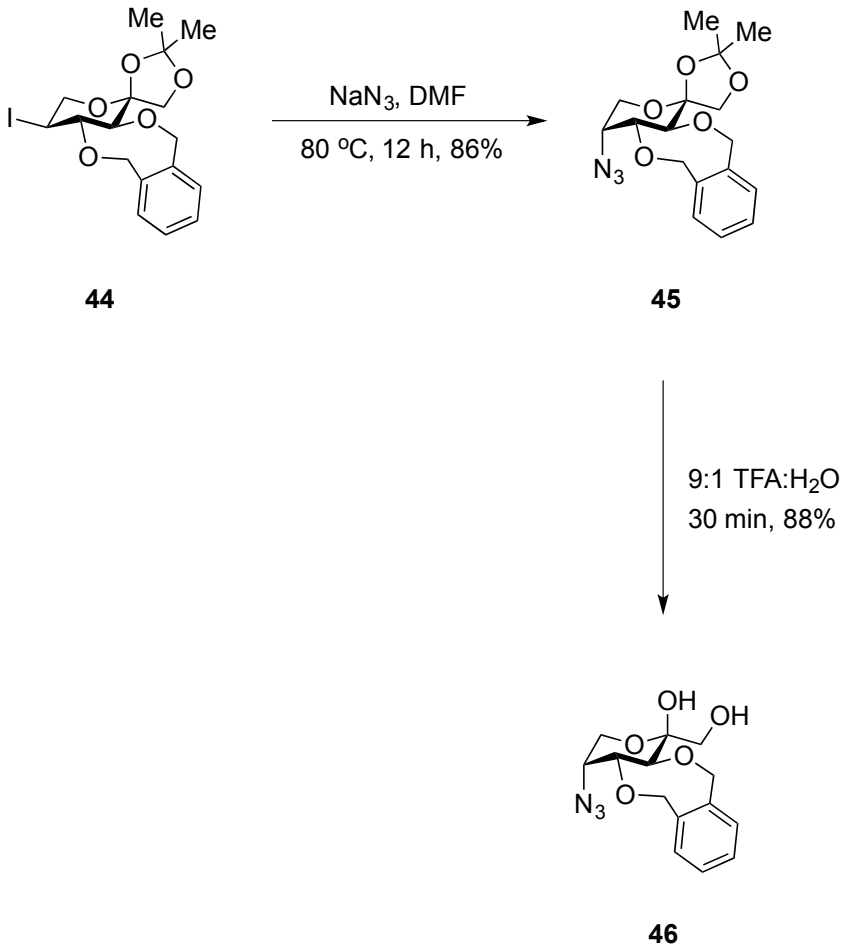

44 **45** **46**

Scheme 5.8.2. Synthesis of key intermediate **46**

Hydrogenation of the key intermediate **46** in the presence of Pd/C in acidified, aqueous MeOH afforded a quantitative amount of DMDP hydrochloride **47** (Scheme 5.8.3). Hydrogenation of **46** cleaves the benzyl ether linkages to yield free alcoholic functionalities at C-3 and C-4 carbons (Intermediate **i**, Scheme 5.8.4). Further, the azide functionality of the intermediate **ii** undergoes reduction to produce the amine functionality to yield amino intermediate **iii**, which immediately undergoes ring contraction reaction by reaction with the anomeric carbon to yield iminium intermediate **iii**. Hydroxyl group directed palladium catalyzed hydrogenation of the iminium ion **iii** provides access to the corresponding amine hydrochloride salt **47**.

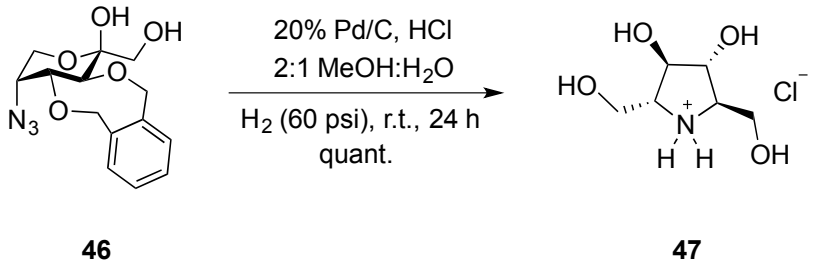

46 **47**

Scheme 5.8.3. Synthesis of DMDP hydrochloride **47**

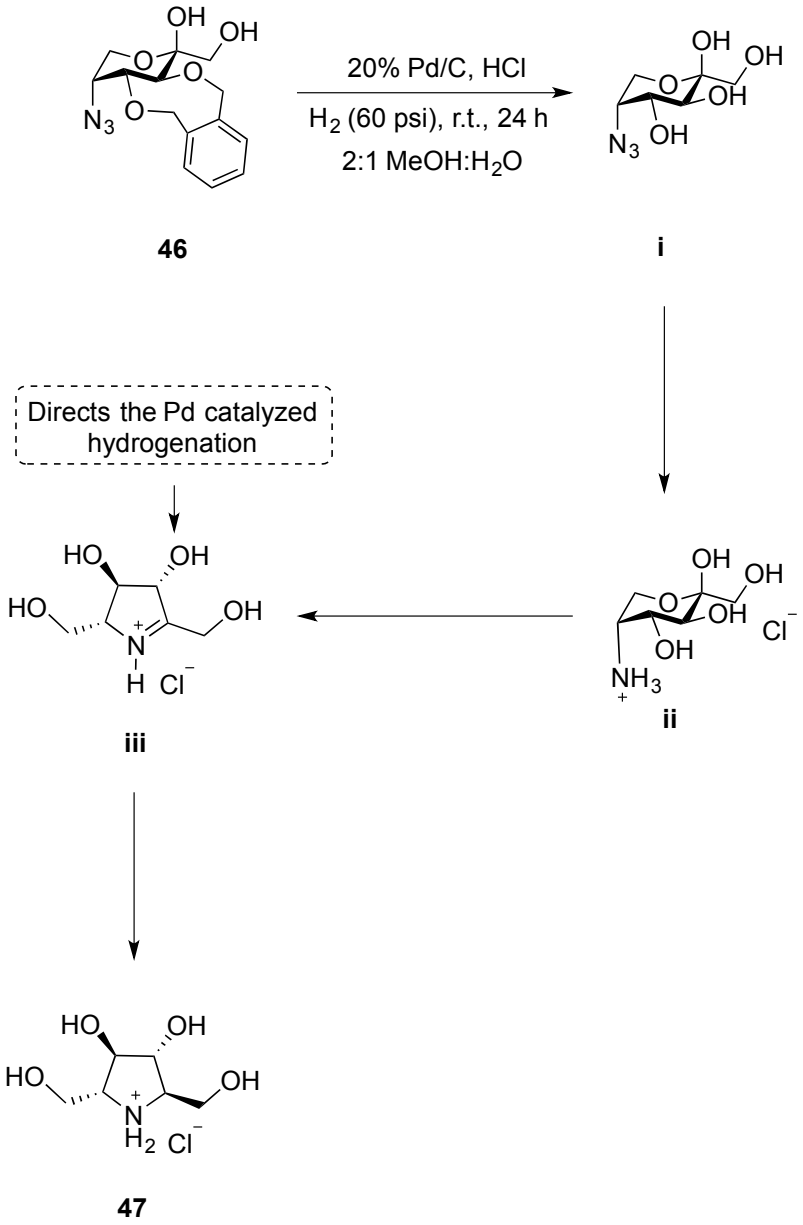

Scheme 5.8.4. Reaction mechanism of formation of DMDP hydrochloride **47** from key intermediate **46** in one chemical transformation

The DMDP hydrochloride salt **52** was stirred in DMF with excess of $NaHCO_3$ to generate the free amine DMDP **42**. After 12 hours of stirring, to the reaction mixture NBD-Cl or active ester was added and stirring was continued for 24 h. Unfortunately, in

both cases we observed no conversion of the **37** to the product (Scheme 5.8.5). The amine functionality of DMDP **37** could be inactive three reasons; i) the inductively electron withdrawing nature of the four hydroxyl substituents, ii) the plausibility of intramolecular hydrogen bonding, which can reduce the nucleophilicity of the amine functionality, iii) reduced nucleophilicity due to steric demands of the more bulky secondary amine.

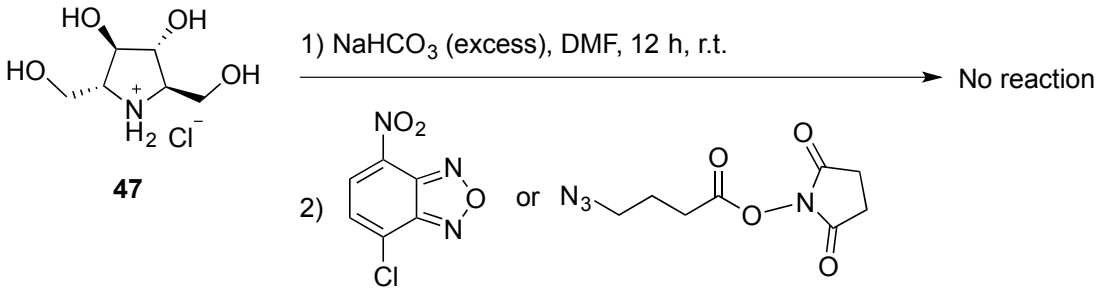

Scheme 5.8.5. Efforts to synthesize the target molecules **38** and **39**

5.9. Conclusion

We successfully synthesized two near-infrared emitting hexoses (3-IR780-AM **8** & 3-IR783-AM **9**) to target GLUT5 transport protein, among which the sulfonate containing near-infrared emitting hexose **9** exhibited GLUT-independent transport into EMT-6 cells. The near-infrared emitting hexose that does not contain anionic sulfonate groups, 3-IR780-AM **8** was identified as the first near-infrared hexose to target GLUT5. Confocal microscopic imaging of EMT-6 cells that are incubated with near-infrared emitting hexoses **8**, **9** and IR-783 dye **36** clearly demonstrated higher accumulation of near-infrared emitting hexose into EMT-6 cells. Our studies not only yielded the first near-infrared hexose that targets GLUT5 transport protein, but also provided preliminary information about the uptake mechanism of such hexose. Furthermore, we designed aza-

sugar moiety containing fluorescent probes **38** and **39** to target GLUT5. Unfortunately, our efforts to synthesize these probes were unsuccessful.

5.10. Future directions

In vitro studies suggest that 3-IR780-AM is potential tracer to diagnose GLUT5 expressing tumors. In order check the efficiency of 3-IR780-AM as a tracer for optical imaging, we need perform *in vivo* imaging with a mice model. EMT-6 tumor-bearing mice will be injected with 3-IR780-AM **8** to study the ability of 3-IR780-AM **8** to accumulate in the tumor region. *In vivo* efflux profile also will be studied over a period of 24 to 48 hours.

We labeled position C-3 modified AM derivatives with IR-78 and IR-783 dyes. However, to increase the efficiency of the tracer molecule, we would like to explore the effect of the dye properties on the uptake mechanism. Furthermore, we would like to synthesize tracer molecules in which hexose moiety is not connected through the central atom of conjugated system (*e.g.* a squaraine dye labeled hexose was shown in Figure 5.10.1) to the dye molecule and such tracer system could enhance the uptake of tracer molecules by tumor cells due to linear arrangement of the conjugate, as compared with T-shape of **8** and **9**.

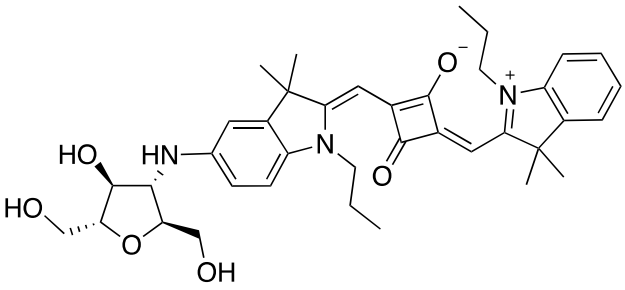

Figure 5.10.1. A squaraine new near-infrared emitting hexose probe for the optical imaging of GLUT5 expressing tumor diagnosis

5.11. Experimental section

Reactions were carried out in flame-dried glassware under a positive argon atmosphere unless otherwise stated. Transfer of anhydrous solvents and reagents was accomplished with oven-dried syringes or cannulae. Solvents were distilled before use (except MeOH and CH_3CN): dichloromethane (CH_2Cl_2) and dimethylformamide (DMF) from calcium hydride, tetrahydrofuran (THF) from sodium/benzophenone ketyl and pyridine from KOH. MeOH and CH_3CN were purchased from Sigma-Aldrich Company, and were used without distillation. All the commercially available solvents and reagents were used without further purification. Reagents were purchased from Sigma-Aldrich company, unless specified. Thin layer chromatography was performed on glass plates precoated with 0.25 mm silica gel. For spot visualization, TLCs were treated with 2.5% *p*-anisaldehyde in AcOH-H_2SO_4-EOH (1:3:86) and heated until color development. Flash chromatography columns were packed with 230–400 mesh silica gel with the indicated eluents. Optical rotations (deg cm^2 g^{-1}) were measured with Perkin Elmer 241 polarimeter, using the D-line of sodium lamp (λ = 589.3 nm) at 22 ± 2 °C. Proton nuclear magnetic resonance spectra (^1H NMR) were recorded at 400 MHz or 500 MHz in indicated deuterated solvents and were reported in ppm in the presence of TMS as

internal standard. The coupling constants (*J*) are reported in hertz (Hz) and standard notation was used to describe the multiplicity of signals observed in ^{1}H NMR spectra: broad (br), multiplet (m), singlet (s), doublet (d), triplet (t), etc. Carbon nuclear magnetic resonance spectra (^{13}C NMR) were recorded at 100 MHz or 125 MHz. The spectra were referenced to the residual solvent present in the deuterated solvent (*e.g.* $CDCl_3$: δ = 77.26 ppm, ^{13}C; 7.26 ppm, ^{1}H). Infrared (IR) spectra were measured with a Nic-Plan FTIR Microscope. IR spectra were recorded neat and reported in cm^{-1}. Mass spectra were determined on a high-resolution electrospray positive ion mode spectrometer.

Beckman LS 6500 multi-purpose scintillation counter was used for the determination ^{14}C isotope concentration. Glucose free Krebs-Ringer buffer solution (120 mM NaCl, 25 mM $NaHCO_3$, 4 mM KCl, 1.2 mM KH_2PO_4, 2.5 mM $MgSO_4$, 70 μM $CaCl_2$, pH 7.4) was used to for the studies with EMT-6 cells. Modified Barth's medium (MBM buffer) was used for the studies with oocytes (88 mM NaCl, 1 mM KCl, 0.33 mM $Ca(NO_3)_2$, 0.82 mM $MgSO_4$, 2.4 mM $NaHCO_3$, 0.4 mM $CaCl_2$, 20 mM HEPES, pH 7.4). [^{14}C]-D-hexoses with specified activity were purchased from Moravek Biochemicals. Cold phosphate-buffered saline (1XPBS) was used to wash the extracellular 3-NBD-AM probe (137 mM NaCl, 2.7 mM KCl, 10 mM Na_2HPO_4, 2 mM KH_2PO_4). All the buffer solutions were mixed with 1% DMSO, prior to the begin of studies with EMT-6 cells. Synergy™ MX BioTek® fluorescent plate reader was used to measure the NBD florescence of EMT-6 cells. Confocal imaging of EMT-6 cells was performed using Leica TCS SP5 fluorescence microscope located in the Katz building, at the University of Alberta.

1,3-*O*-Isopropylidene-2-*O*-methyl-fructofuranoside (24).

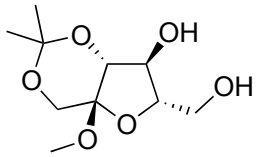

A round bottom flask was charged with 250 mL of MeOH and TsOH•H_2O (0.85 g, 0.50 mmol). The solution was stirred at room temperature for 5 min, before the D-fructose (18.1 g, 0.1 mol) was added. The reaction mixture was stirred for 8 h at room temperature. To the resulting mixture 2,2-dimethoxy propane (70 mL) was added and the stirring was continued for 1 h before being quenched with excess of anhydrous $NaHCO_3$ (ca. 30 g) to neutralize the solution. The mixture was filtered and the filtrate was evaporated. The crude product was purified through silica gel column chromatography, eluting with hexane:EtOAc (a gradient of 100:0 to 60:40) to afford a white crystalline solid (15.9 g, 70% yield). The spectral analysis data matched to the previously reported data.[15] ^{1}H NMR (400 MHz, $CDCl_3$): δ 4.19–3.87 (m, 5H), 3.82 (qd, J = 11.8, 4.3 Hz, 2H), 3.32 (s, 3H), 1.48 (s, 3H), 1.39 (s, 3H).

6-*O*-(*p*-Toluene)sulfonyl-1,3-*O*-isopropylidene-2-*O*-methyl-fructofuranoside (25).

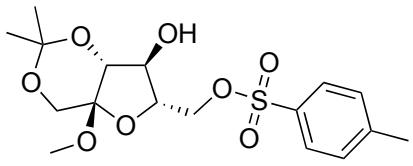

To a round bottom flask, 30 mL pyridine and *N*,*N*-diisopropylethylamine (1.41g, 11.0 mmol) were added. The resulting solvent mixture was charged with compound **24** (2.34

g, 10.0 mmol) and stirred at 0 °C for 10 min. To this mixture tosyl chloride (2.04 g, 11.0 mmol) was added and stirring was continued. After 1 h, the reaction mixture was allowed to attain room temperature and stirred for 4 h at this temperature. The reaction solvent was distilled under vacuum to afford crude compound. The crude compound was subjected to silica gel column chromatography, eluting with hexane:EtOAc (a gradient of 100:0 to 70:30) to yield a pale yellow oil (2.36 g, 61%). The spectral data matched to the reported data.[18] ^{1}H NMR (400 MHz, $CDCl_3$): δ 7.81 (d, J = 8.3 Hz, 2H), 7.33 (d, J = 8.3 Hz, 2H), 4.23 (ddd, J = 6.3, 6.1, 2.0 Hz, 1H), 4.16 (dd, J = 10.3, 6.1 Hz, 1H), 4.12 (dd, J = 10.3, 6.3 Hz, 1H), 3.98 (d, J = 0.7 Hz, 1H), 3.87 (d, J = 12.0 Hz, 1H), 3.85 (d, J = 12.0 Hz, 1H), 3.81-3.83 (m, 1H), 3.27 (s, 3H), 2.68 (s, 1H), 2.44 (s, 3H), 1.40 (s, 3H), 1.23 (s, 3H).

6-Deoxy-6-azido-1,3-*O*-isopropylidene-2-*O*-methyl-fructofuranoside (18).

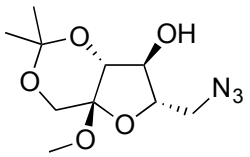

Compound **25** (1.64 g, 5.0 mmol) was added to a round bottom flask that contained 25 mL DMF. After the formation of homogeneous mixture, the flask was charged with an excess of sodium azide (ca. 2g). The resulting heterogeneous mixture was heated to 120 °C and stirred for 8 hours at this temperature, before being cooled to room temperature. The solids were filtered and washed three times with EtOAc. The filtrate fractions were combined and concentrated under reduced pressure to provide the crude compound. Subjection of the crude mixture to silica gel column chromatography, eluting with

hexane:EtOAc (a gradient of 100:0 to 70:30) yielded a colorless oil (1.12 g, 86%). The ^{1}H spectrum of compound **26** matched to the reported data.[15] ^{1}H NMR (500 MHz, CDCl3) δ 4.16 (ddd, *J* = 7.3, 5.0, 2.6 Hz, 1H), 4.04 (d, *J* = 0.6 Hz, 1H), 3.96 (d, *J* = 12.2 Hz, 1H), 3.93 (d, *J* = 12.2 Hz, 1H), 3.90 (dd, *J* = 9.9, 3.4Hz, 1H), 3.54 (dd, *J* = 13.0, 7.5 Hz, 1H), 3.44 (dd, *J* = 13.0, 5.5Hz, 1H), 3.33 (s, 3H), 2.65 (d, *J* =10.0 Hz, 1H), 1.46 (s, 3H), 1.39 (s, 3H).

4-Azido-butanoic acid (28).

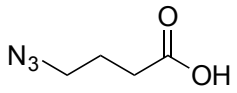

A round bottom flask was charged with ethyl 4-bromobutyrate (1.95 g, 10.0 mmol) and DMF (15 mL). To this solution, an excess of NaN_3 (ca. 2.5 g) was added and the resulting heterogeneous mixture was stirred at 120 °C for 8 h. The cooled reaction mixture was diluted with acetone (30 mL), then the solids were filtered and washed with acetone (3 x 10 mL). The filtrate fractions were combined and concentrated to yield crude ethyl 4-azidobutyrate **27**.

The crude compound **28** was dissolved in ethanol (20 mL) and cooled to 0 °C. To the ice-cold solution, 5 N LiOH (20 mL) was added. The reaction mixture was slowly allowed reach room temperature over a period of 1 h and the stirring was continued for 4 h. Solvents were evaporated and the resulting solid compound was cooled to 0 °C. Ice-cold 2 N HCl was slowly added to the solid compound until the pH of the solution

reached to 1-2 (determined by a pH paper with appropriate range). Then, the solution was transferred into a separatory funnel and was extracted with EtOAc (5 x 30 mL). The organic solvent fractions were combined and dried over anhydrous Na_2SO_4. Filtration of solids and evaporation of the filtrate under high vacuum yielded **28** as a pale yellow oil (0.81 g, 62%), which was used without further purification. Spectral analysis was found match the literature data.[19] ^{1}H NMR (400 MHz, $CDCl_3$): δ 10.71 (br s, 1H), 3.38 (t, J = 6.7 Hz, 2H), 2.48 (t, J = 7.2 Hz, 2H), 1.92 (tt, J = 7.2, 6.7 Hz, 2H).

6-(4-Azido)butyramido-6-deoxy-1,3-*O*-isopropylidene-2-*O*-methyl-fructofuranoside (20).

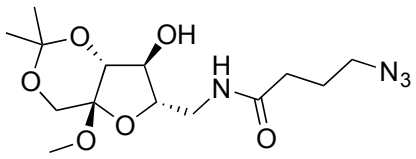

In a 100 mL round bottom flask, compound **18** (0.65g, 2.5 mmol) was dissolved in anhydrous diethylether (30 mL) and cooled to 0 °C. The ice-cold solution was charged with $LiAlH_4$ (0.045 g, 1.25 mmol) in portions. After the careful addition of $LiAlH_4$, the reaction mixture was warmed to room temperature, at which it was stirred for 2 h. The reaction mixture was then cooled to 0 °C and 5 g of $Na_2SO_4 \cdot 10H_2O$ was added in portions to quench the excess $LiAlH_4$. Solids were separated by vacuum filtration and washed with ether (50 mL). Evaporation of diethyl ether resulted a colorless oil in quantitative yield (crude compound **19**).

In a separate round bottom flask, 4-azidobutyric acid was dissolved in 10 mL DCM at room temperature. The solution was charged with 0.5 mL of oxalyl chloride and then 1 drop of DMF. The resulting reaction mixture was stirred at room temperature for 2 h, before the solvents were evaporated under reduced pressure to obtain crude compound **29**. The crude compound **29** was re-dissolved in 15 mL anhydrous DCM and the round bottom flask was cooled to 0 °C using ice. To the cooled solution, *N*-hydroxysuccinimide (0.38 g, 3.3 mmol) and *N*,*N*-diisopropylethylamine (0.54 g, 4.2 mmol) were added. The reaction mixture was allowed to attain room temperature and stirred at this temperature for 1 h. Distillation of DCM under reduced pressure afforded crude compound **30**, which was used without purification.

The crude compound **19** was dissolved in MeOH (5 mL) and $NaHCO_3$ (ca. 1 g) was added to the resulting solution. The heterogeneous mixture was added with the solution of crude compound **30** in DCM (5 mL). After 7 h of stirring at room temperature, the reaction mixture was dilulted with 100 mL of DCM. The solids were separated through vacuum filtration and washed with DCM (3 x 10 mL). Filtrate fractions were combined and concentrated under reduced pressure to afford crude compound **20**. The crude compound was purified by silica gel column chromatography, eluting with DCM:MeOH (a gradient of 100:0 to 95:5) to yield **20** as a colorless oil (0.64 g, 74%). R_f 0.41 (50:50, hexane:EtOAc); $[\alpha]_D^{20}$ +19.9 (*c* 0.21, DCM); IR (cast film) 3340, 3090, 2990, 2940, 2835, 2099, 1651, 1545, 1453, 1376, 1219, 1167, 1098, 858, 761 cm^{-1}; ^1H NMR (500 MHz, $CDCl_3$): δ 6.23 (t, *J* = 4.8 Hz, 1H), 4.16-4.11 (m, 1H), 4.06 (br d, *J* = 0.5 Hz, 1H), 3.97 (d, *J* = 12.1 Hz, 1H) 3.91 (d, *J* = 12.1 Hz, 1H), 3.86 (s, 1H), 3.68-3.61

(m, 1H), 3.55 (dt, J = 14.1, 4.2 Hz, 1H), 3.36 (t, J = 6.6 Hz, 2H), 3.31 (s, 3H), 3.06 (br d, J = 6.3 Hz, 1H), 2.31 (t, J = 6.7, 2H), 1.94 (qint, J = 6.7, 2H), 1.49 (s, 3H), 1.42 (s, 3H); ^{13}C NMR (125 MHz, $CDCl_3$): δ 172.2, 101.2, 98.8, 85.1, 80.0, 78.1, 61.9, 50.8, 48.7, 41.1, 33.1, 28.1, 24.8, 19.2; HRMS (ESI) calcd for $C_{14}H_{24}N_4O_6Na$ [M+Na$^+$] 367.1588; found m/z 367.1587.

Near-infrared emitting fructose derivative (22)

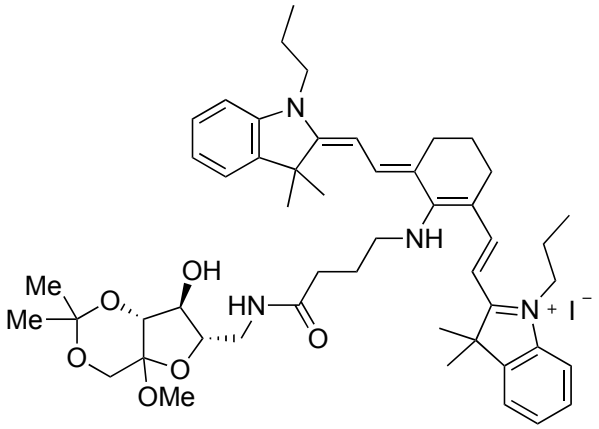

The azide **20** (0.07 g, 0.21 mmol) was taken in a round bottom flask and EtOAc (20 mL) was added. The resulting mixture was charged with 0.03 g of 20% Pd/C and the heterogeneous mixture was sealed with a rubber septum. A rubber balloon was equipped with a valve and syringe was filled with hydrogen gas, and the syringe was inserted into the rubber septum of the round bottom flask to expose the reaction mixture to the hydrogen gas. After the exposure of the reaction mixture to the hydrogen gas for 2 h, the balloon was removed and the rubber septum was unsealed. The reaction mixture was diluted with 50 mL of EtOAc and the solids were filtered by passing the heterogeneous

mixture through a Celite plug. The residual compound remaining in Celite plug was extracted by thorough washing with 20 mL EtOAc. All the EtOAc fractions were combined and concentrated under reduced pressure to provide crude compound **21**.

The crude amine **21**, obtained in the previous step was dissolved in 5 mL of dry DMF. To this solution, 0.25 g of $NaHCO_3$ and IR-780 iodide **17** (0.15 g, 0.22 mmol) was added. The resulting heterogeneous mixture was stirred for 24 h at room temperature, before being diluted with 50 mL DCM. The solids were separated by filtration and removal of solvents under vacuum yielded crude compound. Purification of the crude product was carried out by silica gel column chromatography, eluting with DCM:MeOH (a gradient pf 100:0 to 93:7) to afford a blue gum (0.145 g, 78%). R_f 0.51 (93:7, DCM:MeOH); IR (cast film) 3272, 3052, 2964, 2932, 2869, 1650, 1529, 1485, 1456, 1375, 1293, 1227, 1170, 1127, 1115, 930, 800 cm^{-1}; ^1H NMR (500 MHz, $CDCl_3$): δ 9.80 (br s, 1H), 7.86 (br t, *J* = 5.6 Hz, 1H), 7.60 (d, *J* = 12.7 Hz, 2H), 7.27-7.20 (m, 4H), 7.01 (t, *J* = 7.5 Hz, 2H), 6.81 (d, *J* = 7.8, 2H), 5.56 (d, *J* = 12.20 Hz, 2H), 4.21 (br s, 1H), 4.10 (qint, *J* = 4.2 Hz, 1H), 4.04 (s, 1H), 3.92-3.64 (m, 9H), 3.36-3.29 (m, 1H), 3.24 (s, 3H), 2.94-2.88 (m, 1H), 2.87-2.80 (m, 1H), 2.47 (t, *J* = 6.1 Hz, 4H), 2.03 (br qint, *J* = 6.2, 2H), 1.92-1.74 (m, 7H), 1.66 (s, 12H), 1.39 (s, 3H), 1.31 (s, 3H), 0.99 (t, *J* = 7.5 Hz, 6H); ^{13}C NMR (125 MHz, $CDCl_3$): δ 174.5, 169.5, 166.9, 143.2, 140.0, 136.9, 128.0, 122.5, 122.0, 119.5, 108.3, 102.2, 99.0, 93.7, 83.4, 81.3, 78.9, 62.1, 51.5, 48.7, 47.5, 44.6, 42.3, 35.5, 28.9 (2C), 27.4, 26.0, 25.8, 21.2, 20.3, 20.0, 11.7; HRMS (ESI) calcd for $C_{50}H_{69}N_4O_6$ $[M^+]$ 821.5212; found m/z 821.5210.

1,4,6-Tri-*O*-benzyl-3-azido-3-deoxy-2,5-anhydro-D-mannitol (32).

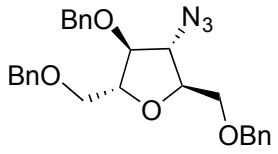

The azide **31** (1.89 g, 10.0 mmol; see Chapter 2 for synthesis) was dissolved in 35 mL of anhydrous DMF and the resulting solution was cooled to 0 °C using an ice-batch. 60% NaH dispersed in mineral oil (1.39 g, 33.0 mmol) was added in portions to the cold solution and stirred for 45 min at 0 °C. To the resulting viscous mixture, BnBr (5.65 g, 33.0 mmol) was added drop wise over 5 min and the solution was allowed to warm to room temperature. After 6 h of stirring at room temperature, the reaction mixture was quenched with saturated ammonium chloride solution. DMF was removed from the reaction mixture and the concentrate was charged with 500 mL diethyl ether. Undissolved salts were filtered and the organic layer was transferred to a separatory funnel. In order to remove residual DMF, the organic layer was washed with brine solution (5 x 100 mL). The diethylether layer was dried over Na_2SO_4, solids were filtered and the filtrate was concentrated under mild vacuum. The crude product obtained was purified by column chromatography, eluting with hexane:EtOAc (a gradient of 100:0 to 95:5) to yield **32** as a plae yellow oil (4.32 g, 94%). R_f 0.71 (90:10, hexane:EtOAc); $[\alpha]_D^{20}$ +51.8 (*c* 0.72, DCM); IR (cast film) 3087, 3063, 3063, 3030, 3004, 2862, 2104, 1496, 1453, 1406, 1259, 1206, 1095, 1027, 988 cm^{-1}; ^1H NMR (500 MHz, $CDCl_3$): δ 7.39-7.29 (m, 15H), 4.68-4.52 (m, 6H), 4.19-4.14 (m, 1H), 4.12-4.04 (m, 3H), 3.69-3.54 (m, 4H); ^{13}C NMR (125 MHz, $CDCl_3$): δ 137.96, 137.87, 137.49, 128.49, 128.44, 128.41, 127.97, 127.86, 127.79, 127.76 (2C), 127.72, 84.1, 81.4, 80.5, 73.6, 73.5, 72.6,

69.9, 69.5, 67.3; HRMS (ESI) calcd for $C_{27}H_{33}N_4O_4$ [M+NH_4^+] 477.2496; found m/z 477.2491.

1,4,6-Tri-*O*-benzyl-3-amino-2,5-anhydro-D-mannitol (33).

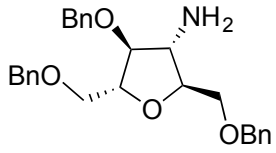

A round bottom flask was charged with azide **32** (2.16 g, 5.0 mmol) and anhydrous diethylether (75 mL). This solution was cooled to 0 °C with ice-bath and $LiAlH_4$ (0.1 g, 2.6 mmol) was added in small portions over 10 min. Then, the reaction mixture was allowed to attain room temperature, at which the stirring was continued for 2 hours. At this stage the reaction mixture was cooled to 0 °C and 10 g of $Na_2SO_4 \bullet 10H_2O$ was added in portions. The solids were filtered and the filtrate was dried under vacuum to afford quantitative amount of analytically pure amine **33**. R_f 0.30 (90:10, DCM:MeOH); $[\alpha]_D^{20}$ +28.5 (*c* 0.60, MeOH); IR (cast film) 3377, 3311, 3087, 3052, 3029, 2861, 1496, 1453, 1364, 1206, 1091, 1027, 737, 697 cm^{-1}; ^1H NMR (500 MHz, $CDCl_3$): δ 7.39-7.26 (m, 15H), 4.64-4.53 (m, 6H), 4.15 (ddd, *J* = 5.0, 4.9, 4.1 Hz, 1H), 3.92 (ddd, *J* = 6.4, 6.1, 5.4 Hz, 1H), 3.86 (t, *J* = 5.0 Hz, 1H), 3.70-3.65 (m, 2H), 3.64-3.58 (m, 2H), 3.39 (dd, *J* = 6.6, 5.1 Hz, 1H); ^{13}C NMR (125 MHz, $CDCl_3$): δ 138.2, 138.0, 128.46, 128.42, 128.38, 128.33, 127.8, 127.7, 127.76, 127.73, 127.71, 127.6, 87.9, 84.1, 81.9, 73.6, 73.5, 72.3, 70.95, 70.93, 60.3; HRMS (ESI) calcd for $C_{27}H_{32}NO_4$ [M+H^+] 434.2326; found m/z 434.2326.

1,4,6-Tri-*O*-benzyl-3-deoxy-3-(4-azido)butyramido-2,5-anhydro-D-mannitol (34).

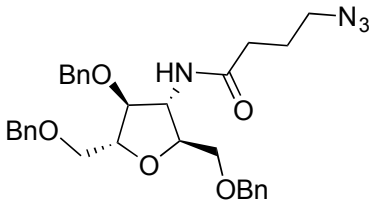

The amine **33** (1.08 g, 2.5 mmol) was added to a round bottom flask containing DCM (20 mL) and *N*,*N*-diisopropylethylamine (0.49 g, 3.75 mmol). The resulting mixture was cooled to 0 °C using ice-bath.

In a separate round bottom flask, 4-azidobutyric acid **28** (0.39 g, 3 mmol) was dissolved in 10 mL DCM at room temperature. The resulting solution was charged with 0.6 mL of oxalyl chloride and then 1 drop of DMF. The resulting reaction mixture was stirred at room temperature for 2 h, before the solvents were evaporated under reduced pressure to obtain crude compound **29**. The crude compound **29** was re-dissolved in 10 mL anhydrous DCM and added to the cold solution of amine **33** in drop-wise manner. After 3 h of stirring at room temperature, the solvents were removed by vacuum distillation. The crude mixture was subjected to silica gel column chromatography, eluting with hexane:EtOAc (a gradient of 100:0 to 50:50) yielded pale yellow oil. R_f 0.43 (50:50, hexane:EtOAc) $[\alpha]_D^{20}$ +53.6 (*c* 0.54, MeOH); IR (cast film) 3320, 3063, 3030, 2864, 2098, 1673, 1654, 1532, 1453, 1272, 1095, 738, 698 cm^{-1}; ^1H NMR (500 MHz, $CDCl_3$): δ 7.41-7.25 (m, 15H), 6.37 (d, *J* = 9.6 Hz, 1H), 4.73-4.41 (m, 7H), 4.29 (q, *J* = 2.0 Hz, 1H), 4.21-4.15 (m, 1H), 3.86 (br s, 1H), 3.84 (dd, *J* = 10.5, 2.2 Hz, 1H), 3.72-3.65

(m, 2H), 3.57 (dd, *J* = 10.5, 4.7 Hz, 1H), 3.14 (td, *J* = 6.8, 2.0 Hz, 2H), 1.71-1.63 (m, 2H), 1.56-1.50 (m, 2H); ^{13}C NMR (125 MHz, CD_3OD): δ 175.1, 137.9 (2C), 137.6, 129.3, 128.0, 127.9, 127.7, 127.5, 127.4, 126.7, 83.8, 81.5, 80.6, 73.1, 72.9, 72.0, 69.7, 69.3, 67.1, 50.3, 48.1, 30.4, 23.9; HRMS (ESI) calcd for $C_{31}H_{37}N_4O_5$ [M+H$^+$] 545.2758; found m/z 545.2761.

3-(4-amino)butyramido-2,5-anhydro-D-mannitol hydrochloride (35).

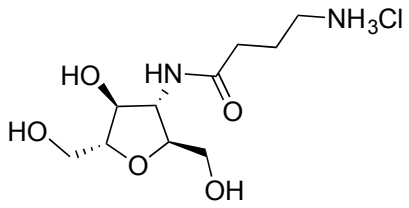

The azide **34** (0.550 g. 1.01 mmol) was taken in a Parr Shaker flask and dissolved in 150 mL MeOH. The resulting solution was carefully charged with 0.5 g of 20% Pd/C, 0.4 g of $Pd(OH)_2$/C (fast addition of these reagents could cause flaming of MeOH) and 4 mL of 2 M HCl in diethyl ether solution. The reaction mixture was exposed to hydrogen gas at 60 psi using parr shaker. After 24 h, the flask containing reaction mixture was carefully removed from the Parr Shaker and solids were filtered using a Celite plug (to obtain Pd/C free, clear solution 3-4 filter papers were used at the bottom of Celite plug). The filtrate was evaporated under reduced pressure and the resulting oil was exposed to high vacuum to obtain quantitative yield colorless gel. $[\alpha]_D^{20}$ +9.8 (*c* 0.10, MeOH); IR (cast film) 3397, 1641, 1564, 1490, 1298, 1069, 965 cm^{-1}; ^{1}H NMR (500 MHz, D_2O): δ 4.25 (app t, *J* = 8.2 Hz, 1H), 4.11 (t, *J* = 7.4 Hz, 1H), 3.95-3.84 (m, 2H), 3.80-3.56 (m, 4H), 3.01 (app t, *J* = 7.5 Hz, 2H), 2.40 (t, *J* = 7.4 Hz, 2H), 1.94 (qin, *J* = 7.6 Hz, 2H); ^{13}C NMR (125

MHz, D_2O): δ 175.4, 82.6, 80.7, 74.7, 61.5, 61.0, 56.7, 38.9, 32.6, 22.9; HRMS (ESI) calcd for $C_{10}H_{21}N_4O_5$ [M^+] 249.1445; found m/z 249.1445.

General procedure to synthesize near-infrared emitting 2,5-AM derivatives 8 and 9.

A round bottom flask was charged with the amine hydrochloride **40** (0.05g, 0.2 mmol), DMF (3 mL) and $NaHCO_3$ (ca. 0.5 g). The resulting heterogeneous mixture was vigorously stirred at room temperature for 6 h, followed by addition of IR780 **17** or **36** (0.20 mmol). The sides of the round bottom were washed with 1 mL DMF and the reaction mixture was stirred for 24 h. The reaction mixture was concentrated under vacuum (during the DMF evaporation process, the temperature must not exceed 30 °C). The crude compound was loaded on to a silica gel column by dissolving in DCM and eluted with DCM:MeOH (a gradient of 100:0 to 94:6, in case of **8**; 100:0 to 80:20, in case of **9**) to afford blue crystals (0.131 g, 75% of **8**; 0.08 g, 44% of **9**)

3-IR780-AM (8).

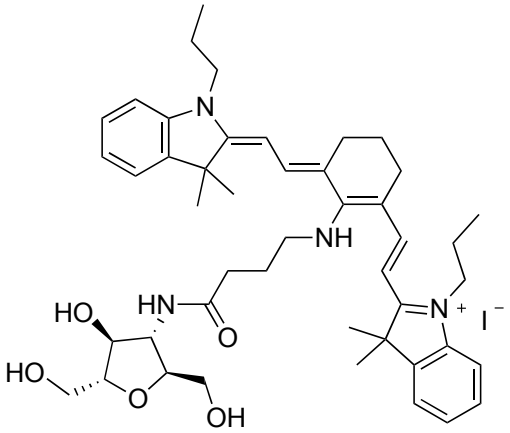

IR (cast film) 3384, 3044, 2927, 1650, 1527, 1486, 1455, 1382, 1324, 1170, 1135, 1042, 922, 799 cm^{-1}; ^1H NMR (500 MHz, CD_3OD): δ 7.74 (d, J = 12.7 Hz, 2H), 7.34 (d, J =

7.1 Hz, 2H), 7.27 (t, *J* = 7.1 Hz, 2H), 7.04 (dd, *J* = 12.9, 7.6 Hz, 4H), 5.79 (d, *J* = 12.9 Hz, 2H), 4.18 (app t, *J* = 7.2 Hz, 1H), 4.02 (app t, *J* = 7.2 Hz, 1H), 3.96-3.42 (m, 12H), 2.59-2.35 (m, 6H), 2.04 (br t, *J* = 6.6 Hz, 2H), 1.80 (br s, 6H), 1.64 (br s, 12H), 1.0 (br t, *J* = 7.2 Hz, 6H); ^{13}C NMR (125 MHz, CD_3OD): δ 175.5, 170.7, 169.3, 144.6, 141.4, 139.9, 129.4, 123.9, 123.1, 121.4, 110.1, 95.7, 85.1, 83.7, 76.7, 64.3, 63.9, 62.9, 59.3, 51.7, 45.5, 34.2, 29.25, 29.23, 27.9, 26.3, 22.9, 21.1, 11.8; HRMS (ESI) calcd for $C_{46}H_{63}N_4O_5$ [M^+] 751.4793; found m/z 751.4791.

3-IR783-AM (9).

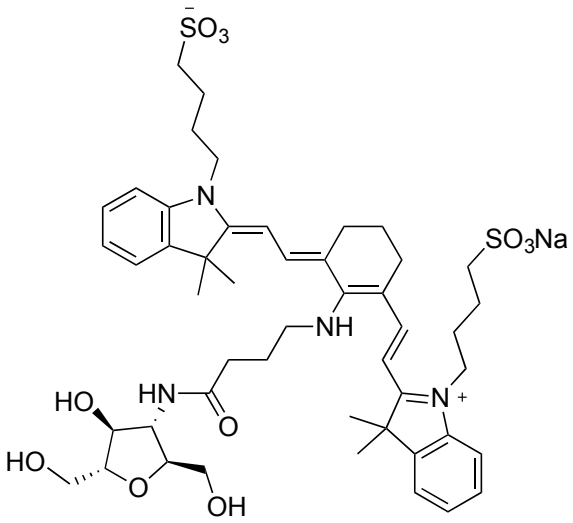

IR (cast film) 3332, 3082, 2920, 1645, 1526, 1456, 1324, 1168, 1131, 1040, 922, 800 cm^{-1}; ^{1}H NMR (500 MHz, CD_3OD): δ 7.73 (d, *J* = 13.2 Hz, 2H), 7.41 (d, *J* = 7.1 Hz, 2H), 7.28 (t, *J* = 7.1 Hz, 2H), 7.06 (dd, *J* = 12.9, 7.6 Hz, 4H), 5.83 (br d, *J* = 12.9 Hz, 2H), 4.22-4.12 (m, 2H), 4.04 (app t, *J* = 7.2 Hz, 1H), 3.8 (br s, 3H), 3.87-3.49 (m, 8H), 2.95-2.81 (m, 5H), 2.53 (app t, *J* = 6.1 Hz, 3H), 2.42 (app q, *J* = 4.2 Hz, 2H), 2.12-1.65 (m,

24H); ^{13}C NMR (125 MHz, CD_3OD): δ 174.0, 169.6, 167.6, 143.1, 139.9, 138.5, 127.9, 122.4, 121.6, 120.3, 108.7, 94.2, 83.5, 82.2, 75.2, 62.4, 61.5, 57.8, 50.6, 50.1, 42.3, 32.7, 27.7, 26.5, 25.3, 24.9, 22.2, 21.4; HRMS (ESI) calcd for $C_{48}H_{65}N_4O_{11}S_2$ [M^-] 937.4097; found m/z 937.4101.

Uptake of near-infrared emitting hexoses into EMT-6 cells and their uptake inhibition by D-hexoses: EMT-6 cells were grown to confluence in 12 well NEST® cell culture plates with media removal every 2 days. One h before performing the flux study, EMT-6 cells were washed twice with Krebs-Ringer buffer solution. To each well 1 mL of Krebs-Ringer buffer was added and incubation at 37 ^oC was continued for one h. After incubation, Krebs-Ringer buffer was removed and 500 μL of 150 μM of freshly prepared solution of (**8** or **9**) or 500 μL solution of (150 μM **8** + 50 mM D-hexose) in Krebs-Ringer buffer (1% DMSO) was added. After incubation for a specified period of time at 37 ^oC, extracellular media was aspirated and each well was rinsed four-times with cold PBS buffer (1% DMSO) over a period of 3 min. To each well 1 mL of PBS buffer was added and fluorescence count in each well was measured *via* fluorescent plate reader (Synergy™ MX BioTek®). Net fluorescence value corresponding to a particular well was calculated by subtracting the background fluorescence value (auto-fluorescence of a well with EMT-6 cells and PBS buffer).

[^{14}C] D-Fructose and [^{14}C] D-glucose transport inhibition study: Radioactive "Hot" flux solutions were prepared by mixing 5 μL of [^{14}C] D-glucose or [^{14}C] D-fructose (solution in EtOH, specific activity approximately 1 mCi/mL), 50 μL of 100 mM D-

fructose or D-glucose and 945 μL Krebs-Ringer solution (1% DMSO) of **8** with specified concentration. EMT-6 cells were grown to confluence in 12 well NEST® cell culture plates with media removal every 2 days. One h before performing the flux study, EMT-6 cells were washed twice with Krebs-Ringer buffer solution. To each well 1 mL of Krebs-Ringer buffer was added and incubation at 37 ^{o}C was continued for one h, in order to deplete the nutrients present in the cells. After one hour of incubation, Krebs-Ringer buffer was removed and 300 μL of radioactive "Hot" flux solution was added into each well. After incubation at 25 ^{o}C for 25 min, media was aspirated and each well was rinsed twice with ice-cold Krebs-Ringer solution. To each well 500 μL of 5% trifluoroacetic acid was added to lyse the cells. After one hour of cell lysing, 400 μL of cell lysate from each well was transferred into scintillation vials containing 5 mL of Scinti-Safe™ liquid scintillation fluid for counting in a liquid scintillation counter.

[^{14}C] D-fructose and [^{14}C] D-glucose transport inhibition study in the presence of CB: Radioactive "Hot" flux solutions were prepared by mixing 5 μL of [^{14}C] D-glucose or [^{14}C]-D-fructose (solution in EtOH, specific activity approximately 1 mCi/mL), 50 μL of 100 mM D-fructose or D-glucose, 10 μL of 10 mM CB and 935 μL of Krebs-Ringer (1% DMSO) solution of **8** with specified concentration. EMT-6 cells were grown to confluence in 12 well NEST® cell culture plates with media removal every 2 days. One hour before performing the flux study, EMT-6 cells were washed twice with Krebs-Ringer buffer solution. To each well 1 mL of Krebs-Ringer buffer was added and incubation at 37 ^{o}C was continued for one hour, in order to deprive the nutrients present in the cells. After one hour of incubation, Krebs-Ringer buffer was removed and 300 μL

of radioactive "Hot" flux solution was added into each well. After incubation at 25 ^{o}C for 25 min, media was aspirated and each well was rinsed twice with ice-cold Krebs-Ringer solution. To each well 500 μL of 5% trifluoroacetic acid was added to lyse the cells. After one hour of cell lysing, 400 μL of cell lysate from each well was transferred into scintillation vials containing 5 mL of Scinti-Safe^{TM} liquid scintillation fluid for counting in a liquid scintillation counter (Beckman LS 6500 multi-purpose scintillation counter).

Study of uptake of 3-IR780-AM (8) into GLUT5 mRNA injected oocytes: Xenopus laevis oocytes were surgically removed, processed and injected with mRNA by D. O′Neill. An equal number of GLUT5 mRNA injected oocytes and water injected oocytes were taken in two separate test tubes. The test tube containing water injected oocytes was labeled as 'W' and the test tube containing GLUT5 mRNA injected oocytes was labeled as 'G'. To each of these test tubes, 500 μL of 300 μM solution of 3-IR780-AM **8** in MBM buffer was added and the incubation was continued for 45 min at room temperature. After the incubation period, extracellular media was carefully removed from each test tube and oocytes were carefully washed six-times with cold MBM buffer solution. After thorough washing, to each test tube 1mL of MBM buffer was added and the oocytes were lysed with the pipette tip. The entire solution from each test tube (W and G) was transferred into two 1.5 mL graduated micro test tubes with sealable top (also labeled as W and G). These micro test tubes were sealed and subjected to centrifugal force for 3 minutes. 900 μL of supernatant from each test tube was transfered to one of the wells of 12 well NEST® cell culture plate. To one the wells 900 μL of MBM buffer was added to obtain background reading. Fluorescence of each well was measured with

fluorescence plate reader (FPR) and subtraction of background value from the crude FPR value provided the net fluorescence value corresponding to a particular well.

Confocal imaging of EMT-6 cells with near-infrared emitting dyes: Murine breast cancer cell line EMT-6 was grown in Gibco DMEM-F-12 supplemented with 15 mM HEPES, L-glutamine, 10% fetal bovine serum and 1% penicillin/streptomycin with media renewal every 2–3 days. Both cell lines were grown in a CO_2 incubator at 37 °C. Prior to the cell imaging experiments, media was removed and cells were washed two times with Krebs-Ringer buffer. Krebs-Ringer buffer, and near-infrared emitting dye (10 μM) or near-infrared emitting dye (10 μM) + D-hexose (50 mM) were added to the coverslips placed in the cell culture plate, respectively. This set up was incubated at 37 °C for 30 min. After incubation, the cells were rinsed two times with Krebs-Ringer buffer. Ethanol (1 mL, 95%) was added to each coverslip to fix the cells in the cell culture plate, and incubation was continued for another 30 min. Cells were rinsed four times with PBS, and PBS-rinsed coverslips were then mounted onto microscopy slides using 20 μL drops of polyvinyl alcohol-based mounting media supplemented with 0.1% n-propyl gallate as anti-fade and 4',6-diamidino-2-phenylindole (DAPI) (50 μgmL^{-1}). Then, cells were imaged using corresponding lasers visualizing DAPI (blue nuclear staining) and Fluorescein isothiocyanate (FITC, green emission) with a Plan-Apochromat 20X/1.3 oil DIC M27 lens on a Leica TCS SP5 confocal laser scanning microscope. Imaging experiments were carried out two times using different batches of cells. (Note: While studying the effect of extracellular D-hexoses on the uptake of near-infrared

emitting dyes or during the comparison among these compounds *via* confocal imaging, all the parameters of microscope must remain the same throughout the study)

Data analysis

In the inhibition experiments performed, counts per minute (CPM) were normalized to standards by the subtraction of the background levels and then plotted against the maximum uptake of the radiolabeled hexose (i.e. [^{14}C]-D-fructose or [^{14}C]-D-glucose). For time courses, values were corrected with standards and to the protein levels present per well. IC_{50} values (concentration at which half maximum inhibition of cellular uptake of a radiotracer was observed) were determined using non-linear regression analysis in GraphPad Prism 5 (GraphPad Software, San Diego, CA, USA), and significance was determined at $p < 0.05$ using a Student's t-test.

5.13. References

1. Ntziachristos, V. Going deeper than microscopy: the optical imaging frontier in biology. *Nat. Methods* **7,** 603–14 (2010).
2. Taruttis, A. & Ntziachristos, V. Translational optical imaging. *AJR. Am. J. Roentgenol.* **199,** 263–71 (2012).
3. Luker, G. D. & Luker, K. E. Optical imaging: current applications and future directions. *J. Nucl. Med.* **49,** 1–4 (2008).
4. Fass, L. Imaging and cancer: A review. *Mol. Oncol.* **2,** 115–152 (2008).

5. Xu, X. Development and Applications of Optical imaging techniques in cancer diagnosis: Diffuse optical tomography and microendoscopy. *Curr. Med. Imaging Rev.* **4,** 125-133 (2016).
6. Hadjipanayis, C. G., Jiang, H., Roberts, D. W. & Yang, L. Current and future clinical applications for optical imaging of cancer: from intraoperative surgical guidance to cancer screening. *Semin. Oncol.* **38,** 109–18 (2011).
7. Penet, M.-F. Mikhaylova, M., Li, C., Krishnamachary, B., Glunde, K., Pathak, A. P. & Bhujwalla, Z. M. Applications of molecular MRI and optical imaging in cancer. *Future Med. Chem.* **2,** 975–88 (2010).
8. Smith, A. M., Mancini, M. C. & Nie, S. Bioimaging: second window for in vivo imaging. *Nat. Nanotechnol.* **4,** 710–1 (2009).
9. Cowles, E. A., Kovar, J. L., Curtis, E. T., Xu, H. & Othman, S. F. Near-infrared optical imaging for monitoring the regeneration of osteogenic tissue-engineered constructs. *Biores.* **2,** 186–91 (2013).
10. Cheng, Z. Levi, J., Xiong, Z., Gheysens, O., Keren, S., Chen, X. & Gambhir S. S. Near-infrared fluorescent deoxyglucose analogue for tumor optical imaging in cell culture and living mice. *Bioconjug. Chem.* **17,** 662–9 (2006).
11. Park, J., Lee, H. Y., Cho, M-H. & Park, S. B. Development of a Cy3-labeled glucose bioprobe and its application in bioimaging and screening for anticancer agents. *Angew. Chem. Int.* **46**, 2018-2022 (2007).
12. Kovar, J. L., Volcheck, W., Sevick-Muraca, E., Simpson, M. A. & Olive, D. M. Characterization and performance of a near-infrared 2-deoxyglucose optical imaging agent for mouse cancer models. *Anal. Biochem.* **384,** 254–62 (2009).

13. Guo, J. Du, C., Shan, L., Zhu, H., Xue, B., Qianz, Z., Achilefu, S. & Gu. Y. Comparison of near-infrared fluorescent deoxyglucose probes with different dyes for tumor diagnosis in vivo. *Contrast Media Mol. Imaging* **7,** 289–301 (2012).

14. For synthesis of IR-780 iodide: Samanta, A., Vendrell, M., Das, R. & Chang, Y.-T. Development of photostable near-infrared cyanine dyes. *Chem. Commun. (Camb).* **46,** 7406–8 (2010); For IR-780 dye applications in PDT: Jiang, C., Cheng, H., Yuan, A., Tang, X., Wu, J. & Hu, Y. Hydrophobic IR780 encapsulated in biodegradable human serum albumin nanoparticles for photothermal and photodynamic therapy. *Acta Biomater.* **14,** 61–9 (2015); Levy, J. G. Photosensitizers in photodynamic therapy. *Semin. Oncol.* **21,** 4–10 (1994); Yuan, A., Wu, J., Tang, X., Zhao, L. Xu. F. & Hu, Y. Application of near-infrared dyes for tumor imaging, photothermal, and photodynamic therapies. *J. Pharm. Sci.* **102,** 6–28 (2013).

15. Yu, K., Zhao, X., Wu, W. & Hong, Z. An efficient procedure for synthesis of fructose derivatives. *Tetrahedron Lett.* **54,** 2788–2790 (2013); Soueidan, O. M., Scully, T. W., Kaur, J., Panigrahi, R. Belovodskiy, A. Do, V., Matier, C., Lemieux, J., Wuest, F., Cheeseman, C. I. & F. G. West. Fluorescent hexose derivatives demonstrate stringent stereochemical requirement for recognition and transport by GLUT1 and GLUT5. *Manuscript in preparation*.

16. Sun, J. Dong, Y., Cao, L., Wang, X., Wang, S. & Hu, Y. Highly efficient chemoselective deprotection of O,O-acetals and O,O-ketals catalyzed by molecular iodine in acetone. *J. Org. Chem.* **69,** 8932–4 (2004).

17. García-Moreno, M. I., Aguilar, M., Ortiz Mellet, C. & García Fernández, J. M. Intramolecular benzyl protection delivery: a practical synthesis of DMDP and DGDP from D-fructose. *Org. Lett.* **8,** 297–9 (2006).
18. Hanaya, T., Sato, N. & Yamamoto, H. An efficient synthesis of methyl 1,3-O-isopropylidene-alpha-D-fructofuranoside and 2,3:5,6-di-O-isopropylidene-D-glucose dimethyl acetal derivatives from sucrose. *Carbohydr. Res.* **340,** 2494–501 (2005).
19. Chouhan, G. & James, K. Efficient Construction of Proline-Containing β-Turn Mimetic Cyclic Tetrapeptides via CuAAC Macrocyclization. *Org. Lett.* **15**, 1206-1209 (2013).

References

Chapter 1

1. Dashty, M. A quick look at biochemistry: Carbohydrate metabolism. *Clin. Biochem.* **46**, 1339-1352 (2013).
2. Thorens, B. & Mueckler, M. Glucose transporters in the 21st century. *Am. J. Physiol. Endocrinol. Metab*. **298**, E141-E145 (2010).
3. Gould, G. & Holman, G. D. The glucose transporter family: Structure, function and tissue specific expression. *Biochem. J*. **295**, 329-341 (1993).
4. Manolescu, A. R., Witkowska, K., Kinnaird, A., Cessford, T. & Cheeseman C. Facilitated hexose transporters: New perspectives on form and function. *Physiology* **22**, 234-240 (2007).
5. McQuade, D. T., Plutschack, M. B. & Seeberger, P. H. Passive fructose transporters in disease: A molecular overview of their structural specificity. *Org. Biomol. Chem*. **11**, 4909-4920 (2013).
6. Mueckler, M. & Thorens, B. The SLC2 (GLUT) family of membrane transporters. *Mol. Aspects Med*. **34**, 121-138 (2013).
7. Long, W. & Cheeseman, C. I. Structure and functional insights into GLUT family of membrane transporters. *Cell Health and Cytoskeleton*. **7**, 167-183 (2015).
8. Deng, D. & Yan, N. GLUT, SGLT, and SWEET: Structural and mechanistic investigation of the glucose transporters. *Protein Sci.* **25**, 546-558 (2016).
9. Kasahara, M. & Hinkle P. C. Recognition and purification of D-glucose transporter from human erythrocytes. *J. Biol. Chem.* **252**, 7384-7390 (1977).

10. Sogin, D. C. & Hinkle, P. C. Characterization of the glucose transporter from human erythrocytes. *J. Supramol. Struct.* **8**, 447-453 (1978).

11. Mueckler, M., Caruso, C., Baldwin, S. A., Panico, M., Blench, I., Morris, H. R., Allard, W. J., Lienhard, G. E. & Lodish, H. F. Sequence and structure of a human glucose transporter. *Science*. **229**, 941-945 (1985).

12. Joost, H-G, Bell, G. I, Best, J. D, Birnbaum, M. J., Charron, M. J., Chen, Y. T., Doege, H., James, D. E., Lodish, H. F., Moley, K. H., Moley, J. F., Mueckler, M., Rogers, S., Schurmann, A. & Seino, S., Thorens, B. Nomenclature of the GLUT/SLC2A family of sugar/poloyl transport facilitators. *Am. J. Physiol. Endocrinol. Metab.* **282**, E974-E976 (2002).

13. Morgello, S., Uson, R. R., Schwartz, E. J. & Haber, R. S. The human blood-brain barrier glucose transporter (GLUT1) is a glucose transporter of gray matter astrocytes. *Glia.* **14**, 43-54 (1995).

14. Kumagai, K. A. Glucose transport in brain and retina: Implications in the management and complications of diabetes. *Diabetes Metab. Res Rev.* **15**, 261-273 (1999).

15. Postic, C., Burcelin, R., Rencurel, F., Pegorier, J-P., Loizeau, M., Girard, J. & Leturque, A. Evidence for a transient inhibitory effect of insulin on GLUT2 expression in the liver: Studies *in vivo* and *in vitro*. *Biochem. J.* **293**, 119-124 (1993).

16. Pang, K., Mukonoweshuro, C. & Wong, G. G. Beta cells arise from glucose transporter 2 (GLUT2)-expressing epithelial cells of the developing rat pancreas. *Proc. Natl. Acad. Sci. USA*. **91**, 9559-9563 (1994).

17. Maher, F., Davies-Hill, T. M., Lysko, P. G., Henneberry, R. C. & Simpson, I. A. Expression of two glucose transporters, GLUT1 and GLUT3, in cultured cerebellar neurons: Evidence for neuron-specific expression of GLUT3. *Mol. Cell. Neurosci.* **2**, 351-360 (1991).

18. Haung, S. & Czech, P. The GLUT4 glucose transporter. *Cell Metab.* **5**, 237-252 (2007).

19. Leto, D. & Saltiel, A. Regulation of glucose transport by insulin: Traffic control of GLUT4. *Mol. Cell Biol.* 13, 383-396 (2012).

20. Band, E. B., Depaoli, A. M., Davidson, N. O, Bell, C. I. & Burant, C. F. Sequence, tissue distribution, and functional characterization of the rat fructose transporter GLUT5. *Am. J. Physiol. Gastrointest. Liver Physiol.* **264**, G1169-1176 (1993).

21. Zhao, F-Q. & Keating, A. F. Functional properties and genomics of glucose transporters. *Curr. Genomics* **8**, 113-128 (2007)

22. Cheeseman, C. GLUT7: A new intestinal facilitated hexose transport. *Am. J. Physiol. Endocrinol. Metab.* **295**, E238-E241(2008).

23. Preitner, F., Bonny, O., Laverriere, A., Rotman, S., Firsov, D., Costa, A. D., Metref, S. & Thorens, B. GLUT9 is a major regulator of urate homostasis and its genetic inactivation induces hyperuricosuria and urate nephropathy. *Proc. Natl. Acad. Sci. USA*. **106**, 15501-15506 (2009).

24. Deng, D., Xu, C., Sun, P., Wu, J., Yan, C., Hu, M. & Yan, N. Crystal structure of the human glucose transporter GLUT1. *Nature.* **510**, 121-125 (2014).

25. Nomura, N., Verdon, G., Kang, H. J., Shimamura, T., Nomura, Y., Sonoda, Y., Hussien, S. A., Qureshi, A. A., Coincon, M., Sato, Y., Abe, H., Nakada-Nakura, Y.,

Hino, T., Arakawa, T., Kusano-Arai, O., Iwanari, H., Murata, T., Kobayashi, T., Hamakubo, T., Kasahara, M., Iwata, S. & Drew, D. Structure and mechanism of mammalian fructose transporter GLUT5. *Nature.* **526**, 397-401 (2015).

26. Deng, D., Xu, C., Sun, P., Yan, C., Ke, M., Jiang, X., Xiong, L., Ren, W., Hirata, K., Yamamoto, M., Fan, S. & Yan, N. Molecular basis of ligand recognition and transport by glucose transporters. *Nature*. **526**, 391-396 (2015).
27. Manolescu, A. R., Augustin, R., Moley, K., & Cheeseman, C. A highly conserved hydrophobic motif in the exofacial vestibule of fructose transporting SLC2A proteins acts as a critical determinant of their substrate selectivity. *Mol. Membr. Biol.* **24**, 455–463 (2007).
28. Sheena, A., Mohan, S. S., Haridas, N. P. A. & Anilkumar, G. Elucidation of the glucose transport pathway in glucose transporter 4 *via* steered molecular dynamics simulations. *PLoS One.* **6**, e25747 (2011).
29. Carruthers, A., DeZutter, J., Ganguly, A. & Devaskar, S. U. Will the original glucose transporter isoform please stand up. Am. J. Physiol. *Endocrinol. Metab.* **297**, E836-E848 (2009).
30. Mueckler, M. & Makepeace, C. Transmembrane segment 12 of the GLUT1 glucose transporter is an outer helix and is not directly involved in the transport mechanism. *J. Biol. Chem.* **281**, 36993-36998 (2006).
31. Gallagher, B. M., Fowler, J. S., Gutterson, N. I., MacGregor, R. R., Wan, C-N. & Wolf, A. P. Metabolic trapping as a principle of radiopharmaceutical design: Some factors responsible for the biodistribution of [^{18}F]-2-deoxy-2-fluoro-D-glucose. *J. Nucl. Med.* **19**, 1154-1161, (1978).

32. Angyal, S. J. The composition and conformation of sugars in solution. *Angew. Chem. Int. Ed. Engl.* ***8***, 157-166 (1969).

33. Tajmir-Riahi, H. A. Carbohydrate complexes with alkaline earth metal ions. Interactions of D-glucono-1,5-lacton with the Mg (II), Ca (II), Sr (II) and Ba (II) cations in the crystalline solid and aqueous solution. *J. Inorg. Chem.* **39**, 33-41 (1990).

34. Gatley, S. J. Labeled glucose analogs in the genomic era. *J. Nucl. Med.* **44**, 1082-1086 (2003).

35. Barnett, J. E. G., Holman, G. D. & Munday, K. A. Structural requirement for binding to the sugar-transport system of the human erythrocyte. *Biochem. J.* **131**, 211-221 (1973).

36. Calvaresi, E. C. & Hergenrother. P. J. Glucose conjugation for specific targeting and treatment of cancer. *Chem. Sci.* **4**, 2319-2333 (2013).

37. Som, P., Atkins, H. L., Bandopadhyay, D., Fowler, J. S., MacGregor, R. R., Matsui, K., Oster, H., Sacker, D. F., Shiue, C. Y., Tuner, H., Wan, C-N., Wolf, A. P. & Zabnski, V. A fluorinated glucose analog, 2-fluoro-2-deoxy-D-glucose (F-18): Nontoxic tracer for tumor detection. *J. Nucl. Med*. **21**, 670-675 (1980).

38. Avril, N. GLUT1 expression in tissue and ^{18}F-FDG uptake. *J. Nucl. Med*. **45**, 930-932 (2004).

39. Guo, J., Du, C., Shan, L., Zhu, H., Xue, B., Quian, Z., Achilefu, S. & Gu, Y. Comparison of near-infrared fluorescent deoxyglucose probes with different dyes for tumor diagnosis in vivo. *Contrast Media Mol. Imaging*. **7**, 289-301 (2012).

40. Z. Cheng, J. Levi, Z. Xiong, O. Gheysens, S. Keren, X. Chen & S. S. Gambhir. Near-infrared fluorescent deoxyglucose analog for tumor optical imaging in cell culture and in living mice. *Bioconjugate Chem.* **17**, 662-669 (2006).

41. Tatibouet, A., Yang, J., Morin, C. & Holman, G. D. Synthesis and evaluation of fructose analogues as inhibitors of the D-fructose transporter GLUT5. *Bioorg. Med. Chem.* **8**, 1825-1833 (2000); Haradahira, T. *et al.* Radiosynthesis, rodent biodistribution, and metabolism of 1-deoxy-1-[^{18}F]-fluoro-D-fructose. *Nucl. Med. Biol.* **22**, 719–725 (1995).

42. Girniene, J., Tatibouët, A., Sackus, A., Yang, J., Holman, G. D. & Rollin, P. Inhibition of the D-fructose transporter protein GLUT5 by fused-ring glycol-1,3-oxazolidin-2-thiones and oxazolidin-2-ones. *Carbohydrate Res.* **338**, 711-719 (2003).

43. Yang, J., Dowden, J., Tatibouet, A., Hatanaka, Y. & Holman, G. D. Development of high-affinity ligands and photoaffinity labels for the D-fructose transporter GLUT5. *Biochem. J.* **367**, 533-539 (2002).

44. Wuest, M., Trayner, B. J., Grant, T. N., Jans, H. S., Mercer, J. R., Murray, D., West, F. G., McEwan, A. J. B., Wuest, F. & Cheeseman, C. I. Radiopharmacological evaluation of 6-deoxy-6-[^{18}F]fluoro-D-fructose as a tracer for PET imaging of breast cancer. *Nucl. Med. Biol.* **38**, 461-475 (2011).

45. Tanasova, M., Plutschack, M., Muroski, M. E., Sturla, S. J., Struouse, G. F. & McQuade, D. T. Fluorescent THF-based fructose analogue exhibits fructose-dependent uptake. *ChemBioChem*. **14**, 1263-1270 (2013).

46. Soueidan, O. M., Trayner, B. J., Grant, T. N., Henderson, J. R., Wuest, F., West, F. G. & Cheeseman, C. I. New fluorinated fructose analogs as selective probes of hexose transport protein GLUT5. *Org. Biomol. Chem.* **13**, 6511-6521 (2015).

47. Medina, R. A. & Owen, G. I. Glucose transporters: Expression, regulation and cancer. *Biol. Res.* **35**, 9-26 (2002).

48. Adekola, K., Rosen, S.T. & Shanmugam M. Glucose transporters in cancer metabolism. *Curr. Opin. Oncol.* **24**, 650-654 (2012).

49. Carvalho, K. C., Cunha, I. W., Rocha, R. M., Ayala, F. R., Cajaiba, M. M., Begnami, M. D., Vilela, R. S., Paiva, G. R., Andrade, R. G. & Soares, F. A. GLUT1 expression in malignant tumors and its use as an immunodiagnostic marker. *Clinics*. **66**, 965-972 (2011).

50. Schwartzenberg-Bar-Yoseph, F., Armoni, M. & Karniel, E. The tumor suppressor p53 down-regulates glucose transporters GLUT1 and GLUT4 gene expression. *Cancer Res.* **64**, 2627-2633 (2004).

51. Krzeslak, A., Wojcik-Krowiranda, K., Forma, E., Jozwiak, P., Romanowicz, A. & Brys, M. Expression of GLUT1 and GLUT3 glucose transporters in endometrial and breast cancer. *Pathol. Oncol. Res.* **18**, 721-728 (2012).

52. Godoy, A., Ulloa, V., Rodriguez, F., Reinicke, K., YaÑez, A. J., GarcÍa, M. A., Medina, R. A., Carrasco, M., Barberis, S., Castro, T., MartÍnez, F., Koch, X., Vera, J. C., Poblete. M. T., Figueroa, C.D., Peruzzo, B., PÉrez, F., Nualart, F. Differential subcellular distribution of glucose transporters GLUT1-6 and GLUT9 in human cancer: Ultrastructural localization of GLUT1 and GLUT5 in breast tumor cells. *J. Cell. Physiol.* **207**, 614-627 (2006).

53. Zamora-Leon, S. P., Golde, D. W., Concha, I. I., Rivas, C. I., Delgado-López, F. & Vera, J. C. Expression of the fructose transporter GLUT5 in human breast cancer. *Proc. Natl. Acad. Sci. USA*. **93**, 1847-1852 (1996).

54. James, M. L. & Gambhir, S. S. A molecular imaging primer: Modalities, imaging agents, and applications. *Physiol. Rev.* **92**, 897-965 (2012).

55. Wang, D. S., Dake, M. D., Park, J. M. & Kuo, M. D. Molecular imaging: A primer for interventionalists and images. *J. Vasc. Interv. Radiol.* **17**, 1405-1423 (2006).

56. Nolting, D. D., Nickels, M. L., Guo, N. & Pham, W. Molecular imaging probe development: A chemistry perspective. *Am. J. Nucl. Med. Mol. Imaging.* **2**, 273-306 (2012).

57. Gambhir, S. S. Molecular imaging of cancer with positron emission tomography. *Nat. Rev. Cancer.* **2**, 683-693 (2002).

58. Imam, S. K. Review of positron emission tomography tracers for imaging of tumor hypoxia. *Cancer Biother. Radiopharm.* **25**, 365–74 (2010).

59. Muehllehner, G. & Karp, J. S. Positron emission tomography. *Phys. Med. Biol.* **51**, R117–37 (2006).

60. Zanzonico, P. Positron emission tomography: a review of basic principles, scanner design and performance, and current systems. *Semin. Nucl. Med.* **34**, 87–111 (2004).

61. Couturier, O., Luxen, A., Chatal, J. F., Vuillez, J. P., Rigo, P. & Hustinx, R. Fluorinated tracers for imaging cancer with positron emission tomography. *Eur. J. Nucl. Med. Mol. Imaging* **31**, 1182–206 (2004); Wood, K. A., Hoskin, P. J. & Saunders, M. I. Positron emission tomography in oncology: a review. *Clin. Oncol. (R. Coll. Radiol).* **19**, 237–55 (2007).

62. Pagani, M., Stone-Elander, S. & Larsson, S. A. Alternative positron emission tomography with non-conventional positron emitters: effects of their physical properties on image quality and potential clinical applications. *Eur. J. Nucl. Med.* **24**, 1301–27 (1997).

63. Maschauer, S. & Prante, O. Sweetening pharmaceutical radiochemistry by ^{18}F fluoroglycosylation: A short review. *BioMed. Res. Int.* Article ID 214748 (2014).

64. Miller, P. W., Long, N. J., Vilar, R. & Gee, A. D. Synthesis of ^{11}C, ^{18}F, ^{15}O, and ^{13}N radiolabels for positron emission tomography. *Angew. Chem. Int. Ed.* **47**, 8998–9033 (2008).

65. Berger, A. How does it work? Positron emission tomography. *Brit. Med. J.* **326,** 1449 (2003).

66. Czernin, J. & Phelps, M. E. Positron emission tomography scanning: current and future applications. *Annu. Rev. Med.* **53**, 89–112 (2002).

67. Rozen, S. Elemental fluorine as a legitimate reagent for selective fluorination of organic compounds. *Acc. Chem. Res.* **21**, 307–312 (1988).

68. Ramsden, C. A. Xenon difluoride in the organic laboratory: a tale of substrates, solvents and vessels. *Arkivoc* **2014**, 109 (2013).

69. Furuya, T., Kamlet, A. S. & Ritter, T. Catalysis for fluorination and trifluoromethylation. *Nature* **473**, 470–7 (2011).

70. Lal, G. S., Pez, G. P. & Syvret, R. G. Electrophilic NF Fluorinating Agents. *Chem. Rev.* **96**, 1737–1756 (1996).

71. Singh, R. P. & Shreeve, J. M. Recent highlights in electrophilic fluorination with 1-chloromethyl-4-fluoro-1,4-diazoniabicyclo[2.2.2]octane bis(tetrafluoroborate). *Acc. Chem. Res.* **37**, 31–44 (2004).

72. Nyffeler, P. T., Durón, S. G., Burkart, M. D., Vincent, S. P. & Wong, C.-H. Selectfluor: mechanistic insight and applications. *Angew. Chem. Int. Ed.* **44**, 192–212 (2004).

73. Umemoto, T., Harasawa, K., Tomizawa, G., Kawada, K. & Tomita, K. N-F 19-fluorine nuclear magnetic resonance of N-fluoropyridinium salts. *J. Fluor. Chem.* **53**, 369–377 (1991).

74. Kiselyov, A. S. Chemistry of N-fluoropyridinium salts. *Chem. Soc. Rev.* **34**, 1031–7 (2005).

75. Stavber, S. Recent advances in the application of Selectfluor™ F-TEDA-BF4 as a versatile mediator or catalyst in organic synthesis. *Molecules* **16**, 6432–64 (2011).

76. Champagne, P. A., Desroches, J., Hamel, J.-D., Vandamme, M. & Paquin, J.-F. Monofluorination of Organic Compounds: 10 Years of Innovation. *Chem. Rev.* **115**, 9073–174 (2015).

77. Umemoto, T. *et al.* Power- and structure-variable fluorinating agents. The N-fluoropyridinium salt system. *J. Am. Chem. Soc.* **112**, 8563–8575 (1990).

78. Waschke, D., Leshch, Y., Thimm, J., Himmelreich, U. & Thiem, J. Synthesis of fluorinated ketoheptoses as specific diagnostic agents. *Eur. J. Org. Chem.* **2012**, 948–959 (2012).

79. Nguyen, T.-H., Abarbri, M., Guilloteau, D., Mavel, S. & Emond, P. Nucleophilic fluorination of alkynyliodonium salts by alkali metal fluorides: access to fluorovinylic compounds. *Tetrahedron* **67**, 3434–3439 (2011).

80. Kim, D. W., Jeong, H. J., Lim, S. T., Sohn, M. H., Katzenellenbogen, J. A. & Chi, D. Y. Facile nucleophilic fluorination reactions using tert-alcohols as a reaction medium: significantly enhanced reactivity of alkali metal fluorides and improved selectivity. *J. Org. Chem.* **73**, 957–62 (2008).

81. Akiyama, Y., Hiramatsu, C., Fukuhara, T. & Hara, S. Selective introduction of a fluorine atom into carbohydrates and a nucleoside by ring-opening fluorination reaction of epoxides. *J. Fluor. Chem.* **127**, 920–923 (2006).

82. Soueidan, O.-M., Trayner, B. J., Grant, T. N., Henderson, J. R., Wuest, F., West, F. G. & Cheeseman, C. I. New fluorinated fructose analogs as selective probes of the hexose transporter protein GLUT5. *Org. Biomol. Chem.* **13**, 6511–21 (2015).

83. Tsuchiya, T., Takahashi, Y., Endo, M., Umezawa, S. & Umezawa, H. Synthesis of 2′,3′-dideoxy-2′-fluorokanamycin A. *J. Carbohydr. Chem.* **4**, 587–611 (2007).

84. Singh, R. P. & Shreeve, J. M. Recent advances in nucleophilic fluorination reactions of organic compounds using deoxofluor and DAST. *Synthesis (Stuttg).* **2002**, 2561–2578 (2002).

85. L'Heureux, A. Beaulieu, F., Bennettl, C., Bill, D. R., Clayton, S., LaFlamme, Mirmehrabi, M., Tadayon, S., Tovell, D. & Couturier, M. Aminodifluorosulfinium salts: selective fluorination reagents with enhanced thermal stability and ease of handling. *J. Org. Chem.* **75**, 3401–11 (2010).

86. Ni, C., Hu, M. & Hu, J. Good partnership between sulfur and fluorine: sulfur-based fluorination and fluoroalkylation reagents for organic synthesis. *Chem. Rev.* **115**, 765–825 (2015).

87. Furuya, T., Kuttruff, C. A. & Ritter, T. Carbon-fluorine bond formation. *Curr. Opin. Drug Discov. Devel.* **11**, 803–19 (2008).

88. Raju, R., Castillo, B. F., Richardson, S. K., Thakur, M., Severins, R., Kronenberg, M. & Howell, A. R. Synthesis and evaluation of 3''- and 4''-deoxy and -fluoro analogs of the immunostimulatory glycolipid, KRN7000. *Bioorg. Med. Chem. Lett.* **19**, 4122–5 (2009).

89. Cole, E. L., Stewart, M. N., Littich, R., Hoareau, R. & Scott, P. J. H. Radiosyntheses using fluorine-18: the art and science of late stage fluorination. *Curr. Top. Med. Chem.* **14**, 875–900 (2014).

90. DeJesus, O. T., Martin, J. A., Yasillo, N. J., Gatley, S. J. & Cooper, M. D. [18F]Fluoride from a small cyclotron for the routine synthesis of [18F]2-Fluoro-2-deoxy-d-glucose. *Int. J. Rad. Appl. Instrum. A.* **37**, 397–401 (1986).

91. Bouvet, V. Jans, H. S., Wuest, M., Soueidan, O.-M., Mercer, J., McEwan, A. J. B., West, F. G., Cheeseman, C.I. & Wuest, F. Automated synthesis and dosimetry of 6-deoxy-6-[(18)F]fluoro-D-fructose (6-[(18)F]FDF): a radiotracer for imaging of GLUT5 in breast cancer. *Am. J. Nucl. Med. Mol. Imaging* **4**, 248–59 (2014).

92. Castellucci, P. Perrone, A. M., Picchio, M., Ghi, R., Farsad, M., Nanni, C., Messa, C., Meriggiola, M. C., Al-Nahhas, A., Rubello, D., Fazio, F. & Fanti, S. Diagnostic accuracy of 18F-FDG PET/CT in characterizing ovarian lesions and staging ovarian

cancer: correlation with transvaginal ultrasonography, computed tomography, and histology. *Nucl. Med. Commun.* **28**, 589–95 (2007).

93. Diksic, M. & Jolly, D. New Synthesis of 2-Deoxy-2-fluoro-D-hexoses by Fluorination in Water. *J. Carbohydr. Chem.* **4**, 265–271 (2006).
94. Haradahira, T., Maeda, M. & Kojima, M. Alternative synthesis of no-carrier-added 2-deoxy-2-[18F]fluoro-D-glucose using [^{18}F] fluoride ion. *J. Label. Compd. Radiopharm.* **25**, 497–507 (1988).
95. Lee, C.-C. *et al.* Multistep synthesis of a radiolabeled imaging probe using integrated microfluidics. *Science* **310**, 1793–6 (2005).
96. Ferrini, K., Ghelfi, F., Mannucci, R. & Titta, L. Lifestyle, nutrition and breast cancer: facts and presumptions for consideration. *Ecancermedicalscience* **9**, 557 (2015).
97. Weigelt, B., Peterse, J. L. & van 't Veer, L. J. Breast cancer metastasis: markers and models. *Nat. Rev. Cancer* **5**, 591–602 (2005).
98. Haradahira, T. *et al.* Radiosynthesis, rodent biodistribution, and metabolism of 1-deoxy-1-[18F]fluoro-D-fructose. *Nucl. Med. Biol.* **22**, 719–725 (1995).
99. Ravshel, F. M. & Cleland, W. W. The substrate and anomeric specificity of fructokinase. *J. Biol. Chem.* **248**, 8174-8177 (1973); Hanson, R. L., Ho, R. S., Wiseberg, J. J., Simpson, R., Younathan, E. S. & Blair, J. B. Inhibition of glucongenesis and glycongenolysis by 2,5-anhydro-D-mannitol. *J. Biol. Chem.* **259**, 218-223 (1984).

Chapter 2

1. Axet, M. R. *et al.* Chiral Diphosphite-Modified Rhodium(0) Nanoparticles: Catalyst reservoir for styrene hydroformylation. *Eur. J. Inorg. Chem.* **2008,** 3460–3466 (2008).
2. Axet, M. R., Benet-Buchholz, J., Claver, C. & Castillón, S. New C2-symmetric diphosphite ligands derived from carbohydrates: Effect of the remote stereocenters on asymmetric catalysis. *Adv. Synth. Catal.* **349,** 1983–1998 (2007); Favier, I. *et al.* Efficient recycling of a chiral palladium catalytic system for asymmetric allylic substitutions in ionic liquid. *Chem. Commun.* **47,** 7869–71 (2011).
3. Balanta Castillo, A. *et al.* An outstanding palladium system containing a C2-symmetrical phosphite ligand for enantioselective allylic substitution processes. *Chem. Commun.* 6197–6199 (2008).
4. Gual, A. *et al.* Diphosphite ligands derived from carbohydrates as stabilizers for ruthenium nanoparticles: promising catalytic systems in arene hydrogenation. *Chem. Commun.* 2759–61 (2008); Gual, A., Godard, C., Claver, C. & Castillón, S. C 1 - Symmetric Diphosphite Ligands Derived from Carbohydrates: Influence of Structural Modifications on the Rhodium-Catalyzed Asymmetric Hydroformylation of Styrene. *Eur. J. Org. Chem.* **2009,** 1191–1201 (2009); Sanhes, D., Gual, A., Castillón, S., Claver, C., Gómez, M. & Teuma, E. New chiral diphosphites derived from substituted 9,10-dihydroanthracene. Applications in asymmetric catalytic processes. *Tetrahedron: Asymmetry* **20,** 1009–1014 (2009).
5. Padwa, A. & Murphree, S. Epoxides and aziridines - a mini review. *ARKIVOC* **2006,** 6-33 (2005).

6. De Faveri, G., Ilyashenko, G. & Watkinson, M. Recent advances in catalytic asymmetric epoxidation using the environmentally benign oxidant hydrogen peroxide and its derivatives. *Chem. Soc. Rev.* **40,** 1722–60 (2011).
7. Xia, Q.-H., Ge, H.-Q., Ye, C.-P., Liu, Z.-M. & Su, K.-X. Advances in homogeneous and heterogeneous catalytic asymmetric epoxidation. *Chem. Rev.* **105,** 1603–62 (2005).
8. Marigo, M., Franzén, J., Poulsen, T. B., Zhuang, W. & Jørgensen, K. A. Asymmetric organocatalytic epoxidation of alpha,beta-unsaturated aldehydes with hydrogen peroxide. *J. Am. Chem. Soc.* **127,** 6964–5 (2005); Corey, E. J., Shibata, S. & Bakshi, R. K. An efficient and catalytically enantioselective route to (S)-(-)-phenyloxirane. *J. Org. Chem.* **53,** 2861–2863 (1988); Kang, J. Y. & Connell, B. T. Synthesis of substituted acetylenic epoxides followed by indium-catalyzed rearrangement to 2,3,5-trisubstituted furans. *J. Org. Chem.* **76,** 2379–83 (2011); Träff, A., Bogár, K., Warner, M. & Bäckvall, J.-E. Highly efficient route for enantioselective preparation of chlorohydrins via dynamic kinetic resolution. *Org. Lett.* **10,** 4807–10 (2008).
9. Tu, Y., Wang, Z.-X. & Shi, Y. An Efficient Asymmetric epoxidation method for trans-olefins mediated by a fructose-derived Ketone. *J. Am. Chem. Soc.* **118,** 9806–9807 (1996); Marigo, M., Franzén, J., Poulsen, T. B., Zhuang, W. & Jørgensen, K. A. Asymmetric organocatalytic epoxidation of α,β-unsaturated aldehydes with hydrogen peroxide. *J. Am. Chem. Soc.* **127,** 6964–5 (2005).
10. Hanazawa, T., Koiwa, M., Hareau, G. P.-J. & Sato, F. Optically active trans-4-(tert-butyldimethylsiloxymethyl)-5-(tert-butyldimethylsiloxy)-2-cyclohexenone as a useful chiral building block for preparation of substituted cyclohexane rings: synthesis and

its highly stereoselective reaction with RCu(CN)Li. *Tetrahedron Lett.* **41,** 2659–2662 (2000).

11. Schneider, C. Synthesis of 1,2-difunctionalized fine chemicals through catalytic, enantioselective ring-opening reactions of epoxides. *Synthesis* **2006,** 3919–3944 (2006); 1. Battistini, C., Crotti, P., Macchia, B., Macchia, F. & DePuy, C. H. Nucleophilic step of ring-opening reactions of cyclopropanes with electrophiles. Electronic substituent effects on stereoselectivity of reactions of some 1-arylbicyclo[4.1.0]heptanes with mercuric salts. *J. Org. Chem.* **43,** 1400–1404 (1978); Bisol, T. B., Bortoluzzi, A. J. & Sá, M. M. Nucleophilic ring-opening of epoxide and aziridine acetates for the stereodivergent synthesis of β-hydroxy and β-amino γ-lactams. *J. Org. Chem.* **76,** 948–62 (2011); Dieter, R. K. & Pounds, S. Ring opening reactions of electrophilic cyclopropanes. *J. Org. Chem.* **47,** 3174–3177 (1982).
12. Ferguson, L. N. Ring strain and reactivity of alicycles. *J. Chem. Educ.* **47,** 46 (1970).
13. Dudev, T. & Lim, C. Ring strain energies from ab initio calculations. *J. Am. Chem. Soc.* **120,** 4450–4458 (1998).
14. Robert D. Bach & Dmitrenko, O. The effect of carbonyl substitution on the strain energy of small ring compounds and their six-member ring reference compounds. *J. Am. Chem. Soc.* **128,** 4598-4611 (2006).
15. Bach, R. D. & Dmitrenko, O. The Effect of substitutents on the strain energies of small ring compounds. *J. Org. Chem.* **67,** 2588–2599 (2002).
16. Cremer, D. & Gauss. Cyclopropane and cyclobutane – CC and CH bond energies, 1,3 interactions and σ-aromaticity. *J. Am. Chem. Soc.* **108,** 7467-7477 (1986); Stirling, C.

J. M. Evaluation of strain effects on the reactivity of small rings. *Isr. J. Chem.* **21,** 111–118 (1981).

17. de Meijere, A. Adolf von Baeyer: winner of the Nobel prize for chemistry 1905. *Angew. Chem. Int. Ed.* **44,** 7836–40 (2005) and cited references.
18. Bonollo, S., Lanari, D. & Vaccaro, L. Ring-opening of epoxides in water. *Eur. J. Org. Chem.* **2011**, 2587–2598 (2011).
19. Nielsen, L. P. C. and Jacobsen, E. N. Catalytic Asymmetric epoxide ring-opening chemistry. In *aziridines and epoxides in organic synthesis* (ed A. K. Yudin), 229-269 (Wiley-VCH Verlag GmbH & Co. KGaA, 2006).
20. Jacobsen, E. N. Asymmetric catalysis of epoxide ring-opening reactions. *Acc. Chem. Res.* **33**, 421–431 (2000).
21. Schaus, S. E. & Jacobsen, E. N. Asymmetric ring opening of meso epoxides with TMSCN catalyzed by (pybox)lanthanide complexes. *Org. Lett.* **2,** 1001–1004 (2000).
22. Hughes, E. D. & Ingold, C. K. Mechanism of substitution at a saturated carbon atom. Part IV. A discussion of constitutional and solvent effects on the mechanism, kinetics, velocity, and orientation of substitution. *J. Chem. Soc.* 244-255 (1935).
23. Martins, F., Leitão, R. E. & Moreira, L. Solvation effects in the heterolyses of 3-X-3-methylpentanes(X = Cl, Br, I). *J. Phys. Org. Chem.* **17,** 1061–1066 (2004).
24. Akeroyd, F. M. The foundations of modern organic chemistry: The rise of the Hughes and Ingold theory from 1930–1942. *Found. Chem.* **2,** 99–125 (2000).
25. Gawley, R. E. A proposal for (slight) modification of the Hughes-Ingold mechanistic descriptors for substitution reactions. *Tetrahedron Lett.* **40,** 4297–4300 (1999).

26. Brown, D. C. Teaching solvent effects on S_N2 reactions by the introduction of ionic liquids. *Chem. Educ.* **11**, 64-66 (2006).

27. Reichardt, C. Empirical parameters of solvent polarity as linear free-energy relationships. *Angew. Chemie Int. Ed. Engl.* **18,** 98–110 (1979).

28. Soueidan, O.-M. *et al.* New fluorinated fructose analogs as selective probes of the hexose transporter protein GLUT5. *Org. Biomol. Chem.* **13,** 6511–21 (2015).

29. Castejón, P., Pastó, M., Moyano, A., Pericàs, M. A. & Riera, A. A convenient, stereodivergent approach to the enantioselective synthesis of N-Boc-aminoalkyl epoxides. *Tetrahedron Lett.* **36,** 3019–3022 (1995).

30. Gutheie, R. D., Jenkins, I. D., Watters, J. J., Wright, M. W. & Yamasaki, R. Synthesis of some derivatives of 2,5-anhydro-D-mannitol. *Aust. J. Chem.* **35**, 2169-21773 (1982).

31. Otero, D. A. & Simpson, R. 2,5-anhydro-D-hexitols: syntheses of 2,5-anhydro-d-altritol and 2,5-anhydro-D-iditol. *Carbohydr. Res.* **128,** 79–86 (1984).

32. Chevallier, O. P. & Migaud, M. E. Investigation of acetyl migrations in furanosides. *Beilstein J. Org. Chem.* **2,** 14 (2006).

33. Amantini, D., Fringuelli, F., Piermatti, O. & Tortoioli, S. Nucleophilic ring opening of 1,2-epoxides in aqueous medium. *ARKIVOC* **2006,** 293-311 (2002); Sabitha, G., Babu, R. S., Rajkumar, M. & Yadav, J. S. Cerium(III) chloride promoted highly regioselective ring opening of epoxides and aziridines using NaN_3 in acetonitrile: A facile synthesis of 1,2-azidoalcohols and 1,2-azidoamines. *Org. Lett.* **4,** 343–345 (2002).

34. Nair, V., Chun, B. K. & Vadakkam J. Ring-expanded analogues of natural oxetanocin. *Tetrahedron* **45**, 10261-10268 (2004).

Chapter 3

1. Wuest, M., Trayner, B. J., Grant, T. N., Jans, H. S., Mercer, J. R., Murray, D., West, F. G., McEwan, A. J. B., Wuest, F. & Cheeseman, C. I. Radiopharmacological evaluation of 6-deoxy-6-[^{18}F]fluoro-D-fructose as a tracer for PET imaging of breast cancer. *Nucl. Med. Biol.* **38**, 461-475 (2011).
2. Soueidan, O. M., Trayner, B. J., Grant, T. N., Henderson, J. R., Wuest, F., West, F. G. & Cheeseman, C. I. New fluorinated fructose analogs as selective probes of hexose transport protein GLUT5. *Org. Biomol. Chem.* **13**, 6511-6521 (2015).
3. Godoy, A., Ulloa, V., Rodriguez, F., Reinicke, K., YaÑez, A. J., GarcÍa, M. A., Medina, R. A., Carrasco, M., Barberis, S., Castro, T., MartÍnez, F., Koch, X., Vera, J. C., Poblete. M. T., Figueroa, C.D., Peruzzo, B., PÉrez, F., Nualart, F. Differential subcellular distribution of glucose transporters GLUT1-6 and GLUT9 in human cancer: Ultrastructural localization of GLUT1 and GLUT5 in breast tumor cells. *J. Cell. Physiol.* **207**, 614-627 (2006); Zamora-Leon, S. P., Golde, D. W., Concha, I. I., Rivas, C. I., Delgado-López, F. & Vera, J. C. Expression of the fructose transporter GLUT5 in human breast cancer. *Proc. Natl. Acad. Sci. USA*. **93**, 1847-1852 (1996).
4. Haradahira, T. *et al.* Radiosynthesis, rodent biodistribution, and metabolism of 1-deoxy-1-[^{18}F]fluoro-D-fructose. *Nucl. Med. Biol.* **22**, 719–725 (1995).
5. Czernin, J. & Phelps, M. E. Positron emission tomography scanning: current and future applications. *Annu. Rev. Med.* **53**, 89–112 (2002).

6. Thorens, B. & Mueckler, M. Glucose transporters in the 21st century. *Am. J. Physiol. Endocrinol. Metab*. **298**, E141-E145 (2010).

7. Gould, G. & Holman, G. D. The glucose transporter family: Structure, function and tissue specific expression. *Biochem. J*. **295**, 329-341 (1993).

8. Manolescu, A. R., Witkowska, K., Kinnaird, A., Cessford, T. & Cheeseman C. Facilitated hexose transporters: New perspectives on form and function. *Physiology* **22**, 234-240 (2007).

9. McQuade, D. T., Plutschack, M. B. & Seeberger, P. H. Passive fructose transporters in disease: A molecular overview of their structural specificity. *Org. Biomol. Chem*. **11**, 4909-4920 (2013).

10. Mueckler, M. & Thorens, B. The SLC2 (GLUT) family of membrane transporters. *Mol. Aspects Med*. **34**, 121-138 (2013).

11. Long, W. & Cheeseman, C. I. Structure and functional insights into GLUT family of membrane transporters. *Cell Health and Cytoskeleton*. **7**, 167-183 (2015).

12. Deng, D. & Yan, N. GLUT, SGLT, and SWEET: Structural and mechanistic investigation of the glucose transporters. *Protein Sci.* **25**, 546-558 (2016).

13. Tatibouet, A., Yang, J., Morin, C. & Holman, G. D. Synthesis and evaluation of fructose analogues as inhibitors of the D-fructose transporter GLUT5. *Bioorg. Med. Chem.* **8**, 1825-1833 (2000); Haradahira, T. *et al.* Radiosynthesis, rodent biodistribution, and metabolism of 1-deoxy-1-[^{18}F]-fluoro-D-fructose. *Nucl. Med. Biol.* **22**, 719–725 (1995).

14. Girniene, J., Tatibouët, A., Sackus, A., Yang, J., Holman, G. D. & Rollin, P. Inhibition of the D-fructose transporter protein GLUT5 by fused-ring glycol-1,3-oxazolidin-2-thiones and oxazolidin-2-ones. *Carbohydrate Res.* **338**, 711-719 (2003).

15. Fileti, E. E., Chaudhuri, P. & Canuto, S. Relative strength of hydrogen bond interaction in alcohol–water complexes. *Chem. Phys. Lett.* **400,** 494–499 (2004).

16. Brammer, L., Bruton, E. A. & Sherwood, P. Understanding the behavior of halogens as hydrogen bond acceptors. *Cryst. Growth Des.* **1,** 277–290 (2001).

17. Schneider, H.-J. Hydrogen bonds with fluorine. Studies in solution, in gas phase and by computations, conflicting conclusions from crystallographic analyses. *Chem. Sci.* **3,** 1381-1394 (2012); Hunter, L. The C-F bond as a conformational tool in organic and biological chemistry. *Beilstein J. Org. Chem.* **6,** 38 (2010).

18. Platts, J. A., Maarof, H., Harris, K. D. M., Lim, G. K. & Willock, D. J. The effect of intermolecular hydrogen bonding on the planarity of amides. *Phys. Chem. Chem. Phys.* **14,** 11944–52 (2012); Johansson, A., Kollman, P., Rothenberg, S. & McKelvey, J. Hydrogen bonding ability of the amide group. *J. Am. Chem. Soc.* **96,** 3794–3800 (1974).

19. Garcia, J. G., Voll, R. J. & Younathan, E. S. Stereoselective carbohydate synthesis *via* palladium hydroxide catalyzed epoxide hydrogenolysis. *Tetrahedron Lett*. **32**, 5273-5276, (1991).

20. Machado, A. S., Olesker, A., Castillon, S. & Lukacs, G. Hydroxy group directed hydrogenation with rhodium and iridium catalysts. Synthesis of a protected chiral carbocyclic analogue of daunosamine. *J. Chem. Soc. Chem. Commun.* 330 (1985);

Stork, G. & Kahne, D. E. Stereocontrol in homogeneous catalytic hydrogenation via hydroxyl group coordination. *J. Am. Chem. Soc.* **105,** 1072–1073 (1983).

21. Steiner, T. The hydrogen bond in the solid state. *Angew. Chem. Int. Ed.* **41,** 49–76 (2002).

22. Bräse, S., Gil, C., Knepper, K. & Zimmermann, V. Organic azides: an exploding diversity of a unique class of compounds. *Angew. Chem. Int. Ed.* **44,** 5188–240 (2005).

23. No direct comparison of the hydrogen bond acceptor strengths between organic fluorides and organic azides was found. Organic azides are 1,3-dipoles with negative charge localization on the nitrogen atom directly attached to carbon (ref. 22), allowing this nitrogen atom to serve as a hydrogen bond acceptor. Based on the observed hydrogen bond acceptor trends (ref. 21) and poor hydrogen bond acceptor ability of organic fluorides (ref. 17), we considered the organic azides to be better hydrogen bond acceptors when compared to organic fluorides.

24. Jung, C. Y. & Rampal, A. L. Cytochalasin B binding sites and glucose transport carrier in human erythrocyte ghosts. *J. Biol. Chem.* **252,** 5456–63 (1977).

25. Nomura, N., Verdon, G., Kang, H. J., Shimamura, T., Nomura, Y., Sonoda, Y., Hussien, S. A., Qureshi, A. A., Coincon, M., Sato, Y., Abe, H., Nakada-Nakura, Y., Hino, T., Arakawa, T., Kusano-Arai, O., Iwanari, H., Murata, T., Kobayashi, T., Hamakubo, T., Kasahara, M., Iwata, S. & Drew, D. Structure and mechanism of mammalian fructose transporter GLUT5. *Nature.* **526**, 397-401 (2015).

Chapter 4

1. Pauwels, E. K. Ribeiro, M. J., Stoot, J. H. M. B, McCready, V. R., Bourguigon, M. & Maziere, B. FDG accumulation and tumor biology. *Nucl. Med. Biol.* **25,** 317–322 (1998); Czernin, J. & Phelps, M. E. Positron emission tomography scanning: current and future applications. *Annu. Rev. Med.* **53**, 89–112 (2002).

2. Medina, R. A. & Owen, G. I. Glucose transporters: Expression, regulation and cancer. *Biol. Res.* **35**, 9-26 (2002); Adekola, K., Rosen, S.T. & Shanmugam M. Glucose transporters in cancer metabolism. *Curr. Opin. Oncol.* **24**, 650-654 (2012); Carvalho, K. C., Cunha, I. W., Rocha, R. M., Ayala, F. R., Cajaiba, M. M., Begnami, M. D., Vilela, R. S., Paiva, G. R., Andrade, R. G. & Soares, F. A. GLUT1 expression in malignant tumors and its use as an immunodiagnostic marker. *Clinics*. **66**, 965-972 (2011).

3. Godoy, A., Ulloa, V., Rodriguez, F., Reinicke, K., YaÑez, A. J., GarcÍa, M. A., Medina, R. A., Carrasco, M., Barberis, S., Castro, T., MartÍnez, F., Koch, X., Vera, J. C., Poblete. M. T., Figueroa, C.D., Peruzzo, B., PÉrez, F., Nualart, F. Differential subcellular distribution of glucose transporters GLUT1-6 and GLUT9 in human cancer: Ultrastructural localization of GLUT1 and GLUT5 in breast tumor cells. *J. Cell. Physiol.* **207**, 614-627 (2006).

4. Tanasova, M., Plutschack, M., Muroski, M. E., Sturla, S. J., Struouse, G. F. & McQuade, D. T. Fluorescent THF-based fructose analogue exhibits fructose-dependent uptake. *ChemBioChem*. **14**, 1263-1270 (2013).

5. Wuest, M., Trayner, B. J., Grant, T. N., Jans, H. S., Mercer, J. R., Murray, D., West, F. G., McEwan, A. J. B., Wuest, F. & Cheeseman, C. I. Radiopharmacological

evaluation of 6-deoxy-6-[^{18}F]fluoro-D-fructose as a tracer for PET imaging of breast cancer. *Nucl. Med. Biol.* **38**, 461-475 (2011); Soueidan, O. M., Trayner, B. J., Grant, T. N., Henderson, J. R., Wuest, F., West, F. G. & Cheeseman, C. I. New fluorinated fructose analogs as selective probes of hexose transport protein GLUT5. *Org. Biomol. Chem.* **13**, 6511-6521 (2015).

6. Zamora-Leon, S. P., Golde, D. W., Concha, I. I., Rivas, C. I., Delgado-López, F. & Vera, J. C. Expression of the fructose transporter GLUT5 in human breast cancer. *Proc. Natl. Acad. Sci. USA*. **93**, 1847-1852 (1996).
7. Gowrishankar, G., Zitzmann-Kolbe, S., Junutula, A., Reeves, R., Levi, J., Srinivasan, A., Bruus-Jensen, K., Cry, J., Dinkelborg, L. & Gambhir, S. S. GLUT 5 is not over-expressed in breast cancer cells and patient breast cancer tissues. *PLoS One* **6,** e26902-e26902 (2011).
8. Loaiza, A., Porras, O. H. & Barros, L. F. Glutamate triggers rapid glucose transport stimulation in astrocytes as evidenced by real-time confocal microscopy. *J. Neurosci.* **23,** 7337–42 (2003).
9. Visualizing sweetness: increasingly diverse applications for fluorescent-tagged glucose bioprobes and their recent structural modifications. *Sensors (Basel).* **12,** 5005–27 (2012).
10. TeSlaa, T. & Teitell, M. A. Techniques to monitor glycolysis. *Methods Enzymol.* **542,** 91-114 (2014).
11. Yoshioka, K., Takashashi, H., Homma, T., Saito, M., Oh, K. B., Nemomoto, Y. & Matsuoka, H. A novel fluorescent derivative of glucose applicable to the assessment of glucose uptake activity of Escherichia coli. *Biochim. Biophys. Acta* **1289,** 5–9

(1996); Cheng, Z., Levi, J., Xiong, Z., Gheysens, O., Keren, S., Chen, X. & Gambhir, S. S. Near-Infrared fluorescent deoxyglucose analog for tumor optical imaging in cell culture and in living mice. *Bioconjugate Chem.* **17**, 662-669 (2006).

12. Soueidan, O. M., Scully, T. W., Kaur, J., Panigrahi, R. Belovodskiy, A. Do, V., Matier, C., Lemieux, J., Wuest, F., Cheeseman, C. I. & F. G. West. Fluorescent Hexose Derivatives Demonstrate Stringent Stereochemical Requirement for Recognition and Transport by GLUT1 and GLUT5. *Manuscript in preparation*.

13. Levi, J. Cheng, Z., Gheysens, O., Patel, M., Chan, C. T., Wang, Y., Namavari, M. & Gambhir, S. S. Fluorescent fructose derivatives for imaging breast cancer cells. *Bioconjug. Chem.* **18,** 628–34

14. Ghosh, P. B. & Whitehouse, M. W. 7-chloro-4-nitrobenzo-2-oxa-1,3-diazole: a new fluorigenic reagent for amino acids and other amines. *Biochem. J.* **108,** 155–6 (1968).

15. Toyo'oka, T., Watanabe, Y. & Imai, K. Reaction of amines of biological importance with 4-fluoro-7-nitrobenzo-2-oxa-1,3-diazole. *Anal. Chim. Acta* **149,** 305–312 (1983).

16. del Rosso, M. D., di Nunno, L., Florio, S. & Amorese, A. Reactivity of 7-halogeno-4-nitrobenzofurazans towards thiophenols. A kinetic investigation. *J. Chem. Soc. Perkin Trans. 2* 239 (1980).

17. Instrumentation for fluorescence spectroscopy. In *Principles of Fluorescence Spectroscopy*. Edn. 3. (eds. Lakowicz, J. R.) 27-61 (Springer Science+Business Media, LLC, 233 Spring Street, New York, NY 10013, USA, 2006).

18. Jung, C. Y. & Rampal, A. L. Cytochalasin B binding sites and glucose transport carrier in human erythrocyte ghosts. *J. Biol. Chem.* **252,** 5456–63 (1977).

19. Song, J. *et al.* Flavonoid inhibition of sodium-dependent vitamin C transporter 1 (SVCT1) and glucose transporter isoform 2 (GLUT2), intestinal transporters for vitamin C and Glucose. *J. Biol. Chem.* **277,** 15252–60 (2002); Kwon, O. *et al.* Inhibition of the intestinal glucose transporter GLUT2 by flavonoids. *FASEB J.* **21,** 366–77 (2007) and cited references.

20. Manolescu, A. R., Witkowska, K., Kinnaird, A., Cessford, T. & Cheeseman C. Facilitated hexose transporters: New perspectives on form and function. *Physiology* **22**, 234-240 (2007).

21. Ravshel, F. M. & Cleland, W. W. The substrate and anomeric specificity of fructokinase. *J. Biol. Chem.* **248**, 8174-8177 (1973); Hanson, R. L., Ho, R. S., Wiseberg, J. J., Simpson, R., Younathan, E. S. & Blair, J. B. Inhibition of gluconeogenesis and glycogenolysis by 2,5-anhydro-D-mannitol. *J. Biol. Chem.* **259**, 218-223 (1984).

Chapter 5

1. Ntziachristos, V. Going deeper than microscopy: the optical imaging frontier in biology. *Nat. Methods* **7,** 603–14 (2010).
2. Taruttis, A. & Ntziachristos, V. Translational optical imaging. *AJR. Am. J. Roentgenol.* **199,** 263–71 (2012).
3. Luker, G. D. & Luker, K. E. Optical imaging: current applications and future directions. *J. Nucl. Med.* **49,** 1–4 (2008).
4. Fass, L. Imaging and cancer: A review. *Mol. Oncol.* **2,** 115–152 (2008).

5. Xu, X. Development and applications of optical imaging techniques in cancer diagnosis: Diffuse optical tomography and microendoscopy. *Curr. Med. Imaging Rev.* **4,** 125-133 (2016).
6. Hadjipanayis, C. G., Jiang, H., Roberts, D. W. & Yang, L. Current and future clinical applications for optical imaging of cancer: from intraoperative surgical guidance to cancer screening. *Semin. Oncol.* **38,** 109–18 (2011).
7. Penet, M.-F. Mikhaylova, M., Li, C., Krishnamachary, B., Glunde, K., Pathak, A. P. & Bhujwalla, Z. M. Applications of molecular MRI and optical imaging in cancer. *Future Med. Chem.* **2,** 975–88 (2010).
8. Smith, A. M., Mancini, M. C. & Nie, S. Bioimaging: second window for in vivo imaging. *Nat. Nanotechnol.* **4,** 710–1 (2009).
9. Cowles, E. A., Kovar, J. L., Curtis, E. T., Xu, H. & Othman, S. F. Near-infrared optical imaging for monitoring the regeneration of osteogenic tissue-engineered constructs. *Biores.* **2,** 186–91 (2013).
10. Cheng, Z. Levi, J., Xiong, Z., Gheysens, O., Keren, S., Chen, X. & Gambhir S. S. Near-infrared fluorescent deoxyglucose analogue for tumor optical imaging in cell culture and living mice. *Bioconjug. Chem.* **17,** 662–9 (2006).
11. Park, J., Lee, H. Y., Cho, M-H. & Park, S. B. Development of a Cy3-labeled glucose bioprobe and its application in bioimaging and screening for anticancer agents. *Angew. Chem. Int.* **46**, 2018-2022 (2007).
12. Kovar, J. L., Volcheck, W., Sevick-Muraca, E., Simpson, M. A. & Olive, D. M. Characterization and performance of a near-infrared 2-deoxyglucose optical imaging agent for mouse cancer models. *Anal. Biochem.* **384,** 254–62 (2009).

13. Guo, J. Du, C., Shan, L., Zhu, H., Xue, B., Qianz, Z., Achilefu, S. & Gu. Y. Comparison of near-infrared fluorescent deoxyglucose probes with different dyes for tumor diagnosis in vivo. *Contrast Media Mol. Imaging* **7,** 289–301 (2012).

14. For synthesis of IR-780 iodide: Samanta, A., Vendrell, M., Das, R. & Chang, Y.-T. Development of photostable near-infrared cyanine dyes. *Chem. Commun. (Camb).* **46,** 7406–8 (2010); For IR-780 dye applications in PDT: Jiang, C., Cheng, H., Yuan, A., Tang, X., Wu, J. & Hu, Y. Hydrophobic IR780 encapsulated in biodegradable human serum albumin nanoparticles for photothermal and photodynamic therapy. *Acta Biomater.* **14,** 61–9 (2015); Levy, J. G. Photosensitizers in photodynamic therapy. *Semin. Oncol.* **21,** 4–10 (1994); Yuan, A., Wu, J., Tang, X., Zhao, L. Xu. F. & Hu, Y. Application of near-infrared dyes for tumor imaging, photothermal, and photodynamic therapies. *J. Pharm. Sci.* **102,** 6–28 (2013).

15. Yu, K., Zhao, X., Wu, W. & Hong, Z. An efficient procedure for synthesis of fructose derivatives. *Tetrahedron Lett.* **54,** 2788–2790 (2013); Soueidan, O. M., Scully, T. W., Kaur, J., Panigrahi, R. Belovodskiy, A. Do, V., Matier, C., Lemieux, J., Wuest, F., Cheeseman, C. I. & F. G. West. Fluorescent hexose derivatives demonstrate stringent stereochemical requirement for recognition and transport by GLUT1 and GLUT5. *Manuscript in preparation*.

16. Sun, J. Dong, Y., Cao, L., Wang, X., Wang, S. & Hu, Y. Highly efficient chemoselective deprotection of O,O-acetals and O,O-ketals catalyzed by molecular iodine in acetone. *J. Org. Chem.* **69,** 8932–4 (2004).

17. García-Moreno, M. I., Aguilar, M., Ortiz Mellet, C. & García Fernández, J. M. Intramolecular benzyl protection delivery: a practical synthesis of DMDP and DGDP from D-fructose. *Org. Lett.* **8,** 297–9 (2006).
18. Hanaya, T., Sato, N. & Yamamoto, H. An efficient synthesis of methyl 1,3-O-isopropylidene-alpha-D-fructofuranoside and 2,3:5,6-di-O-isopropylidene-D-glucose dimethyl acetal derivatives from sucrose. *Carbohydr. Res.* **340,** 2494–501 (2005).
19. Chouhan, G. & James, K. Efficient Construction of proline-containing β-turn mimetic cyclic tetrapeptides via CuAAC macrocyclization. *Org. Lett.* **15**, 1206-1209 (2013).

Appendix I: Selected NMR spectra (Chapter 2)

399.795 MHz H1 1D in d2o (ref. to external acetone @ 2.225 ppm), temp 26.5 C -> actual temp = 27.0 C, autoxdb probe

date: Nov 4 2013 sweep width: 4802Hz acq.time: 3.0s relax.time: 2.0s # scans: 16 dig.res.: 0.1 Hz/pt hz/mm:20.0
spectrometer:d300 file:/mnt/d600/home13/westnmr/nmrdata/Venkata/venkata-dt-pb/2013.11.04.i4_3-FDAM-protom_H1_presat

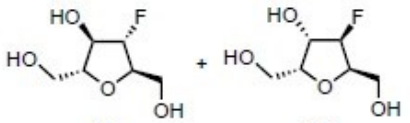

(96:4)

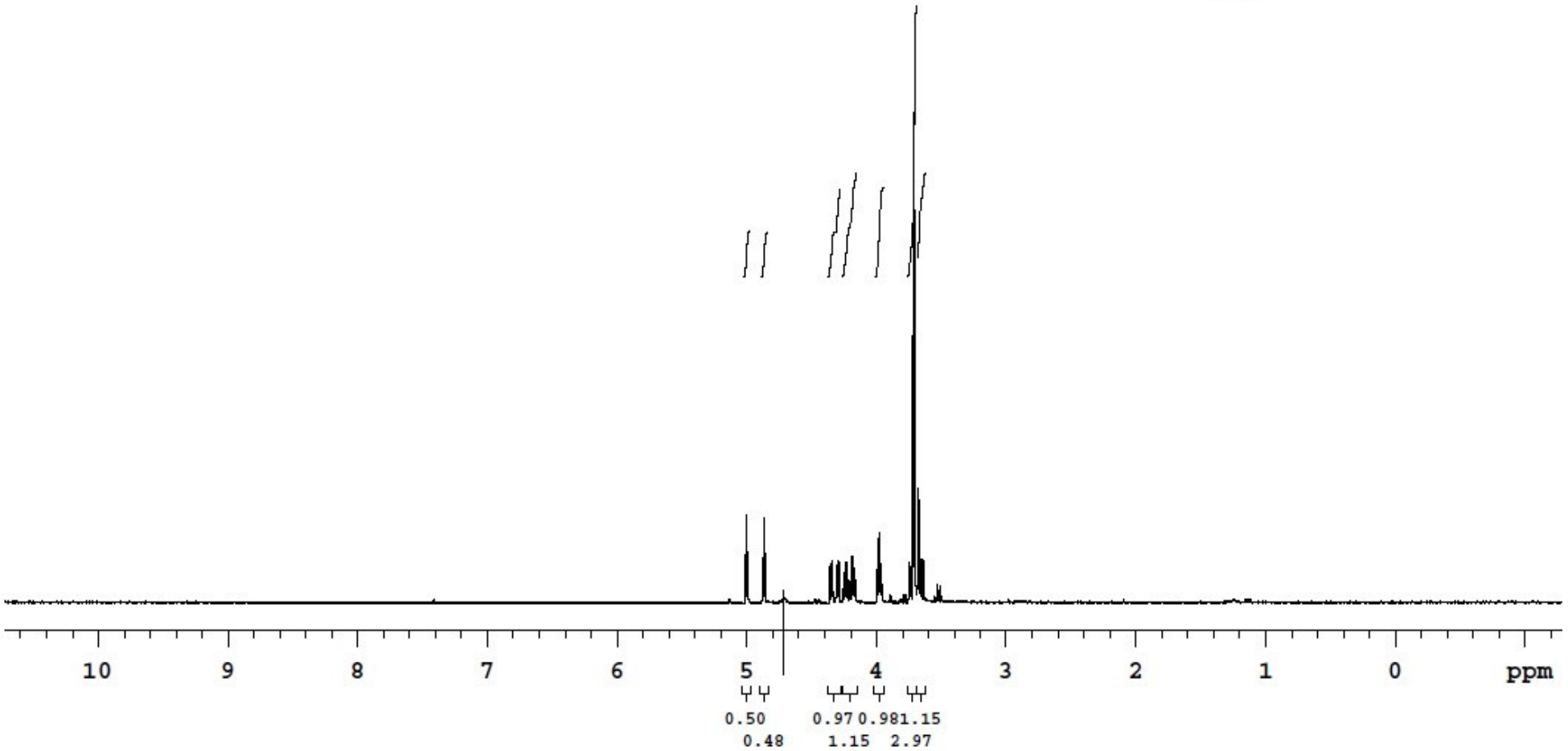

Pulse Sequence: presat

100.587 MHz C13[H1] 1D in d2o (ref. to external acetone @ 31.07 ppm), temp 25.9 C -> actual temp = 27.0 C, onenmr probe

date: Nov 4 2013 sweep width: 27174Hz acq.time: 2.5s relax.time: 0.1s # scans: 168 dig.res.: 0.2 Hz/pt hz/mm:113.2
spectrometer:d300 file:/mnt/d600/home13/westnmr/nmrdata/Venkata/venkata-dt-pb/2013.11.04.mr4_3FDAM-c13-f19coupled_C13_1D

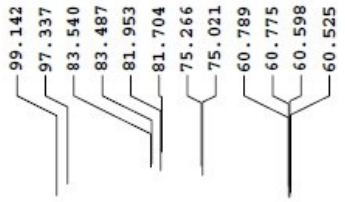

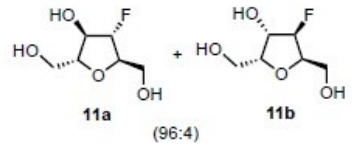

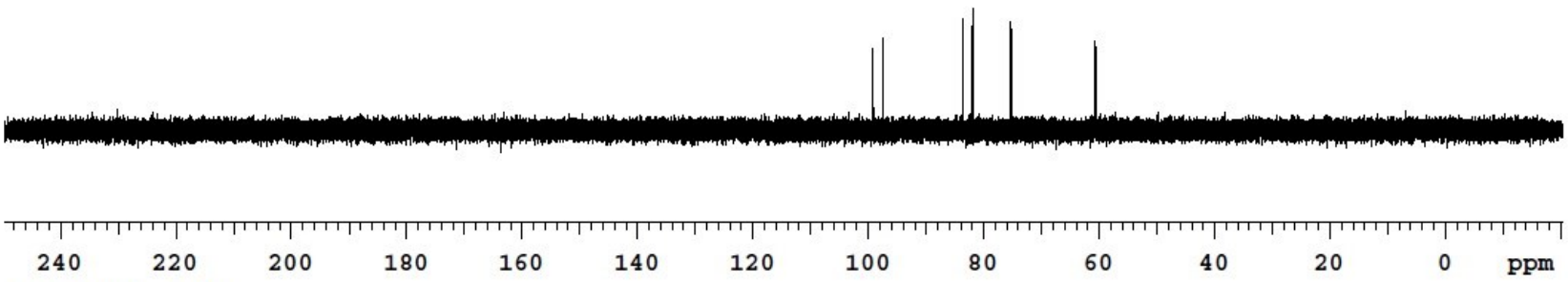

Pulse Sequence: s2pul

venkata, mes-AM
100.690 MHz C13[H1] 1D in d2o (ref. to external acetone @ 31.07 ppm), temp 27.0 C -> actual temp = 27.0 C, m400gz probe

date: Jan 5 2014 sweep width: 25189Hz acq.time: 2.5s relax.time: 1.1s # scans: 4348 dig.res.: 0.2 Hz/pt hz/mm:83.3
spectrometer:d300 file:/mnt/d600/home13/westnmr/nmrdata/DATA_FROM_NMRSERVICE/venkata/2014.01/2014.01.5.m4_mes-AM_20.33_C13_1D

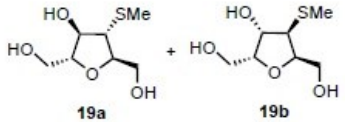

(90:10)

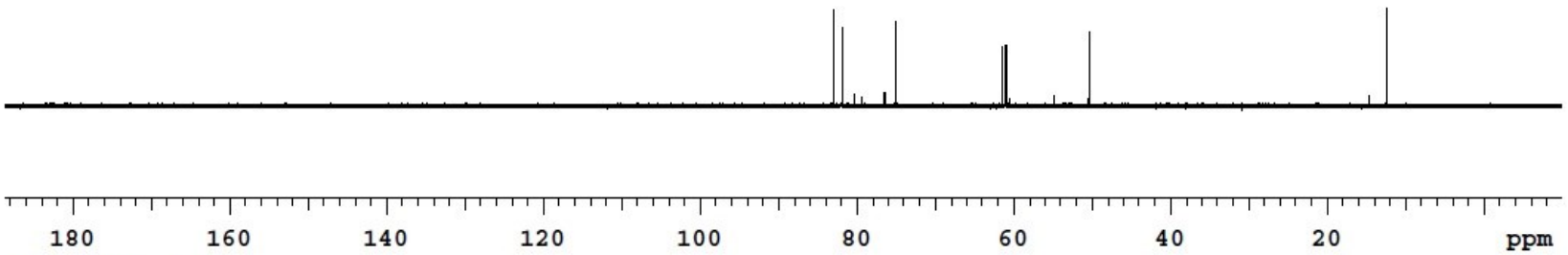

Pulse Sequence: s2pul

Department of Chemistry, University of Alberta

Agilent Technologies

Recorded on: **m400, Jan 5 2014**	Sweep Width(Hz): **4807.69**	Acquisiton Time(s): **3**	Relaxation Delay(s): **0.1**
Pulse Sequence: **PRESAT**	Digital Res.(Hz/pt): **0.29**	Hz per mm(Hz/mm): **20.03**	Completed Scans **212**

venkata, mes-AM

400.393 MHz H1 PRESAT in d2o (ref. to external acetone @ 2.225 ppm), temp 27.0 C -> actual temp = 27.0 C, m400gz probe

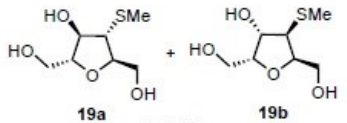

19a (90:10) **19b**

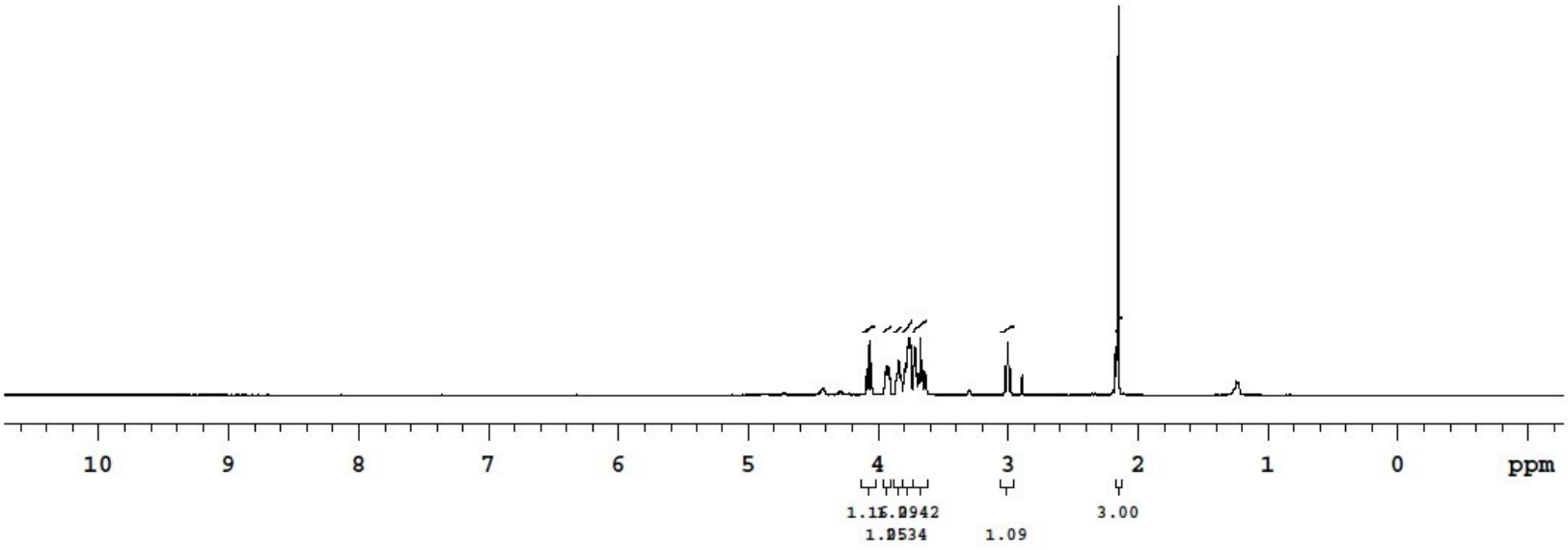

File: /mnt/d600/home13/westnmr/nmrdata/DATA_FROM_NMRSERVICE/venkata/2014.01/2014.01.5.m4_mes-AM_20.04_H1_1D

125.690 MHz C13[H1] 1D in d2o (ref. to external acetone @ 31.07 ppm), temp 27.7 C -> actual temp = 27.0 C, colddual probe

date: Mar 2 2012 sweep width: 33784Hz acq.time: 2.5s relax.time: 0.1s # scans: 8 dig.res.: 0.3 Hz/pt hz/mm:140.8
spectrometer:d300 file:/mnt/d600/home13/westnmr/nmrdata/Venkata/venkata-dt-pb/N3-man-c13-pure

82.294
80.454
75.061
66.377
61.084
60.789

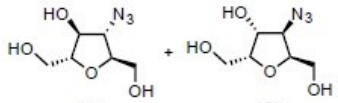

16a (95:5) 16b

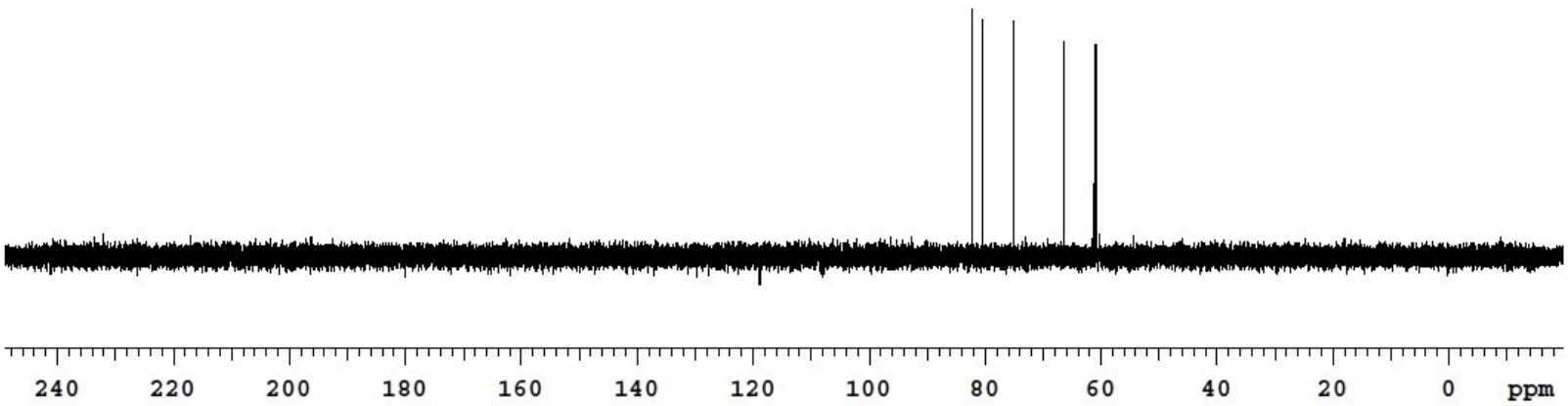

Pulse Sequence: s2pul

498.123 MHz H1 1D in d2o (ref. to external acetone @ 2.225 ppm), temp 27.2 C -> actual temp = 27.0 C, autoxdb probe

date: Jan 9 2012 sweep width: 6001Hz acq.time: 3.0s relax.time: 2.0s # scans: 16 dig.res.: 0.1 Hz/pt hz/mm:25.0
spectrometer:d300 file:/mnt/d600/home13/westnmr/nmrdata/Venkata/venkata-dt-pb/n3-oh-man

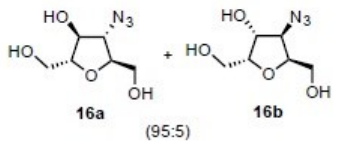

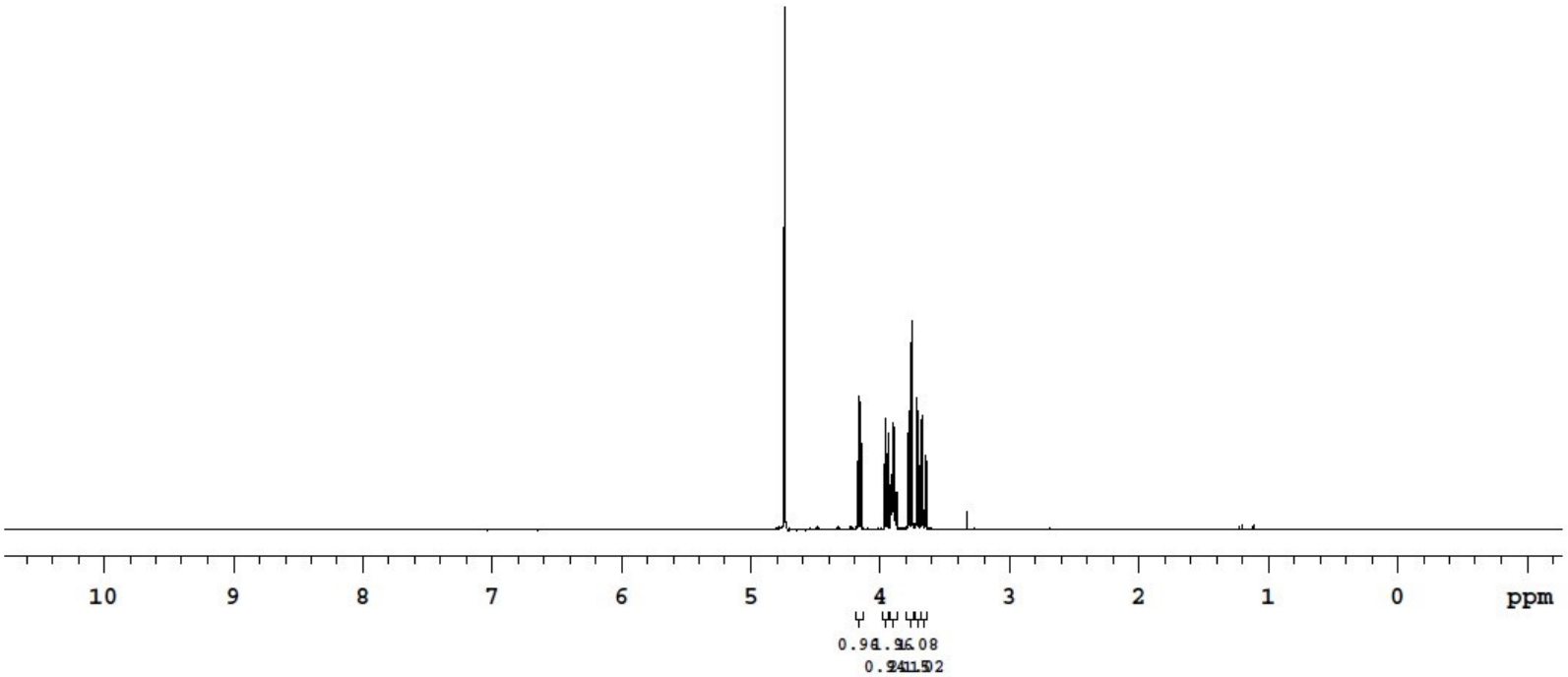

Pulse Sequence: s2pul

499.816 MHz H1 1D in d2o (ref. to external acetone @ 2.225 ppm), temp 27.7 C -> actual temp = 27.0 C, colddual probe

date: Mar 1 2012 sweep width: 6010Hz acq.time: 5.0s relax.time: 2.0s # scans: 16 dig.res.: 0.1 Hz/pt hz/mm:25.0
spectrometer:d300 file:/mnt/d600/home13/westnmr/nmrdata/Venkata/venkata-dt-pb/Iodo-man-proton1

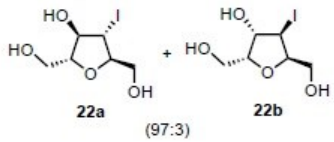

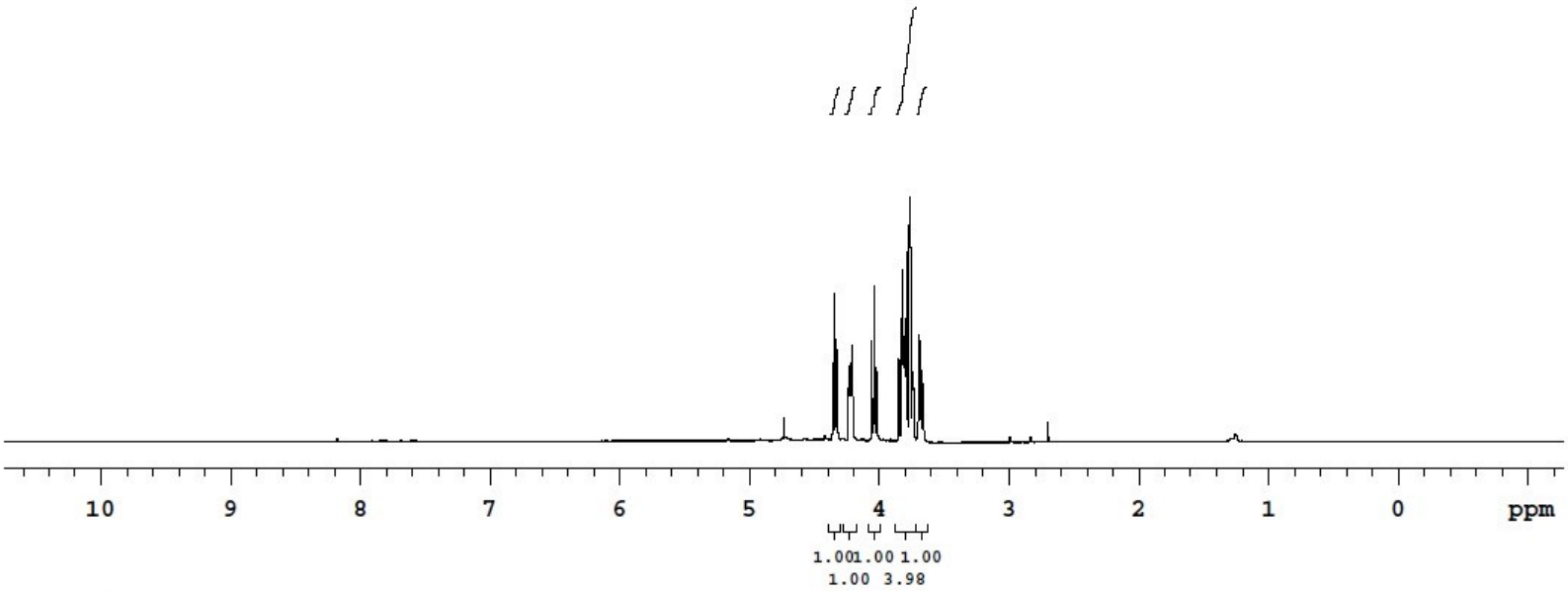

Pulse Sequence: presat

125.690 MHz C13[H1] 1D in d2o (ref. to external acetone @ 31.07 ppm), temp 27.7 C -> actual temp = 27.0 C, colddual probe

date: Mar 1 2012 sweep width: 33784Hz acq.time: 2.5s relax.time: 0.1s # scans: 44 dig.res.: 0.3 Hz/pt hz/mm:140.8
spectrometer:d300 file:/mnt/d600/home13/westnmr/nmrdata/Venkata/venkata-dt-pb/Iodo-man-c13-publish

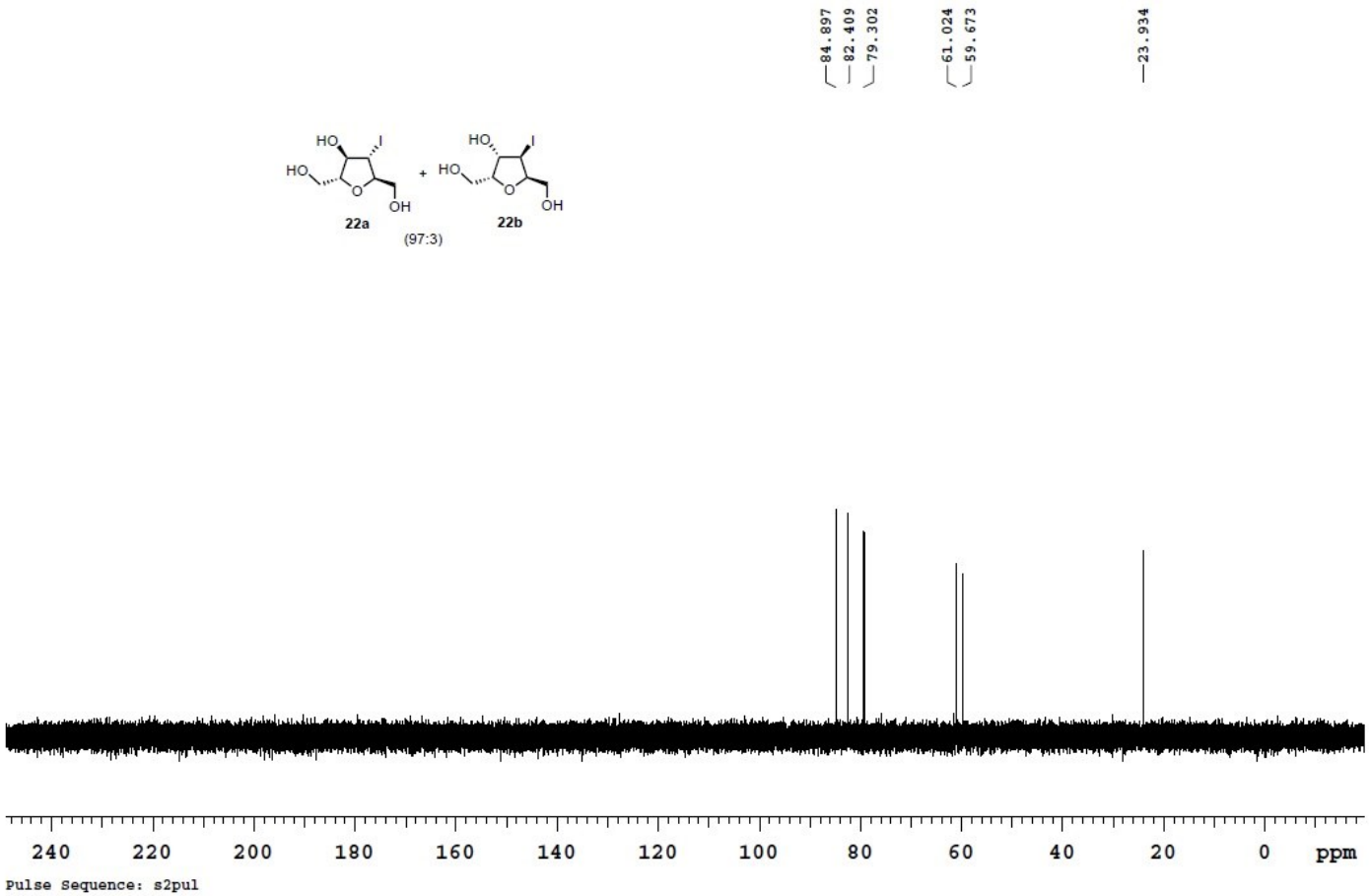

498.123 MHz H1 1D in d2o (ref. to external acetone @ 2.225 ppm), temp 27.2 C -> actual temp = 27.0 C, autoxdb probe

date: Feb 14 2012 sweep width: 6001Hz acq.time: 3.0s relax.time: 5.0s # scans: 32 dig.res.: 0.1 Hz/pt hz/mm:25.0
spectrometer:d300 file:/mnt/d600/home13/westnmr/nmrdata/Venkata/venkata-dt-pb/Br-man-proton

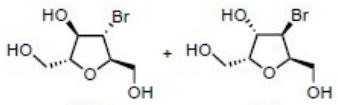

21a (97:3) **21b**

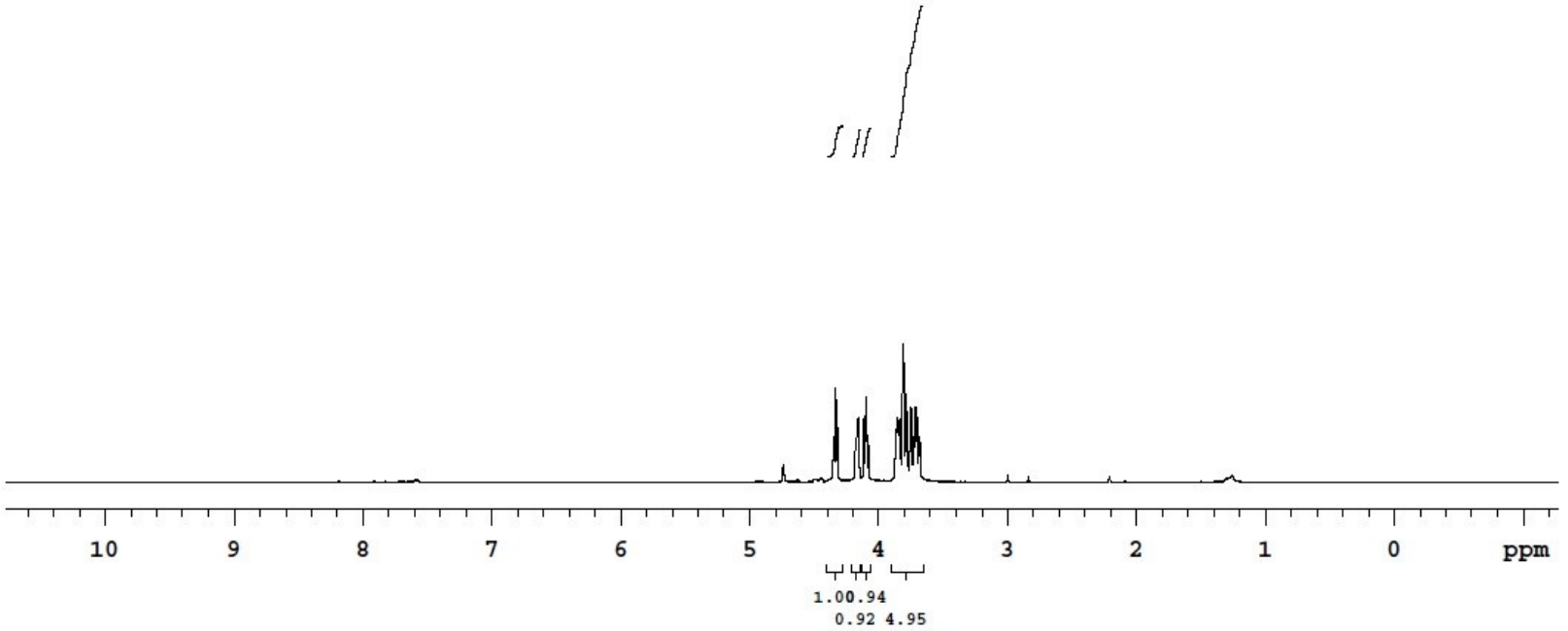

Pulse Sequence: s2pul

125.264 MHz C13[H1] 1D in d2o (ref. to external acetone @ 31.07 ppm), temp 27.2 C -> actual temp = 27.0 C, autoxdb probe

date: Feb 14 2012 sweep width: 33827Hz acq.time: 2.5s relax.time: 0.1s # scans: 316 dig.res.: 0.3 Hz/pt hz/mm:140.9
spectrometer:d300 file:/mnt/d600/home13/westnmr/nmrdata/Venkata/venkata-dt-pb/2012.02.14.15_Br-man-c13-publishable_C13_1D

84.285
83.119
78.547
61.851
60.695
49.910

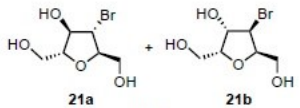

21a (97:3) **21b**

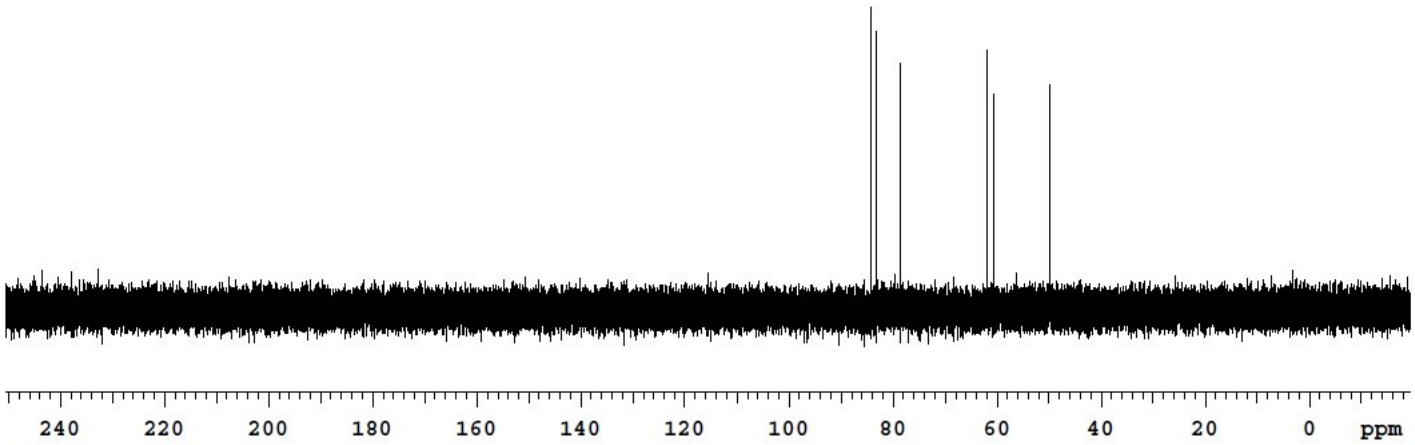

Pulse Sequence: s2pul

399.985 MHz H1 1D in d2o (ref. to external acetone @ 2.225 ppm), temp 25.9 C -> actual temp = 27.0 C, onenmr probe

date: Mar 31 2014 sweep width: 4808Hz acq.time: 3.0s relax.time: 2.0s # scans: 16 dig.res.: 0.1 Hz/pt hz/mm:20.0
spectrometer:d300 file:/mnt/d600/home13/westnmr/nmrdata/Venkata/2014.03.31.mr4_CH3-amide-AM-pure-proton_H1_presat

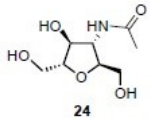

24

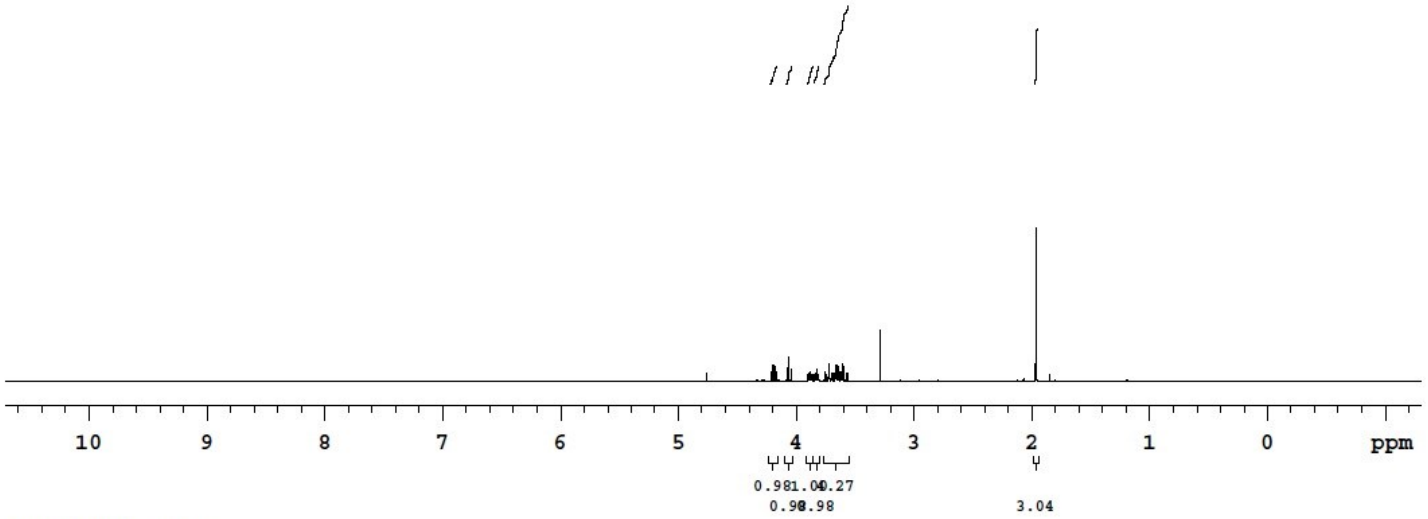

Pulse Sequence: presat

100.587 MHz C13[H1] 1D in d2o (ref. to external acetone @ 31.07 ppm), temp 25.9 C -> actual temp = 27.0 C, onenmr probe

date: Mar 31 2014 sweep width: 27174Hz acq.time: 2.5s relax.time: 0.1s # scans: 72 dig.res.: 0.2 Hz/pt hz/mm:113.2
spectrometer:d300 file:/mnt/d600/home13/westnmr/nmrdata/Venkata/2014.03.31.mr4_CH3-amide-AM-pure-C13_C13_1D

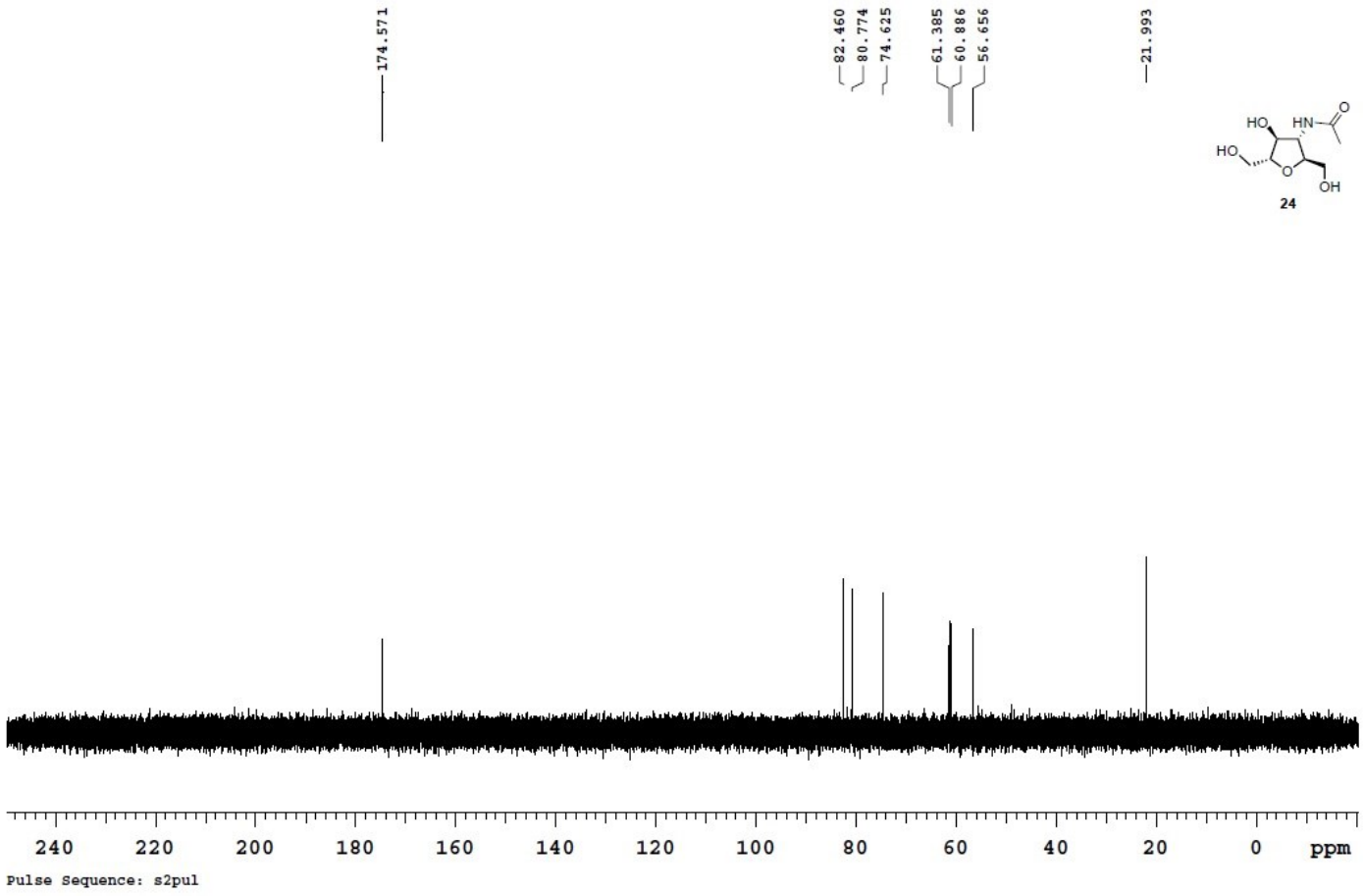

Pulse Sequence: s2pul

Appendix II: Selected NMR spectra (Chapter 3)

498.119 MHz H1 1D in d2o (ref. to external acetone @ 2.225 ppm), temp 26.4 C -> actual temp = 27.0 C, autoxdb probe

date: Jan 21 2014 sweep width: 6001Hz acq.time: 3.0s relax.time: 5.0s # scans: 36 dig.res.: 0.1 Hz/pt hz/mm:25.0
spectrometer:d300 file:/mnt/d600/home13/westnmr/nmrdata/Venkata/2014.01.21.15_CF3-NH-Amide-AM_H1_presat

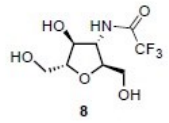

8

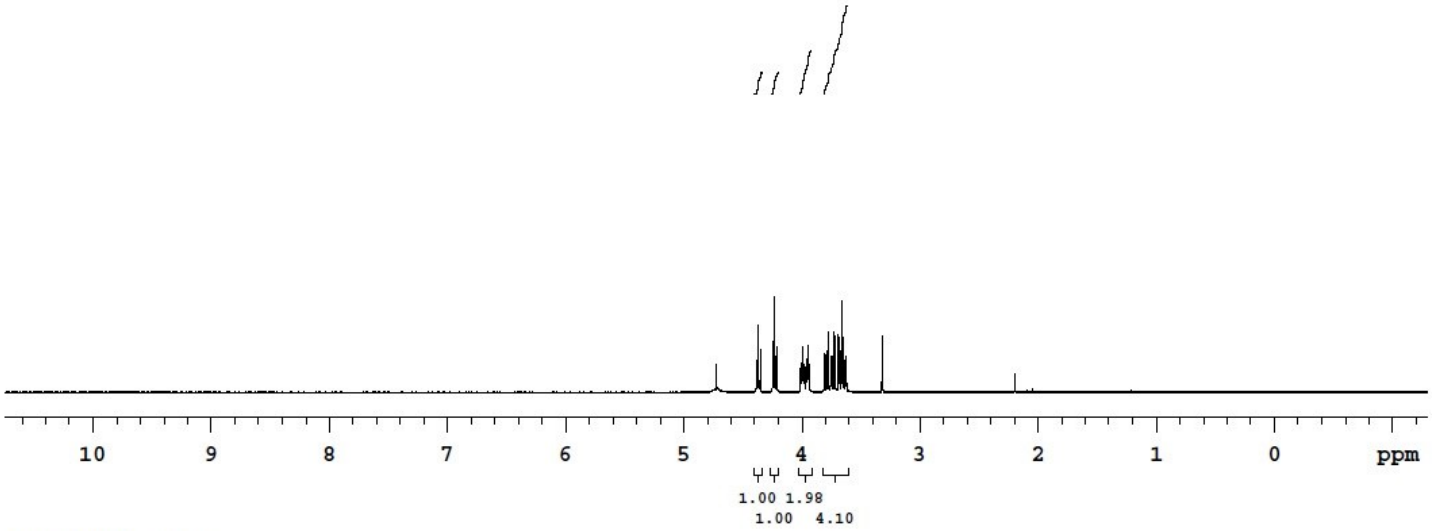

Pulse Sequence: presat

venkata, cf3-c13
125.691 MHz C13[H1] 1D in d2o (ref. to external acetone @ 31.07 ppm), temp 27.7 C -> actual temp = 27.0 C, colddual probe

date: Feb 7 2014 sweep width: 32895Hz acq.time: 2.5s relax.time: 0.2s # scans: 2188 dig.res.: 0.3 Hz/pt hz/mm:137.1
spectrometer:d300 file:/mnt/d600/home13/westnmr/nmrdata/DATA_FROM_NMRSERVICE/venkata/2014.02/2014.02.7.u5_cf3-c13_03.02_C13_1D

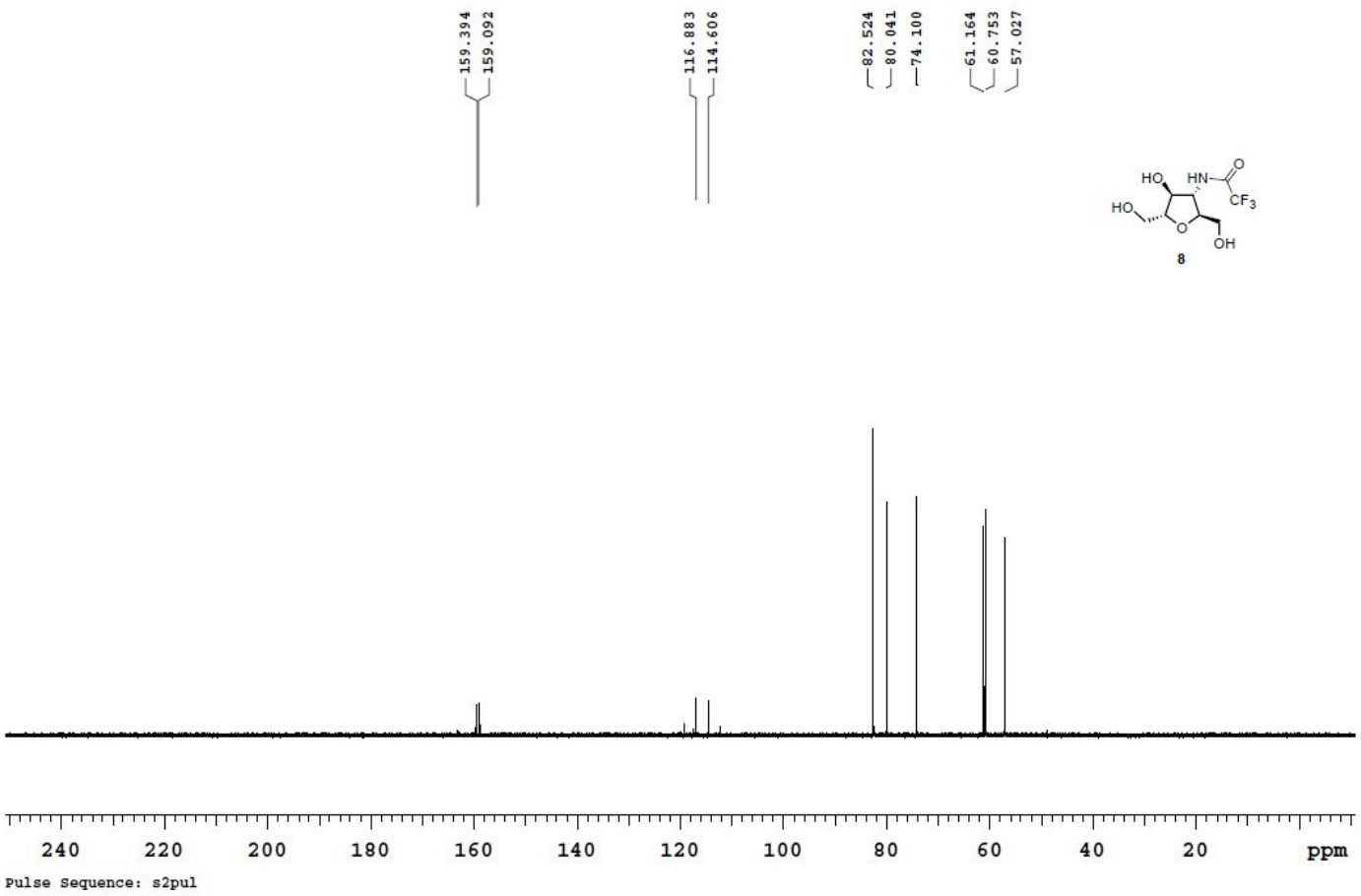

Pulse Sequence: s2pul

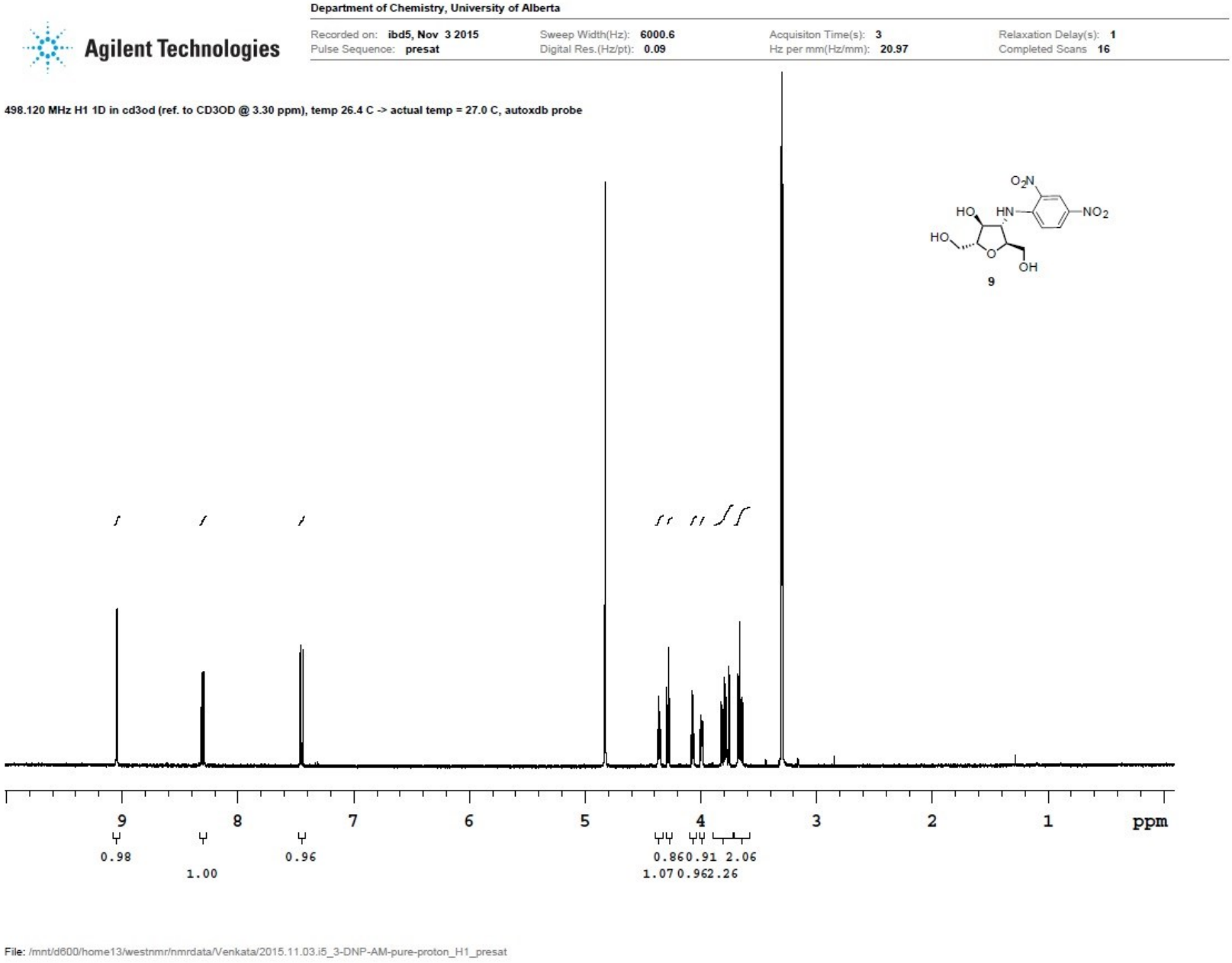
Department of Chemistry, University of Alberta
Agilent Technologies
Recorded on: ibd5, Nov 3 2015
Pulse Sequence: presat
Sweep Width(Hz): 6000.6
Digital Res.(Hz/pt): 0.09
Acquisiton Time(s): 3
Hz per mm(Hz/mm): 20.97
Relaxation Delay(s): 1
Completed Scans 16
498.120 MHz H1 1D in cd3od (ref. to CD3OD @ 3.30 ppm), temp 26.4 C -> actual temp = 27.0 C, autoxdb probe
O2N
HO
HN
NO2
HO
O
OH
9
9
8
7
6
5
4
3
2
1
ppm
0.98
1.00
0.96
0.86
0.91
2.06
1.07
0.96
2.26
File: /mnt/d600/home13/westnmr/nmrdata/Venkata/2015.11.03.i5_3-DNP-AM-pure-proton_H1_presat

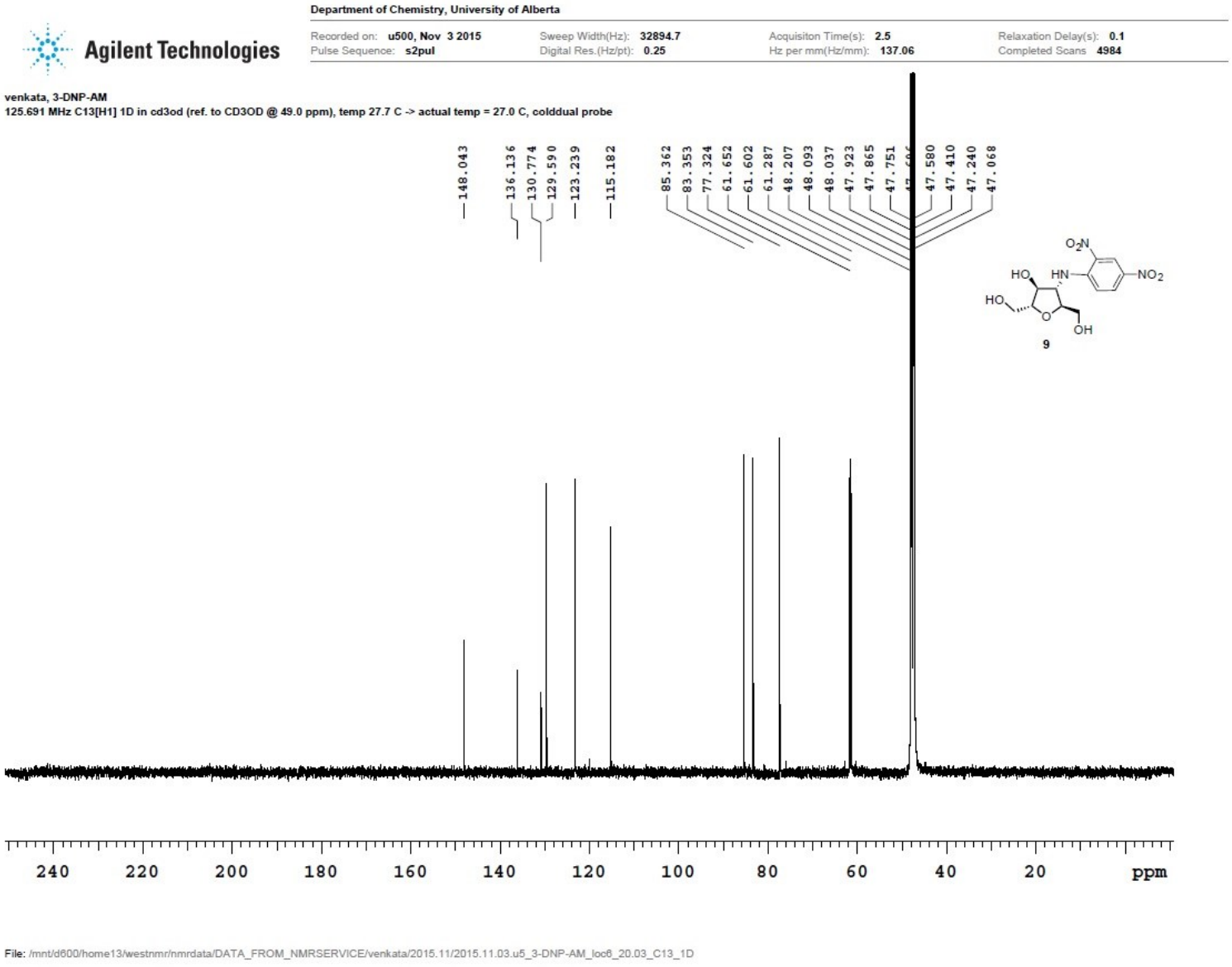
Department of Chemistry, University of Alberta
Agilent Technologies
Recorded on: u500, Nov 3 2015
Pulse Sequence: s2pul
Sweep Width(Hz): 32894.7
Digital Res.(Hz/pt): 0.25
Acquisiton Time(s): 2.5
Hz per mm(Hz/mm): 137.06
Relaxation Delay(s): 0.1
Completed Scans 4984
venkata, 3-DNP-AM
125.691 MHz C13[H1] 1D in cd3od (ref. to CD3OD @ 49.0 ppm), temp 27.7 C -> actual temp = 27.0 C, colddual probe
148.043
136.136
130.774
129.590
123.239
115.182
85.362
83.353
77.324
61.652
61.602
61.287
48.207
48.093
48.037
47.923
47.865
47.751
47.580
47.410
47.240
47.068
HO
HN
O2N
NO2
HO
O
OH
9
240
220
200
180
160
140
120
100
80
60
40
20
ppm
File: /mnt/d600/home13/westnmr/nmrdata/DATA_FROM_NMRSERVICE/venkata/2015.11/2015.11.03.u5_3-DNP-AM_loc6_20.03_C13_1D

Appendix III: Selected NMR spectra (Chapter 4)

Agilent Technologies

Department of Chemistry, University of Alberta

Recorded on:	Apr 30 2014	Sweep Width(Hz):	6000.6	Acquisiton Time(s):	3	Relaxation Delay(s):	2
Pulse Sequence:	presat	Digital Res.(Hz/pt):	0.09	Hz per mm(Hz/mm):	25	Completed Scans	56

498.120 MHz H1 1D in cd3od (ref. to CD3OD @ 3.30 ppm), temp 26.4 C -> actual temp = 27.0 C, autoxdb probe

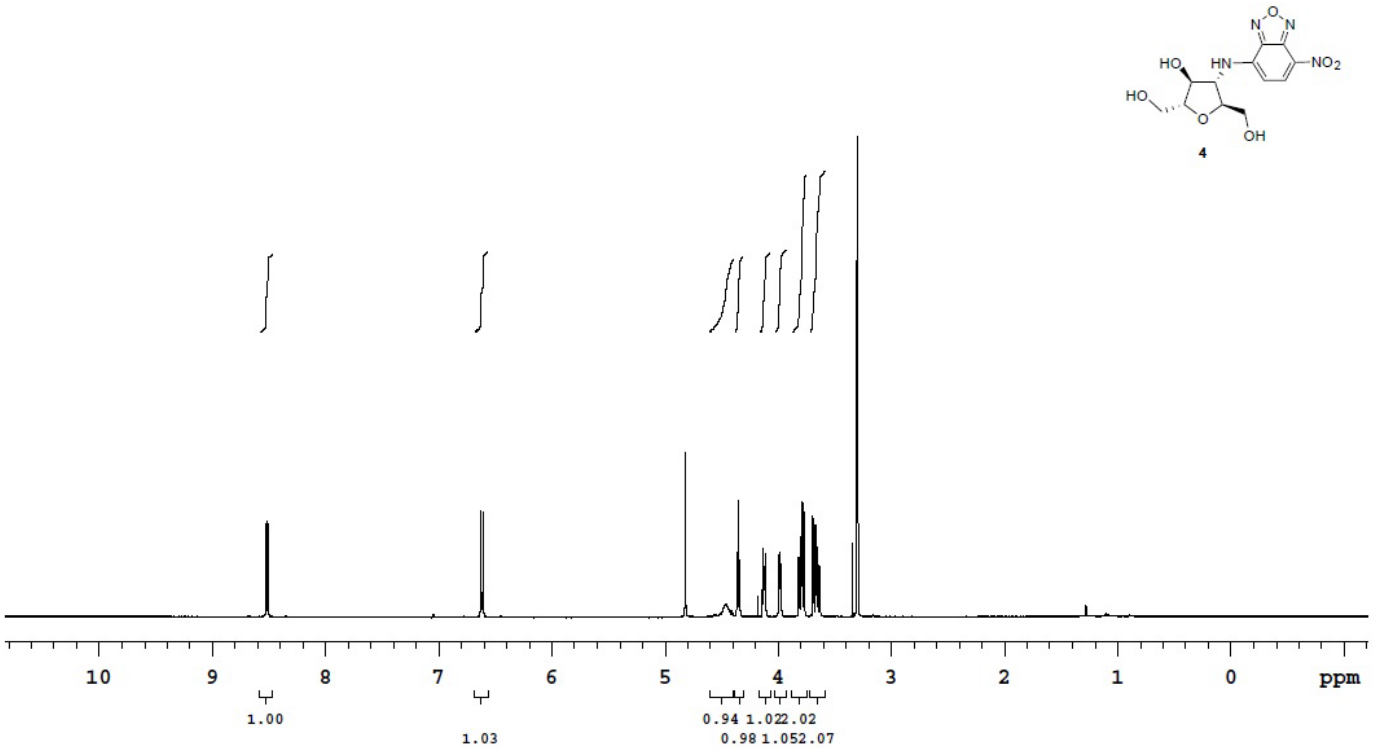

File: /mnt/d600/home13/westnmr/nmrdata/Venkata/2014.04.30.i5_3-NH-NBD-AM-PURE_H1_presat

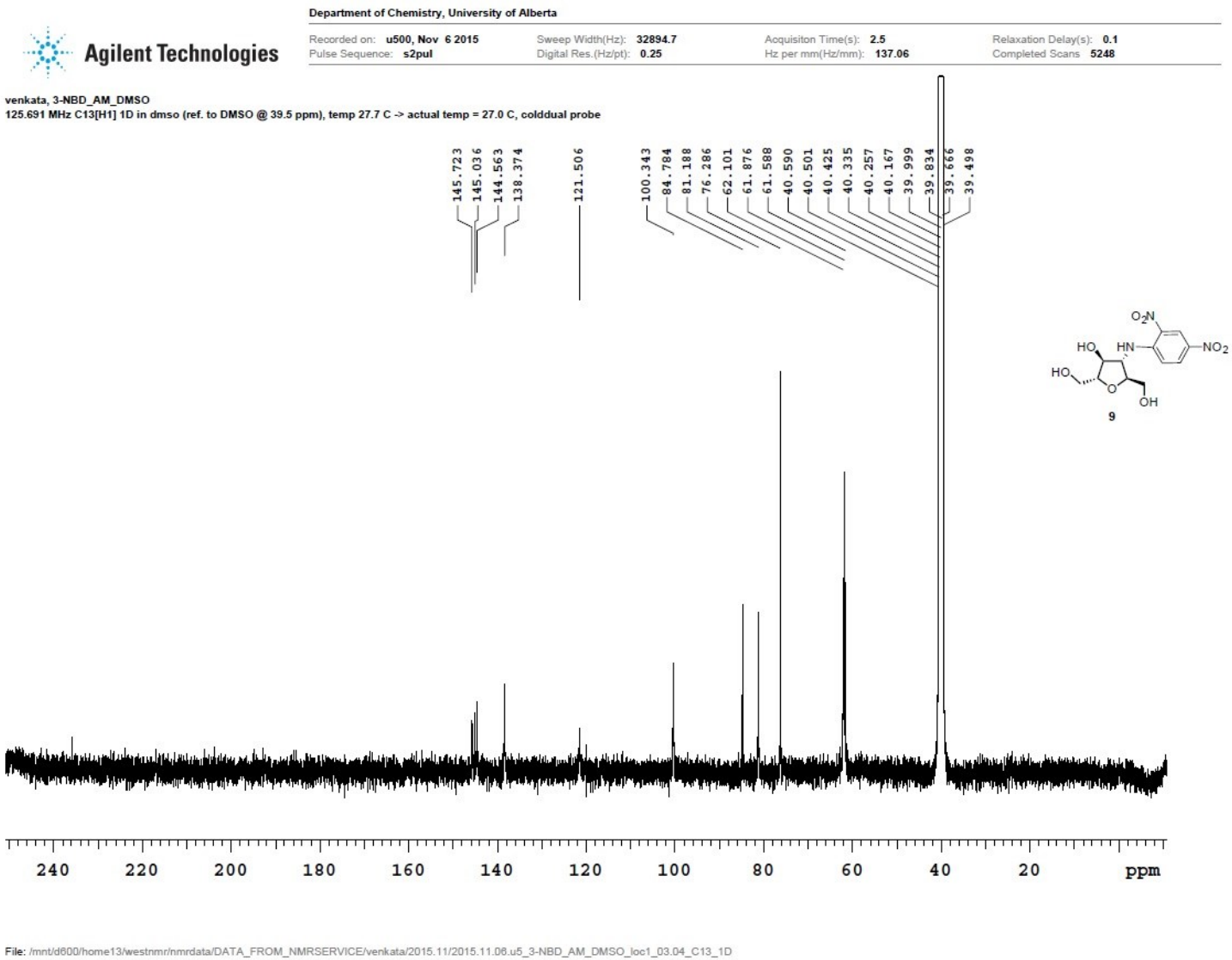
Department of Chemistry, University of Alberta
Agilent Technologies
Recorded on: u500, Nov 6 2015
Pulse Sequence: s2pul
Sweep Width(Hz): 32894.7
Digital Res.(Hz/pt): 0.25
Acquisiton Time(s): 2.5
Hz per mm(Hz/mm): 137.06
Relaxation Delay(s): 0.1
Completed Scans 5248
venkata, 3-NBD_AM_DMSO
125.691 MHz C13[H1] 1D in dmso (ref. to DMSO @ 39.5 ppm), temp 27.7 C -> actual temp = 27.0 C, colddual probe
145.723
145.036
144.563
138.374
121.506
100.343
84.784
81.188
76.286
62.101
61.876
61.588
40.590
40.501
40.425
40.335
40.257
40.167
39.999
39.834
39.666
39.498
9
240
220
200
180
160
140
120
100
80
60
40
20
ppm
File: /mnt/d600/home13/westnmr/nmrdata/DATA_FROM_NMRSERVICE/venkata/2015.11/2015.11.06.u5_3-NBD_AM_DMSO_loc1_03.04_C13_1D

Appendix IV: Selected NMR spectra (Chapter 5)

Agilent Technologies

Department of Chemistry, University of Alberta

Recorded on: ibd5, Jul 1 2015	Sweep Width(Hz): 6000.6	Acquisiton Time(s): 5	Relaxation Delay(s): 0.1
Pulse Sequence: s2pul	Digital Res.(Hz/pt): 0.09	Hz per mm(Hz/mm): 25	Completed Scans 16

498.118 MHz H1 1D in cdcl3 (ref. to CDCl3 @ 7.26 ppm), temp 26.4 C -> actual temp = 27.0 C, autoxdb probe

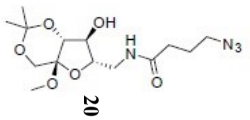

20

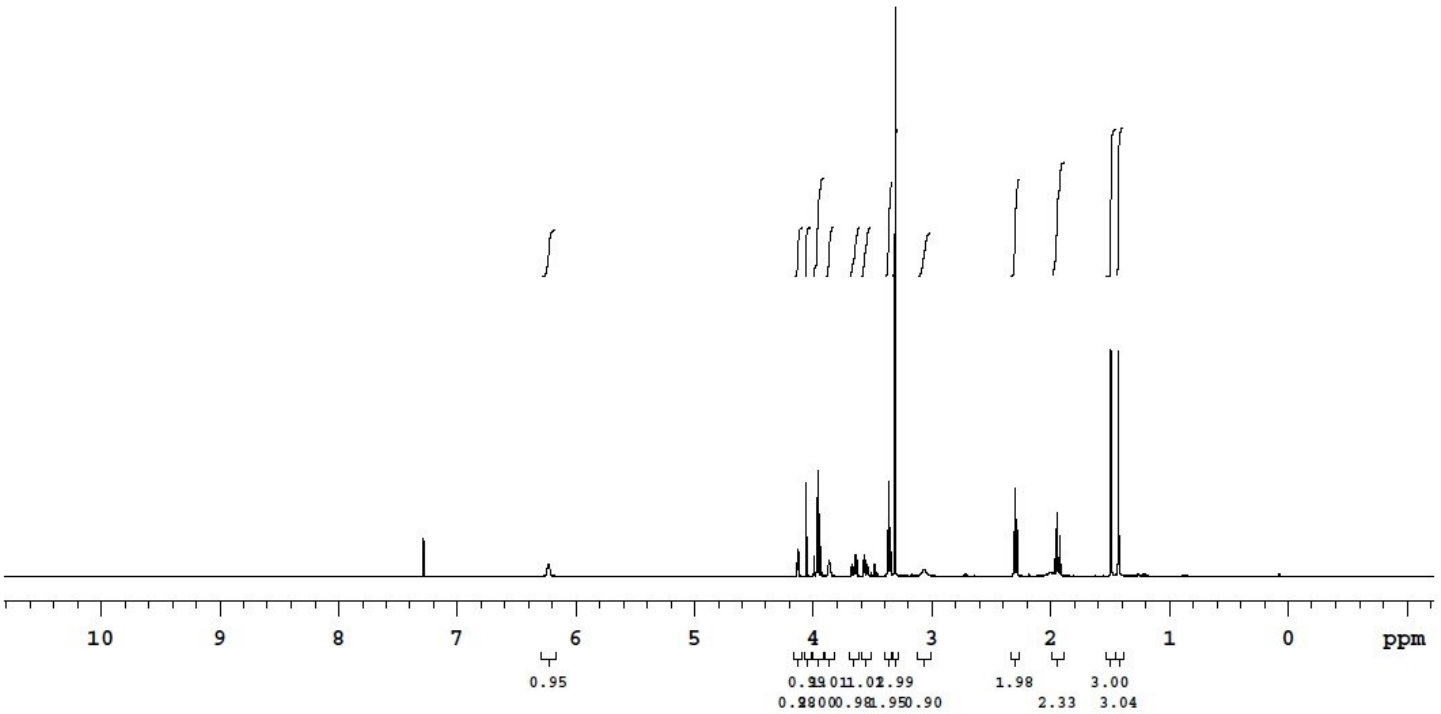

File: /mnt/d600/home13/westnmr/nmrdata/pavan/2015.07.01.i5_fru-prot-n3-liker_H1_1D

Agilent Technologies

Department of Chemistry, University of Alberta

Recorded on:	ibd5, Jul 1 2015	Sweep Width(Hz):	33826.6	Acquisiton Time(s):	2.495	Relaxation Delay(s):	0.1
Pulse Sequence:	s2pul	Digital Res.(Hz/pt):	0.26	Hz per mm(Hz/mm):	140.94	Completed Scans	2524

125.266 MHz C13[H1] 1D in cdcl3 (ref. to CDCl3 @ 77.06 ppm), temp 26.4 C -> actual temp = 27.0 C, autoxdb probe

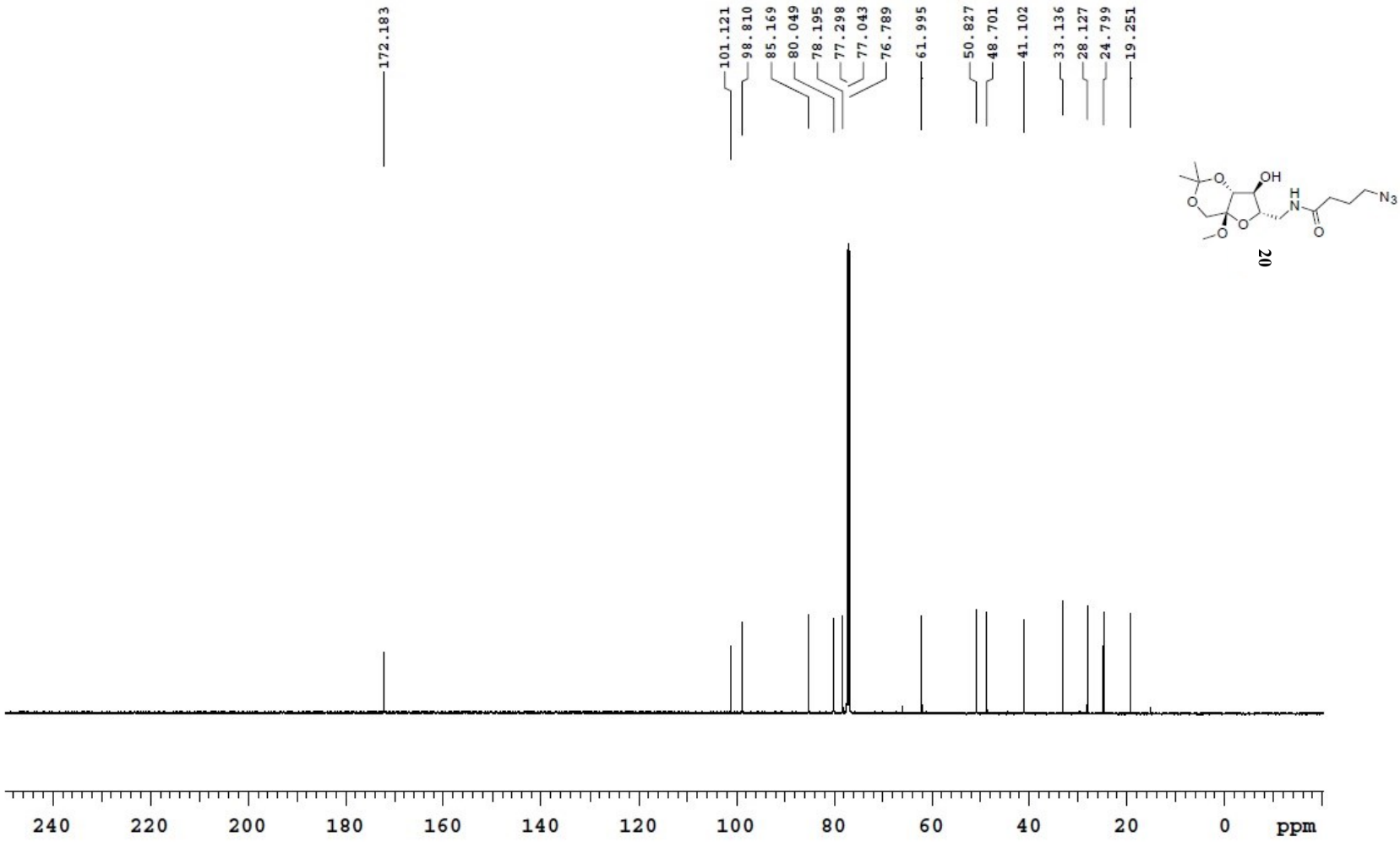

File: /mnt/d600/home13/westnmr/nmrdata/pavan/2015.07.01.i5_fru-prot-n3-liker-c13_C13_1D

venkata, P-F-NIR
699.769 MHz H1 PRESAT in cdcl3 (ref. to CDCl3 @ 7.26 ppm), temp 27.5 C -> actual temp = 27.0 C, coldid probe

date: May 27 2015 sweep width: 8389Hz acq.time: 5.0s relax.time: 2.1s # scans: 340 dig.res.: 0.1 Hz/pt hz/mm:35.0
spectrometer:d300 file:/mnt/d600/home13/westnmr/nmrdata/DATA_FROM_NMRSERVICE/venkata/2015.05/2015.05.27.v7_P-F-NIR_loc77_15.28_H1_1D

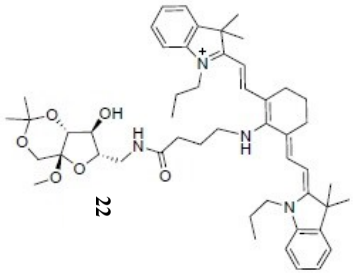

22

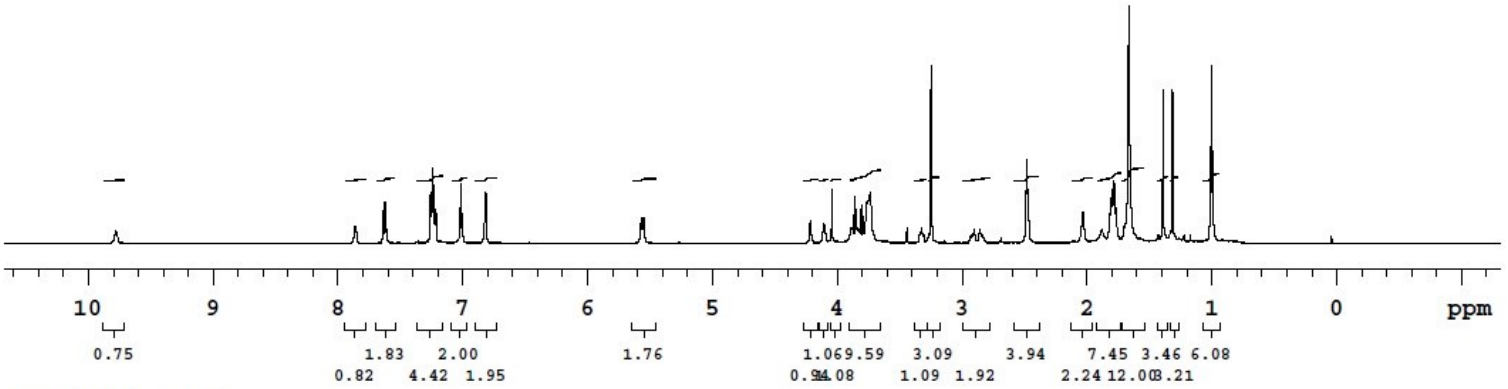

Pulse Sequence: PRESAT

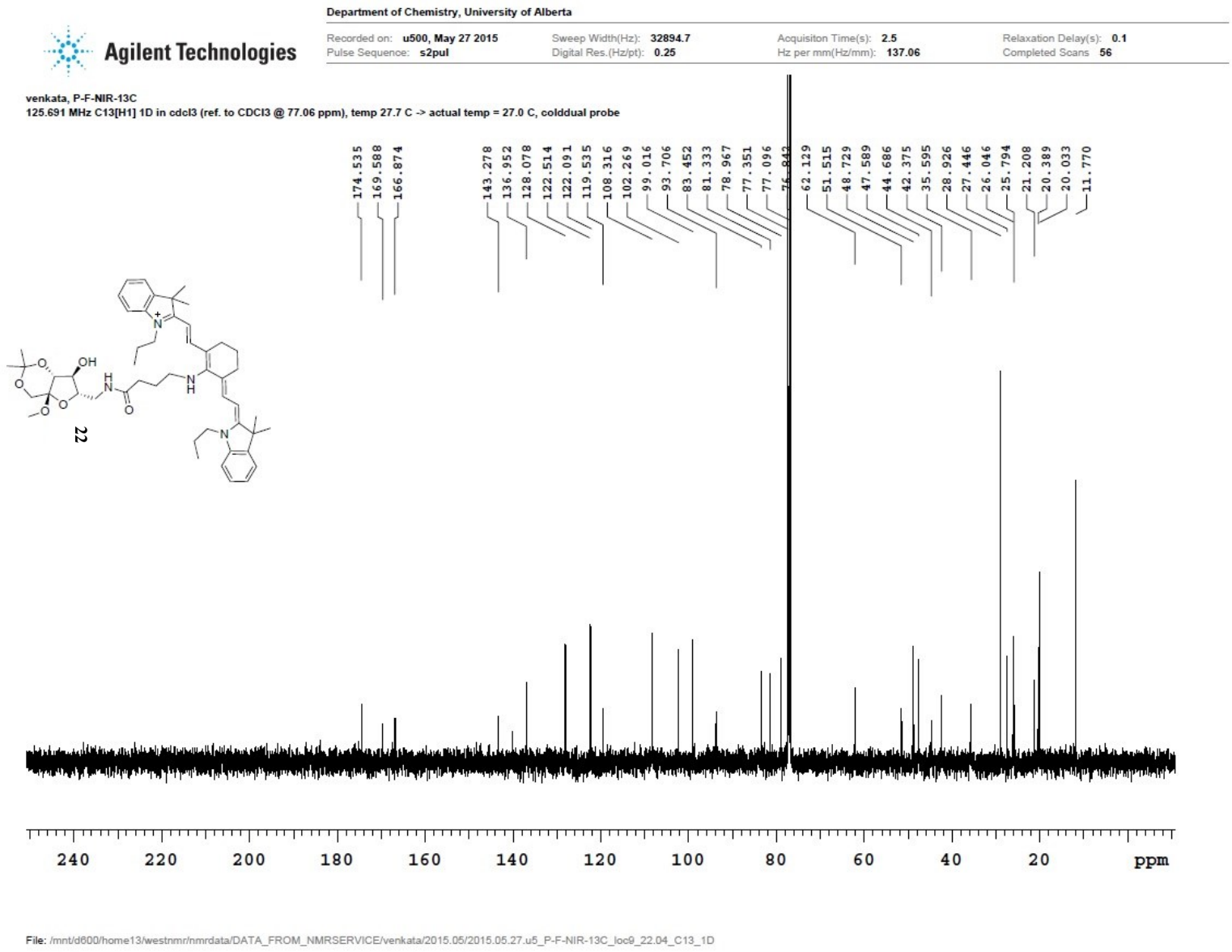
Department of Chemistry, University of Alberta
Agilent Technologies
Recorded on: u500, May 27 2015
Pulse Sequence: s2pul
Sweep Width(Hz): 32894.7
Digital Res.(Hz/pt): 0.25
Acquisiton Time(s): 2.5
Hz per mm(Hz/mm): 137.06
Relaxation Delay(s): 0.1
Completed Scans 56
venkata, P-F-NIR-13C
125.691 MHz C13[H1] 1D in cdcl3 (ref. to CDCl3 @ 77.06 ppm), temp 27.7 C -> actual temp = 27.0 C, colddual probe
174.535
169.588
166.874
143.278
136.952
128.078
122.514
122.091
119.535
108.316
102.269
99.016
93.706
83.452
81.333
78.967
77.351
77.096
76.843
62.129
51.515
48.729
47.589
44.686
42.375
35.595
28.926
27.446
26.046
25.794
21.208
20.389
20.033
11.770
22
240
220
200
180
160
140
120
100
80
60
40
20
ppm
File: /mnt/d600/home13/westnmr/nmrdata/DATA_FROM_NMRSERVICE/venkata/2015.05/2015.05.27.u5_P-F-NIR-13C_loc9_22.04_C13_1D

Department of Chemistry, University of Alberta

Agilent Technologies

Recorded on: u500, May 27 2015	Sweep Width(Hz): 32894.7	Acquisiton Time(s): 2.5	Relaxation Delay(s): 0.1
Pulse Sequence: s2pul	Digital Res.(Hz/pt): 0.25	Hz per mm(Hz/mm): 137.06	Completed Scans 56

venkata, P-F-NIR-13C

125.691 MHz C13[H1] 1D in cdcl3 (ref. to CDCl3 @ 77.06 ppm), temp 27.7 C -> actual temp = 27.0 C, colddual probe

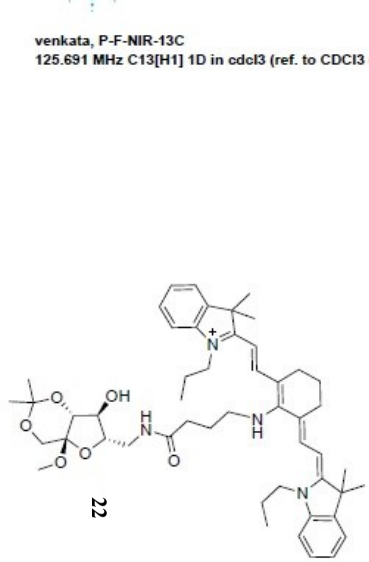

22

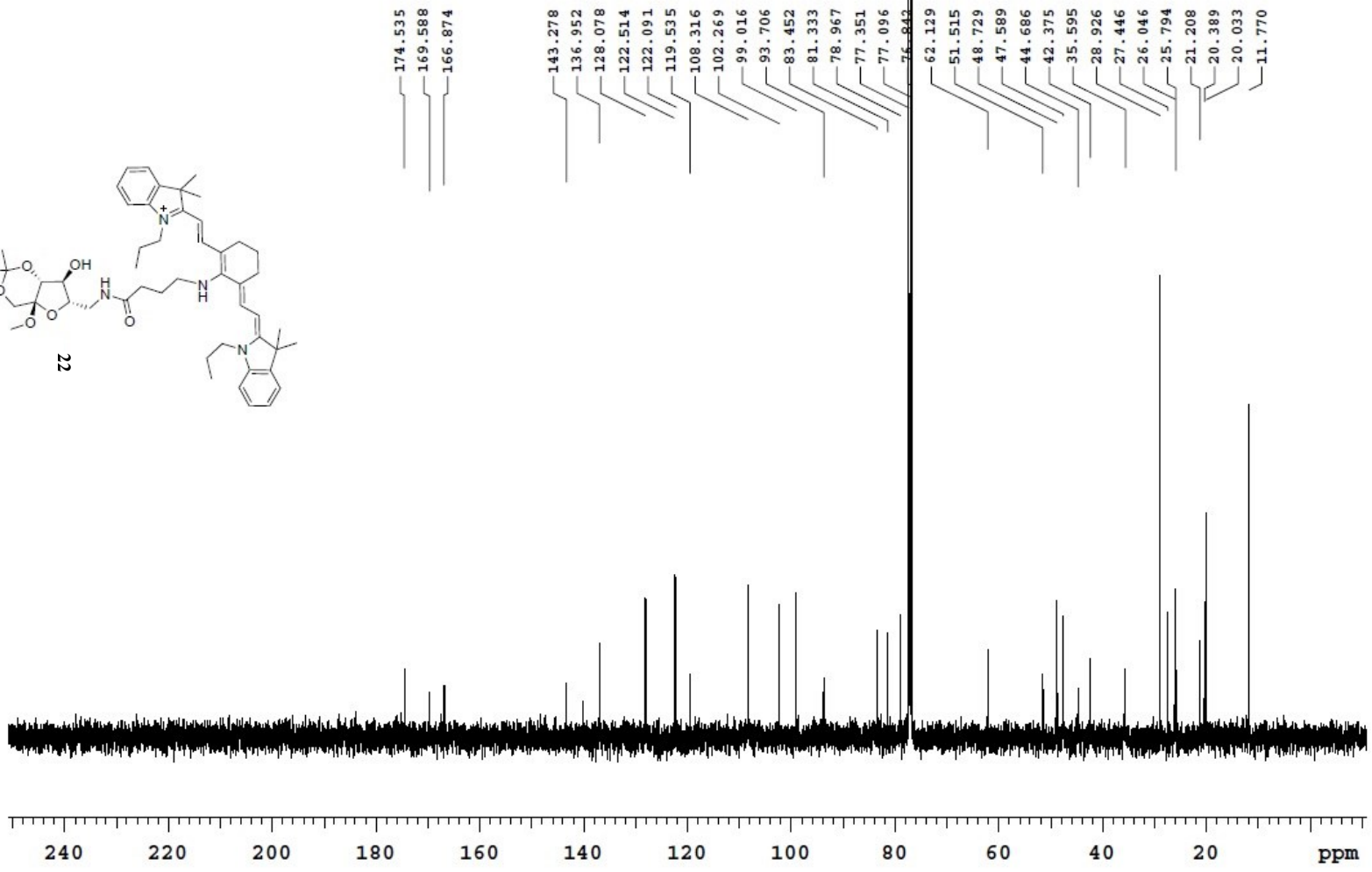

File: /mnt/d600/home13/westnmr/nmrdata/DATA_FROM_NMRSERVICE/venkata/2015.05/2015.05.27.u5_P-F-NIR-13C_loc9_22.04_C13_1D

Agilent Technologies

Department of Chemistry, University of Alberta

Recorded on: u500, Oct 4 2014	Sweep Width(Hz): 6009.62	Acquisiton Time(s): 5	Relaxation Delay(s): 0.1
Pulse Sequence: PRESAT	Digital Res.(Hz/pt): 0.18	Hz per mm(Hz/mm): 25.04	Completed Scans 52

venkata, tri-o-bn-nh-mno-AM
499.806 MHz H1 PRESAT in cdcl3 (ref. to CDCl3 @ 7.26 ppm), temp 27.7 C -> actual temp = 27.0 C, colddual probe

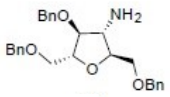

33

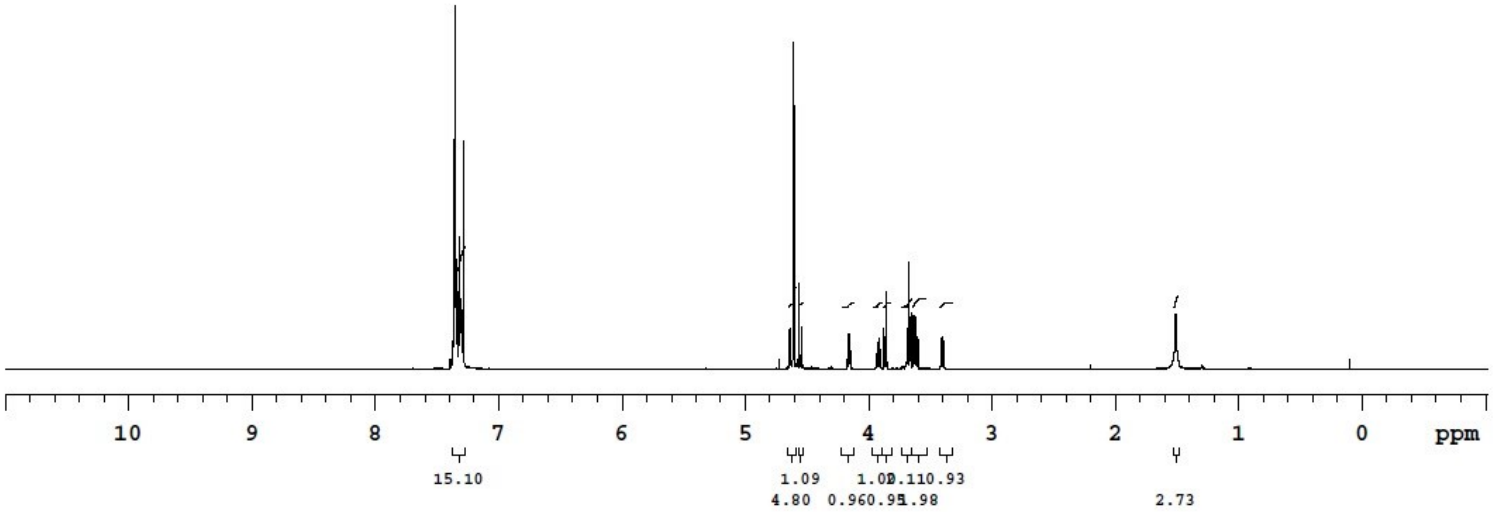

File: /mnt/d600/home13/westnmr/nmrdata/DATA_FROM_NMRSERVICE/venkata/2014.10/2014.10.4.u5_tri-o-bn-nh-mno-AM_loc6_13.19_H1_1D

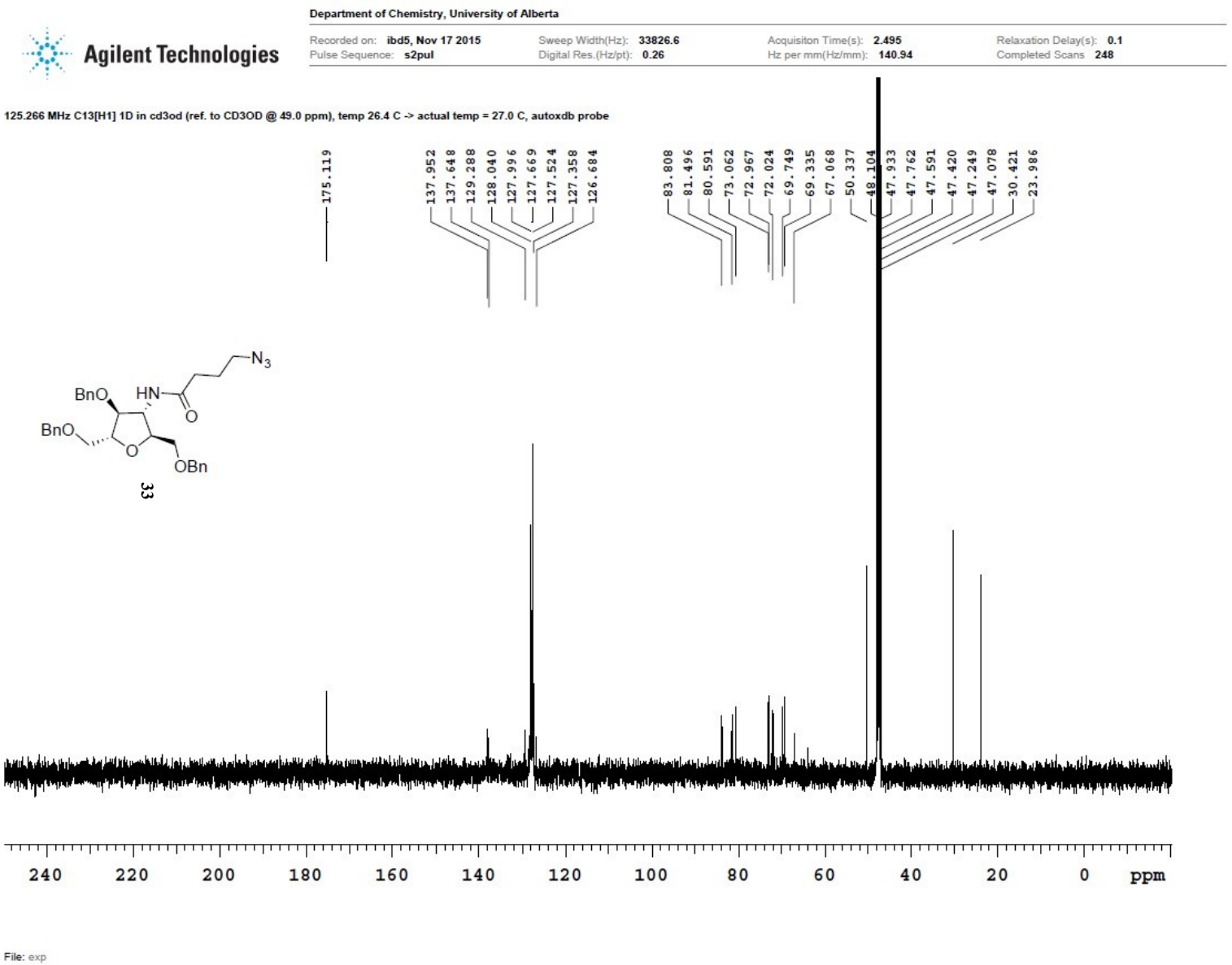
Department of Chemistry, University of Alberta
Agilent Technologies
Recorded on: ibd5, Nov 17 2015
Pulse Sequence: s2pul
Sweep Width(Hz): 33826.6
Digital Res.(Hz/pt): 0.26
Acquisiton Time(s): 2.495
Hz per mm(Hz/mm): 140.94
Relaxation Delay(s): 0.1
Completed Scans 248
125.266 MHz C13[H1] 1D in cd3od (ref. to CD3OD @ 49.0 ppm), temp 26.4 C -> actual temp = 27.0 C, autoxdb probe
175.119
137.952
137.648
129.288
128.040
127.996
127.669
127.524
127.358
126.684
83.808
81.496
80.591
73.062
72.967
72.024
69.749
69.335
67.068
50.337
48.104
47.933
47.762
47.591
47.420
47.249
47.078
30.421
23.986
BnO
HN
N3
O
BnO
O
OBn
33
240
220
200
180
160
140
120
100
80
60
40
20
0
ppm
File: exp

399.986 MHz H1 1D in cd3od (ref. to CD3OD @ 3.30 ppm), temp 25.9 C -> actual temp = 27.0 C, onenmr probe

date: Jul 6 2015 sweep width: 4808Hz acq.time: 3.0s relax.time: 3.0s # scans: 68 dig.res.: 0.1 Hz/pt hz/mm:20.0
spectrometer:d300 file:/mnt/d600/home13/westnmr/nmrdata/pavan/2015.07.06.mr4_3-IR780-AM-pure_H1_presat

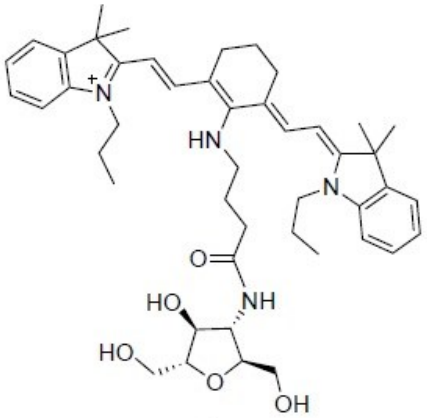

8

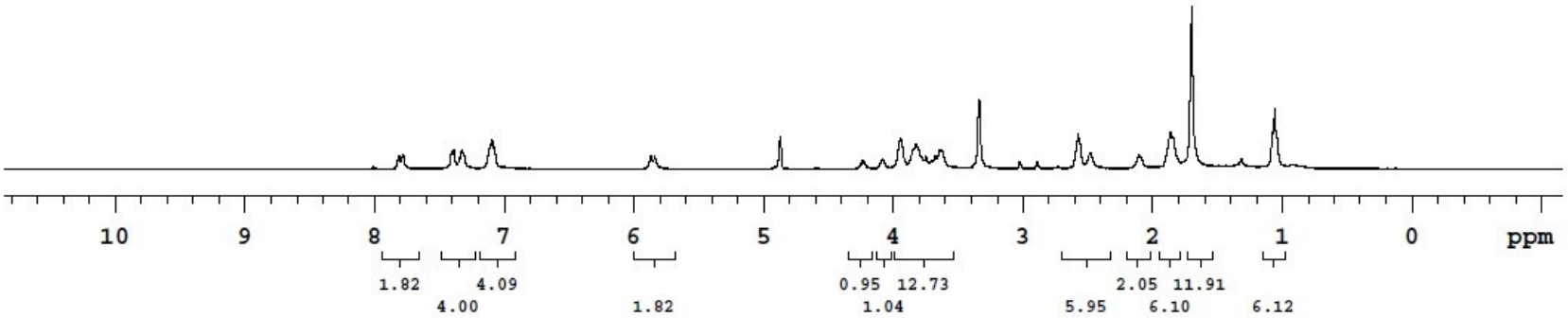

Pulse Sequence: presat

venkata, 3-IR-780-AM-pure
125.691 MHz C13[H1] 1D in cd3od (ref. to CD3OD @ 49.0 ppm), temp 27.7 C -> actual temp = 27.0 C, colddual probe

date: Jul 6 2015 sweep width: 32895Hz acq.time: 2.5s relax.time: 0.2s # scans: 5184 dig.res.: 0.3 Hz/pt hz/mm 137.1
spectrometer:d300 file:/mnt/d600/home13/westnmr/nmrdata/DATA_FROM_NMRSERVICE/venkata/2015.07/2015.07.06.u5_3-IR-780-AM-pure_loc5_21.15_C13_1D

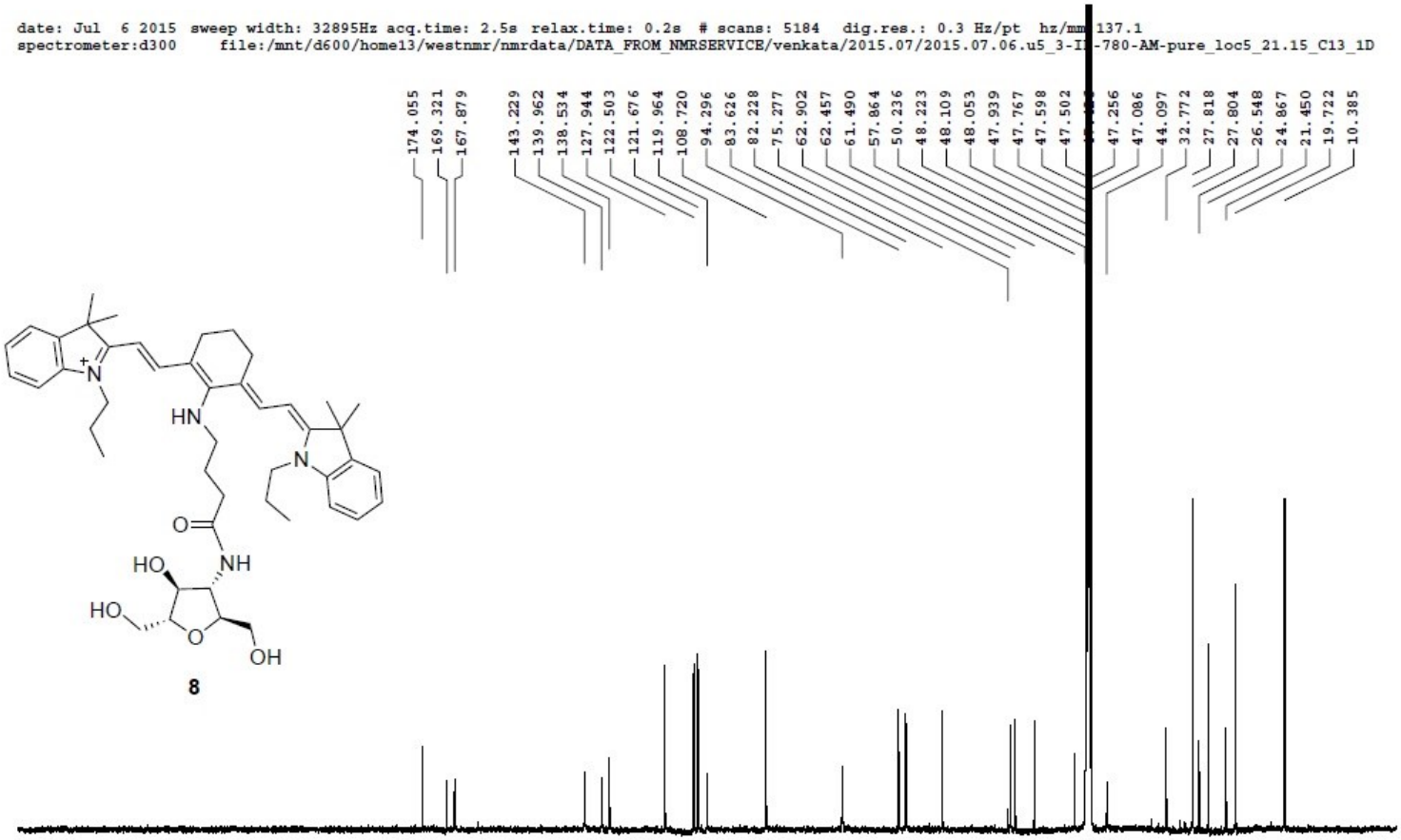

Pulse Sequence: s2pul

498.120 MHz H1 1D in cd3od (ref. to CD3OD @ 3.30 ppm), temp 26.4 C -> actual temp = 27.0 C, autoxdb probe

date: May 27 2015 sweep width: 6001Hz acq.time: 3.0s relax.time: 4.0s # scans: 112 dig.res.: 0.1 Hz/pt hz/mm:25.0
spectrometer:d300 file:/mnt/d600/home13/westnmr/nmrdata/Venkata/2015.05.27.15_3-IR-783-AM_H1_presat

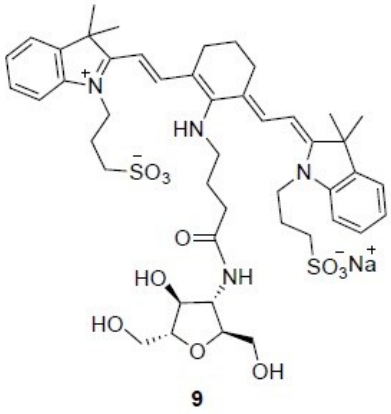

9

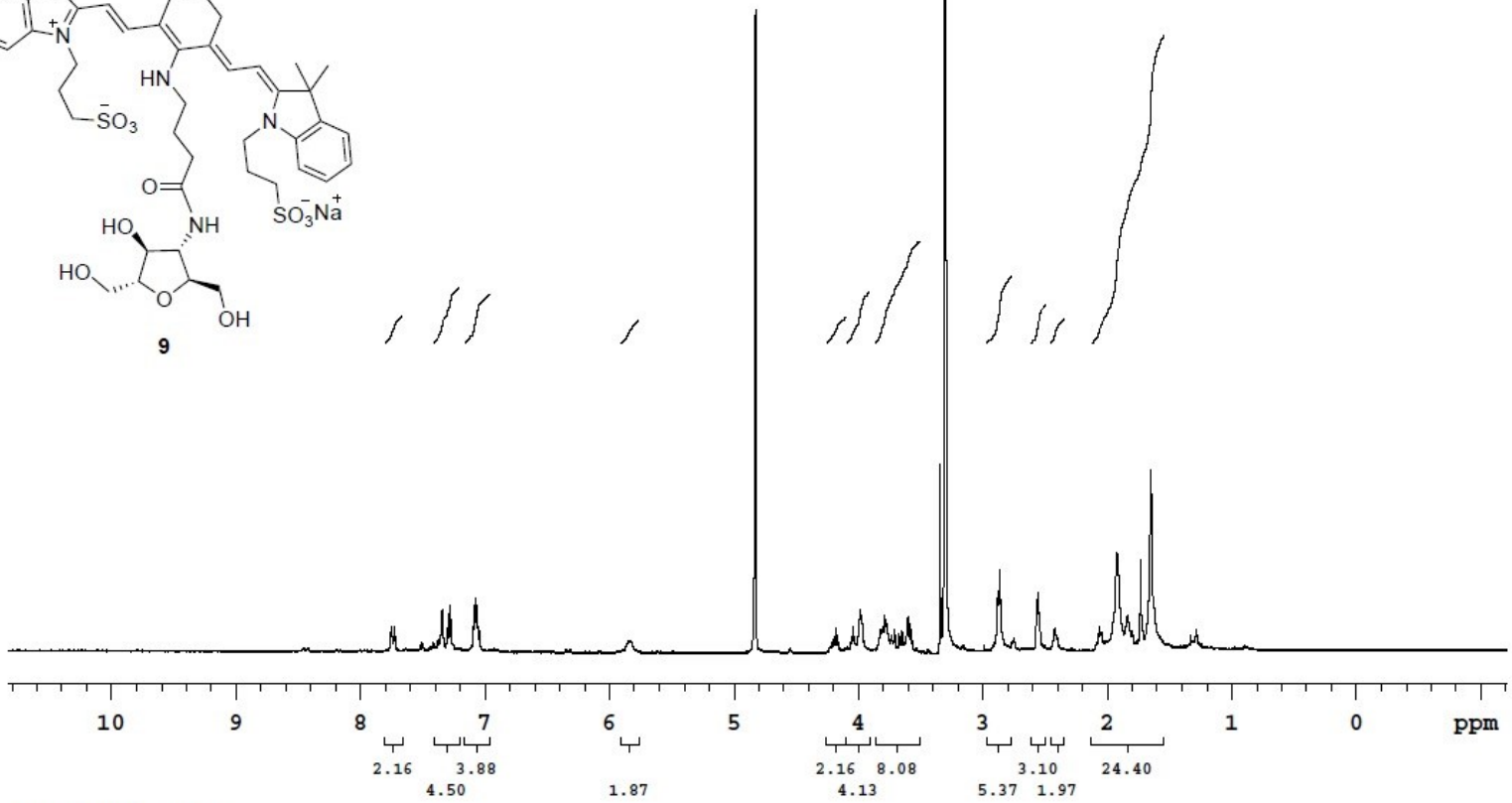

Pulse Sequence: presat

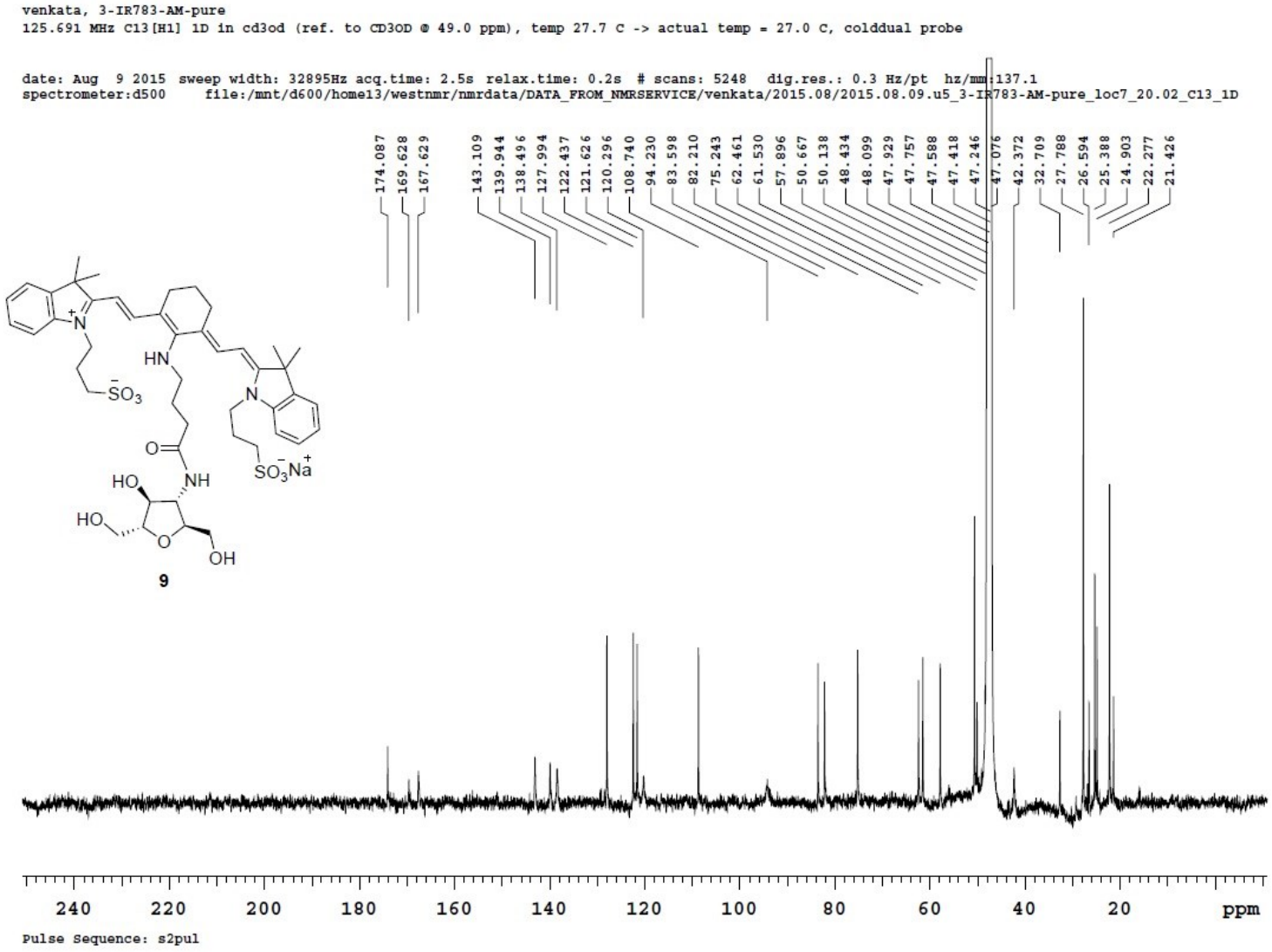
venkata, 3-IR783-AM-pure
125.691 MHz C13[H1] 1D in cd3od (ref. to CD3OD @ 49.0 ppm), temp 27.7 C -> actual temp = 27.0 C, colddual probe
date: Aug 9 2015 sweep width: 32895Hz acq.time: 2.5s relax.time: 0.2s # scans: 5248 dig.res.: 0.3 Hz/pt hz/mm:137.1
spectrometer:d500 file:/mnt/d600/home13/westnmr/nmrdata/DATA_FROM_NMRSERVICE/venkata/2015.08/2015.08.09.u5_3-IR783-AM-pure_loc7_20.02_C13_1D
174.087
169.628
167.629
143.109
139.944
138.496
127.994
122.437
121.626
120.296
108.740
94.230
83.598
82.210
75.243
62.461
61.530
57.896
50.667
50.138
48.434
48.099
47.929
47.757
47.588
47.418
47.246
47.076
42.372
32.709
27.788
26.594
25.388
24.903
22.277
21.426
HN
N
SO3
O
NH
HO
HO
O
OH
N
SO3Na
9
240
220
200
180
160
140
120
100
80
60
40
20
ppm
Pulse Sequence: s2pul

STRUCTURE REPORT

XCL Code: FGW1403 **Date:** 15 April 2014

Compound: 3-(acetylamino)-2,5-anhydro-3-deoxyhexitol
Formula: $C_8H_{15}NO_5$

Supervisor: F. G. West **Crystallographer:** R. McDonald

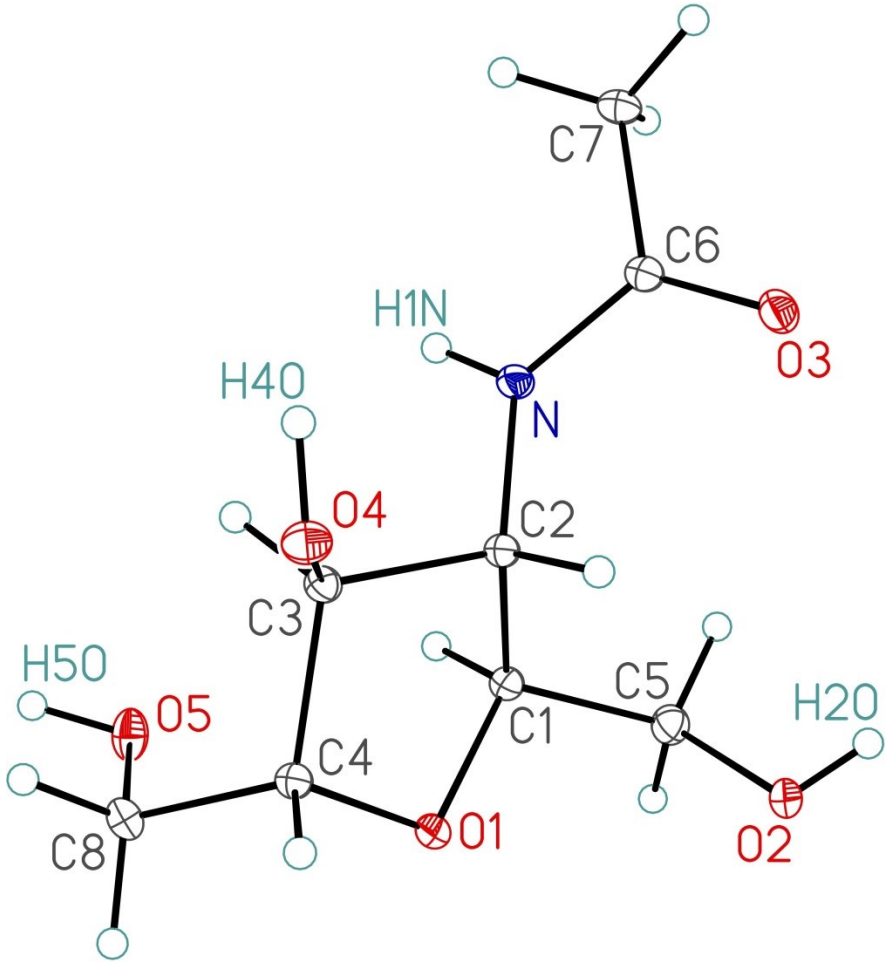

Figure Legends

Figure 1. Perspective view of the 3-(acetylamino)-2,5-anhydro-3-deoxyhexitol molecule showing the atom labelling scheme. Non-hydrogen atoms are represented by Gaussian ellipsoids at the 30% probability level. Hydrogen atoms are shown with arbitrarily small thermal parameters.

Figure 2. Illustration of hydrogen-bonded interactions between adjacent molecules of 3-(acetylamino)-2,5-anhydro-3-deoxyhexitol within the crystal lattice. Primed atoms are related to unprimed ones via the crystallographic symmetry operation ($\bar{x}$, $^{-1}/_{2}+y$, $\bar{z}$). Double-primed atoms are related to unprimed ones via the crystallographic symmetry operation (x, $1+y$, z). Starred (*) atoms are related to unprimed ones via the crystallographic symmetry operation ($\bar{x}$, $^{1}/_{2}+y$, $1-z$). Atoms marked with an octothorpe (#) are related to unprimed ones via the crystallographic symmetry operation ($-1+x$, y, z). See Table 6 for a listing of hydrogen-bonded interactions.

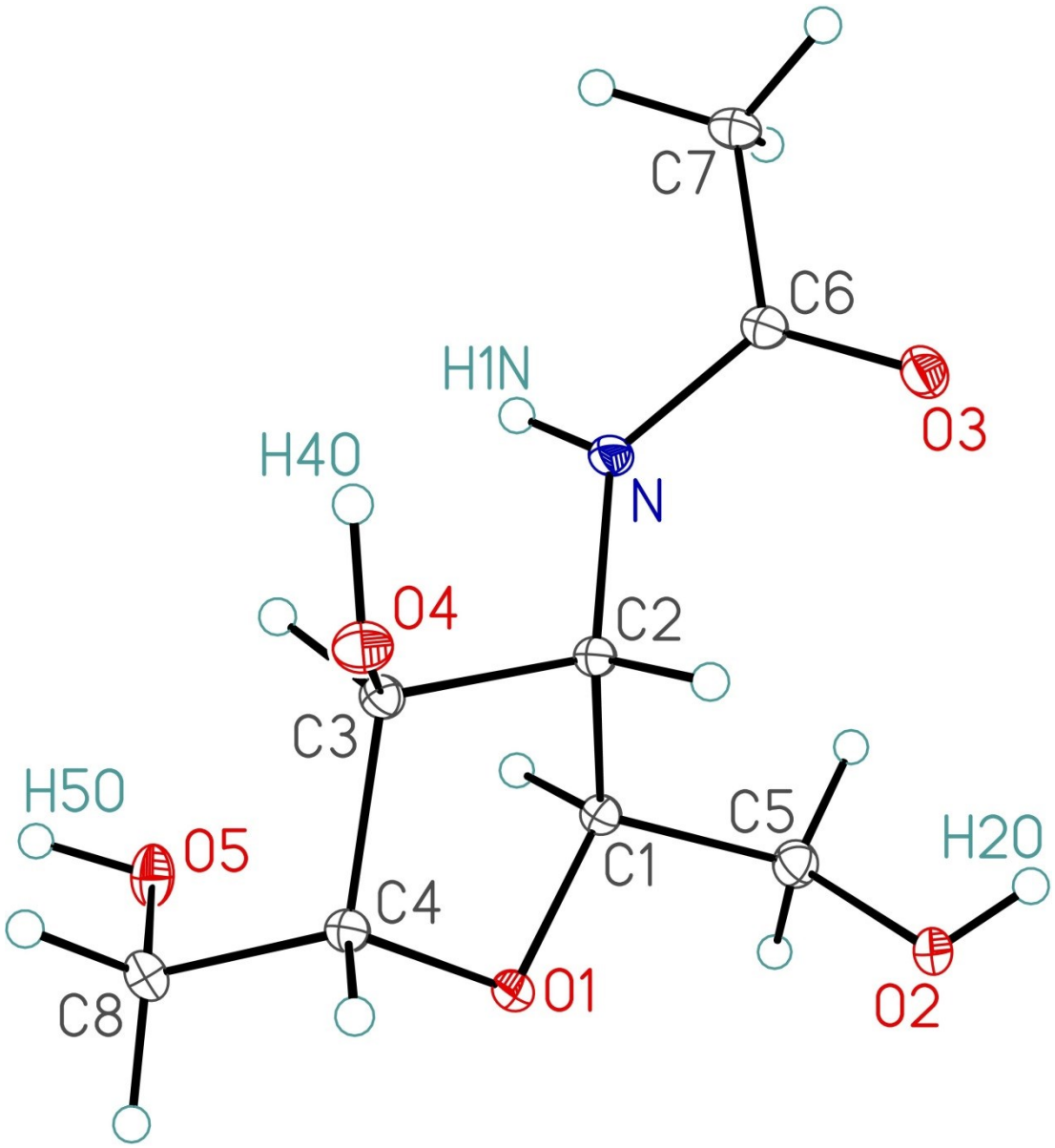
C7
C6
H1N
O3
H40
N
O4
C2
C3
H50
C5
H20
O5
C1
C4
O1
O2
C8

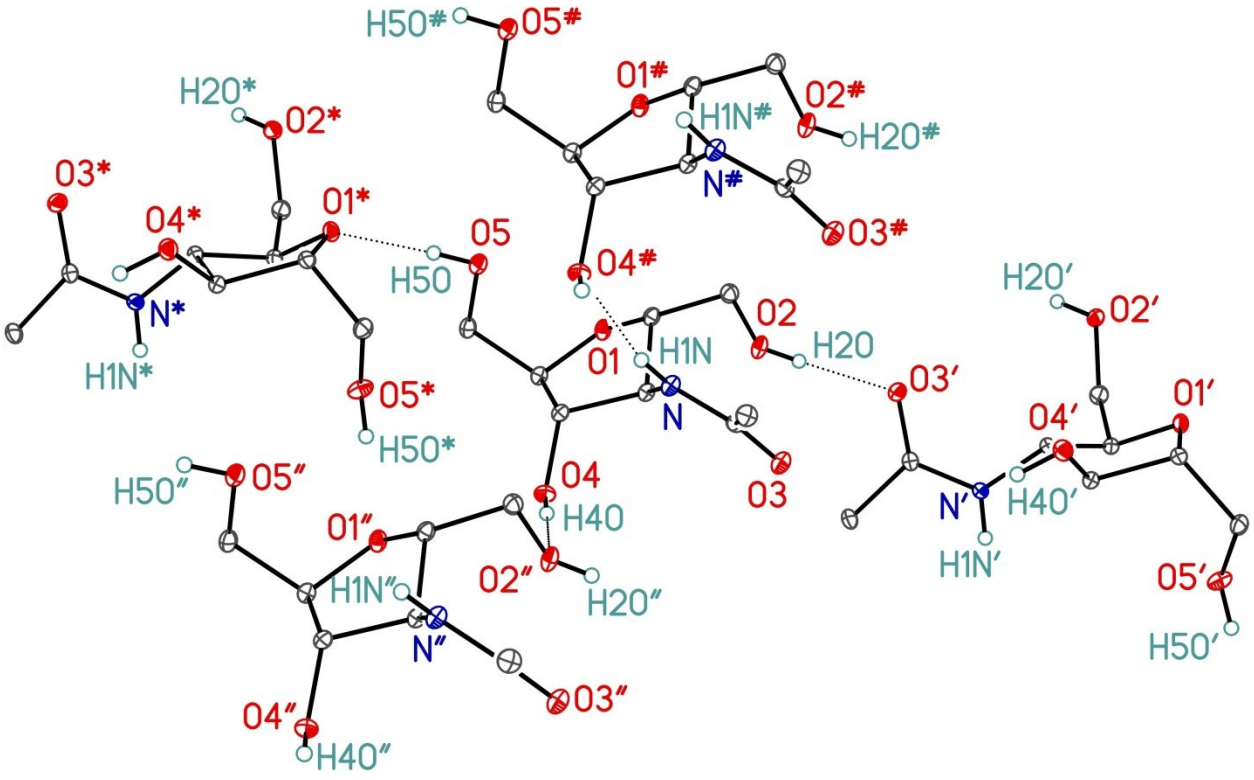
H50#
05#
01#
02#
H1N#
H20#
N#
03#
H20*
02*
03*
04*
01*
05
H50
04#
N*
H1N*
01
H1N
02
H20
03′
H20′
02′
01′
04′
05*
H50*
N
03
H50″
05″
04
H40
01″
H1N″
02″
H20″
N″
03″
04″
H40″
N′
H40′
H1N′
05′
H50′

List of Tables

Table 1. Crystallographic Experimental Details

A. Crystal Data	
formula	$C_8H_{15}NO_5$
formula weight	205.21
crystal dimensions (mm)	0.43 × 0.33 × 0.23
crystal system	monoclinic
space group	$P2_1$ (No. 4)
unit cell parameters[a]	
a (Å)	5.0350 (2)
b (Å)	6.8128 (3)
c (Å)	13.3504 (5)
β (deg)	95.2304 (4)
V (Å^3)	456.04 (3)
Z	2
ρ_{calcd} (g cm^{-3})	1.494
μ (mm^{-1})	0.124
B. Data Collection and Refinement Conditions	
diffractometer	Bruker D8/APEX II CCD[b]
radiation (λ [Å])	graphite-monochromated Mo Kα (0.71073)
temperature (°C)	–100
scan type	ω scans (0.3°) (15 s exposures)
data collection 2θ limit (deg)	56.77
total data collected	4186 (-6 ≤ h ≤ 6, -9 ≤ k ≤ 8, -17 ≤ l ≤ 17)
independent reflections	2191 (R_{int} = 0.0083)
number of observed reflections (*NO*)	2171 [$F_o^2 \geq 2\sigma(F_o^2)$]
structure solution method	intrinsic phasing (*SHELXT-2013*[c])
refinement method	full-matrix least-squares on F^2 (*SHELXL–2013*[c])
absorption correction method	Gaussian integration (face-indexed)
range of transmission factors	1.0000–0.9108
data/restraints/parameters	2191 / 0 / 144
Flack absolute structure parameter[d]	-0.21(14)
goodness-of-fit (*S*)[e] [all data]	1.094
final *R* indices[f]	
R_1 [$F_o^2 \geq 2\sigma(F_o^2)$]	0.0275
wR_2 [all data]	0.0705
largest difference peak and hole	0.269 and –0.202 e Å^{-3}

[a]Obtained from least-squares refinement of 7290 reflections with 6.12° < 2θ < 56.76°.

(continued)

Table 1. Crystallographic Experimental Details (continued)

[b]Programs for diffractometer operation, data collection, data reduction and absorption correction were those supplied by Bruker.

[c]Sheldrick, G. M. *Acta Crystallogr.* **2008**, *A64*, 112–122.

[d]Flack, H. D. *Acta Crystallogr.* **1983**, *A39*, 876–881; Flack, H. D.; Bernardinelli, G. *Acta Crystallogr.* **1999**, *A55*, 908–915; Flack, H. D.; Bernardinelli, G. *J. Appl. Cryst.* **2000**, *33*, 1143–1148. The Flack parameter will refine to a value near zero if the structure is in the correct configuration and will refine to a value near one for the inverted configuration. The low anomalous scattering power of the atoms in this structure (none heavier than oxygen) implies that the data cannot be used for absolute structure assignment, thus the Flack parameter is provided for informational purposes only. The absolute configuration was established from the relative stereochemistry determined herein along with the known stereochemistry at several stereogenic centers within the precursor compounds.

[e]$S = [\Sigma w(F_o^2 - F_c^2)^2/(n - p)]^{1/2}$ (n = number of data; p = number of parameters varied; $w = [\sigma^2(F_o^2) + (0.0419P)^2 + 0.0896P]^{-1}$ where $P = [\mathrm{Max}(F_o^2, 0) + 2F_c^2]/3$).

[f]$R_1 = \Sigma||F_o| - |F_c||/\Sigma|F_o|$; $wR_2 = [\Sigma w(F_o^2 - F_c^2)^2/\Sigma w(F_o^4)]^{1/2}$.

Table 2. Atomic Coordinates and Equivalent Isotropic Displacement Parameters

Atom	x	y	z	U_{eq}, Å^2
O1	0.2033(2)	-0.17361(17)	0.36152(8)	0.0169(2)*
O2	0.1656(2)	-0.39395(17)	0.18114(9)	0.0198(3)*
O3	-0.0446(2)	0.07382(19)	0.01857(8)	0.0200(2)*
O4	0.3973(2)	0.29020(18)	0.28615(9)	0.0185(2)*
O5	-0.0539(2)	0.0471(2)	0.50045(9)	0.0228(3)*
N	-0.1657(3)	0.1340(2)	0.17488(10)	0.0159(3)*
C1	-0.0179(3)	-0.1455(2)	0.28685(11)	0.0150(3)*
C2	0.0593(3)	0.0376(2)	0.23011(10)	0.0141(3)*
C3	0.1897(3)	0.1667(2)	0.31529(11)	0.0146(3)*
C4	0.3035(3)	0.0179(2)	0.39461(11)	0.0151(3)*
C5	-0.0660(3)	-0.3311(2)	0.22580(12)	0.0188(3)*
C6	-0.1972(3)	0.1522(2)	0.07420(11)	0.0144(3)*
C7	-0.4310(3)	0.2766(2)	0.03436(12)	0.0183(3)*
C8	0.2284(3)	0.0597(3)	0.50016(11)	0.0187(3)*
H2O	0.132(5)	-0.401(4)	0.122(2)	0.029(6)
H4O	0.324(5)	0.388(5)	0.253(2)	0.035(7)
H5O	-0.105(5)	0.132(5)	0.5434(19)	0.030(6)
H1N	-0.275(5)	0.191(4)	0.2076(17)	0.022(5)

Anisotropically-refined atoms are marked with an asterisk (*). The form of the anisotropic displacement parameter is: $\exp[-2\pi^2(h^2a^{*2}U_{11} + k^2b^{*2}U_{22} + l^2c^{*2}U_{33} + 2klb^*c^*U_{23} + 2hla^*c^*U_{13} + 2hka^*b^*U_{12})]$.

Table 3. Selected Interatomic Distances (Å)

Atom1	Atom2	Distance	Atom1	Atom2	Distance
O1	C1	1.4382(18)	N	C6	1.345(2)
O1	C4	1.4531(19)	C1	C2	1.528(2)
O2	C5	1.423(2)	C1	C5	1.512(2)
O3	C6	1.2375(19)	C2	C3	1.537(2)
O4	C3	1.4236(18)	C3	C4	1.538(2)
O5	C8	1.4243(19)	C4	C8	1.519(2)
N	C2	1.4511(18)	C6	C7	1.507(2)

Table 4. Selected Interatomic Angles (deg)

Atom1	Atom2	Atom3	Angle	Atom1	Atom2	Atom3	Angle
C1	O1	C4	108.45(11)	C2	C3	C4	103.87(12)
C2	N	C6	124.42(13)	O1	C4	C3	106.56(12)
O1	C1	C2	103.68(12)	O1	C4	C8	109.98(13)
O1	C1	C5	109.76(13)	C3	C4	C8	113.99(13)
C2	C1	C5	116.81(13)	O2	C5	C1	112.35(13)
N	C2	C1	113.55(12)	O3	C6	N	122.46(14)
N	C2	C3	112.21(12)	O3	C6	C7	122.58(14)
C1	C2	C3	102.18(11)	N	C6	C7	114.95(13)
O4	C3	C2	114.27(12)	O5	C8	C4	108.90(12)
O4	C3	C4	109.94(12)				

Table 5. Torsional Angles (deg)

Atom1	Atom2	Atom3	Atom4	Angle	Atom1	Atom2	Atom3	Atom4	Angle
C4	O1	C1	C2	35.10(14)	O1	C1	C5	O2	-55.69(17)
C4	O1	C1	C5	160.60(12)	C2	C1	C5	O2	61.90(18)
C1	O1	C4	C3	-16.57(15)	N	C2	C3	O4	-89.78(15)
C1	O1	C4	C8	107.46(13)	N	C2	C3	C4	150.45(12)
C6	N	C2	C1	-116.13(16)	C1	C2	C3	O4	148.25(12)
C6	N	C2	C3	128.63(15)	C1	C2	C3	C4	28.47(13)
C2	N	C6	O3	5.8(2)	O4	C3	C4	O1	-131.22(12)
C2	N	C6	C7	-173.77(14)	O4	C3	C4	C8	107.27(14)
O1	C1	C2	N	-160.04(11)	C2	C3	C4	O1	-8.54(14)
O1	C1	C2	C3	-38.98(13)	C2	C3	C4	C8	-130.05(13)
C5	C1	C2	N	79.11(17)	O1	C4	C8	O5	-57.09(17)
C5	C1	C2	C3	-159.84(13)	C3	C4	C8	O5	62.50(17)

Table 6. Hydrogen-Bonded Interactions

D–H···A	D–H (Å)	H···A (Å)	D···A (Å)	∠D–H···A (deg)	Note
O2–H2O···O3[a]	0.79(3)	1.90(3)	2.6892(16)	178(3)	[a]At $\bar{x}$, $-1/2+y$, $\bar{z}$.
O4–H4O···O2[b]	0.86(3)	1.91(3)	2.7674(17)	179(3)	[b]At x, $1+y$, z.
O5–H5O···O1[c]	0.87(3)	1.93(3)	2.7993(17)	178(2)	[b]At $\bar{x}$, $1/2+y$, $1-z$.
N–H1N···O4[d]	0.83(3)	2.15(3)	2.9626(18)	169(2)	[a]At $-1+x$, y, z.

Table 7. Anisotropic Displacement Parameters (U_{ij}, Å^2)

Atom	U_{11}	U_{22}	U_{33}	U_{23}	U_{13}	U_{12}
O1	0.0231(5)	0.0147(5)	0.0123(5)	0.0003(4)	-0.0012(4)	0.0029(4)
O2	0.0273(6)	0.0194(6)	0.0127(5)	-0.0024(4)	0.0015(4)	0.0062(5)
O3	0.0204(5)	0.0255(6)	0.0143(5)	-0.0002(5)	0.0020(4)	0.0038(5)
O4	0.0180(5)	0.0169(6)	0.0207(6)	0.0037(4)	0.0025(4)	-0.0009(4)
O5	0.0227(6)	0.0262(6)	0.0204(5)	-0.0075(5)	0.0073(5)	-0.0021(5)
N	0.0155(6)	0.0186(6)	0.0136(6)	0.0011(5)	0.0012(4)	0.0053(5)
C1	0.0173(6)	0.0149(7)	0.0129(6)	0.0006(6)	0.0017(5)	0.0026(5)
C2	0.0151(6)	0.0147(7)	0.0124(6)	0.0007(5)	0.0011(5)	0.0029(5)
C3	0.0155(7)	0.0155(7)	0.0128(6)	0.0009(5)	0.0020(5)	0.0013(5)
C4	0.0154(6)	0.0160(7)	0.0137(6)	0.0002(5)	0.0006(5)	0.0024(5)
C5	0.0218(7)	0.0167(7)	0.0178(7)	-0.0004(6)	0.0020(5)	-0.0007(6)
C6	0.0144(6)	0.0132(7)	0.0153(6)	0.0011(5)	-0.0006(5)	-0.0024(5)
C7	0.0172(7)	0.0193(7)	0.0178(7)	0.0035(6)	-0.0023(5)	0.0023(6)
C8	0.0215(7)	0.0210(7)	0.0132(6)	-0.0015(6)	-0.0007(5)	0.0002(6)

The form of the anisotropic displacement parameter is:
$\exp[-2\pi^2(h^2a^{*2}U_{11} + k^2b^{*2}U_{22} + l^2c^{*2}U_{33} + 2klb^*c^*U_{23} + 2hla^*c^*U_{13} + 2hka^*b^*U_{12})]$

Table 8. Derived Atomic Coordinates and Displacement Parameters for Hydrogen Atoms

Atom	x	y	z	U_{eq}, Å^2
H1	-0.1809	-0.1158	0.3216	0.018
H2	0.1948	0.0021	0.1829	0.017
H3	0.0501	0.2485	0.3439	0.017
H4	0.5023	0.0175	0.3957	0.018
H5A	-0.1238	-0.4366	0.2699	0.023
H5B	-0.2119	-0.3079	0.1722	0.023
H7A	-0.4013	0.3252	-0.0328	0.022
H7B	-0.4496	0.3881	0.0796	0.022
H7C	-0.5941	0.1975	0.0304	0.022
H8A	0.3153	-0.0368	0.5479	0.022
H8B	0.2898	0.1926	0.5215	0.022